Peter Knippertz
Jan-Berend W. Stuut *Editors*

Mineral Dust

A Key Player in the Earth System

Springer

Mineral Dust

Peter Knippertz • Jan-Berend W. Stuut
Editors

Mineral Dust

A Key Player in the Earth System

Springer

Editors
Peter Knippertz
School of Earth & Environment
University of Leeds
Leeds, UK

Institute for Meteorology
and Climate Research
Karlsruhe Institute of Technology
Karlsruhe, Germany

Jan-Berend W. Stuut
NIOZ – Royal Netherlands
Institute for Sea Research
Department of Marine
Geology and Chemical Oceanography
Texel, The Netherlands

MARUM – Center for Marine
Environmental Sciences
Department of Marine Sedimentology
University of Bremen
Bremen, Germany

ISBN 978-94-017-8977-6 ISBN 978-94-017-8978-3 (eBook)
DOI 10.1007/978-94-017-8978-3
Springer Dordrecht Heidelberg New York London

Library of Congress Control Number: 2014947241

Cover image: Jutta Leyrer (NIOZ)

Printed on acid-free paper

Springer is part of Springer Science+Business Media (www.springer.com)

Preface

This is a book about mineral dust in the Earth's atmosphere. Atmospheric dust consists of tiny mineral particles, which mostly originate from soils in the arid and semi-arid parts of the Earth and can be transported over distances of many thousands of kilometres to be finally deposited on soil, plants and glaciers or into the ocean. Dust is a fascinating, truly interdisciplinary and rapidly growing research topic for many reasons. Dust storms are dramatic meteorological events that can have considerable impacts on human activities reaching from health and agriculture to industrial production, (air-)traffic and military operations. Dust changes the global energy and carbon budgets and thereby affects climate and even weather in multiple ways. The amounts of dust in the atmosphere, its sources and transport patterns have changed considerably through climate history, providing an important source of information for reconstructions. It is currently debated what role dust may play in manmade climate change. This book attempts to give a comprehensive overview of the full range of current dust research and the underpinning fundamental scientific concepts while at the same time explaining concrete applications of this science. It mainly addresses researchers from the postgraduate to the senior level, but at least parts of it should be useful for specialised teaching activities (e.g. summer schools).

The idea for this book was born in a recurrent session at the annual General Assembly of the European Geosciences Union (EGU) entitled "Aeolian dust: Initiator, Player, and Recorder of Environmental Change". Jan-Berend Stuut and Maarten Prins (both from the Climate division of EGU) started this session in 2004. It has successfully run every year since then with up to 60 contributions per session. Peter Knippertz was invited to join as a convener in 2008 to enhance the involvement of the Atmospheric Sciences division. Since then, the role of dust in climate and atmospheric sciences has been the backbone of the session, while participation from the soil science and geomorphology community has varied, as also reflected in changes to the convener group (Andreas Baas participating in 2008 and 2009, Sue McLaren joining in 2013). There are very few long-running, recurrent conference sessions or meetings solely dedicated to dust, such that this session has created an important interdisciplinary forum for this type of research. Over the years, a great number of internationally recognized experts on dust have attended and presented

at the session, many of which are now authors of this book. Many presentations and the subsequent discussions have inspired new research and collaborations, and it has been a true pleasure to be involved in this activity over the years. We hope that the readers of this book will find it an inspiring and interesting lecture and that at least part of the fascination that brought the authors and editors of this book together in the first place can be conveyed on the following pages.

For those interested to learn more about aeolian dust, please visit the website of the International Society for Aeolian Research (ISAR) at www.aeolianresearch.org. The International Society of Aeolian Research was created to promote contacts among scientists undertaking research in aeolian processes, landforms, and modeling, to stimulate scientific research in aeolian topics and related fields, and to further the application of the results of such research into practical applications.

Personal Notes by the Editors

We, the editors, had a long discussion about how to write personal notes in the preface of this book. In the end we agreed that one important aspect should be to attempt to inspire the reader by telling how our careers developed and how the mixture of curiosity, enthusiasm, collaboration and pure chance have made our jobs so fascinating . . . .

Peter Knippertz

Looking back at my scientific career so far, it is interesting to reflect upon how I increasingly became involved in dust research. The initial spark was the extraordinary dust storm of 3–6 March 2004, which affected almost entire northern Africa for several days. By the time of this event I had just completed my PhD at the University of Cologne (Germany) on rainfall variability in northwestern Africa and had moved on to a postdoc fellowship at the University of Wisconsin–Madison (USA). The first Meteosat Second Generation satellite (Meteosat-8) had just become operational in time for this event on 29 January 2004. The extension to 12 channels, several of which in the infrared part of the electromagnetic spectrum, allowed for the first time visualizing dust plumes over land and water in a clear and consistent way with 15-min time resolution. Watching animations of this storm over and over again, I decided to conduct a detailed case study, which led to my first publication on dust (Knippertz and Fink, 2006, Quart. J. Roy. Meteorol. Soc.). After my return to Germany in 2005, I became involved with the SAMUM (Saharan Mineral Dust Experiment) project that brought me to Morocco and the Cape Verde Islands for dust-related fieldwork and led to numerous new contacts, collaborations and publications across Europe. In 2010, after my move to the University of Leeds (UK), I was granted my first own project on dust entitled "Desert Storms" through the European Research Council Starting Grant scheme, which allowed me to focus very strongly on meteorological aspects of dust uplift. Today, after another move back to Germany, dust science makes up an important part of my research portfolio,

demonstrating how the invention of new technology (Meteosat) in combination with a spectacular single meteorological event (the March 2004 dust storm) can shape a research career for years. This book is yet another step in the growing importance that dust research has taken in my scientific interest and research work.

Of course, a book of this breadth of topics can hardly be assembled by one person alone. Therefore I am very grateful to Jan-Berend Stuut for the long-term fruitful and enjoyable collaboration, both for organising the EGU dust sessions and for editing this book. Only this collaboration made it possible to fully bridge the wide gap from dust particles acting as ice nuclei to the evolution of the Chinese Loess Plateau. I'm also thankful to the fantastic team of chapter authors that brought the fascinating range of dust research to life in this book. It is an honour to be an editor for such an excellent group of international experts, who have not only put together their own chapters but also contributed substantially by reviewing the chapters of others. I would like to thank the EGU for providing a great forum over the years to assemble the dust community at their annual meetings and all the scientists that have contributed to make the dust sessions lively and inspiring. Many of those have contributed significantly to my interest in and research on dust through fruitful collaborations and joint papers, and I won't be able to provide an exhaustive list here. To mention at least a few I would like to thank Andreas Fink for sharing the enthusiasm about the March 2004 storm and many other interesting meteorological events; Lothar Schütz, Konrad Kandler, Albert Ansmann and many others involved in SAMUM for opening the project up generously and widely for my participation; Amato Evan and Helen Brindley for giving me a better satellite perspective on dust; Martin Todd, Cyrille Flamant and Diana Bou Karam for fruitful discussions and joint papers; as well as my students, postdocs and colleagues at the Universities of Mainz (Carmen Emmel née Deutscher, Gregor Gläser) and Leeds (John Marsham, Bernd Heinold, Kerstin Schepanski, Carl Gilkeson, Sophie Cowie, Alex Roberts, Stephanie Fiedler, Bradley Jemmett-Smith) as well as at the Karlsruhe Institute of Technology (Florian Pantillon) for their fantastic research on dust and collaboration. Last but not least I am much obliged to those that funded this research over the past 10 years: the European Research Council (ERC), the German Science Foundation (DFG) and the Johannes Gutenberg University Mainz (JGU).

Leeds, UK
Karlsruhe, Germany
July 2014

Peter Knippertz

Jan-Berend W. Stuut

Ever since my Master's project, during which I tried to recognise and quantify wind-blown dust in marine sediments from the Indian Ocean, I have been fascinated by aeolian dust. Together with and supervised by Maarten Prins, we managed to characterise and quantify dust in marine sediments from both the Indian- and south-eastern Atlantic oceans, simply by studying the grain-size distribution of

deep-marine sediments. A powerful proxy indeed! I continued studying mineral dust for my PhD studies offshore Namibia and established a reconstruction of environmental changes in south-western Africa. It turned out that climate in this part of Africa was related to ocean circulation but showed a pattern that was exactly opposite to the well-established paleoclimate records from the northern hemisphere. When looking at these records I am literally still amazed how the patterns in the grain size of the terrigenous sediments and those in the $\delta^{18}O$ of surface-ocean unicellular calcifiers line up so nicely although they are totally independent proxies! After finishing my PhD in 2001, I moved on to the University of Bremen, Germany, for a postdoc to study mineral dust in marine sediments offshore Chile to see if climate throughout the late Quaternary followed the same southern-hemisphere pattern, which it did! I thank both Gerold Wefer and Dierk Hebbeln for their unrelenting support and for giving me the freedom to go my own way "chasing dust" during two more postdoc phases in Bremen.

While studying dust in marine sediment archives, I found that it is quite possible and of vital importance to ground-truth observations inferred from dust deposits by comparing them with present-day processes of dust mobilisation, dispersal, and deposition. I am much obliged to Ralph Schneider who invited me to join his research cruise on board RV *Meteor* in 1998 to collect Saharan dust from the atmosphere while sailing from southern Spain to Gabon all along the west African coast. This was a typical example of being at the right place at the right time because we happened to sail through a few giant dust outbreaks: an amazing experience and probably a trigger similar to Peter's observation of the March 2004 dust storm. For the first time we managed to combine the set of actual dust samples collected on board the ship with satellite data and the daily meteorological observations done by the German Weather Service on board the ship. By studying back-trajectories of the different air masses we located with the weather-balloon data, we managed to trace the different dust particles back to their sources. Many ship cruises and dust sampling campaigns later we still have more questions than answers regarding dust dispersal and deposition and also the marine environmental effects of dust deposition: enough work to be done!

One more colleague that played a critical role in my dusty career is Patrick De Deckker who picked up and stimulated my curiosity after the role of the southern hemisphere on global climate. Within weeks after we met, he managed to transfer our ideas into an ARC (the Australian NSF) proposal to study Australian dust sources. We got funded to go into the Australian outback to fingerprint the many different dust sources based on geology, mineralogy, chemistry and microbiology. These field trips were truly amazing and they broadened my horizon in many ways.

Another event that I think has been essential in shaping my dusty career is a project by the Dutch TV channel VPRO, who organised a trip on board the clipper *Stad Amsterdam* in 2010, retracing Charles Darwin's travels on board HMS *Beagle*. They allowed me to participate in this cruise by installing a dust collector on deck sampling the atmosphere offshore the large deserts they passed, just like Darwin did. The trip made me aware of how easily scientific results can be misused to make money. On the ship I discussed a lot with a so-called geo-engineer who wanted to make money by fertilising the ocean with powdered iron ore in order to combat

global warming. His motivation was based on John Martin's iron hypothesis which states that phytoplankton can sequester CO_2 from the atmosphere, and that there are certain iron-limited parts of the ocean in which phytoplankton can benefit from iron additions. These discussions convinced me of the fact that fundamental research is of vital importance for applied sciences as well and that great care should be taken when disturbing natural balances. As a result I am now working on three parallel projects in which we collect Saharan dust along a transatlantic transect between NW Africa and the Caribbean using tethered surface buoys and moored submarine sediment traps to study the marine environmental effects of dust deposition.

When I wanted to present my results in a big meeting like the European Geosciences Union, I found that actually there were no sessions in which my work fitted very well. As a result, the EGU program committee (by then still called EGS) was kind enough to allow Maarten Prins and me to organise our first dust session in Nice in 2004. It came down to us writing emails to invite people that we only knew from their dusty papers and ask them to join us in Nice to discuss mineral dust. The incredible thing was: virtually all these famous people (e.g., Grant McTainsh a.k.a. "Dr Dust", Joe Prospero, Ed Derbyshire, Martin Iriondo, Misao Mikami, Ina Tegen, Slobodan Markovic, Jean Robert Petit, Ludwig Zöller, Patrick De Deckker, Dennis Rousseau, Ian Smalley, to name a few) responded enthusiastically and came! From the first one on, our dust session was a great success with many very interesting contributions from almost all scientific disciplines one can think of related to mineral dust, which are also presented in this book. Throughout the years I had the pleasure to have worked together with different co-convenors (Maarten Prins, Andreas Baas, Peter Knippertz, Sue McLaren) and our sessions have been a continuous success, supported by many contributors presenting their fascinating work and ideas. I have enjoyed bringing people together in workshops and sessions like this and this book is just another result from this exercise of bridging gaps between scientific disciplines.

I wish to explicitly thank my co-editor Peter Knippertz who also put a lot of energy in organising the sessions in Vienna and came up with the idea to produce a state-of-the-art overview of the interdisciplinary studies of mineral dust in the form of this book.

Last but not least I would like to thank my direct dusty teammates in Bremen and at NIOZ, Inka Meyer, Conny Saukel, Carmen Friese, Malte Jäger, Felix Temmesfeld, Michelle van der Does, Laura Korte, Chris Munday, Geert-Jan Brummer, Esmee Geerken, Yvo Witte, Edwin Keijzer, and Bob Koster as well as generous funding by NIOZ and MARUM and by the German Science Foundation (DFG) through the DFG-Research Center/Cluster of Excellence "The Ocean in the Earth System", the Dutch Science Foundation (NWO), the Qatari Science Foundation (QNRF), the Australian Science Foundation (ARC), and the European Research Council (ERC).

Texel, The Netherlands — Jan-Berend W. Stuut
Bremen, Germany
July 2014

Acknowledgements

Many of the contributors to this book did a peer review of other chapters, for which they are greatly acknowledged. In addition, the editors we would like to acknowledge the external reviewers: Ed Sholkovitz, Jef Vandenberghe, and Anna Wegner.

In addition, there are a number of acknowledgments from the individual chapter authors:

Peter Knippertz and Jan-Berend Stuut (Chap. 1) would explicitly like to thank Slobodan Nickovic for helpful ideas and literature for their chapter. PK acknowledges funding from ERC grant 257543 Desert Storms. JBS acknowledges funding from ERC grant 311152 DUSTTRAFFIC, from the NWO grant TRAFFIC, and funding from the German Science Foundation (DFG) through the DFG-Research Center/Cluster of Excellence "The Ocean in the Earth System".

Dan Muhs et al. (Chap. 3) explicitly thank Randy Schumann, Gene Ellis and Tom Judkins for helpful comments on an earlier version of Chap. 3. Muhs' work (Chaps. 3 and 16) is supported by the Climate and Land Use Change Program of the U.S. Geological Survey.

Beatrice Marticorena (Chap. 5) explicitly thanks colleagues and students from LISA: Gilles Bergametti, Stéphane Alfaro, Jean Louis Rajot, Florence Fécan, Benoit Laurent, Christel Bouet and Caroline Pierre.

Peter Knippertz (Chap. 6) explicitly acknowledges funding from ERC grant 257543 Desert Storms. He would like to thank Michael Reeder for his advice on Australian dust storms and relevant literature as well as John Marsham, Stephanie Fiedler, and Carl Gilkeson for helpful comment on an earlier version of the manuscript.

Gilles Bergametti and Gilles Forêt (Chap. 8) explicitly thank B. Gaubert for his help with illustrations.

Claire Ryder (Chap. 11) explicitly acknowledges funding by the Natural Environment Research Council Grant NE/G015937/1 (FENNEC). The authors also would like to thank all the FENNEC team, and the staff and pilots of the FAAM BAe146 for insights gained during the project and for the data which they have used in their chapter.

Athanasios Nenes (Chap. 12) explicitly acknowledges support from Georgia Power chair funds, NSF CAREER, NASA, NOAA and DOE awards. Ben Murray would like to acknowledge the European Research Council (FP7, 240449 ICE) and the Natural Environment Research Council (NE/I020059/1, NE/I013466/1, NE/H001050/1) for funding. Aikatarini Bougiatioti is supported by the "Supporting of Postdoctoral Researchers" of the Operational Program "Education and Life-long Learning" (Action's Beneficiary: General Secretariat for Research and Technology), and is co-financed by the European Social Fund (ESF) and the Greek State.

Ron L. Miller et al. (Chap. 13) explicitly thank Brian Cairns and Andy Lacis for their expertise regarding the influence of dust upon radiation. This work was supported by the NASA Modeling, Analysis and Prediction Program. Computational resources were provided by the NASA High-End Computing (HEC) Program through the NASA Center for Climate Simulation (NCCS) at Goddard Space Flight Center. CP and JPP received additional support from the Earth System Modeling Program of the Department of Energy, Project DE-SC0006713. PK acknowledges funding from European Research Council grant 257543 "Desert Storms". Thanks to Lilly Del Valle for redrafting Fig. 13.3.

Dan Muhs et al. (Chap. 16) explicitly thank Robert Thompson, Tom Judkins and Eugene Ellis for helpful reviews of an earlier version of their chapter. From D.-D. Rousseau, this is Lamont-Doherty Earth Observatory contribution #7801.

Jan-Berend Stuut (Chap. 17) explicitly acknowledges funding from ERC grant 311152 DUSTTRAFFIC, funding from NWO grant TRAFFIC, and funding from the German Science Foundation (DFG) through the DFG-Research Center/Cluster of Excellence "The Ocean in the Earth System".

Contents

Contributors

Matthew C. Baddock Atmospheric Environment Research Centre, Griffith School of Environment, Griffith University, Brisbane, QLD, Australia

Alex R. Baker Centre for Ocean and Atmospheric Sciences, School of Environmental Sciences, University of East Anglia, Norwich, UK

José Maria Baldasano Barcelona Supercomputer Center-Centro Nacional de Supercomputación (BSC-CNS), Barcelona, Spain

Sara Basart Barcelona Supercomputer Center-Centro Nacional de Supercomputación (BSC-CNS), Barcelona, Spain

Angela Benedetti European Centre for Medium-Range Weather Forecasts, Reading, UK

Francesco Benincasa Barcelona Supercomputer Center-Centro Nacional de Supercomputación (BSC-CNS), Barcelona, Spain

Gilles Bergametti LISA, UMR CNRS 7583 – Université Paris Est Créteil – Université Paris Diderot, Paris, France

Olivier Boucher Laboratoire de Météorologie Dynamique, Paris, France

Aikaterini Bougiatioti School of Earth and Atmospheric Sciences, Georgia Institute of Technology, Atlanta, GA, USA

Laser Remote Sensing Laboratory, National Technical University of Athens, Athens, Greece

Philip Boyd University of Tasmania, Hobart, Australia

Otago University, Dunedin, New Zealand

Malcolm E. Brooks Met Office, Exeter, UK

Stephen R. Cattle Faculty of Agriculture and Environment, The University of Sydney, Sydney, NSW, Australia

Jen-Ping Chen Department of Atmospheric Science, National Taiwan University, Taipei, Taiwan

Isabelle Chiapello LOA, CNRS/Université Lille 1, Villeneuve d'Ascq, France

Peter R. Colarco NASA Goddard Space Flight Center, Greenbelt, MD, USA

Onn Crouvi Geological Survey of Israel, Jerusalem, Israel

Gilles Forêt LISA, UMR CNRS 7583 – Université Paris Est Créteil – Université Paris Diderot, Paris, France

Thomas E. Gill Department of Geological Sciences, University of Texas at El Paso, El Paso, TX, USA

Sunlin Gong Chinese Academy of Meteorological Sciences, Beijing, China

Vicki H. Grassian Department of Chemistry, University of Iowa, Iowa City, IA, USA

Eleanor J. Highwood Department of Meteorology, University of Reading, Reading, UK

Nicolas Huneeus Department of Geophysics and Center for Climate and Resilience Research, University of Chile, Santiago, Chile

Keith A. Hunter Otago University, Dunedin, New Zealand

Tim Jickells School of Environmental Sciences, University of East Anglia, Norwich Research Park, Norwich, UK

Luke Jones European Centre for Medium-Range Weather Forecasts, Reading, UK

Konrad Kandler Institute of Applied Geosciences, Technical University Darmstadt, Darmstadt, Germany

Peter Knippertz School of Earth & Environment, University of Leeds, Leeds, UK

Institute for Meteorology and Climate Research, Karlsruhe Institute of Technology, Karlsruhe, Germany

Olga Laskina Department of Chemistry, University of Iowa, Iowa City, IA, USA

Sarah Lu National Centers for Environmental Prediction, College Park, MD, USA

Beatrice Marticorena Laboratoire Interuniversitaire des Systèmes Atmosphériques, UMR CNRS 7583, Universités Paris Est – Paris Diderot, IPLS, Créteil, France

Laurent Menut Laboratoire de Météorologie Dynamique, Paris, France

Ron L. Miller NASA Goddard Institute for Space Studies, New York, NY, USA

Department of Applied Physics and Applied Mathematics, Columbia University, New York, NY, USA

Jean-Jacques Morcrette European Centre for Medium-Range Weather Forecasts, Reading, UK

Suzette A. Morman United States Geological Survey, Denver, CO, USA

Daniel R. Muhs U.S. Geological Survey, Federal Center, Denver, CO, USA

Jane Mulcahy Met Office, Exeter, UK

Benjamin Murray Institute for Climate and Atmospheric Science, School of Earth and Environment, University of Leeds, Leeds, UK

Athanasios Nenes School of Earth and Atmospheric Sciences, School of Chemical and Biomolecular Engineering, Georgia Institute of Technology, Atlanta, GA, USA

Institute of Chemical Engineering Sciences (ICE-HT), FORTH, Patras, Greece

Slobodan Nickovic Institute of Physics Belgrade, Serbia and University of Arizona, Tucson, AZ, USA

Carlos Pérez García-Pando Department of Applied Physics and Applied Maths, NASA Goddard Institute for Space Studies, Columbia University, New York, NY, USA

Jan P. Perlwitz NASA Goddard Institute for Space Studies, New York, NY, USA

Department of Applied Physics and Applied Mathematics, Columbia University, New York, NY, USA

Geoffrey S. Plumlee United States Geological Survey, Denver, CO, USA

Joseph M. Prospero Rosenstiel School of Marine and Atmospheric Sciences, University of Miami, Miami, FL, USA

Jeffrey S. Reid Naval Research Laboratory, Monterey, CA, USA

Denis-Didier Rousseau Ecole Normale Supérieure, Laboratoire de Météorologie Dynamique, UMR CNRS-ENS 8539 & CERES-ERTI, Paris Cedex 5, France

Lamont-Doherty Earth Observatory, Columbia University, Palisades, USA

Claire L. Ryder Department of Meteorology, University of Reading, Reading, UK

Dirk Scheuvens Institute of Applied Geosciences, Technical University Darmstadt, Darmstadt, Germany

Michael Schulz Norwegian Meteorological Institute, Oslo, Norway

Thomas T. Sekiyama Japan Meteorological Agency/Meteorological Research Institute, Tsukuba, Japan

Jan-Berend W. Stuut NIOZ – Royal Netherlands Institute for Sea Research, Department of Marine Geology and Chemical Oceanography, Texel, The Netherlands

MARUM – Center for Marine Environmental Sciences, Department of Marine Sedimentology, University of Bremen, Bremen, Germany

Jimin Sun Institute of Geology and Geophysics, Chinese Academy of Sciences, Beijing, China

Anders Svensson Centre for Ice and Climate, Niels Bohr Institute, University of Copenhagen, Copenhagen, Denmark

Taichu Y. Tanaka Japan Meteorological Agency/Meteorological Research Institute, Tsukuba, Japan

Ina Tegen Leibniz Institute for Tropospheric Research, Leipzig, Germany

Enric Terradellas Spanish Meteorological Agency, AEMET, Barcelona, Spain

Paul Vallelonga Centre for Ice and Climate, Niels Bohr Institute, University of Copenhagen, Copenhagen, Denmark

Douglas L. Westphal Naval Research Laboratory, Monterey, CA, USA

Marcelo A. Zárate Instituto de Ciencias de la Tierra y Ambientales de la Pampa (INCITAP), Avenida Uruguay 151, Santa Rosa, La Pampa, Argentina

Xiao-Ye Zhang Chinese Academy of Meteorological Sciences, Beijing, China

Chun-Hong Zhou Chinese Academy of Meteorological Sciences, Beijing, China

About the Editors

Peter Knippertz is an expert in meteorological aspects of dust storms. He received his Ph.D. in Meteorology from the University of Cologne (Germany) in 2003 and was a researcher at the Universities of Wisconsin-Madison (USA, 2003–2005), Mainz (Germany, 2005–2009), where he received his habilitation in 2008, and Leeds (UK, 2009–2013). In 2013 he moved to the Karlsruhe Institute of Technology (Germany), where he is now a Professor of Meteorology. He is currently leading a major 5-year project on dust emission funded by the European Research Council and a large European consortium on cloud-aerosol interactions in West Africa funded by the European Union.

Jan-Berend W. Stuut has been working on aeolian dust from a marine perspective since his Ph.D., which he received from Utrecht University (the Netherlands) in 2001. After his Ph.D., he worked as a postdoctoral researcher at the Research Center Ocean Margins and the MARUM – Center for Marine Environmental Sciences, both at the University of Bremen, focusing on marine archives of mineral dust. He then moved to the NIOZ – Royal Netherlands Institute for Sea Research in 2009 to further study modern dust deposition processes in and offshore deserts around the world. Since 2012 he is leading two projects on the marine environmental effects of Saharan dust funded by both the Dutch NSF (NWO) and the European Research Council (ERC). He is still affiliated to MARUM, Bremen, where he also leads a project on Saharan dust deposition in the Atlantic Ocean, funded by the German NSF (DFG).

Chapter 1
Introduction

Peter Knippertz and Jan-Berend W. Stuut

Abstract Mineral dust is a key player in the Earth system with important impacts on the global energy and carbon cycles, acting on timescales of minutes to millennia. Megatons of dust are lifted each year into the atmosphere by strong near-surface winds over the world's arid regions. Such winds can be generated by short-lived small-scale dust devils, cold outflow from thunderstorms up to continental-scale dust storms. The tiny dust particles can be lifted to great heights and transported thousands of kilometres across the globe. Once airborne, dust affects radiation and clouds and thereby also precipitation. Dust also alters chemical processes in the atmosphere and deteriorates air quality and visibility for aviation. Dust is removed from the atmosphere by gravitational settling, turbulence or precipitation. Deposition on plants, snow and ice changes the amount of reflected solar radiation. Iron and other nutrients contained in dust fertilise both terrestrial and marine ecosystems. Dust deposits in glaciers, soils and ocean or lake sediments constitute an important archive of past environmental changes. For the first time, this book gives a detailed account of the state of the art in the fascinating, highly interdisciplinary and dynamically evolving area of dust research including results from field campaigns,

P. Knippertz (✉)
School of Earth & Environment, University of Leeds, Leeds, UK

Institute for Meteorology and Climate Research, Karlsruhe Institute of Technology, Karlsruhe, Germany
e-mail: peter.knippertz@kit.edu

J.-B.W. Stuut
NIOZ – Royal Netherlands Institute for Sea Research, Department of Marine Geology and Chemical Oceanography, Texel, The Netherlands

MARUM – Center for Marine Environmental Sciences, Department of Marine Sedimentology, University of Bremen, Bremen, Germany
e-mail: jbstuut@nioz.nl

P. Knippertz and J.-B.W. Stuut (eds.), *Mineral Dust: A Key Player in the Earth System*, DOI 10.1007/978-94-017-8978-3_1,

laboratory, aircraft, satellite, modelling and theoretical studies. This chapter gives a short introduction into the topic, placing several recent developments in dust research into a historical context.

Keywords Overview • History • Chapter • Publications • Observations • Modelling • Field campaigns • Player • Recorder • Environmental change

1.1 Why Study Dust?

Airborne dust, mostly emitted from soils in arid and semi-arid regions, is a key atmospheric constituent and represents an important natural source of atmospheric particulate matter. In comparison to soot from natural fires, sulphates from industrial exhaust, ash from volcanic eruptions and sea salt, dust is the most important aerosol by mass (Fig. 1.1).

Atmospheric dust is considered to be a harmful air pollutant causing respiratory diseases and infections, and in some regions dust can also contribute to trigger serious epidemics through carrying pathogens (De Deckker et al. 2008), such as foot-and-mouth disease in the UK (Griffin et al. 2001) and meningitis in the Sahel (Thomson et al. 2006). Significant dust events have a substantial economic impact as reduced visibility can affect air traffic, road transportation and military operations. The aerial erosion of soils is a major problem in agriculture (McTainsh et al. 1990). Reduced radiation at the surface has an impact on the output from solar power plants, especially those that rely on direct solar radiation (Schroedter-Homscheidt et al. 2013).

Dust also interacts with continental and maritime ecosystems by being a source of micronutrients (e.g. Okin et al. 2004; Jickells et al. 2005; Schulz et al. 2012;

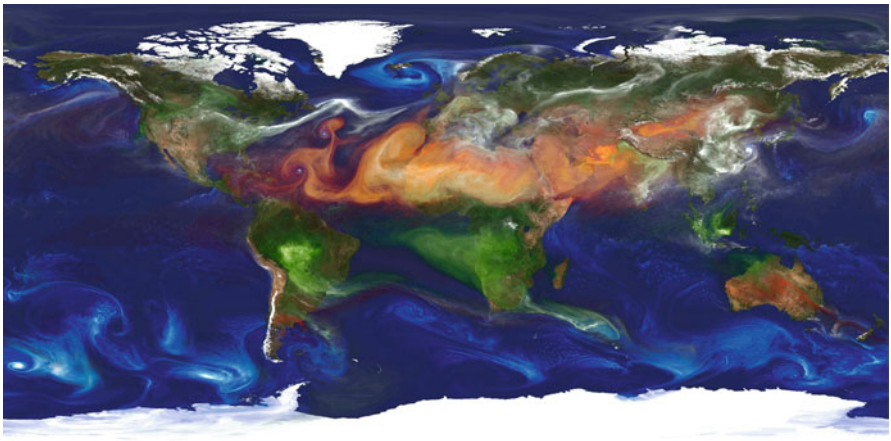

Fig. 1.1 NASA's GEOS-5 simulation, showing the four main aerosols: mineral dust from deserts (*red*), sea salt from spray (*blue*), soot and smoke from fires (*green*) and sulphate particles from fossil fuel combustion and volcanoes (*white*). Source: http://geos5.org

Martinez-Garcia et al. 2011). It has been hypothesised that the Amazon rainforest is fertilised significantly by Saharan dust (e.g. Bristow et al. 2010) and that the fertilising effect on the ocean is potentially so large that it plays an important role in global climate (Martin 1990).

In addition, dust plays an important role in different aspects of weather and climate dynamics, the Earth's radiative budget, cloud microphysics and atmospheric chemistry. The radiative heating of airborne dust modifies the energetics of the atmosphere, including possible modifications of easterly waves and tropical cyclone development over the Atlantic Ocean, downwind of the Sahara Desert (Karyampudi and Carlson 1988; Karyampudi and Pierce 2002).

As stressed by both the fourth and recent fifth assessment of the International Panel of Climate Change, the level of scientific understanding of the effects of aerosols, both natural and anthropogenic, on climate is generally low (Forster et al. 2007; Myhre et al. 2013). Considerable advances in the knowledge of dust mobilisation, dispersal and deposition as well as impacts of atmospheric dust have been made, but many open questions remain.

1.2 A Short History of Dust Research

Dust storms and atmospheric dust processes have attracted societal attention for millennia. In ancient Korea, for example, dust events caused concern because they were considered as God's punishment or a warning to the ruler. Historical records of dust observations are preserved from as early as the first century BC (Chun et al. 2008). Two millennia later, Alexander von Humboldt (1807) discussed how dust particles could be taken up into the atmosphere after viewing a wind spout in South America. Charles Darwin (1846) published the first scientific record of intercontinental transport of Saharan dust across the Atlantic Ocean. A Royal Society Colleague of Darwin had encountered Saharan dust along the African coast transported by the Harmattan winds much earlier, but he did not recognise that the 'troublesome sensation of prickling on the skin' he felt was probably caused by dust particles (Dobson 1781). Samples of dust collected by Darwin on the Beagle near the Cape Verde Islands were sent to Berlin, where they were analysed with regard to their microscopic content. Ehrenberg hypothesised that at least parts of the dust originated from a dry lake due to findings of freshwater diatoms and terrestrial plant material, thereby excluding volcanic sources as previously suggested (Ehrenberg 1849). In 1925 Sutton published a paper on the meteorology of haboob dust storms in Sudan, including a limited climatology based on surface station data. A few years later, Semmelhack (1934) described some details of the long-range transport and deposition patterns of mineral dust over the tropical Atlantic.

An important milestone of modern dust research was the publication of *The physics of blown sand and desert dunes* by Bagnold in 1941, which has been a main reference in the field of dust uplift ever since. The following 1940s–1960s saw a number of studies on dust emission and its dependence on soil characteristics (e.g.

Bisal and Hsieh 1966) and wind, including some work on dust devils (e.g. Sinclair 1969). Much of this was conducted in the field but also increasingly in wind tunnels (e.g. Marshall 1971). At the same time, researchers began to look more into characteristics of dust after long-range transport (Pitty 1968), while Policard and Collet (1952) published an early study of dust impacts on human health in the Sahara.

The first large field campaign with a dust component was the GARP Atlantic Tropical Experiment (GATE) during the summer of 1974, which included aerosol and turbidity measurements from a network of five land stations and ten ships. The 1970s also saw the advent of satellite technology capable of estimating dust loads from space (e.g. Fraser 1976). A number of publications authored by Prospero and Carlson discussed details of the transport of dust from Africa to America and its impacts on radiation (e.g. Carlson and Prospero 1972; Prospero and Nees 1976; Prospero and Carlson 1980), while Schütz and Jaenicke extensively analysed physical and chemical properties of dust particles sampled in the field (Schütz and Jaenicke 1974; Jaenicke and Schütz 1978). Work by Gillette and colleagues from the 1970s onwards established some of the concepts of dust emission still used today, such as sandblasting efficiency (e.g. Gillette 1974, 1977; Gillette et al. 1982). In 1979, Christer Morales edited a book entitled *Saharan dust: Mobilization, Transport, Deposition*. Based on a workshop held in Gothenburg, Sweden, this book gave a first comprehensive account of the state of the art in dust research at the time. In the following years, more detailed overviews were presented in two books by Pye (1987) and Goudie and Middleton (2006). In 2008, Shao published a book with a more specific focus on wind erosion.

In the 1980s many fundamental concepts of dust emission and deposition were developed further, including some classical work on dry and wet removal (e.g. Slinn and Slinn 1980; Giorgi 1988). Also during this time, Koopmann and Sarnthein conducted some pioneering work on Saharan dust deposited in the equatorial north Atlantic (Sarnthein and Koopmann 1980; Sarnthein et al. 1981; Koopmann 1981). This decade also saw the development of the first computer models for dust processes. While, for example, Lee (1983) looked specifically at the transport and removal processes of dust, Westphal et al. (1988) studied the importance of low-level nocturnal jets and the midlevel easterly jet on dust mobilisation and transport, using the first multidimensional, size-resolving, full physics numerical dust transport model. This implementation demonstrated the practicality of computer simulations of dust storms, as they are still used today.

The development of numerical dust models and the refinement of satellite retrievals have led to a rapid growth in the scientific interest in atmospheric dust over the past two decades. To illustrate this, Fig. 1.2 shows the development in publications and citations of papers on Saharan dust from 1985 to 2012. The number of publications per year grew exponentially from a handful of papers in the mid-1980s to almost 250 in 2009 with an even steeper increase in citations, as expected. This exponential increase corresponds to a doubling of the publication (citation) rate every 6 (4) years, which can be compared to the 11-year doubling time of the publication rate for climate change articles found by Stanhill (2001). These numbers are an impressive demonstration of the dynamic development of dust as a research topic of international relevance.

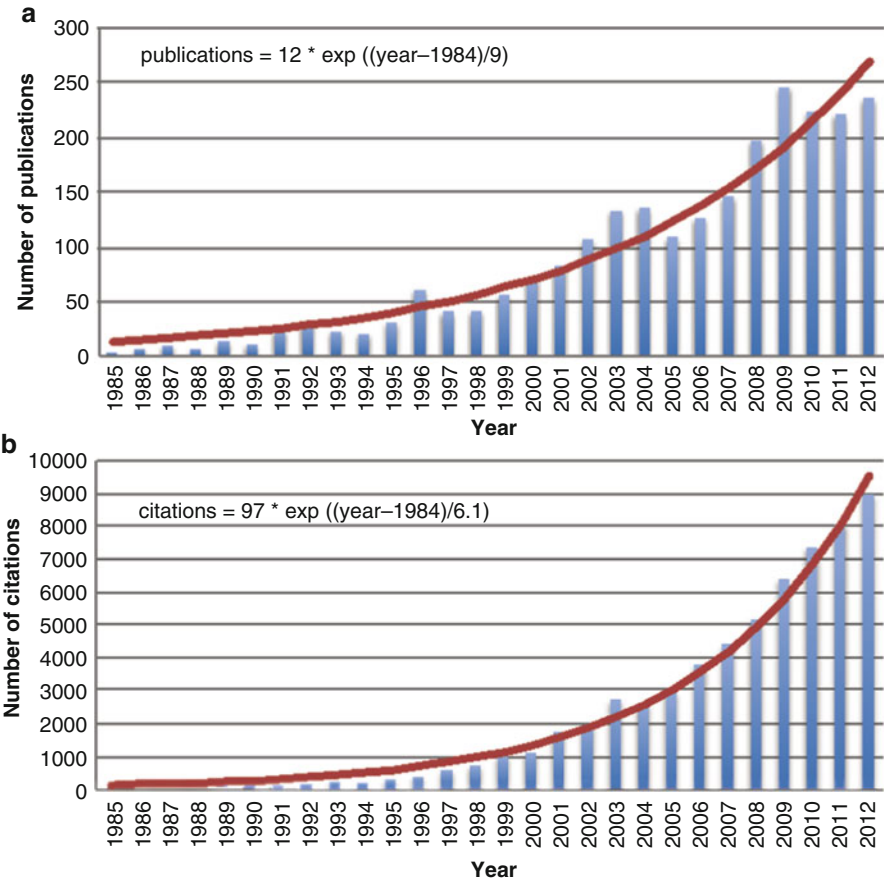

Fig. 1.2 Increase in (**a**) publications and (**b**) citations of papers on Saharan dust. *Blue* bars give actual numbers and red lines best-fit exponential growths. The latter correspond to doubling of the publication (citation) rate every 6 (4) years. The publication search was performed on 14 August 2013 using Thompson Reuters Web of Knowledge under the term 'dust and Sahar*' and was conducted on the title, abstract and keywords. The figure is an update and extension of a similar plot in Kaufman et al. (2005)

1.3 Recent Developments: Timeliness of This Book

As demonstrated by Fig. 1.2, dust research has accelerated massively since the late 1990s. This is to some extent a reflection of the development of the field of Earth system science as a new interdisciplinary research area. The Earth system concept is built on the idea that a full understanding of the climate system and its natural and anthropogenic changes over time is not possible without considering couplings to other 'spheres'. This concept has led to a stronger linkage between the more classical areas of climate research, atmospheric and oceanic sciences and

research on the cryosphere, land surface, vegetation, marine ecosystems and human activity, to name a few. In many ways dust is a topic par excellence for this evolving research area, as it depends on and interacts with several spheres of the Earth system: originating from the land surface, dust sources depend on geological and geomorphological processes such as weathering and sediment transport (Chap. 3). On shorter timescales, vegetation, soil moisture and snow cover play a role, which in turn depend on precipitation and temperature (Chap. 5). Meteorology has a strong control on dust emission and distribution through the generation of deflating winds near the surface (Chap. 6), as well as through vertical mixing and long-range horizontal transport (Chap. 7), through alterations during suspension (Chap. 4) and finally through dry and wet deposition processes (Chap. 8), the former depending again on the land surface and vegetation. Once airborne, dust can change the radiation budget (Chap. 11), the properties of clouds and precipitation (Chap. 12) and thus regional circulations (Chap. 13), with potential feedbacks on the land surface. Many of these processes crucially depend on the size distribution and composition of the dust particles (Chap. 2). Dust depositions into the ocean and on land potentially fertilise ecosystems and impact on the carbon cycle (Chap. 14), which then feeds back on climate. Dust depositions on ice and snow change the albedo and can therefore affect melting rates. Such depositions together with those in soils, lakes and oceans are increasingly used to reconstruct past climates (Chaps. 16, 17, 18). Last but not least, it is still a topic of debate to what extent human activities (land-use change, agriculture, stock grazing, mining, off-road transport, etc.) have changed and will change the distribution, strength and characteristics of dust sources. This has potential ramifications for the quality of life in affected regions through respiratory and eye diseases (Chap. 15) and reduced visibility. In contrast, there is growing evidence that airborne dust reacts chemically with anthropogenically emitted substances, which contributes to an ageing of natural particles, changing their optical and microphysical properties (Chap. 4).

In addition to its prominent role in Earth system science, several new developments in dust research itself have contributed to the rapidly growing interest in this topic. Dust is a quantity that is difficult to observe in situ, particularly near source regions, which tend to be remote and inaccessible due to harsh climate conditions, the lack of infrastructure and even political instability. Therefore the advance of spaceborne remote-sensing capabilities has allowed fascinating new insights into the distribution and characteristics of atmospheric dust (see Chap. 7). Several new developments are particularly noteworthy (in rough order of occurrence):

- The Multi-angle Imaging SpectroRadiometer (MISR) onboard the Terra satellite became operational in February 2000. Its innovative configuration of nine separate digital cameras, which gather data in four different spectral bands of the solar spectrum, allowed for the first time to view the same dust plume from different angles. This makes it possible to retrieve a plume height together with aspects such as optical thickness, a-sphericity of particles and optical properties (Kalashnikova et al. 2005).

- With the first satellite of the Meteosat Second Generation becoming operational in January 2004, the tracking of individual dust plumes with high resolution in time and space became possible, both during day and night, at least in a qualitative sense. This has significantly enhanced our understanding of sources (e.g. Schepanski et al. 2007) as well as dust storm dynamics (e.g. Knippertz and Todd 2012).
- The first spaceborne lidar, which allowed the retrieval of a detailed vertical profile of the dust distribution, is the Cloud-Aerosol Lidar with Orthogonal Polarization (CALIOP) onboard the Cloud-Aerosol Lidar and Infrared Pathfinder Satellite Observations (CALIPSO) satellite, which was launched in April 2006. Despite its low space-time coverage, CALIOP data give unprecedented insight into vertical mixing and layering processes (Winker et al. 2009).
- New retrieval development: Traditional satellite retrievals in the visible part of the spectrum struggle to see dust over bright desert areas due to the small contrast to the underlying surface and are only available during the day. Recent years have seen the development of new retrievals for optical thickness that overcome this problem by (additionally) using channels outside the visible band such as in the near-ultraviolet (Deep Blue algorithm, Hsu et al. 2004) and infrared (Spinning Enhanced Visible and Infrared Imager (SEVIRI), Brindley and Ignatov 2006; Infrared Atmospheric Sounding Interferometer (IASI), Klüser et al. 2011; Atmospheric Infrared Sounder (AIRS), Peyridieu et al. 2010).

Recent years have also seen a considerable increase in the number and complexity of dust models used both for research and for forecasting purposes (Chap. 9). Due to the increase of computer power, these models can be run in higher horizontal and vertical resolution to allow for investigations of smaller-scale meteorological processes such as effects of cold outflows from thunderstorms on dust emission (Reinfried et al. 2009; Heinold et al. 2013; Chap. 6). At the same time there have been some new approaches to treat emission processes in models at high resolution (Kok 2011; Klose and Shao 2012; Chap. 5). An important new development from an operational perspective is the introduction of dust prediction models at several modelling centres around the world, which generate daily forecasts of parameters such as near-surface concentrations and optical thickness for air-quality and weather warning purposes (Chap. 10). These include both regional and global models. In contrast to research models, these new systems include the assimilation of satellite and ground-based observations, making them an important tool for climatological monitoring as well. The new capabilities in dust observations also play a role in model evaluation and development. Many of the latest versions of both operational and research models include couplings between dust and radiation fields (Chaps. 11 and 13), while couplings with cloud microphysics (Chap. 12) have become more widespread in specialised research models.

The increasing complexity in both models and satellite retrievals has led to the recognition that more detailed information on the characteristics and size distribution of dust particles (Chap. 2) are needed to determine necessary input parameters and to evaluate the credibility of our approaches. Therefore, a number

of field campaigns have recently been conducted to measure dust particles and their impacts in natural environments, both near source and after long-range transport. Prominent examples include:

- The Bodélé Dust Experiment (BoDEx) in February and March 2005 (Washington et al. 2006) with a dedicated small-scale field campaign to the world's largest dust source, the Bodélé Depression in Chad.
- The Japanese Australian Dust Experiment (JADE) that took place on an Australian farm in February and March 2006, measuring atmospheric, land-surface and soil variables as well as size-resolved saltation and dust fluxes (Ishizuka et al. 2008).
- The African Monsoon Multidisciplinary Analysis (AMMA), a large international programme that involved a multitude of different organisations and platforms. AMMA's main field campaign took place in West Africa and surrounding waters in 2006 (Lebel et al. 2011) and was coordinated with the Dust and Biomass Experiment (DABEX; Haywood et al. 2008) and Dust Outflow and Deposition to the Ocean (DODO; McConnell et al. 2008). Some monitoring stations continued for several years, such as the AMMA Sahelian Dust Transect (Marticorena et al. 2010).
- The Geostationary Earth Radiation Budget Intercomparison of Longwave and Shortwave Radiation (GERBILS) campaign in June 2007 (Haywood et al. 2011) that combined in situ aircraft measurements over West Africa with satellite data.
- The Saharan Mineral Dust Experiment (SAMUM), which organised two major field campaigns including aircraft and ground-based measurements and satellite data dedicated mostly to radiative impacts of dust. The campaign in May and June 2006 was based in southern Morocco (Heintzenberg 2009), while the one in January and February 2008 took place on the Cape Verde Islands (Ansmann et al. 2011).
- Fennec was the first campaign to take comprehensive measurements of atmospheric and dust-related parameters in the Central Sahara with aircraft campaigns in April 2011, June 2011 and June 2012, accompanied by two supersites and an array of automatic weather stations in Algeria and Mauritania (Hobby et al. 2013; Marsham et al. 2013; Todd et al. 2013).

1.4 Outline and Structure of This Book

The exciting new developments discussed in Sect. 1.3 have substantially expanded and changed the nature of modern research on dust. Therefore, the time is ripe to follow up on previous overviews of dust research in the books by Morales (1979), Pye (1987), and Goudie and Middleton (2006). The increased range of involved timescales, applications and scientific disciplines makes it challenging for individual scientists to stay on top of the developments in the ever-widening field of mineral-dust studies and to see where their own work fits into the bigger picture.

This evolution was a strong motivation to compile this book, which aims to give a detailed account of the state of the art in the highly interdisciplinary and dynamically evolving area of dust research. This book is meant to allow researchers working directly on mineral dust and closely related topics to quickly obtain an overview of the full range of roles that dust plays in the Earth system. It is mainly aimed at an expert audience (postgraduate to senior researcher level). Parts of this book, however, could also be used for specialised teaching activities, such as summer schools, training courses for operational forecasters in regions prone to dust storms or modules specialising on aerosol science or climate reconstructions. This book covers aspects of dust research reaching from timescales of minutes (e.g. dust devils, cloud processes, radiation) to millennia (e.g. loess formation, dust in subaquatic sediment archives) including theoretical concepts, observations and results from computer modelling and operational forecasts.

Given the breadth and quick evolution of dust research, it would have been challenging for a single author or a small team of authors to cover enough ground for an exhaustive treatment of the topic, making it almost unavoidable that this volume has become an edited book. This approach has the clear and important advantage of allowing the direct involvement of a larger number of leading experts of dust research to cover specific aspects in much detail. The most significant disadvantage is that of a greater variety in style, depth and approach between the individual chapters. Naturally, some chapters are therefore closer to full-blown scientific reviews and others more similar to classical textbook writings. However, the editors have worked closely with the authors to reduce overlap between chapters, improve the overall narrative and to remove inconsistencies in terms of terminology and mathematical symbols used, but some such instances may have remained. It is hoped that the increase of scientific rigour and breadth brought about by the approach of an edited book far outweighs such minor flaws.

This book is structured into four main parts: Part I: Characteristics of natural dust particles (Chaps. 2, 3, 4) details the chemical and physical properties of dust and how those can evolve from the sources through processing in the atmosphere. In Chap. 2, Dirk Scheuvens and Konrad Kandler give a detailed account of the mineral and chemical composition of natural dust together with information on typical shapes and size distributions, thereby providing a foundation for subsequent chapters. The following chapter by Daniel Muhs et al. provides information on geographical and geomorphological aspects of global dust sources in current times, but also describes situations in past climates. The discussion of the mineralogical characteristics of sources provides a direct link to Chap. 2. The specification of source areas and their characteristics is a great challenge for the numerical modelling of dust emission as discussed in Chap. 9. Finally, Chap. 4 by Alex Baker et al. reports about how the freshly emitted dust particles, as discussed in Chaps. 2 and 3, can be processed in the atmosphere, for example, through chemical reactions with other aerosol particles or liquids or through physical processes in clouds. These changes cause a so-called ageing of dust particles, creating coatings with, for example, sulphate and nitrate or aggregation of particles.

The largest of the four parts of this book is Part II, which describes the global dust budget (Chaps. 5, 6, 7, 8, 9, 10). This involves the three key elements of the dust cycle, emission, transport and deposition, as well as information on how the dust budget is monitored and modelled. Naturally, this part begins with dust emission processes in Chap. 5, where Béatrice Marticorena explains the fundamental concept of an erosion threshold and key physical processes like saltation and self-abrasion, which ultimately lead to the release of fine particles available for long-range transport. The theoretical concepts presented here are a key ingredient in numerical models of dust that are used for weather and climate forecasts and analyses (Chaps. 9, 10 and 13). One of the most important controlling parameters of dust emission is near-surface wind speed, and therefore Chap. 6 by Peter Knippertz describes the meteorological systems and phenomena that create sufficiently high winds in dust source regions. These systems span scales from thousands of kilometres (cyclones and anticyclones, fronts) to less than a few tens of metres (dust devils) and are also involved in the vertical and horizontal transport of freshly emitted dust, often with strong diurnal cycles. Observing and documenting the resulting 3D dust distribution and its changes in time is a great challenge as detailed in Chap. 7 by Isabelle Chiappello. It requires an ever-increasing range of spaceborne remote-sensing techniques and platforms in concert with ground-based instruments such as sun photometers and lidars. The final stage of the dust cycle is deposition, the physical mechanisms of which are explained by Gilles Bergametti and Gilles Forêt in Chap. 8. Deposition is typically divided into dry deposition through gravitational settling, impaction and diffusion and wet deposition through in-cloud and sub-cloud scavenging. Particular in-cloud processes are strongly dependent on characteristics of individual particles (Part I) and how they can interact with cloud microphysics (Chap. 12). In Chap. 9, Ina Tegen and Michael Schulz explain how the fundamental concepts of emission, transport and deposition are implemented into numerical dust models that can be used for climate and weather simulations following different approaches for how the dust is treated in the model. Finally in Chap. 10, Angela Benedetti et al. document how the dust models described in Chap. 9 are used in operational forecast systems around the world to produce daily predictions of dust fields. This includes a discussion of key new approaches like multimodel ensembles and assimilation of satellite data of the type discussed in Chap. 7.

Part III is entitled *Impacts of dust* and comprises the Chaps. 11, 12, 13, 14, 15. The two most important direct impacts of dust on the atmosphere and climate system are those connected to radiation and clouds, both discussed at the beginning of this Part. In Chap. 11, Ellie Highwood and Claire Ryder explain the fundamental optical properties of dust (dust optical thickness, single-scattering albedo etc.) and their dependence on composition and size distribution, which links back to Chap. 2. In the following Chap. 12, Athanasios Nenes et al. discuss how dust particles affect characteristics of clouds (and therefore precipitation) through acting as cloud condensation nuclei or ice nuclei. These aspects are equally dependent on composition and size distribution, with ageing processes being of great importance, as they tend to change the hygroscopicity of dust (see Chap. 4). The following three chapters discuss more indirect impacts of dust. In Chap. 13,

Ron Miller et al. explain how direct radiative forcing through dust affects climate on a regional to global scale. Emphasis is given to key parameters like sea-surface temperature, near-surface temperature over land, wind, precipitation, stability and regional circulations. Chapter 14 by Tim Jickells et al. reports how the deposition of dust particles can increase bioactivity through iron and phosphorus fertilisation of both terrestrial and oceanic ecosystems (e.g. plankton, algae). This has ramifications for the uptake of carbon into soils and the ocean, which in turn affects climate. This chapter has strong links with Chap. 8. Finally, Chap. 15 by Suzette Morman and Geoffrey Plumlee discusses impacts of dust particles on human health, which range from respiratory diseases such as asthma to connections with meningitis outbreaks and long-range transport of microbes on dust particles.

The final part, Part IV is entitled *Dust archives* (Chaps. 16, 17, 18) and covers the three main areas where dust deposits are used for climate reconstructions. Chapter 16 by Daniel Muhs et al. looks at deposits in soils, that is, records from the main Loess regions around the world (China, eastern and western Europe, North and South America). In Chap. 17, Jan-Berend Stuut discusses subaquatic dust records focusing on lacustrine and marine sediment archives. The former typically allow a relatively detailed view into the recent climate history of a relatively small region and the latter offering opportunities to study dust over millions of years and from larger source areas. Mineral-dust archives in ice cores cover slightly shorter timescales as discussed by Paul Vallelonga and Anders Svensson in Chap. 18. The most prominent such cores were taken from Antarctica and Greenland allowing reconstructions for both hemispheres, but also tropical ice cores, for example, from South America, are discussed.

The editors are convinced that they have assembled a comprehensive and fascinating overview of the state of the art of mineral-dust research and hope that the readers will enjoy it as much the editors did compiling it.

References

Ansmann A, Petzold A, Kandler K et al (2011) Saharan mineral dust experiments SAMUM-1 and SAMUM-2: what have we learned? Tellus B 63:403–429

Bagnold RA (1941) The physics of blown sand and desert dunes. Methuen, London

Bisal F, Hsieh J (1966) Influence of moisture on erodibility of soil by wind. Soil Sci 102:143–146

Brindley H, Ignatov A (2006) Retrieval of mineral aerosol optical depth and size information from Meteosat Second Generation solar reflectance bands. Remote Sens Environ 102:344–363

Bristow CS, Hudson-Edwards KA, Chappell A (2010) Fertilizing the Amazon and equatorial Atlantic with West African dust. Geophys Res Lett 37:L14807

Carlson TN, Prospero JM (1972) The large-scale movement of Saharan air outbreaks over the northern equatorial Atlantic. J Appl Meteorol 11(2):283–297

Chun J, Cho H, Chung H, Lee M (2008) Historical records of Asian dust events (*Hwansa*) in Korea. Bull Am Meteorol Soc 89(6):823–827

Darwin CR (1846) An account of the fine dust which often falls on vessels in the Atlantic ocean. Q J Geol Soc Lond 2:26–30

De Deckker P, Abed RMM, de Beer D et al (2008) Geochemical and microbiological fingerprinting of airborne dust that fell in Canberra, Australia, in October 2002. Geochem Geophys Geosyst 9. doi:10.1029/2008GC002091

Dobson M (1781) An account of the Harmattan, a singular African wind. Phil Trans R Soc Lond 71:46–57

Ehrenberg CG (1849) Passatstaub und Blutregen – ein großes organisches unsichtbares Wirken und Leben in der Atmosphäre. Druckerei der Königlichen Akademie der. Wissenschaften, Berlin

Forster P, Ramaswamy V, Artaxo P et al (2007) Changes in atmospheric constituents and in radiative forcing. In: Solomon S, Quin D, Manning M et al (eds) Climate change 2007: the physical science basis. Cambridge University Press, Cambridge

Fraser RS (1976) Satellite measurement of mass of Sahara dust in the atmosphere. Appl Opt 15(10):2471–2479

Gillette DA (1974) On the production of soil wind erosion aerosols having the potential for long range transport. J Rech Atmos 8:735–744

Gillette DA (1977) Fine particulate emissions due to wind erosion. Trans Am Soc Agric Eng 20:890–897

Gillette DA, Adams J, Muhs DR, Khil R (1982) Threshold friction velocities and rupture moduli for crusted desert soils for the input of soil particles into the air. J Geophys Res 87:9003–9015

Giorgi F (1988) Dry deposition velocities of atmospheric aerosols as inferred by applying a particle dry deposition parameterization to a general circulation model. Tellus 40B:23–41

Goudie AS, Middleton NJ (2006) Desert dust in the global system. Springer, Berlin/Heidelberg/New York

Griffin DW, Kellogg CA, Shinn EA (2001) Dust in the wind: long range transport of dust in the atmosphere and its implications for global public and ecosystem health. Glob Change Hum Health 2(1):20–33

Haywood JM, Pelon J, Formenti P et al (2008) Overview of the dust and biomass-burning experiment and African monsoon multidisciplinary analysis special observing period-0. J Geophys Res 113:D00C17. doi:10.1029/2008JD010077

Haywood JM, Johnson BT, Osborne SR et al (2011) Motivation, rationale and key results from the GERBILS Saharan dust measurement campaign. Q J R Meteorol Soc 137:1106–1116

Heinold B, Knippertz P, Marsham JH et al (2013) The role of deep convection and low-level jets for dust emissions in West Africa. J Geophys Res 118(10):4385–4400. doi:10.1002/jgrd.50402

Heintzenberg J (2009) The SAMUM-1 experiment over Southern Morocco: overview and introduction. Tellus 61B:2–11

Hobby M, Gascoyne M, Marsham JH (2013) The Fennec automatic weather station (AWS) network: monitoring the Saharan climate system. J Atmos Ocean Technol 30:709–724

Hsu NC, Tsay SC, King MD, Herman JR (2004) Aerosol properties over bright-reflecting source regions. IEEE Trans Geosci Rem Sens 42:557–569

Ishizuka M, Mikami M, Leys JF et al (2008) Effects of soil moisture and dried rain droplet crust on saltation and dust emission. J Geophys Res 113:D24212. doi:10.1029/2008JD009955

Jaenicke R, Schütz L (1978) Comprehensive study of physical and chemical properties of the surface aerosols in the Cape Verde Islands region. J Geophys Res 83(C7):3585–3599

Jickells TD, An ZS, Andersen KK et al (2005) Global iron connections between desert dust, ocean biogeochemistry, and climate. Science 308:67–71

Kalashnikova OV, Kahn RA, Sokolik IN, Li W-H (2005) The ability of multi-angle remote sensing observations to identify and distinguish mineral dust types: Part 1. Optical models and retrievals of optically thick plumes. J Geophys Res 110:D18(27). doi:10.1029/2004JD004550

Karyampudi VM, Carlson TN (1988) Analysis and numerical simulations of the Saharan air layer and its effect on easterly wave disturbances. J Atmos Sci 45:3103–3136

Karyampudi VM, Pierce HF (2002) Synoptic-scale influence of the Saharan air layer on tropical cyclogenesis over the Eastern Atlantic. Mon Weather Rev 130:3100–3128

Kaufman YJ, Koren I, Remer LA et al (2005) Dust transport and deposition observed from the Terra-Moderate Resolution Imaging Spectroradiometer (MODIS) spacecraft over the Atlantic Ocean. J Geophys Res 110:D10S12. doi:10.1029/2003JD004436

Klose M, Shao Y (2012) Stochastic parameterization of dust emission and application to convective atmospheric conditions. Atmos Chem Phys 12:7309–7320

Klüser L, Martynenko D, Holzer-Popp T (2011) Thermal infrared remote sensing of mineral dust over land and ocean: a spectral SVD based retrieval approach for IASI. Atmos Meas Tech 4:757–773

Knippertz P, Todd MC (2012) Mineral dust aerosols over the Sahara: processes of emission and transport, and implications for modeling. Rev Geophys 50:RG1007. doi:10.1029/2011RG000362

Kok JF (2011) A scaling theory for the size distribution of emitted dust aerosols suggests climate models underestimate the size of the global dust cycle. Proc Natl Acad Sci U S A 108:1016–1021

Koopmann B (1981) Sedimentation von Saharastaub im subtropischen Nordatlantik während der letzten 25.000 Jahre. Meteor Forsch C 35:23–59

Lebel T, Parker DJ, Flamant C et al (2011) The AMMA field campaigns: accomplishments and lessons learned. Atmos Sci Lett 12(1):123–128

Lee I-Y (1983) Simulation of transport and removal processes of the Saharan dust. J Clim Appl Meteorol 22:632–639

Marshall J (1971) Drag measurements in roughness areas of varying density and distribution. Agric Meteorol 8:269–292

Marsham JH, Hobby M, Allen CJT et al (2013) Meteorology and dust in the central Sahara: observations from Fennec supersite-1 during the June 2011 Intensive Observation Period. J Geophys Res. doi:10.1002/jgrd.50211

Marticorena B, Chatenet B, Rajot JL (2010) Temporal variability of mineral dust concentrations over West Africa: analyses of a pluriannual monitoring from the AMMA Sahelian Dust Transect. Atmos Chem Phys 10:8899–8915

Martin JH (1990) Glacial-interglacial CO2 change: the iron hypothesis. Paleocean 5:1–13

Martinez-Garcia A, Rosell-Mele A, Jaccard SL et al (2011) Southern Ocean dust-climate coupling over the past four million years. Nature 476:312–315

McConnell CL, Highwood EJ, Coe H et al (2008) Seasonal variations of the physical and optical characteristics of Saharan dust: results from the Dust Outflow and Deposition to the Ocean (DODO) experiment. J Geophys Res 113:D14S05. doi:10.1029/2007JD009606

McTainsh GH, Lynch AW, Burgess RC (1990) Wind erosion in eastern Australia. Aust J Soil Res 28:323–339

Morales C (1979) Saharan dust, mobilization, transport, deposition, vol 14, SCOPE. Wiley, Chichester/New York/Brisbane/Toronto

Myhre G, Shindell D, Bréon F-M, Collins W, Fuglestvedt J, Huang J, Koch D, Lamarque J-F, Lee D, Mendoza B, Nakajima T, Robock A, Stephens G, Takemura T, Zhang H (2013) Anthropogenic and natural radiative forcing. In: Stocker TF et al (eds) Climate change 2013: the physical science basis. Cambridge University Press, Cambridge/New York

Okin GS, Mahowald N, Chadwick OA, Artaxo P (2004) Impact of desert dust on the biogeochemistry of phosphorus in terrestrial ecosystems. Glob Biogeochem Cycle 18, GB2005. doi:10.1029/2003GB002145

Peyridieu S, Chédin A, Tanré D et al (2010) Saharan dust infrared optical depth and altitude retrieved from AIRS: a focus over North Atlantic – comparison to MODIS and CALIPSO. Atmos Chem Phys 10:1953–1967

Pitty AF (1968) Particle size of the Saharan dust which fell in Britain in July 1968. Nature 220:364–365

Policard A, Collet A (1952) Deposition of siliceous dust in the lungs of the inhabitants of the Saharan regions. AMA Arch Ind Hyg Occup Med 5(6):527–534

Prospero JM, Carlson TN (1980) Saharan air outbreaks over the tropical North Atlantic. Pure Appl Geophys 119(3):677–691

Prospero JM, Nees RT (1976) Dust concentration in the atmosphere of the equatorial North Atlantic: possible relationship to Sahelian drought. Science 196:1196–1198

Pye K (1987) Aeolian dust and dust deposits. Academic Press, London/Orlando/San Diego/New York/Austin/Boston/Sydney/Tokyo/Toronto, ix+ 334pp. ISBN 0125686900

Reinfried F, Tegen I, Heinold B et al (2009) Density currents in the Atlas Region leading to dust mobilization: a model sensitivity study. J Geophys Res 114:D08127. doi:10.1029/2008JD010844

Sarnthein M, Koopmann B (1980) Late quaternary deep-sea record on northwest African dust supply and wind circulation. Palaeoecol Afr Surr Isl 12:239–253

Sarnthein M, Tetzlaff G, Koopmann B et al (1981) Glacial and interglacial wind regimes over the eastern subtropical Atlantic and North-West Africa. Nature 293:193–196

Schepanski K, Tegen I, Laurent B et al (2007) A new Saharan dust source activation frequency map derived from MSG-SEVIRI IR-channels. Geophys Res Lett 34. doi:10.1029/2007GL030168

Schroedter-Homscheidt M, Oumbe A, Benedetti A, Morcrette J-J (2013) Aerosols for concentrating solar electricity production forecasts: requirement quantification and ECMWF/MACC aerosol forecast assessment. Bull Am Meteorol Soc 94:903–914

Schulz M, Prospero JM, Baker AR et al (2012) The atmospheric transport and deposition of mineral dust to the ocean: implications for research needs. Environ Sci Technol 46:10390–10404. doi:10.1021/es300073u

Schütz L, Jaenicke R (1974) Particle number and mass distributions above 10^{-4} cm radius in sand and aerosol of the Sahara Desert. J Appl Meteorol 13:863–870

Semmelhack W (1934) Die Staubfälle im Nordwestafrikanischen Gebiet des atlantischen Ozeans. Ann Hydrogr 62:273–277

Sinclair PC (1969) General characteristics of dust devils. J Appl Meteorol 8:32–45

Slinn SA, Slinn WGN (1980) Prediction for particle deposition on natural waters. Atmos Environ 14:1013–1016

Stanhill G (2001) The growth of climate change science: a scientometric study. Clim Change 48:515–524

Sutton LJ (1925) Haboobs. Q J R Meteorol Soc 51:25–30

Thomson MC, Molesworth A, Djingarey MH et al (2006) Potential of environmental models to predict meningitis epidemics in Africa. Trop Med Int Health 11:781–788

Todd MC, Allen CJT, Bart M et al (2013) Meteorological and dust aerosol conditions over the Western Saharan region observed at Fennec supersite-2 during the Intensive Observation Period in June 2011. J Geophys Res. doi:10.1002/jgrd.50470

von Humboldt A (1807) Ansichten der Natur. Verlag der J. G. Cotta'schen Buchhandlung, Stuttgart

Washington R, Todd MC, Engelstaedter S, Mbainayel S, Mitchell F (2006) Dust and the low-level circulation over the Bodélé Depression, Chad: observations from BoDEx 2005. J Geophys Res 111(D3). doi:10.1029/2005JD006502

Westphal DL, Toon OB, Carlson TN (1988) A case study of mobilization and transport of Saharan dust. J Atmos Sci 45:2145–2175

Winker DM, Vaughan MA, Omar A et al (2009) Overview of the CALIPSO mission and CALIOP data processing algorithms. J Atmos Ocean Technol 26:2310–2323

Chapter 2
On Composition, Morphology, and Size Distribution of Airborne Mineral Dust

Dirk Scheuvens and Konrad Kandler

Abstract Mineral dust is a key player in the Earth system. The uplift, transport, and deposition of mineral dust have large impacts on different Earth's compartments such as the deserts, oceans, rain forests, and, last but not least, the atmosphere. The mineral dust cycle influences the fertility of soils and the biological activity in oceans and may cause harm to flora and fauna including human beings. Moreover, it changes the climate system directly by absorption and scattering of radiation and indirectly by influencing the life cycle of clouds.

The type and intensity of the consequences of mineral dust transport mainly depend on the chemical and physical properties of the dust. This chapter reviews data on the chemical composition, the shape and morphology of particles, and the size distribution of airborne dust. It focuses on the description and comparison of dust samples from northern Africa and eastern Asia, the two strongest dust source areas on Earth. From the compilation it gets obvious that an "average" mineral dust does not exist and that the physicochemical properties of a dust sample depend, for example, on the composition and grain-size distribution of sediments in the source area, on fractionation processes during entrainment and transport, and on mixing and reactions with other aerosol types and trace gases. Nevertheless, most mineral dust samples are mineralogically dominated by (alumino) silicates such as quartz, feldspar, and clay minerals with varying amounts of carbonates, sulfates, and iron-bearing minerals. Individual-particle analysis shows that dust particles are internally mixed, predominantly nonspherical, and morphologically complex, meaning that the usage of oversimplified compositional and physical parameters in radiative modeling will lead to inaccurate or even erroneous results.

D. Scheuvens (✉) • K. Kandler
Institute of Applied Geosciences, Technical University Darmstadt, Darmstadt, Germany
e-mail: dscheuvens@geo.tu-darmstadt.de; kzk@gmx.de

P. Knippertz and J.-B.W. Stuut (eds.), *Mineral Dust: A Key Player in the Earth System*, DOI 10.1007/978-94-017-8978-3_2,

Keywords Composition • Mineralogy • Chemistry • Elements • Isotopes • Particle shape • Particle morphology • Single-particle analysis • Radiative forcing • Size distribution

2.1 Introduction

Mineral dust is an omnipresent constituent of the Earth's atmosphere. It is mainly uplifted in the large desert regions of the Earth and may be transported hundreds to several thousand of kilometers around the globe. The uplift, transport, and final deposition of mineral dust have severe consequences on climate and many important ecosystems. One can distinguish between impacts in the source regions, the atmosphere, and the zones of dust settlement, respectively.

Source regions of mineral dust are often affected by heavy dust storms coupled with extremely high concentrations of particulate matter resulting in negative health effects for the population, a degradation of visibility, damages to crops and machinery, and the deflation and degradation of surface sediments (see Goudie and Middleton 2006, their Table 3.1).

The input of mineral dust into the atmosphere largely influences the radiative budget of the Earth through absorption and scattering of the incoming solar and outgoing terrestrial radiation (direct effect, e.g., Balkanski et al. 2007). Mineral dust particles may also act as cloud condensation nuclei (CCN) or ice nuclei (IN) and consequently will change in-cloud processes (see Chap. 12, Rosenfeld et al. 2001; Yin et al. 2002; DeMott et al. 2003; Toon 2003; Zimmermann et al. 2008; Koehler et al. 2009; Kumar et al. 2011). The detailed characteristics and the extent of this so-called indirect effect is a matter of intense research. During transport, mineral dust will also inevitably react with other components including heterogeneous reactions with trace gases which will in turn alter the chemical balance of the atmosphere (Bauer et al. 2004). Especially calcium-rich dusts will partly buffer an elevated acidity of the atmosphere and increase pH values of precipitation (e.g., Rodá et al. 1993; Cao et al. 2005; Ooki and Uematsu 2005).

In regions of dust settlement, several impacts are also observed, and many terrestrial soils and marine surface sediments contain significant fractions of aeolian material. Mineral dust may be also a carrier of different nutrients, and the supply of iron and phosphorus to terrestrial and marine ecosystems will modify the primary bio-productivity and finally the biogeochemical cycle in regions far apart from the dust source regions (see Chap. 14 and, e.g., Swap et al. 1992; Jickells et al. 2005; Mahowald et al. 2008b; Paytan et al. 2009; Okin et al. 2011). On the other hand, living microorganisms (including pathogens) are often carried along with mineral dust which may cause diseases leading, for example, to the demise of coral reefs (Shinn et al. 2000; Garrison et al. 2003; Griffin and Kellogg 2004). Furthermore, the remaining size fraction of mineral dust after long-range transport will be comparatively small and therefore may affect human health through inhalation and transport deep into the lungs (see Chap. 15, Prospero et al. 2008; De Longueville et al. 2010).

Most of the impacts described above depend on the chemical and mineralogical composition, the external and internal mixing state of the dust, the absolute aerosol mass concentration, the particle number concentration, the particle size distribution, and/or the morphology and shape of the particles (see also Formenti et al. 2011b). This chapter describes and compares the composition of northern African and eastern Asian dust based on bulk composition and individual-particle analysis and presents data on size distribution and morphological parameters. Northern Africa and eastern Asia are the two major source regions for mineral dust supplying about 700 Tg year^{-1} (Laurent et al. 2008) and 250 Tg year^{-1} (Laurent et al. 2006) of dust to the Earth's atmosphere, respectively, amounting to one third to more than half of the total dust burden of 1,000 to 3,000 Tg year^{-1} (Cakmur et al. 2006).

When it comes to interpretation of literature data of mineral dust properties measurements and their representation of total mineral dust, a cautious approach is necessary. First, measurements were usually not performed during the highest concentrations situations like haboobs or synoptically induced dust storms, as modern instrumentation or an aircraft carrying this instrumentation is usually not very robust in these situations. Second, dust is usually measured away from its source, as the source regions are often nearly inaccessible for logistical or political reasons. As a result, the dust properties in closest vicinity to its source still remain rather unknown. Instead, we know more on transported and aged mineral dust.

As a technical remark, in this work we would like to distinguish between "mineral dust," meaning the fraction of airborne particulates deriving from the soil and consisting of inorganic minerals, and "desert aerosol" consisting of the airborne particulates found in the outflow of a mineral dust source, possibly containing additional material from natural and anthropogenic sources. Although it would be desirable to distinguish strictly between these, for many methods of measurement, it is commonly not possible, for example, for size distribution or aerosol-integral measurements. Even single-particle-based measurements like electron microscopical individual-particle analysis cannot strictly perform this discrimination, as particles become internal mixtures of different sources or composition by processes like cloud processing or gas phase reactions. As a result, we usually observe a desert aerosol.

2.2 Composition

In the following, the discussion of the composition of bulk samples is separated from individual-particle analysis. The bulk composition of mineral dust is mainly determined by three different methodological approaches and yields variable compositional parameters.

2.2.1 Mineralogical Data

The mineralogical composition of mineral dust samples is predominantly analyzed by X-ray diffractometry (XRD) and has been now used for more than 40 years for the characterization of mineral dust samples and their possible source sediments. By means of XRD techniques, the crystalline compounds of a sample are determined, neglecting noncrystalline phases such as opaline diatoms or volcanic glass fragments which may constitute a significant fraction in some dust samples. However, XRD has to be viewed as a semiquantitative technique with high detection limits (>3–5 wt%) and comparatively large analytical errors. The amount of mass required for analysis (>800 μg; Formenti et al. 2011b) is usually much larger than the sample mass obtained by short-time impactor sampling and hence, X-ray diffractometry has been mainly applied to source sediments and to long-term deposited samples. X-ray diffractometry is used for the mineralogical characterization of non-oriented bulk samples and for the determination of the fine-grained phases (<2 μm; clay mineral size spectrum) on oriented samples. A summary of results obtained by XRD techniques on mineral dust samples (aerosols and deposited samples) mainly from northern Africa and eastern Asia will be provided in the following paragraphs.

Bulk dust samples from all over the Earth are mainly composed of silicates and carbonates. The major mineralogical phases are the silicates quartz (SiO_2), feldspar, and members of the group of phyllosilicates (see below) and the carbonates calcite ($CaCO_3$) and dolomite ($CaMg((CO_3)_2)$). The amount of quartz significantly varies but mainly falls in a range between 15 and 60 wt% with exceptional high amounts reaching 80 wt% and more in some deposited samples in northern Africa (Nigeria: Adedokun et al. 1989, Libya: O'Hara et al. 2006). The different feldspar minerals K-feldspar ($KAlSi_3O_8$) and plagioclase (solid solution series between albite ($NaAlSi_3O_8$) and anorthite ($CaAl_2Si_2O_8$)) are present in most mineral dust samples but rarely exceed 10 wt%. Considering the present data set, neither the abundance of quartz or feldspar in a dust sample nor any ratio between quartz and feldspar or between both feldspars are characteristic for a specific source area and hence they cannot be recommended for any source apportionment studies. On the other hand, the abundance of the carbonates calcite and dolomite in mineral dust samples is clearly correlated to the composition of the soils and sediments in the source area and can be used as a compositional fingerprint in northern African as well as in eastern Asian dust samples (Formenti et al. 2011b; Scheuvens et al. 2013). In northern Africa, mineral dusts with the highest carbonate contents (occasionally more than 50 wt%) are reported from the northwestern part of northern Africa (northern Algeria, Morocco) and are probably associated with source sediments deposited along the foothills of the Atlas mountains. Mineral dusts uplifted in this area are mainly transported northwards to the Mediterranean region and southwestern Europe or to the west towards the Canary Islands. Hence, it can be expected that mineral dusts sampled in this regions should be generally rich in carbonates (if no solution or transformation processes have taken place). In eastern Asia, a general trend with higher carbonate contents in western source

regions (e.g., Taklamakan Desert) to very low carbonate contents in eastern source regions can be observed (Shen et al. 2009b). Furthermore, Li et al. (2007) proposed that the occurrence of dolomite in Asian dusts is characteristic for specific potential source areas. Other minerals detected by XRD in minor or trace amounts are, for example, hematite, gypsum, halite, or amphibole.

The amount of clay minerals in bulk samples varies considerably from trace amounts to 60 wt% or more. It is suggested that this parameter does not only depend on the composition of the source sediments but also reflects the conditions during dust uplift (e.g., wind speed) and transport (e.g., transport distance).

XRD analysis of oriented specimen of the fine fraction (<2 μm) offers the possibility to characterize the occurring clay minerals in more detail. The dominating clay minerals in mineral dust samples are members of the illite, kaolin, and smectite group, respectively. Other more rarely observed phyllosilicates are chlorite, palygorskite, and white mica (muscovite). Only sporadically were clay minerals of the mixed layer type or halloysite detected. As particles of the clay mineral groups occur (by definition) in approximately the same size class, a significant segregation during uplift, transport, and deposition is not expected (however, for a more detailed discussion, see Scheuvens et al. 2013). Hence, the ratio between the amounts of different clay minerals was proposed as a compositional fingerprint of the source region (Schütz and Sebert 1987; Caquineau et al. 2002). The illite/kaolinite (I/K) ratio was repeatedly claimed as a viable source marker. In northern Africa, mineral dusts with I/K ratios >1.0 are mainly restricted to source areas located in northern and western Algeria, Morocco, and Western Sahara. A trend with decreasing I/K ratios to the south can also be seen off the coast of western Africa by numerous analyses from different ship cruises (Chester et al. 1971, 1972; Chester and Johnson 1971a, b; Stuut et al. 2005). Mineral dust samples from the sub-Saharan (Sahelian) zone are mainly characterized by I/K ratios <0.5 (Caquineau et al. 2002; Formenti et al. 2008; Kandler et al. 2011b). On average, I/K ratios of eastern Asian dust samples are higher compared to northern African dust samples (often >5.0). Highest values are reported from samples from the Taklamakan Desert (Shen et al. 2005). Hence, Asian mineral dust samples that are characterized by elevated carbonate contents and high illite abundances most probably derive from the westernmost source region of eastern Asia. In many northern African dust samples, chlorite is not detected at all or only occurs in trace amounts (see Scheuvens et al. 2013; their Fig. 10), whereas in eastern Asian dust samples, the abundance of chlorite is mostly greater than the abundance of kaolinite. However, significant overlapping in the chlorite/kaolinite (C/K) ratios of Asian and African dust samples prevents any assignment of far-travelled dusts to one of both major source regions solely based on the C/K ratio. In many dust samples from northern Africa, members of the smectite group (e.g., montmorillonite) or illite-smectite mixed layers were not detected at all or only occur in minor and trace amounts. However, mineral dust samples that had their origin in the region of southern Algeria and northern Mali exhibit significantly elevated smectite contents (>40 wt% of the fine fraction; Paquet et al. 1984; Skonieczny et al. 2011). These high smectite abundances are probably coupled with intensely weathered basic volcanics of this region (Coudé-Gaussen 1989).

In eastern Asia, elevated smectite contents were not reported so far. However, Shao et al. (2007) detected extremely high contents of illite-smectite mixed layers in the fine fraction of Asian dust samples collected in Beijing in 2002. Further XRD data is needed to clarify if the data of Shao et al. (2007) is representative for Asian dust in general or if it represents a single unusual event. Palygorskite, an Mg-bearing fibrous clay mineral, has not been detected in Asian dusts. In northern Africa, it is only rarely found in Sahelian dusts but is frequently observed as a minor phase in mineral dusts uplifted in the region of Morocco, Algeria, and Tunisia. Hence, palygorskite was proposed as a source tracer for dusts originating in the northwestern part of northern Africa (e.g., Schütz and Sebert 1987). Far-travelled palygorskite-bearing African dusts were found, for example, in western Europe (e.g., Avila et al. 1997) and on the Canary islands (Menéndez et al. 2007).

2.2.2 Isotope Data

Isotope data of mineral dusts are mainly used for source apportionment analyses. Studies in the last two decades have shown that the analysis of Nd and Sr isotopes is an especially valuable tool to assign actual and paleo-dust samples (e.g., marine sediments, ice core samples) to a specific source region. For northern Africa, there exists an impressive data set of calculated $\varepsilon_{Nd}(0)$ and $^{87}Sr/^{86}Sr$ values from continental and marine surface sediments, which were mainly measured by Grousset and coworkers (Grousset et al. 1988, 1990, 1992, 1998; Grousset and Biscaye 2005; see also compilation by Scheuvens et al. 2013). However, isotope analyses of mineral dust or deposited samples are much rarer (Grousset et al. 1988, 1992, 1998; Rognon et al. 1996; Meyer et al. 2011, 2013), owing to the high amount of particulate mass required. Northern African dusts which were mainly sampled off the western coast of northern Africa exhibit $\varepsilon_{Nd}(0)$ values between -15 and -10 (with the exception of data from Goldstein et al. 1984; Frost et al. 1986) and $^{87}Sr/^{86}Sr$ values between 0.713 and 0.725. In conjunction with analyses from marine surface sediments, an indistinct trend with decreasing $\varepsilon_{Nd}(0)$ values to the south can be observed along the western coast of northern Africa. However, the extremely low $\varepsilon_{Nd}(0)$ values (< -16.0) that were obtained in northern Mauretania and Western Sahara on surface sediment samples (Grousset et al. 1998) were not detected in African dust samples so far.

Isotope analyses of mineral dusts from other regions are rare. For example, Kanayama et al. (2005) presented isotope data from aerosol samples collected with a high-volume sampler at different sites in China and their data can be compared to the numerous analyses of potential source sediment and loess samples in eastern Asia (see Formenti et al. 2011b). On average, Asian dusts and source sediments exhibit slightly higher $\varepsilon_{Nd}(0)$ values and lower $^{87}Sr/^{86}Sr$ values than northern African dusts. However, the interregional variability within a continent is much more pronounced than the differences between African and Asian dusts. Hence, it is suggested that isotope data are best suited for regional source apportionment studies and that some

care should be taken in assigning far-travelled dusts (e.g., paleo dusts in ice cores) to "continental source areas" without other evidence. Finally, it should be borne in mind that especially $^{87}Sr/^{86}Sr$ analyses are grain-size sensitive and that only similar (carbonate-free) size fractions can be compared in a strict sense (Meyer et al. 2011).

2.2.3 Elemental Data

The third important bulk analytical technique to characterize mineral dust samples is the chemical analysis of major and/or trace elements. However, the compilation and evaluation of this data set is hampered, for example, by the different types of data obtained (mass fraction [wt%] versus aerosol mass concentration [$\mu g/m^3$]), the different analytical methods used (atomic absorption spectroscopy (AAS), inductively coupled plasma mass spectrometry (ICP-MS), inductively coupled plasma optical (atomic) emission spectroscopy (ICP-OES or ICP-AES), X-ray fluorescence spectrometry (XRF), particle-induced X-ray emission (PIXE), or instrumental neutron activation analysis (INAA)), and the grain-size dependence of the elemental composition. Nevertheless, the elemental analyses of northern African dust samples were compiled and discussed in detail by Scheuvens et al. (2013) and will be briefly reviewed in the following (starting with the mass fraction data set). As expected, in many northern African dust samples, Si is the most abundant element and is in average slightly enriched compared to the composition of the upper continental crust. Si/Al ratios fall mainly into a range between 2 and 7, pointing to mixtures between quartz and aluminosilicates in agreement with the mineralogical data. Regional trends in the Si/Al ratio are not observed. Scheuvens et al. (2013) could show that especially the ratio (Ca + Mg)/Fe has a high potential for the discrimination between the different potential source areas in northern Africa (see their Fig. 2). Mineral dusts from the Atlas region, central Algeria, Libya, and Egypt are generally characterized by (Ca + Mg)/Fe ratios >1, whereas dust samples collected in the sub-Saharan belt (including the Bodélé depression in Chad) mainly exhibit (Ca + Mg)/Fe ratios <1 in agreement with the mineralogical data presented above (carbonate-rich mineral dusts in more northern latitudes). All other major elements (e.g., K, Na, Fe, Mn, Ti, P) and elemental ratios (with the "crustal" element Al as the denominator) do not show any distinct regional trends and should not be used for any source apportionment in northern Africa. In average, northern African dusts are slightly depleted in K and Na and slightly enriched in Ti and P when compared to the average composition of the upper continental crust. The abundance of Fe in mineral dusts arouses interest because of its possible capability to serve as nutrient in downwind marine (Atlantic ocean) and terrestrial ecosystems (Amazon forest) and its significant influence on the optical properties of mineral dust in the visible range of the spectrum (e.g., Arimoto et al. 2002). Meanwhile, a series of studies focused on the partitioning of Fe between iron oxides (e.g., hematite) and iron hydroxides (e.g., goethite), on one hand, and crystal-bound Fe (mainly in clay minerals), on the other hand, mainly using the CBD extraction

method (Lafon et al. 2004, 2006, for Asian dust: Shen et al. 2006; Formenti et al. 2008, 2011a; Lázaro et al. 2008). They could show that in mineral dusts approximately one half of the total iron content is associated with the (hydr)oxides goethite and hematite (with usually goethite > hematite).

In principle, aerosol mass concentration data [$\mu g/m^3$] of ground-based and airborne samples which were mainly collected in the Mediterranean region and off the western coast of northern Africa (but see also Formenti et al. 2008 and Paris et al. 2010 for continental airborne samples from Niger, Formenti et al. 2011a) reveal comparable trends to the mass fraction data. Si/Al ratios constantly fall into a range between 2.0 and 4.0 with slightly elevated values for dust originated in the Bodélé depression in Chad (Formenti et al. 2011a). Fe/Al (mainly 0.4–0.8) and Na/Al ratios (large scatter of data is probably due to occasional uptake of sea salt) do not exhibit any unequivocal trends. K/Al and Mg/Al ratios are slightly lower in dust samples from the Sahelian region (mainly <0.35 and <0.20, respectively) compared to samples from more northern latitudes. The opposite trend is observed for Ti/Al ratios (south: > 0.1; north: < 0.1), opening up the possibility that these elemental ratios may be used as additional source tracers in the future. However, it should be remembered that, in southern latitudes, an additional K component might be introduced by biomass burning. One of the best parameters for the discrimination of different potential source areas in northern Africa is the ratio (Ca + Mg)/Fe (Scheuvens et al. 2013), which is <1.2 for Sahelian dust samples and mostly >2.0 for dust samples from the northern regions of northern Africa.

The elemental composition of eastern Asian dust samples (aerosol mass concentration data in [$\mu g/m^3$], neglecting the analyzed size fraction) shows many similarities to northern African dust samples (see also Formenti et al. 2011b). The Si/Al ratios of eastern Asian dust mainly fall in the range between 1.0 and 5.0 and hence are comparable to northern African dust samples. Highest Si/Al ratios are reported from dust samples collected in the surroundings of the Taklamakan Desert (Zhang et al. 1996; Makra et al. 2002) and from the Horqin sandy desert in northeastern China (Shen et al. 2007) with Si/Al ratios generally above 3.5. As expected, dust storm samples are mainly characterized by higher Si/Al ratios pointing to elevated quartz contents in these samples (Zhang et al. 1996). Fe/Al and K/Al ratios exhibit a comparatively large range of values and do not yield any significant regional trends from the westernmost potential source area (Taklamakan Desert) to the east. In contrast, the Ca/Al ratio can be used as a compositional fingerprint for different source regions in eastern Asia with high ratios (>2.0) in dust samples from the Taklamakan Desert and lower ratios (<1.0) in the deserts of Mongolia and northeastern China (e.g., Cheng et al. 2005; Sun et al. 2005). A detailed study of deposited dust in the eastern source regions by Wang et al. (2009) also showed a trend with decreasing Ca/Al ratios from the Mu Us and Hobq Deserts towards the northeast.

Based on the S/Al ratio, Alfaro et al. (2003) separated aerosols from dust episodes (S/Al <0.15) from aerosols of pollution episodes (S/Al >0.20). This can be compared to northern African dust samples where near-source "pristine" dust samples from Niger exhibit S/Al ratios <0.20 (Paris et al. 2010), whereas

transported dusts collected, for example, at Fuerteventura (Canary islands) are characterized by much higher values (Bergametti et al. 1989).

Finally it is important to note that the calculation of the fraction of "pure" desert dust in Asian aerosol samples shows that even during heavy dust-storm conditions, the amount of mineral dust at maximum reaches about 80 % and that 20 % of the aerosol concentration are still of non-crustal origin (Zhang et al. 2003b; Shen et al. 2007). Comparable studies of northern African dust are not available at the moment.

Today, only a comparatively small number of studies is devoted to the (inorganic) ionic composition of northern African (e.g., Viana et al. 2002; Formenti et al. 2003; Alastuey et al. 2005; Müller et al. 2010; Paris et al. 2010) and eastern Asian (e.g., Arimoto et al. 2004; Cheng et al. 2005; Shen et al. 2009a; Wang et al. 2012) mineral dust. This data is mainly helpful to decipher the alteration and processing of mineral dust and its mixing with different pollution aerosols. The obtained data is extremely heterogeneous concerning absolute values and ratios between different ions and will here not be considered further.

2.3 Individual-Particle Analysis

For several decades now, scanning electron microscopy (mainly coupled with energy-dispersive X-ray microanalysis) sometimes accompanied by transmission electron microscopy (TEM) was used to characterize individual particles of mineral dust samples in more detail. However, only recently techniques become available enabling the automated measurement of several 10,000 particles in a single study. Particles are collected on different substrates by active (e.g., impactor) or passive (e.g., dry and/or wet deposition) sampling. Subsequently, particles are analyzed for their chemical elements (usually atomic number ≥ 6), their size (area, diameter), and their shape (aspect ratio, shape factor). Based on net counts or after some correction procedures (e.g., standardless ZAF correction), the chemical analyses of the particles are interpreted in terms of particle classes (e.g., Si rich, Ca(Mg) rich, S rich, etc.) grossly comparable to mineralogical groups (e.g., quartz, calcite + dolomite, sulfates, etc.) or are further evaluated by statistical treatments such as principal component analysis (PCA) (e.g., Anderson et al. 1996). Automated individual-particle analysis offers the possibility to determine the size-segregated composition and shape of aerosols in more detail and is helpful for a better understanding of the external and internal mixing state of mineral dust. Furthermore, from the obtained data set, it is possible to derive an average complex refractive index (Kandler et al. 2007) which can be compared with direct optical measurements.

For northern African dust, a series of studies exist using automated individual-particle analysis for a robust characterization of mineral dust samples (Reid et al. 2003; Moreno et al. 2006; Kandler et al. 2007, 2009, 2011a; Chou et al. 2008; Deboudt et al. 2010; Matsuki et al. 2010a, b; Lieke et al. 2011; Scheuvens et al. 2011; Deboudt et al. 2012; Pósfai et al. 2013). Their results are summarized in the following paragraphs, and some images of "typical" mineral dust particles

are shown in Fig. 2.1. In principle, individual-particle analysis confirms the XRD results of bulk samples. It demonstrates that the major fraction of the particle number abundance consists of Si-dominated particles (mainly quartz, Fig. 2.1a; occasionally diatoms, Fig. 2.1i), different aluminosilicates (Fig. 2.1b–d), and carbonates (Fig. 2.1e), whereas sulfates (Fig. 2.1e), Fe-dominated particles (Fig. 2.1f), Cl-bearing, and carbonaceous particles only occur in minor amounts. Minor components such as Ca sulfates (gypsum), sodium chloride (halite), and C-dominated components may or may not be of desert origin. Size-segregated analysis of Kandler et al. (2009) clearly shows that sulfates and carbonaceous particles are significantly enriched in the smallest size fraction (<500 nm) and at least in their samples cannot be classified as mineral dust particles in a strict sense. Furthermore, it is important to note that the majority of particles are represented by internal mixtures between different phases and that "pure" end-member particles are rather rare (Falkovich et al. 2001; Deboudt et al. 2010). For example, a detailed study by Deboudt et al. (2012) shows that Fe oxides and Fe hydroxides in dust samples stemming from northwestern Africa are mostly internally mixed with aluminosilicates (see also Lieke et al. 2011; Scheuvens et al. 2011). Iron-bearing particles often seem to be positioned at the surface of silicate particles probably due to rubification processes in the parent soil. Other studies emphasize the role of coatings of sulfur-, nitrogen-, and phosphorus-bearing or carbonaceous phases on northern African mineral dust particles (Falkovich et al. 2001; Kandler et al. 2007, 2011a; Crumeyrolle et al. 2008; Dall'Osto et al. 2010; Scheuvens et al. 2011; Pósfai et al. 2013) due to post-entrainment processing in the atmosphere. It is somehow surprising that even freshly emitted near-source mineral dust collected in Morocco contains significant amounts of internally mixed silicate-sulfate particles (Kandler et al. 2011a; Scheuvens et al. 2011). An extraordinary case study was presented by Matsuki et al. (2010b) from airborne dust samples collected in southwestern Niger where calcium carbonate particles completely reacted to form spherical (aqueous) calcium nitrate particles.

Concerning the characterization of potential source areas, different SEM/EDX studies indicate that samples originating in the northwestern regions of northern Africa (Morocco, northern Algeria) exhibit elevated abundances of Ca-rich particles (calcite, dolomite) and palygorskite and are characterized by illite/kaolinite ratios >1 in full agreement with the mineralogical data obtained by XRD (Blanco et al. 2003; Moreno et al. 2006; Kandler et al. 2007, 2009; Coz et al. 2009; Scheuvens et al. 2011; Deboudt et al. 2012). On the other hand, SEM-EDX analysis was used to determine a shift in source area with time (2002–2005) for sediment trap material in the north Atlantic (Brust and Waniek 2010) based on the estimated abundances of different phyllosilicates (illite, palygorskite, smectite). Manual inspection of individual particles have also yielded some hints to specific source regions (e.g., findings of the diatoms Aulacoseira and Stephanodiscus as source markers for the Bodélé depression in samples from Niger, Chou et al. 2008).

An important topic for northern African mineral dust (especially from more southern latitudes) is its mixing state with aerosols stemming from biomass burning (and/or urban emissions). Several large field campaigns were dedicated to this problem. In summary, it could be shown that biomass burning aerosol (mainly

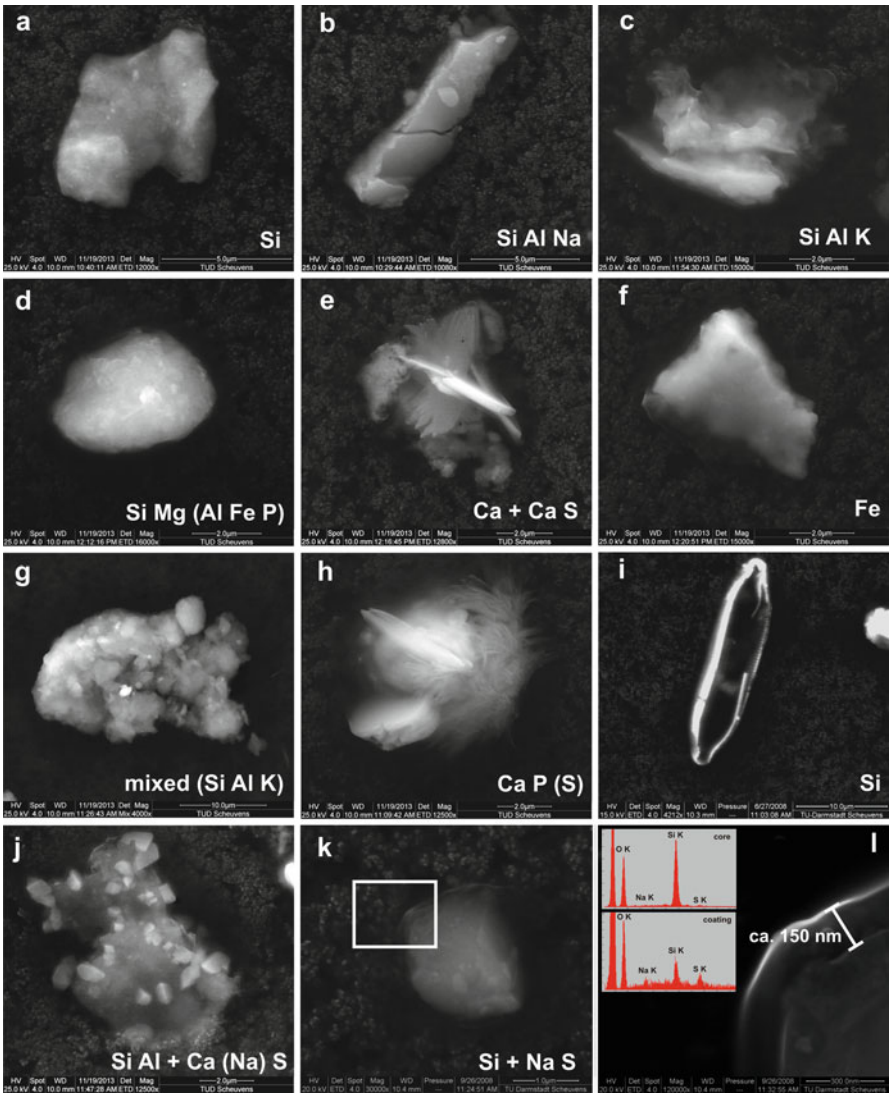

Fig. 2.1 Secondary electron images of typical dust particles of northern Africa collected during the SAMUM I campaign in Morocco. At the bottom of the images, the major elements analyzed by energy-dispersive X-ray technique (EDX) are labelled. In the following, common atmospheric minerals with the specified composition (and matching the morphology of the particle) are given in parenthesis. (**a**) Si-rich particle (quartz), (**b**) Na-bearing aluminosilicate (albite), (**c**) K-bearing aluminosilicate (illite), (**d**) Mg-dominated silicate (palygorskite), (**e**) Ca sulfate and Ca-dominated mineral (gypsum on calcite), (**f**) Fe-dominated mineral (iron oxide or iron hydroxide), (**g**) complex internally mixed aluminosilicate with individual Fe-dominated phase (bright spot in center), (**h**) Ca-P-S-bearing particle (biological?), (**i**) Si-dominated particle (opaline diatom), (**j**) aluminosilicate (kaolin group?) with Ca(Na) sulfate (gypsum, thenardite, glauberite?), and (**k**) Si-rich particle (quartz) with sulfate coating (overview). (**l**) Detail of coating with EDX spectra for rim and core of the particle

C-dominated (soot, "tar balls") and K-S rich particles) is mostly restricted to the fine (submicron) size fractions and is in most case studies mainly externally mixed with mineral dust (Chou et al. 2008; Formenti et al. 2008; Deboudt et al. 2010, but see also Hand et al. 2010; Matsuki et al. 2010a; Kandler et al. 2011a; Lieke et al. 2011).

Individual-particle analysis on Asian dust mainly focused on the interaction between (long-range) transported dust and urban (polluted) aerosols of mega-cities as Xi'an and Beijing and/or mixing and processing during transport towards eastern China and Korea and further to Japan and the North Pacific. On the other hand, a number of studies exist that investigate near-ground or balloon-borne dust samples collected in the most important potential source areas of eastern Asia (e.g., Taklamakan) although the number of analyzed particles is often low (<500). In general, individual-particle analysis shows that Asian dust is composed of external and internal mixtures of quartz, aluminosilicates (mainly different clay minerals), and carbonates to varying amounts (Okada and Kai 1995; Gao and Anderson 2001; Trochkine et al. 2003; Matsuki et al. 2005a; Yuan et al. 2006; Jeong 2008) comparable to northern African dust. Jeong (2008) describes the occurring clay minerals in more detail and shows their association with nanosized calcite, iron oxides, and other minerals. In dusts from the Taklamakan Desert, elevated amounts of halite particles were detected (Okada and Kai 2004). The older idea that freshly emitted Asian dust is mostly devoid of sulfates (Iwasaka et al. 2003) has recently been challenged by a study of Wu et al. (2012) who could show that the sulfur content in samples from the Taklamakan Desert is of primary soil-derived origin (see also Shi et al. 2005; Yuan et al. 2006; Wang et al. 2012). Yuan et al. (2006) also proposed that elevated phosphorus and chlorine contents in their dust samples are related to saline soils in the source area (here: Inner Mongolia).

In particular, the carbonate calcite is subjected to heterogeneous reactions at the particle surface and readily reacts during transport to form calcium sulfate (Gao and Anderson 2001; Trochkine et al. 2003; Matsuki et al. 2005a), calcium nitrate, and/or calcium chloride (Tobo et al. 2009) depending mainly on the abundance of the different acidic gases H_2SO_4, HCl, and HNO_3 in the atmosphere. Whereas the reaction from calcite to calcium nitrate under participation of nitric acid is a self-reinforcing process resulting in complete transformation and genesis of spherical (aqueous) particles, the conversion from calcium carbonate to calcium sulfate occurs more slowly and is often incomplete (Matsuki et al. 2005a, b; Formenti et al. 2011a). During long-range transport (alumino)silicate particles are also strongly affected by internal mixing with non-crustal components (e.g., sea salt, Niimura et al. 1998; Zhang et al. 2003a; Zhang and Iwasaka 2004; Ma and Choi 2007) and/or uptake of sulfur, nitrogen, chlorine or organic compounds on the particle surface (Ma et al. 2001, 2012; Zhang et al. 2003a; Matsuki et al. 2005a; Sullivan et al. 2007). The internal mixing of Asian dust with sea salt on its way to Japan is mainly restricted to near-ground samples and is not found in the cloud-free troposphere (Trochkine et al. 2003).

2.3.1 *Particle Shape and Morphology*

Generally, mineral dust particles are nonspherical. Their shapes[1] vary between crystals without defects and aggregates of small irregular grains, but also near-spherical shapes are found for processed dust particles (Laskin et al. 2005a, b). The shape of the dust particles has importance for their radiative interaction (e.g., Kalashnikova and Sokolik 2002; Nousiainen 2009) and for their settling behavior (Ginoux 2003; Li and Osada 2007a), though for both influences, high uncertainties exist (Nousiainen et al. 2011). Surface roughness influences active remote sensing (Zubko et al. 2007; Gasteiger et al. 2011). Shape and morphology also affect the effective surface area and therefore might modify heterogeneous chemical reactions.

Currently, there are mainly three approaches to measure the particle shape: microscopy, radiation scattering, and measurement of aerodynamic properties. Light microscopy, electron microscopy, and atomic force microscopy have been used in many cases to study the shape of single mineral dust particles collected on substrates. The depolarization of scattered or transmitted radiation has been used to retrieve information on effective particles shapes (e.g., Dubovik et al. 2006; Müller et al. 2012). However, the retrieved results do not necessarily resemble real particles shapes (Nousiainen et al. 2011). Aerodynamic measurements have also been used to determine the effective particle shape parameter (Kaaden et al. 2009). While the latter two approaches lack the close connection to real geometrical shape, the microscopy approach instead is usually limited by the comparatively small number of analyzed particles, a limitation which is somewhat overcome by the use of automated instruments (e.g., Reid et al. 2003; Kandler et al. 2007; Coz et al. 2009).

From the microscopic techniques, primarily a two-dimensional projected shape of the particle is retrieved, which then is usually parameterized by several shape descriptors. Mainly the aspect ratio is used, in principle defined as the ratio of the longer to the shorter axis of an ellipse fitted to the particles shape but often also calculated as the ratio of four times the squared particle's longest projection to pi times the projected area. We will use the latter definition for the data presented here. It must be emphasized that the difference between these two definitions are significant for non-elliptic shapes like those of dust particles. In addition, other shape descriptors like fractal dimension, circularity, roundness, shape factor, and solidity are sometimes used. The shape descriptors are usually derived from discretized images; the latter four – depending on shape perimeter or holes – are more prone to resolution-dependent artifacts (Podczeck et al. 1999; Almeida-Prieto et al. 2007). An illustration of several shape descriptors applied

[1]The expressions particle shape and particle morphology are used interchangeably throughout the literature with slightly different meanings. We will use the term particle shape to describe the general outline of a particle, and the term particle morphology shall refer to small-scale structures like surface roughness.

to mineral dust is given by Kalashnikova and Sokolik (2004). Three-dimensional information can be obtained by using laser scanning microscopy (Osada 2013), shadowing techniques in electron microscopy (Okada et al. 2001), scanning electron microscope stereogrammetry (Lindqvist et al. 2013), and atomic force microscopy (Gwaze et al. 2007; Chou et al. 2008). The latter techniques are, however, quite work intensive, and as a result only information on small particle numbers is available.

In contrast to shape, morphology is currently only described qualitatively, and no measure for size and amount of small scale structures of roughness of mineral dust particles is available, unlike for other aerosol types like, for example, soot (Yehliu et al. 2011).

Aspect ratio measurements of several regions are summarized in Table 2.1. Note that the aspect ratio measurements for African dust are based on the longest projection/area method mentioned above, while for the Asian dust the ratio of the particle's longest projection to the orthogonally measured width is used; this explains the generally lower aspect ratios found in Asian dust. Conversion between the two definitions is not possible without further information on particle shape. A considerable trend in aspect ratio as function of particle size is absent. Long-range transported particles seem to have a higher aspect ratio than those found close to the source, which would indicate a preferential settling of particles that are more spherical. Where the particle length-to-height ratio has been determined, it exhibits significantly larger values than the aspect ratio. For these cases we can conclude that the majority of particles are elongated and platelike, resembling the shape of clay minerals. In addition, from a methodical point of view, it means that the particles are orientated "flat" on the substrate and that the commonly applied two-dimensional projected area diameter is likely to overestimate the particle volume. Besides the median values displayed here, dust aerosol consists usually of an ensemble of particles having a broader distributions. This was illustrated, for example, by Okada et al. (2001) and Kandler et al. (2007) who have shown that this aspect ratio distribution can be readily parameterized by a modified log-normal distribution.

As mentioned above, shape factors are difficult to compare for different investigations and image resolutions. A general trend, however, seems to exist of increasing shape factors with increasing particle size, indicating a more complex geometrical structure of larger dust particles (i.e., aggregates).

Particle shapes are mostly a function of particle composition (Kandler et al. 2007, 2009, 2011a; Coz et al. 2009; Scheuvens et al. 2011). In dry conditions, soluble compounds not containing sulfate and iron and titanium (oxyhydr)oxides as well as partly carbonates tend to have lower aspect ratios than silicates, whereas crystallized sulfate-containing particles – except for ammonium (hydrogen)sulfate – are usually elongated. Consequently, an internal mixture of dust with, for example, sodium sulfate usually leads to a growth of the aspect ratio. Besides the atmospheric alteration of the shape of single particles, the shape distribution of a dust aerosol could also be changed by shape-sensitive atmospheric processes, for example, heterogeneous processing due to higher surface area or material selectivity (Matsuki et al. 2010b) or preferential settling due to different settling velocities (Li and Osada 2007a).

Table 2.1 Median aspect ratios and shape factors for African and Asian dust particles

Location	Size range, μm	Median aspect ratio[a]	Length-to-height ratio	Median shape factor[b]	Number of analyzed particles	Reference
Airborne, over Niger	0.1–0.75	1.7		1.53	31,000	Chou et al. (2008)
	0.75–2			1.61		
	2–10			1.76		
			3.6/5.5		2	
Mountain station, Tenerife	0.7–10	1.64			22,000	Kandler et al. (2007)
Ground-based, Morocco	0.7–200	1.58			45,000	Kandler et al. (2009)
High-altitude airborne, over Morocco	0.5–3	1.74			7,000	Kandler et al. (2009)
Low-altitude airborne, over Morocco	1–30	1.57		1.23	22,000	Scheuvens et al. (2011)
Ground-based, dust component only, Cape Verde	0.5–20	1.63			16,000	Kandler et al. (2011a)
Airborne, dust over Cape Verde	0.4–20	1.69		1.40	48,000	Lieke et al. (2011)
Ground-based, dust episodes in Spain	2.4–4	1.87			30,000	Coz et al. (2009)
	4–10	1.81				
Airborne, African dust over Puerto Rico	0.3–0.75	1.9		1.25	60,000	Reid et al. (2003)
	0.75–5			1.35		
	5–10			1.58		
Ground-based, Asian dust, Japan			>1.59[c]		1,600	Osada (2013)

(continued)

Table 2.1 (continued)

Location	Size range, μm	Median aspect ratio[a]	Length-to-height ratio	Median shape factor[b]	Number of analyzed particles	Reference
Ground-based, arid locations, western and central China	0.2–0.4	1.38[d]	3.4–4.0	1.33–1.37	5,000 (estimate)	Okada et al. (2001)
	0.4–1	1.38–1.42[d]	5.9–7.1	1.52–1.54		
	1–2	1.41–1.43[d]	5.9–7.1	1.71–1.84		
	2–4	1.27–1.41[d]	5.0–7.7	2.05–2.07		
Ground-based, eastern China	0.2–0.4	1.34[d]	2.5	1.32	2,000 (estimate)	Okada et al. (2001)
	0.4–1	1.37[d]	2.9	1.48		
	1–2	1.36[d]	2.5	1.53		
	2–4	1.37[d]	4.2	1.70		
Ground-based, dust component in central China	>1 (estimate)			1.55	1,000 (estimate)	Gao and Anderson (2001)
Ground-based, dust in eastern coastal China	>1 (estimate)			1.06	1,500 (estimate)	Gao and Anderson (2001)
Insoluble Asian and African dust in snow deposition, Japan	2.5–15	1.22–1.30[d]		1.08–1.16	11,000	Li and Osada (2007b)
Ship-borne, Asian dust, western North Pacific	0.4–5			1.12–1.24	11,000	Gao et al. (2007)

[a] Aspect ratio: ratio of four times the squared particle's longest projection to pi times the projected area
[b] Shape factor: ratio of squared particle's perimeter to four pi times the projected area
[c] 0.63 is reported as ratio of particle height to projected area diameter
[d] Lower values due to different definition of aspect ratio

2.4 Size Distributions

The size distribution of an aerosol is one of its most important properties, as it governs its impact on any process, in particular on its radiative impact – for example, the scattering cross section scaling with powers of 3–5 of particle size – its impact on multiphase chemical reactions (particle surface area/surface to volume ratio) and on cloud processes (threshold sizes), but also its removal processes efficiencies (sedimentation, wet removal) and as a consequence transport distances. The mineral dust size distribution, which usually ranges from less than 100 nm to more than 100 μm, is notoriously difficult to measure. A major problem is the collection efficiency of any instrument for particle sizes larger than a few micrometers, particularly for airborne measurements. This can be in part overcome by using inlet-free instruments like free-path optical-scattering instruments or body impactor techniques for particle collection. Another problem arises from the sizing technique itself, which usually uses a secondary measure – that is, light-scattering, aerodynamic behavior – to determine particle size. While the relationship of these secondary measures for spherical particles of known composition is generally well known, this does not necessarily apply to mineral dust particles, which are highly nonspherical and consist of mixtures of many different minerals in different shapes.

Geometric sizing techniques analyze samples collected by filtration or impactor sampling by means of optical or electron microscopy (Fletcher et al. 2011). They usually measure the two-dimensional projected shape of the particles (projected area diameter). As a result, they are sensitive to particle orientation on the substrate and overestimate particle size for flatly oriented, platelike particles (e.g., clay minerals). However, this is the only major technique directly assessing the particle's geometrical size. Aerodynamic and electrical methods determine the quantity of particle with certain vacuum stopping distances and mechanical (super-micron range) or electrical (submicron) mobilities. These measured quantities are then translated into a geometrical size assuming spherical or spheroidal particles of homogeneous, known density. Nonsphericity of the particles is assessed for aerodynamic methods with a shape factor (e.g., like done by Kaaden et al. 2009), but still dust particles are usually undersized (Reid et al. 2008). Light-scattering methods measure an optically equivalent diameter with the same scattering properties. Thus, they are sensitive to the particle shape and to its refractive index, imaginary as well as real part. Assumption of sphericity usually leads to a slight oversizing (Collins et al. 2000). Particle light absorption can strongly influence light-scattering sizing, especially for forward scattering (Weinzierl et al. 2009; Schumann et al. 2011). Quality control of size distribution measurements can be achieved by comparison with a reliable integral measure, for example, mass concentration or optical extinction properties (Collins et al. 2000; Esselborn et al. 2009; Schladitz et al. 2011).

A compilation of coarse mode modal diameters for desert aerosol in and downwind of major deserts is compiled in Fig. 2.2. In the Saharan Desert and downwind, there is a gradient of decreasing modal diameters from ground-based over airborne to medium-/long-range transported dust as it would be expected

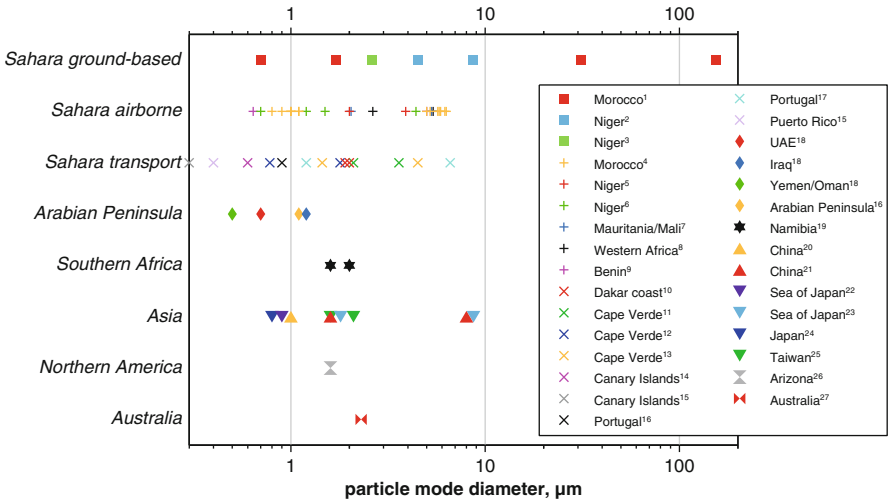

Fig. 2.2 Number modal diameters detected by atmospheric measurements for different dust situations. *1* Kandler et al. (2009), *2* Rajot et al. (2008), *3* Sow et al. (2009), *4* Weinzierl et al. (2009), *5* Osborne et al. (2008), *6* Chou et al. (2008), *7* Ryder et al. (2013), *8* Johnson and Osborne (2011), *9* Crumeyrolle et al. (2011), *10* McConnell et al. (2008), *11* Haywood et al. (2003a), *12* Schladitz et al. (2011), *13* Weinzierl et al. (2011), *14* de Reus et al. (2000), *15* Maring et al. (2003), *16* Bates et al. (2002), *17* Wagner et al. (2009), *18* Reid et al. (2008), *19* Haywood et al. (2003b), *20* Kim et al. (2004), *21* Zhou et al. (2012), *22* Quinn et al. (2004), *23* Clarke et al. (2004), *24* Kobayashi et al. (2007), *25* Chang et al. (2010), *26* Peters (2006), *27* Shao et al. (2011)

from the preferential settling of the large particles (e.g., Schütz et al. 1981). The latter gradient, however, is smaller. After 1,000 km or a few days of transport, no modal diameter larger than 3 µm particle diameter is detected and the change in size distribution for mineral dust becomes very small (cf. also Reid et al. 2008). However, this does not mean that large particles cannot be transported over long distances; for example, over Portugal, in the Caribbean, and over the Pacific Ocean, particles measuring tens of micrometers were observed (Betzer et al. 1988; Formenti et al. 2001; Wagner et al. 2009).

In principle, Asian dust covers a similar range of observations like the lifted/transported Saharan dust, so no different microphysical behavior for dust dynamics should be expected. Only sparse data is available for other deserts, so no conclusion can be drawn from them.

Figure 2.3 illustrates the difference between the desert aerosol and mineral dust size distribution as defined previously. The mineral dust fraction of the total size distributions in desert regions starts to decrease from unity at particle sizes smaller than one micrometer. At 100 nm particle diameter, even comparatively close to strong dust sources most of the airborne particles are non-dust.

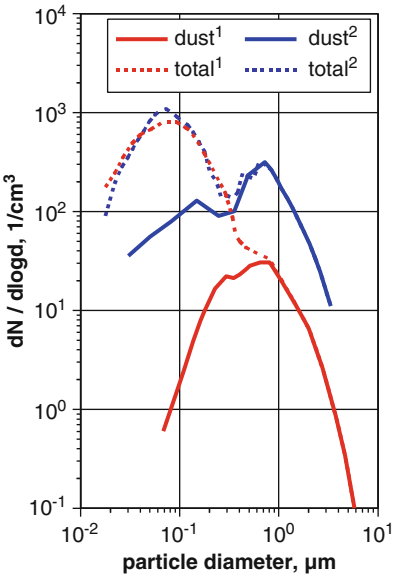

Fig. 2.3 Total desert aerosol and mineral dust size distributions for two different situations in northwestern Africa (PM_{10} inlet); *1* dust size distribution inferred from spectral absorption measurements ("period 1" of Müller et al. 2009); *2* inferred from hygroscopic growth measurements ("dust event" of Kaaden et al. 2009)

Thus, the lower end of the mineral dust size distribution is often set at 100 nm. However, even considerably smaller mineral dust particles have been identified in desert aerosol (Lieke et al. 2011) in low concentrations.

2.5 Discussion and Conclusions

The uplift, transport, and final deposition of mineral dust from the major source regions in northern Africa and eastern Asia have severe environmental and climatic impacts, depending on various physicochemical parameters such as composition, mixing state, or size and shape of the dust particles. In the following, first, the possibilities for an assignment of mineral dust samples to specific source regions are given. Afterwards, the specific physicochemical parameters, which are important for the evaluation of the impacts of mineral dust on Earth's climate, and different ecosystems are briefly discussed.

The uplift or entrainment of mineral dust in northern Africa and eastern Asia is restricted to several main regions, which can cover sometimes areas of thousands of square kilometers (see Chap. 3). In the past, these so-called potential source areas have been determined by vastly differing methods including personal meteorological observations, backward trajectory analyses, remote sensing data, and last but not least by the use of compositional fingerprints. Only the last method is able to attribute paleo-dust samples (e.g., from terrestrial or marine surface sediments or

ice cores) to specific source areas and is therefore helpful for a better understanding of paleoclimatic conditions. Meanwhile, several studies have shown that some "source tracers" perform much better than others (see compilation by Scheuvens et al. 2013). For mineral dust samples that have originated in northern Africa and eastern Asia, a combination of different analytical techniques is probably the most promising approach to assign even far-travelled mineral dusts to a specific source area. Especially the different isotopes of Nd and Sr, the abundance of carbonates (calcite + dolomite), the illite/kaolinite ratio, and the elemental ratio (Ca + Mg)/Fe are valuable tools for mineral dust source apportionment. However, it has to be claimed that at present some partial data sets are at best rudimentary and should be improved in the future. A compilation of the compositional data also reveals that mineral dust is compositionally heterogeneous and that a "typical" dust composition does not exist. However, the observed regional compositional trends in northern Africa and eastern Asia show that average mineral dusts from the different regional source areas are characterized by specific compositional features (Formenti et al. 2011b; Scheuvens et al. 2013) that in turn will determine their impacts on Earth's climate, ecosystems, and human health.

2.5.1 Direct Radiative Forcing

Besides the absolute dust concentration and the height and structure of a dust layer in the atmosphere, the radiative characteristics (direct radiative effect) of "pure" mineral dust are mainly determined by its particle size distribution, the composition, and the shape of the particles (see Chap. 11, Sokolik and Toon 1999; Nousiainen 2009). Concerning composition, the abundance and mixing state of the main light-absorbing minerals in dust – iron-bearing ones like hematite (Fe_2O_3) and goethite (FeOOH) – is of prime importance for estimation of the optical properties (e.g., Sokolik and Toon 1999). However, as the elemental Fe content is only a rough proxy for the amount of Fe (hydr)oxides in a given sample and the abundance of hematite/goethite often falls below the detection limit of XRD analysis, other methods have to be applied to analyze the amount and speciation of iron-bearing phases (e.g., Lafon et al. 2004). Furthermore, individual-particle analysis revealed that pure Fe (hydr)oxide particles are rare in mineral dust and that these minerals are more often internally mixed with different (alumino)silicates (e.g., Kandler et al. 2009; Lieke et al. 2011; Scheuvens et al. 2011). The detailed structure of these internally mixed particles and hence their radiative characteristics are far from being understood. Nevertheless, for northern Africa, an indistinct trend with higher abundances of iron (hydr)oxides towards southern latitudes was shown by Formenti et al. (2008), resulting in an elevated value for the imaginary part of the refractive index for sub-Saharan/Sahelian dust (Kandler et al. 2009, Table 6, Kandler et al. 2011a, Fig. 12, Müller et al. 2011). A more detailed closure is currently limited

by the lack of detailed particle structure information and the resulting ambiguity of the shape and structure influence on the radiative properties (Merikallio et al. 2011; Nousiainen et al. 2011).

Particle size strongly influences the shortwave direct radiative forcing of mineral dust by changing the effective scattering cross section, in particular in the absence of clouds (Liao and Seinfeld 1998). In contrast to other aerosol types, the contribution of large mineral dust particles is non-negligible for the radiative forcing in a size range, where exact measurement is more difficult and variability is high (Miller et al. 2004). As a result, the aerosol size distribution is still a considerable uncertainty in determining the dust radiative forcing (see Chap. 11, Claquin et al. 1998; Miller et al. 2004; Durant et al. 2009; Zhao et al. 2010; Köhler et al. 2011; Osborne et al. 2011). Although a better modeling based on more exact measurements of the size distribution decreased the uncertainties in the last decade (e.g., Heinold et al. 2011; Johnson et al. 2012), there still seems to be some way to go (e.g., Haustein et al. 2009; Kok 2011; Müller et al. 2012).

The shape and morphology of the particles is another important parameter influencing the optical properties of mineral dust. The dust particle's nonspherical shape exhibits quite different radiative characteristics compared to the formerly assumed spherical particles (Nousiainen 2009; see, e.g., Otto et al. 2009 for a forcing simulation as function of particle shape; Redmond et al. 2010). The largest database is available for the aspect ratio of the particles (see compilation above), but except for a characteristic distribution function, the variability seems to be low; however, a shape-preferential particle removal (Li and Osada 2007a) will change the radiative properties. More complex shapes and morphologies have been investigated recently (Nousiainen et al. 2009; Gasteiger et al. 2011; Kahnert and Rother 2011; Lindqvist et al. 2013), but for a broad application of these methods, more knowledge on the real particle shape and morphology has to be acquired.

2.5.2 Indirect Radiative Forcing

The indirect effects of aerosol particles are associated with their ability to provide surfaces for the nucleation of cloud droplets (cloud condensation nuclei, CCN) or ice crystals (ice nuclei, IN; see also Chap. 12). Based on the classical Köhler theory, dust particles are considered to represent poor CCN (Pruppacher and Klett 1997). However, several experimental and field studies revealed that mineral dust in general (Twohy et al. 2009; Kumar et al. 2011) and (aged) calcite in particular may act as CCN (Gibson et al. 2006). Hence, the CCN activity of pristine mineral dust may largely depend on its carbonate (or Ca) content. On the other hand, individual-particle studies for northern African and eastern Asian dust reveal that pure mineral dust hardly exists and that, even shortly after entrainment, dust particles are the sites of heterogeneous reactions finally resulting in the deposition of highly soluble

phases at their surface (e.g., coatings). Meanwhile, different types of coatings (sulfate, nitrate, phosphate, organic; see Chap. 4) were verified by several studies (Shi et al. 2008; Li and Shao 2009; Matsuki et al. 2010a, b), and even a combination of different coatings has to be taken into account. The deposition of highly soluble material at the (dust) particle surface will significantly change the hygroscopicity and hence enhance their ability to act as cloud condensation nuclei (CCN).

In contrast to its possibly restricted CCN activity, dust particles are readily activated as ice nuclei (DeMott et al. 2003; Sassen et al. 2003) so that the long-range transport of mineral dust is associated with elevated IN number concentrations (Klein et al. 2010; Chou et al. 2008). However, a soluble coating acquired through atmospheric processing during transport may suppress the initiation of ice formation at the same time as enhancing their action as CCN (Hoose et al. 2008; Möhler et al. 2008; Niedermeier et al. 2011; Reitz et al. 2011; Tobo et al. 2012). A high atmospheric burden of dust particles, that is, readily available CCN or IN, may have a significant impact on cloud processes (Rosenfeld et al. 2001; Yin et al. 2002; Levin et al. 2005), so the absolute number concentration of mineral dust plays a considerable role. The mineral dust size distribution should, in contrast, not affect activation, as most of the dust particles are larger than the usual activation size for cloud droplets (Pruppacher and Klett 1997). However, for particle cloud dynamic and precipitation development, the presence of large CCN and a large number of IN should have an influence, which most probably depends on the actual thermodynamic situation and cannot be generalized.

2.5.3 Ecosystem Nutrient Supply and Human Health Effects

The major nutrients that may control the functionality of marine and terrestrial ecosystems are iron, phosphorus, and nitrogen (Duce and Tindale 1991; Mills et al. 2004). Nitrogen concentrations in freshly emitted mineral dust are generally low. However, several studies emphasized that especially calcite particles may react to form calcium nitrate under conditions of elevated NO_x and/or HNO_3 concentrations in the atmosphere. These nitrate (or internally mixed calcite/nitrate) particles are highly soluble and may be an important source for nitrogen when finally deposited (Fan et al. 2004; Doney et al. 2007). Northern African dust is generally enriched in phosphorus with respect to the composition of the upper continental crust (Scheuvens et al. 2013). Special attention has recently been drawn to large phosphorite deposits in northwestern Africa which may be the source of P-enriched dust deposits (Rodríguez et al. 2011). The major carrier of phosphorus in dust samples is the mineral apatite which is in general only slightly soluble. Studies on the determination and conditions of phosphorus solubility in dust samples are comparatively rare (see also Mahowald et al. 2008a, e.g., Nenes et al. 2011; Okin et al. 2011) and will be a challenge for future studies due to the comparatively low P abundance and the high fraction of generally insoluble apatite in dust samples.

The most important nutrient that is transported with mineral dust is iron (see Chap. 14, Jickells et al. 2005; Mahowald et al. 2005). The major carriers of Fe in mineral dust are iron oxide (e.g., hematite), iron hydroxide (e.g., goethite), and/or Fe-bearing sheet silicates (mainly members of the smectite and chlorite group). Journet et al. (2008) emphasized that the soluble iron (Fe^{2+}) in mineral dust is mainly derived from the different clay minerals and not from the iron oxides and hydroxides. Hence, the primary fraction of clay minerals in a dust sample (and its evolution during transport) is crucial for the supply of bioavailable iron to the different ecological compartments. However, as mentioned above, this fraction largely varies from a few wt% to more than 60 wt% (Lawrence and Neff 2009; Scheuvens et al. 2013) and is only partly determined by the soil type of the source region. The clay mineral fraction probably also strongly depends on the wind speed during emission (with higher wind speed favoring lower abundance of clay minerals). During transport of mineral dust, its mass concentration generally decreases due to deposition and dispersion, whereas the fraction of clay minerals increases relatively, owing to preferential settling of larger particles (mainly quartz, carbonates, and feldspar) during the early stages of transport. As result, an increase in dust "fertility" is expected.

The relationship between human health and environmental mineral dust exposure is not well defined (see also Chap. 15), and studies are often restricted to a comparison of elevated mass concentrations during dust events (e.g., PM_{10}) and their effects on health or mortality (e.g., Chen et al. 2004; Yang et al. 2005; Prospero et al. 2008; Dadvand et al. 2011; Tobías et al. 2011; Thalib and Al-Taiar 2012). In southern Europe, the input of Saharan dust is also responsible for exceedances of PM_{10} (and $PM_{2.5}$) limit values set by the directive for air quality in Europe (Querol et al. 2009; Remoundaki et al. 2012). For future studies, it would be highly desirable to include more often compositional parameters (especially obtained by individual-particle analysis) and particle size distributions to gain a deeper understanding of the health effects of mineral dust intrusions, despite the fact that anthropogenic emissions (e.g., traffic related) are clearly more toxic than dust particles (e.g., Samoli et al. 2011).

In Table 2.2, we list the major topics that are associated with the uplift, transport, and settlement of mineral dust and assign a preferred physicochemical analytical method for each field of investigation. It becomes obvious that determination of the dust mineralogy by XRD and (automated) chemical and morphological analysis of dust particles are powerful tools for a better understanding of origin and impacts of mineral dust. It is suggested that a combination of both techniques (e.g., automated particle analysis in a transmission electron microscope) could be very helpful in impact studies of mineral dust and will be hopefully available in the future.

Table 2.2 Fields of research and preferred chemical and physical methods

	Preferred chemical method	Preferred physical method
Source identification	Nd and Sr isotopes	
	XRD	
	[Elemental]	
	[Individual-particle analysis]	
Direct effect	XRD	Determination of PSD
	Individual-particle analysis (chemistry, mixing state)	Individual-particle analysis (shape)
	CBD extraction	
	[Elemental]	
Indirect effect (CCN)	Individual-particle analysis (mixing state)	Determination of PSD
Indirect effect (IN)	XRD	Determination of PSD
	[Individual-particle analysis]	Individual-particle analysis
Nutrient supply	XRD	Determination of MC
	Elemental	
	CBD extraction	
	[Individual-particle analysis]	
Human health	[Individual-particle analysis]	Determination of MC
		Determination of PSD

CCN cloud condensation nuclei; *IN* ice nuclei; *XRD* X-ray diffraction; *CBD extraction* selective dissolution of free iron with citrate, bicarbonate, and dithionite; *PSD* particle size distribution; *MC* mass concentration

References

Adedokun JA, Emofurieta WO, Adedeji OA (1989) Physical, mineralogical and chemical properties of harmattan dust at Ile-Ife. Nigeria Theor Appl Climatol 40:161–169

Alastuey A, Querol X, Castillo S, Escudero M, Avila A, Cuevas E et al (2005) Characterisation of TSP and PM2.5 at Izaña and Sta. Cruz de Tenerife (Canary Islands, Spain) during a Saharan Dust Episode (July 2002). Atmos Environ 39:4715–4728

Alfaro SC, Gomes L, Rajot JL, Lafon S, Gaudichet A, Chatenet B et al (2003) Chemical and optical characterization of aerosols measured in spring 2002 at the ACE-Asia supersite, Zhenbeitai, China. J Geophys Res 108:8641

Almeida-Prieto S, Blanco-Méndez J, Otero-Espinar FJ (2007) Microscopic image analysis techniques for the morphological characterization of pharmaceutical particles: influence of the software, and the factor algorithms used in the shape factor estimation. Eur J Pharm Biopharm 67:766–776

Anderson JR, Buseck PR, Patterson TL, Arimoto R (1996) Characterization of the Bermuda tropospheric aerosol by combined individual-particle and bulk-aerosol analysis. Atmos Environ 30:319–338

Arimoto R, Balsam W, Schloesslin C (2002) Visible spectroscopy of aerosol particles collected on filters: iron-oxide minerals. Atmos Environ 36:89–96

Arimoto R, Zhang XY, Huebert BJ, Kang CH, Savoie DL, Prospero JM et al (2004) Chemical composition of atmospheric aerosols from Zhenbeitai, China, and Gosan, South Korea, during ACE-Asia. J Geophys Res 109, D19S04

Avila A, Queralt-Mitjans I, Alarcón M (1997) Mineralogical composition of African dust delivered by red rains over northeastern Spain. J Geophys Res 102:21977–21996

Balkanski Y, Schulz M, Claquin T, Guibert S (2007) Reevaluation of Mineral aerosol radiative forcings suggests a better agreement with satellite and AERONET data. Atmos Chem Phys 7:81–95

Bates TS, Coffman DJ, Covert DS, Quinn PK (2002) Regional marine boundary layer aerosol size distributions in the Indian, Atlantic, and Pacific Oceans: a comparison of INDOEX measurements with ACE-1, ACE-2, and Aerosols99. J Geophys Res 107:8026

Bauer SE, Balkanski Y, Schulz M, Hauglustaine DA, Dentener F (2004) Global modeling of heterogeneous chemistry on mineral aerosol surfaces: influence on tropospheric ozone chemistry and comparison to observations. J Geophys Res 109, D02304

Bergametti G, Gomes L, Coudé-Gaussen G, Rognon P, Coustumer M-NL (1989) African dust observed over Canary Islands: source-regions identification and transport pattern for some summer situations. J Geophys Res 94:14855–14864

Betzer PR, Carder KL, Duce RA, Merrill JT, Tindale NW, Uematsu M et al (1988) Long-range transport of giant mineral aerosol particles. Nature 336:568

Blanco A, De Tomasi F, Filippo E, Manno D, Perrone MR, Serra A et al (2003) Characterization of African dust over southern Italy. Atmos Chem Phys 3:2147–2159

Brust J, Waniek JJ (2010) Atmospheric dust contribution to deep-sea particle fluxes in the subtropical Northeast Atlantic. Deep-Sea Res I 57:988–998

Cakmur RV, Miller RL, Perlwitz J, Geogdzhayev IV, Ginoux P, Koch D et al (2006) Constraining the magnitude of the global dust cycle by minimizing the difference between a model and observations. J Geophys Res 111, D06207

Cao JJ, Lee SC, Zhang XY, Chow JC, An ZS, Ho KF et al (2005) Characterization of airborne carbonate over a site near Asian dust source regions during spring 2002 and its climatic and environmental significance. J Geophys Res 110, D03203

Caquineau S, Gaudichet A, Gomes L, Legrand M (2002) Mineralogy of Saharan dust transported over northwestern tropical Atlantic Ocean in relation to source regions. J Geophys Res 107:4251

Chang S-C, Chou CCK, Chen W-N, Lee C-T (2010) Asian dust and pollution transport – a comprehensive observation in the downwind Taiwan in 2006. Atmos Res 95:19–31

Chen Y-S, Sheen P-C, Chen E-R, Liu Y-K, Wu T-N, Yang C-Y (2004) Effects of Asian dust storm events on daily mortality in Taipei. Taiwan Environ Res 95:151–155

Cheng T, Lu D, Wang G, Xu Y (2005) Chemical characteristics of Asian dust aerosol from Hunshan Dake Sandland in Northern China. Atmos Environ 39:2903–2911

Chester R, Johnson LR (1971a) Atmospheric dusts collected off the Atlantic coasts of North Africa and the Iberian Peninsula. Mar Geol 11:251–260

Chester R, Johnson LR (1971b) Atmospheric dusts collected off the West African Coast. Nature 229:105–107

Chester R, Elderfield H, Griffin JJ (1971) Dust transported in the North-east and South-east trade winds in the Atlantic Ocean. Nature 233:474–476

Chester R, Elderfield H, Griffin JJ, Johnson LR, Padgham RC (1972) Eolian dust along the eastern margins of the Atlantic Ocean. Mar Geol 13:91–105

Chou C, Formenti P, Maille M, Ausset P, Helas G, Harrison M, Osborne S (2008) Size distribution, shape, and composition of mineral dust aerosols collected during the African Monsoon Multidisciplinary Analysis Special Observation Period 0: Dust and Biomass-Burning Experiment field campaign in Niger, January 2006. J Geophys Res 113, D00C10

Claquin T, Schulz M, Balkanski Y, Boucher O (1998) Uncertainties in assessing radiative forcing by mineral dust. Tellus 50B:491–505

Clarke AD, Shinozuka Y, Kapustin VN, Howell S, Huebert B, Doherty S et al (2004) Size distributions and mixtures of dust and black carbon aerosol in Asian outflow: physiochemistry and optical properties. J Geophys Res 109, D15S09

Collins DR, Johnsson HH, Seinfeld JH, Flagan RC, Gassó S, Hegg DA et al (2000) In situ aerosol-size distributions and clear-column radiative closure during ACE-2. Tellus B 52: 498–525

Coudé-Gaussen G (1989) Local, proximal and distal Saharan dusts: characterization and contribution to the sedimentation. In: Leinen M, Sarnthein M (eds) Palaeoclimatology and palaeometeorology: modern and past patterns of global atmospheric transport. Kluwer Academic Publishers, Dordrecht, pp 339–358

Coz E, Gómez-Moreno FJ, Pujadas M, Casuccio GS, Lersch TL, Artíñano B (2009) Individual particle characteristics of North African dust under different long-range transport scenarios. Atmos Environ 43:1850–1863

Crumeyrolle S, Gomes L, Tulet P, Matsuki A, Schwarzenboeck A, Crahan K (2008) Increase of the aerosol hygroscopicity by cloud processing in a mesoscale convective system: a case study from the AMMA campaign. Atmos Chem Phys 8:6907–6924

Crumeyrolle S, Tulet P, Gomes L, Garcia-Carreras L, Flamant C, Parker DJ et al (2011) Transport of dust particles from the Bodélé region to the monsoon layer – AMMA case study of the 9–14 June 2006 period. Atmos Chem Phys 11:479–494

Dadvand P, Basagana X, Figueras F, Amoly E, Tobias A, de Nazelle A et al (2011) Saharan dust episodes and pregnancy. J Environ Monit 13:3222–3228

Dall'Osto M, Harrison RM, Highwood EJ, O'Dowd C, Ceburnis D, Querol X et al (2010) Variation of the mixing state of Saharan dust particles with atmospheric transport. Atmos Environ 44:3135–3146

De Longueville F, Hountondji Y-C, Henry S, Ozer P (2010) What do we know about effects of desert dust on air quality and human health in West Africa compared to other regions? Sci Total Environ 409:1–8

de Reus M, Dentener F, Thomas A, Borrmann S, Ström J, Lelieveld J (2000) Airborne observations of dust aerosol over the North Atlantic Ocean during ACE 2: indications for heterogeneous ozone destruction. J Geophys Res 105:15263–15275

Deboudt K, Flament P, Choël M, Gloter A, Sobanska S, Colliex C (2010) Mixing state of aerosols and direct observation of carbonaceous and marine coatings on African dust by individual particle analysis. J Geophys Res 115, D24207

Deboudt K, Gloter A, Mussi A, Flament P (2012) Red-ox speciation and mixing state of iron in individual African dust particles. J Geophys Res 117, D12307

DeMott P, Sassen K, Poellot M, Baumgardner D, Rogers D, Brooks S et al (2003) African dust aerosols as atmospheric ice nuclei. Geophys Res Lett 30:1732

Doney SC, Mahowald N, Lima I, Feely RA, Mackenzie FT, Lamarque J-F et al (2007) Impact of anthropogenic atmospheric nitrogen and sulfur deposition on ocean acidification and the inorganic carbon system. Proc Natl Acad Sci U S A 104:14580–14585

Dubovik O, Sinyuk A, Lapyonok T, Holben BN, Mishchenko M, Yang P et al (2006) Application of spheroid models to account for aerosol particle nonsphericity in remote sensing of desert dust. J Geophys Res 111, D11208

Duce RA, Tindale NW (1991) Atmospheric transport of iron and its deposition in the ocean. Limnol Oceanogr 36:1715–1726

Durant AJ, Harrison SP, Watson IM, Balkanski Y (2009) Sensitivity of direct radiative forcing by mineral dust to particle characteristics. Prog Phys Geog 33:80–102

Esselborn M, Wirth M, Fix A, Weinzierl B, Rasp K, Tesche M et al (2009) Spatial distribution and optical properties of Saharan dust observed by airborne high spectral resolution lidar during SAMUM 2006. Tellus B 61:131–143

Falkovich AH, Ganor E, Levin Z, Formenti P, Rudich Y (2001) Chemical and mineralogical analysis of individual mineral dust particles. J Geophys Res 106:18029–18036

Fan S-M, Horowitz LW, Levy H II, Moxim WJ (2004) Impact of air pollution on wet deposition of mineral dust aerosols. Geophys Res Lett 31, L02104

Fletcher RA, Ritchie NWM, Anderson IM, Small JA (2011) Microscopy and microanalysis of individual collected particles. In: Kulkarni P, Baron PA, Willeke K (eds) Aerosol measurement: principles, techniques, and applications. Wiley, Hoboken, pp 179–232

Formenti P, Andreae MO, Lange L, Roberts G, Cafmeyer J, Rajta I et al (2001) Saharan dust in Brazil and Suriname during the Large-Scale Biosphere-Atmosphere Experiment in Amazonia (LBA)-Cooperative LBA Airborne Regional Experiment (CLAIRE) in March 1998. J Geophys Res 106:14919–14934

Formenti P, Elbert W, Maenhaut W, Haywood J, Andreae MO (2003) Chemical composition of mineral dust aerosol during the Saharan Dust Experiment (SHADE) airborne campaign in the Cape Verde region, September 2000. J Geophys Res 108:8576

Formenti P, Rajot JL, Desboeufs K, Caquineau S, Chevaillier S, Nava S et al (2008) Regional variability of the composition of mineral dust from western Africa: results from the AMMA SOP0/DABEX and DODO field campaigns. J Geophys Res 113, D00C13

Formenti P, Rajot JL, Desboeufs K, Saïd F, Grand N, Chevaillier S et al (2011a) Airborne observations of mineral dust over western Africa in the summer Monsoon season: spatial and vertical variability of physico-chemical and optical properties. Atmos Chem Phys 11:6387–6410

Formenti P, Schütz L, Balkanski Y, Desboeufs K, Ebert M, Kandler K et al (2011b) Recent progress in understanding physical and chemical properties of mineral dust. Atmos Chem Phys 11:8231–8256

Frost CD, O'Nions RK, Goldstein SL (1986) Mass balance for Nd in the Mediterranean Sea. Chem Geol 55:45–50

Gao Y, Anderson JR (2001) Characteristics of Chinese aerosols determined by individual-particle analysis. J Geophys Res 106:18037–18045

Gao Y, Anderson JR, Hua X (2007) Dust characteristics over the North Pacific observed through shipboard measurements during the ACE-Asia experiment. Atmos Environ 41:7907–7922

Garrison VH, Shinn EA, Foreman WT, Griffin DW, Holmes CW, Kellogg CA et al (2003) African and Asian Dust: from desert soils to coral reefs. BioScience 53:469–480

Gasteiger J, Wiegner M, Groß S, Freudenthaler V, Toledano C, Tesche M et al (2011) Modeling lidar-relevant optical properties of complex mineral dust aerosols. Tellus 63B

Gibson ER, Hudson PK, Grassian VH (2006) Aerosol chemistry and climate: laboratory studies of the carbonate component of mineral dust and its reaction products. Geophys Res Lett 33, L13811

Ginoux P (2003) Effects of nonsphericity on mineral dust modeling. J Geophys Res 108, D4052

Goldstein SL, O'Nions RK, Hamilton PJ (1984) A Sm-Nd isotopic study of atmospheric dusts and particulates from major river systems. Earth Planet Sci Lett 70:221–236

Goudie AS, Middleton NJ (2006) Desert dust in the global system. Springer, Berlin

Griffin DW, Kellogg CA (2004) Dust storms and their impact on ocean and human health: dust in Earth's atmosphere. Ecohealth 1:284–295

Grousset FE, Biscaye PE (2005) Tracing dust sources and transport patterns using Sr, Nd and Pb isotopes. Chem Geol 222:149–167

Grousset FE, Biscaye PE, Zindler A, Prospero J, Chester R (1988) Neodymium isotopes as tracers in marine sediments and aerosols: North Atlantic. Earth Planet Sci Lett 87:367–378

Grousset FE, Henry F, Minster JF, Monaco A (1990) Nd isotopes as tracers in water column particles: the western Mediterranean Sea. Mar Chem 30:389–407

Grousset F, Rognon P, Coudé-Gaussen G, Pedemay P (1992) Origins of peri-Saharan dust deposits traced by their Nd and Sr isotopic composition. Paleogeog Paeloclim Paleoecol 93:201–212

Grousset FE, Parra M, Bory A, Martinez P, Bertrand P, Shimmield G et al (1998) Saharan wind regimes traced by the Sr-Nd isotopic composition of subtropical Atlantic sediments: last glacial maximum vs today. Quaternary Sci Rev 17:395–409

Gwaze P, Annegarn HJ, Huth J, Helas G (2007) Comparison of particle sizes determined with impactor, AFM and SEM. Atmos Res 86:93–104

Hand VL, Capes G, Vaughan DJ, Formenti P, Haywood JM, Coe H (2010) Evidence of internal mixing of African dust and biomass burning particles by individual particle analysis using electron beam techniques. J Geophys Res 115, D13301

Haustein K, Pérez C, Baldasano JM, Müller D, Tesche M, Schladitz A et al (2009) Regional dust model performance during SAMUM 2006. Geophys Res Lett 36, L03812

Haywood J, Francis P, Osborne S, Glew M, Loeb N, Highwood E et al (2003a) Radiative properties and direct radiative effect of Saharan dust measured by the C-130 aircraft during SHADE: 1. Solar spectrum. J Geophys Res 108:8577

Haywood JM, Osborne SR, Francis PN, Keil A, Formenti P, Andreae MO et al (2003b) The mean physical and optical properties of regional haze dominated by biomass burning aerosol measured from the C-130 aircraft during SAFARI 2000. J Geophys Res 108:8473

Heinold B, Tegen I, Schepanski K, Tesche M, Esselborn M, Freudenthaler V et al (2011) Regional modelling of Saharan dust and biomass burning smoke. Part I: Model description and evaluation. Tellus 63B:781

Hoose C, Lohmann U, Erdin R, Tegen I (2008) The global influence of dust mineralogical composition on heterogeneous ice nucleation in mixed-phase clouds. Environ Res Lett 3, 025003

Iwasaka Y, Shi GY, Shen Z, Kim YS, Trochkine D, Matsuki A et al (2003) Nature of atmospheric aerosols over the desert areas in the Asian continent: chemical state and number concentration of particles measured at Dunhuang, China. Water Air Soil Pollut 3:129–145

Jeong GY (2008) Bulk and single-particle mineralogy of Asian dust and a comparison with its source soils. J Geophys Res 113, D02208

Jickells TD, An ZS, Andersen KK, Baker AR, Bergametti G, Brooks N et al (2005) Global iron connection between desert dust, ocean biogeochemistry, and climate. Science 308:67–71

Johnson BT, Osborne SR (2011) Physical and optical properties of mineral dust aerosol measured by aircraft during the GERBILS campaign. Q J Roy Meteorol Soc 137:1117–1130

Johnson MS, Meskhidze N, Praju Kiliyanpilakkil V (2012) A global comparison of GEOS-Chem-predicted and remotely-sensed mineral dust aerosol optical depth and extinction profiles. J Adv Model Earth Syst 4, M07001

Journet E, Desboeufs KV, Caquineau S, Colin J-L (2008) Mineralogy as a critical factor of dust iron solubility. Geophys Res Lett 35, L07805

Kaaden N, Maßling A, Schladitz A, Müller T, Kandler K, Schütz L et al (2009) State of mixing, shape factor, number size distribution, and hygroscopic growth of the Saharan anthropogenic and mineral dust aerosol at Tinfou, Morocco. Tellus 61B:51–63

Kahnert M, Rother T (2011) Modeling optical properties of particles with small-scale surface roughness: combination of group theory with a perturbation approach. Opt Express 19:11138–11151

Kalashnikova OV, Sokolik IN (2002) Importance of shapes and compositions of wind-blown dust particles for remote sensing at solar wavelengths. Geophys Res Lett 29

Kalashnikova OV, Sokolik IN (2004) Modeling the radiative properties of nonspherical soil-derived mineral aerosols. J Quant Spectrosc Radiat Transf 87:137–166

Kanayama S, Yabuki S, Zeng F, Liu M, Shen Z, Liu L et al (2005) Size-dependent geochemical characteristics of Asian dust – Sr and Nd isotope compositions as tracers for source identification. J Meteor Soc Japan II 83A:107–120

Kandler K, Benker N, Bundke U, Cuevas E, Ebert M, Knippertz P et al (2007) Chemical composition and complex refractive index of Saharan Mineral Dust at Izaña, Tenerife (Spain) derived by electron microscopy. Atmos Environ 41:8058–8074

Kandler K, Schütz L, Deutscher C, Hofmann H, Jäckel S, Knippertz P et al (2009) Size distribution, mass concentration, chemical and mineralogical composition, and derived optical parameters of the boundary layer aerosol at Tinfou, Morocco, during SAMUM 2006. Tellus 61B:32–50

Kandler K, Lieke K, Benker N, Emmel C, Küpper M, Müller-Ebert D et al (2011a) Electron microscopy of particles collected at Praia, Cape Verde, during the Saharan Mineral dust experiment: particle chemistry, shape, mixing state and complex refractive index. Tellus 63B:475–496

Kandler K, Schütz L, Jäckel S, Lieke K, Emmel C, Müller-Ebert D et al (2011b) Ground-based off-line aerosol measurements at Praia, Cape Verde, during the Saharan Mineral Dust Experiment: microphysical properties and mineralogy. Tellus 63B:459–474

Kim KW, He Z, Kim YJ (2004) Physicochemical characteristics and radiative properties of Asian dust particles observed at Kwangju, Korea, during the 2001 ACE-Asia intensive observation period. J Geophys Res 109, D19S02

Klein H, Nickovic S, Haunold W, Bundke U, Nillius B, Ebert M, Weinbruch S, Schütz L, Levin Z, Barrie LA, Bingemer H (2010) Saharan dust and ice nuclei over Central Europe. Atmos Chem Phys 10:10211–10221

Kobayashi H, Arao K, Murayama T, Iokibe K, Koga R, Shiobara M (2007) High-resolution measurement of size distributions of Asian dust using a coulter multisizer. J Atmos Oceanic Tech 24:194–205

Koehler KA, Kreidenweis SM, DeMott PJ, Petters MD, Prenni AJ, Carrico CM (2009) Hygroscopicity and cloud droplet activation of mineral dust aerosol. Geophys Res Lett 36, L08805

Köhler CH, Trautmann T, Lindermeir E, Vreeling W, Lieke K, Kandler K et al (2011) Thermal IR radiative properties of mixed mineral dust and biomass aerosol during SAMUM-2. Tellus 63B

Kok JF (2011) A scaling theory for the size distribution of emitted dust aerosols suggests climate models underestimate the size of the global dust cycle. Proc Natl Acad Sci U S A 108:1016–1021

Kumar P, Sokolik IN, Nenes A (2011) Measurements of cloud condensation nuclei activity and droplet activation kinetics of fresh unprocessed regional dust samples and minerals. Atmos Chem Phys 11:3527–3541

Lafon S, Rajot J-L, Alfaro SC, Gaudichet A (2004) Quantification of iron oxides in desert aerosol. Atmos Environ 38:1211–1218

Lafon S, Sokolik IN, Rajot JL, Caquineau S, Gaudichet A (2006) Characterization of iron oxides in mineral dust aerosols: implications for light absorption. J Geophys Res 111, D21207

Laskin A, Iedema MJ, Ichkovich A, Graber ER, Taraniukb I, Yinon R (2005a) Direct observation of completely processed calcium carbonate dust particles. Faraday Discuss 130:453–468

Laskin A, Wietsma TW, Krueger BJ, Grassian VH (2005b) Heterogeneous chemistry of individual mineral dust particles with nitric acid: a combined CCSEM/EDX, ESEM, and ICP-MS study. J Geophys Res 110, D10208

Laurent B, Marticorena B, Bergametti G, Mei F (2006) Modeling mineral dust emissions from Chinese and Mongolian deserts. Global Planet Change 52:121–141

Laurent B, Marticorena B, Bergametti G, Léon JF, Mahowald NM (2008) Modeling mineral dust emissions from the Sahara desert using new surface properties and soil database. J Geophys Res 113, D14218

Lawrence CR, Neff JC (2009) The contemporary physical and chemical flux of aeolian dust: a synthesis of direct measurements of dust deposition. Chem Geol 267:46–63

Lázaro FJ, Gutiérrez L, Barrón V, Gelado MD (2008) The speciation of iron in desert dust collected in Gran Canaria (Canary Islands): combined chemical, magnetic and optical analysis. Atmos Environ 42:8987–8996

Levin Z, Teller A, Ganor E, Yin Y (2005) On the interactions of mineral dust, sea-salt particles, and clouds: a measurement and modeling study from the Mediterranean Israeli Dust Experiment campaign. J Geophys Res 110, D20202

Li J, Osada K (2007a) Preferential settling of elongated mineral dust particles in the atmosphere. Geophys Res Lett 34, L17807

Li J, Osada K (2007b) Water-insoluble particles in spring snow at Mt. Tateyama, Japan: characteristics of the shape factors and size distribution in relation with their origin and transportation. J Meteor Soc Japan 85:137–149

Li WJ, Shao LY (2009) Observation of nitrate coatings on atmospheric mineral dust particles. Atmos Chem Phys 9:1863–1871

Li G, Chen J, Chen Y, Yang J, Ji J, Liu L (2007) Dolomite as a tracer for the source regions of Asian dust. J Geophys Res 112, D17201

Liao H, Seinfeld JH (1998) Radiative forcing by mineral dust aerosols: sensitivity to key variables. J Geophys Res 103:31637–31645

Lieke K, Kandler K, Scheuvens D, Emmel C, Von Glahn C, Petzold A et al (2011) Particle chemical properties in the vertical column based on aircraft observations in the vicinity of Cape Verde Islands. Tellus 63B:497–511

Lindqvist H, Jokinen O, Kandler K, Scheuvens D, Nousiainen T (2013) Single scattering by realistic, inhomogeneous mineral dust particles with stereogrammetric shapes. Atmos Chem Phys Discuss 13:18451–18488

Ma C-J, Choi K-C (2007) A combination of bulk and single particle analyses for Asian dust. Water Air Soil Pollut 183:3–13

Ma C-J, Kasahara M, Höller R, Kamiya T (2001) Characteristics of single particles sampled in Japan during the Asian dust-storm period. Atmos Environ 35:2707–2714

Ma Q, Liu Y, Liu C, Ma J, He H (2012) A case study of Asian dust storm particles: chemical composition, reactivity to SO_2 and hygroscopic properties. J Environ Sci 24:62–71

Mahowald NM, Baker AR, Bergametti G, Brooks N, Duce RA, Jickells TD et al (2005) Atmospheric global dust cycle and iron inputs to the ocean. Global Biogeochem Cy 19, GB4025

Mahowald N, Jickells TD, Baker AR, Artaxo P, Benitez-Nelson CR, Bergametti G et al (2008a) Global distribution of atmospheric phosphorus sources, concentrations and deposition rates, and anthropogenic impacts. Global Biogeochem Cy 22, GB4026

Mahowald NM, Engelstaedter S, Luo C, Sealy A, Artaxo P, Benitez-Nelson C et al (2008b) Atmospheric iron deposition: global distribution, variability, and human perturbations. Ann Rev Mar Sci 1:245–278

Makra L, Borbély-Kiss I, Koltay E, Chen Y (2002) Enrichment of desert soil elements in Takla Makan dust aerosol. Nucl Instrum Meth B 189:214–220

Maring H, Savoie DL, Izaguirre MA, Custals L, Reid JS (2003) Mineral dust aerosol size distribution change during atmospheric transport. J Geophys Res 102, D8592

Matsuki A, Iwasaka Y, Shi G-Y, Chen H-B, Osada K, Zhang D et al (2005a) Heterogeneous sulfate formation on dust surface and its dependence on mineralogy: balloon-borne observations from balloon-borne measurements in the surface atmosphere of Beijing, China. Water Air Soil Pollut 5:101–132

Matsuki A, Iwasaka Y, Shi G, Zhang D, Trochkine D, Yamada M et al (2005b) Morphological and chemical modification of mineral dust: observational insight into the heterogeneous uptake of acidic gases. Geophys Res Lett 32, L22806

Matsuki A, Quennehen B, Schwarzenboeck A, Crumeyrolle S, Venzac H, Laj P et al (2010a) Temporal and vertical variations of aerosol physical and chemical properties over West Africa: AMMA aircraft campaign in summer 2006. Atmos Chem Phys 10:8437–8451

Matsuki A, Schwarzenboeck A, Venzac H, Laj P, Crumeyrolle S, Gomes L (2010b) Cloud processing of mineral dust: direct comparison of cloud residual and clear sky particles during AMMA aircraft campaign in summer 2006. Atmos Chem Phys 10:1057–1069

McConnell CL, Highwood EJ, Coe H, Formenti P, Anderson B, Osborne S et al (2008) Seasonal variations of the physical and optical characteristics of Saharan dust: results from the Dust Outflow and Deposition to the Ocean (DODO) experiment. J Geophys Res 113, D14S05

Menéndez I, Díaz-Hernández JL, Mangas J, Alonso I, Sánchez-Soto PJ (2007) Airborne dust accumulation and soil development in the North-East sector of Gran Canaria (Canary Islands, Spain). J Arid Environ 71:57–81

Merikallio S, Lindqvist H, Nousiainen T, Kahnert M (2011) Modelling light scattering by mineral dust using spheroids: assessment of applicability. Atmos Chem Phys 11:5347–5363

Meyer I, Davies GR, Stuut J-BW (2011) Grain size control on Sr-Nd isotope provenance studies and impact on paleoclimate reconstructions: an example from deep-sea sediments offshore NW Africa. Geochem Geophys Geosyst 12, Q03005

Meyer I, Davies GR, Vogt C, Kuhlmann H, Stuut J-BW (2013) Changing rainfall patterns in NW Africa since the Younger Dryas. Aeolian Res 10:111–123

Miller RL, Tegen I, Perlwitz J (2004) Surface radiative forcing by soil dust aerosols and the hydrologic cycle. J Geophys Res 109, D04203

Mills MM, Ridame C, Davey M, La Roche J, Geider RJ (2004) Iron and phosphorus co-limit nitrogen fixation in the eastern tropical North Atlantic. Nature 429:292–294

Möhler O, Benz S, Saathoff H, Schnaiter M, Wagner R, Schneider J, Walter S, Ebert V, Wagner S (2008) The effect of organic coating on the heterogeneous ice nucleation efficiency of mineral dust aerosols. Environ Res Lett 3, 025007

Moreno T, Querol X, Castillo S, Alastuey A, Cuevas E, Herrmann L et al (2006) Geochemical variations in aeolian mineral particles from the Sahara–Sahel Dust Corridor. Chemosphere 65:261–270

Müller T, Schladitz A, Maßling A, Kaaden N, Wiedensohler A, Kandler K (2009) Spectral absorption coefficients and refractive index of Saharan dust during SAMUM 2006. Tellus 61B:79–95

Müller K, Lehmann S, van Pinxteren D, Gnauk T, Niedermeier N, Wiedensohler A et al (2010) Particle characterization at the Cape Verde atmospheric observatory during the 2007 RHaMBLe intensive. Atmos Chem Phys 10:2709–2721

Müller T, Schladitz A, Kandler K, Wiedensohler A (2011) Spectral particle absorption coefficients, single scattering albedos, and imaginary parts of refractive indices from ground based in-situ measurements at Cape Verde Island during SAMUM-2. Tellus 63B:573–588

Müller D, Lee K-H, Gasteiger J, Tesche M, Weinzierl B, Kandler K et al (2012) Comparison of optical and microphysical properties of pure Saharan mineral dust observed with AERONET Sun photometer, Raman lidar, and in situ instruments during SAMUM 2006. J Geophys Res 117, D07211

Nenes A, Krom MD, Mihalopoulos N, Van Cappellen P, Shi Z, Bougiatioti A et al (2011) Atmospheric acidification of mineral aerosols: a source of bioavailable phosphorus for the oceans. Atmos Chem Phys 11:6265–6272

Niimura N, Okada K, Fan X-B, Kai K, Arao K, Shi G-Y et al (1998) Formation of Asian dust-storm particles mixed internally with sea salt in the atmosphere. J Meteor Soc Japan 76:275–288

Niedermeier D, Hartmann S, Clauss T, Wex H, Kiselev A, Sullivan RC, DeMott PJ, Petters MD, Reitz P, Schneider J, Mikhailov E, Sierau B, Stetzer O, Reimann B, Bundke U, Shaw RA, Buchholz A, Mentel TF, Stratmann F (2011) Experimental study of the role of physicochemical surface processing on the IN ability of mineral dust particles. Atmos Chem Phys 11:11131–11144

Nousiainen T (2009) Optical modeling of mineral dust particles: a review. J Quant Spectrosc Radiat Transf 110:1261–1279

Nousiainen T, Zubko E, Niemi JV, Kupiainen K, Lehtinen M, Muinonen K et al (2009) Single-scattering modeling of thin, birefringent mineral-dust flakes using the discrete-dipole approximation. J Geophys Res 114, D07207

Nousiainen T, Kahnert M, Lindqvist H (2011) Can particle shape information be retrieved from light-scattering observations using spheroidal model particles? J Quant Spectrosc Radiat Transf 112:2213–2225

O'Hara SL, Clarke ML, Elatrash MS (2006) Field measurements of desert dust deposition in Libya. Atmos Environ 40:3881–3897

Okada K, Kai K (1995) Features and elemental composition of mineral particles collected in Zhangye, China. J Meteor Soc Japan 73:947–957

Okada K, Kai K (2004) Atmospheric mineral particles collected at Qira in the Taklamakan Desert, China. Atmos Environ 38:6927–6935

Okada K, Heintzenberg J, Kai K, Qin Y (2001) Shape of atmospheric mineral particles collected in three Chinese arid-regions. Geophys Res Lett 28:3123–3126

Okin GS, Baker AR, Tegen I, Mahowald NM, Dentener FJ, Duce RA et al (2011) Impacts of atmospheric nutrient deposition on marine productivity: roles of nitrogen, phosphorus, and iron. Global Biogeochem Cy 25, GB2022

Ooki A, Uematsu M (2005) Chemical interactions between mineral dust particles and acid gases during Asian dust events. J Geophys Res 110, D03201

Osada K (2013) Water soluble fraction of Asian dust particles. Atmos Res 124:101–108

Osborne SR, Johnson BT, Haywood JM, Baran AJ, Harrison MAJ, McConnell CL (2008) Physical and optical properties of mineral dust aerosol during the Dust and Biomass-burning Experiment. J Geophys Res 113, D00C3

Osborne SR, Baran AJ, Johnson BT, Haywood JM, Hesse E, Newman S (2011) Short-wave and long-wave radiative properties of Saharan dust aerosol. Q J Roy Meteorol Soc 137:1149–1167

Otto S, Bierwirth E, Weinzierl B, Kandler K, Esselborn M, Tesche M et al (2009) Solar radiative effects of a Saharan dust plume observed during SAMUM assuming spheroidal model particles. Tellus 61B:270–296

Paquet H, Coudé-Gaussen G, Rognon P (1984) Etude minéralogique de poussieres sahariennes le long d'un itinéraire entre 19° et 35° de latitude nord. Rev Geol Dyn Geogr Phys 25:257–265

Paris R, Desboeufs KV, Formenti P, Nava S, Chou C (2010) Chemical characterisation of iron in dust and biomass burning aerosols during AMMA-SOP0/DABEX: implication for iron solubility. Atmos Chem Phys 10:4273–4282

Paytan A, Mackey KRM, Chen Y, Lima ID, Doney SC, Mahowald N et al (2009) Toxicity of atmospheric aerosols on marine phytoplankton. Proc Natl Acad Sci U S A 106:4601–4605

Peters TM (2006) Use of the aerodynamic particle sizer to measure ambient p M10–2.5: the coarse fraction of PM10. J Air Waste Manage Assoc 56:411–416

Podczeck F, Rahman SR, Newton JM (1999) Evaluation of a standardised procedure to assess the shape of pellets using image analysis. Int J Pharm 192:123–138

Pósfai M, Axisa D, Tompa É, Freney E, Bruintjes R, Buseck PR (2013) Interactions of mineral dust with pollution and clouds: an individual-particle TEM study of atmospheric aerosol from Saudi Arabia. Atmos Res 122:347–361

Prospero J, Blades E, Naidu R, Mathison G, Thani H, Lavoie M (2008) Relationship between African dust carried in the Atlantic trade winds and surges in pediatric asthma attendances in the Caribbean. Int J Biometeorol 52:823–832

Pruppacher HR, Klett JD (1997) Microphysics of clouds and precipitation, 2nd edn. Kluwer Academic Publishers, Dordrecht

Querol X, Pey J, Pandolfi M, Alastuey A, Cusack M, Pérez N et al (2009) African dust contributions to mean ambient PM10 mass-levels across the Mediterranean Basin. Atmos Environ 43:4266–4277

Quinn PK, Coffman DJ, Bates TS, Welton EJ, Covert DS, Miller TL et al (2004) Aerosol optical properties measured on board the Ronald H. Brown during ACE-Asia as a function of aerosol chemical composition and source region. J Geophys Res 109, D19S01

Rajot JL, Formenti P, Alfaro S, Desboeufs K, Chevaillier S, Chatenet B et al (2008) AMMA dust experiment: an overview of measurements performed during the dry season special observation period (SOP0) at the Banizoumbou (Niger) supersite. J Geophys Res 113, D00C14

Redmond HE, Dial KD, Thompson JE (2010) Light scattering and absorption by wind blown dust: theory, measurement, and recent data. Aeolian Res 2:5–26

Reid EA, Reid JS, Meier MM, Dunlap MR, Cliff SS, Broumas A et al (2003) Characterization of African dust transported to Puerto Rico by individual particle and size segregated bulk analysis. J Geophys Res 108:8591

Reid JS, Reid EA, Walker A, Piketh S, Cliff S, Al Mandoos A et al (2008) Dynamics of southwest Asian dust particle size characteristics with implications for global dust research. J Geophys Res 113, D14212

Reitz P, Spindler C, Mentel TF, Poulain L, Wex H, Mildenberger K, Niedermeier D, Hartmann S, Clauss T, Stratmann F, Sullivan RC, Demott PJ, Petters MD, Sierau B, Schneider J (2011) Surface modification of mineral dust particles by sulphuric acid processing: implications for ice nucleation abilities. Atmos Chem Phys 11:7839–7858

Remoundaki E, Papayannis A, Kassomenos P, Mantas E, Kokkalis P, Tsezos M (2012) Influence of Saharan dust transport events on PM2.5 concentrations and composition over Athens. Water Air Soil Pollut 224:1–14

Rodá F, Bellot J, Avila A, Escarré A, Piñol J, Terradas J (1993) Saharan dust and the atmospheric inputs of elements and alkalinity to Mediterranean ecosystems. Water Air Soil Pollut 66:277–288

Rodríguez S, Alastuey A, Alonso-Pérez S, Querol X, Cuevas E, Abreu-Afonso J et al (2011) Transport of desert dust mixed with North African industrial pollutants in the subtropical Saharan Air Layer. Atmos Chem Phys 11:6663–6685

Rognon P, Coudé-Gaussen G, Revel M, Grousset FE, Pedemay P (1996) Holocene Saharan dust deposition on the Cape Verde Islands: sedimentological and Nd-Sr isotopic evidence. Sedimentology 43:359–366

Rosenfeld D, Rudich Y, Lahav R (2001) Desert dust suppressing precipitation: a possible desertification feedback loop. Proc Natl Acad Sci U S A 98:5975–5980

Ryder CL, Highwood EJ, Rosenberg PD, Trembath J, Brooke JK, Bart M et al (2013) Optical properties of Saharan dust aerosol and contribution from the coarse mode as measured during the Fennec 2011 aircraft campaign. Atmos Chem Phys 13:303–325

Samoli E, Kougea E, Kassomenos P, Analitis A, Katsouyanni K (2011) Does the presence of desert dust modify the effect of PM_{10} on mortality in Athens, Greece? Sci Total Environ 409:2049–2054

Sassen K, DeMott PJ, Prospero JM, Poellot MR (2003) Saharan dust storms and indirect aerosol effects on clouds: CRYSTAL-FACE results. Geophys Res Lett 30:1633

Scheuvens D, Kandler K, Küpper M, Lieke K, Zorn S, Ebert M et al (2011) Individual-particle analysis of airborne dust samples collected over Morocco in 2006 during SAMUM 1. Tellus 63B:512–530

Scheuvens D, Schütz L, Kandler K, Ebert M, Weinbruch S (2013) Bulk composition of northern African dust and its source sediments – a compilation. Earth-Sci Rev 116:170–194

Schladitz A, Müller T, Nowak A, Kandler K, Lieke K, Massling A et al (2011) In situ aerosol characterization at Cape Verde Part 1: particle number size distributions, hygroscopic growth and state of mixing of the marine and Saharan dust aerosol. Tellus 63B:531–548

Schumann U, Weinzierl B, Reitebuch O, Schlager H, Minikin A, Forster C et al (2011) Airborne observations of the Eyjafjalla volcano ash cloud over Europe during air space closure in April and May 2010. Atmos Chem Phys 11:2245–2279

Schütz L, Sebert M (1987) Mineral aerosols and source identification. J Aerosol Sci 18:1–10

Schütz L, Jaenicke R, Pietrek H (1981) Saharan dust transport over the North Atlantic Ocean. Geol Soc Am Spec Paper 186:87–100

Shao L, Li W, Yang S, Shi Z, Lü S (2007) Mineralogical characteristics of airborne particles collected in Beijing during a severe Asian dust storm period in spring 2002. Sci China Ser D 50:953–959

Shao Y, Ishizuka M, Mikami M, Leys JF (2011) Parameterization of size-resolved dust emission and validation with measurements. J Geophys Res 116, D08203

Shen Z, Li X, Cao J, Caquineau S, Wang Y, Zhang X (2005) Characteristics of clay minerals in Asian dust and their environmental significance. China Particuol 3:260–264

Shen ZX, Cao JJ, Zhang XY, Arimoto R, Ji JF, Balsam WL et al (2006) Spectroscopic analysis of iron-oxide minerals in aerosol particles from northern China. Sci Total Environ 367:899–907

Shen ZX, Cao JJ, Arimoto R, Zhang RJ, Jie DM, Liu SX et al (2007) Chemical composition and source characterization of spring aerosol over Horqin sand land in northeastern China. J Geophys Res 112, D14315

Shen Z, Cao J, Arimoto R, Han Z, Zhang R, Han Y et al (2009a) Ionic composition of TSP and $PM_{2.5}$ during dust storms and air pollution episodes at Xi'an, China. Atmos Environ 43:2911–2918

Shen Z, Caquineau S, Cao J, Zhang X, Han Y, Gaudichet A et al (2009b) Mineralogical characteristics of soil dust from source regions in northern China. Particuology 7:507–512

Shi Z, Shao L, Jones TP, Lu S (2005) Microscopy and mineralogy of airborne particles collected during severe dust storm episodes in Beijing, China. J Geophys Res 110. doi:D01303

Shi Z, Zhang D, Hayashi M, Ogata H, Ji H, Fujiie W (2008) Influences of sulfate and nitrate on the hygroscopic behaviour of coarse dust particles. Atmos Environ 42:822–827

Shinn EA, Smith GW, Prospero JM, Betzer P, Hayes ML, Garrison V et al (2000) African dust and the demise of Caribbean coral reefs. Geophys Res Lett 28:3029–3032

Skonieczny C, Bory A, Bout-Roumazeilles V, Abouchami W, Galer SJG, Crosta X et al (2011) The 7–13 March 2006 major Saharan outbreak: multiproxy characterization of mineral dust deposited on the West African margin. J Geophys Res 116, D18210

Sokolik IN, Toon OB (1999) Incorporation of mineralogical composition into models of the radiative properties of mineral aerosol from UV to IR wavelengths. J Geophys Res 104:9423–9444

Sow M, Alfaro SC, Rajot JL, Marticorena B (2009) Size resolved dust emission fluxes measured in Niger during 3 dust storms of the AMMA experiment. Atmos Chem Phys 9:3881–3891

Stuut J-B, Zabel M, Ratmeyer V, Helmke P, Schefuss E, Lavik G et al (2005) Provenance of present-day eolian dust collected off NW Africa. J Geophys Res 110, D04202

Sullivan RC, Guazzotti SA, Sodeman DA, Prather KA (2007) Direct observations of the atmospheric processing of Asian mineral dust. Atmos Chem Phys 7:1213–1236

Sun Y, Zhuang G, Wang Y, Zhao X, Li J, Wang Z et al (2005) Chemical composition of dust storms in Beijing and implications for the mixing of mineral aerosol with pollution aerosol on the pathway. J Geophys Res 110, D24209

Swap R, Garstang M, Greco S, Talbot R, Kållberg P (1992) Saharan dust in the Amazon Basin. Tellus 44B:133–149

Thalib L, Al-Taiar A (2012) Dust storms and the risk of asthma admissions to hospitals in Kuwait. Sci Total Environ 433:347–351

Tobías A, Pérez L, Díaz J, Linares C, Pey J, Alastruey A et al (2011) Short-term effects of particulate matter on total mortality during Saharan dust outbreaks: a case-crossover analysis in Madrid (Spain). Sci Total Environ 412–413:386–389

Tobo Y, Zhang D, Nakata N, Yamada M, Ogata H, Hara K et al (2009) Hygroscopic mineral dust particles as influenced by chlorine chemistry in the marine atmosphere. Geophys Res Lett 36, L05817

Tobo Y, DeMott PJ, Raddatz M, Niedermeier D, Hartmann S, Kreidenweis SM, Stratmann F, Wex H (2012) Impacts of chemical reactivity on ice nucleation of kaolinite particles: a case study of levoglucosan and sulfuric acid. Geophys Res Lett 39, L19803

Toon OB (2003) African dust in Florida clouds. Nature 424:623–624

Trochkine D, Iwasaka Y, Matsuki A, Yamada M, Kim Y-S, Nagatani T et al (2003) Mineral aerosol particles collected in Dunhuang, China, and their comparison with chemically modified particles collected over Japan. J Geophys Res 108:8642

Twohy CH, Kreidenweis SM, Eidhammer T, Browell EV, Heymsfield AJ, Bansemer AR et al (2009) Saharan dust particles nucleate droplets in eastern Atlantic clouds. Geophys Res Lett 36, L01807

Viana M, Querol X, Alastuey A, Cuevas E, Rodríguez S (2002) Influence of African dust on the levels of atmospheric particulates in the Canary Islands air quality network. Atmos Environ 36:5861–5875

Wagner F, Bortoli D, Pereira S, Costa MJ, Silva AM, Weinzierl B et al (2009) Properties of dust aerosol particles transported to Portugal from the Sahara desert. Tellus B 61:297–306

Wang X, Dong Z, Zhang C, Qian G, Luo W (2009) Characterization of the composition of dust fallout and identification of dust sources in arid and semiarid North China. Geomorphology 112:144–157

Wang X, Hua T, Zhang C, Lang L, Wang H (2012) Aeolian salts in Gobi deserts of the western region of Inner Mongolia: gone with the dust aerosols. Atmos Res 118:1–9

Weinzierl B, Petzold A, Esselborn M, Wirth M, Rasp K, Kandler K et al (2009) Airborne measurements of dust layer properties, particle size distribution and mixing state of Saharan dust during SAMUM 2006. Tellus 61B:96–117

Weinzierl B, Sauer D, Esselborn M, Petzold A, Veira A, Rose M et al (2011) Microphysical and optical properties of dust and tropical biomass burning aerosol layers in the Cape Verde region – an overview of the airborne in situ and lidar measurements during SAMUM-2. Tellus B 63:589–618

Wu F, Zhang D, Cao J, Xu H, An Z (2012) Soil-derived sulfate in atmospheric dust particles at Taklimakan desert. Geophys Res Lett 39, L24803

Yang C-Y, Chen Y-S, Chiu H-F, Goggins WB (2005) Effects of Asian dust storm events on daily stroke admissions in Taipei. Taiwan Environ Res 99:79–84

Yehliu K, Vander Wal RL, Boehman AL (2011) Development of an HRTEM image analysis method to quantify carbon nanostructure. Combust Flame 158:1837–1851

Yin Y, Wurzler S, Levin Z, Reisin TG (2002) Interactions of mineral dust particles and clouds: effects on precipitation and cloud optical properties. J Geophys Res 107:4724

Yuan H, Zhuang G, Rahn KA, Zhang X, Li Y (2006) Composition and mixing of individual particles in dust and nondust conditions of north China, spring 2002. J Geophys Res 111, D20208

Zhang D, Iwasaka Y (2004) Size change of Asian dust particles caused by sea salt interaction: measurements in southwestern Japan. Geophys Res Lett 31, L15102

Zhang X, Zhang G, Zhu G, Zhang D, An Z, Chen T et al (1996) Elemental tracers for Chinese source dust. Sci China Ser D 39:512–521

Zhang D, Zang J, Shi G, Iwasaka Y, Matsuki A, Trochkine D (2003a) Mixture state of individual Asian dust particles at a coastal site of Qingdao, China. Atmos Environ 37:3895–3901

Zhang XY, Gong SL, Shen ZX, Mei FM, Xi XX, Liu LC et al (2003b) Characterization of soil dust aerosol in China and its transport and distribution during 2001 ACE-Asia: 1. Network observations. J Geophys Res 108:4261

Zhao C, Liu X, Leung LR, Johnson B, McFarlane SA, Gustafson WI Jr et al (2010) The spatial distribution of mineral dust and its shortwave radiative forcing over North Africa: modeling sensitivities to dust emissions and aerosol size treatments. Atmos Chem Phys 10:8821–8838

Zhou B, Zhang L, Cao X, Li X, Huang J, Shi J et al (2012) Analysis of the vertical structure and size distribution of dust aerosols over the semi-arid region of the Loess Plateau in China. Atmos Chem Phys Discuss 12:6113–6143

Zimmermann F, Weinbruch S, Schütz L, Hofmann H, Ebert M, Kandler K et al (2008) Ice nucleation properties of the most abundant mineral dust phases. J Geophys Res 113, D23204

Zubko E, Muinonen K, Shkuratov Y, Videen G, Nousiainen T (2007) Scattering of light by roughened Gaussian random particles. J Quant Spectrosc Radiat Transf 106:604–615

Chapter 3
Identifying Sources of Aeolian Mineral Dust: Present and Past

Daniel R. Muhs, Joseph M. Prospero, Matthew C. Baddock, and Thomas E. Gill

Abstract Aeolian mineral dust is an important component of the Earth's environmental systems, playing roles in the planetary radiation balance, as a source of fertilizer for biota in both terrestrial and marine realms and as an archive for understanding atmospheric circulation and paleoclimate in the geologic past. Crucial to understanding all of these roles of dust is the identification of dust sources. Here we review the methods used to identify dust sources active at present and in the past. Contemporary dust sources, produced by both glaciogenic and non-glaciogenic processes, can be readily identified by the use of Earth-orbiting satellites. These data show that present dust sources are concentrated in a global dust belt that encompasses large topographic basins in low-latitude arid and semiarid regions. Geomorphic studies indicate that specific point sources for dust in this zone include dry or ephemeral lakes, intermittent stream courses, dune fields, and some bedrock surfaces. Back-trajectory analyses are also used to identify dust sources, through modeling of wind fields and the movement of air parcels over periods of several days. Identification of dust sources from the past requires novel approaches

D.R. Muhs (✉)
U.S. Geological Survey, Federal Center, MS 980, Box 25046, Denver, CO 80225, USA
e-mail: dmuhs@usgs.gov

J.M. Prospero
Rosenstiel School of Marine and Atmospheric Sciences, University of Miami,
4600 Rickenbacker Causeway, Miami, FL 33149, USA
e-mail: jprospero@rsmas.miami.edu

M.C. Baddock
Atmospheric Environment Research Centre, Griffith School of Environment,
Griffith University, Brisbane, QLD 4111, Australia
e-mail: m.baddock@griffith.edu.au

T.E. Gill
Department of Geological Sciences, University of Texas at El Paso,
500 West University Avenue, El Paso, TX 79968, USA
e-mail: tegill@utep.edu

P. Knippertz and J.-B.W. Stuut (eds.), *Mineral Dust: A Key Player in the Earth System*, DOI 10.1007/978-94-017-8978-3_3,

that are part of the geologic toolbox of provenance studies. Identification of most dust sources of the past requires the use of physical, mineralogical, geochemical, and isotopic analyses of dust deposits. Physical properties include systematic spatial changes in dust deposit thickness and particle size away from a source. Mineralogy and geochemistry can pinpoint dust sources by clay mineral ratios and Sc-Th-La abundances, respectively. The most commonly used isotopic methods utilize isotopes of Nd, Sr, and Pb and have been applied extensively in dust archives of deep-sea cores, ice cores, and loess. All these methods have shown that dust sources have changed over time, with far more abundant dust supplies existing during glacial periods. Greater dust supplies in glacial periods are likely due to greater production of glaciogenic dust particles from expanded ice sheets and mountain glaciers, but could also include dust inputs from exposed continental and insular shelves now submerged. Future dust sources are difficult to assess, but will likely differ from those of the present because of global warming. Global warming could bring about shifts in dust sources by changes in degree or type of vegetation cover, changes in wind strength, and increases or decreases in the size of water bodies. A major uncertainty in assessing dust sources of the future is related to changes in human land use, which could affect land surface cover, particularly due to increased agricultural endeavors and water usage.

Keywords Composition • Mineralogy • Chemistry • Elements • Isotopes • Arid regions • Semiarid regions • Glaciated regions • Satellite imagery • Back-trajectory analysis

3.1 Introduction

Aeolian mineral dust is an important component of the atmosphere, geosphere, hydrosphere, and biosphere. Recent reviews (Kohfeld and Harrison 2001; Harrison et al. 2001; Tegen 2003; Goudie and Middleton 2006; Kohfeld and Tegen 2007; Maher et al. 2010; Shao et al. 2011; Muhs 2013a, b) summarize a number of important aspects of aeolian mineral dust on the Earth-atmosphere system. Dust can change the overall planetary radiation balance through direct effects on radiation at both solar (shortwave) and terrestrial (longwave) portions of the electromagnetic spectrum (Tegen 2003). Dust, acting as condensation and ice nuclei (Creamean et al. 2013; Karydis et al. 2011; Twohy et al. 2009), can affect climate and meteorology by changing cloud lifetime, cloud fraction, and precipitation processes. Aeolian dust is a significant carrier of Fe, a limiting nutrient in many ocean regions; dust deposition can significantly increase ocean primary productivity and, consequently, impact the global carbon cycle (Falkowski et al. 1998; Jickells et al. 2005; Mahowald et al. 2009). There are important effects that dust can have on the biogeochemical cycle of terrestrial ecosystems, adding nutrients to soils and the vegetation they support (Ravi et al. 2011).

Critical to understanding the importance of dust in all aspects of the Earth's physical and biological systems is identification of the sources of dust. Knowledge of dust sources is the fundamental first step in recognizing the entire pathway of dust entrainment, transport, and deposition. Because dust has importance in so many scientific disciplines, a surprisingly diverse set of tools has been generated for identification of dust sources. In this chapter, we review what is known about global dust sources, but with a particular emphasis on methods of *identifying* dust sources, both directly and indirectly. With this background, we review the geography of present dust sources and in addition, we review methods of identifying dust sources from the geologic record. Finally, we discuss how dust sources can change over time, with an emphasis on such changes over geologic time scales.

3.2 Processes of Dust Particle Formation

In order to provide the context for understanding dust sources, it is important to consider those processes that generate dust-sized particles (Kok et al. 2012). Formation of dust-sized mineral particles can be classified broadly into four groups of processes: (1) volcanogenic, (2) physical mechanisms of coarse particle reduction, (3) chemical mechanisms of coarse particle reduction, and (4) inheritance from fine-grained rocks. Much of what we observe as mineral dust in the atmosphere is produced by coarse particle size reduction either by physical or chemical means. Loess, which is sediment dominated by aeolian silt and clay, has long been considered to be produced primarily by physical reduction of coarse particles through glacial grinding. Prime examples of glaciogenic silt production can be found today where glaciers still exist, such as in Svalbard, Iceland, Canada, and Alaska (Bullard 2013). Satellite images often capture dust plumes emanating from these sources (Crusius et al. 2011; Prospero et al. 2012). Bullard (2013) gives an excellent overview of modern glaciogenic dust-forming environments that are good analogs for what was a much more important process in the last glacial period.

It has been observed that there is little loess that accumulates in non-glacial settings, such as desert regions (Tsoar and Pye 1987). Thus, some investigators have proposed that glacial grinding is the only efficient means by which silt-sized particles can be produced (Smalley 1966, 1995). Nevertheless, non-glacial loess has been identified in many desert regions (Coudé-Gaussen 1987; Crouvi et al. 2010). Furthermore, experimental work has shown that although glacial grinding is indeed an efficient method of silt particle production, other processes, including fluvial and aeolian abrasion, are surprisingly effective mechanisms; silt particles can also be produced by frost and salt weathering (Smith et al. 2002; Wright and Smith 1993; Wright et al. 1998; Wright 2001). In many of the world's desert regions, where there is no history of glacial erosion, fluvial comminution in stream valleys, aeolian abrasion and ballistic impacts in dune fields, and salt weathering in playas and on alluvial fans have all been shown to produce silt-sized particles (Fig. 3.1).

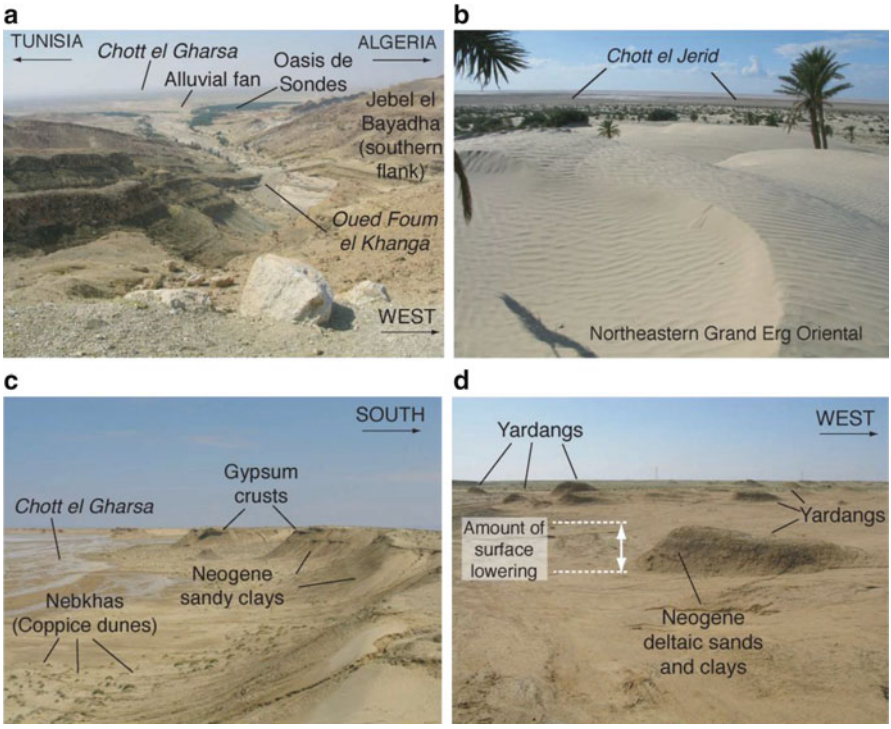

Fig. 3.1 Geomorphic settings in the Sahara Desert that are common dust sources: (**a**) wadi and alluvial fan of the Oued Foum el Khanga, draining the Atlas Mountains of Tunisia and Algeria; (**b**) dunes of northernmost part of Grand Erg Oriental adjacent to southeastern side of Chott (playa) el Jerid, Tunisia; (**c**) fine-grained sediments in Chott el Gharsa, derived from sandy clays of Neogene age, northeast of Tozeur, Tunisia; (**d**) yardangs eroded into Neogene deltaic sands and clays, southern Tunisia (Photographs by D.R. Muhs)

For example, in the northern part of the Saharan Desert in southern Tunisia, fluvial comminution can take place in large wadis or dry washes that drain major upland terrain such as the Atlas Mountains (Fig. 3.1a).

Despite the importance of physical processes of silt production and the dominance of silt in many source regions, much long-range transport (LRT) dust consists of clay-sized particles with diameters less than 2 μm. Such fine-grained particles are difficult to generate by the physical processes described above. LRT dust derived from Africa, carried across the Atlantic, and collected on Barbados and Miami, Florida, consists almost entirely of particles less than 20 μm (Prospero et al. 1970). About half of this mass comprises particles with diameters less than 2–3 μm (Li-Jones and Prospero 1998; Prospero et al. 2001; Reid et al. 2003a, b).

Many (though not all) clay-sized particles, including those found in dust, have a very different mineralogy compared to that of coarser particles (Glaccum and Prospero 1980). Coarse particles, greater than ~2 μm, consist largely of primary,

rock-forming minerals produced by igneous rock formation. These include quartz, plagioclase, K-feldspar, amphibole, biotite, and muscovite. Metamorphic rocks contribute many of these same minerals plus chlorite. Common dust minerals from noncrystalline rocks include calcite and dolomite from carbonate terrain and evaporite minerals, such as gypsum and halite. In contrast, many clay-sized particles are phyllosilicates or layered aluminosilicate minerals, such as mica, kaolinite, smectite, vermiculite, and chlorite, and occasionally non-phyllosilicate clays such as palygorskite or sepiolite.

With the exception of micas, other phyllosilicate clay minerals, such as kaolinite, smectite, vermiculite, and many chlorites, as well as Al-dominated minerals such as gibbsite and boehmite, form at low temperatures at or near the Earth's surface, primarily in soils (Birkeland 1999). The process of clay mineral formation is typically alteration of primary rock-forming minerals, such as feldspars, to phyllosilicate clay minerals by hydrolysis. Phyllosilicate clay minerals form a very important component of LRT dust (Glaccum and Prospero 1980; Biscaye et al. 1997; Stuut et al. 2005; Scheuvens et al. 2013) and identifying dust source areas requires a good understanding of how clay minerals form in soils and how clay mineralogy changes with soil geography. Dust sources can sometimes be identified by examination of clay mineralogy, which we illustrate later.

Finally, studies of dust origins often overlook the process of simple particle inheritance from sedimentary rocks such as siltstones or shales. Silt is abundant in the sedimentary rock record. Indeed, Blatt (1987) estimates that fully half of the detrital quartz in the world's sedimentary rocks consists of silt-sized particles. In Australia, for example, siltstones may be the primary source of much of the silt-sized dust derived from arid basins (McTainsh 1989). In the Great Plains of North America, Aleinikoff et al. (1999, 2008) show that sedimentary rock (volcaniclastic siltstone) is the most important source of silt-sized particles in loess of last-glacial age, which we discuss in more detail below.

3.3 Methods of Identifying Contemporary Dust Sources

3.3.1 Geomorphic Perspectives on Dust Sources

In a recent study, Bullard et al. (2011) developed a useful conceptual geomorphic scheme for dust sources. Recognizing that most dust sources occur in arid regions, these investigators identified six geomorphic systems (see examples in Fig. 3.1) that could be considered as possible dust-emitting sources. These include (1) lakes, (2) high-relief alluvial systems, (3) low-relief alluvial systems, (4) stony surfaces (not including those connected to fluvial sources of fine-grained particles), (5) aeolian systems, and (6) low-emission surfaces (including bedrock surfaces, rocky slopes, and duricrusted surfaces). Bullard et al. (2011) further classified these geomorphic systems into subgroups that demonstrate a range of dust emission potentials.

For example, lakes can be considered in four different states: wet, ephemeral, dry (with consolidated sediments), and dry (with nonconsolidated sediments), all characterized by a variable propensity to emit dust due to different degrees of sediment availability and supply. A good review of studies focusing on the geomorphic controls on dust emission processes is provided by Bryant (2013).

3.3.2 *Aerosol Indexes (AI) Derived from the Orbiting TOMS (Total Ozone Mapping Spectrometer)*

Launch of the Nimbus 7 satellite with the onboard Total Ozone Mapping Spectrometer (TOMS) in 1978 became a milestone in our ability to identify dust sources on a global scale. Aerosol indexes (AI) derived from TOMS data demonstrated that broad source areas for dust can be identified (Goudie and Middleton 2006; Middleton and Goudie 2001; Prospero et al. 2002; Washington et al. 2003). Prospero et al. (2002) used TOMS imagery from several years to generate a global map of dust source areas. This, combined with observations made from MODIS and MISR imagery (see discussion below), gives a worldwide picture of dust sources and their dominant transport pathways. Indeed, what Prospero et al. (2002) refer to as a "global dust belt" has been identified by this process (Fig. 3.2) with major dust source areas including the Sahara and Sahel regions of Africa. The two most important dust source areas in the world at present are in the Sahara: the Bodélé depression in Chad and an area in the southwestern Sahara Desert region of Mali, Mauritania, and Algeria. In addition, however, the Arabian Peninsula, Central Asia, desert basins in China and central and southeastern Australia, the Mojave, Sonoran, and Chihuahuan deserts and Great Plains region of western North America, and the Pampas and Patagonian regions of southern South America also have been identified as major dust sources over the past couple of decades. An important finding in the study by Prospero et al. (2002) is that most dust source areas identified by interpretation of TOMS imagery are dominantly in topographic depressions and remote from areas of human settlement. Thus, they conclude that *most* areas of dust generation (~75 %) at present are the result of natural processes, rather than anthropogenic causes, such as agriculture or urban development. Continued monitoring using TOMS and other sensors can test whether this generalization holds true in the future. New studies have already shown that different platforms, different algorithms for dust assessment, and different time periods of imaging can change the picture of what we consider to be the dominant dust sources globally. For example, Ginoux et al. (2012), using the moderate resolution imaging spectroradiometer (MODIS) "Deep Blue" aerosol capability, report that a significant part of the Great Plains region of North America is an important dust source, a region not identified as such in the earlier study by Prospero et al. (2002), with TOMS.

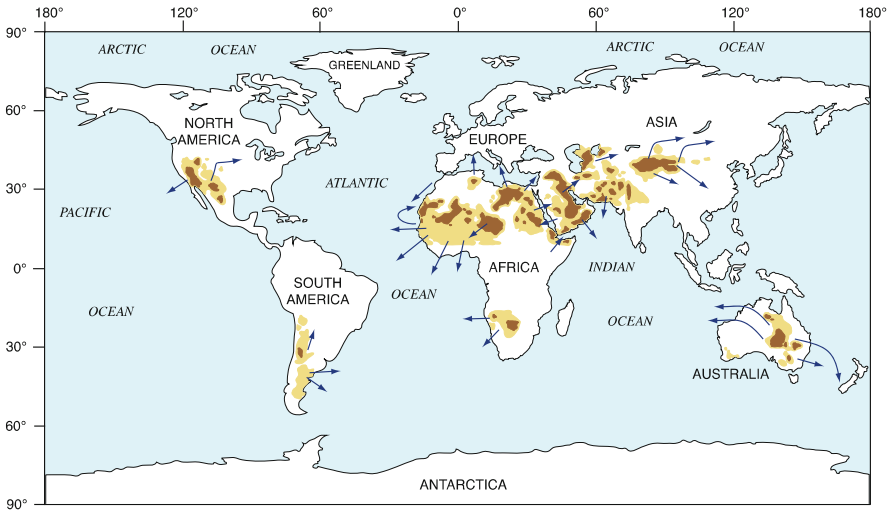

Fig. 3.2 Map of global dust sources, based on multiple years of satellite imagery, derived from frequency of occurrence (number of days) where the TOMS absorbing aerosol index (*AAI*) is greater than 0.7 (significant amounts of dust or smoke) or 1.0 (abundant dust or smoke). For comparison, nonabsorbing aerosols such as sulfate and sea salt yield negative AAI values; clouds yield values near zero; ultraviolet-absorbing aerosols such as dust and smoke yield positive values (Prospero et al. 2002). *Dark brown* is 21–31 days; *yellow* is 7–21 days (Redrawn from Fig. 4 of Prospero et al. 2002). *Blue arrows* indicate typical dust transport pathways, based on interpretation of MODIS imagery from Terra and Aqua satellites by the authors

3.3.3 MODIS and MISR Imagery from the Terra and Aqua Satellites

Gillette (1999) pointed out that many of the world's most important dust sources are not always large regions with uniform emissions of dust across them. He coined the phrase "hot spot" to identify relatively small areas that have a particularly favorable set of characteristics for dust emission. This concept was developed further by Okin et al. (2006) and with the subbasin geomorphology approach of Bullard et al. (2011). The past couple of decades have added greatly to our identification of contemporary "hot spot" dust sources. Here we present examples of identification of dust sources using satellite imagery (Fig. 3.3), set within the context of the "hot spot" concept of Gillette (1999) and the preferential-dust-emission geomorphic scheme of Bullard et al. (2011).

Dry lakebeds with abundant fine-grained sediments that are unconsolidated constitute one of the most important dust emission sources throughout the world (Gill 1996) (e.g., Figs. 3.1b, c and 3.3a, c). These lakebed sources are especially prominent in North Africa, where today there is evidence that during the Holocene,

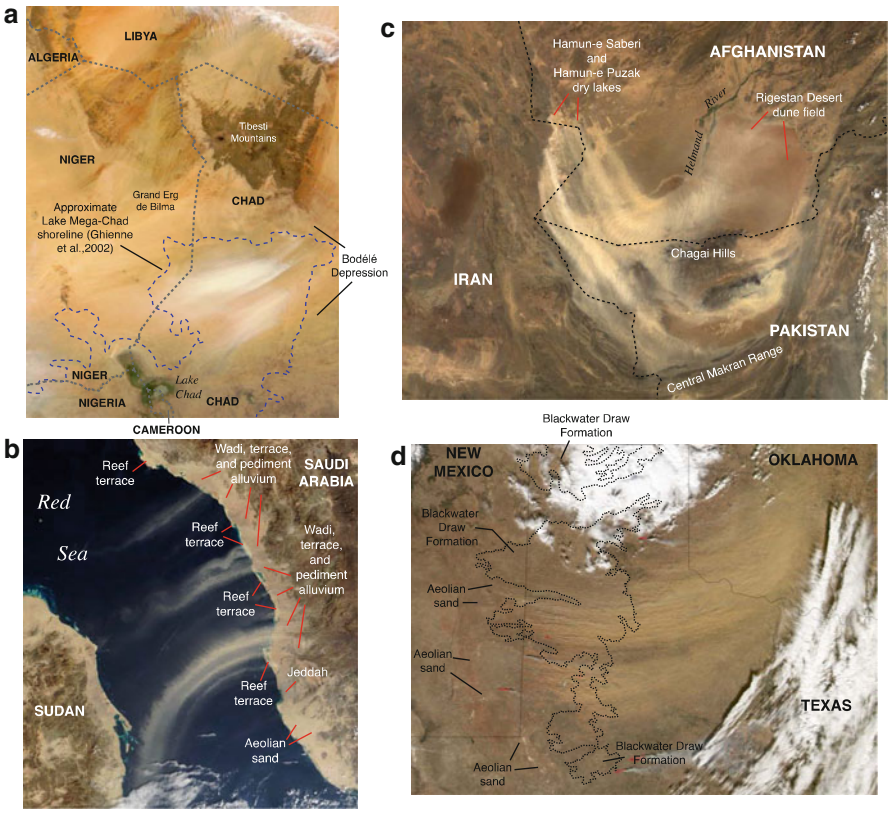

Fig. 3.3 (**a**) MODIS image from the Terra satellite showing dust originating from the Bodélé Depression of the Chad Basin, 11 April 2007. *Dashed line* indicates the approximate extent of former Lake Mega-Chad (Ghienne et al. 2002) (Image courtesy of the NASA MODIS Rapid Response Team, Goddard Space Flight Center). (**b**) MODIS image from the Terra satellite acquired on 15 January 2009 showing dust plumes from Saudi Arabia moving over the Red Sea in the direction of Sudan (Image courtesy of MODIS Rapid Response, NASA Goddard Space Flight Center). Geologic features from Brown et al. (1989). (**c**) MODIS image from the Terra satellite acquired on 20 August 2003, showing dust from the Hamun dry lakes of Afghanistan and Iran (Image courtesy of Jacques Descloitres, MODIS Land Rapid Response Team, NASA Goddard Space Flight Center). (**d**) MODIS image from the Aqua satellite acquired on 1 January 2006 showing dust plumes originating in the panhandle of Texas and moving eastward; also shown is the extent of the Blackwater Draw Formation of Quaternary age, thought to be the source of much of the dust (MODIS image courtesy of Jesse Allen, NASA Earth Observatory and the MODIS Rapid Response Team; extent of the Blackwater Draw Formation taken from Texas Bureau of Economic Geology (1992))

watercourses and lakes were widespread (Drake et al. 2011). A prominent example is Lake Chad, which today occupies a small area of the central part of the Sahara Desert, straddling the boundaries of Chad, Nigeria, and Niger. However, in the early-to-mid Holocene, Paleolake Chad (Fig. 3.3a) was a much larger water body

(Ghienne et al. 2002; Drake and Bristow 2006). The northern portion of this former lakebed, south of the Tibesti Mountains, is a topographic low, the Bodélé Depression, which is estimated to be the largest single source of dust on the Earth at present based on TOMS and other data (Middleton and Goudie 2001; Prospero et al. 2002; Washington et al. 2003, 2009). Recent field studies in the basin itself, where there are abundant erosional remnant yardangs, composed of diatomaceous sediments, confirm the dramatic amount of sediment removal by wind (Warren et al. 2007; Bristow et al. 2009).

Earlier, we alluded to the study of Ginoux et al. (2012) identifying the Great Plains region of North America as an important source of dust. Much of the area where these dust plumes originate is covered by a Quaternary-age aeolian sediment known as the Blackwater Draw Formation (Holliday 1989) (Fig. 3.3d) and is disturbed by extensive agriculture (Lee et al. 2012). Alluvial sources in desert regions have also been identified in MODIS imagery, such as dust seen on the western Saudi Arabian coast, moving southwestward over the Red Sea and toward Sudan (Fig. 3.3b). The outermost part of the Saudi Arabian coast is an emergent coral reef terrace, with silt-rich sabkhah deposits, just landward of the terrace. However, it appears that the main dust sources are alluvial deposits that are landward of the coast. Drainage development in the mountains that parallel the Red Sea coast of Saudi Arabia has generated not only wadis that are filled with alluvium but also older alluvial terraces and pediment surfaces (Brown et al. 1989), all of which are potential dust sources.

3.3.4 Back-Trajectory Analyses to Identify Dust Sources

The analysis of the atmospheric trajectories taken by parcels of air has also assisted in the investigation of dust sources. In this approach, models are used to reconstruct the route that an air mass takes to, or from, a given point in time and space. Trajectories can therefore be examined both "backward" and "forward," and assessments in both directions have provided considerable insight into dust source location and behavior.

Trajectory models typically use three-dimensional input datasets of remodeled gridded wind fields, available in varying spatial and temporal resolutions; thus, performance of the analysis is dependent on the quality of input data (Gebhart et al. 2005). The model outcomes also depend on the specified initial conditions, with key variables including the starting height above the surface for the air parcel, because this affects mean speed of the advected parcel. Studies commonly run trajectories at more than one height to show the potential variation associated with the start height or where atmospheric structure is known to be important for dust transport routes (Engelstaedter et al. 2009; Alonso-Perez et al. 2012). The length of time for which the air parcel is simulated is another important issue in the reliability of the trajectories produced. With increased time, the accuracy of the modeled route depreciates, but the distance between dust source and sampling

point is the determining factor in the length of run. When investigating transatlantic dust advection to Barbados, Engelstaedter et al. (2009) used 12-day model runs, calculating the transit time of air parcels and therefore dust from West Africa to the West Indies to be 6–7 days. For back trajectories, the passage of an air parcel is determined through time before its arrival at a location. Backward trajectory analysis is typically used therefore in cases where an aerosol has been sampled at some receptor location, and the provenance of the dust emission needs to be estimated (e.g., Stuut et al. 2005, Fig. 3.4). In the Lake Eyre Basin of Australia, Radhi et al. (2011) also used back-trajectory analysis to interpret the chemistry of captured dust and provide corroborating evidence that Cl/Na correlations of samples indeed indicated dry lake sources.

3.4 Identification of Past Dust Sources

Direct observation of dust storms and dust pathways using satellite imagery is obviously not possible when studying dust records in the geologic past. Dust archives in geologic records can take many forms, including those in deep-sea sediments, lake sediments, ice cores, loess deposits, and soils. The nature of these records is reviewed by Muhs (2013a), but here we examine the methods geologists have used in identifying sources of dust in such records.

3.4.1 Geomorphic Evidence of Past Dust Sources

There are some forms of geomorphic evidence that can be used to identify past (and present) dust sources, landscape settings that would be classified as being of "high potential for dust emissions," by Bullard et al. (2011). These include pans, yardangs, and stone pavements. Laity (1994) and Goudie (2008) provide good reviews of landforms of aeolian erosion, some of which help identify dust sources.

Pans, also called "playas," are relatively small (on the order of a few kilometers or usually less in diameter), generally circular, closed depressions (Shaw and Bryant 2011). They often occur in clusters, or fields, which can number in the thousands. Pans are found extensively in South America (Pampas and Patagonia), in the Great Plains of North America, and in parts of Africa, Australia, Siberia, and China (Gill 1996; Goudie 2008). Because fields of pans often occur in semiarid climates, they are commonly thought to form primarily by aeolian excavation and therefore can be considered dust sources. The association of many pans with lunette dunes on the downwind sides provides good evidence that at least some pans may have formed by aeolian erosion.

More direct forms of geomorphic evidence for dust sources are landforms called yardangs (McCauley et al. 1977). Yardangs are erosional remnants resulting from

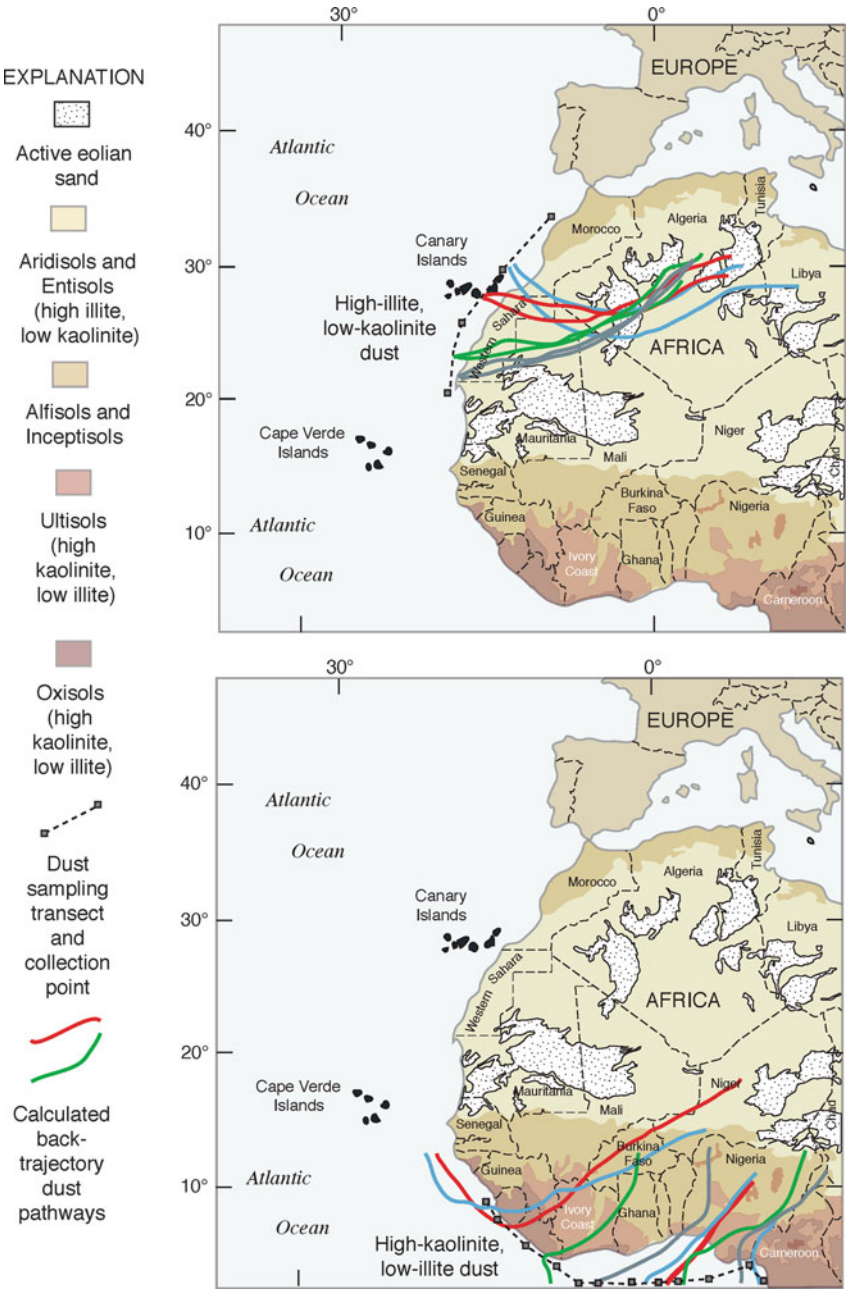

Fig. 3.4 Soil geography of western Africa, redrawn and generalized from U.S. Department of Agriculture, Natural Resources Conservation Service "Global Soil Regions" map (http://www.soils.usda.gov/use/worldsoils/mapindex/order.html) and clay minerals typically found in each soil type. Also shown are calculated back trajectories of dust samples with contrasting clay mineral compositions collected off the coast of Africa in 1998 (Redrawn from Stuut et al. 2005)

aeolian removal of material, resulting in a streamlined, linear ridge (Fig. 3.1d). Yardangs can develop in bedrock or sediment, as long as there is sufficient particle-to-particle binding that a remnant landform can persist after erosion. They are thought to form primarily by aeolian abrasion from saltating sand, which explains their common occurrence near (and particularly downwind of) dunefields.

Stone pavements, also known as "gobi" and "gibber" (see Laity 2011), are concentrations of gravel-sized clasts on the surface of a landform that is composed (usually) of unconsolidated materials. Traditionally, they have been interpreted to be the lag deposits left behind after aeolian deflation has removed all the finer-grained material. Thus, under this interpretation, stone pavements can be regarded as evidence for a former dust source. We use the word "former" here as a modifier, because after its creation, the pavement itself serves as an armor that prevents further aeolian erosion. Some investigators have proposed that stone pavements actually form by aeolian *accretion*, rather than deflation, thus making them dust sinks rather than sources (McFadden et al. 1987). It is likely that pavements can form by more than one process, and they are not mutually exclusive. Thus, stone pavements are not always reliable indicators of dust sources.

3.4.2 Physical Properties of Dust Deposits

Smith (1942) developed the use of physical properties of loess to identify ancient dust sources in North America. He studied glaciogenic loess that is found southeast of the Mississippi and Illinois rivers in the North American mid-continent. This sediment, now called Peoria Loess, is of last-glacial age and for many decades was hypothesized to have its origins in fine-grained glacial outwash in river valleys draining the last-glacial-age Laurentide Ice Sheet (e.g., the Mississippi and Illinois rivers) during the last glacial period. In a series of transects to the southeast of both rivers, Smith (1942) reported systematic decreases in loess thickness, which he interpreted to be the result of a reduction in sediment load in a downwind direction. He also reported that particle size changed along the same transects, with eastward-decreasing coarse silt (50–30 μm) content and increasing fine silt and clay contents, reflecting a winnowing of coarse particles in a downwind direction, consistent with the thickness trend. This pioneering study clearly identified these major river systems as the source of dust that generated Peoria Loess and has served as the foundation for many source-to-sink studies of loess around the world. Systematic decreases in loess thickness away from hypothesized sources have been observed elsewhere in North America, such as Iowa and Alaska, as well as in China (see examples in Muhs 2013b). In the cases of Iowa and Alaska, hypothesized loess sources are, as in the Illinois case, major outwash-bearing river systems. In the case of China, the hypothesized immediate sources are thought to be desert basins that occur to the northwest of the Loess Plateau region.

3.4.3 Mineralogy as a Guide to Dust Sources

Mineralogy is potentially one of the most fundamental methods of identifying past dust sources, but unfortunately, it is one of the most difficult to apply. Much of the difficulty in using mineralogy to identify sources is that most dust (Glaccum and Prospero 1980; Reid et al. 2003a, b; Trapp et al. 2010) and loess sediments have a composition similar to average upper continental crust (Taylor and McLennan 1985; Gallet et al. 1996; Muhs et al. 2007). Thus, dust and loess have a mineralogy similar to many of the rocks found on the Earth's surface. Nevertheless, detailed mineralogical analyses combined with consideration of potential source areas can often identify points of dust origin.

Mineralogy has been exploited in many studies simply to recognize that a nonlocal dust component exists within a soil or a sediment body. Good examples of this kind of approach include the recognition of exotic quartz in soils that occur on basaltic or andesitic bedrock, lithologies that lack quartz. Such studies have confirmed the existence of aeolian quartz in soils on mafic volcanic rocks of the Hawaiian Islands (Jackson et al. 1971), Australia (Hesse and McTainsh 2003), the California Channel Islands (Muhs et al. 2008), and the Canary Islands of Spain (Muhs et al. 2010).

For the purpose of identifying dust sources, mineralogy of the clay (<2 μm) fraction is the approach that has been used most commonly. Special attention has been paid to the clay mineral composition of dust sources in Africa, which have a clear geographic trend. Scheuvens et al. (2013) provide an excellent review of studies that have been done thus far on mineralogical, geochemical, and isotopic composition of dust sources in Africa. One of the earliest observations was a shipboard dust collection campaign in 1971 along the west coast of Africa, from the Canary Islands to southern Africa (Chester et al. 1972). This study found that the clay mineralogy of dust varied from north to south, with illite (mica) contents high at extratropical latitudes, and kaolinite contents highest in tropical latitudes (Fig. 3.4). This clay mineral zonation corresponds closely to the soil geography of the continent, with Aridisols and Entisols supplying the illite (mica) in the extratropical regions and Ultisols and Oxisols supplying the kaolinite from farther south. Chiapello et al. (1997) and Caquineau et al. (1998, 2002) used back-trajectory analyses, geochemistry, and clay mineralogy to define three distinct dust source areas in western Africa (Fig. 3.5). The northwestern sector of the Sahara, including Western Sahara, Morocco, and western Algeria, has relatively low kaolinite and relatively high illite. The central Sahara and southern Sahara, including Mauritania, northern Mali, and southern Algeria, have somewhat lower illite content and higher kaolinite content. Finally, the Sahel sector, including Senegal, southern Mauritania, and southern Mali, has the lowest illite and highest kaolinite content.

Using these source areas with their characteristic mineralogy, it is possible to infer the origins of dust at more distant localities. Dust collected on Barbados has a mix of clay mineral types with values intermediate between the illite/kaolinite ranges of the northwestern Sahara and the central and southern Sahara (Fig. 3.5).

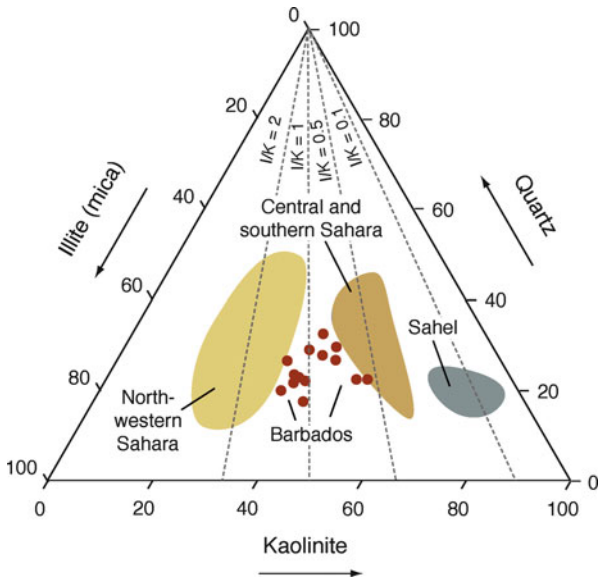

Fig. 3.5 Ternary diagram showing abundances of quartz, illite (mica), and kaolinite in dust samples collected off the coast of Africa attributed to various regions of origin (*shaded polygons*) based on back-trajectory analyses. Also shown are values of dust samples collected on Barbados. I/K = illite/kaolinite lines (Data from Caquineau et al. 1998, 2002)

These results are consistent with the concept that dust collected on Barbados is likely the result of integration of many individual dust sources in Saharan Africa and the Sahel, well mixed after transport over not only much of Africa but also the breadth of the Atlantic Ocean (Prospero and Lamb 2003).

3.4.4 Geochemical Methods of Identifying Dust Sources

Geochemical methods of identifying dust sources are highly complementary to mineralogical methods because geochemistry is a direct reflection of mineralogy. The advantage of the geochemical approach is that it is highly quantitative; analytical methods are now rapid, accurate, and precise, and trace elements can often yield data about sources that are not apparent with mineralogy. Here we give some examples of using this approach for identifying dust sources using samples from both the marine and terrestrial environments. We caution, however, that the mineralogy (and hence, the geochemistry) of dust being emitted from even a small source area can change significantly from day to day and point source to point source (Rojo et al. 2008).

Olivarez et al. (1991), in a study of fine-grained sediments found in Pacific deep-sea cores, sought to determine whether the particles were derived from LRT dust or volcanic sources. Oceanic crust and other mafic volcanic rocks are enriched in Sc and depleted in Th and La compared to average upper continental crust. Thus, mafic rocks or particles derived from them will plot near the Sc pole on a ternary diagram, whereas felsic rocks or particles derived from them will plot near the

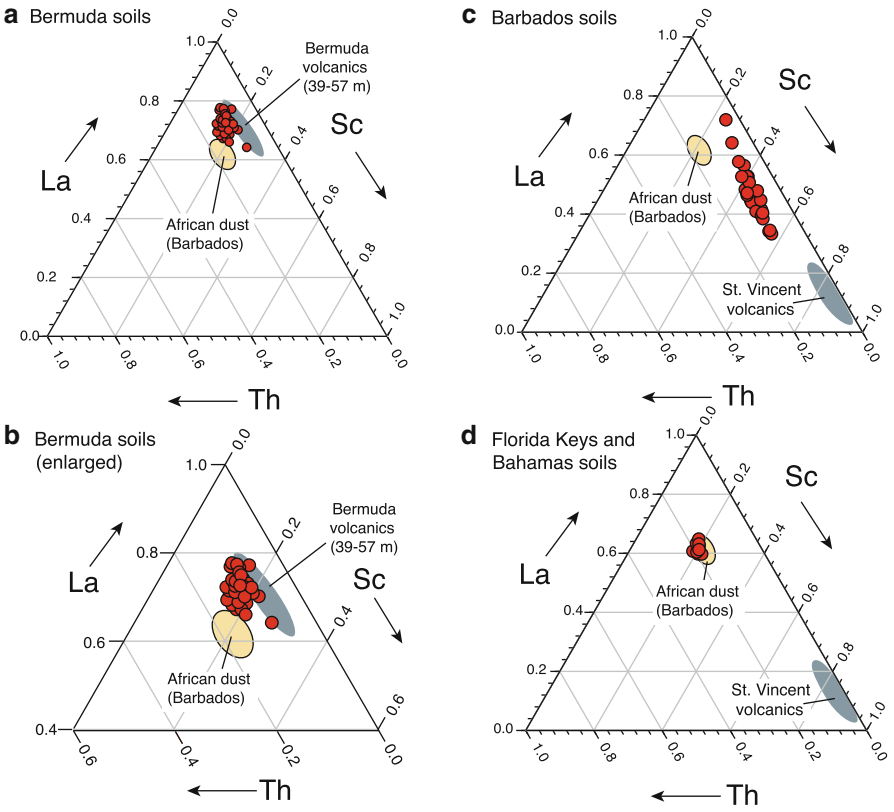

Fig. 3.6 Ternary diagrams showing abundances of Sc-Th-La in soils from (**a**) Bermuda, (**b**) Bermuda [enlarged from (**a**)], (**c**) Barbados, and (**d**) the Florida Keys and Bahamas. Shown for comparison are compositions of African dust collected on Barbados and competing volcanic parent materials (Data from Muhs et al. 2007, 2012)

La pole. Olivarez et al. (1991) found that fine-grained sediments from cores in the northwestern Pacific Ocean had Sc-Th-La compositions that fell between these two extremes, although the majority of core samples have compositions closer to average continental crust (proxied by Chinese loess). They infer from these observations that Asian dust is a likely source for much of what is seen in northwestern Pacific cores. On the other hand, cores from the equatorial Pacific, although also showing a hybrid composition, plot closer to the composition of oceanic crust and other mafic volcanic rocks, suggesting lesser amounts of input from Asian dust. This interpretation is consistent with the greater distance of travel for Asian dust to reach the equatorial latitudes of the Pacific. A similar approach has been used to identify African dust in soils of western Atlantic islands (Fig. 3.6).

3.4.5 Isotopic Methods of Identifying Dust Sources

One of the most powerful methods of identifying dust sources is through isotopic "fingerprinting." This approach has become so important that many dust provenance studies, particularly for LRT dust, routinely incorporate isotopic analyses in their analyses. Isotopic studies have formed the foundation for some of our current understanding of the sources of loess, deep-sea sediments, and dust particles found in polar ice caps.

Commonly used elements for identifying dust sources are all radiogenic isotopes, Sr, Nd, and Pb. Taylor et al. (1983) were among the first to show the relation of Nd and Sr isotopes in loess to possible source rocks. Grousset and Biscaye (2005) review the use of these isotope systems in dust provenance studies in general, and Scheuvens et al. (2013) review the Sr-Nd-Pb data that have been generated specifically for major dust sources in Africa. Sr-Nd-Pb-isotopic compositions of dust grains are highly dependent on particle size, as we show below with examples from China (Chen et al. 2007) and Africa (Meyer et al. 2011).

The source or sources of silt particles on the Loess Plateau of China (Fig. 3.7a) have been debated for decades. Here, $^{87}Sr/^{86}Sr$ vs. $^{143}Nd/^{144}Nd$ studies provide a means to evaluate hypothesized sources, and a recent study not only applies this approach but also provides a cautionary note in the methodology. Particle size trends in the Loess Plateau suggest that loess could have originated from any or all of several desert basins found to the north of the loess body. Chen et al. (2007) analyzed sediment samples from most of these basins, which here we collapse into three groups, the "western deserts" (Taklimakan Desert, Qaidam Basin, Badain Jaran Desert, and Tengger Desert), the "northeastern deserts," and the two deserts immediately to the north of the Loess Plateau (Mu Us and Hobq Deserts). Analytical results show that the $^{87}Sr/^{86}Sr$ and $^{143}Nd/^{144}Nd$ compositions of sediments from these three desert-basin groups are distinct from one another (Fig. 3.7b). Further, Chen et al. (2007) show that the $^{87}Sr/^{86}Sr$ and $^{143}Nd/^{144}Nd$ compositions of sediments in all three deserts are a function of particle size. Although the $^{143}Nd/^{144}Nd$ compositions are not significantly different for the <75 μm fraction compared to the <5 μm fraction, $^{87}Sr/^{86}Sr$ values are consistently more radiogenic for the <5 μm fraction. For samples from the Loess Plateau, both size fractions show $^{87}Sr/^{86}Sr$ and $^{143}Nd/^{144}Nd$ compositions that fall closest to the western deserts. Given the close geographic association of the Loess Plateau to the Mu Us and Hobq Deserts, this interesting result shows the interpretive power of this isotopic approach to identifying loess or dust sources, as long as due attention is paid to the potential effects of particle size on isotopic composition. Similar effects of grain size on $^{87}Sr/^{86}Sr$ composition were reported for aeolian and fluvial sediments analyzed from cores off northwestern Africa (Meyer et al. 2011).

The Pb-isotopic system has also been employed to identify dust and loess sources. Dust source sediments will have Pb-isotopic signatures that reflect the rocks they are derived from, although care must be taken to avoid local urban and industrial anthropogenic additions of Pb (from gasoline, mining, and smelting

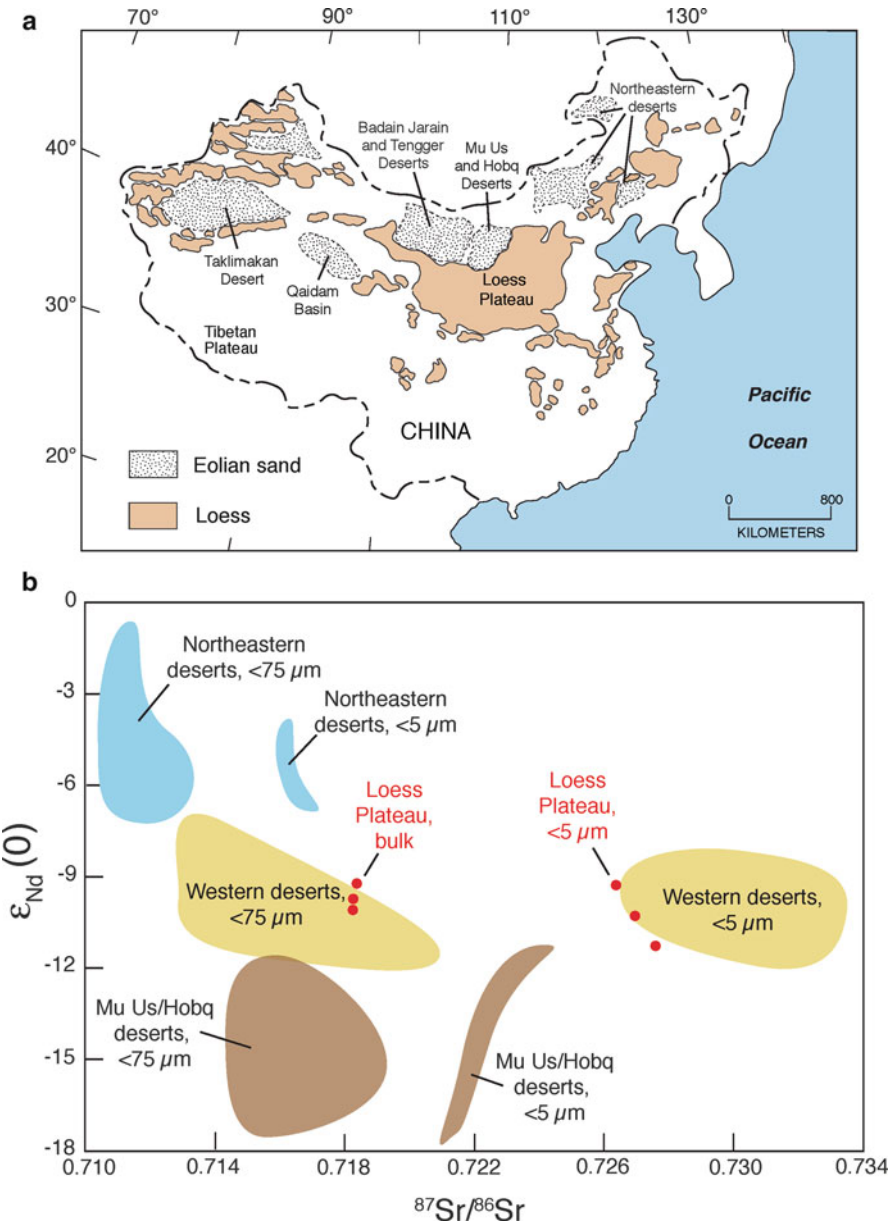

Fig. 3.7 (**a**) Map of loess bodies and aeolian sand in China (Redrawn from Liu 1985; Sun and Muhs 2007); (**b**) Nd and Sr isotopic compositions of desert source sediments and loess from the Loess Plateau of China (Data from Chen et al. 2007)

activities). Studies by Aleinikoff et al. (1999, 2008) in the Great Plains region of North America utilized this method in identifying sources of loess in Nebraska and Colorado. Although loess in Nebraska lies downwind of the Nebraska Sand Hills dune field, little or no loess appears to be derived from it, based on Pb-isotopic compositions of K-feldspar. In fact, even the Platte River is an important source only for those loess deposits that are very close to this fluvial source. The vast majority of loess sediments in Nebraska are derived from silts of the White River Group, a tertiary volcaniclastic siltstone that resulted from a major eruption ~34 Ma (hence its highly radiogenic composition).

3.4.6 Biologic Methods of Identifying Dust Sources

Our emphasis has been on physical properties of sediments or their mineralogical, chemical, or isotopic compositions to identify dust sources. Biological materials can also give important clues for mineral dust origins, because organic materials that are in the form of fine-grained particles can be transported from the same sources as mineral dust, can travel along the same pathways, can adhere to dust particles, and can be deposited in the same geologic archives. Interestingly, one of the first written observations of dust, linked to sources in Africa, was made by Charles Darwin, and was based on biological materials. On his *Beagle* voyage in 1833, Darwin observed dust aboard ship while in the vicinity of the Cape Verde Islands (Darwin 1846). Examination of this dust by Darwin himself and by Christian Gottfried Ehrenberg of Berlin showed that the samples contained abundant "infusoria" (obsolete term for certain protozoans), but also phytoliths. Darwin (1846) speculated that the source of the dust was Africa.

An interesting blend of both aquatic and terrestrial biological markers to identify dust sources comes from a study of sediments in deep-sea cores in the eastern Atlantic Ocean. In a core retrieved off northwestern Africa, Pokras and Mix (1985) generated an oxygen isotope stratigraphy (from foraminifera) of warm and cool periods of the last interglacial/glacial cycle and determined the abundances of *Melosira* and phytoliths in each depth interval. *Melosira* is a genus of freshwater diatoms that includes many species that are abundant in all the large lakes of Africa. Phytoliths are silica bodies produced in plants and are most abundant in grasses, such as those that occur in the transitional zones between humid tropical forest and desert regions of Africa. Pokras and Mix (1985) found that the greatest abundances of *Melosira* occur in time periods that correspond either to glacial periods (marine isotope stages [MIS] 6, 4 and 2) or cool interstadial periods (MIS 5.2 and 5.4). They interpret these results to indicate that aeolian input of diatoms increased during cool periods due to the desiccation of African lakes under arid conditions. In contrast, during warm interglacial or interstadial periods (MIS 5.5, 5.3, 5.1, 3, and 1), more-humid conditions prevailed, African lakes were extant, and aeolian diatom input diminished. However, phytolith input increased during these times, due to northward

migration of grasslands into former desert regions. Pokras and Mix (1985) note that the *Melosira* maximum in the late Holocene interglacial period is anomalous over the past ~150,000 year.

3.5 Conclusion

The study of dust is important, because this sediment has important effects on the planetary radiation balance and biogeochemical cycles. Furthermore, geologic records of past dust deposition have tremendous importance in paleoclimate studies. Crucial to most investigations of dust in these contexts is identification of source regions as the physical and chemical characteristics of suspended dust are strongly governed by their surface provenance.

Particular geomorphic settings are the most favorable dust sources. These include desiccated or ephemeral lakes, high- and low-relief alluvial systems, and aeolian systems. Different landform systems exhibit varying potential as dust sources due to the limitations on emission imposed by differences in the supply of fine sediment (e.g., some geomorphic settings receiving sediment recharge from periodic flood deposition) and in the availability of this sediment for entrainment. For example, dry or ephemeral lakes may contain abundant fine-grained sediment, but will not generate much dust if the surface is moist or if particles are cemented by salts or clay minerals.

Many contemporary dust sources have been identified using high-resolution, Earth-orbiting satellites. Satellites have provided a global assessment, establishing topographic depressions in arid regions, usually far from populated areas, as the most important dust sources and the presence of a "global dust belt." MODIS and MISR imagery give high-resolution records of dust sources on a regular basis. The resolution of this imagery is sufficient that point sources ("hot spots") of dust within broader desert regions can be identified.

For studies of dust records of the past, identification of source areas requires imaginative approaches. Physical properties of dust deposits, particularly loess, have been used to identify aeolian sources for several decades. Mineralogy can also be used to determine dust sources, even in deep-sea core records that are distant from their sources on the continents. Dust collected along the African coast shows a latitudinally variable clay mineral composition that closely matches the changes in clay mineralogy of the major soil types of the African source regions, which are in turn a function of the dominant soil-forming processes along a climatic gradient. Geochemical methods have also been used to identify dust sources and isotopic compositions (commonly for Nd, Sr, and Pb) have helped determine the sources of dust in the Loess Plateau of China and Antarctic ice cores.

Dust sources can change over time, particularly on the scale of interglacial/glacial cycles of the Quaternary. During glacial periods, growth of continental ice sheets and expanded valley glaciers and mountain ice caps generated abundant glaciogenic silt to a degree much greater than today. The record of this glacial-age dust source

is found in the vast loess deposits of North America, South America, and Eurasia, as well as in many deep-sea cores. In addition, growth of continental ice sheets lowered sea level and exposed many continental and insular shelves that today are submerged. The importance of this potential glacial-age dust source has yet to be realized with field studies, but would be a fruitful area of research in the future. Other land surface changes promoting dust also occurred during the last glacial period including desiccation of lakes and reduction in overall vegetation cover.

Assessing future dust sources is not easy and such efforts require modeling. Modeling suggests that climate change will likely bring about shifts in dust sources through changes in degree or kind of vegetation cover, variations in wind strength, and changes in the size of water bodies. Human land use is a major uncertainty in assessing dust sources of the future, as changes in land use could affect land surface erodibility significantly, particularly due to increased agricultural endeavors and water usage.

References

Aleinikoff JN, Muhs DR, Sauer R, Fanning CM (1999) Late Quaternary loess in northeastern Colorado Part II–Pb isotopic evidence for the variability of loess sources. Geol Soc Am Bull 111:1876–1883

Aleinikoff JN, Muhs DR, Bettis EA III, Johnson WC, Fanning CM, Benton R (2008) Isotopic evidence for the diversity of late Quaternary loess in Nebraska: glaciogenic and non-glaciogenic sources. Geol Soc Am Bull 120:1362–1377

Alonso-Perez S, Cuevas E, Querol X, Guerra JC, Perez C (2012) African dust source regions for observed dust outbreaks over the Subtropical Eastern North Atlantic region above 25°N. J Arid Environ 78:100–109

Birkeland PW (1999) Soils and geomorphology. Oxford University Press, New York

Biscaye PE, Grousset FE, Revel M, Van der Gaast S, Zielinski GA, Vaars A, Kukla G (1997) Asian provenance of glacial dust (stage 2) in the Greenland Ice Sheet Project 2 Ice Core Summit Greenland. J Geophys Res 102(C12):26765–26781

Blatt H (1987) Oxygen isotopes and the origin of quartz. J Sediment Petrol 57:373–377

Bristow CS, Drake N, Armitage S (2009) Deflation in the dustiest place on Earth: the Bodélé Depression Chad. Geomorphology 105:50–58

Brown GF, Schmidt DL, Huffman AC Jr (1989) Geology of the Arabian Peninsula: shield area of western Saudi Arabia. US Geological Survey Professional Paper 560-A

Bryant RG (2013) Recent advances in our understanding of dust source emission processes. Prog Phys Geogr 37:397–421

Bullard JE (2013) Contemporary glacigenic inputs to the dust cycle. Earth Surf Proc Landforms 38:71–89

Bullard JE, Harrison SP, Baddock MC, Drake N, Gill TE, McTainsh G, Sun Y (2011) Preferential dust sources: a geomorphological classification designed for use in global dust-cycle models. J Geophys Res 116, F04034. doi:10.1029/2011JF002061

Bureau of Economic Geology (1992) Geology of Texas. University of Texas at Austin Bureau of Economic Geology, Austin

Caquineau S, Gaudichet A, Gomes L, Magonthier M-C, Chatenet B (1998) Saharan dust: clay ratio as a relevant tracer to assess the origin of soil-derived aerosols. Geophys Res Lett 25:983–986

Caquineau S, Gaudichet A, Gomes L, Legrand M (2002) Mineralogy of Saharan dust transported over northwestern tropical Atlantic Ocean in relation to source regions. J Geophys Res 107(D15):4251. doi:10.1029/2000JD247

Chen J, Li G, Yang J, Rao W, Lu H, Balsam W, Sun Y, Ji J (2007) Nd and Sr isotopic characteristics of Chinese deserts: implications for the provenances of Asian dust. Geochim Cosmochim Acta 71:3904–3914

Chester R, Elderfield H, Griffin JJ, Johnson LR, Padgham RC (1972) Eolian dust along the eastern margins of the Atlantic Ocean. Mar Geol 13:91–105

Chiapello I, Bergametti G, Chatenet B, Bousquet P, Dulac F, Santos Soares ES (1997) Origins of African dust transported over the northeastern tropical Atlantic. J Geophys Res 102:13701–13709

Coudé-Gaussen G (1987) The perisaharan loess: sedimentological characterization and paleoclimatical significance. GeoJournal 15:177–183

Creamean JM, Suski KJ, Rosenfeld D, Cazorla A, DeMott PJ, Sullivan RC, White AB, Ralph FM, Minnis P, Comstock JM, Tomlinson JM, Prather KA (2013) Dust and biological aerosols from the Sahara and Asia influence precipitation in the western US. Science 339:1572–1578

Crouvi O, Amit R, Enzel Y, Gillespie AR (2010) Active sand seas and the formation of desert loess. Quaternary Sci Rev 29:2087–2098

Crusius J, Schroth AW, Gasso S, Moy CM, Levy RC, Gatica M (2011) Glacial flour dust storms in the Gulf of Alaska: hydrologic and meteorological controls and their importance as a source of bioavailable iron. Geophys Res Lett 38, L06602

Darwin C (1846) An account of the fine dust which falls upon vessels in the Atlantic Ocean. Q J Geol Soc Lond 2:26–30

Drake NA, Bristow C (2006) Shorelines in the Sahara: geomorphological evidence for an enhanced monsoon from palaeolake Megachad. Holocene 16:901–911

Drake NA, Blench RM, Armitage SJ, Bristow CS, White KH (2011) Ancient watercourses and biogeography of the Sahara explain the peopling of the desert. Proc Natl Acad Sci U S A 108:458–462

Engelstaedter S, Washington R, Mahowald N (2009) Impact of changes in atmospheric conditions in modulating summer dust concentration at Barbados: a back-trajectory analysis. J Geophys Res 114, D17111

Falkowski PG, Barber RT, Smetacek V (1998) Biogeochemical controls and feedbacks on ocean primary production. Science 281:200–206

Gallet S, Jahn B, Torii M (1996) Geochemical characterization of the Luochuan loess-paleosol sequence China and paleoclimatic implications. Chem Geol 133:67–88

Gebhart KA, Schichtel BA, Barna MG (2005) Directional biases in back trajectories caused by model and input data. J Air Waste Manage Assoc 55:1649–1662

Ghienne J-F, Schuster M, Bernard A, Duringer P, Brunet M (2002) The Holocene giant Lake Chad revealed by digital elevation models. Quaternary Int 87:81–85

Gill TE (1996) Eolian sediments generated by anthropogenic disturbance of playas: human impacts on the geomorphic system and geomorphic impacts on the human system. Geomorphology 17:207–228

Gillette DA (1999) A qualitative geophysical explanation for “hot spot” dust emitting source regions. Contrib Atmos Phys 72:67–77

Ginoux P, Prospero JM, Gill TE, Hsu NC, Zhao M (2012) Global-scale attribution of anthropogenic and natural dust sources and their emission rates based on MODIS deep blue aerosol products. Rev Geophys 50, RG3005. doi:10.1029/2012RG000388

Glaccum RA, Prospero JM (1980) Saharan aerosols over the tropical north Atlantic – mineralogy. Mar Geol 37:295–321

Goudie AS (2008) The history and nature of wind erosion in deserts. Annu Rev Earth Planet Sci 36:97–119

Goudie AS, Middleton NJ (2006) Desert dust in the global system. Springer, Heidelberg

Grousset FE, Biscaye PE (2005) Tracing dust sources and transport patterns using Sr Nd and Pb isotopes. Chem Geol 222:149–167

Harrison SP, Kohfeld KE, Roelandt C, Claquin T (2001) The role of dust in climate changes today at the last glacial maximum and in the future. Earth-Sci Rev 54:43–80

Hesse PP, McTainsh GH (2003) Australian dust deposits: modern processes and the Quaternary record. Quaternary Sci Rev 22:2007–2035

Holliday VT (1989) The Blackwater Draw Formation (Quaternary): a 1.4-plus-m.y. record of eolian sedimentation and soil formation on the Southern High Plains. Geol Soc Am Bull 101:1598–1607

Jackson ML, Levelt TWM, Syers JK, Rex RW, Clayton RN, Sherman GD, Uehara G (1971) Geomorphological relationships of tropospherically derived quartz in the soils of the Hawaiian islands. Soil Sci Soc Am Proc 35:515–525

Jickells TD, An ZS, Andersen KK, Baker AR, Bergametti G, Brooks N, Cao JJ, Boyd PW, Duce RA, Hunter KA, Kawahata H, Kubilay N, LaRoche J, Liss PS, Mahowald N, Prospero JM, Ridgwell AJ, Tegen I, Torres R (2005) Global iron connections between desert dust ocean biogeochemistry and climate. Science 308:67–71

Karydis V, Kumar AP, Barahona D, Sokolik IN, Nenes A (2011) On the effect of dust particles on global cloud condensation nuclei and cloud droplet number. J Geophys Res 116(D23), D23204

Kohfeld KE, Harrison SP (2001) DIRTMAP: the geological record of dust. Earth-Sci Rev 54:81–114

Kohfeld KE, Tegen I (2007) Record of mineral aerosols and their role in the Earth system. In: Holland HD, Turekian KK (eds) Treatise on geochemistry. Elsevier, Amsterdam

Kok JF, Parteli EJR, Michaels TI, Karam DB (2012) The physics of wind-blown sand and dust. Rep Prog Phys 75

Laity JE (1994) Landforms of aeolian erosion. In: Abrahams A, Parsons A (eds) Geomorphology of desert environments. Chapman & Hall, London, pp 506–535

Laity JE (2011) Pavements and stone mantles. In: Thomas DSG (ed) Arid zone geomorphology: process form and change in drylands, 3rd edn. Wiley, Chichester, pp 181–207

Lee JA, Baddock MC, Mbuh MJ, Gill TE (2012) Geomorphic and land cover characteristics of aeolian dust sources in West Texas and eastern New Mexico USA. Aeolian Res 3:459–466

Li-Jones X, Prospero JM (1998) Variations in the size distribution of non-sea-salt sulfate aerosol in the marine boundary layer at Barbados: impact of African dust. J Geophys Res D Atmos 103:16073–16084

Liu T (1985) Loess in China, 2nd edn. China Ocean Press/Springer, Beijing/Berlin

Maher BA, Prospero JM, Mackie D, Gaiero D, Hesse P, Balkanski Y (2010) Global connections between aeolian dust climate and ocean biogeochemistry at the present day and at the last glacial maximum. Earth-Sci Rev 99:61–97

Mahowald NM, Engelstaedter S, Luo C, Sealy A, Artaxo P, Benitez-Nelson C, Bonnet S, Chen Y, Chuang PY, Cohen DD, Dulac F, Herut B, Johansen AM, Kubilay N, Losno R, Maenhaut W, Paytan A, Prospero JM, Shank LM, Siefert RL (2009) Atmospheric iron deposition: global distribution variability and human perturbations. Ann Rev Mar Sci 1:245–278

McCauley JF, Grolier MJ, Breed CS (1977) Yardangs. In: Doehring DO (ed) Geomorphology in arid regions. Allen and Unwin, London, pp 233–269

McFadden LD, Wells SG, Jercinovich MJ (1987) Influences of eolian and pedogenic processes on the origin and evolution of desert pavements. Geology 15:504–508

McTainsh GH (1989) Quaternary aeolian dust processes and sediments in the Australian region. Quaternary Sci Rev 8:235–253

Meyer I, Davies GR, Stuut J-BW (2011) Grain size control on Sr-Nd isotope provenance studies and impact on paleoclimate reconstructions: an example from deep-sea sediments offshore NW Africa. Geochem Geophys Geosyst 12, Q03005

Middleton NJ, Goudie AS (2001) Saharan dust: sources and trajectories. Trans Inst Br Geogr 26:165–181

Muhs DR (2013a) Geologic records of dust in the Quaternary. Aeolian Res 9:3–48

Muhs DR (2013b) Loess and its geomorphic stratigraphic and paleoclimatic significance in the Quaternary. In: Shroder JF (ed) Treatise on geomorphology, vol 11. Academic Press, San Diego, pp 149–183

Muhs DR, Budahn J, Prospero JM, Carey SN (2007) Geochemical evidence for African dust inputs to soils of western Atlantic islands: Barbados, the Bahamas, and Florida. J Geophys Res 112, F02009

Muhs DR, Budahn J, Johnson DL, Reheis M, Beann J, Skipp G, Fisher E, Jones JA (2008) Geochemical evidence for airborne dust additions to soils in Channel Islands National Park California. Geol Soc Am Bull 120:106–126

Muhs DR, Budahn J, Skipp G, Prospero JM, Patterson D, Bettis EA III (2010) Geochemical and mineralogical evidence for Sahara and Sahel dust additions to Quaternary soils on Lanzarote, eastern Canary Islands, Spain. Terra Nova 22:399–410

Muhs DR, Budahn J, Prospero JM, Skipp G, Herwitz SR (2012) Soil genesis on the island of Bermuda in the Quaternary: the importance of African dust transport and deposition. J Geophys Res 117, F03025

Okin GS, Gillette DA, Herrick JE (2006) Multi-scale controls on and consequences of aeolian processes in landscape change in arid and semi-arid environments. J Arid Environ 65:253–275

Olivarez AM, Owen RM, Rea DK (1991) Geochemistry of eolian dust in Pacific pelagic sediments: implications for paleoclimatic interpretations. Geochim Cosmochim Acta 55:2147–2158

Pokras EM, Mix AC (1985) Eolian evidence for spatial variability of late Quaternary climates in tropical Africa. Quatern Res 24:137–149

Prospero JM, Lamb PJ (2003) African droughts and dust transport to the Caribbean: climate change implications. Science 302:1024–1027

Prospero JM, Bonatti E, Schubert C, Carlson TN (1970) Dust in the Caribbean atmosphere traced to an African dust storm. Earth Planet Sci Lett 9:287–293

Prospero JM, Olmez I, Ames M (2001) Al and Fe in PM 2.5 and PM 10 suspended particles in south-central Florida: the impact of the long range transport of African mineral dust. Water Air Soil Pollut 125:291–317

Prospero JM, Ginoux P, Torres O, Nicholson SE, Gill TE (2002) Environmental characterization of global sources of atmospheric soil dust identified with the Nimbus 7 Total Ozone Mapping Spectrometer (TOMS) absorbing aerosol product. Rev Geophys 40:1002

Prospero JM, Bullard JE, Hodgkins R (2012) High-latitude dust over the North Atlantic: inputs from Icelandic proglacial dust storms. Science 335:1078–1082

Radhi M, Box MA, Box GP, Keywood MD, Cohen DD, Stelcer E, Mitchell RM (2011) Size-resolved chemical composition of Australian dust aerosol during winter. Environ Chem 8:248–262

Ravi S, D'Odorico P, Breshears DD, Field JP, Goudie AS, Huxman TE, Li J, Okin GS, Swap RJ, Thomas AD, Van Pelt S, Whicker JJ, Zobeck TM (2011) Aeolian processes and the biosphere. Rev Geophys 49, RG3001

Reid EA, Reid JS, Meier MM, Dunlap MR, Cliff SS, Broumas A, Perry K, Maring H (2003a) Characterization of African dust transported to Puerto Rico by individual particle and size segregated bulk analysis. J Geophys Res 108(D19):8591

Reid JS, Jonsson HH, Maring HB, Smirnov A, Savoie DL, Cliff SS, Reid EA, Livingston JM, Meier MM, Dubovik O, Tsay S-C (2003b) Comparison of size and morphological measurements of coarse mode dust particles from Africa. J Geophys Res 108(D19):8593

Rojo L, Gill TE, Gillette DA (2008) Particle size/composition relationships of wind-eroding sediments Owens (dry) Lake California USA. X-Ray Spectrom 37:111–115

Scheuvens D, Schütz L, Kandler K, Ebert E, Weinbruch S (2013) Bulk composition of northern African dust and its source sediments – a compilation. Earth-Sci Rev 116:170–194

Shao Y, Wyrwoll K-H, Chappell A, Huang J, Lin Z, McTainsh GH, Mikami M, Tanaka TY, Wang X, Yoon S (2011) Dust cycle: an emerging theme in Earth system science. Aeolian Res 2:181–204

Shaw PA, Bryant RG (2011) Pans playas and salt lakes. In: Thomas DSG (ed) Arid zone geomorphology: process form and change in drylands, 3rd edn. Wiley, Chichester, pp 373–401

Smalley IJ (1966) The properties of glacial loess and the formation of loess deposits. J Sediment Petrol 36:669–676

Smalley IJ (1995) Making the material: the formation of silt-sized primary mineral particles for loess deposits. Quaternary Sci Rev 14:645–651

Smith GD (1942) Illinois loess: variations in its properties and distribution a pedologic interpretation. Univ Ill Agric Exp Stn Bull 490:139–184

Smith BJ, Wright JS, Whalley WB (2002) Sources of non-glacial loess-size quartz silt and the origins of "desert loess". Earth-Sci Rev 59:1–26

Stuut J-BW, Zabel M, Ratmeyer V, Helmke P, Schefuß E, Lavik G, Schneider R (2005) Provenance of present-day eolian dust collected off NW Africa. J Geophys Res 110, D04202

Sun J, Muhs DR (2007) Dune fields: mid-latitudes. In: Elias S (ed) The encyclopedia of Quaternary sciences. Elsevier, Amsterdam, pp 607–626

Taylor SR, McLennan SM (1985) The continental crust: its composition and evolution. Blackwell Scientific Publications, Oxford

Taylor SR, McLennan SM, McCulloch MT (1983) Geochemistry of loess, continental crustal composition and crustal model ages. Geochim Cosmochim Acta 47:1897–1905

Tegen I (2003) Modeling the mineral dust aerosol cycle in the climate system. Quaternary Sci Rev 22:1821–1834

Trapp JM, Millero FJ, Prospero JM (2010) Temporal variability of the elemental composition of African dust measured in trade wind aerosols at Barbados and Miami. Mar Chem 120:71–82

Tsoar H, Pye K (1987) Dust transport and the question of desert loess formation. Sedimentology 34:139–153

Twohy CH, Kreidenweis SM, Eidhammer T, Browell EV, Heymsfield AJ, Bansemer AR, Anderson BE, Chen G, Ismail S, DeMott PJ, Van Den Heever SC (2009) Saharan dust particles nucleate droplets in eastern Atlantic clouds. Geophys Res Lett 36, L01807

Warren A, Chappell A, Todd MC, Bristow C, Drake N, Engelstaedter S, Martins V, M'bainayel S, Washington R (2007) Dust-raising in the dustiest place on earth. Geomorphology 92:25–37

Washington R, Todd M, Middleton NJ, Goudie AS (2003) Dust-storm source areas determined by the Total Ozone Monitoring Spectrometer and surface observations. Ann Assoc Am Geogr 93:297–313

Washington R, Bouet C, Cautenet G, Mackenzie E, Ashpole I, Engelstaedter S, Henderson GM, Schepanski K, Tegan I (2009) Dust as a tipping element: the Bodélé Depression, Chad. Proc Natl Acad Sci 106:20564–20571

Wright JS (2001) "Desert" loess versus "glacial" loess: quartz silt formation, source areas and sediment pathways in the formation of loess deposits. Geomorphology 36:231–256

Wright J, Smith B (1993) Fluvial comminution and the production of loess-sized quartz silt: a simulation study. Geogr Ann 75A:25–34

Wright J, Smith BJ, Whalley WB (1998) Mechanisms of loess-sized quartz silt production and their relative effectiveness: laboratory simulations. Geomorphology 23:15–34

Chapter 4
Processing and Ageing in the Atmosphere

Alex R. Baker, Olga Laskina, and Vicki H. Grassian

Abstract Transport through the atmosphere exposes mineral dust to a number of processes that alter its physicochemical properties, which in turn affects its direct and indirect impacts on climate. In this chapter, we review the physical and chemical processes that alter dust properties and their impacts on dust's radiative properties, cloud condensation nucleus activity, morphology, nutrient and trace element solubility and the impacts of heterogeneous chemistry on dust surfaces on atmospheric composition.

Keywords Physical processing • Chemical processing • Dust dispersal • Solubility • Iron • Nitrogen • Nitric acid • Nitrogen oxides • Sulphur • Ozone • Chemical properties • Particle surface • Ageing

4.1 Introduction

Mineral dust aerosol is an abundant component of the Earth's atmosphere. Once suspended in the atmosphere, dust can be subjected to a number of processes that influence its transport, deposition and impact on the environment. Effects range from purely physical, e.g. winnowing, to those associated with heterogeneous chemistry on dust particle surfaces. Heterogeneous chemistry during long-range

A.R. Baker (✉)
Centre for Ocean and Atmospheric Sciences, School of Environmental Sciences, University of East Anglia, Norwich NR4 7TJ, UK
e-mail: Alex.Baker@uea.ac.uk

O. Laskina • V.H. Grassian
Department of Chemistry, University of Iowa, Iowa City, IA, 52242-1294, USA
e-mail: olga-laskina@uiowa.edu; Vicki-grassian@uiowa.edu

P. Knippertz and J.-B.W. Stuut (eds.), *Mineral Dust: A Key Player in the Earth System*, DOI 10.1007/978-94-017-8978-3_4,

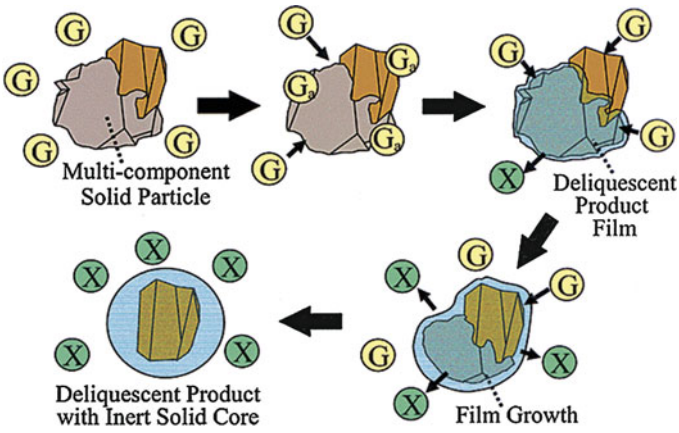

Fig. 4.1 Pictorial representation of changes in a composite mineral dust particle as it is processed in the atmosphere (Reprinted with permission from Usher et al. (2003). Copyright (2003) American Chemical Society)

transport may alter hygroscopicity (and hence removal mechanisms), reactivity of dust constituents and the composition of the atmosphere, as illustrated schematically in Fig. 4.1. In this chapter, we examine these processes using data from field observations and laboratory measurements. Field studies allow us to assess the net effect of the various complex processes involved, while laboratory work provides the means to study fundamental chemical and physical mechanisms under controlled conditions.

4.2 Physical Processing

As discussed in Chaps. 8 and 17, winnowing leads to shifts in the size spectrum of suspended dust during transport away from source areas (Maring et al. 2003; Mahowald et al. 2005). Large particles (>10 μm) are removed rather rapidly and do not contribute appreciably to long-range transport (Formenti et al. 2011). This shift also potentially affects the mineralogy of transported dust, as large quartz grains are removed close to source (Glaccum and Prospero 1980).

The modal size of long-range transported dust is generally considered to be 1–3 μm (Arimoto et al. 1997; Schulz et al. 1998; Reid et al. 2003), but there are reports of giant particles (>75 μm) being transported many thousands of kilometres away from sources (see Chap. 17, Betzer et al. 1988).

4.3 Chemical Processing

4.3.1 Impacts on Physical Properties of Dust

Heterogeneous chemistry and photochemistry of mineral dust aerosol is extremely important as these reactions change the properties of the particles and their direct and indirect climate forcing, thus impacting climate (see Chap. 13 for a detailed discussion of the impact of dust on radiative forcing). There are still many uncertainties associated with the role of mineral dust aerosol on climate, in part due to its inherent heterogeneity and in part due to the incomplete understanding of the influence of ageing processes on climate-related properties of mineral dust. Processing may alter the chemical composition of particles and, ultimately, may change the optical properties, hygroscopicity, cloud condensation nuclei (CCN) and ice nuclei (IN) activity (see Chap. 12).

For example, sulphate coatings on mineral dust particles are known to have a cooling effect by effectively scattering radiation and to promote CCN activity (Yin et al. 2002); at the same time, the presence of sulphuric acid leads to a decrease in the dust particles' ice nucleation ability (Sullivan et al. 2010). Cloud processing of dust particles with sea-salt species and anthropogenic pollutants is an important pathway in the formation of hygroscopic species (Kim and Park 2012). Calcite particles reacted with nitric or oxalic acids show an increase in the hygroscopicity due to the formation of hygroscopic species (Gierlus et al. 2012). Coating of mineral particles with soluble materials such as sulphate, nitrate and chloride also increases cloud condensation nuclei activity (Crumeyrolle et al. 2008); however, the exact effect (enhancement or inhibition) on cloud formation depends on the particular chemical interactions (Sullivan et al. 2009). Coated mineral particles may accelerate the formation of precipitation particles in continental clouds (Yin et al. 2002).

For calcium carbonate ($CaCO_3$), reaction with HNO_3 in the presence of water leads to the formation of calcium nitrate droplets. This causes a significant change in particle morphology, size, scattering properties and hygroscopic growth relative to calcium carbonate (Gibson et al. 2006), as shown in Fig. 4.2.

4.3.2 Impacts on Dust Reactivity

Chemical processing has some potentially important impacts on the reactivity of dust in the environment. The most significant of these is the potential to increase the solubility of nutrients, such as iron (Fe) and phosphorus (P) contained in dust, and thus to enhance their bioavailability once deposited onto marine and terrestrial ecosystems (see Chap. 14).

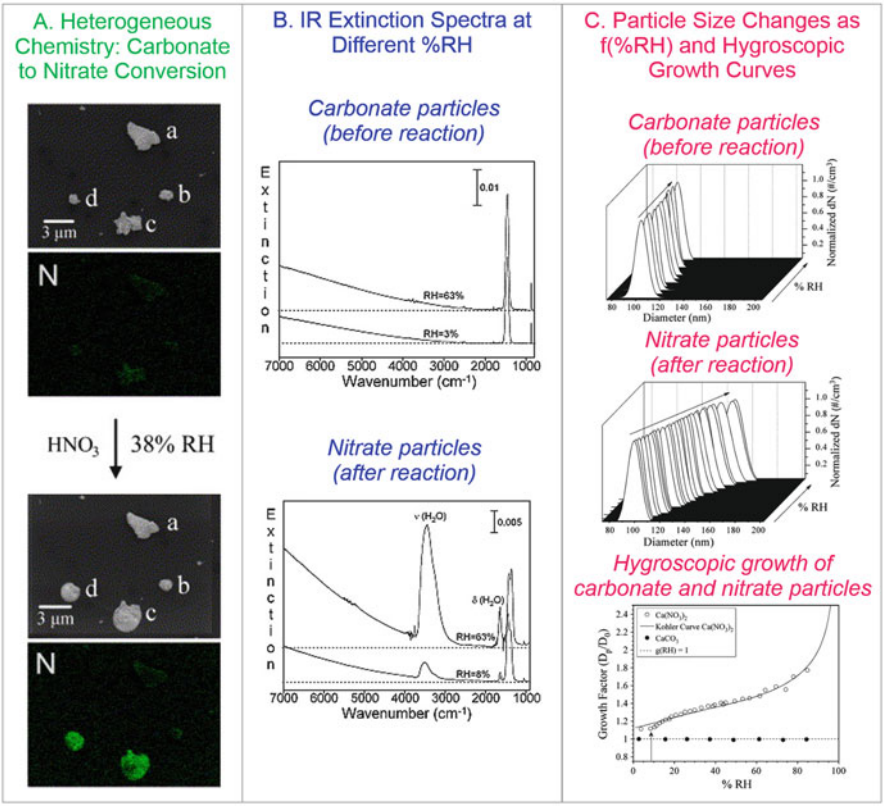

Fig. 4.2 (**a**) Heterogeneous chemistry of mineral dust measured with scanning electron microscopy and energy dispersive X-ray analysis. These data show that carbonate particles "c" and "d" have unique reactivity with gas-phase nitric acid to form nitrate particles that take up water as shown by the change in particle size and shape (*spherical*). (**b**) Infrared extinction spectra at 2 % RHs for carbonate and nitrate particles showing that nitrate particles scatter light to a greater extent at higher relative humidity due to the size change and increased water content of the particles. (**c**) Increase in particle size for a 0.1 micron-sized dry particle as a function of relative humidity for carbonate compared to nitrate particles. The growth factor (ratio of particle diameter at a given relative humidity to the dry particle diameter) for carbonate particles is one at all % RH, whereas the growth factor of nitrate particles is greater than one and increases with relative humidity

Several potential mechanisms which might lead to changes in the chemical properties of dust during atmospheric transport have been proposed (see Baker and Croot 2010). The interaction of dust with both mineral and organic acids has been suggested to enhance dissolution of trace metals (Pehkonen et al. 1993; Spokes et al. 1994; Spokes and Jickells 1996; Desboeufs et al. 2001; Mackie et al. 2005; Shi et al. 2011) and phosphorus (Nenes et al. 2011). Although this enhancement appears to be largely reversible when pH is raised (Spokes et al. 1994; Spokes and Jickells 1996; Mackie et al. 2005; Shi et al. 2011), it appears that newly precipitated

Fe takes the form of amorphous ferrihydrite nanoparticles, which are more soluble than the Fe originally associated with dust particle surfaces (Shi et al. 2009). Acid-processing reactions have formed the basis of several attempts to model changes in Fe solubility in atmospheric dust, with a variety of iron-containing minerals being used as models for dust (Meskhidze et al. 2003; Johnson et al. 2010; Ito 2013). Photochemical redox changes (e.g. reduction of Fe (III) to the more soluble Fe (II)), often enhanced by organic components, such as oxalate, have also been suggested to enhance the solubility of Fe in the atmosphere (Erel et al. 1993; Pehkonen et al. 1993; Siefert et al. 1994).

Dust reactivity changes as a result of atmospheric transport have also been linked to the physical consequences of winnowing. Baker and Jickells (2006) suggested that decreasing particle size spectrum during transport led to increasing particle surface area to volume ratios and hence to higher fractional solubility of iron and other dust components. Journet et al. (2008) linked changes in mineralogy to changes in overall solubility of Fe in dust and suggested that >96 % of soluble Fe was derived from clay minerals, rather than Fe oxides. Cwiertny et al. (2008) also suggested in a study on authentic dust samples that clay minerals played an important role in Fe solubility. Furthermore, it was also noted that Fe present as Fe(II) in clays were particularly soluble.

The extent to which atmospheric processing enhances trace element solubility is not very well defined. Measurements of solubility in dust actually at source are very scarce and measurements on source soil materials (also few in number) are probably not representative of suspended dust at source because abrasion and fractionation during dust uplift significantly alter the dust with respect to the parent soil (Bullard et al. 2004; Mackie et al. 2006). Nevertheless, analysis of atmospheric dust collected over a broad range of dust concentrations appears to show a general hyperbolic increase in Fe solubility as dust concentration (or total Fe concentration, as a proxy for dust concentration) decreases (e.g. Chen and Siefert 2004; Baker and Jickells 2006; Sedwick et al. 2007; Theodosi et al. 2010). Sholkovitz et al. (2012) compiled (∼1,000) available measurements of iron solubility and total Fe concentration from more than 20 studies of (marine) aerosols and showed that this hyperbolic relationship is observed consistently on a global scale. In Fig. 4.3, we replot the Sholkovitz data set (excluding samples extracted with strong acid solutions, which have been shown to release a significantly higher fraction of Fe from dust than the majority of methods used in the data set (Witt et al. 2010)). It is apparent from Fig. 4.3 that similar behaviour is exhibited under four, rather different, conditions for the extraction of soluble Fe (ultrapure water, ammonium acetate, formate and seawater leaching solutions) and that there is considerable scatter about the general solubility – concentration trend within, and between, these methods.

Several authors have suggested that non-dust Fe might contribute to elevated Fe solubility values, particularly at low dust concentrations (e.g. Guieu et al. 2005; Sedwick et al. 2007; Sholkovitz et al. 2012). In Fig. 4.4, we compare Fe solubility for subsets of the data in Fig. 4.3 for total Fe concentration ranges of 30–100 ng TFe m^{-3} and 300–1,000 ng TFe m^{-3}. These data appear to indicate that Fe solubility increases as total Fe decreases, even when non-dust sources of Fe are unlikely to be

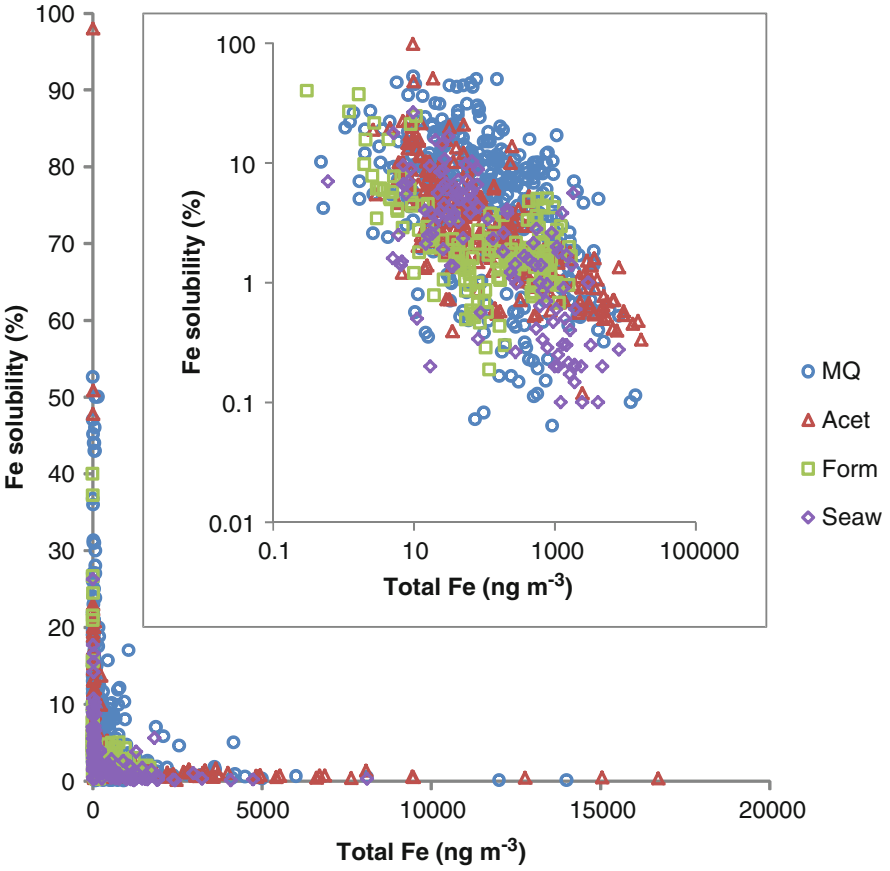

Fig. 4.3 Percentage of soluble Fe in ~1,000 aerosol samples plotted as a function of total atmospheric Fe concentration. Data is taken from the compilation of Sholkovitz et al. (2012) and *symbols* indicate the leaching solutions in which the aerosol samples were solubilised. Inset shows the same data replotted on a log–log scale

significant. This effect seems to be common to most of the analytical methods used to determine soluble Fe concentrations, except for leaching in formate solutions. The presentation of the data in Fig. 4.4 does not allow for variations due to other factors, such as dust source. In Table 4.1, we break the Sholkovitz data set down further to show variations in median solubility between soluble Fe extraction methods in different oceans over a broader range of total Fe concentrations. This table shows similar trends in solubility between methods to those evident in Fig. 4.4 and may point to differences in solubility between different ocean basins (e.g. MQ solubility in the North Pacific may be slightly higher than in the North Atlantic). However, some of the apparent solubility differences in Table 4.1 (e.g. MQ solubility is higher than acetate solubility) are probably artefacts. Indeed, a recent direct

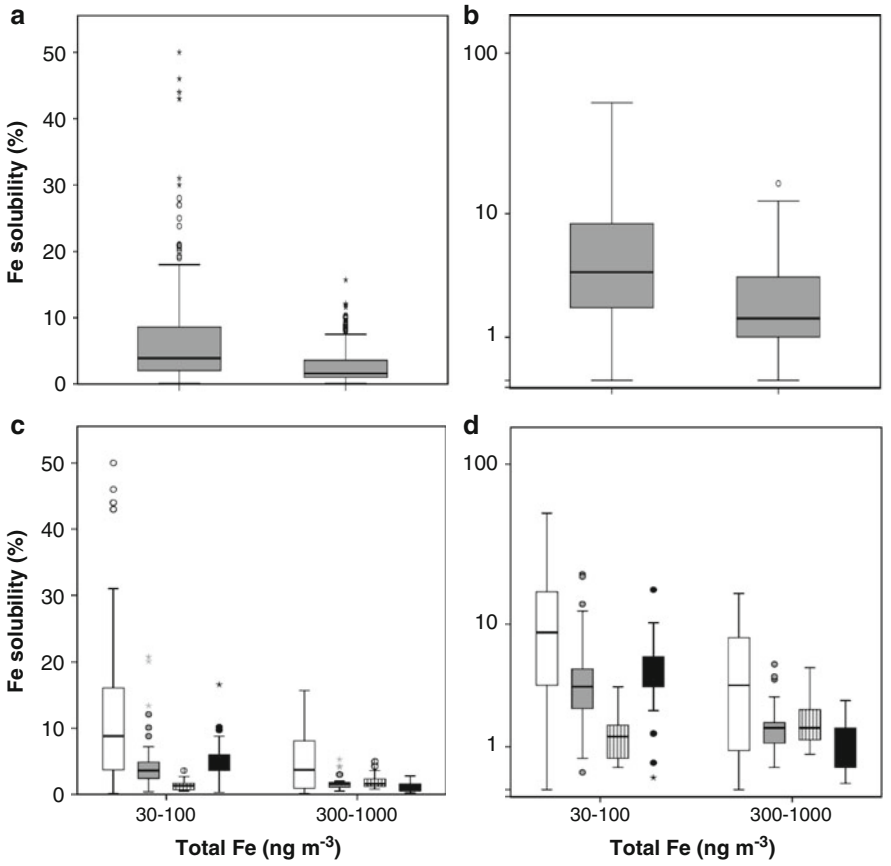

Fig. 4.4 *Box and whisker plots* showing percentage soluble Fe for two subsets of the Sholkovitz et al. (2012) data compilation: total Fe concentrations of 30–100 ng TFe m^{-3} and 300–1,000 ng TFe m^{-3}. Characteristics of all the data in those concentration ranges are shown in (**a**) (linear y-axis scale) and (**b**) (log y-axis scale). In panels (**c**) and (**d**), the data is further subdivided according to the leaching solution used for soluble Fe determination (ultrapure water (*white*), ammonium acetate (*grey*), formate (*vertical stripes*), seawater (*black*))

intercomparison exercise showed that acetate leaching solubilised more Fe than did MQ (Morton et al. 2013). Overall, the inter-method comparison shown in Table 4.1 provides further support to the observation of Aguilar-Islas et al. (2010) that inter-sample variability is a more significant contributor to the wide range of observed aerosol Fe solubility values than is inter-method variability.

Baker and Croot (2010) pointed out that it is very difficult to identify the mechanisms responsible for the hyperbolic solubility relationship from field observations of Fe solubility alone. Further insight can be gained by examining the behaviour of other dust components and related chemical tracers in field data and through controlled laboratory studies. Sholkovitz and co-workers (Sedwick et al. 2007;

Table 4.1 Median percentage Fe solubility values for aerosol samples contained in the Sholkovitz et al. (2012) data set

	Region				
Method	N. Atlantic	S. Atlantic	N. Pacific	N. Indian	All oceans
All TFe concentrations					
All methods	2.6 (419)	3.2 (91)	4.2 (270)	3.6 (157)	3.1 (960)
MQ	5.0 (150)		7.0 (122)	6.6 (112)	6.0 (384)
Acetate	2.0 (198)	3.2 (91)			2.5 (296)
Formate	2.2 (66)		1.4 (58)	1.4 (26)	1.7 (150)
Seawater	3.2 (5)		3.6 (90)	0.3 (19)	2.3 (121)
1–<10 ng TFe m^{-3}					
MQ	9.6 (34)		20 (5)		10.0 (39)
Acetate	15 (13)	10 (9)			10.0 (25)
Formate	4.6 (8)		6.1 (15)		6.1 (23)
Seawater			7.0 (7)		6.6 (12)
10–<100 ng TFe m^{-3}					
MQ	5.8 (79)		8.1 (46)	24 (26)	8.6 (151)
Acetate	4.1 (64)	3.6 (69)			3.7 (137)
Formate	2.3 (13)		1.2 (31)		1.5 (44)
Seawater	3.5 (4)		5.0 (46)		4.6 (52)
100–<1,000 ng TFe m^{-3}					
MQ	1.0 (32)		7.8 (44)	5.3 (77)	5.2 (153)
Acetate	1.7 (79)	2.3 (13)			1.8 (92)
Formate	1.7 (41)		1.1 (12)	1.5 (22)	1.5 (75)
Seawater	2.6 (1)		1.4 (17)	1.0 (11)	1.2 (29)
1,000–<10,000 ng TFe m^{-3}					
MQ	5.0 (5)		0.9 (27)	1.7 (9)	1.2 (41)
Acetate	0.7 (42)				0.7 (42)
Formate	2.4 (4)			1.0 (4)	1.4 (8)
Seawater			0.6 (20)	0.2 (8)	0.3 (28)

Values are given for the whole data and for subsets of the data obtained using Fe dissolution into ultrapure water (MQ), pH 4.7 ammonium acetate buffer (Acetate), pH 4.2 formate buffer (Formate) and seawater (Seawater). The data is also further subdivided according to the total atmospheric Fe concentration of the samples

Sholkovitz et al. 2009, 2012) have linked high Fe solubility in samples collected from the western North Atlantic region to anthropogenic Fe emissions, using V (and Ni) as tracers for combustion-derived Fe. While this source is not strictly "dust", this does suggest that there is some anthropogenic influence on Fe solubility, and this influence is most likely to be significant at low dust concentrations.

Similar hyperbolic solubility – concentration relationships have been identified for other dust components (e.g. Al, P and Si in aerosol (Baker and Jickells 2006), Al in rainfall (Prospero et al. 1987)). In Fig. 4.5, we show percentage solubility – total element concentration relationships for Fe, Al, Mn, P and Si for samples collected over the Atlantic Ocean. Symbols in Fig. 4.5 indicate source regions for the samples, based on 5-day air mass back trajectories (see Baker et al. 2006). While these

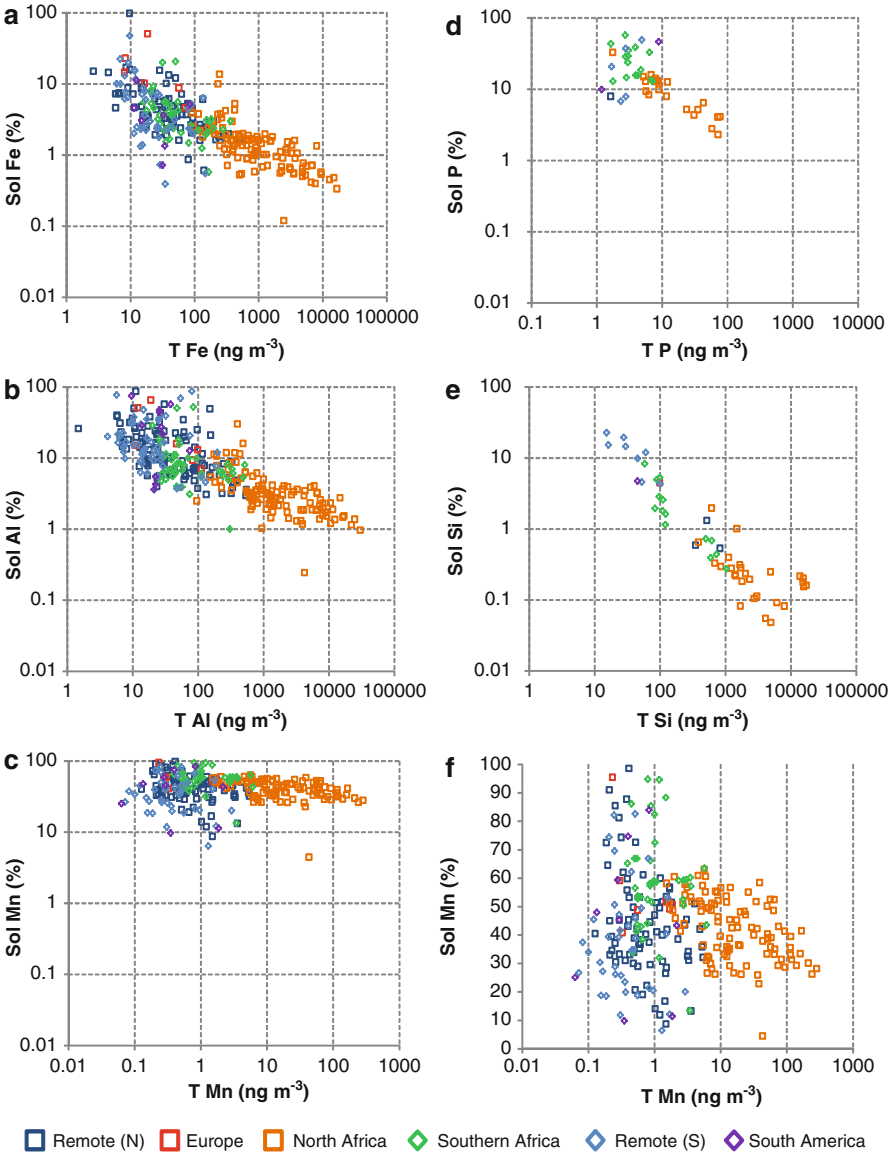

Fig. 4.5 Percentage elemental solubility plotted as a function of total atmospheric elemental concentration for (**a**) Fe, (**b**) Al, (**c**) Mn, (**d**) P and (**e**) Si (all on log–log scales) for aerosol samples collected over the North and South Atlantic. Fe data (**a**) is the ammonium acetate leach data from Fig. 4.3, and the Al and Mn data (**b**, **c**) were obtained from the same samples, using the same methods. P and Si data are from a subset of the samples in **a**–**c** (n = 44 and 54 for P and Si, respectively), using a solution buffered at pH 7 for extraction of soluble P and Si. Total Si (**e**) was estimated from total Al, using the Si/Al ratio of Saharan dust aerosol at Sal, Cape Verde (Chiapello et al. 1997). (**f**) is the same as (**c**) with a linear scale for the y-axis

indicate that different source regions appear to have characteristic solubilities (see Baker et al. 2006), for Fe, Al, P and Si, it would appear that solubility varies strongly with total element concentration, as noted above. The solubility of Mn, however, does not exhibit the same hyperbolic relationship with total concentration. Mn solubility varies over a much more restricted range than the other elements and appears to be much less dependent on total Mn concentration (Fig. 4.5c, f). This difference may be related to the association of Mn with different mineral phases and to the tendency of Mn to form oxide coatings on other particles (Potter and Rossman 1979; Guest et al. 2002).

The similarity of the hyperbolic solubility relationships for Fe, Al, P and Si imply that the overall impact of atmospheric processing on solubility is similar for these elements, even if the relationship itself does not give clear evidence for which, if any, of the potential processing mechanisms dominate. However, redox changes can probably be discounted as a major control on solubility (Baker and Croot 2010), since there are no significant differences between redox-active Fe (Fig. 4.5a) and the non-redox-active elements Al, P and Si (Fig. 4.5b, d, e).

If acid processing is a significant control on solubility, some significant differences in dust–acid interactions might be expected in different regions of the world. North African dust is uplifted into air influenced by European and North African sulphur and nitrogen oxide emissions before transport over the Atlantic. In contrast, dust from the great Asian deserts is transported significant distances before encountering high concentrations of acid precursors emitted from the industrialised regions of Southeast Asia. These two regimes imply rather different mechanisms for the interaction of dust and anthropogenic acids, with direct uptake of gaseous species likely to be more important for Asian dust.

4.3.3 Impacts on Atmospheric Composition

Heterogeneous chemistry on dust surfaces leads to uptake and release of several atmospherically important trace gas species, as well as the formation or alteration of secondary coatings on mineral particles. Controlled laboratory experiments on model mineral phases and authentic dusts have demonstrated that these processes can be sensitive to relative humidity, photolysis and the nature of the reactive surface.

Nitric Acid and Nitrogen Oxides

Nitric acid reacts with mineral dust resulting in formation of surface nitrate and gas-phase species including NO, NO_2 and N_2O (Rubasinghege and Grassian 2009). Studies performed on clays and authentic dust samples from Africa and Asia show efficient uptake of nitric acid onto these samples (Hanisch and Crowley 2001).

When oxide surfaces are exposed to NO_2, it reacts with the surface to form nitrite or nitrate at higher NO_2 pressure. In addition, gas-phase NO is produced. Relative humidity and temperature influence the uptake of NO_2 by clays and soil samples (Zhang et al. 2012). Heterogeneous hydrolysis of NO_2 on silicate surfaces produces HONO and NO, and it was proposed that this reaction does not depend strongly on the nature of surface (Finlayson-Pitts et al. 2003). This suggests that any mineral dust can provide a surface for this reaction. Trace amounts of TiO_2 in the authentic dust can play an important role in NO_2 uptake. When NO_3^- adsorbed on mineral dust surfaces containing TiO_2 is irradiated, NO and NO_2 (NO_x) are detected; however, SiO_2 does not show NO_x formation. Consequently, TiO_2 is responsible for NO_x production (Ndour et al. 2009). NO_2 uptake on TiO_2 as well as Saharan sand samples shows a significant increase under irradiation.

NO adsorption on TiO_2 in the presence of molecular oxygen leads to the formation of surface adsorbed nitrate and NO^+ (Hadjiivanov and Knozinger 2000). Heterogeneous reaction of NO with adsorbed nitric acid is a significant source of HONO in polluted areas. Besides, this reaction also converts nitric acid to NO_x (Saliba et al. 2000). The exposure of surface nitrate-coated aluminium oxide to gaseous hydrogen chloride (HCl) yields several gas-phase products, including NOCl, NO_2 and HNO_3 under dry or NO and N_2O under humid conditions.

Daytime photochemistry of dust-adsorbed nitrogen species can be responsible for formation of HONO, a precursor to the hydroxyl radical. Adsorbed molecular HNO_3 undergoes photolysis to form HONO or HONO and H_2O_2 in the presence of water (Ramazan et al. 2006). As the relative humidity decreases, the adsorbed HONO reacts with adsorbed nitric acid to form NO_2. Photolysis of surface nitrate yields only NO_2, NO and N_2O on Al_2O_3 (Rubasinghege and Grassian 2009), but HONO on SiO_2 (Ma et al. 2011). The latter can account for the presence of HONO in the dust-laden atmosphere. TiO_2 photocatalysis is another potential source of daytime HONO, a process which shows a strong dependence on the relative humidity (RH) (Gustafsson et al. 2006). Another mechanism of HONO formation involves heterogeneous photochemistry of NO_2 on soil particles and ice films coated with humic substances (Bartels-Rausch et al. 2010).

Sulphur Species

Sulphur dioxide adsorbs irreversibly on mineral oxides and authentic aerosol samples to form surface sulphite, bisulphite and sulphate, and this process is significantly enhanced in the presence of adsorbed water. Atmospheric sulphur dioxide can be oxidised to sulphate or sulphuric acid on dust surfaces (Usher et al. 2002; Wu et al. 2011). Iron compounds are responsible for the removal of SO_2 from gas mixtures with uptake limited to the outer layer of the particles. Adsorbed SO_2 oxidises on the surface of most iron oxides to form a bidentate or monodentate surface sulphate species. The reaction of SO_2 on the surface of mixed particles of Fe_2O_3 and NaCl mainly produces sulphate/bisulphate species. Oxidation of sulphur dioxide into sulphate readily occurs on TiO_2 yielding adsorbed sulphite in the dark

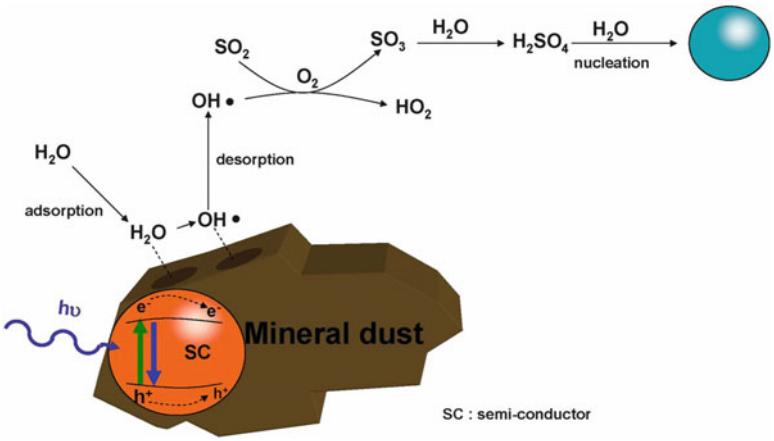

Fig. 4.6 The semiconductor (SC) components of dust under UV irradiation are producing OH radicals that can desorb and oxidise SO_2. The produced sulphuric acid may then initiate nucleation events (Reprinted with permission from Dupart et al. (2012). Copyright (2012) National Academy of Sciences, USA)

and adsorbed sulphate under irradiation (Rubasinghege et al. 2010). Reaction of calcium carbonate with sulphur dioxide leads to formation of adsorbed sulphite. This reaction is enhanced in the presence of water as reviewed in Rubasinghege and Grassian (2013).

Carbonyl sulphide (OCS) is one of the most abundant sulphur compounds in the atmosphere. It can be catalytically oxidised on mineral oxides to produce surface SO_4^{2-} species and gaseous CO_2. Reversible and irreversible adsorption of OCS is observed on α-Fe_2O_3 and ZnO, respectively, whereas no uptake is observed on SiO_2 and TiO_2. On kaolinite OCS can only be reversibly adsorbed at Al-OH sites. The hydrolysis of OCS and succeeding oxidation of intermediate products readily takes place on α-Al_2O_3, MgO and CaO (Liu et al. 2010). On the surface of hematite, the adsorbed OCS is oxidised, forming surface hydrogen thiocarbonate, carbonate and sulphate species and gaseous CO_2 (Chen et al. 2007).

We have discussed above that sulphur dioxide forms sulphate ions on the surface of dust particles. However, there is evidence for an alternate pathway in which a series of reactions under solar light causes formation of gaseous sulphuric acid as an intermediate product leading either to surface-bound sulphate production or nucleation. This photocatalytic mechanism is based on the presence of semiconductor metal oxides in mineral dust with a band gap (the difference in energy between the valence and conduction bands) within the solar spectrum. The production of electron–hole pairs at the semiconductor surface upon excitation enables these minerals to act as photocatalysts, leading to the formation of reactive species such as OH radicals in the gas phase. These OH radicals can initiate the conversion of SO_2 to H_2SO_4 and subsequently new particle formation as shown in Fig. 4.6 (Dupart et al. 2012). New particle formation is usually inhibited during a dust event; however,

there is a decoupling between nucleation and growth (Kulmala et al. 2000), which allows formation of new aerosol particles even during high dust loadings.

Ozone

Trace amounts of TiO_2 may be responsible for ozone loss. Doping of SiO_2 with TiO_2 increases ozone decomposition (Nicolas et al. 2009), and TiO_2-containing Saharan dust shows irreversible ozone uptake (Hanisch and Crowley 2003). Ozone decay rate is significantly higher under irradiation compared to dark conditions, indicating that this reaction is also photoinduced.

Heterogeneous photochemistry of O_3 depends on the surface properties of oxides. For example, Fe_2O_3 shows high uptake capacity and catalytic decomposition towards O_3, but Al_2O_3 is deactivated by O_3 exposure. The photoenhancement of O_3 decomposition on Fe_2O_3 is explained by its semiconductor properties. Irradiation of Fe_2O_3 with UV photons having energies higher than 2.2 eV creates electron–hole pairs, which initiate photochemical reactions. Since mineral dust aerosol can contain a variety of semiconductor metal oxides, such as TiO_2, ZnO and Fe_2O_3, heterogeneous photodecomposition of O_3 may be an important path of ozone loss in the troposphere.

Other Inorganic and Organic Species

Adsorption of hydrogen peroxide on SiO_2 and $CaCO_3$ is mainly reversible. Metal oxides exhibit catalytic behaviour towards the decomposition of hydrogen peroxide, while SiO_2 does not (Wang et al. 2011). The uptake of hydrogen peroxide by TiO_2 was found to decrease at higher RH, while irradiation enhances H_2O_2 decomposition with formation of HO_2 intermediate (Yi et al. 2012).

Adsorption of acidic gases on calcium carbonate under dry conditions shows the formation of carbonic acid on the calcite surface (Al-Hosney and Grassian 2004). The acid is stable over long periods at low temperatures even in the presence of water vapour (Bernard et al. 2012). Thus, in the high troposphere, H_2CO_3 may be adsorbed on mineral dust particles.

Organic compounds are often associated with dust particles (Lee et al. 2002; Russell et al. 2002) and adsorption of organics on minerals is an important process. Adsorption of carbonyls on SiO_2 particles is nonreactive and reversible (Carlos-Cuellar et al. 2003), but it is irreversible on other oxides (α-Al_2O_3, TiO_2, α-Fe_2O_3, SiO_2 and CaO) (Xu et al. 2006). Carbonyl compounds can undergo photolysis and react with OH radicals, yielding peroxy radicals and peroxyacetyl nitrates (PAN) (Li et al. 2001).

Multiple studies show that tropospheric particles are often associated with organic acids (Lee et al. 2002). Dissociation of formic acid yields mono- and bidentate formate species. The adsorption of acetic acid produces both molecularly adsorbed acetic acid and acetate groups (Takeuchi et al. 2010). The extent of the

reaction varies with the mineral phase of the particles. For α-Al_2O_3, the reaction is limited to the surface, while for MgO the bulk of the particle is involved. For $CaCO_3$, acetic acid uptake is limited to the surface under dry conditions, but penetrates to the bulk under humid conditions (Ma et al. 2012). Illumination of environmental surfaces including Fe_2O_3, TiO_2, Mauritanian sand and Icelandic volcanic ash with adsorbed oxalic acid produces gas-phase CO_2 (Styler and Donaldson 2012).

4.4 Conclusion

Atmospheric processing of mineral dust leads to evolution of many dust physicochemical properties during transport. Heterogeneous chemistry, in particular, has profound effects on dust morphology, optical properties and nutrient availability and alters atmospheric composition. These changes influence the direct and indirect effects of dust on climate. Therefore, comprehensive understanding of the effect of mineral dust on climate requires detailed knowledge of dust mineralogy and the changes in chemical composition and properties that take place during global transport and atmospheric processing.

References

Aguilar-Islas AM, Wu JF, Rember R, Johansen AM, Shank LM (2010) Dissolution of aerosol-derived iron in seawater: leach solution chemistry, aerosol type, and colloidal iron fraction. Mar Chem 120:25–33

Al-Hosney HA, Grassian VH (2004) Carbonic acid: an important intermediate in the surface chemistry of calcium carbonate. J Am Chem Soc 126:8068–8069

Arimoto R, Ray BJ, Lewis NF, Tomza U, Duce RA (1997) Mass-particle size distributions of atmospheric dust and the dry deposition of dust to the remote ocean. J Geophys Res 102:15867–15874

Baker AR, Croot PL (2010) Atmospheric and marine controls on aerosol iron solubility in seawater. Mar Chem 120:4–13

Baker AR, Jickells TD (2006) Mineral particle size as a control on aerosol iron solubility. Geophys Res Lett 33, L17608. doi:10.1029/2006GL026557

Baker AR, Jickells TD, Witt M, Linge KL (2006) Trends in the solubility of iron, aluminium, manganese and phosphorus in aerosol collected over the Atlantic Ocean. Mar Chem 98:43–58

Bartels-Rausch T, Brigante M, Elshorbany YF, Ammann M, D'Anna B, George C et al (2010) Humic acid in ice photo-enhanced conversion of nitrogen dioxide into nitrous acid. Atmos Environ 44:5443–5450

Bernard J, Seidl M, Mayer E, Loerting T (2012) Formation and stability of bulk carbonic acid (H_2CO_3) by protonation of tropospheric calcite. Chemphyschem 13:3087–3091

Betzer PR, Carder KL, Duce RA, Merrill JT, Tindale NW, Uematsu M et al (1988) Long-range transport of giant mineral aerosol particles. Nature 336:568–571

Bullard JE, McTainsh GH, Pudmenzky C (2004) Aeolian abrasion and modes of fine particle production from natural red dune sands: an experimental study. Sedimentology 51:1103–1125

Carlos-Cuellar S, Li P, Christensen AP, Krueger BJ, Burrichter C, Grassian VH (2003) Heterogeneous uptake kinetics of volatile organic compounds on oxide surfaces using a Knudsen cell reactor: adsorption of acetic acid, formaldehyde, and methanol on α-Fe_2O_3, α-Al_2O_3, and SiO_2. J Phys Chem A 107:4250–4261

Chen Y, Siefert RL (2004) Seasonal and spatial distributions and dry deposition fluxes of atmospheric total and labile iron over the tropical and subtropical North Atlantic Ocean. J Geophys Res-Atmos 109, D09305. doi:10.1029/2003JD003958

Chen HH, Kong LD, Chen JM, Zhang RY, Wang L (2007) Heterogeneous uptake of carbonyl sulfide on hematite and hematite-NaCl mixtures. Environ Sci Technol 41:6484–6490

Chiapello I, Bergametti G, Chatenet B, Bousquet P, Dulac F, Santos Soares E (1997) Origins of African dust transported over the northeastern tropical Atlantic. J Geophys Res 102:13701–13709

Crumeyrolle S, Gomes L, Tulet P, Matsuki A, Schwarzenboeck A, Crahan K (2008) Increase of the aerosol hygroscopicity by cloud processing in a mesoscale convective system: a case study from the AMMA campaign. Atmos Chem Phys 8:6907–6924

Cwiertny DM, Baltrusaitis J, Hunter GJ, Laskin A, Scherer MM, Grassian VH (2008) Characterization and acid-mobilization study of iron-containing mineral dust source materials. J Geophys Res 113, D05202. doi:10.1029/2007JD009332

Desboeufs KV, Losno R, Colin JL (2001) Factors influencing aerosol solubility during cloud processes. Atmos Environ 35:3529–3537

Dupart Y, King SM, Nekat B, Nowak A, Wiedensohler A, Herrmann H et al (2012) Mineral dust photochemistry induces nucleation events in the presence of SO_2. Proc Natl Acad Sci U S A 109:20842–20847

Erel Y, Pehkonen SO, Hoffmann MR (1993) Redox chemistry of iron in fog and stratus clouds. J Geophys Res 98:18423–18434

Finlayson-Pitts BJ, Wingen LM, Sumner AL, Syomin D, Ramazan KA (2003) The heterogeneous hydrolysis of NO_2 in laboratory systems and in outdoor and indoor atmospheres: an integrated mechanism. Phys Chem Chem Phys 5:223–242

Formenti P, Schütz L, Balkanski Y, Desboeufs K, Ebert M, Kandler K et al (2011) Recent progress in understanding physical and chemical properties of African and Asian mineral dust. Atmos Chem Phys 11:8231–8256

Gibson ER, Hudson PK, Grassian VH (2006) Physicochemical properties of nitrate aerosols: implications for the atmosphere. J Phys Chem A 110:11785–11799

Gierlus KM, Laskina O, Abernathy TL, Grassian VH (2012) Laboratory study of the effect of oxalic acid on the cloud condensation nuclei activity of mineral dust aerosol. Atmos Environ 46:125–130

Glaccum RA, Prospero JM (1980) Saharan aerosols over the tropical North Atlantic – mineralogy. Mar Geol 37:295–321

Guest CA, Schulze DG, Thompson IA, Huber DM (2002) Correlating manganese X-ray absorption near-edge structure spectra with extractable soil manganese. Soil Sci Soc Am J 66:1172–1181

Guieu C, Bonnet S, Wagener T, Loye-Pilot MD (2005) Biomass burning as a source of dissolved iron to the open ocean? Geophys Res Lett 32, L19608. doi:10.1029/2005GL022962

Gustafsson RJ, Orlov A, Griffiths PT, Cox RA, Lambert RM (2006) Reduction of NO_2 to nitrous acid on illuminated titanium dioxide aerosol surfaces: implications for photocatalysis and atmospheric chemistry. Chem Commun 37:3936–3938

Hadjiivanov K, Knozinger H (2000) Species formed after NO adsorption and $NO + O_2$ co-adsorption on TiO_2: an FTIR spectroscopic study. Phys Chem Chem Phys 2:2803–2806

Hanisch F, Crowley JN (2001) Heterogeneous reactivity of gaseous nitric acid on Al_2O_3, $CaCO_3$, and atmospheric dust samples: a Knudsen cell study. J Phys Chem A 105:3096–3106

Hanisch F, Crowley JN (2003) Ozone decomposition on Saharan dust: an experimental investigation. Atmos Chem Phys 3:119–130

Ito A (2013) Global modeling study of potentially bioavailable iron input from shipboard aerosol sources to the ocean. Global Biogeochem Cycles 27:1–10. doi:10.1029/2012GB004378

Johnson MS, Meskhidze N, Solmon F, Gasso S, Chuang PY, Gaiero DM et al (2010) Modeling dust and soluble iron deposition to the South Atlantic Ocean. J Geophys Res 115, D15202. doi:10.1029/2009JD013311

Journet E, Desboeufs KV, Caquineau S, Colin JL (2008) Mineralogy as a critical factor of dust iron solubility. Geophys Res Lett 35, L07805. doi:10.1029/2007GL031589

Kim J-S, Park K (2012) Atmospheric aging of Asian dust particles during long range transport. Aerosol Sci Tech 46:913–924

Kulmala M, Pirjola U, Makela JM (2000) Stable sulphate clusters as a source of new atmospheric particles. Nature 404:66–69

Lee SH, Murphy DM, Thomson DS, Middlebrook AM (2002) Chemical components of single particles measured with Particle Analysis by Laser Mass Spectrometry (PALMS) during the Atlanta SuperSite Project: focus on organic/sulfate, lead, soot, and mineral particles. J Geophys Res-Atmos 107:4003. doi:10.1029/2000JD000011

Li P, Perreau KA, Covington E, Song CH, Carmichael GR, Grassian VH (2001) Heterogeneous reactions of volatile organic compounds on oxide particles of the most abundant crustal elements: surface reactions of acetaldehyde, acetone, and propionaldehyde on SiO_2, Al_2O_3, Fe_2O_3, TiO_2, and CaO. J Geophys Res-Atmos 106:5517–5529

Liu Y, Ma J, He H (2010) Heterogeneous reactions of carbonyl sulfide on mineral oxides: mechanism and kinetics study. Atmos Chem Phys 10:10335–10344

Ma J, Liu Y, He H (2011) Heterogeneous reactions between NO_2 and anthracene adsorbed on SiO_2 and MgO. Atmos Environ 45:917–924

Ma Q, Liu Y, Liu C, He H (2012) Heterogeneous reaction of acetic acid on MgO, α-Al_2O_3, and $CaCO_3$ and the effect on the hygroscopic behaviour of these particles. Phys Chem Chem Phys 14:8403–8409

Mackie DS, Boyd PW, Hunter KA, McTainsh GH (2005) Simulating the cloud processing of iron in Australian dust: pH and dust concentration. Geophys Res Lett 32, L06809. doi:10.1029/2004GL022122

Mackie DS, Peat JM, McTainsh GH, Boyd PW, Hunter KA (2006) Soil abrasion and eolian dust production: implications for iron partitioning and solubility. Geochem Geophys Geosyst 7, Q12Q03. doi:10.1029/2006GC001404

Mahowald NM, Baker AR, Bergametti G, Brooks N, Duce RA, Jickells TD et al (2005) The atmospheric global dust cycle and iron inputs to the ocean. Global Biogeochem Cycles 19, GB4025. doi:10.1029/2004GB002402

Maring H, Savoie DL, Izaguirre MA, Custals L, Reid JS (2003) Mineral dust aerosol size distribution change during atmospheric transport. J Geophys Res 108:8592. doi:10.1029/2002JD002536

Meskhidze N, Chameides WL, Nenes A, Chen G (2003) Iron mobilization in mineral dust: can anthropogenic SO_2 emissions affect ocean productivity? Geophys Res Lett 30:2085. doi:10.1029/2003GL018035

Morton P, Landing WM, Hsu SC, Milne A, Aguilar-Islas AM, Baker AR et al (2013) Methods for sampling and analysis of marine aerosols: results from the 2008 GEOTRACES aerosol intercalibration experiment. Limnol Oceanogr-Methods 11:62–78

Ndour M, Conchon P, D'Anna B, Ka O, George C (2009) Photochemistry of mineral dust surface as a potential atmospheric renoxification process. Geophys Res Lett 36, L05816. doi:10.1029/2008GL036662

Nenes A, Krom MD, Mihalopoulos N, Van Cappellen P, Shi Z, Bougiatioti A et al (2011) Atmospheric acidification of mineral aerosols: a source of bioavailable phosphorus for the oceans. Atmos Chem Phys 11:6265–6272

Nicolas M, Ndour M, Ka O, D'Anna B, George C (2009) Photochemistry of atmospheric dust: ozone decomposition on illuminated titanium dioxide. Environ Sci Technol 43:7437–7442

Pehkonen SO, Siefert R, Erel Y, Webb S, Hoffmann MR (1993) Photoreduction of iron oxyhydroxides in the presence of important atmospheric organic-compounds. Environ Sci Technol 27:2056–2062

Potter RM, Rossman GR (1979) The manganese- and iron-oxide mineralogy of desert varnish. Chem Geol 25:79–94

Prospero JM, Nees RT, Uematsu M (1987) Deposition rate of particulate and dissolved aluminum derived from Saharan dust in precipitation at Miami, Florida. J Geophys Res 92:14723–14731

Ramazan KA, Wingen LM, Miller Y, Chaban GM, Gerber RB, Xantheas SS et al (2006) New experimental and theoretical approach to the heterogeneous hydrolysis of NO_2: key role of molecular nitric acid and its complexes. J Phys Chem A 110:6886–6897

Reid JS, Jonsson HH, Maring HB, Smirnov A, Savoie DL, Cliff SS et al (2003) Comparison of size and morphological measurements of coarse mode dust particles from Africa. J Geophys Res 108:8593. doi:10.1029/2002JD002485

Rubasinghege G, Grassian VH (2009) Photochemistry of adsorbed nitrate on aluminum oxide particle surfaces. J Phys Chem A 113:7818–7825

Rubasinghege G, Grassian VH (2013) Role(s) of adsorbed water in the surface chemistry of environmental interfaces. Chem Commun 30:3071–3094

Rubasinghege G, Lentz RW, Scherer MM, Grassian VH (2010) Simulated atmospheric processing of iron oxyhydroxide minerals at low pH: roles of particle size and acid anion in iron dissolution. Proc Natl Acad Sci U S A 107:6628–6633

Russell LM, Maria SF, Myneni SCB (2002) Mapping organic coatings on atmospheric particles. Geophys Res Lett 29:1779. doi:10.1029/2002GL014874

Saliba NA, Mochida M, Finlayson-Pitts BJ (2000) Laboratory studies of sources of HONO in polluted urban atmospheres. Geophys Res Lett 27:3229–3232

Schulz M, Balkanski YJ, Guelle W, Dulac F (1998) Role of aerosol size distribution and source location in a three-dimensional simulation of a Saharan dust episode tested against satellite-derived optical thickness. J Geophys Res-Atmos 103:10579–10592

Sedwick PN, Sholkovitz ER, Church TM (2007) Impact of anthropogenic combustion emissions on the fractional solubility of aerosol iron: evidence from the Sargasso Sea. Geochem Geophys Geosyst 8, Q10Q06. doi:10.1029/2007GC001586

Shi Z, Krom MD, Bonneville S, Baker AR, Jickells TD, Benning LG (2009) Formation of iron nanoparticles and increase in iron reactivity in mineral dust during simulated cloud processing. Environ Sci Technol 43:6592–6596

Shi Z, Bonneville S, Krom MD, Carslaw KS, Jickells TD, Baker AR et al (2011) Iron dissolution kinetics of mineral dust at low pH during simulated atmospheric processing. Atmos Chem Phys 11:995–1007

Sholkovitz ER, Sedwick PN, Church TM (2009) Influence of anthropogenic combustion emissions on the deposition of soluble aerosol iron to the ocean: empirical estimates for island sites in the North Atlantic. Geochim Cosmochim Acta 73:3981–4003

Sholkovitz ER, Sedwick PN, Church TM, Baker AR, Powell CF (2012) Fractional solubility of aerosol iron: synthesis of a global-scale data set. Geochim Cosmochim Acta 89:173–189

Siefert RL, Pehkonen SO, Erel Y, Hoffmann MR (1994) Iron photochemistry of aqueous suspensions of ambient aerosol with added organic acids. Geochim Cosmochim Acta 58:3271–3279

Spokes LJ, Jickells TD (1996) Factors controlling the solubility of aerosol trace metals in the atmosphere and on mixing into seawater. Aquat Geochem 1:355–374

Spokes LJ, Jickells TD, Lim B (1994) Solubilisation of aerosol trace metals by cloud processing: a laboratory study. Geochim Cosmochim Acta 58:3281–3287

Styler SA, Donaldson DJ (2012) Heterogeneous photochemistry of oxalic acid on Mauritanian sand and Icelandic volcanic ash. Environ Sci Technol 46:8756–8763

Sullivan RC, Moore MJK, Petters MD, Kreidenweis SM, Roberts GC, Prather KA (2009) Effect of chemical mixing state on the hygroscopicity and cloud nucleation properties of calcium mineral dust particles. Atmos Chem Phys 9:3303–3316

Sullivan RC, Petters MD, DeMott PJ, Kreidenweis SM, Wex H, Niedermeier D et al (2010) Irreversible loss of ice nucleation active sites in mineral dust particles caused by sulphuric acid condensation. Atmos Chem Phys 10:11471–11487

Takeuchi M, Deguchi J, Sakai S, Anpo M (2010) Effect of H_2O vapor addition on the photocatalytic oxidation of ethanol, acetaldehyde and acetic acid in the gas phase on TiO_2 semiconductor powders. Appl Catal B-Environ 96:218–223

Theodosi C, Markaki Z, Mihalopoulos N (2010) Iron speciation, solubility and temporal variability in wet and dry deposition in the Eastern Mediterranean. Mar Chem 120:100–107

Usher CR, Al-Hosney H, Carlos-Cuellar S, Grassian VH (2002) A laboratory study of the heterogeneous uptake and oxidation of sulfur dioxide on mineral dust particles. J Geophys Res-Atmos 107:4713. doi:10.1029/2002JD002051

Usher CR, Michel AE, Grassian VH (2003) Reactions on mineral dust. Chem Rev 103(12):4883–4939

Wang W-G, Ge M-F, Sun Q (2011) Heterogeneous uptake of hydrogen peroxide on mineral oxides. Chin J Chem Phys 24:515–520

Witt MLI, Mather TA, Baker AR, de Hoog C-J, Pyle DM (2010) Atmospheric trace metals over the south-west Indian Ocean: total gaseous mercury, aerosol trace metal concentrations and lead isotope ratios. Mar Chem 121:2–16

Wu LY, Tong SR, Wang WG, Ge MF (2011) Effects of temperature on the heterogeneous oxidation of sulfur dioxide by ozone on calcium carbonate. Atmos Chem Phys 11:6593–6605

Xu B-Y, Zhu T, Tang X-Y, Ding J, Li H-J (2006) Heterogeneous reaction of formaldehyde on surface of α-Al_2O_3 particles. Chem J Chin Univ-Chin 27:1912–1917

Yi J, Bahrini C, Schoemaecker C, Fittschen C, Choi W (2012) Photocatalytic decomposition of H_2O_2 on different TiO_2 surfaces along with the concurrent generation of HO_2 radicals monitored using cavity ring down spectroscopy. J Phys Chem C 116:10090–10097

Yin Y, Wurzler S, Levin Z, Reisin TG (2002) Interactions of mineral dust particles and clouds: effects on precipitation and cloud optical properties. J Geophys Res-Atmos 107:4724. doi:10.1029/2001JD001544

Zhang Z, Shang J, Zhu T, Li H-J, Zhao D, Liu Y et al (2012) Heterogeneous reaction of NO_2 on the surface of montmorillonite particles. J Environ Sci-China 24:1753–1758

Chapter 5
Dust Production Mechanisms

Beatrice Marticorena

Abstract This chapter is concerned with dust production mechanisms, that is, the interactions between the wind and the surface that lead to the emission of fine soil particles. Mineral dust emissions mainly result from wind erosion in the arid and semi-arid regions of the world. Wind is thus the main driver of emissions, but surface characteristics also play a key role for their spatial distribution, intensity and frequency. This chapter describes the main stages involved in dust emission: the erosion threshold, the saltation flux and the dust production by sandblasting, with a focus on the influence of the surface characteristics. For each of these stages, the involved physical processes and their parameterisations are described with a discussion on their limitations. The first stage, the erosion threshold, corresponds to the minimum wind velocity that must be reached for the initiation of soil particle movement. This threshold depends on the soil properties (size distribution and moisture) and surface roughness. It is a key parameter for dust emission, since it controls the frequency of dust emission events. The horizontal motion of soil particles close to the surface is mainly a saltation motion, where soil particles rebound on the surface and initiate the movement of other soil particles. These rebounds also lead to the ejection of fine dust particles from the surface or the saltating aggregates, which correspond to the sandblasting process. Recent field measurements show that saltation is a prerequisite for intense dust emissions. While the erosion threshold and the saltation flux are well understood and reasonably quantified, the amount and size of the dust emitted by sandblasting and their dependence on soil properties and wind intensity are still insufficiently described to provide reliable parameterisations. Significant progresses in the description and parameterisation of dust emission processes have been achieved in the last 20 years, which allow a better understanding of the properties that makes specific areas active

B. Marticorena (✉)
Laboratoire Interuniversitaire des Systèmes Atmosphériques, UMR CNRS 7583, Universités Paris Est – Paris Diderot, IPLS, Créteil, France
e-mail: beatrice.marticorena@lisa.u-pec.fr

P. Knippertz and J.-B.W. Stuut (eds.), *Mineral Dust: A Key Player in the Earth System*, DOI 10.1007/978-94-017-8978-3_5,

or non-active dust sources. However, additional investigation on the saltation and sandblasting processes, both from a theoretical and experimental point of view, is still needed. Special attention must be paid to the link with soil properties and its implications on the size distribution of the emitted dust.

Keywords Erosion threshold • Dust production • Soil moisture • Surface roughness • Particle size • Dust emission • Surface • Saltation • Numerical models • Field observations

5.1 Introduction

Aeolian erosion in arid and semi-arid regions is the main source of atmospheric dust particles. Mineral dust represents about 40 % of the global annual emissions of tropospheric aerosols (IPCC 2007). Mineral dust can be transported thousands of kilometres away from its sources. In the atmosphere, mineral dust has a significant impact on the Earth radiative budget by scattering radiation in the visible range and absorbing it in the infrared (IR) (see Chaps. 11 and 13). This radiative impact induces interactions with local and regional dynamics that can affect, for example, the quality of meteorological forecasts over West Africa (Tompkins et al. 2005). Mineral dust is now included in forecasting models (e.g. Milton et al. 2008) to improve climate projections and the simulations of dust storms and visibility (see Chap. 10). On a longer timescale, the soil loss due to dust export from arid and semi-arid regions contributes to desertification processes (Rajot 2001). On the opposite, dust deposition can be a significant source of nutrients or micronutrients (phosphorus, iron, etc.) for remote oceanic or continental ecosystems (e.g. Jickells et al. 2005; Mahowald et al. 2008; see Chap. 14). Inside and close to source regions, dust storms are responsible for severe reductions of the horizontal visibility, which induce social and economical impacts by affecting, for example, aerial and terrestrial traffic (e.g. Pauley et al. 1996). Finally, mineral dust can have sanitary impacts in source and transport regions (see Chap. 15). As an example, mineral dust is suspected to play a role in meningitis epidemics in the Sahelian region (e.g. Thomson et al. 2006; Agier et al. 2013; Martiny and Chiapello 2013).

Uncertainties in the evaluation of mineral dust impacts are in large part due to its spatial and temporal distribution. Surface concentrations vary over several orders of magnitude (0.001–1,000 $\mu g\ m^{-3}$) as a function of the distance to the dust sources (Marticorena and Formenti 2013). This variability is largely due to dust emission. Current estimates of mineral dust emissions are mainly derived from modelling approaches. The simulated global dust emissions reported from the intercomparison exercise of the AEROCOM project (http://aerocom.met.no/) range between 500 and 3,000 Mt $year^{-1}$ with a median value of ~1,500 Mt $year^{-1}$ and a standard deviation of 1,000 Mt $year^{-1}$ (Huneeus et al. 2011). The ratio between the median estimation and the standard deviation is lower than 80 % for the main dust source regions of the northern hemisphere (North Africa, Middle East, Asia) but much higher for the

dust sources of the southern hemisphere (Australia, South America, South Africa). These numbers show that the quantification of dust emissions is very uncertain, both at the regional and at the global scale. These uncertainties are largely due to the way dust emissions are represented in 3-D models, which in turn depends on our understanding of dust production mechanisms and our capability to parameterise them. In the following, the general understanding of the dust emission processes, the way the different physical processes involved in dust emissions are modelled, and the present limitations are discussed. The link between dust production mechanisms and actual dust sources is also discussed briefly.

5.2 General Understanding

Dust emission is the final "product" of a succession of processes involved in aeolian erosion of soils. Subsequently, describing dust emission means describing the physical processes involved in soil erosion and the environmental factors that influence them (e.g. Greeley and Iversen 1985). A detailed description of the physics of sand movement and dust emission processes and their modelling can be found in Shao (2001).

Aeolian erosion is a direct function of the wind velocity, but occurs only when a threshold value has been reached. This erosion threshold results from the fact that soil particles are subject to forces holding them at the surface: their weight and interparticle cohesion forces I_p. Interparticle forces can be reinforced by the presence of water in the soil and as a result, the erosion threshold increases when soil moisture increases. This threshold also depends on the presence of non-erodible roughness elements, which cover and protect part of the surface and absorb a fraction of the wind momentum, which otherwise would have been available to initiate particle motion.

The wind shear stress τ acting on a horizontal surface can be related to the vertical gradient of wind velocity U (Greeley and Iversen 1985), as schematically illustrated in Fig. 5.1 and expressed in Eq. 5.1:

$$\tau = \mu \, (\partial U / \partial z) \tag{5.1}$$

Where U is the wind velocity at the height z, and μ is the dynamical viscosity of the air.

The wind shear stress can also be expressed as a function of the wind friction velocity U^*, which is the parameter most commonly used in aeolian erosion studies:

$$\tau = \rho_a U^{*2} \tag{5.2}$$

where ρ_a is the air density.

The wind velocity is defined at a given height z above the surface, while U^* is related to the vertical gradient of the wind velocity. In neutral conditions (no gradient

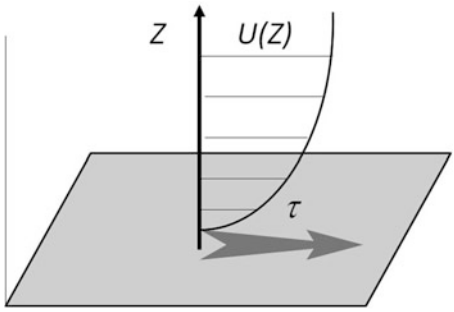

Fig. 5.1 Schematic representation of the surface wind shear stress and of the vertical profile of wind velocity (Alfaro 1997)

in air potential temperature), the wind velocity can be expressed by a logarithmic profile (Priestley 1959):

$$\text{for } z > Z_0, \quad U(z) = \frac{U^*}{k} \ln (z/Z_0) \tag{5.3}$$

with k the von Karman constant ($= 0.4$) and Z_0 the aerodynamic roughness length.

The momentum partitioning due to roughness elements leads to a decrease of the wind shear stress acting on the erodible surface and thus an apparent increase of the threshold wind friction velocity U_t^*. Finally, U_t^* is generally expressed as a combination of a size-dependent term weighted by additional functions describing the influence of surface roughness, soil moisture or other environmental factors (e.g. snow).

Once in motion, the movement of a soil particle depends on its size, shape and density, being controlled by the balance between its terminal fall velocity and the air vertical velocity. The largest or heaviest particles (approx. $D_p > 1{,}000$ μm) generally move along the surface with a creeping motion. Particles with diameters between 70 and 1,000 μm are entrained in a saltating motion: they are ejected from the surface, follow a ballistic trajectory and finally impact the surface downwind. These impacts eject other particles that follow a similar saltation motion. The total amount of material mobilised by the wind in this horizontal movement depends mainly on U^* and the size of the soil particles.

Theoretically, dust particles can directly be lifted from the surface by aerodynamic entrainment (Fig. 5.2, top panel). However, wind-tunnel measurements performed on a dust bed show that such a direct entrainment requires very high U^* ($\sim$0.6–1 m s^{-1}) and that the resulting dust fluxes are one order of magnitude lower than those measured in the field (Loosemore and Hunt 2000). On the opposite, as saltating particles hit the surface, their impacts are strong enough to overcome the binding forces acting upon dust particles, leading to dust emission (Fig. 5.2, middle panel). This mechanism is also known as sandblasting (Gomes et al. 1990; Alfaro et al. 1997). The released particles can originate either from the impacted surface or from the disaggregation of the saltating soil grains (Fig. 5.2, bottom panel). This process is also called "auto-abrasion" (Warren et al. 2007). Recent field campaigns

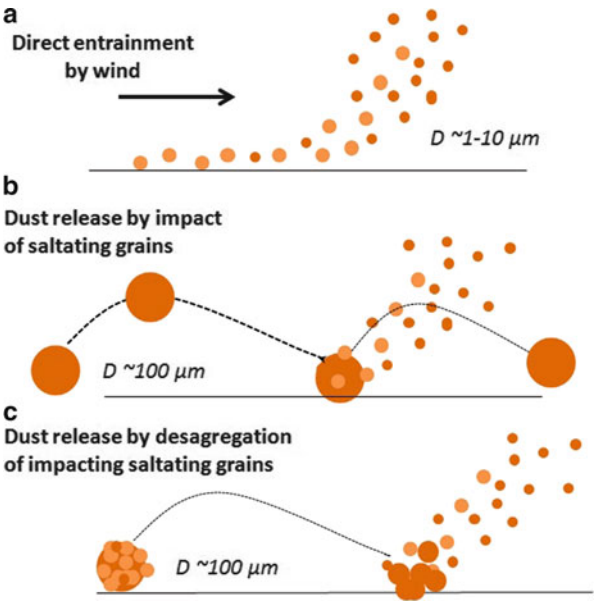

Fig. 5.2 Mechanisms for dust emission. (**a**) Dust emission by aerodynamic lift, (**b**) by saltation bombardment and (**c**) through disaggregation (Adapted from Shao et al. 2011)

have highlighted the importance of saltation as a prerequisite for dust emission (Sow et al. 2009; Shao et al. 2011). Once produced, particles smaller than ~70 μm can be entrained by suspension because their terminal fall velocity is lower than the vertical wind velocity; the smallest fraction ($D < 20$ μm) can easily be uplifted and transported long-range.

In the following sections, the physical processes involved in the main stages of dust emission and the soil and surface properties or environmental factors that influence them are described.

5.3 Erosion Threshold

The threshold for particle motion results from the balance between the wind shear stress, τ, and the forces acting on the soil particles to hold them on the surface. These forces include the particle weight P, interparticle cohesion forces I_p and cohesion forces induced by soil moisture F_c. U_t^* is thus a function of the parameters that control these forces, mainly the particle size and density and the soil moisture.

The generic expression "wind erosion threshold" encompasses several different concepts. First, it corresponds either to a wind velocity at a given height $U(z)$ or to a wind friction velocity U^*, both defined and measured at the erosion threshold. Second, the definition of the threshold can depend on the way it is experimentally determined. Theoretically, it should be the threshold of movement of the first particles set in motion by the action of the fluid (also called the "fluid threshold").

Practically, the erosion threshold determined from experiments is generally a "saltation threshold", that is, the minimal wind velocity for which a sustained particle movement is detected (Iversen and White 1982). This is also the case for field measurements of erosion thresholds performed with sensors that detect the impacts of grains in saltation. Such sensors have detection limits, which generally prevent the detection of the very first particle movement but provide an estimation of the saltation threshold defined as the wind velocity below which the saltation flux is negligible.

5.3.1 *Influence of Soil Particle Size*

For loose and dry soil particles, Bagnold (1941) first proposed an expression of the threshold of movement of soil particles initiated by the wind. It is derived from the balance between τ and particle weight. It expresses the dependence of the erosion threshold with particle diameter D_p and the air and particle density ρ_a and ρ_p, assuming soil particles have a spherical shape. Wind-tunnel measurements have shown an increase of the erosion threshold with decreasing particle size below ~100 μm (Chepil 1951). This increase is explained by an increase of the interparticle cohesion due to electrostatic forces (Iversen et al. 1976). Due to inverse size dependencies of the cohesion forces and particle weight force, there is an optimum particle size (~60 μm) for wind erosion, that is, a particle size for which U_t^* is at a minimum. Assuming the electrostatic cohesion forces as a power function of D_p, Iversen and White (1982) proposed a formulation to predict the saltation U_t^*, fitted on a large set of wind-tunnel measurements for various particle densities and diameters. Shao and Lu (2000) proposed an improved formulation of the erosion threshold based on an explicit physical formulation of the Van der Waals and electrostatic forces involved in the interparticle cohesion forces.

$$U_t^*\left(D_p\right) = \left[A_N\left(\frac{\rho_p g D_p}{\rho_a} + \frac{\gamma}{\rho_a D_p}\right)\right]^{0.5} \tag{5.3}$$

with $A_N = \sqrt{f\left(\mathrm{Re}_{*t}\right)} \approx 0.0123$.

Re_t is the Reynolds number at the erosion threshold, that is, $\mathrm{Re}_t = (U_t^*.D_p)/\nu$,, where ν is the kinematic viscosity of the air. The term $\gamma/\rho_a D_p$ accounts for the interparticle forces, γ being adjusted to wind-tunnel measurements (from 1.65 10^{-4} to 5.10^{-4} kg s^{-2}). Figure 5.3 illustrates the dependence of U_t^* on D_p. The general shape of the curve is similar for the expressions of Iversen and White (1982) and Shao and Lu (2000). Differences appear for small particles (<100 μm) and for the minimal threshold and the associated particle diameter. The minimum erosion U_t^* of ~20 cm s^{-1}, predicted by Iversen and White (1982), is in agreement with wind-tunnel measurements for $D_p < 100$ μm and with field measurements (Gillette and Stockton 1989). The minimum U_t^* predicted by the expression of

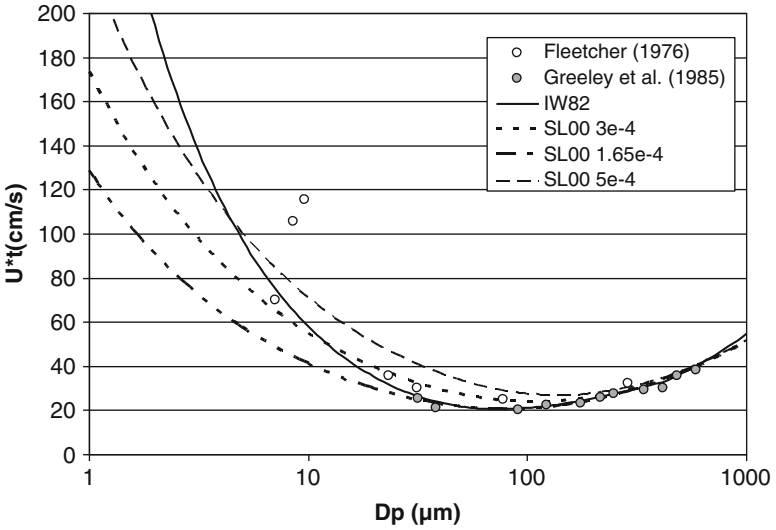

Fig. 5.3 Threshold wind friction velocity (U_t^*) as a function of particle diameter based on Iversen and White (1982) (IW82) and Shao and Lu (2000) (SL00) for different values of γ (3, 1.62 or 5×10^{-4} kg s^{-2}). *White dots* are experimental data from Fletcher (1976a, b) and *grey dots* from Greeley and Iversen (1985)

Shao and Lu (2000) increases with the value of γ. It is slightly higher than that predicted by Iversen and White (1982) for the value of γ recommended by the authors, but γ can be adjusted to reach a similar minimum value. Differences in the minimum threshold may have significant implications, especially on the dust emissions frequency. Indeed, for a smooth and flat surface such as that encountered in active dust source areas, a minimum U_t^* of 20 cm s^{-1} corresponds to a wind velocity of 7 m s^{-1} at 10 m height above the ground (in neutral conditions, assuming a Z_0 of 10^{-3} cm, typical of a smooth surface), while a U_t^* of 24 cm s^{-1} corresponds to a wind velocity of more than 8 m s^{-1} at 10 m height.

These theoretical curves have several implications for our understanding of dust emission processes. Firstly, both theoretical and experimental results show very high U_t^* (>100 cm s^{-1}) for particles in the single-micron range, that is, for typical dust-sized particles. This corresponds to a wind velocity at 10 m height on the order of 35 m s^{-1} for a smooth surface ($Z_0 = 10^{-3}$ cm) in neutral conditions. Such a wind velocity is hardly ever reached during dust storms. This explains why direct suspension or "uplifting" of dust-sized particles from the surface is not commonly observed. Secondly, the existence of an optimum threshold for sizes on the order of 60–100 µm makes soils containing particles in this range (fine sand in sedimentology) the most easily erodible. Thirdly, U_t^* increases with D_p for particles with diameters larger than 100 µm and decreases for particles with diameters smaller than 60 µm. This implies that mobilisation of soil particles by wind is a size-segregating process, in which the size distribution of the mobilised

particles will differ from that of the parent soil and, moreover, will change as a function of U^*. As U^* increases, it becomes possible to mobilise larger and smaller particles and thus to broaden the size distribution of the mobilised soil particles.

Because the dependence of the threshold on particle size is non-linear, a precise description of the soil size distribution is required. The various forces that define the erosion threshold act on individual particles in their natural state of aggregation. As a result, what must be documented is the size distribution of in situ particles. This distribution cannot be determined based on techniques that lead to disaggregation of soil particles, as classically used to determine soil texture. Soil texture determination provides the size distribution of the elementary particles composing a soil but does not necessarily reflect the available in situ soil size distribution except if in situ soil particles are individual elementary particles. Such a situation can be encountered, for example, for sandy soils composed of individual quartz grains, but for loamy and clayey soils, the two distributions are very different. Here, the undisturbed distribution is mainly composed of particles in the range of 50–100 μm, while fully disturbed size distributions exhibit large fractions of particles in the single-micron range (Shao 2000). In fact, fine dust particles are generally not present as loose individual particles in soils. They are present in super-micron soil aggregates or they are attached to larger solid soil grains (e.g. quartz grains). It must be noted that there is no standard technique to measure the in situ soil size distribution and that these soil characteristics are typically not documented in soil datasets. In addition, there is no simple relationship to convert soil texture into in situ or undisturbed, soil size distributions (Laurent et al. 2006). The in situ size distribution of the soil may be affected by its composition. As an example, salts or organic matter can increase the level of aggregation of soils.

Practically speaking, soils from arid or semi-arid regions usually do not lack particles in the optimum size range (see the soil size distribution in Chatenet et al. 1996; Laurent et al. 2006). As a result, in the field, the erosion threshold is often controlled by the influence of other factors such as soil moisture and surface roughness.

5.3.2 Influence of Soil Moisture

Soil moisture generally increases U_t^* (Chepil 1956; Bisal and Hsieh 1966; Saleh and Fryrear 1995). McKenna-Neuman and Nickling (1989) show that sand grains are held together by the capillary effect of soil moisture. Fécan et al. (1999) notice that the minimal soil moisture, for which an increase of U_t^* is measured, varies as a function of the soil texture. This can be explained by the capability of soil particles to retain soil water. Soil water usually takes the form of a water film around the grains, and the amount of water contained in this film increases with the soil clay content because clay minerals can absorb water in the interlayer positions. When the water absorption capacity of mineral grains is reached, the excess water can accumulate to form interstitial water between the soil grains where then capillarity

forces can develop. This conceptual view of water partitioning in the soil is reflected in the parameterisation of the increase of the erosion threshold due to soil moisture depending on the soil clay content proposed by Fécan et al. (1999).

$$\text{for } w < w' : \quad U^*_{tw}/U^*_{td} = 1 \tag{5.4a}$$

$$\text{for } w > w' : \quad U^*_{tw}/U^*_{td} = \left[1 + 1.21(w - w')^{0.68}\right]^{0.5} \tag{5.4b}$$

with U^*_{tw} the threshold wind friction in wet conditions, U^*_{td}, the threshold wind friction in dry conditions, w the gravimetric soil moisture content and w' the minimal soil moisture for which the erosion threshold increases, which depends on soil texture and more specifically on soil clay content:

$$w' = 0.0014(\%\text{Clay})^2 + 0.17\,(\%\text{Clay}) \tag{5.5}$$

Cornelis et al. (2004) proposed a different approach based on a complete analysis of the forces acting to maintain the particles at the surface, including capillary forces due to soil moisture. They proposed a single expression for the dependence of the erosion threshold as a function of the size, particle density and the soil moisture content. This expression was adjusted on wind-tunnel measurements performed over dry and wet soils, but including mainly sandy and loamy soils.

There are very few field measurements of erosion thresholds over wet soils in the literature. The increase of the erosion thresholds for wet soils compared to dry conditions measured in the Taklamakan Desert (Ishizuka et al. 2005) was found to be in agreement with the parameterisation of Fécan et al. (1999). Experimental results of Wiggs et al. (2004) for field measurements of threshold erosion velocities for sand showed that moisture contents of less than 2 % had little or no effect on sand flux. Gillette et al. (2001) observed vigorous wind erosion 10–30 minutes after a rainstorm on sandy soil. The reason for such a short time reduction of wind erosion in the field is that the eroding soil layer is thin and can dry rapidly under conditions of low humidity, high temperature and high winds. Consequently, soil moisture may have a limited influence on the erosion threshold in sandy deserts under a hot and dry climate, such as the Sahara, while it can significantly inhibit the dust emissions in more temperate climate for soils with higher silt and clay soil content such as Asian deserts (e.g. Laurent et al. 2006, 2008).

5.3.3 *Influence of Surface Roughness*

U^*_t values measured over rough surfaces are higher than those measured over smooth surfaces (e.g. Gillette et al. 1982). Non-erodible roughness elements absorb part of the wind momentum that would otherwise be available to initiate particle motion. To reach the erosion threshold, the shear stress component acting on the erodible

part of the surface must at least be equal to the shear stress corresponding to U_t^* in a "smooth" situation. This explains why U_t^* measured in settings with roughness elements are apparently higher than those in smooth surface settings. However, for a given wind velocity at a fixed height, the surface wind shear stress and thus U^* both increase with Z_0. The increase of the erosion threshold is generally predominant, and a decrease of the soil losses due to wind erosion is generally observed when Z_0 increases (e.g. Fryrear 1985). This partition of wind shear stress can be theoretically investigated by describing the forces exerted on the roughness elements, which is a function of their surface exposed to the wind and their aerodynamic properties or drag coefficients. This explains why the description of the drag partition generally involves the roughness density or lateral cover, defined as the sum of the frontal surface of the exposed roughness elements divided by a reference of unit horizontal surface S: $\lambda = nbh/S$, where n is the number of roughness elements, and b and h are the mean width and height, of the roughness elements.

To determine predictive expressions for practical applications, Raupach (1992) proposed an analytical treatment of the drag partition on a rough surface based on a dimensional analysis and physical hypothesis. The proposed equation gives the ratio of the overall shear stress to the shear stress on the uncovered and erodible surface as a function of the roughness density λ_r, the ratio of the drag coefficients of the roughness elements C_R and of the erodible surface C_S ($\beta_r = C_R/C_S$), σ_r the ratio of basal and frontal surfaces of the roughness elements and m_r, a coefficient accounting for the local shear stress acceleration ($0 > m_r > 1$).

$$f_R(\lambda) = (1 - \sigma_r\lambda)^{-1/2}(1 + m_r\beta_r\lambda)^{-1/2} \tag{5.6}$$

Predictions based on this equation agree well with the wind-tunnel dataset of Marshall (1971), for β_r ranging from 0.0002 to 0.2 and other measurements performed in wind tunnels or for natural sites (Raupach et al. 1993). Roughly, the wind shear stress on the erodible part of the surface decreases as β_r increases and becomes negligible for a value of 0.03. This provides an estimation of the critical value of β_r for which the decrease of the wind shear stress on the uncovered surface is such that it should inhibit erosion. When applied to field situations, this formulation requires the introduction of an empirical parameter (m_r in Eq. 5.6) that reflects the differences between the average and the maximum stress on the surface (Raupach et al. 1993). The practical use of this equation as a predictive tool is not evident because of the difficulty in estimating the empirical parameter and the drag coefficients of the obstacles. For example, to represent the shear stress partition in sparsely vegetated desert canopies, Wolfe and Nickling (1996) tested various combinations of values for these parameters and determined the appropriate values, a posteriori, as those matching the experimental data.

Alternative approaches of the drag partition use a more integrative parameter to represent the effect of roughness elements, Z_0. In micrometeorology, Z_0 is the length scale that characterises the loss of wind momentum attributable to roughness elements. For aerodynamic roughness lengths ranging from 10^{-4} to

10^{-1} cm, Gillette et al. (1982) measured U_t^* from 20 to 100 cm s^{-1} over loose or disturbed surfaces with a portable wind tunnel. A similar approach was used by Arya (1975) to determine the wind stress on Arctic pack ice. Marticorena and Bergametti (1995) extended this concept to aeolian studies. As suggested by Arya (1975), they assumed that an internal boundary layer (IBL) develops behind the roughness elements, similarly to the development of the IBL occurring after a sudden change in roughness. At the intersection of the IBL and the boundary layer produced by the roughness elements, the ratio of local to total wind shear stress (or the ratio of U^*s) can be expressed as a function of the roughness length of the smooth erodible surface and of the roughness length characterising the overall surface, including the effect of the roughness elements. This drag partition scheme predicts that the efficiency for eroding particles is greatly reduced for Z_0 of about 0.1 cm, above which one would not expect dust emissions under most natural conditions (Marticorena and Bergametti 1995). Compared to the wind-tunnel dataset of Marshall (1971), this parameterisation gives a comparable level of agreement to that of Raupach et al. (1993). It also reproduces the erosion threshold measured with a portable wind tunnel (Gillette et al. 1980) over natural non-vegetated surface across a large range of Z_0 (Marticorena et al. 1997a):

$$f_R(Z_0, z_{0s}) = 1 - \left(\ln(Z_0/z_{0s}) / \ln\left(a(X/z_{0s})^b\right)\right) \tag{5.7}$$

where z_{0s} is the aerodynamic roughness length of the erodible surface, and a and b are empirical coefficient describing the evolution of the IBL as a function of the distance (X) estimated, respectively, to be $a = 0.35$, $b = 0.8$ and $X = 10$ (with Z, Z_0 and z_{0s} in cm).

These two drag partition schemes are now widely used and have allowed significant progress in the prediction of erosion threshold over natural rough surfaces. As an example, Laurent et al. (2005) used such a partition scheme and Z_0 derived from satellite to estimate erosion thresholds over East Asian deserts. The estimated values, expressed as wind velocity at a height of 10 m, vary from 7 m s^{-1} in smooth sandy deserts such as the Taklamakan to 15–18 m s^{-1} in the stony Gobi Desert, in agreement with field observations (Natsagdorj et al. 2003; Wang et al. 2003). The spatial distribution of these thresholds is in remarkable agreement with wind velocities associated with synoptic records of dust storms (Kurosaki and Mikami 2007).

The partition schemes discussed above have been developed for relatively low roughness densities and assume an isotropic arrangement of roughness elements. An extensive comparison performed by Darmenova et al. (2009) shows that when using consistent input data, the two models give similar results for loose soils and for rough surfaces with sparse roughness elements, that is, the most easily erodible surfaces. In contrast, large discrepancies are found in the case of dense vegetation or solid elements, such as stony surfaces (regs or gobi deserts) and grasslands. More generally, these schemes do not reproduce the erosion thresholds over complex surfaces, such as surfaces with dense vegetation cover and/or specific

arrangement of the vegetation (MacKinnon et al. 2004). For example, in the Chihuahuan Desert, measurements or erosion fluxes over surfaces with different vegetation type and density have shown that the highest fluxes were measured over surfaces with very dense mesquite vegetation, but arranged as linear "streets" parallel to the wind direction of the highest winds (Gillette and Pitchford 2004). Such vegetated surfaces exhibit high saltation thresholds and consequently low dust emission frequencies. But under extremely high wind conditions, source regions with high erosion thresholds can be responsible for extremely intense dust events (Laurent et al. 2008). Grasslands and shrublands represent significant fractions of the semi-arid areas and can be subject to large seasonal or interannual variability of the vegetation cover and thus erosion thresholds. Such surfaces may also be the most impacted by climate change. Better constrains on the parameterisation of the saltation thresholds over vegetated surfaces are needed that account for the specific arrangement of the vegetation that allow wind erosion to occur even over densely vegetated surfaces and that account for the specific properties (porosity, flexibility) of the different vegetation types in arid and semi-arid areas (herbaceous vegetation, shrubs, etc.).

5.3.4 Other Factors

Crusts are thin soil surface layers more compact and harder than the material directly beneath, produced by physical or biological binding agents (e.g. Valentin and Bresson 1992). They are often formed following a thorough wetting by precipitation. Surface crusts may be thick and hard and protective of the surface from almost all winds. However, crusts may also be thin, weak and destroyed by winds that are occasionally experienced in many environments. Observations of crust formation and destruction on Owens Lake (California, USA) show extreme differences in the amount of crusted sediment from year to year and from season to season (Gillette et al. 2001). Additionally, biological crusts can form that provide sufficient surface aggregation to protect the surface from wind erosion (Belnap and Gillette 1997). Physical properties of crusts appear to be strongly influenced by soil texture and soil composition. For natural crusts found in desert soils in the Southwestern USA, Gillette et al. (1982) observed that silt and clay sediments form thicker and stronger crusts than predominantly sandy sediments. For clay-rich soils, Breuninger et al. (1989) observed that increased organic matter content correlates with lack of crusting and breakage of the clay into increasingly smaller peds (i.e. soil aggregates), which are vulnerable to wind erosion. For many of these broken clay crusts, however, the pieces are large and hard enough to resist erosion (Gillette et al. 1982). Surface crusting can be one of the main effects of precipitation on dust emissions. Indeed, a fully crusted surface provides cover for possibly more vulnerable soil beneath. Partially or fully crusted surfaces may modify soil sediment supply and limit erosion fluxes (Lopez 1998). On the contrary, any process that acts to break crusts or prevent their formation will increase the potential for

dust emission. Such processes can be natural processes, such as intense rainfall or anthropogenic processes such as soil trampling by livestock or vehicle traffic. The dynamics of crust formation and destruction can induce temporal and spatial variability of dust emissions in semi-arid areas.

Some arid or semi-arid areas are located at sufficiently high latitudes to experience snow. In East Asia (35°N–50°N), for example, areas covered with snow can persist in the spring, during the period when the highest frequency of dust storms is recorded (Kurosaki and Mikami 2004). Snow protects the soil from wind erosion, but the physical mechanisms involved have not been investigated extensively. Based on a statistical analysis of synoptic reports, Kurosaki and Mikami (2004) proposed an empirical parameterisation of the change of the erosion threshold as a function of the degree of snow cover. Laurent et al. (2005) also found that for specific Asian dust sources, snow cover could influence the modelled simulated dust emissions significantly during the winter months.

5.4 Saltation

The amount of soil material set in a horizontal movement by the wind is generally quantified through the so-called horizontal flux. The horizontal flux is the mass of soil particles crossing a vertical surface of unit width and infinite height perpendicular to the eroding surface and to the wind direction per unit time. The saltation process has been investigated thoroughly both from a theoretical and experimental point of view, in the field and in wind tunnels. In addition to the prediction of saltation thresholds, numerous studies have been dedicated to the quantification of the horizontal mass flux of saltating particles and its dependence on U^* and the influence of soil particle size and surface characteristics. Several numerical expressions of the saltation flux have been proposed that generally include a power dependence on U^* and U_t^*.

Assuming that above the erosion threshold the entire wind momentum is transferred to the surface by the saltating grains and based on dimensional arguments, Bagnold (1941) suggested that the horizontal flux is proportional to U^* to the power of 3. Most of the expressions in the literature also exhibit a third power law of U^* to express the horizontal flux (e.g. White 1979; Owen 1964; Kawamura 1964). Such dependence has been experimentally observed as well in natural situations as in wind tunnels, especially for large values of U^* (Gillette 1974, 1977, 1979; Gillette and Stockton 1989; Sörensen 1985; Leys and Raupach 1991; Shao et al. 1993). These expressions are supported by theoretical considerations on the mean path trajectories of the saltating particles as a function of U^* and on the efficiency of momentum transfer to the surface. Most of these expressions assume that the saltation layer has reached equilibrium and provide the horizontal flux as a function of the wind velocity. In the field for a steady wind, the equilibrium can be reached at a distance of about 600 m (Gillette et al. 1996). Horizontal flux measurements performed with a high confidence level (5 % in mass) by

Greeley et al. (1994) allowed tests of these different expressions. These authors found that Bagnold's (1941) model and White's (1979) formulations most closely agree with the experimental data. However, as noted by Shao (2000), regarding the uncertainties associated with the estimation of the erosion threshold, it is difficult to determine the agreement of different expressions of the saltation flux with field measurements. White's equation, which includes a threshold term, is given here as a typical example for the vertically integrated horizontal flux, Q:

$$Q = c\frac{\rho}{g}U^{*3}\left(1-\frac{U_t^*}{U^*}\right)\left(1+\frac{U_t^{*2}}{U^{*2}}\right) \tag{5.8}$$

where c is an adjustment constant.

The problem in applying this formulation to natural situations is that the soil grains are generally not characterised by a uniform diameter. As the equation of U_t^* is non-linearly dependent on particle diameter, the adequate size-dependent threshold value will be affected by each size range, and thus the soil grain size distribution must be represented by a continuous function. Both Marticorena and Bergametti (1995) and Shao et al. (1996) included a size-dependent expression of the erosion threshold in the horizontal flux equation. The flux produced by each particle size range is weighted by its relative mass (Shao et al. 1996) or relative basal surface (Marticorena and Bergametti 1995). An illustration of the influence of the soil size distribution on the computed horizontal flux is given in Fig. 5.4. The horizontal flux is according to Marticorena and Bergametti (1995) for a soil mass size distribution composed of two log-normal populations: a fine and a coarse mode representing, respectively, 30 and 70 % of the soil mass size distribution. The comparison between the relative mass and surface size distribution shows that weighting the flux by the relative surface distribution increases the contribution of the finer mode compared to the coarse mode. This predominance of the finer mode is reinforced by the fact that this size range has a lower erosion threshold. As a result, when U^* is close to the minimum erosion threshold, only the fine mode contributes to the erosion flux. When the wind friction velocity increases, the size distribution of the horizontal flux broadens and progressively tends towards the size distribution of the parent soil. This parameterisation reproduces the change in size distribution between the eroding soil and the horizontal flux as a function of U^* observed in wind-tunnel experiments (Williams 1964) for simple soil size distributions (Marticorena and Bergametti 1995). However, its application in the field, with poly-disperse soil size distribution reveals some difficulties in reproducing the size distribution of the horizontal flux. As an example, Flores-Aqueveque et al. (2010) noted that the model satisfyingly retrieved the total mass flux, while the measured size distribution of the horizontal mode was much coarser than the predicted one. Reproducing the size distribution of the horizontal flux is a key issue in representing dust emission because the energy required for releasing fine dust particles from the surface or from soil aggregates will be supplied mainly by the kinetic energy of the saltating soil particles. The size distribution of the saltation flux and its dependence

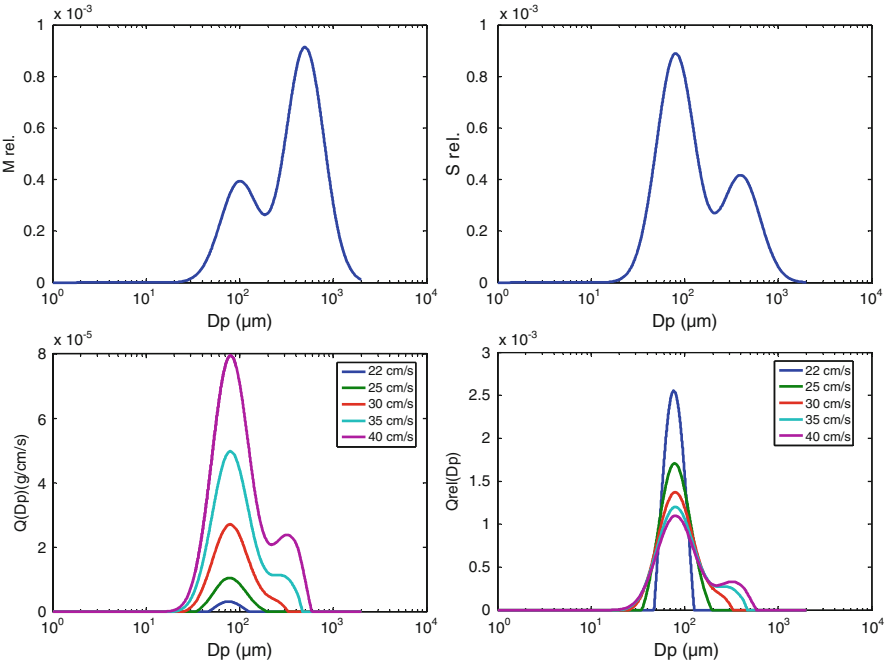

Fig. 5.4 Relative mass size distribution (*top left*), relative surface distribution (*top right*), size distribution of the horizontal flux (*bottom left*) and relative size distribution of the horizontal flux (*bottom right*) computed for wind friction velocities ranging from 22 to 40 cm s^{-1} (*right*) for a soil mass size distribution composed of two log-normal modes: a fine mode ($Ds_{\mathrm{med1}} = 100$ µm, $\sigma s_1 = 1.3$) representing 30 of the soil mass size distribution and a coarse mode ($Ds_{\mathrm{med2}} = 500$, $\sigma s_2 = 1.6$) representing 70 %. The horizontal flux is computed assuming a smooth erodible surface using the Marticorena and Bergametti (1995) model

on the size distribution of the parent soil and the U^* clearly deserve additional investigations. Such investigations would also help representing the entrainment of coarse particles (∼100 µm) from the saltation layer ("modified saltation") to quantify their contribution to local and long-range transport (e.g. Alfaro et al. 2011).

Saltating particles set in motion by the wind cause a feedback mechanism, called the "Owen Effect", by which they increase the Z_0 of the surface. A demonstration of this effect is given by the increase of the ratio of U^* to mean wind velocity U. Raupach (1991) incorporated the theory of Owen (1964) to provide an expression for the aerodynamic roughness length, $z_{0\mathrm{salt}}$, when saltation occurred on smooth or rough surfaces, that has been validated by field measurements (Gillette et al. 1998).

Despite their capability to provide reliable estimates of the saltation flux at equilibrium, the available simple flux equations mentioned above are not appropriate to give a very detailed description of the saltation process. Specific and more complex models have thus been developed to describe the characteristics of the particle movement, the development of the equilibrium layer, the interactions between soil

particles and the fluid and the intermittency of the saltation induced by turbulent flows or surface heterogeneity (e.g. Shao and Li 1999; Kok and Renno 2009; Dupont et al. 2013). Another limitation of these simple saltation flux models is that they are not designed to estimate the erosion fluxes properly for supply limited sources. Supply limitation is often encountered in semi-arid areas and is often associated to areas or time periods when soil crusts protect the surface soil against erosion. In such cases, the measured horizontal flux is lower than the expected potential flux a non-supply limited soil would have for the same wind conditions (Gillette et al. 2001) and can evolve with time as a function of sediment depletion. Accounting for sediment supply is also an issue when addressing climatic timescales (e.g. Kocurek and Lancaster 1999). Similarly, classical saltation models fail to reproduce the erosion fluxes over complex surfaces such as vegetated or cultivates surfaces, where trapping can occur on surfaces roughened by vegetation or ridged soil. Trapping is especially important for agricultural soils where ploughing causes both non-erodible surface clods and furrows. As an example, the reduction of the erosion flux measured in wind tunnels over sandy ridged surfaces ranges between 65 and 85 % under high wind conditions (>14 m s^{-1}) regardless of the height and spacing of the ridges (Kardous et al. 2005). Despite these limitations, which mainly concern semi-arid areas, saltation can be considered as the best understood and well-described stage of the dust emissions processes.

5.5 Dust Emission

Dust production by sandblasting results from the balance between the kinetic energy of the saltating particles and the cohesion of the dust particles to the soil aggregates. The efficiency of this process is thus dependent on the intensity of the saltation flux and of the cohesive properties of the dust particles or the resistance of the soil. While the description of the saltation bombardment can be derived from the size-dependent computation of the saltation flux, an explicit description of dust entrainment by the impact of saltating grains is not straightforward. In addition, the estimation of the amount of dust particles available in a soil that can be released by sandblasting or disaggregation is also a major difficulty.

5.5.1 Empirical Approaches

Up to now, the most complete and comprehensive dataset available for dust mass flux is that from Gillette (1977), which includes synchronous measurements of the saltation and dust emission fluxes as a function of U^* for several soils in the USA with different textures. This dataset shows different behaviour of the ratio of dust and saltation fluxes, the so-called sandblasting efficiency, depending on the soil: for some soils, the efficiency tends to vary with U^*, while for others, it

seems relatively insensitive. In agreement with these measurements, Gillette and Passi (1988) proposed a very simple expression to describe dust emission fluxes, F, similar to the expression of the saltation flux but proportional to U^* to the power of 3–5. It includes an empirical proportionality coefficient, in which various wind erosion factors are lumped together. This scheme is attractive due to its simplicity, but the definition of the proportionality coefficient and the power of U^* must be empirically determined based on pre-existing knowledge of the soil and surface properties. For a quantitative estimate, Marticorena and Bergametti (1995) assumed that, to first order, dust emission flux can be considered as a constant fraction of the saltation flux depending on the amount of dust particles present within the soil. The percentage of clay-size particles in the soil was used as a proxy for the amount of potentially available dust in the soil. An empirical relationship between the sandblasting efficiency and the soil clay content has thus been established by fitting the sandblasting efficiency on the dataset from Gillette (1977) for soils having clay contents ranging from 1.8 to 19 %. Average sandblasting efficiencies vary from 10^{-4} to 10^{-6} cm^{-1}, highlighting the fact that only a tiny fraction of the soil particles in motion near the surface is susceptible to be entrained in vertical motion and long-range transport. This empirical approach captures two aspects of the dust emission process: dust emission is proportional to saltation intensity, and the sandblasting efficiency depends on soil properties. However, it oversimplifies dust emission processes by assuming that the sandblasting efficiency only depends on soil properties. A major limitation of this scheme is that it cannot provide size-resolved estimates of dust emissions. Its main advantage is to provide reasonable estimates of the dust mass fluxes as a function of soil type and U^* (through the saltation flux) when applied at the regional scale (e.g. Marticorena et al. 1997b; Laurent et al. 2005, 2008).

5.5.2 *Physically Based Models*

Several approaches have been developed to describe dust emission processes though bombardment by saltating grains. Shao et al. (1993, 1996) considered the energy balance of a saltating particle during its collision with the surface with the binding strength of the dust particles, which was then estimated to be proportional to U_t^*. The process of dust emission is assumed as a linear combination of saltation bombardment of various sand particle sizes. A specific problem with this scheme is that the proportionality coefficients have been derived based on a small set of idealised wind-tunnel experiments. Alfaro et al. (1997, 1998) used a similar concept to model sandblasting efficiency, but they estimated the binding energy of dust particles based on wind-tunnel measurement performed with several soils from arid or semi-arid regions. The measured dust size distribution and its evolution as a function of U^* were used as a constraint to determine the binding energy of each mode composing the emitted dust size distribution.

These descriptions of the sandblasting processes are based on two main assumptions. The first assumption is that the impact velocity of the saltating particles increases as a function of U^*, such that the available kinetic energy increases as U^* to the power of two and as a function of the diameter of saltating particles. The second assumption is that, like the erosion threshold, the dust binding energy increases as the particle size decreases. As a result, these models predict a coarser dust size distribution for weak U^* and an increasing proportion of fine dust for higher wind velocities. This behaviour is consistent with the difference in the dust size distribution measured during intense dust emission events compared to background conditions (d'Almeida and Schütz 1983; Gomes et al. 1990). Based on wind-tunnel measurements, Alfaro et al. (1998) determined three typical modes for the size distribution of emitted dust whose relative contribution depends on U^*. For weak events, only the coarse mode, having the lowest binding energy, is emitted. With increasing U^*, the relative proportion of the finest modes increases once the kinetic energy of the saltating particles exceeds the binding energy associated with each mode. This scheme predicts that the sandblasting efficiency depends on the soil size distribution and on U^*. The variation of the sandblasting efficiency with U^* is very sensitive close to the erosion threshold, but for high U^*, it is relatively constant or slightly decreasing for coarse soil size distribution (Alfaro and Gomes 2001). This may explain the different behaviour of the experimentally determined sandblasting efficiency (Gillette 1977). The capability of this scheme to reproduce mass dust flux measurements has been tested by comparison with measurements obtained in Spain, Niger (Gomes et al. 2003) and the USA (Nickling and Gillies 1989). As a result of these studies, an adjustment of the binding energy initially determined from wind-tunnel studies has been proposed (Alfaro et al. 2004).

Shao (2001, 2004) proposed the most complete and physically explicit description of dust emission processes. His model takes into consideration the three dust emission mechanisms: aerodynamic entrainment, saltation bombardment and aggregate disintegration. It reflects the fact that dust emission is proportional to saltation mass transport, but also depends on soil texture and soil "resistance" expressed by the soil plastic pressure, p, characterising the flowing behaviour of the soil subject to the particle impact. The bombardment efficiency, defined as the ratio between the mass ejected by bombardment and the mass of impacting particles, is estimated as a function of the soil bulk density and of the soil plastic pressure. Both the range of bombardment efficiency and the soil plastic pressure have been estimated from the data of Rice et al. (1995, 1996). The amount of emitted dust is assumed to be proportional to the amount of dust potentially available in the soil and quantified by the soil texture. The size distribution of the emitted dust evolves between two limits defined by the "undisturbed" soil size distribution and the "fully disturbed" size distribution. This approach implies that during weak erosion events, only emission of free dust is possible, while during strong erosion events, aggregated dust can be released. The capability of this model to reproduce all the measurements of mass dust emission fluxes available at this time (Gillette 1977; Nickling 1983; Nickling and Gillies 1993; Nickling et al. 1999; Gomes et al. 2003; Rajot et al. 2003) has been evaluated by Shao (2004). They found that the model has the capacity to

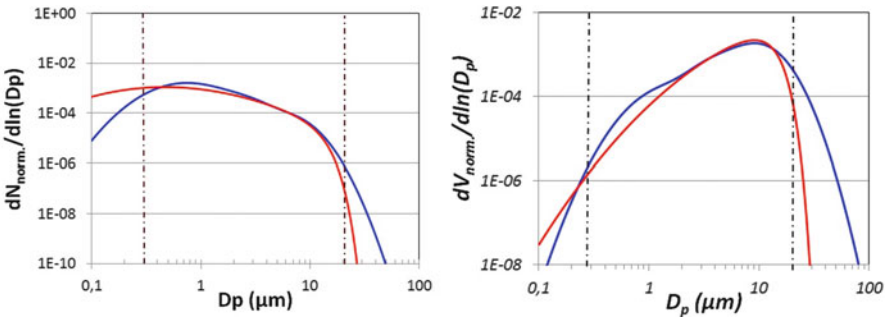

Fig. 5.5 Relative number (*right*) and volume size distribution computed as a combination of 3 log-normal functions adjusted on field measurements from Sow et al. (2009) (number size distribution parameter: $D_1 = 0{,}73$ µm; $\sigma_1 = 1.84$; $p_1 = 84$ %; $D_2 = 2.32$ µm; $\sigma_2 = 1.65$; $p_2 = 14$ %; $D_3 = 6.51$ µm; $\sigma_3 = 1.48$; $p_3 = 2$ %. Volume size distribution parameters: $D_1 = 1{,}5$ µm; $\sigma_1 = 1.79$; $p_1 = 8$ %; $D_2 = 5.1$ µm; $\sigma_2 = 1.68$; $p_2 = 40$ %; $D_3 = 10.4$ µm; $\sigma_3 = 1.52$; $p_3 = 52$ %; corresponding to the ME4 event in Sow et al. (2009)) (*blue line*) and computed with the size distribution from Kok (2011a, b) (with $\lambda =$, 12; $D_{soil} = 3.4$ µm; $\sigma_{soil} = 3$; $C_N = 0.9539$ and $C_V = 12.62$). The *dotted lines* correspond to the lower (0.3 µm) and higher (20 µm) particle size sampled by Sow et al. (2009)

predict dust emission rates from various soils, once the input soil properties has been set to reasonable values, which can be estimated by adjustment of the computed flux on the measured one.

A different approach has recently been proposed based on an analogy between the processes of dust emission by sandblasting and the fragmentation of brittle materials (Kok 2011a). When a brittle material, such as glass or gypsum, receives a very large input of energy, it can fragment into a wide range of smaller particle sizes. Disaggregation of soil aggregates or the release of fine dust particles attached to sand grains can thus be considered as a similar process. The advantage of this theory is that the size distribution of the resulting fragments follows a power law and is thus "scale invariant". The application of this fragmentation theory to the case of dust emission by saltating particles requires accounting for the size of the released indivisible constituents (i.e. the dust particles) and estimating the main parameter of the power law: the propagation length, λ, that is, the limited length to which side cracks propagate, that depends on the density of the main cracks (Kok 2011a). The production of dust particles of a given size is assumed to be proportional to the cumulated volume fraction of soil particles smaller than this size, estimated by the fully dispersed soil size distribution.

Figure 5.5 compares the normalised size distribution in number and volume obtained assuming dust size distribution as a combination of 3 log-normal functions (as in Alfaro and Gomes (2001)) adjusted on field measurements from Sow et al. (2009) (dust event referred to as ME4) and using the "fragmentation" model from Kok (2011a), whose parameters have been adjusted on a series of field measurements, among which the data from Sow et al. (2009) encompass the largest size range. When considering the size range of the measurements (vertical

dotted lines), the two representations do not differ much. The largest differences correspond to the finest dust fraction (<0.3 μm) in the number size distribution and the coarse dust fraction (>20 μm) in the volume size distribution. This clearly highlights the need for documenting the full size spectra of mineral dust at emission.

5.5.3 Models Versus Observations

While several conceptual approaches for dust emission have been developed, a main limitation for their improvement is the availability of experimental data to test and validate these different models. Most of the available datasets are total mass dust emission fluxes measured as a function of U^* (Gillette 1977; Nickling 1983; Nickling and Gillies 1993; Nickling et al. 1999; Gomes et al. 2003; Rajot et al. 2003). Several of them include simultaneous measurements of the saltation and dust emission fluxes, which limit some uncertainty in the simulation of the saltation fluxes. All these comparisons lead to the conclusion that the developed models are able to reproduce the measured total dust emission flux, after adjustment of the main input parameters. Indeed, the soil properties required as input parameters in most of the models are generally not provided in the experimental datasets. As a result, there is always a combination of input parameters that allows reproducing the measured dust fluxes. This leads to the conclusion that measurements of the dust emission fluxes in terms of total mass only are not sufficient to constrain these models and in particular the physical processes they aim to reproduce. From this point of view, a key point is to test the capability of the physically explicit dust models to predict the size distribution of the emitted dust.

This analysis has lead to the implementation of field campaigns dedicated to the measurements of size-resolved dust emission fluxes such as recently made during the JADE (Japanese Australian Dust Experiment; Ishizuka et al. 2008) and AMMA (African Monsoon Multidisciplinary Analysis; Sow et al. 2009) programmes. The size-resolved dust emission fluxes measured during AMMA show significant differences between weak and intense dust events, with a much higher contribution of the finest modes for the latter (Sow et al. 2009). The higher relative contribution of the finest dust fraction to the total dust size distribution for high U^* is in agreement with the sandblasting models of Alfaro and Gomes (2001) and Shao (2004). However, the airborne dust size distributions measured during JADE (Shao et al. 2011) appear to be independent of the wind speed. Such an invariant behaviour is reproduced by Kok's model (2011b), with a constant propagation length and assuming a typical fully dispersed soil size distribution for soils from arid and semi-arid regions. However, to reproduce the measurements corresponding to the intense dust event from Sow et al. (2009) properly, a different adjustment of the propagation length is required, that was attributed to changes in surface properties between the different events (Kok 2011b). Part of the differences between the models can be due to the representation of the saltation processes. Kok (2011b) argues that the dependence of the dust size distribution on U^* in the models of

Alfaro and Gomes (2001) or Shao (2001, 2004) results from the assumption that the impact velocity of saltating particles is proportional to U^*, in disagreement with some wind-tunnel results. Assuming a constant impact velocity of the saltating particles, only a limited change in the kinetic energy of the saltation particles can be expected as a function of U^*, due to the enlargement of the horizontal flux size distribution. Further investigation of the characteristics of individual particle trajectories and of the size distribution of the saltation flux as a function of U^* could provide additional constrains for the description of the sandblasting process.

In essence, no definitive conclusion can be given on the capability of the different dust emission models to reproduce the size-resolved measurements. Whatever conceptual description is used (sandblasting, fragmentation), the link between soil properties and dust size distribution is not sufficiently understood and parameterised. All models include several input parameters, mainly related to soil characteristics, which have not necessarily been experimentally determined, such that they can be adjusted to fit the observations. Additional measurements of size-resolved dust emission fluxes over large size spectra and for a wide range of dynamical conditions with an extensive description of soil properties are necessary to improve sandblasting models.

5.6 Conclusion

The understanding and modelling of dust emission processes have benefitted greatly from a large body of theoretical and experimental studies on wind erosion processes and, in particular, on saltation processes. The knowledge of these processes provides some guidance in understanding the behaviour of dust sources and supporting classifications of dust sources based on their geomorphological and pedological characteristics (Callot et al. 2000; Bullard et al. 2011). Typically, from a physical point of view, smooth surfaces with dry, sandy soils have the lowest erosion thresholds and thus the highest probability to be frequent dust emission sources. This explains why dust emission is frequent in sandy deserts such as Taklamakan (Laurent et al. 2006; Bullard et al. 2011). On long timescales, such properties may lead to soil depletion in dust-sized particles unless external sediment supply is provided to the system. On the contrary, dust emission from rough surfaces, characterised by high erosion thresholds, occurs less frequently since it requires higher winds, but may be very intense. As an example, Laurent et al. (2006) found that the annual dust emission from northeastern Asian deserts can be increased by a factor of 2 due to a few unusually intense dust events originating from the Gobi Desert. In terms of dust emission intensity, certain soil properties are favourable. Because saltation is a prerequisite for intense dust emission, soils with undisturbed particles in the optimum size range in terms of erosion threshold are good candidates. But the intensity of dust emission is also influenced by the amount of dust particles within the soil, as quantified by its fully dispersed size distribution or its texture. This association of sand-sized ($\sim$100 μm) and dust-sized ($\sim$1 μm)

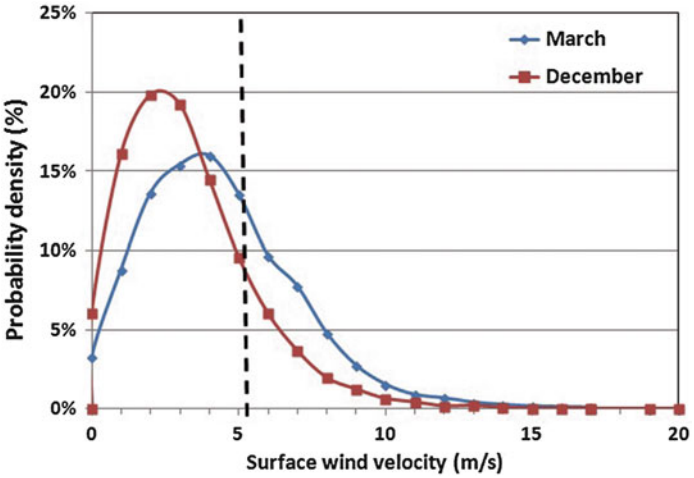

Fig. 5.6 Probability density function of the 10 m wind velocity fields from the ECMWF meteorological model over the Western Sahara for March and December 1991 (Adapted from Marticorena and Bergametti 1996)

particles in a soil is often encountered in salty or silty depressions, such as dry lakes, which explain their high potential for dust emissions (Callot et al. 2000; Bullard et al. 2011; see also Chap. 3).

However, a high potential for dust emission is not sufficient to make a dust source; sufficiently, high winds are needed. The activity of a dust source depends on the fraction of surface winds exceeding the erosion threshold defined by the local surface properties and its intensity depends on the local wind velocity and erosion thresholds and on the soil properties. The distribution of the surface wind velocities (at 10 m height) from the analysis of the European Centre for Medium-Range Weather Forecast over the Western Sahara is illustrated in Fig. 5.6 for the month of March and December 1991. A small fraction of the surface winds corresponds to velocities higher than the minimum erosion threshold (29 % $>$ 6 m s^{-1} in March and 15 % in December). The fraction of high winds, responsible for the most intense dust emissions, is even smaller (4 % $>$ 10 m s^{-1} in March and 2 % in December). Representing the surface winds in dust source regions is thus a challenging issue (see Chap. 6). Finally, a proper description of both the surface characteristics and the surface wind distribution is required to estimate whether a source region is a "preferential source" or not, either in terms of frequency or in terms of intensity.

The knowledge of dust emission processes has allowed the establishment of conceptual and numerical models that describe the dependence of the emission fluxes on U^* and surface and soil parameters. When all input parameters are measured or fixed in reasonable and realistic ranges, dust mass fluxes can be properly estimated by physical dust emission models as a function of U^* (Shao et al. 2011). The major weakness in the present description of dust emission processes

lies in the physical understanding of the dust released by the impact of saltating grains, which has implications for the capability of dust emission models to predict the size distribution of the emitted dust. Different models predict different dust size distributions as a function of U^* and of the soil properties. Available field experimental data of size-resolved dust emission fluxes are not sufficient to estimate these dependences correctly. Thus, a rigorous intercomparison of the dust emission models remains to be done, based on experiments of size-resolved dust emission fluxes where all input parameters are experimentally determined and independently constrained. Among the required input data, specific attention must be paid to the determination of the undisturbed and fully disturbed soil size distributions. Such an experiment should also cover the largest possible range of dust particle sizes. As a matter of fact, dust emission flux measurements, especially those resolved in size, remain a difficult task. The experimental determination of emission fluxes is generally based on the method of gradients, which has theoretical limitations (Shao 2008) and is often difficult to implement in the field. Alternatives such as eddy-covariance methods (Porch and Gillette 1977; Fratini et al. 2007) could help to limit the uncertainties associated with the gradient method to provide more reliable size-resolved dust fluxes. Differences in the prediction of the emitted dust size distribution may also be explained by the way in which saltation processes are modelled (Kok 2011b). Revisiting the description of the saltation processes with respect to dust emission may significantly improve the capability of dust emission models to simulate the dust size distribution and its dependence on soil properties and dynamical conditions. Lastly, a better quantification of dust emission in semi-arid areas is required, which implies further efforts in the description of the impact of vegetation and cultivation on dust emission processes. Indeed, the contribution of anthropogenic sources to the total atmospheric dust load and the evolution of the dust emissions in semi-arid areas resulting from climate changes are still very uncertain.

References

Agier L, Deroubaix A, Martiny N, Yaka P, Djibo A, Broutin H (2013) Seasonality of meningitis in Africa and climate forcing: aerosols stand out. J R Soc Interface 10(79):20120814. doi:10.1098/rsif.2012.0814

Alfaro SC (1997) Simulation expérimentale et modélisation de la production d'aérosol minéral par érosion éolienne. Thèse de doctorat, Université Paris 12 Val-de-Marne, 176 pp

Alfaro SC, Gomes L (2001) Modeling mineral aerosol production by wind erosion: emission intensities and aerosol distributions in source areas. J Geophys Res 106:18075–18084

Alfaro SC, Gaudichet A, Gomes L, Maillé M (1997) Modeling the size distribution of a soil aerosol produced by sandblasting. J Geophys Res 102(D10):11239–11249

Alfaro SC, Gaudichet A, Gomes L, Maillé M (1998) Mineral aerosol production by wind erosion: aerosol particle sizes and binding energies. Geophys Res Lett 25(7):991–994

Alfaro SC, Rajot JL, Nickling W (2004) Estimation of PM20 emissions by wind erosion: main sources of uncertainties. Geomorphology 59:63–74

Alfaro SC, Flores-Aqueveque V, Foret G, Caquineau S, Vargas G, Rutllant JA (2011) A simple model accounting for the uptake, transport, and deposition of wind-eroded mineral particles in the hyperarid coastal Atacama Desert of northern Chile. Earth Surf Process Landf 36:923–932. doi:10.1002/esp.2122

Arya SPS (1975) A drag partition theory for determining the large-scale roughness parameter and wind stress on Arctic pack ice. J Geophys Res 80:3447–3454

Bagnold RA (1941) The physics of blown sand and desert dunes. Methuen, London, 265 pp

Belnap J, Gillette DA (1997) Vulnerability of desert biological soil crusts to wind erosion: the influences of crust development, soil texture, and disturbance. J Arid Environ 39:133–142, Article No. ae980388, 1998

Bisal F, Hsieh J (1966) Influence of moisture on erodibility of soil by wind. Soil Sci 102:143–146

Breuninger RH, Gillette DA, Khil R (1989) Formation of wind-erodible aggregates for salty soils and soils with less than 50 % sand composition in natural terrestrial environments. In: Leinen M, Sarthein M (eds) Paleoclimatology and paleometeorology: modern and past patterns of global atmospheric transport. Kluwer, Norwell, pp 31–63

Bullard JE, Harrison SP, Baddock MC, Drake N, Gill TE, McTainsh G, Sun Y (2011) Preferential dust sources: a geomorphological classification designed for use in global dust-cycle models. J Geophys Res 116, F04034. doi:10.1029/2011JF002061

Callot Y, Marticorena B, Bergametti G (2000) Geomorphologic approach for modelling the surface features of arid environments in a model of dust emissions: application to the Sahara desert. Geodin Acta 13:245–270

Chatenet B, Marticorena B, Gomes L, Bergametti G (1996) Assessing the micropeds size-distributions of desert soils erodible by wind. Sedimentology 43:901–911

Chepil WS (1951) Properties of soil which influence wind erosion: IV. State or dry aggregate structure. Soil Sci 72:387–401

Chepil WS (1956) Influence of soil moisture on erodibility of soil by wind. Proc Soil Sci Soc Am 20:288–292

Cornelis WM, Gabriels D, Hartmann R (2004) A parameterisation for the threshold shear velocity to initiate deflation of dry and wet sediment. Geomorphology 59:43–51

d'Almeida GA, Schütz L (1983) Number, mass and volume distributions of mineral aerosol and soils of the Sahara. J Clim Appl Meteorol 22:233–243

Darmenova K, Sokolik IN, Shao Y, Marticorena B, Bergametti G (2009) Development of a physically-based dust emission module within the Weather Research and Forecasting (WRF) model: assessment of dust emission parameterizations and input parameters for source regions in Central and East Asia. J Geophys Res 114, D14201

Dupont S, Bergametti G, Marticorena B, Simoens S (2013) Modelling saltation intermittency. J Geophys Res 118:7109–7128

Fécan F, Marticorena B, Bergametti G (1999) Soil-derived dust emissions from semi-arid lands: 1. Parameterization of the soils moisture effect on the threshold wind friction velocities. Ann Geophys 17:149–157

Fletcher B (1976a) The erosion of dust by an airflow. J Phys Appl Phys 9(17):913–924

Fletcher B (1976b) The incipient motion of granular materials. J Phys Appl Phys 9(17):2471–2478

Flores-Aqueveque V, Alfaro SC, Muñoz R, Rutllant J, Caquineau S, LeRoux J, Vargas G (2010) Aeolian sand transport over the Pampa Mejillones in the coastal Atacama Desert of northern Chile. Geomorphology 120(3–4):312–325

Fratini G, Ciccioli P, Febo A, Forgione A, Valentini R (1997) Size-segregated fluxes of mineral dust from a desert area of northern China by eddy covariance. Atmos Chem Phys 7:2839–2854

Fryrear DW (1985) Soil cover and wind erosion. Trans ASAE 28:781–784

Gillette DA (1974) On the production of soil wind erosion aerosols having the potential for long range transport. J Rech Atmos 8:735–744

Gillette DA (1977) Fine particulate emissions due to wind erosion. Trans Am Soc Agric Eng 20:890–897

Gillette DA (1979) Environmental factors affecting dust emission by wind erosion. In: Morales C (ed) Saharan dust. Wiley, New York, pp 71–94

Gillette DA, Passi R (1988) Modeling dust emission caused by wind erosion. J Geophys Res 93:14233–14242

Gillette DA, Pitchford A (2004) Sand flux in the northern Chihuahuan Desert, New Mexico, USA and the influence of mesquite-dominated landscapes. J Geophys Res 109, F04003. doi:10.1029/2003JF000031

Gillette DA, Stockton PH (1989) The effect of nonerodible particles on wind erosion of erodible surfaces. J Geophys Res 94:12885–12893

Gillette DA, Adams J, Endo A, Smith D, Khil R (1980) Threshold velocities for input of soil particles into the air by desert soils. J Geophys Res 85:5621–5630

Gillette DA, Adams J, Muhs DR, Khil R (1982) Threshold friction velocities and rupture moduli for crusted desert soils for the input of soil particles into the air. J Geophys Res 87:9003–9015

Gillette DA, Herbert G, Stockton P, Owen P (1996) Causes of the fetch effect in wind erosion. Earth Surf Process Landf 21:641–659

Gillette DA, Marticorena B, Bergametti G (1998) Changing the roughness length by saltating grains: experimental assessment, test of theory and operational parameterization. J Geophys Res 103:6203–6210

Gillette DA, Niemeyer TC, Helm PJ (2001) Supply-limited horizontal sand drift at an ephemerally crusted, unvegetated saline playa. J Geophys Res 106(D16):P18085–P18098

Gomes L, Bergametti G, Coudé-Gaussen G, Rognon P (1990) Submicron desert dust: a sandblasting process. J Geophys Res 95:13927–13935

Gomes L, Rajot JL, Alfaro SC, Gaudichet A (2003) Validation of a dust production model from measurements performed in semi-arid agricultural areas of Spain and Niger. Catena 52:257–271

Greeley R, Iversen JD (1985) Wind as a geological process, Cambridge planetary science series. Cambridge University Press, Cambridge, 333 pp

Greeley R, Blumberg DG, Williams SH (1994) Field measurements of active windblown sand. In: Abstract of the workshop on response of eolian processes to global change. Occasional paper No. 2, The Desert Research Institute, Reno

Huneeus N, Schulz M, Balkanski Y, Griesfeller J, Prospero J, Kinne S, Bauer S, Boucher O, Chin M, Dentener F, Diehl T, Easter R, Fillmore D, Ghan S, Ginoux P, Grini A, Horowitz L, Koch D, Krol MC, Landing W, Liu X, Mahowald N, Miller R, Morcrette J-J, Myhre G, Penner J, Perlwitz J, Stier P, Takemura T, Zender CS (2011) Global dust model intercomparison in AeroCom phase I. Atmos Chem Phys 11:7781–7816

Intergovernmental Panel on Climate Change (IPCC) (2007) Fourth assessment report: climate change 2007. In: Solomon S et al (ed) Contribution of Working Group I to the fourth assessment report of the Intergovernmental Panel on Climate Change. Cambridge University Press, Cambridge/New York

Ishizuka M, Mikami M, Yamada Y, Zeng F, Gao W (2005) An observational study of soil moisture effects on wind erosion at a gobi site in the Taklimakan Desert. J Geophys Res 110, D18S03. doi:10.1029/2004JD004709

Ishizuka M, Mikami M, Leys J, Yamada Y, Heidenreich S, Shao Y, McTainsh GH (2008) Effects of soil moisture and dried raindroplet crust on saltation and dust emission. J Geophys Res 113, D24212. doi:10.1029/2008JD009955

Iversen JD, White BR (1982) Saltation threshold on Earth, Mars and Venus. Sedimentology 29:111–119

Iversen JD, Pollack JB, Greeley R, White BR (1976) Saltation threshold on Mars: The effect on interparticle force, surface roughness, and low atmospheric density. Icarus 29:381–393

Jickells TD, An ZS, Andersen KK, Baker AR, Bergametti G, Brooks N, Cao JJ, Boyd PW, Duce RA, Hunter KA, Kawahata H, Kubilay N, La Roche J, Liss PS, Mahowald N, Prospero JM, Ridgwell AJ, Tegen I, Torres R (2005) Global iron connections: between desert dust, ocean biogeochemistry and climate. Science 308(5708):67–71

Kardous M, Bergametti G, Marticorena B (2005) Wind tunnel experiments on the effects of tillage ridge features on wind erosion horizontal fluxes. Ann Geophys 23:3195–3206

Kawamura R (1964) Study of sand movement by wind. In: Hydraulic Engineering Laboratory Technical Report, HEL-2-8, University of California, Berkeley, pp 99–108
Kocurek G, Lancaster N (1999) Aeolian system sediment state: theory and Mojave Desert Kelso dune field example. Sedimentology 46:505–515
Kok JF (2011a) A scaling theory for the size distribution of emitted dust aerosols suggests climate models underestimate the size of the global dust cycle. Proc Natl Acad Sci U S A 108:1016–1021
Kok JF (2011b) Does the size distribution of mineral dust aerosols depend on the wind speed at emission? Atmos Chem Phys 11:10149–10156. doi:10.5194/acp-11-10149-2011
Kok JF, Renno NO (2009) A comprehensive numerical model of steady-state saltation (COMSALT). J Geophys Res 114, D17204. doi:10.1029/2009JD011702
Kurosaki Y, Mikami M (2004) Effect of snow cover on threshold wind velocity of dust outbreak. Geophys Res Lett 31, L03106. doi:10.1029/2003GL018632
Kurosaki Y, Mikami M (2007) Threshold wind speed for dust emission in east Asia and its seasonal variations. J Geophys Res 112, D17202. doi:10.1029/2006JD007988
Laurent B, Marticorena B, Bergametti G, Chazette P, Maignan F, Schmechtig C (2005) Simulation of the mineral dust emission frequencies from desert areas of China and Mongolia using an aerodynamic roughness length map derived from the POLDER/ADEOS 1 surface products. J Geophys Res 110, D18S04. doi:10.1029/2004JD005013
Laurent B, Marticorena B, Bergametti G, Mei F (2006) Modeling mineral dust emissions from Chinese and Mongolian deserts. Glob Planet Change 52:121–141
Laurent B, Marticorena B, Bergametti G, Léon JF, Mahowald NM (2008) Modeling mineral dust emissions from the Sahara desert using new surface properties and soil database. J Geophys Res 113, D14218. doi:10.1029/2007JD009484
Leys JF, Raupach MR (1991) Soil flux measurements with a portable wind erosion tunnel. Aust J Soil Res 29:533–552
Loosemore GA, Hunt JR (2000) Dust resuspension without saltation. J Geophys Res 105(D16):20663–20671
Lopez MV (1998) Wind erosion in agricultural soil: an example of limited supply of particles available for erosion. Catena 33:17–28
MacKinnon DJ, Clow GD, Tigges RK, Reynolds RL, Chaves PS Jr (2004) Comparison of aerodynamically and model-derived roughness lengths (z0) over diverse surfaces, central Mojave desert, California, USA. Geomorphology 63:103–113. doi:10.1016/j.geomorph.2004.03.009
Mahowald N, Jickells TD, Baker AR, Artaxo P, Benitez-Nelson CR, Bergametti G, Bond TC, Chen Y, Cohen DD, Herut B, Kubilay N, Losno R, Luo C, Maenhaut W, McGee KA, Okin GS, Siefert RL, Tsukuda S (2008) The global distribution of atmospheric phosphorus sources, concentrations and deposition rates and anthropogenic impacts. Glob Biogeochem Cycles 22, GB4026. doi:10.1029/2008GB003240
Marshall JK (1971) Drag measurements in roughness arrays of varying density and distribution. Agric Meteorol 8:269–292
Marticorena B, Bergametti G (1995) Modeling the atmospheric dust cycle: 1. Design of a soil-derived dust production scheme. J Geophys Res 100:16415–16430
Marticorena B, Bergametti G (1996) Two-year simulations of seasonal and interannual changes of the Saharan dust emissions. Geophys Res Lett 23:1921–1924
Marticorena B, Formenti P (2013) Fundamentals of aeolian sediment transport: long-range transport of dust. In: Shroder JF (ed) Treatise on geomorphology, vol 11. Academic, San Diego, pp 64–84
Marticorena B, Bergametti G, Gillette DA, Belnap J (1997a) Factors controlling threshold friction velocity in semi-arid and arid areas of the United States. J Geophys Res 102:23277–23287
Marticorena B, Bergametti G, Aumont B, Callot Y, N'Doumé C, Legrand M (1997b) Modeling the atmospheric dust cycle: 2. Simulation of Saharan dust sources. J Geophys Res 102:4387–4404
Martiny N, Chiapello I (2013) Assessments for the impact of mineral dust on the meningitis incidence in West Africa. Atmos Environ 70:245–253. doi:10.1016/j.atmosenv.2013.01.016

McKenna-Neuman C, Nickling WG (1989) A theoretical and wind tunnel investigation of the effect of capillarity water on the entrainment of sediment by wind. Can J Soil Sci 69:79–96
Milton SF, Greed G, Brooks ME, Haywood J, Johnson B, Allan RP, Slingo A, Grey WMF (2008) Modeled and observed atmospheric radiation balance during the West African dry season: role of mineral dust, biomass burning aerosol, and surface albedo. J Geophys Res 103, D00C02. doi:10.1029/2007JD009741
Natsagdorj L, Jugder D, Chung YS (2003) Analysis of dust storms observed in Mongolia during 1937–1999. Atmos Environ 37:1401–1411
Nickling WG (1983) Grain-size characteristics of sediment transported during dust storms. J Sediment Petrol 53:1011–1024
Nickling WG, Gillies JA (1989) Emission of fine-grained particulates from desert soils. In: Leinen M, Sarnthein M (eds) Paleoclimatology and paleometeorology: modern and past patterns of global atmospheric transport. Kluwer, Dordrecht, pp 133–165
Nickling WG, Gillies JA (1993) Dust emission and transport in Mali, West Africa. Sedimentology 40:859–868
Nickling WG, McTainsh GH, Leys JF (1999) Dust emissions from the channel country of western Queensland, Australia. Z Geomorphol NF 116:1–17
Owen PR (1964) Saltation of uniform grains in air. J Fluid Mech 20(2):225–242
Pauley PM, Baker NL, Barker EH (1996) An observational study of the "Interstate 5" dust storm case. Bull Am Meteorol Soc 77:693–720
Porch WM, Gillette DA (1977) A comparison of aerosol and momentum mixing in dust storms using fast-response instruments. J Appl Meteorol 16(12):1273–1281
Priestley CHB (1959) Turbulent transfer in the lower atmosphere. University of Chicago Press, Chicago, 130 pp
Rajot JL (2001) Wind blown sediment mass budget of Sahelian village land units in Niger. Bull Soc Géol France 172:523–531
Rajot JL, Alfaro SC, Gomes L, Gaudichet A (2003) Soil crusting on sandy soils and its influence on wind erosion. Catena 53:1–16
Raupach MR (1991) Saltation layers, vegetation canopies and roughness lengths. Acta Mech 1(Suppl):83–96
Raupach MR (1992) Drag and drag partition on rough surfaces. Bound Layer Meteorol 60:375–395
Raupach MR, Gillette DA, Leys JF (1993) The effect of roughness elements on wind erosion threshold. J Geophys Res 98:3023–3029
Rice MA, Willetts BB, McEwan IK (1995) An experimental study of multiple grain-size ejecta produced by collisions of saltating grains with a flat bed. Sedimentology 42:695–706
Rice MA, Willetts BB, McEwan IK (1996) Wind erosion of crusted sediments. Earth Surf Process Landf 21:279–293
Saleh A, Fryrear DW (1995) Threshold wind velocities of wet soils as affected by wind blown sand. Soil Sci 160:304–309
Shao Y (2000) Physics and modelling of wind erosion. Kluwer, Dordrecht, 393 pp
Shao Y (2001) A model for mineral dust emission. J Geophys Res 106:20239–20254
Shao Y (2004) Simplification of a dust emission scheme and comparison with data. J Geophys Res 109, D10202. doi:10.1029/2003JD004372
Shao Y (2008) Physics and modelling of wind erosion. Springer, Heidelberg. 452 pp
Shao Y, Li A (1999) Numerical modelling of saltation in the atmospheric surface layer. Bound Layer Meteorol 91:199–225
Shao Y, Lu H (2000) A simplified expression for threshold friction velocity. J Geophys Res 105:22437–22443
Shao Y, Raupach MR, Findlater PA (1993) Effect of saltation bombardment on the entrainment of dust by wind. J Geophys Res 98:12719–12726
Shao Y, Raupach MR, Leys JF (1996) A model for predicting aeolian sand drift and dust entrainment on scales from paddock to region. Aust J Soil Res 34:309–342
Shao Y, Ishizuka M, Mikami M, Leys JF (2011) Parameterization of size-resolved dust emission and validation with measurements. J Geophys Res 116, D08203. doi:10.1029/2010JD014527

Sörensen M (1985) Estimation of some Aeolian saltation transport parameters from transport rate profiles. In: Barndorff-Nielsen OE, Möller JT, Römer Rasmussen K, Willets BB (eds) Proceedings of the international workshop on the physics of blown sand. University of Aarhus, Aarhus, pp 141–190

Sow M, Alfaro SC, Rajot JL, Marticorena B (2009) Size resolved dust emission fluxes measured in Niger during 3 dust storms of the AMMA experiment. Atmos Chem Phys 9(12):3881–3891

Thomson MC, Molesworth AM, Djingarey MH, Yameogo KR, Belanger F, Cuevas LE (2006) Potential of environmental models to predict meningitis epidemics in Africa. Trop Med Int Health 11(6):781–788

Tompkins AM, Cardinali C, Morcrette J-J, Rodwell M (2005) Influence of aerosol climatology on forecasts of the African easterly jet. Geophys Res Lett 32, L10801. doi:10.1029/2004GL022189

Valentin C, Bresson L-M (1992) Morphology, genesis and classification of surface crusts in loamy and sandy soils. Geoderma 55:225–245

Wang X, Ma Y, Chen H, Wen G, Chen S, Tao Z, Chung YS (2003) The relation between sandstorms and strong winds in Xinjiang, China. Water Air Soil Pollut 3:67–79

Warren A, Chappell A, Todd MC, Bristow C, Drake N, Engelstaedter S, Martins V, M'bainayel S, Washington R (2007) Dust-raising in the dustiest place on earth. Geomorphology 92:25–37

White BR (1979) Soil transport by winds on Mars. J Geophys Res 84:4643–4651

Wiggs GFS, Baird AJ, Atherton RJ (2004) The dynamic effects of moisture on the entrainment and transport of sand by wind. Geomorphology 59(1–4):13–30

Williams G (1964) Some aspects of the aeolian saltation load. Sedimentology 3:253–256

Wolfe SA, Nickling WG (1996) Shear stress partitioning in sparsely vegetated desert canopies. Earth Surf Process Landf 21:607–619

Chapter 6
Meteorological Aspects of Dust Storms

Peter Knippertz

Abstract Dust emission requires the combination of deflatable soil material and near-surface wind speeds above the local emission threshold. Across the many dust source regions on Earth a number of generic meteorological phenomena can be identified and classified: (1) Large-scale monsoon-type flows associated with an acceleration towards a continental heat low, predominantly in late spring and early summer; (2) mobile synoptic-scale systems such as anticyclones, cyclones and their cold fronts, typically in late winter and spring; (3) gust fronts generated by outflow from moist convective storms, most common during the beginning of the summer rainy season; (4) intense dry convection in the daytime planetary boundary layer particularly during summer, leading to the generation of dust devils and dusty plumes. These processes can locally be modified by topographic effects and are usually characterised by marked diurnal cycles, for example caused by the development and subsequent breakdown of nocturnal low-level jets in areas of sufficiently large pressure gradients and stable nighttime conditions. In this chapter the different meteorological phenomena listed above will be explained and illustrated using ground-based observations, satellite data and measurements from field campaigns as well as data from meteorological models.

Keywords Meteorology • Large-scale circulations • Cyclones • Anticyclones • Moist convection • Dry convection • Diurnal variations • Topographic effects • Modelling • Cold front • Dust emission • Wind

P. Knippertz (✉)
School of Earth & Environment, University of Leeds, Leeds, UK

Institute for Meteorology and Climate Research, Karlsruhe Institute of Technology, Karlsruhe, Germany
e-mail: peter.knippertz@kit.edu

P. Knippertz and J.-B.W. Stuut (eds.), *Mineral Dust: A Key Player in the Earth System*, DOI 10.1007/978-94-017-8978-3_6,

6.1 Introduction

Dust emission occurs from multiple sources around the globe (Chap. 3), when the near-surface wind exceeds the emission threshold determined by the local soil conditions (Chap. 5). This threshold is strongly influenced by factors such as rainfall, soil moisture, flooding (e.g. of ephemeral lakes), vegetation and snow cover. Soil and wind related factors in combination create strong regional, seasonal, interannual and longer-term variations in dust emissions. This chapter concentrates on meteorological mechanisms for the generation of strong winds over dust sources during the parts of the year, when the soil is typically dry and exposed enough to be deflated, leading to local peaks in the annual dust emission (for an overview, see Littmann 1991).

These meteorological drivers will be separated by their spatial scales into continental-scale circulation systems like monsoons (Sect. 6.2), synoptic-scale weather systems in the southern midlatitudes, subtropics and tropics (Sect. 6.3), mesoscale moist convective systems (Sect. 6.4) and microscale processes in the dry-convective planetary boundary layer (PBL; Sect. 6.5). Subsequently, diurnal variations (Sect. 6.6) and topographic effects such as lee cyclogenesis and orographic channelling (Sect. 6.7) will be described. Section 6.8 discusses how well the multi-scale processes involved in dust lifting and transport are captured in state-of-the-art computer models (see also Chaps. 9 and 10).

While there is no doubt that each dust source region has its own particular local characteristics as discussed in many other articles and books, this chapter does not aim to describe and discuss all these in any detail. Instead it aims at conveying a general understanding of the meteorological mechanisms of greatest importance to dust emission and subsequent transport, which are in fact common to many dust source regions. A certain focus will be placed on the world's most significant dust source regions in the so called dust belt, reaching from northern Africa across the Middle East and central Asia to northern India, as well as those in China and Mongolia (see Chap. 3 for more details). Additional discussion will be devoted to sources in North America and Australia, while the understudied weaker dust regions in South America and southern Africa are covered less.

Many of the dust emission regions mentioned above, particularly the single most important one, the Sahara, have a sparse observational network, as population density tends to be low in source areas. Recent fieldwork on different continents (see list in Chap. 1), together with significant advances in dust remote sensing (Chap. 7) and dust modelling (Chaps. 9 and 10), has improved our understanding of the role of the multi-scale meteorological processes involved in dust emission and transport as well as their relative importance. Given the highly non-linear dependence of emitted dust mass on peak wind speeds, a better understanding of the meteorological processes involved is not only key to interpreting observations of dust, but crucially also to successful modelling of the global dust budget and its climatic impact (see Chap. 13), as many of the processes described in the following occur at scales below that of a typical climate or Earth system model.

6.2 Large-Scale Circulations

Many dust sources around the world are located in areas influenced by monsoon circulations, most notably the Indian and West African monsoons. These regions are characterised by a reversal of the mean wind direction from summer to winter, associated with the formation of marked continental heat lows during the hottest part of the year (marked 'L' in Fig. 6.1). For the Indian summer monsoon, the lowest mean-sea level pressure is typically found near the Pakistan-Indian border around 30°N, 73°E. The strong interhemispheric pressure gradient to the subtropical anticyclone over the southern Indian Ocean drives a powerful circulation with strong and persistent winds affecting dust sources on the Horn of Africa, the eastern flank of the Arabian Peninsula as well as in southern parts of Pakistan and northwestern parts of India (marked by red lines in Fig. 6.1). At the same time, there is a north–south corridor of strong northerly winds across Turkmenistan, eastern Iran and Afghanistan directed into the heat low, which is sometimes referred to as the "wind of 120 days" (Middleton 1986). There is a maximum occurrence of dust days with

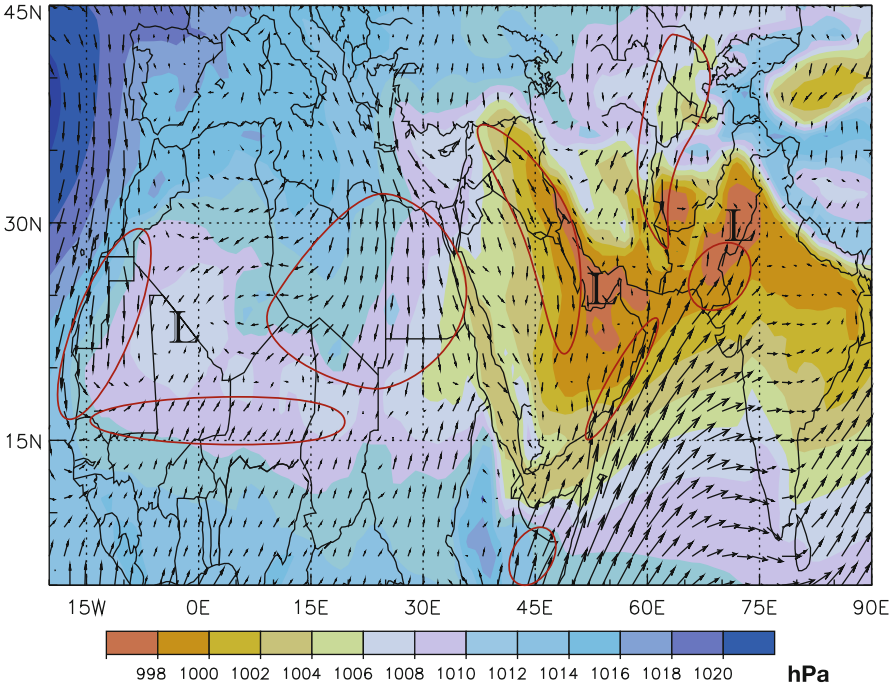

Fig. 6.1 Boreal summer (June–August) average mean sea-level pressure (*shaded*) and 10 m vector winds. The three main continental heat lows over West Africa, the Arabian Peninsula and the border of India and Pakistan are marked with 'L's. Areas with strong inflow into these heat lows prone to dust generation are marked in red. The plot is based on 1979–2012 ERA-Interim analyses produced by the European Centre for Medium-Range Weather Forecasts (ECMWF)

visibility of less than 1,000 m near the area of convergence in the Sistan region, where the borders of Iran, Afghanistan and Pakistan meet (Fig. 2 in Middleton 1986). Farther to the west, the northwesterly summer Shamal winds, which frequently carry dust, blow across the Tigris and Euphrates river valleys of Iraq and the Persian Gulf states into the heat low over the Arabian Peninsula (Fig. 6.1).

In a similar way, the weaker West African or Saharan heat low generates marked circulations and convergence from late spring into summer (Fig. 6.1). Due to the orographic barriers of the Atlas and Hoggar Mountains the three most important inflow regions are the very strong and persistent Atlantic inflow over Western Sahara and Mauritania (Knippertz 2008; Grams et al. 2010; Todd et al. 2013), the southerly monsoon flow over the Sahel (Parker et al. 2005; Flamant et al. 2007; Bou Karam et al. 2008) and the northeasterly inflow from the eastern and central Mediterranean Sea (Knippertz et al. 2009a) (all marked in Fig. 6.1). All three airstreams pass over dust source regions, leading to a marked maximum near the centre of the heat low, where low-level convergence is strong (Engelstaedter and Washington 2007). Similar but weaker inflows into continental heat lows are found for other monsoon regions with less pronounced dust activity such as Australia with its persistent southerly winds over the southern coastal region in austral summer, and North America with persistent inflow from the Gulf of Mexico into the southern Great Plains (not shown).

6.3 Synoptic-Scale Aspects

Synoptic-scale weather systems are the primary control on episodic, large, intense dust events in many source regions. The most important prerequisite is the establishment of a sufficiently large low-level pressure gradient to drive strong winds capable of dust emission and often also long-range transport. On the synoptic scale, these are frequently associated with extratropical cyclonic disturbances and particularly the trailing cold fronts associated with them, but can also occur in connection with strong winds around anticyclones or with tropical African easterly waves (AEWs; Knippertz and Todd 2010). AEWs are disturbances that frequently form along the midlevel easterly jet over the Sahel during summer.

The importance of individual dust storm types is a strong function of season and position relative to the main stormtracks and subtropical anticyclones. The former are located over the North Atlantic/Europe, the Mediterranean/Middle East, Siberia, the North Pacific and a circumpolar band in the southern hemisphere between about 40 and 60°S. Activity maxima typically occur in the local winter and spring. Naturally, most dust source regions are found on the equatorward side of the stormtracks, where precipitation is low. The subtropical anticyclones are centred over the eastern parts of all major ocean basins in both hemispheres year-round, typically around 30° latitude with moderate seasonal shifts. In addition, there are shallow, cold continental highs over central Asia and Canada during winter.

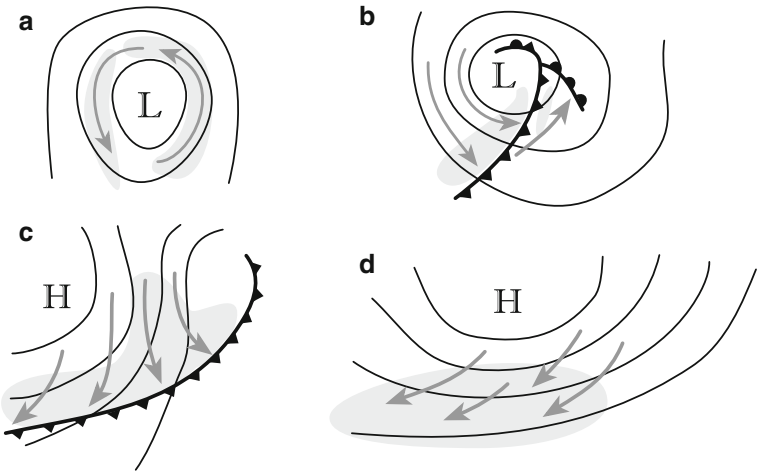

Fig. 6.2 Different generic types of synoptic-scale dust storms (here depicted for the northern hemisphere): (**a**) Type I: Continental desert depression without a clear frontal structure; (**b**) Type II: Well developed cyclone with dust emission behind (and sometimes also ahead of) the cold front; (**c**) Type III: Weak cyclonic disturbance with long trailing cold front and strong post-frontal ridge formation causing highly isallobaric flow; (**d**) Type IV: Intensified subtropical (or sometimes mid-latitude) high-pressure system. *Black lines* are isobars with 'L' and 'H' marking low- and high-pressure centres. *Grey arrows* show areas of strong surface winds with resulting dust plumes in grey shading. Fronts are marked with standard symbols

Many case studies of significant dust events and statistical analyses of long-term records have contributed to our understanding of the dominant synoptic types and their seasonal variations. The different mechanisms of dust lifting and transport documented in the literature can sometimes occur in isolation, but are often part of a succession of events, leading to prolonged and widespread dust episodes, which can last several days and affect areas of almost continental scale. Figure 6.2 categorises the different types/stages of synoptic-scale dust events. Most of these occur from late winter to early summer with spring being the most active season in large parts of northern Africa, Asia, Australia and North America. This seasonality is related to the transition from the winter to the summer circulation, which is often accompanied by episodes of rapid equatorward transport of cold airmasses from high latitudes into the subtropics, where most dust sources are located (Chap. 3). In spring, the mid and high latitudes are still covered with snow and sea ice, and sea surface temperatures are at a minimum, while the dry subtropical landmasses heat up quickly in response to the increased solar radiation, leading to large temperature contrasts. The resulting baroclinicity provides energy for strong synoptic-scale disturbances that can lead to cyclonic storms with sharp cold fronts. These often generate an eastward and sometimes poleward transport of dust (Fig. 6.2a, b).

The advection of air from high-latitude origin behind the cold front can lead to rapid pressure increase and anticyclogenesis. These events have been termed cold

intrusions, cold surges or even pressure surges with dust typically being lifted and transported in northerly or northwesterly winds (southerly or southwesterly in the southern hemisphere) (Fig. 6.2c). In addition waves on the upper-level subtropical jet can intensify and shift subtropical anticyclones into nearby continental regions and increase winds there without a surface cyclogenesis. These situations tend to enhance the trade wind circulations creating equatorward and westward dust transport (Fig. 6.2d). The following subsections provide more detail and regional examples of these four types.

6.3.1 Cyclone Dominated Dust Events

Cyclonic dust storms are most prominent near stormtrack areas, usually mainly affecting the poleward parts of hot deserts. Figure 6.3a shows an example of an intense cyclonic dust storm over India and Pakistan in April 2005 (Badarinath et al. 2007; Prasad and Singh 2007). The associated low-pressure system forms on the eastern side of an upper-trough extending equatorwards from a more intense midlatitude system (Fig. 6.3b). There are sharp pressure gradients on the northwestern and northeastern flanks of the low, both associated with dust activity (Fig. 6.3a). The formation of such a cyclone over hot and dry land is typically associated with frontal and cloud structures that are much less pronounced than those of a typical midlatitude cyclone (Fig. 6.3a). A similar phenomenon is the Khamsin (Libya and Egypt) or Sharav cyclone (Middle East) that forms along the northern margin of the Sahara (Alpert and Ziv 1989; Bou Karam et al. 2010). These systems are often related to lee cyclogenesis to the south of the Atlas Mountains and then track eastward along the Mediterranean coast. Many tracks turn northwards into Turkey (Hannachi et al. 2010), but some systems continue moving eastwards (Saeed and Al-Dashti 2011). Incorporating moisture from the Mediterranean Sea can lead to a rapid intensification of the systems, associated with significant rainfall. Khamsin cyclones often resemble Type I (Fig. 6.2a) in their early stages. Other examples are heat troughs over Australia (Strong et al. 2011).

Many low-latitude cyclones, however, develop sharp cold fronts with dust emission in the westerly or even northwesterly (southwesterly in the southern hemisphere) flow behind them (Type II, see Fig. 6.2b). Khamsin cyclones in their late stages are often of this type as the example shown in Fig. 6.3c with its core over Turkey and widespread dust emission behind the cold front over Libya and Egypt. In a similar way, dust storms from the northern Negev to Iraq are associated with cold fronts from lows between Cyprus and the Turkish-Syrian border (Offer and Goossens 2001; Liu et al. 2007; Saeed and Al-Dashti 2011). These situations are sometimes referred to as winter Shamal in Iraq. Mobile cold fronts with dust emission and transport to the west and south also dominate dust sources in the interior parts of southern and central Australia in spring and summer (Ekström et al. 2004; McTainsh et al. 2005; Leslie and Speer 2006; Wain et al. 2006; Shao et al. 2007; Baddock et al. 2009; Gabric et al. 2010; Strong et al. 2011). Dust storms over

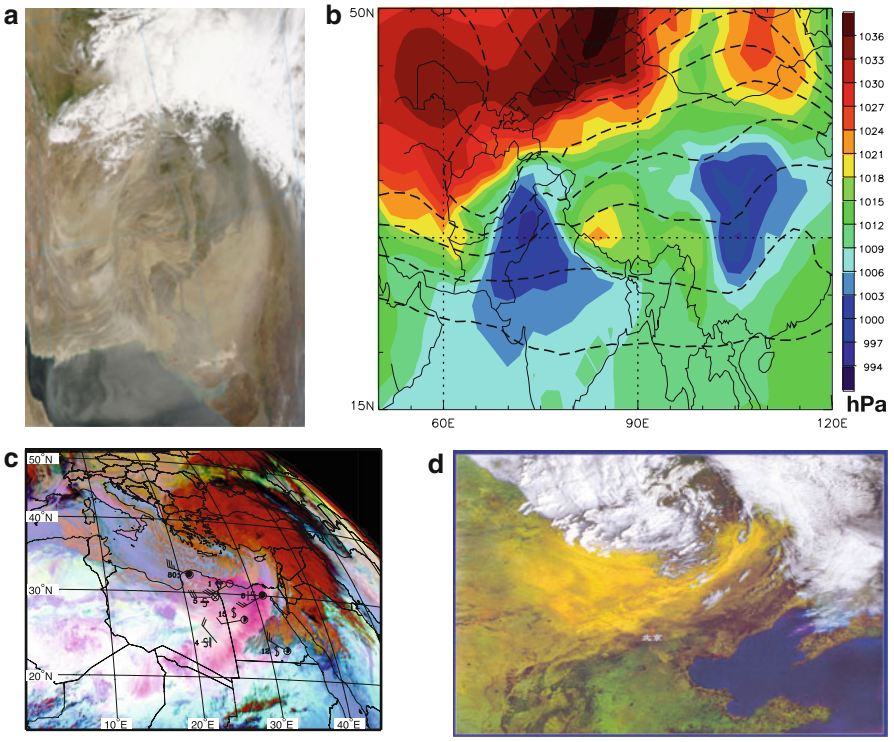

Fig. 6.3 Examples of synoptic dust storm Types I (*top*) and II (*bottom*). (**a**) MODIS Terra visible image at 0610 UTC 7 April 2005 showing an intense dust storm over India and Pakistan. (**b**) Associated patterns (at 00 UTC 7 April) of mean sea-level pressure (*shading*) and geopotential height at 500 hPa (contoured every 60 gpm) from ECMWF data. (**c**) Meteosat dust product showing a Khamsin cyclone on 22 January 2004 including some synoptic station reports indicating dust storms and strong winds (Fig. 9b in Knippertz and Todd 2012). The *dark red colours* show the main cloud mass of the cyclone and cold front, while *pink colours* indicate dust emission. (**d**) Dust storm over China as seen by the Chinese Geostationary Satellite FY-1C in the morning of 6 April 2000 (Fig. 12 in Shao et al. 2002)

the Gobi Desert (Mongolia and China) show a sharp activity peak associated with spring cyclones with a secondary maximum in autumn, while winter is dominated by the cold Siberian anticyclone (Qian et al. 2002; Shao and Wang 2003; Yamamoto et al. 2007). Dust emissions mostly occur in the cold northwesterly and sometimes westerly winds behind the front (Fig. 6.3d; Sun et al. 2001; Shao et al. 2002; Liu et al. 2003; Natsagdory et al. 2003; Shao et al. 2003; Takemi and Seino 2005; Tao et al. 2006).

North American dust events are also dominated by Type II cyclones during winter and spring, often associated with marked upper-level troughs and jets (Orgill and Sehmel 1976; Novlan et al. 2007). Most activity occurs over the southern Great Plains including the Chihuahuan Desert in northern Mexico (Yin et al. 2005;

Novlan et al. 2007; Rivera Rivera et al. 2009), and southwestern USA (Brazel and Nickling 1986; Bach et al. 1996). Dust events associated with mobile cyclones and associated cold fronts are observed as far north as the northern Great Plains (Godon and Todhunter 1998) and Canadian Prairies (Wheaton and Chakravarti 1990), and as far south as Mexico City (Jauregui 1989). Dust from Type II cyclones is often transported polewards, particularly if the surface low is connected to a midlevel trough that provides the extensive meridional flow for long-range transport. Example cases have been documented for Europe (DeSouza-Machado et al. 2010; Wiegand et al. 2011; Cabello et al. 2012; White et al. 2012) or the Asian states of the former USSR (Middleton 1986).

During summertime, when monsoon circulations are strongest (see Sect. 6.2), the midlatitude stormtrack is weak and shifted polewards, and only dust sources located at higher latitudes are occasionally affected by cyclonic dust storms. For example, Orlovsky et al. (2005) describe intrusions of cooler air into the thermal depression over southeastern Turkmenistan. Pre-frontal troughs can occasionally affect coastal areas in south and west Australia during summer and autumn in drought conditions (Garratt 1984; Ekström et al. 2004; Gibson 2007; Strong et al. 2011). Weak summer cyclones also affect the Canadian Prairies (Wheaton and Chakravarti 1990). Tropical cyclones are frequent during this time of year but only rarely and indirectly affect dust source regions (e.g. Brazel and Nickling 1986), as they are generally associated with too much precipitation to allow dust generation.

Interesting examples of tropical synoptic-scale weather systems causing summertime dustiness are the cyclonic surface vortices associated with AEWs over the Sahel/southern Sahara. AEWs also contribute to dust emission through convective cold pools (see Sect. 6.4), favoured by the moist southerlies to the east of the AEW trough. These are sometimes enhanced through interactions with subtropical upper-level troughs (Knippertz and Todd 2010), which have been proposed to create mobile, dust generating, cyclonic surface disturbances called Soudano-Saharan Depressions, but this concept has recently been questioned on the basis of modern re-analysis and satellite data (Schepanski and Knippertz 2011). In addition, AEWs modify dust transport over the continent and downstream tropical Atlantic (Karyampudi and Carlson 1988).

6.3.2 Anticyclone Dominated Dust Events

Some of the cyclonic storms affecting dust regions develop long, trailing cold fronts with marked post-frontal anticyclogenesis, which dominates low-level pressure patterns, winds and dust emission, typically taking place in equatorward and eastward flow in these cases (Type III, Fig. 6.2c). Through the deep penetration of cold air and high winds into lower latitudes, such situations can create long-lasting and extensive events with high dust amounts. Prominent examples of this type over the Sahara occurred during 02–07 March 2004 (Knippertz and Fink 2006; Min et al. 2009; Mangold et al. 2011; Shao et al. 2010) and 07–13 March 2006 (Slingo et al.

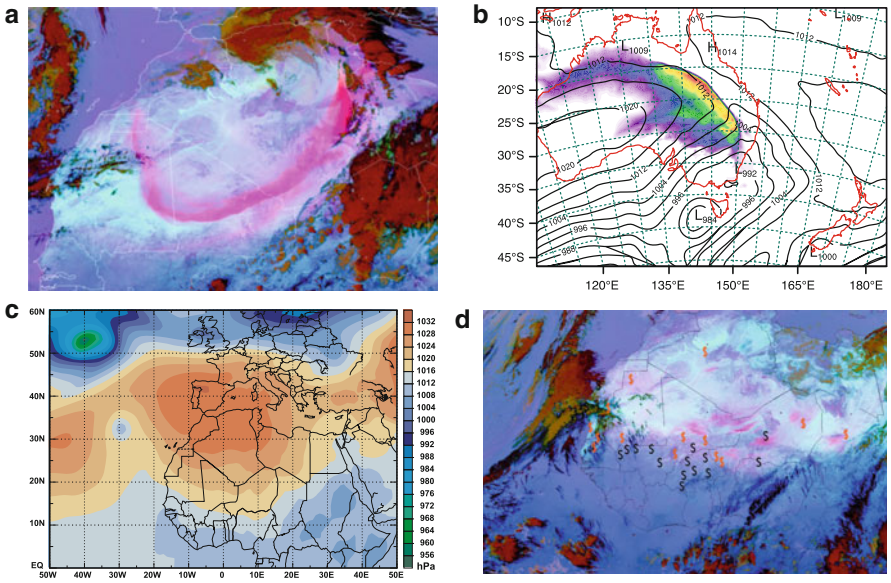

Fig. 6.4 Examples of synoptic dust storm Types III (*top*) and IV (*bottom*). (**a**) Meteosat dust product (as in Fig. 6.3c) at 1800 UTC 24 April 2013. (**b**) Simulated mean sea-level pressure (contour interval of 4 hPa) and surface PM_{10} concentrations (up to 7,500 mg m^{-3}) at 1600 UTC on 22 September 2009 (Fig. 2a in Alizadeh Choobari et al. 2012a). (**c**) Mean sea-level pressure and (**d**) Meteosat dust product overlaid with station reports of 'dust in suspension' (*black*) and "dust raised by the wind" (*orange*) at 1200 UTC on 21 January 2008 (Figs. 7a, d from Knippertz et al. 2011)

2006; Tulet et al. 2008; Cavazos et al. 2009; Mallet et al. 2009; Kocha et al. 2012; Stanelle et al. 2010). The satellite image of a recent case in April 2013 (Fig. 6.4a) shows a well-developed cyclonic cloud feature near the coasts of Algeria, Tunisia and Libya, while an elongated cloud-free band of enhanced dust loadings stretches far into the Sahara along the trailing cold front.

Examples of cold northerlies associated with winter anticyclones and fronts have been documented for Central Asia (Orlovsky et al. 2005), the Middle East and Arabian Peninsula (de Villiers and van Heerden 2011; Maghrabi et al. 2011; sometimes referred to as Nashi dust storms), and North America (Novlan et al. 2007). Being surrounded by ocean on the poleward side, Australia is not as strongly affected by wintertime continental high-pressure systems as the African-Asian dust belt and North America, but still many cyclonic storms generate marked high-pressure ridges behind the cold front with dust being lifted and transported in post-frontal southerlies like in the extreme cases of October 2002 and September 2009 (Fig. 6.4b; Leslie and Speer 2006; Shao et al. 2007; Baddock et al. 2009; Alizadeh Choobari et al. 2012a).

In source regions equatorward of the mean subtropical anticyclones dust can be generated through an intensification of the trade wind circulation towards

the tropical low-pressure trough without a clear low-pressure centre (Type IV, Fig. 6.2d). For the central and southern Sahara and Sahel, for example, ridging of the Azores and Libyan Highs increases the south–north pressure gradient and leads to a surge in the northeasterly harmattan or Etesian winds that amongst other areas affect the Bodélé Depression, the most important single dust source region on the planet (Washington and Todd 2005; Washington et al. 2006; Klose et al. 2010; Knippertz et al. 2011). Figures 6.4c, d shows a typical case with multiple local dust emission events across the entire Sahel as revealed by both satellite data and station observations.

6.3.3 Dynamics and Character of Dust Fronts

The passage of dust-generating cold fronts discussed in the previous subsections (particularly Types II and III) is typically associated with a marked drop in temperature and visibility and increases in wind speed and pressure (e.g. Knippertz and Fink 2006; Maghrabi et al. 2011). Depending on the season and region as well as the evolution of the cyclone, however, the depth and shape of the frontal zone can vary significantly. Smirnov et al. (1993) categorised two different types of cold fronts in central Asia, which are common in many other dust regions around the world: While some fronts have a more typical midlatitude character with a rearward sloping frontal surface and deep frontal circulation associated with cloud formation (Fig. 6.5b), others develop into shallow density current-like features that may not generate any clouds at all (Fig. 6.5a; see cloud distributions in Figs. 6.3 and 6.4). The deep frontal type may generate precipitation and it has been suggested that evaporative cooling from moderate rain can help to sharpen the front, while not suppressing dust generation through wet soils (Gläser et al. 2012). The shallow type is frequently found in the equatorward portion of cold fronts or fronts in very dry continental regions. Dust storms with a characteristic density-current shape as in Fig. 6.5a have been termed ‘haboobs’ (from the Arab word for wind), which is also used for dust fronts generated by moist convection (see Sect. 6.4). Numerous examples have been documented in the literature, particularly for Australia (Garratt 1984; Smith et al. 1995; Gibson 2007; Gabric et al. 2010).

Due to the slow geostrophic adjustment at low latitudes, the rapid increase of pressure behind the cold front can lead to highly isallobaric winds, blowing almost perpendicular to the isobars (see schematic in Fig. 6.2c; Knippertz and Fink 2006; Wain et al. 2006; Kaplan et al. 2011; Lewis et al. 2011). For dust storms in the western USA Lewis et al. (2011) document a high degree of flow imbalance and complex adjustment processes around strong upper-level jets streaks and troughs with marked secondary circulations (see also Pauley et al. 1996), which ultimately create the near-surface gust front (Fig. 6.6). In addition, recent modelling case studies suggest that dust-radiative effects can modify the temperature, stability and winds in synoptic-scale dust outbreaks and therefore alter the characteristics of fronts (Alizadeh Choobari et al. 2012b; Kocha et al. 2012).

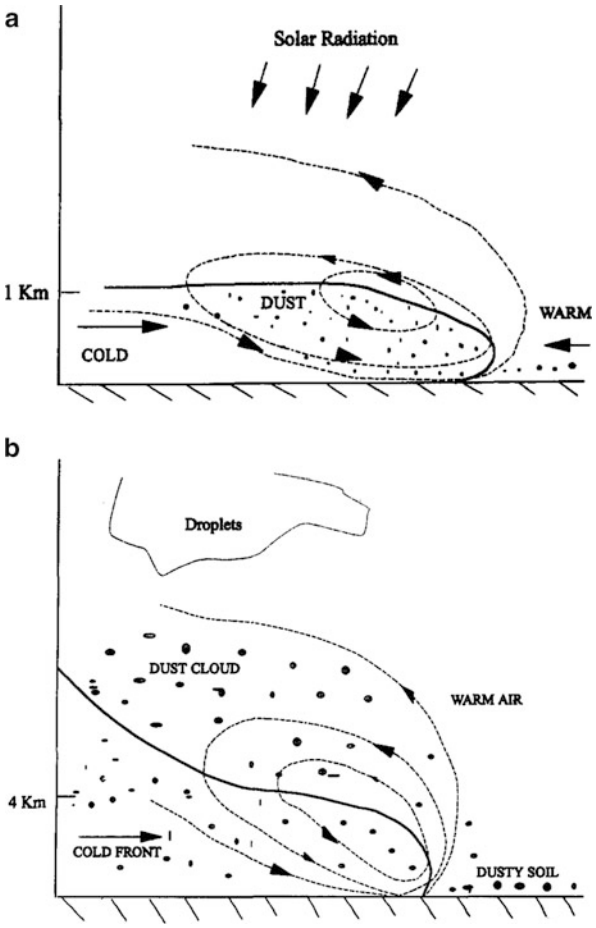

Fig. 6.5 Schematic depiction of the vertical structure of different types of dust-generating cold fronts (Fig. 1 from Smirnov et al. 1993)

6.4 Moist Convection

Evaporationally driven, cold near-surface outflow from moist convection frequently causes dust storms. These range in scale from weak events caused by individual precipitating clouds to outflows from mesoscale convective systems that span hundreds of kilometers. This type of storm is very prominent during the pre-monsoon season, when convective instability is building through an increase in low-level moisture, but when soils are still dry. In addition, dry air at midlevels allows for strong evaporation and downdrafts (Marsham et al. 2008a). In fact, in some of these systems, evaporation is so large that very little or no precipitation is observed at the ground. Convective cold pool-related dust storms belong to the most dramatic of their kind, creating moving "walls of dust" and very sharp increases in wind speed and particle concentrations. As the cold pools behave like density

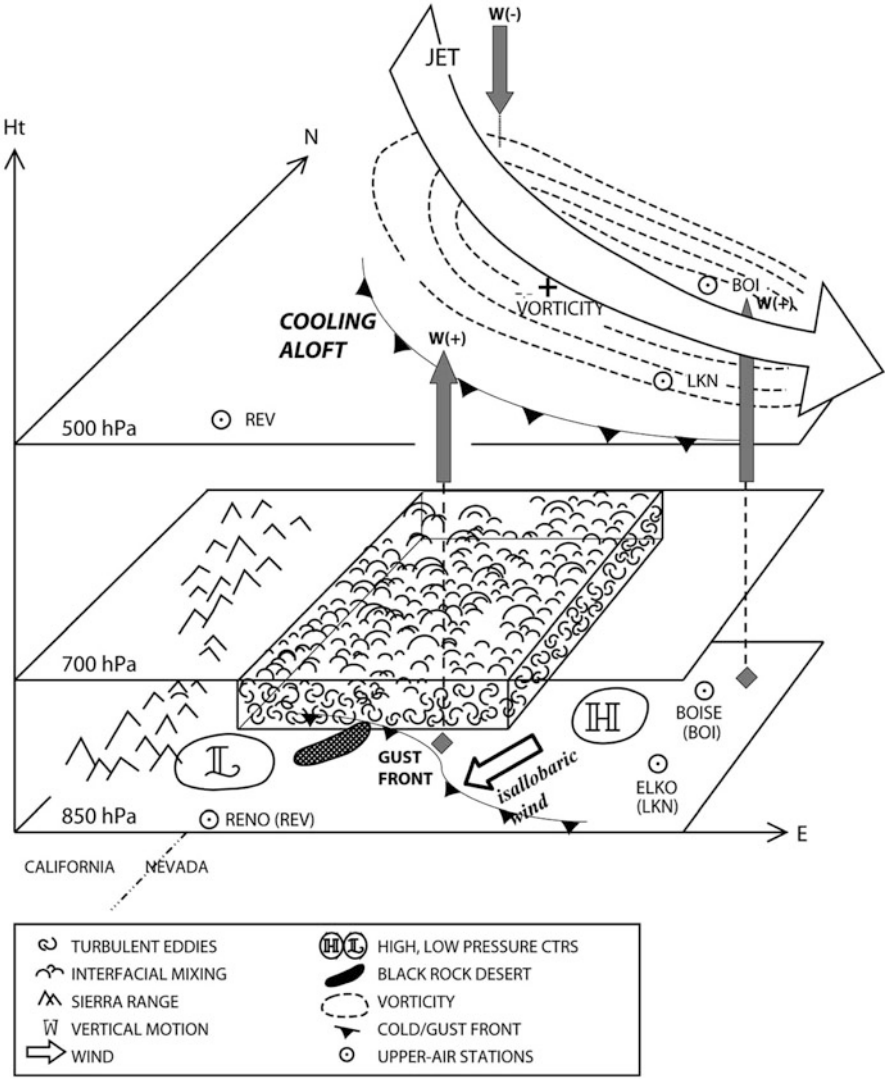

Fig. 6.6 Schematic depiction of the vertical three-dimensional structure of a dust storm over the western USA (Fig. 18 from Lewis et al. 2011)

currents, they are also termed 'haboobs' in the literature (see Sect. 6.3.3). An important element in convective haboobs is the separation of up- and downdrafts through vertical shear, which enhances evaporation (Fig. 6.7). In contrast to many cold-frontal haboobs, those associated with convection may be accompanied by a shelf or arc cloud over the head of the density current, where moist and warm air is lifted over the advancing cooler air (Fig. 6.7).

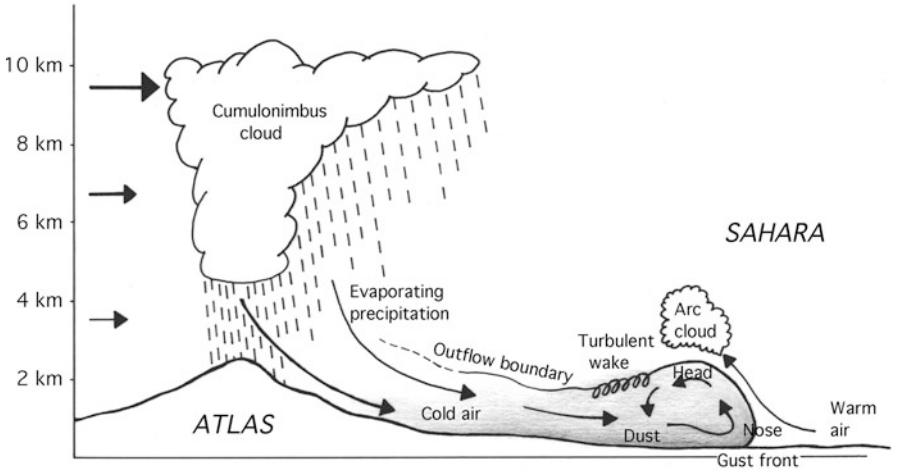

Fig. 6.7 Schematic depiction of a convective dust storm in the foothills of the Atlas Mountains in northwestern Africa. The mountains serve as a trigger for deep moist convection. Evaporation on the dry Saharan side leads to evaporative cooling and the generation of a dust density current. (Fig. 2 from Knippertz et al. 2007)

Convective haboobs have been documented for all major dust source regions of the planet. In particular the squall lines of the Sudan have long been connected to this kind of dust storm during spring and summer (Sutton 1925; Farquharson 1937; Freeman 1952), but haboobs frequently occur throughout the entire Sahel/southern Sahara, where convective organisation is supported by shear underneath a midlevel jet (Lawson 1971; Marsham et al. 2008a; Williams et al. 2008; Knippertz and Todd 2010; Marsham et al. 2013a; Roberts and Knippertz 2014). Other active haboob regions during the pre-monsoon and monsoon seasons include northwestern India (Andhi dust storms, see Middleton 1986 and reference to Joseph 1982), the Middle East (Membery 1985; Offer and Goossens 2001; Miller et al. 2008) and the southern Great Plains of North America (Orgill and Sehmel 1976; Chen and Fryrear 2002; Novlan et al. 2007) as well as central Mexico (Jauregui 1989). Once the monsoon has fully set in, the soil is typically too wet for dust generation, which can create a negative correlation between dust and the frequency of thunderstorms on a seasonal basis (Littmann 1991). Away from main monsoon rains, haboobs tend to occur in the foothills of mountain ranges, which provide a trigger for convective initiation, as for example along the Atlas chain in northern Africa (Fig. 6.7; Knippertz et al. 2007; Emmel et al. 2010) and in the southwestern USA (Orgill and Sehmel 1976; Brazel and Nickling 1986; Bach et al. 1996). Convective dust storms appear to be more localised and infrequent in China (Takemi 2005), Australia (Leslie and Speer 2006; Strong et al. 2011) and the northern Great Plains of the USA (Godon and Todhunter 1998).

There is an ongoing debate on the relative importance of convective haboobs (Engelstaedter and Washington 2008; Williams 2008). Recent modelling studies

strongly suggest that they are a major contributor to dust generation over summertime northern Africa and that many (particularly smaller) events go unnoticed due to the sparse observational network and cloud contamination in satellite data (Marsham et al. 2011; Heinold et al. 2013; Kocha et al. 2013). This is supported by recent in-situ observations of the role of haboobs to dust uplift in the central Sahara (Marsham et al. 2013a). Another aspect of debate is wet deposition of dust particles by convective rains (e.g. Takemi 2005). Satellite imagery suggests that at least the northern parts of many large dusty cold pools over the Sahara can move sufficiently far away from the precipitation areas (Knippertz and Todd 2010), consistent with recent modelling work (Heinold et al. 2013).

6.5 Dry Convection

Turbulent circulations in the dry convective daytime PBL over deserts during summertime can cause considerable dust emission over mostly bare dry lands on days with high insolation and weak background winds (Sinclair 1969; Balme and Greeley 2006). These can take the form of more compact rotating dust devils (typically 10 m in diameter persisting for a few minutes; Fig. 6.8a) and larger, longer-lived non-rotating dusty plumes (typically 100 m in diameter persisting for up to an hour; Koch and Renno 2005). Due to their short lifetime and small scale, as well as logistical problems, systematic observation of these features is a challenge. Consequently, it is not surprising that the majority of studies concentrate on more accessible arid areas in North America (Sinclair 1964; Ryan and Carroll 1970; Ryan 1972; Snow and McClelland 1990; Balme et al. 2003; Renno et al. 2004),

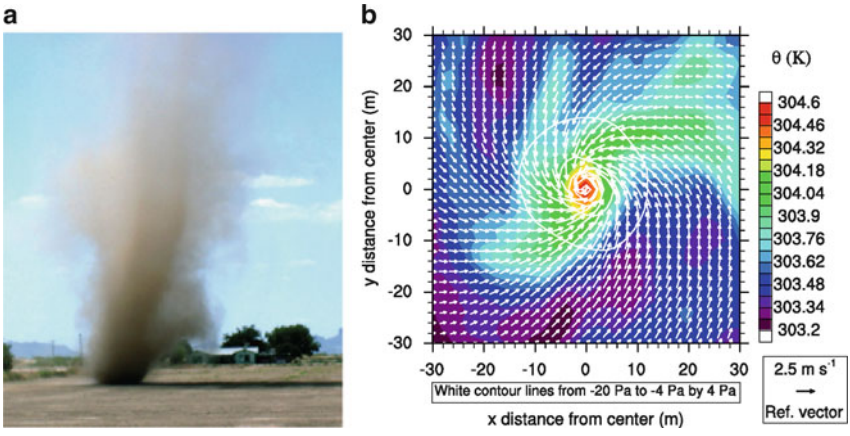

Fig. 6.8 (**a**) Photograph of a dust devil in Eloy, Arizona (Fig. 1c from Balme and Greeley 2006). (**b**) Horizontal distribution of potential temperature (*shading*), perturbation pressure (*contours*) and the horizontal component of wind vectors (*arrows*) at 1 m above ground using 2 m grid spacing (Fig. 8a from Raasch and Franke 2011)

South America (Kurgansky et al. 2011), Australia (Hess and Spillane 1990; Oke et al. 2007; Lyons et al. 2008) and the northern fringes of the Sahara (McGinnigle 1966; Mattsson et al. 1993; Ansmann et al. 2009). Dust devils are a fascinating hydrodynamical problem, which has been investigated by many authors from a theoretical (e.g. Renno et al. 1998; Kurgansky 2006) or more recently also from a high-resolution modelling point of view (Kanak 2005; Ohno and Takemi 2010; Raasch and Franke 2011; Sullivan and Patton 2011; Ito et al. 2013). Figure 6.8b shows an example of a model-generated dust devil indicated by the abruptly increasing cyclonic winds and hot core. Both theoretical and observational studies show large sensitivities of dust devil frequency, intensity and characteristics to aspects such as sensible heat flux, background wind, PBL depth, surface roughness and inhomogeneities, vegetation and terrain slope. The contribution of dust devils and dusty plumes to the global dust emission (in particular of dust available for long-range transport) is unknown. While extrapolations of limited observations in North America by Koch and Renno (2005) suggest values of up to 35 %, Balme and Greeley (2006) regard dust devils as a "nuisance level phenomenon".

6.6 Diurnal Variations

Luo et al. (2004) show that 35–70 % of dust mobilisation in the world's major dust source regions is associated with diurnal variability, dominating over synoptic-scale variability in all major dust regions but East Asia and Australia, where cyclones and fronts are of greater importance. Diurnal variations in the meteorological mechanisms described in previous subsections have different causes, but are mostly related to the build-up and decay of the PBL. This is most obvious for dust devils and dusty plumes, which only occur during the hottest hours of the day, typically from 10 to 16 LT (e.g. Ansmann et al. 2009). Deep moist convection typically peaks in the afternoon hours, but the organisation into mesoscale convective systems or regional scale circulations can extend the occurrence of haboobs well into the night (Knippertz et al. 2007; Emmel et al. 2010; Marsham et al. 2011, 2013a; Heinold et al. 2013). Daytime heating can also set up land-sea or mountain-valley circulations that can be important in certain regions.

A large body of work discusses the importance of nocturnal low-level jets (NLLJs) for dust emission (e.g. Knippertz 2008; Todd et al. 2008a,b). These form due to a decoupling of the air above the radiative surface inversion from surface friction, which then oscillates around the geostrophic wind (Blackadar 1957; van de Wiel et al. 2010). The amplitude of this inertial oscillation depends on the magnitude of the ageostrophic component at the time of decoupling and therefore on the background pressure gradient, the latitude and the roughness of the underlying surface. The oscillation period depends on the Coriolis parameter, favouring highly supergeostrophic NLLJs around 25° latitude (Todd et al. 2008b). After sunrise, the growing PBL mixes momentum from the jet level to the surface, which leads to gusty winds and potentially dust emission (Fig. 6.9a; Engelstaedter and Washington 2007;

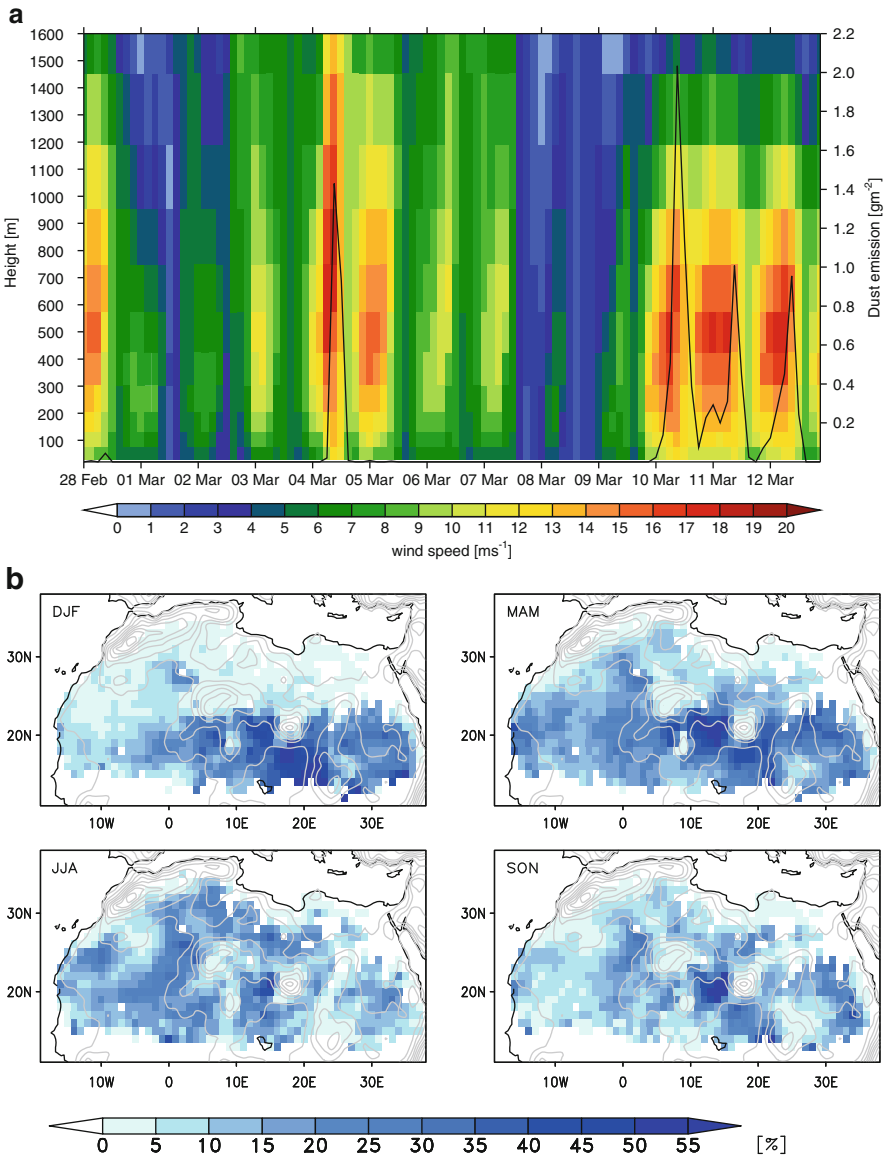

Fig. 6.9 Dust storms related to NLLJs. (**a**) Time series of the low-level profile of horizontal wind speed (*shaded*) at Chicha (Bodélé Depression, Chad) for 28 February to 13 March 2005. *Black lines* show dust emission flux. (**b**) Seasonal mean NLLJ contribution to dust emission. *Contours* show the terrain height in steps of 200 m. All plots are based on ECMWF ERA-Interim data. (Figs. 6 and 16 from Fiedler et al. 2013)

Knippertz 2008). The degree of decoupling depends on the nighttime radiative cooling and therefore on cloud cover, column water vapour and dust loading. In situations of very large pressure gradients (or weak stability), vertical shear can drive mechanical mixing and lead to a breakdown of the NLLJ before sunrise (for a more detailed discussion, see Knippertz and Todd 2012). In addition, the diurnal cycle in surface heating, pressure and turbulence leads to a continental-scale pulsation of the monsoon circulation (Parker et al. 2005; Abdou et al. 2010) that affects winds around the Saharan heat low. In higher latitudes, where NLLJs are less prominent and where the strongest winds tend to be near the tropopause, the largest downward momentum transport occurs when the PBL is deepest in the afternoon, but such effects have been observed over Africa as well (e.g. Marsham et al. 2008b; Todd et al. 2013).

The mechanisms described above suggest a daytime maximum in dustiness in most source regions. This has been confirmed by station observations around the world (Mbourou et al. 1997; Offer and Goossens 2001; Natsagdory et al. 2003; Orlovsky et al. 2005; Marticorena et al. 2010). While North American stations tend to show an afternoon maximum when the PBL is deepest (Orgill and Sehmel 1976; Hahnenberger and Nicoll 2012), many areas in northern Africa show morning peaks related to the breakdown of the NLLJ, in particular in winter and spring (Mbourou et al. 1997; Washington et al. 2006), while summer has an important contribution from afternoon convective storms (Marticorena et al. 2010; Marsham et al. 2013a). Recently, satellite products have become available whose time resolution allows an assessment of the diurnal cycle. Twice-daily time series of MODIS data revealed a strong diurnal pulsing of emission from the Bodélé Depression during winter, indicating discrete 'packets' of emission during daytime hours (Koren and Kaufman 2004). The beginning of dust plume trajectories from 15-min Meteosat imagery suggests a dominance of the mid-morning period in all North African source regions in all seasons (Schepanski et al. 2007, 2009), while estimates based on re-analysis data suggest a fairly small contribution of NLLJs along the Mediterranean Coast in winter and spring (Fig. 6.9b). The NLLJs over northern Africa are typically related to the harmattan and Etesian winds in winter and the Saharan heat low in summer (Fiedler et al. 2013).

However, satellite retrievals struggle to detect very shallow dust layers, dust over bright surfaces or dust below clouds, leading to some important biases (Kocha et al. 2013; see also Chap. 7). Therefore the diurnal cycle in dust emission has also been investigated in high-resolution models. These reveal an important contribution from afternoon and nighttime convective systems (Marsham et al. 2011; see Fig. 6.10), which can even support NLLJ formation through the creation of pressure gradients around ageing cold pools from the previous day (Heinold et al. 2013).

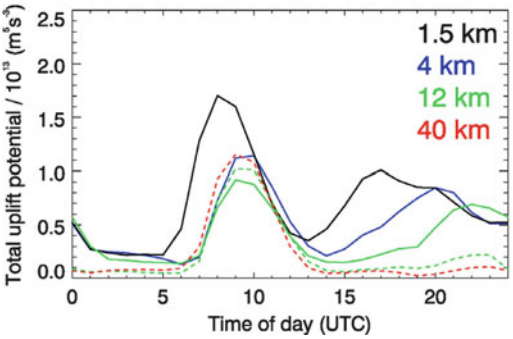

Fig. 6.10 Diurnal cycle of peak winds in model simulations using different horizontal grid spacing (*colours*) and representation of deep moist convection (dashed = parameterised; solid = explicit). The parameter "uplift potential" is closely related to the cube of the wind speed at 10 m height above a constant threshold of 7 m s^{-1}, this way representing the dependency of dust uplift on wind speed for constant soil conditions. Shown are averages over the Sahel and southern Sahara for 25–26 July 2006. The morning peak is related to the breakdown of NLLJs, while the afternoon peak is related to convective activity, which is substantially weaker in models with parameterised convection. (Fig. 3a from Marsham et al. 2011)

6.7 Topographic Effects

Topography alters the meteorology of dust emission and transport in many ways, reaching from influences on monsoon circulations to the triggering of moist convection (Fig. 6.7) or the suppression of dust devil formation on steep terrain. Prominent examples on how terrain affects dust storms include the formations of lee cyclones to the east of the Rocky Mountains (Orgill and Sehmel 1976; Hahnenberger and Nicoll 2012) and to the south of the Atlas Mountains (Alpert and Ziv 1989; Hannachi et al. 2010) in situations of approaching upper-level troughs. Wind channelling has been documented for the Bodélé Depression (Tibesti and Ennedi Mountains; Washington et al. 2006), Owen's Lake in California (Reid et al. 1994) and the Gansu Corridor in China (Goudie and Middleton 1992). Orgill and Sehmel (1976) also discuss the importance of katabatic flows and föhn for parts of the western USA. The Tarim Basin within the Taklamakan Desert in northwest China is a particularly interesting example of a dust source strongly influenced by topography. In contrast to other Chinese sources, the high mountains around the basin reduce the influence of passing cyclones and lead to dust emissions in easterly flow and due to local topographic circulations (Sun et al. 2001; Qian et al. 2002; Shao and Wang 2003; Seino et al. 2005; Mikami et al. 2006). In fact Liu and Westphal (2001) show that wind and dust simulations over Asia improve measurably due to better resolved topography.

6.8 Modelling

Accurate simulation of dust emission and transport is a large challenge for current state-of-the-art models as discussed in detail in Chaps. 9 and 10. Here the representation of specific meteorological features will briefly be summarised. The key process on the continental scale is the representation of the summertime monsoon circulation and specifically the strength of the heat low. For northern Africa, many coarse-resolution models struggle to represent the correct intensity and northward propagation of the monsoon (e.g. Cook and Vizy 2006), which is to some degree related to accumulated effects of errors introduced through the parameterisation of deep moist convection (Marsham et al. 2011, 2013b). In contrast, the synoptic-scale dust outbreaks in winter and spring are usually satisfactorily reproduced (Shao et al. 2002; Laurent et al. 2006; Cavazos et al. 2009; Shao et al. 2010; Alizadeh Choobari et al. 2012a). Synoptic-scale AEWs are also reasonably well represented in state-of-the-art weather prediction models, although interactions with moist convection and the land surface can lead to errors in both strength and propagation (Sander and Jones 2008; Shen et al. 2010). However, systematic biases in the monsoon circulation affect AEWs, too.

The largest deficits of current dust models are arguably associated with deep moist convection and PBL processes. Accurately modelling haboob dust storms is closely tied to a realistic representation of organised moist convection (Knippertz et al. 2009b; Reinfried et al. 2009; Cavazos-Guerra and Todd 2012; Marsham et al. 2011). Practically all weather and climate models used for dust simulations have grid spacings that require a parameterisation of deep convection. These are designed to release convective instability within a model grid box and therefore do not allow for the spatial separation of up- and downdrafts that are crucial to mesoscale organisation and the formation of cold pools, which in reality can reach dimensions of many grid boxes of a typical regional model (up to several 100 km). Other issues are the sensitivity of convective initiation to topography and soil moisture and the occurrence of convectively generated small-scale and short-lived wind events that are not well represented by coarse-resolution models (Heinold et al. 2013). As a consequence, a key meteorological mechanism in areas like the Sahel is not satisfactorily represented in most models (Fig. 6.10) and sometimes not even in analyses due to a lack of observations and difficulties of the model to generate the parent convection (Knippertz et al. 2009a).

While models often reproduce the large-scale pressure gradients that drive NLLJs satisfactorily, they often struggle to capture the distinct diurnal cycle in near-surface winds. Several studies have shown model weaknesses with temperature inversions over arid areas being underestimated, leading to too little decoupling and therefore too much vertical dispersion during the night, even in analysis data (Fiedler et al. 2013). Simulations of NLLJs over the Sahara are sensitive to vertical resolution, PBL scheme and roughness length (Todd et al. 2008b), but less so to horizontal

resolution (Fig. 6.10). Effects of dust devils and PBL turbulence are usually not considered in dust models that use grid point winds to drive emissions (see Chap. 9). Some authors, however, have used simple gust parameterisations to represent effects of dry and moist convection on the probability to exceed dust emission thresholds in a given grid box, which leads to model improvement (Cakmur et al. 2004; Morcrette et al. 2008; Ridley et al. 2013).

6.9 Conclusion

The spatial and temporal scales of the meteorological processes involved in dust storms span several orders of magnitude from microscale dust devils to almost continental-scale dust outbreaks associated with trailing cold fronts. Despite large differences in topography and climate between the world's most important dust source regions, some common meteorological features can be identified. Synoptic-scale dust storms cover a spectrum of types, reaching from cyclonic desert depressions with weak frontal features to well-developed cyclones with marked post-frontal ridges to strong winds around the fringes of subtropical highs or cold continental highs at higher latitudes, often locally modified by topographic channelling. These types of storms are usually most active in spring and well represented in regional dust models. At low latitudes dust emission and transport is affected by synoptic-scale features like AEWs or through interactions with extratropical weather systems.

On the mesoscale, convective dust storms are found in many dust regions, particularly during the pre-monsoon season in West Africa and India/Pakistan and in the vicinity of orographic triggers (e.g. Atlas and Rocky Mountains). An accurate representation of these storms requires explicitly resolving moist convection and its organisation into squall lines, which is beyond the computational limits for most current dust models, creating a fundamental bias over convectively active regions like summertime West Africa. On even smaller scales dry convection in the daytime PBL can create dusty plumes or dust devils, whose contribution to the global dust cycle is unknown and which are typically not represented in dust models other than through a simple gust parameterisation. Daytime mixing in the PBL creates a distinct diurnal cycle in many dust regions. At low latitudes, nighttime acceleration in the stable PBL lead to NLLJs throughout the year whose breakdown causes distinct emission peaks in the morning, while midlatitude areas are often characterised by a dust maximum in the afternoon when the PBL is deepest and taps into momentum from deep baroclinic jets. Improvements to the understanding and model representation of moist convective and PBL processes in the future will further enhance our capabilities of simulating dust storms and their interactions with weather and climate.

References

Abdou K, Parker DJ, Brooks B et al (2010) The diurnal cycle of lower boundary-layer wind in the West African monsoon. Q J Roy Meteorol Soc 136:66–76

Alizadeh Choobari O, Zawar-Reza P, Sturman A (2012a) Atmospheric forcing of the three-dimensional distribution of dust particles over Australia: A case study. J Geophys Res 117, D11206. doi:10.1029/2012JD017748

Alizadeh Choobari O, Zawar-Reza P, Sturman A (2012b) Feedback between windblown dust and planetary boundary-layer characteristics: sensitivity to boundary and surface layer parameterizations. Atmos Environ 61:294–304

Alpert P, Ziv B (1989) The Sharav cyclone: observations and some theoretical considerations. J Geophys Res 94(D15):18495–18514

Ansmann A, Tesche M, Knippertz P et al (2009) Vertical profiling of convective dust plumes in southern Morocco during SAMUM. Tellus 61B:340–353

Bach AJ, Brazel AJ, Lancaster N (1996) Temporal and spatial aspects of blowing dust in the Mojave and Colorado deserts of southern California, 1973–1994. Phys Geogr 17(4):329–353

Badarinath KVS, Kharol SK, Kaskaoutis DG, Kambezidis AH (2007) Case study of a dust storm over Hyderabad area, India: its impact on solar radiation using satellite data and ground measurements. Sci Total Environ 384(1–3):316–332

Baddock MC, Bullard JE, Bryant RG (2009) Dust source identification using MODIS: a comparison of techniques applied to the Lake Eyre Basin, Australia. Remote Sens Environ 113(7):1511–1528

Balme M, Greeley R (2006) Dust devils on Earth and Mars. Rev Geophys 44, RG3003. doi:10.1029/2005RG000188

Balme M, Metzger S, Towner M et al (2003) Friction wind speeds in dust devils: a field study. Geophys Res Lett 30(16):1830. doi:10.1029/2003GL017493

Blackadar AK (1957) Boundary layer wind maxima and their significance for the growth of nocturnal inversions. Bull Am Meteorol Soc 38:282–290

Bou Karam D, Flamant C, Knippertz P (2008) Dust emissions over the Sahel associated with the West African Monsoon inter-tropical discontinuity region: a representative case study. Q J Roy Meteorol Soc 134:621–634

Bou Karam D, Flamant C, Cuesta J et al (2010) Dust emission and transport associated with a Saharan depression: the February 2007 case. J Geophys Res 115, D00H27. doi:10.1029/2009JD012390

Brazel AJ, Nickling WG (1986) The relationship of weather types to dust storm generation in Arizona (1965–1980). J Climatol 6(3):255–275

Cabello M, Orza JAG, Barrero MA et al (2012) Spatial and temporal variation of the impact of an extreme Saharan dust event. J Geophys Res 117, D11204. doi:10.1029/2012JD017513

Cakmur RV, Miller RL, Torres O (2004) Incorporating the effect of small-scale circulations upon dust emission in an atmospheric general circulation model. J Geophys Res 109, D07201. doi:10.1029/2003JD004067

Cavazos C, Todd MC, Schepanski K (2009) Numerical model simulation of the Saharan dust event of 6–11 March 2006 using the Regional Climate Model version 3 (RegCM3). J Geophys Res 114, D12109. doi:10.1029/2008JD011078

Cavazos-Guerra C, Todd MC (2012) Model simulations of complex dust emissions over the Sahara during the West African monsoon onset. Adv Meteorol 2012. doi:10.1155/2012/351731

Chen W, Fryrear D (2002) Sedimentary characteristics of a haboob dust storm. Atmos Res 61:75–85

Cook KH, Vizy EK (2006) Coupled model simulations of the West African monsoon system: 20th century simulations and 21st century predictions. J Clim 19:3681–3703

de Villiers M, van Heerden J (2011) Nashi dust storm over the United Arab Emirates. Weather 66(3):79–81

DeSouza-Machado SG, Strow LL, Imbiriba B et al (2010) Infrared retrievals of dust using AIRS: comparisons of optical depths and heights derived for a North African dust storm to other collocated EOS A-Train and surface observations. J Geophys Res 115, D15201. doi:10.1029/2009JD012842

Ekström M, McTainsh GH, Chappell A (2004) Australian dust storms: temporal trends and relationships with synoptic pressure distributions (1960–99). Int J Climatol 24(12):1581–1599

Emmel C, Knippertz P, Schulz O (2010) Climatology of convective density currents in the southern foothills of the Atlas mountains. J Geophys Res 115, D11115. doi:10.1029/2009JD011819

Engelstaedter S, Washington R (2007) Atmospheric controls on the annual cycle of North African dust. J Geophys Res 112. doi:10.1029/2006JD007195

Engelstaedter S, Washington R (2008) Reply to comment by E. Williams on "Atmospheric controls on the annual cycle of North African dust". J Geophys Res 113, D23110. doi:10.1029/2008JD010275

Farquharson M (1937) Haboobs and instability in the Sudan. Q J Roy Meteorol Soc 63:393–414

Fiedler S, Schepanski K, Heinold B et al (2013) Climatology of nocturnal low-level jets over North Africa and implications for modeling mineral dust emission. J Geophys Res 118(12):6100–6121. doi:10.1002/jgrd.50394

Flamant C, Chaboureau J-P, Parker DJ (2007) Airborne observations of the impact of a convective system on the planetary boundary layer thermodynamics and aerosol distribution in the inter-tropical discontinuity region of the West African Monsoon. Q J Roy Meteorol Soc 133:1175–1189

Freeman M (1952) Duststorms of the Anglo-Egyptian Sudan, Meteorological Reports 11. Her Majesty's Stn. Off, London, p 22

Gabric AJ, Cropp RA, McTainsh GH et al (2010) Australian dust storms in 2002–2003 and their impact on Southern Ocean biogeochemistry. Global Biogeochem Cycles 24, GB2005. doi:10.1029/2009GB003541

Garratt JR (1984) Cold fronts and dust storms during the Australian summer 1982–1983. Weather 39:98–103

Gibson B (2007) Examination of a density current with severe winds and extensive dust: South Australia case study. 2 April 2005. Aust Meteorol Mag 56(4):267–283

Gläser G, Knippertz P, Heinold B (2012) Orographic effects and evaporative cooling along a subtropical cold front: the case of the spectacular Saharan dust outbreak of March 2004. Mon Weather Rev 140(8):2520–2533

Godon NA, Todhunter PE (1998) A climatology of airborne dust for the Red River Valley of North Dakota. Atmos Environ 32(9):1587–1594

Goudie AS, Middleton NJ (1992) The changing frequency of dust storms through time. Clim Change 20(3):197–225

Grams CM, Jones SC, Marsham JM et al (2010) The Atlantic inflow to the Saharan heat low: observations and modelling. Q J Roy Meteorol Soc 136:125–140

Hahnenberger M, Nicoll K (2012) Meteorological characteristics of dust storm events in the eastern Great Basin of Utah, U.S.A. Atmos Environ 60:601–612

Hannachi A, Awad A, Ammar K (2010) Climatology and classification of spring Saharan cyclone tracks. Clim Dyn. doi:10.1007/s00382-010-0941-9

Heinold B, Knippertz P, Marsham JH et al (2013) The role of deep convection and low-level jets for dust emissions in West Africa. J Geophys Res 118(10):4385–4400. doi:10.1002/jgrd.50402

Hess GD, Spillane KT (1990) Characteristics of dust devils in Australia. J Appl Meteorol 29:498–507

Ito J, Niino H, Nakanishi M (2013) Formation mechanism of dust devil–like vortices in idealized convective mixed layers. J Atmos Sci 70:1173–1186

Jauregui E (1989) The dust storms of Mexico-City. Int J Climatol 9(2):169–180

Joseph PV (1982) A tentative model of Andhi. Mausam 33:417

Kanak K (2005) Numerical simulation of dust devil-scale vortices. Q J Roy Meteorol Soc 131:1271–1292

Kaplan ML, Vellore RK, Lewis JM et al (2011) The role of unbalanced mesoscale circulations in dust storms. J Geophys Res 116, D23101. doi:10.1029/2011JD016218
Karyampudi VM, Carlson TN (1988) Analysis and numerical simulations of the Saharan air layer and its effect on easterly wave disturbances. J Atmos Sci 45:3102–3136
Klose M, Shao Y, Karremann MK, Fink AH (2010) Sahel dust zone and synoptic background. Geophys Res Lett 37, L09802. doi:10.1029/2010GL042816
Knippertz P (2008) Dust mobilization in the West African heat trough – the role of the diurnal cycle and of extratropical synoptic disturbances. Meteorol Z 17:553–563
Knippertz P, Fink AH (2006) Synoptic and dynamic aspects of an extreme springtime Saharan dust outbreak. Q J Roy Meteorol Soc 132:1153–1177
Knippertz P, Todd MC (2010) The central west Saharan dust hot spot and its relation to African easterly waves and extratropical disturbances. J Geophys Res 115, D12117. doi:10.1029/2009JD012819
Knippertz P, Todd MC (2012) Mineral dust aerosols over the Sahara: processes of emission and transport, and implications for modeling. Rev Geophys 50, RG1007. doi:10.1029/2011RG000362
Knippertz P, Deutscher C, Kandler K et al (2007) Dust mobilization due to density currents in the Atlas region: observations from the SAMUM 2006 field campaign. J Geophys Res 112, D21109. doi:10.1029/2007JD008774
Knippertz P, Ansmann A, Althausen D et al (2009a) Dust mobilization and transport in the northern Sahara during SAMUM 2006 – a meteorological overview. Tellus 61B:12–31
Knippertz P, Trentmann J, Seifert A (2009b) High-resolution simulations of convective cold pools over the northwestern Sahara. J Geophys Res 114, D08110. doi:10.1029/2008JD011271
Knippertz P, Tesche M, Heinold B (2011) Dust mobilization and aerosol transport from West Africa to Cape Verde – a meteorological overview of SAMUM-2. Tellus 63B:430–447
Koch J, Renno NO (2005) The role of convective plumes and vortices on the global aerosol budget. Geophys Res Lett 32. doi:10.1029/2005GL023420
Kocha C, Lafore J-P, Tulet P et al (2012) High-resolution simulation of a major West African dust-storm: comparison with observations and investigation of dust impact. Q J Roy Meteorol Soc 138:455–470
Kocha C, Tulet P, Lafore J-P, Flamant C (2013) The importance of the diurnal cycle of Aerosol Optical Depth in West Africa. Geophys Res Lett 40:785–790
Koren I, Kaufman YJ (2004) Direct wind measurements of Saharan dust events from Terra and Aqua satellites. Geophys Res Lett 31, L06122. doi:10.1029/2003GL019338
Kurgansky MV (2006) Steady-state properties and statistical distribution of atmospheric dust devils. Geophys Res Lett 33, L19S06. doi:10.1029/2006GL026142
Kurgansky MV, Montecinos A, Villagran V, Metzger SM (2011) Micro-meteorological conditions for dust devil occurrence in the Atacama Desert. Bound Layer Meteorol 138(2):285–298
Laurent B, Marticorena B, Bergametti G, Mei D (2006) Modeling mineral dust emissions from Chinese and Mongolian deserts. Global Planet Change 52(1–4):121–141
Lawson TJ (1971) Haboob structure at Khartoum. Weather 26:105–112
Leslie LM, Speer MS (2006) Modelling *dust* transport over central eastern Australia. Meteorol App 13(2):141–167
Lewis JM, Kaplan ML, Vellore R et al (2011) Dust storm over the Black Rock Desert: larger-scale dynamic signatures. J Geophys Res 116, D06113. doi:10.1029/2010JD014784
Littmann T (1991) Dust storm frequency in Asia – climatic control and variability. Int J Climatol 11(4):393–412
Liu M, Westphal DL (2001) A study of the sensitivity of simulated mineral dust production to model resolution. J Geophys Res 106(D16):18099–18112
Liu M, Westphal DL, Wang SG et al (2003) A high-resolution numerical study of the Asian dust storms of April 2001. J Geophys Res 108(D23):8653. doi:10.1029/2002JD003178
Liu M, Westphal DL, Walker AL et al (2007) COAMPS real-time dust storm forecasting during operation Iraqi freedom. Weather Forecast 22(1):192–206

Luo C, Mahowald NM, Jones C (2004) Temporal variability of dust mobilization and concentration in source regions. J Geophys Res 109, D20202. doi:10.1029/2004JD004861
Lyons TJ, Nair US, Foster IJ (2008) Clearing enhances dust devil formation. J Arid Environ 72(10):1918–1928
Maghrabi A, Alharbi B, Tapper N (2011) Impact of the March 2009 dust event in Saudi Arabia on aerosol optical properties, meteorological parameters, sky temperature and emissivity. Atmos Environ 45(13):2164–2173
Mallet M, Tulet P, Serça D et al (2009) Impact of dust aerosols on the radiative budget, surface heat fluxes, heating rate profiles and convective activity over West Africa during March 2006. Atmos Chem Phys 9:7143–7160
Mangold A, De Backer H, De Paepe B et al (2011) Aerosol analysis and forecast in the European Centre for Medium-Range Weather Forecasts Integrated Forecast System: 3. Evaluation by means of case studies. J Geophys Res 116, D03302. doi:10.1029/2010JD014864
Marsham JH, Parker DJ, Grams CM (2008a) Uplift of Saharan dust south of the inter-tropical discontinuity. J Geophys Res 113, D21102. doi:10.1029/2008JD009844
Marsham JH, Parker DJ, Grams CM et al (2008b) Observations- of mesoscale and boundary-layer scale circulations affecting dust transport and uplift over the Sahara. Atmos Chem Phys 8:6979–6993
Marsham JH, Knippertz P, Dixon N et al (2011) The importance of the representation of deep convection for modeled dust-generating winds over West Africa during summer. Geophys Res Lett 38, L16803. doi:10.1029/2011GL048368
Marsham JH, Hobby M, Allen CJT et al (2013a) Meteorology and dust in the central Sahara: observations from Fennec supersite-1 during the June 2011 Intensive Observation Period. J Geophys Res. doi:10.1002/jgrd.50211
Marsham J, Dixon N, Garcia-Carreras L et al (2013b) The role of moist convection in the West African monsoon system – insights from continental-scale convection-permitting simulations. Geophys Res Lett 40(9):1843–1849. doi:10.1002/grl.50347
Marticorena B, Chatenet B, Rajot JL (2010) Temporal variability of mineral dust concentrations over West Africa: analyses of a pluriannual monitoring from the AMMA Sahelian Dust Transect. Atmos Chem Phys 10:8899–8915
Mattsson JO, Nihlén T, Yue W (1993) Observations of dust devils in a semi-arid district of southern Tunisia. Weather 48:359–363
Mbourou GN, Bertrand JJ, Nicholson SE (1997) The diurnal and seasonal cycles of wind-borne dust over Africa north of the equator. J Appl Meteorol 36:868–882
McGinnigle JB (1966) Dust whirls in north-west Libya. Weather 21:272–276
McTainsh G, Chan Y-C, McGowan H et al (2005) The 23rd October 2002 dust storm in eastern Australia: characteristics and meteorological conditions. Atmos Environ 39(7):1227–1236
Membery D (1985) A gravity-wave haboob? Weather 40:214–221
Middleton NJ (1986) A geography of dust storms in southwest Asia. J Climatol 6(2):183–196
Mikami M, Shi GY, Uno I et al (2006) Aeolian dust experiment on climate impact: an overview of Japan–China joint project ADEC. Global Planet Change 52(1–4):142–172
Miller SSD, Kuciauskas AP, Liu M et al (2008) Haboob dust storms of the southern Arabian Peninsula. J Geophys Res 113, D01202. doi:10.1029/2007JD008550
Min Q-L, Li R, Lin B et al (2009) Evidence of mineral dust altering cloud microphysics and precipitation. Atmos Chem Phys 9:3223–3231
Morcrette J-J, Beljaars A, Benedetti A et al (2008) Seasalt and dust aerosols in the ECMWF IFS model. Geophys Res Lett 35, L24813. doi:10.1029/2008GL036041
Natsagdory L, Jugder D, Chung YS (2003) Analysis of dust storms observed in Mongolia during 1937–1999. Atmos Environ 37:1401–1411
Novlan DJ, Hardiman M, Gill TE (2007) A synoptic climatology of blowing dust events in El Paso, Texas from 1932–2005. Preprints 16th Conference on Applied Climatology, Am Meteorol Soc, J3.12

Offer ZY, Goossens D (2001) Ten years of aeolian dust dynamics in a desert region (Negev desert, Israel): analysis of airborne dust concentration, dust accumulation and the high-magnitude dust events. J Arid Environ 47(2):211–249

Ohno H, Takemi T (2010) Mechanisms for intensification and maintenance of numerically simulated dust devils. Atmos Sci Lett 11:27–32

Oke AMC, Tapper NJ, Dunkerley D (2007) Willy-willies in the Australian landscape: the role of key meteorological variables and surface conditions in defining frequency and spatial characteristics. J Arid Environ 71(2):201–215

Orgill MM, Sehmel GA (1976) Frequency and diurnal-variation of dust storms in contiguous USA. Atmos Environ 10(10):813–825

Orlovsky L, Orlovsky N, Durdyev A (2005) Dust storms in Turkmenistan. J Arid Environ 60(1):83–97

Parker DJ, Burton RR, Diongue-Niang A et al (2005) The diurnal cycle of the West African monsoon circulation. Q J Roy Meteorol Soc 131:2839–2860

Pauley PM, Baker NL, Barker EH (1996) An observational study of the "Interstate 5" dust storm case. Bull Am Meteorol Soc 77(4):693–720

Prasad AK, Singh RP (2007) Changes in aerosol parameters during major dust storm events (2001–2005) over the Indo-Gangetic Plains using AERONET and MODIS data. J Geophys Res 112(D9), D09208. doi:10.1029/2006JD007778

Qian W, Quan L, Shi S (2002) Variations of the dust storm in China and its climatic control. J Clim 15:1216–1229

Raasch S, Franke T (2011) Structure and formation of dust devil–like vortices in the atmospheric boundary layer: a high-resolution numerical study. J Geophys Res 116, D16120. doi:10.1029/2011JD016010

Reid JS, Flocchini RG, Cahill TA et al (1994) Local meteorological, transport, and source aerosol characteristics of late autumn Owens Lake (dry) dust storms. Atmos Environ 28(9):1699–1706

Reinfried F, Tegen I, Heinold B et al (2009) Density currents in the Atlas Region leading to dust mobilization: a model sensitivity study. J Geophys Res 114, D08127. doi:10.1029/2008JD010844

Renno NO, Burkett ML, Larkin MP (1998) A simple thermodynamical theory for dust devils. J Atmos Sci 55:3244–3252

Renno NO, Abreu VJ, Koch J et al (2004) MATADOR 2002: a pilot field experiment on convective plumes and dust devils. J Geophys Res 109, E07001. doi:10.1029/2003JE002219

Ridley DA, Heald CL, Pierce JR, Evans MJ (2013) Towards resolution-independent dust emissions in global models: impacts on the seasonal and spatial distribution of dust. Geophys Res Lett. doi:10.1002/grl.50409

Rivera Rivera NI, Gill TE, Gebhart KA et al (2009) Wind modeling of Chihuahuan Desert dust outbreaks. Atmos Environ 43(2):347–354

Roberts A, Knippertz P (2014) The formation of a large summertime Saharan dust plume: convective and synoptic-scale analysis. J Geophys Res. doi:10.1002/2013JD020667

Ryan JA (1972) Relation of dust devil frequency and diameter to atmospheric temperature. J Geophys Res 77:7133–7137

Ryan JA, Carroll JJ (1970) Dust devil wind velocities: mature state. J Geophys Res 75(3):531–541

Saeed TM, Al-Dashti H (2011) Optical and physical characterization of "Iraqi freedom" dust storm, a case study. Theor Appl Climatol 104(1–2):123–137

Sander N, Jones SC (2008) Diagnostic measures for assessing numerical forecasts of African easterly waves. Meteorol Z 17:209–220

Schepanski K, Knippertz P (2011) Soudano-Saharan depressions and their importance for precipitation and dust: a new perspective on a classical synoptic concept. Q J Roy Meteorol Soc 137:1431–1445

Schepanski K, Tegen I, Laurent B et al (2007) A new Saharan dust source activation frequency map derived from MSG-SEVIRI IR-channels. Geophys Res Lett 34. doi: 10.1029/2007GL030168

Schepanski K, Tegen I, Todd MC et al (2009) Meteorological processes forcing Saharan dust emission inferred from MSG-SEVIRI observations of subdaily dust source activation and numerical models. J Geophys Res 114, D10201. doi:10.1029/2008JD010325
Seino N, Sasaki H, Yamamoto A et al (2005) Numerical simulation of mesoscale circulations in the Tarim Basin associated with dust events. J Meteorol Soc Japan 83A:205–218
Shao Y, Wang JJ (2003) A climatology of Northeast Asian dust events. Meteorol Z 12(4):187–196
Shao Y, Jung E, Leslie LM (2002) Numerical prediction of northeast Asian dust storms using an integrated wind erosion modeling system. J Geophys Res 107(D24):4814. doi:10.1029/2001JD001493
Shao Y, Yang Y, Wang JJ et al (2003) Northeast Asian dust storms: real-time numerical prediction and validation. J Geophys Res 108(D22):4691. doi:10.1029/2003JD003667
Shao Y, Leys JF, McTainsh GH, Tews K (2007) Numerical simulation of the October 2002 dust event in Australia. J Geophys Res 112, D08207. doi:10.1029/2006JD007767
Shao Y, Fink AH, Klose M (2010) Numerical simulation of a continental-scale Saharan dust event. J Geophys Res 115, D13205. doi:10.1029/2009JD012678
Shen B-W, Tao W-K, Wu M-LC (2010) African easterly waves in 30-day high-resolution global simulations: a case study during the 2006 NAMMA period. Geophys Res Lett 37, L18803. doi:10.1029/2010GL044355
Sinclair PC (1964) Some preliminary dust devil measurements. Mon Weather Rev 22(8):363–367
Sinclair PC (1969) General characteristics of dust devils. J Appl Meteorol 8:32–45
Slingo A et al (2006) Observations of the impact of a major Saharan dust storm on the atmospheric radiation balance. Geophys Res Lett 33, L24817. doi:10.1029/2006GL027869
Smirnov VV, Johnson TC, Krapivtseva GM et al (1993) Synoptic meteorological conditions during the U.S.S.R./U.S. dust experiment in Tadzhikistan in September 1989. Atmos Environ 27(16):2471–2479
Smith RK, Reeder J, Tapper NJ, Christie DR (1995) Central Australian cold fronts. Mon Weather Rev 123:16–38
Snow JT, McClelland TM (1990) Dust devils at White Sands Missile Range, New Mexico: 1. Temporal and spatial distributions. J Geophys Res 95:13707–13721
Stanelle T, Vogel B, Vogel H et al (2010) Feedback between dust particles and atmospheric processes over West Africa during dust episodes in March 2006 and June 2007. Atmos Chem Phys 10:10771–10788
Strong CL, Parsons K, McTainsh GH, Sheehan A (2011) Dust transporting wind systems in the lower Lake Eyre Basin, Australia: a prelimary study. Aeolian Res 2:205–214
Sullivan PP, Patton EG (2011) The effect of mesh resolution on convective boundary layer statistics and structures generated by large-eddy simulation. J Atmos Sci 68:2395–2415
Sun JM, Zhang MY, Liu TS (2001) Spatial and temporal characteristics of dust storms in China and its surrounding regions, 1960–1999: relations to source area and climate. J Geophys Res 106(D10):10325–10333
Sutton LJ (1925) Haboobs. Q J Roy Meteorol Soc 51:25–30
Takemi T (2005) Explicit simulations of convective-scale transport of mineral dust in severe convective weather. J Meteorol Soc Japan 83A:187–203
Takemi T, Seino N (2005) Dust storms and cyclone tracks over the arid regions in east Asia in spring. J Geophys Res 110(D18), D18S11. doi:10.1029/2004JD004698
Tao G, Yongfu X, Yuhua B, Xiao Y (2006) Synoptic characteristics of dust storms observed in Inner Mongolia and their influence on the downwind area (the Beijing–Tianjin Region). Meteorol Appl 13:393–403
Todd M, Bou Karam D, Cavazos C et al (2008a) Quantifying uncertainty in estimates of mineral dust flux: an intercomparison of model performance over the Bodélé Depression, northern Chad. J Geophys Res 113, D24107. doi:10.1029/2008JD010476
Todd MC, Washington R, Raghavan S et al (2008b) Regional model simulations of the Bodélé low-level jet of northern Chad during the Bodélé Dust Experiment (BoDEx 2005). J Clim 21:995–1012

Todd MC, Allen CJT, Bart M et al (2013) Meteorological and dust aerosol conditions over the Western Saharan region observed at Fennec supersite-2 during the Intensive Observation Period in June 2011. J Geophys Res. doi:10.1002/jgrd.50470

Tulet P, Mallet M, Pont V et al (2008) The 7–13 March 2006 dust storm over West Africa: generation, transport, and vertical stratification. J Geophys Res 113, D00C08. doi:10.1029/2008JD009871

van de Wiel BJH, Moene AF, Steeneveld GJ et al (2010) A conceptual view on inertial oscillations and nocturnal low-level jets. J Atmos Sci 67:2679–2689

Wain AG, Lee S, Mills GA et al (2006) Meteorological overview and verification of HYSPLIT and AAQFS dust forecasts for the duststorm of 22–24 October 2002. Aust Meteorol Mag 55(1):35–46

Washington R, Todd MC (2005) Atmospheric controls on mineral dust emission from the Bodélé Depression, Chad: the role of the low level jet. Geophys Res Lett 32, L17701. doi:10.1029/2005GL023597

Washington R, Todd MC, Engelstaedter S et al (2006) Dust and the low-level circulation over the Bodélé Depression, Chad: observations from BoDEx 2005. J Geophys Res 111(D3). doi:10.1029/2005JD006502

Wheaton EE, Chakravarti AK (1990) Dust storms in the Canadian prairies. Int J Climatol 10(8):829–837

White JR, Cerveny RS, Balling RC Jr (2012) Seasonality in European Red Dust/"Blood" rain events. Bull Am Meteorol Soc 93(4):471–476

Wiegand L, Twitchett A, Schwierz C, Knippertz P (2011) Heavy precipitation at the Alpine south side and Saharan dust over central Europe: a predictability study using TIGGE. Weather Forecast 26:958–974

Williams E (2008) Comment on "Atmospheric controls on the annual cycle of North African dust" by S. Engelstaedter and R. Washington. J Geophys Res 113, D23109. doi:10.1029/2008JD009930

Williams E, Nathou N, Hicks E et al (2008) The electrification of dust-lofting gust fronts ('haboobs') in the Sahel. Atmos Res. doi:10.1016/j.atmosres.2008.05.017

Yamamoto T, Yoshino M, Suzuki J (2007) The relationship between occurrence of dust events and synoptic climatological condition in East Asia, 1999–2003. J Meteorol Soc Japan 85(2):81–99

Yin D, Nickovic S, Barbaris B et al (2005) Modeling wind-blown desert dust in the Southwestern United States for public health warning: a case study. Atmos Environ 39:6243–6254

Chapter 7
Dust Observations and Climatology

Isabelle Chiapello

Abstract Along with a growing research interest for aerosols, a variety of methods have been developed in the last two decades to observe airborne mineral dust. Both remote sensing from spaceborne sensors and associated ground-based networks have played important roles. An increasing number of satellite sensors have been used either singly or in association with models, aircraft and ground-based measurements. The relevance of these techniques is to provide regional/global pictures of dust storm activity, allowing significant progress in the identification of dust sources, understanding of transport processes and assessment of variability at different timescales, from the diurnal cycle to interannual changes. More recently the development of lidar techniques has provided further advances in dust monitoring. The vertical profiling allows a 4D view of dust properties, a crucial point for progress on the assessment of aerosol radiative impact and aerosol-cloud interaction research. The algorithms associated to advanced sensors dedicated to aerosols, as well as the reliability of retrievals, have been improved in the last decade, giving more detailed and accurate description of dust properties. This chapter provides a brief review of the main observational techniques that have been used for dust survey (Sect. 7.2) with a focus on remote sensing observations. Applications of these data for research on dust source regions (Sect. 7.3.1), transport (Sect. 7.3.2), climatology (Sect. 7.3.3) and vertical structure (Sect. 7.3.4) are presented. Historical context and recent progress are shown alongside remaining limitations determining the needs for future improvements.

Keywords Satellite • Aerosol optical depth • Total ozone mapping spectrometer • Source regions • Interannual variability • Vertical structure • Environmental conditions • Dust transport

I. Chiapello (✉)
LOA, CNRS/Université Lille 1, Villeneuve d'Ascq, France
e-mail: Isabelle.Chiapello@univ-lille1.fr

P. Knippertz and J.-B.W. Stuut (eds.), *Mineral Dust: A Key Player in the Earth System*, DOI 10.1007/978-94-017-8978-3_7,

7.1 Introduction

Mineral dust particles emitted from arid and semi-arid regions of the globe are one of the major aerosol components in the troposphere, especially in tropical to mid-latitude regions of the Northern Hemisphere. Desert dust has a number of complex environmental effects, including substantial changes in radiative budget and climate (Chap. 13), and influence on ocean biogeochemistry (Chap. 15). Recently, the contribution of dust particles to air quality degradation has been emphasized (Prospero 1999; Escudero et al. 2007; Querol et al. 2009), as well as their possible role on specific regional health problems, especially in North Africa (Martiny and Chiapello 2013; Chap. 16).

Desert dust has interested observers of the natural world for a long time, as indicated by early scientific reports like those of Charles Darwin (1846) off the west coast of Africa (Goudie and Middleton 2006). A number of dust studies have been performed through the analysis of observational data recorded at meteorological stations. N'tchayi Mbourou et al. (1997) studied dust storm frequency and variability over North Africa using horizontal visibility data as an indicator of dust. Based on similar approaches, Goudie and Middleton (1992) investigated dust storm frequency trends by analysing long-term meteorological records for a large number of arid areas.

Today, long-term in situ measurements of dust remain rare over both remote arid and semi-arid areas prone to emissions and oceanic regions affected by transport, such that only sparse pluriannual time series of quantitative ground-based observations exist (Schulz et al. 2012; Rodriguez et al. 2012). The Barbados site in the Caribbean Sea is unique, since it has recorded Saharan dust concentrations transported across the north tropical Atlantic since 1965 (Prospero and Lamb 2003), this way constituting the longest current quantitative mineral dust dataset.

Both field campaigns providing detailed measurements of specific dust events for limited periods (generally weeks to months) and long-term monitoring stations are essential for dust research, but alone they do not provide enough observational constraints for a comprehensive quantification of dust loads, associated impacts and understanding of dust processes (Knippertz and Todd 2012). One additional tool that has become increasingly important in recent years for identifying, tracking and analysing large-scale dust events is remote sensing from space. Indeed, the satellite repetitive and global measurement is the only way to monitor the complex spatial pattern (horizontally and vertically) and high temporal variability of mineral dust.

In the 1990s the first operational algorithms that allowed retrieving dust/aerosol optical depth (DOD/AOD; see Table 7.1 for abbreviations) over oceanic surfaces were developed, especially from the European Meteorological Satellite (Meteosat; Jankowiak and Tanré 1992) and the NOAA AVHRR (Swap et al. 1996; Husar et al. 1997). In parallel, the development of the global ground-based aerosol network of sun/sky photometers AERONET (Holben et al. 2001; Dubovik et al. 2002) has allowed constant assessment, validation and improvement of these satellite aerosol products. Since then, the number of space sensors including several techniques

Table 7.1 Acronyms and abbreviations of satellites, sensors, products, networks and field campaigns

AD-Net	Asian Dust Network
AERONET	Aerosol Robotic Network
AI (from TOMS and OMI)	Aerosol index
AIRS	Atmospheric Infrared Sounder
AMMA	African Monsoon Multidisciplinary Analysis
AOD	Aerosol optical depth
AVHRR	Advanced Very High Resolution Radiometer
CALIOP	Cloud-Aerosol Lidar with Orthogonal Polarization
CALIPSO	Cloud-Aerosol Lidar and Infrared Pathfinder Satellite Observation
DOD or dust AOD	Dust optical depth
EARLINET	European Aerosol Research Lidar Network
GOES	Geostationary Operational Environmental Satellite
IASI	Infrared Atmospheric Sounding Interferometer
IDDI	Infrared difference dust index
IR	Infrared
Meteosat	European Geostationary Meteorological Satellites
Metop	Meteorological operational satellite programme
MISR	Multiangle Imaging Spectroradiometer
MODIS	Moderate-Resolution Imaging Spectroradiometer
MSG	Meteosat Second Generation
MVIRI	Meteosat Visible and Infrared Imager
NOAA	National Oceanic and Atmospheric Administration
OMI	Ozone Monitoring Instrument
PARASOL	Polarization and Anisotropy of Reflectances for Atmospheric Science Coupled with Observations from a Lidar
PM2.5, PM10	Mass concentrations of particulate matter with an aerodynamic diameter smaller than 2.5, 10 μm
POLDER	Polarization and Directionality of the Earth's Reflectances
PRIDE	Puerto Rico Dust Experiment
SAMUM	Saharan Mineral Dust Experiment
SeaWiFS	Sea-Viewing Wide Field of View Sensor
SEVIRI	Spinning Enhanced Visible and Infrared Imager
SHADE	Saharan Dust Experiment
TEOM	Tapered element oscillating microbalance
TOMS	Total ozone mapping spectrometer
UV	Ultraviolet

of passive and active remote sensing in different spectral ranges has considerably increased. The associated algorithms and methods of inversions are still being improved (Dubovik et al. 2011), allowing to progress towards more comprehensive, detailed and accurate monitoring of dust from space for the entire globe.

Satellite observations of mineral dust have been used singly or combined with other measurements from space (Cakmur et al. 2001) or from ground-based networks and field campaigns. In recent years, several field experiments in West Africa (AMMA; Haywood et al. 2008; Cuesta et al. 2008) and the Sahara (Fennec; Todd

et al. 2013; SAMUM; Ansmann et al. 2011) used in situ dust measurements in synergy with satellite observations. Likewise, remote sensing data are essential for constraining, evaluating and improving aerosol and dust simulations with global and regional models (Mangold et al. 2011; Yu et al. 2013; Chap. 9) and for progressing towards operational predictions (Chap. 10). The global (or regional) repetitive view provided by satellite measurements is valuable to investigate the high spatial and temporal variability of mineral dust, allowing to progress in the understanding of transport pathways and identification of main source regions. Current algorithms allow deriving more detailed information, such as size parameters (Tanré et al. 2011) and optical properties (Chap. 12). A better knowledge of all these parameters is highly needed to reduce current uncertainties with respect to the radiative effects of mineral dust, both direct and indirect through interactions with clouds (Chap. 11).

In this chapter, we first present a brief review of measurement systems that have been applied for dust monitoring (Sect. 7.2). The main scientific applications of dust observations, focusing on satellite remote sensing techniques, are presented in Sect. 7.3. Section 7.3.1 shows their use for studies of dust source regions and Sect. 7.3.2 for dust transport monitoring. Long-term satellite dust records that have been used to explore interannual variability and trends will be presented in Sect. 7.3.3, while Sect. 7.3.4 discusses recent progress on observing the vertical distribution of dust. Conclusion will be given in Sect. 7.4.

7.2 Observational Systems

The first available dust observations were from synoptic meteorological stations (Goudie and Middleton 1992; Mahowald et al. 2007), based on either visibility reduction or dust weather code analysis (Klose et al. 2010; Table 7.2). Dust weather conditions are subjectively determined by trained observers but have the advantage to be available for decades at many stations located in the arid and semi-arid areas of Africa and Asia (Cowie et al. 2013; Kurosaki and Mikami 2003).

More recent dust measurements can generally be divided into two broad categories: in situ and remote sensing. Remote sensing systems include ground-based and space-based instruments. Both of these may be performed with either passive or active techniques. Examples of these different types of observations for dust monitoring are given in Table 7.2. Rodriguez et al. (2012) present a recent review of long-term in situ measurements of dust. These authors report that only four sites have been active during at least the last two decades for continuous in situ dust monitoring, three being in the North Atlantic (Barbados, Miami, Izaña) and one in the South Pacific (Samoa).

In situ measurements to determine surface dust concentrations generally consist of collecting particles on filters followed by weighting or chemical analysis in the laboratory. Table 7.2 lists some examples of in situ dust data that have been available for more than 1 year, focusing on dust load monitoring, that is, mass concentrations, derived from various sampling systems (TEOM, filters). Besides surface air quality

Table 7.2 Examples of measurements available for dust monitoring including in situ data and ground-based and satellite-based remote sensing observations. Studies based on at least 1 year of dust record are favoured, this way excluding case study analyses and results from field campaigns

Parameter relevant for dust	Measurement type: Instrument network or platform	Region	Selected references
	Meteorological		
Reduction of horizontal visibility (<1, 5 or 10 km)	Surface meteorological stations (WMO)	Arid areas of the globe	Goudie and Middleton (1992); Mahowald et al. (2007)
		North West Africa	N'tchayi MBourou et al. (1997)
		China	Sun et al. (2001) and Wang et al. (2004)
SYNOP weather codes (ww = 6, 7–9, 30–35 and 98)		Sahel	Cowie et al. (2013) and Klose et al. (2010)
		East Asia	Kurosaki and Mikami (2003)
	In situ		
Surface dust mass concentration, TSP, PM10 or PM2.5 ($\mu g/m^3$)	Sampling filter – TEOM – gravimetric method	Barbados	Prospero and Lamb (2003)
		Miami	Prospero (1999)
		Canary Islands, Bermuda	Arimoto et al. (1995)
		Canary Islands	Alonso-Pérez et al. (2007)
		Cape Verde Islands	Chiapello et al. (1995, 1997)
		Crete Island	Kalivitis et al. (2007)
		West Sahel (3 stations)	Marticorena et al. (2010)
		Sede Boker, Israel	Derimian et al. (2006)
		Air quality networks (USA, South Europe, Asia, etc.)	Escudero et al. (2007) and Querol et al. (2009)
	Remote sensing from ground		
AOD + Angström, AOD coarse mode	Sun/sky photometer/ AERONET	Roughly 450 sites (2009)	Holben et al. (2001)
	Radiometer	Lampedusa	Meloni et al. (2007)
	Satellite retrievals		
DOD	AVHRR/NOAA	Northern Tropical Atlantic Ocean	Evan and Mukhopadhyay (2010)
DOD + Dust Column Conc.	MODIS/Terra	Atlantic Ocean	Kaufman et al. (2005)
AOD + Angström	SeaWiFS and MODIS	East Asia	Hsu et al. (2004)
DOD	MODIS	Global bright surfaces	Ginoux et al. (2012)
AOD	MISR	Global	Martonchik et al. (2004)

(continued)

Table 7.2 (continued)

Parameter relevant for dust	Measurement type: Instrument network or platform	Region	Selected references
AOD + Angström and Coarse nonspherical AOD	POLDER-1, POLDER-2, POLDER-3/ PARASOL	Global ocean	Herman et al. (2005) and Tanré et al. (2011)
DOD + night	IASI/Metop	Northern Africa and Arabia	Klüser et al. (2011)
AOD	MVIRI/Meteosat	Atlantic Ocean	Jankowiak and Tanré (1992)
DOD		Atlantic Ocean, Mediterranean Sea	Moulin et al. (1997)
AOD + Angström	SEVIRI/MSG	Atlantic Ocean, Mediterranean Sea	Thieuleux et al. (2005)
	Satellite retrievals		
UV AI	TOMS/Nimbus 7 and Earth Probe	Global (land and ocean)	Herman et al. (1997)
UV AI		Global (land and ocean)	Prospero et al. (2002)
UV AI + AOD	OMI/Aura	Global (land and ocean)	Torres et al. (2007)
	Satellite retrievals		
IDDI	MVIRI/Meteosat	Continental Africa	Brooks and Legrand (2000) and Legrand et al. (2001)
IR dust index	SEVIRI/MSG	Sahara, Sahel	Schepanski et al. (2007, 2009)
	Satellite retrievals		
DOD, dust layer altitude	AIRS/Aqua	Atlantic Ocean	Pierangelo et al. (2004)
DOD, dust layer altitude		Atlantic Ocean, Arabian Sea	Peyridieu et al. (2010)
	Remote sensing from ground		
Dust vertical profile, DOD	Lidar/EARLINET	Europe (∼25 stations)	Papayannis et al. (2008) and Pappalardo et al. (2010)
		West Africa (AMMA)	Léon et al. (2009) and Cavalieri et al. (2010)
		Lampedusa	Di Iorio et al. (2009)
	Satellite retrievals		
Dust vertical profile	CALIOP/CALIPSO	Global	Liu et al. (2008b)
		Atlantic Ocean	Ben-Ami et al. (2009)
		Asia	Uno et al. (2008)

networks providing continuous PM10 and/or PM2.5 measurements, from which dust loads can be derived, only a few sites have been dedicated to dust mass concentration recording over long periods. Many of the available dust datasets cover periods of 10 years or less, especially in the marine regions surrounding North Africa, as in the Cape Verde Islands (Chiapello et al. 1995, 1997) and in a few Mediterranean stations. Long-term dust mass concentration records are especially rare over arid and semi-arid regions located close to sources. To fill this gap, a transect of ground-based dust concentration measurements at three sites in the Sahel, one of the dustiest places on Earth, has been started in 2006 in the framework of AMMA (Marticorena et al. 2010). As highlighted by many studies, due to the sporadic nature of dust events, the regional and daily variability of surface dust loads provided by this kind of measurements is huge. The mass concentrations in desert areas where (and when) dust is raised have been reported in the range 100–100,000 $\mu g/m^3$ (Goudie and Middleton 2006), varying between 0.1 and 100 $\mu g/m^3$ in other oceanic and continental regions.

The AERONET with hundreds of identical sun/sky photometer sites around the world, the first starting in the mid-1990s, is a key reference observational system for aerosols. The photometer measurements provide vertically integrated aerosol records during daily clear sky conditions, given as AODs at different wavelengths. Angström exponents are generally used to distinguish the large particles during dust events (i.e. low Angström values) from other aerosol types. These high-quality data have been used to investigate dust variability and properties over different regions of the world (Kim et al. 2011). Figure 7.1 shows two illustrations of multiyear dust observations performed at the site of Banizoumbou (Niger) in West Africa, with (a) AOD (and Angström exponent) from an AERONET photometer and (b) surface mass concentrations from a TEOM. These measurements illustrate the large variability of dust at daily and seasonal timescales.

There are currently more than 20 separate satellite sensors available for aerosol studies (Lenoble et al. 2013), allowing to spatially extend the point observations from the ground sites. These sensors, because they allow repetitive large-scale observations and monitoring of dust events, have been widely used in recent years. Table 7.2 gives selected examples of the main satellite sensors suitable and applied to dust studies, especially for dust load monitoring. As for sun photometers, the main retrieved aerosol parameter is AOD (i.e. an information of the total amount of aerosol weight by their extinction coefficient, at one or several wavelengths), which includes the contribution of all aerosol species. Some algorithms allow specific retrieval of the dust contribution to AOD (i.e. dust optical depth, DOD). Other algorithms, especially in the UV (with TOMS and OMI) and in the IR (with Meteosat and MSG), only provide semi-quantitative indices that have been used as proxy of dust events or loads, especially over arid regions. Thus, the different spectral ranges that have been used, that is, besides the visible, the UV and IR, allow to extent the monitoring to arid and semi-arid surfaces, which is of primary importance for a better understanding of desert dust emissions (Legrand et al. 2001; Prospero et al. 2002, and Sect. 7.3.1). Observations from geostationary sensors, that is, Meteosat and MSG, have been applied for studies of North African

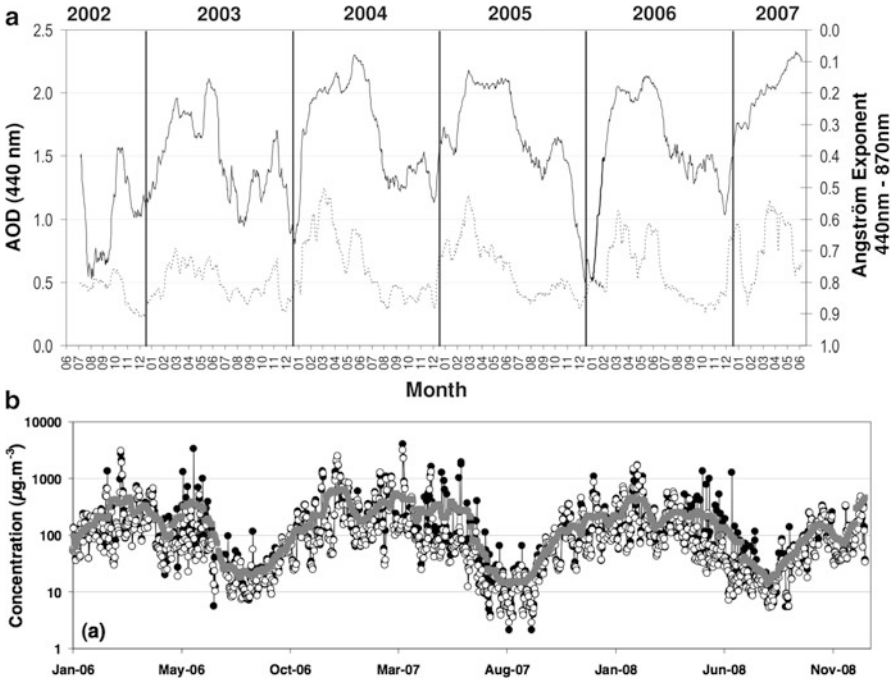

Fig. 7.1 Examples of multiyear measurements available for dust studies in West Africa at the station of Banizoumbou (Niger). (**a**) *AOD and Angström exponent*: 30-day sliding averages of daily AOD (440 nm, *dotted line*) and Angström exponent (440–870 nm, *solid line*) derived from the AERONET sun photometer for 2002–2007. From Rajot et al. (2008). (**b**) *PM10*: daily mean (*black circle*) and median (*open circle*) concentration and 30-day sliding average of the daily mean (*grey line*) from 2006 to 2008 (From Marticorena et al. 2010)

dust emissions and transport over surrounding oceanic regions. Although they are restricted to a part of the globe, the frequency of measurements (15 min with MSG) is of great benefit for research on dust (Schepanski et al. 2007, 2009; Thieuleux et al. 2005). Most of the sensors on polar-orbiting platforms are limited to one observation of aerosol per day, a frequency which may, at least in certain cases, prevent a representative measurement of daily dust content (Kocha et al. 2013). The spatial resolution also differs from one sensor to another, generally in the range between ∼10 km and ∼100 km (or 0.1–1°). Besides differences in the measurement techniques (especially spectral range) and algorithms used for aerosol retrievals, the specific spatio-temporal coverage of each sensor may generate differences in the dust load retrievals as well. So, as shown in Table 7.2 and in Sect. 7.3 of this chapter, each sensor and product (from semi-quantitative indices to DOD) has been used with specific purposes for dust studies. Since the launch of the CALIOP/CALIPSO mission in 2006, vertically resolved observations of dust have become available, at a global scale, a huge progress in dust observations (Sect. 7.3.4). Remote sensing data from global ground-based networks with sun photometers (i.e. AERONET)

and other regional networks (i.e. EARLINET with lidars over Europe) are of primary importance for the validation and interpretation of the satellite-derived dust products. Likewise, the quality and length of the aerosol records they provide at certain sites make them by themselves well adapted for application to dust research.

7.3 Applications

7.3.1 Source Regions

As mineral dust sources are mostly located in remote and arid regions where ground-based aerosol measurements are difficult, observations from both geostationary (Sect. 7.3.1) and earth-orbiting (Sect. 7.3.1) satellites have played an important role to identify contemporary dust sources (see also Chap. 3). Among the first aerosol satellite products used for this aspect are semi-quantitative indices such as the AI derived from the TOMS/Nimbus 7 (Prospero et al. 2002) and the IDDI derived from Meteosat (Brooks and Legrand 2000; see Table 7.2). The analysis of global aerosol satellite observations, especially the TOMS AI (Prospero et al. 2002), has highlighted that the Sahara desert is by far the most important dust source of the world. More recently, data from sensors such as MODIS and SEVIRI/MSG have provided more detailed information on dust sources (Ginoux et al. 2012; Schepanski et al. 2009).

Regional Data from Geostationary Satellite

The IDDI is a dust product firstly derived from daily noontime IR images of Meteosat-1 available over continental Africa over the period 1984–1993 (Brooks and Legrand 2000; Legrand et al. 2001). It has been applied for dust source identification in the Sahara and Sahel, as well as the description of seasonal and interannual variability (Brooks and Legrand 2000). Thanks to the shift of Meteosat-5–63°E, 1 year of Meteosat-IDDI (1999) is available to monitor dust sources in the arid and semi-arid areas surrounding the North Indian Ocean, highlighting the *Rub Al Khali* Desert in central Saudi Arabia as one of the largest dust sources in this region (Léon and Legrand 2003). Vergé-Dépré et al. (2006) have investigated methods to improve the IDDI, which is sensitive to water vapour and surface temperature. A recent progress for the investigation of North African dust sources is based on the SEVIRI/MSG thermal IR radiance measurements (Schepanski et al. 2007). One of the main advantages of this product is to provide observations of dust source activation at 3-hourly resolution (Schepanski et al. 2009). Thus the diurnal cycle of dust emission over the Sahara has been investigated and better understood in view of meteorological controls. Based on 2 years of SEVIRI/MSG dust index data, Schepanski et al. (2009) show that emissions peak in the hours after sunrise

related to the breakdown of nocturnal low-level jets (see Chap. 6). However, no quantitative optical depth or source strength can be derived with this approach. Banks and Brindley (2013) have developed a more quantitative approach from SEVIRI/MSG observations in the 10.8 and 13.4 μm channels that allows inferring DOD at a half-hourly temporal resolution during the daytime. Such an approach offers a new perspective for quantitative analysis of mineral dust source variability at high temporal resolution over North Africa and the Middle East.

Global Data from Polar-Orbiting Satellite

The AI derived from TOMS/Nimbus 7 measurements (Herman et al. 1997) in the UV part of the spectrum has been the first satellite dataset applied to identification and characterization of mineral dust sources at a global scale (Prospero et al. 2002). In contrast to the visible range, surface reflectivity is low and constant in the UV. Thus, TOMS measurements allowed retrieving the loading of absorbing aerosols (i.e. mainly mineral dust and carbonaceous particles) at a global scale, over both oceanic and land surfaces, including arid and semi-arid areas of the globe. Regions of maximum AI or high frequency of high AI occurrences have been used as a proxy for dust source identification. Such an analysis has highlighted both the importance of topographic depressions as the strongest sources and the dominance of dust sources located in the Northern Hemisphere, mainly in a broad "dust belt" over North Africa, the Middle East and Asia. Figure 3.2 in Chap. 3 nicely illustrates the global map of dust source areas generated by analysis of the TOMS AI dataset. From this approach, the Bodélé Depression in Chad has been identified to be the most intense source region in the world (Prospero et al. 2002; Goudie and Middleton 2006). However, since the TOMS AI is known to be less sensitive to aerosols at low altitude, the application of this index for dust source identification is questionable in some cases (Mahowald and Dufresne 2004). Despite the large progress provided by global TOMS AI analyses, the general difficulty of determining whether the dust derived from satellite corresponds to transport or emission has been emphasized. Thus, a more accurate identification of the sources of mineral dust from satellite may require more sophisticated approaches. Hsu et al. (2004) have developed the Deep Blue algorithm based on MODIS measurements in the 412 nm channel, which has been applied to global dust source identification (Ginoux et al. 2012). The advantage of Deep Blue compared to UV techniques is that it can detect dust close to the surface and at a higher spatial resolution (0.1°). Using criteria on size distribution and optical properties allows distinction of DOD from AOD. However, as the dust retrieval is limited to bright surfaces, dust sources as those in the Northern Hemisphere high latitudes (Iceland, Alaska) may be underrepresented (Ginoux et al. 2012). The analysis of dust sources based on Deep Blue DOD retrievals tends to confirm the results of Prospero et al. (2002), especially the remarkably little dust activity in the Southern Hemisphere (Ginoux et al. 2012; Fig. 7.2).

Figure 7.2 highlights that the highest DOD values occur during spring and summer season over arid areas in the Northern Hemisphere. High-resolution

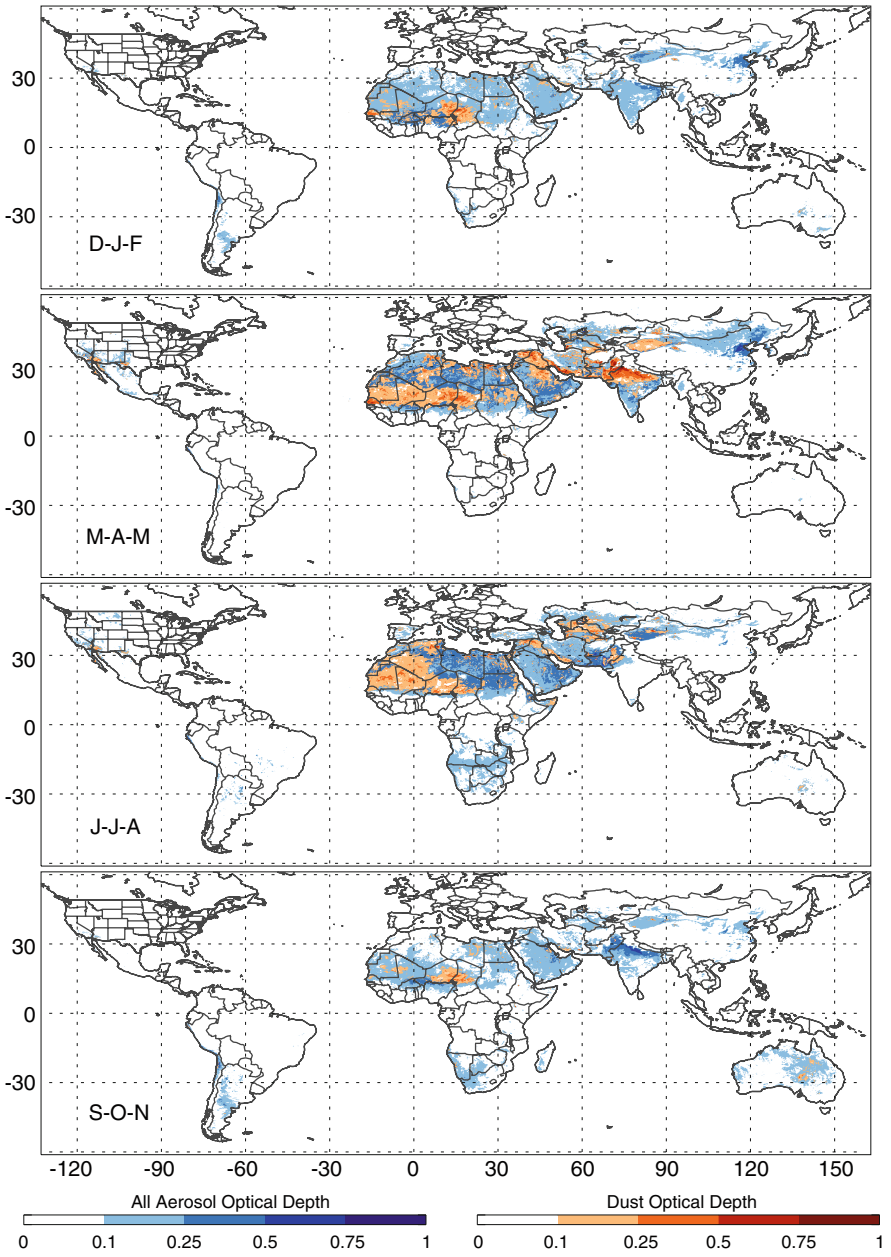

Fig. 7.2 Global distribution of MODIS Deep Blue seasonal mean AOD (*blue*) overplotted by DOD (*red*) at 550 nm, for values greater than 0.1. The retrieval is restricted to bright land surfaces. The data are from MODIS/Aqua at $0.1° \times 0.1°$ resolution averaged over the period 2003–2009 (From Ginoux et al. 2012)

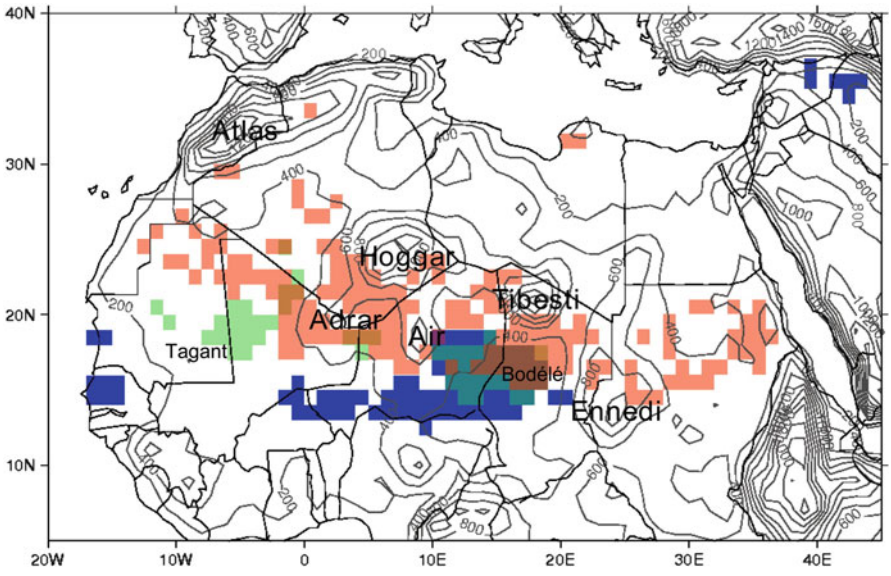

Fig. 7.3 Summary of main dust source areas inferred from satellite observations. Different colours indicate the three satellite dust products: *blue* MODIS Deep Blue AOD frequency >40 %, *green* OMI AI frequency >40 % and *red* MSG dust source activation frequency >6 %. *Contour lines* represent topography and are given at 200 m intervals. The figure illustrates the differences between the three satellite datasets in terms of identification of dust source regions (except for the Bodélé Depression) (From Schepanski et al. 2012)

MODIS dust observations have also been related to land use in order to provide new estimates of the contribution of anthropogenic dust sources (25 % globally, 8 % in North Africa; Ginoux et al. 2012).

Despite the undeniable potential of the satellite approaches for source identification and characterization, it must be underlined that the interpretation of individual satellite dust products may be complicated by a number of factors. The difficulties of interpreting coarse-resolution satellite data and of differentiating between transported and emitted dust are some of them. In certain cases, the restriction to clear sky conditions and the contribution of aerosol species other than dust to the satellite retrieval can be problematic. Schepanski et al. (2012) compared Saharan dust source areas observed from three different satellites, the 15-min MSG IR dust product, daily noontime Aqua MODIS Deep Blue AOD and Aura OMI AI. Their analysis highlights that differences in temporal resolution are a critical factor and concludes that different satellite methods lead to the identification of different source areas (Fig. 7.3). Finally, although each satellite dust product has limitations that must be accounted for in the analysis, observations from space remain one of the most powerful tools to locate and study dust sources, particular in combination with numerical models (Huneeus et al. 2012; Ginoux et al. 2012).

Other satellite datasets may also be applied to global dust source identification. The MISR/Terra measurements, despite limited temporal coverage (3 or 4 over-

passes per month), have been shown to provide reliable AOD over bright desert surfaces (Martonchik et al. 2004) and can complement past and current satellite analysis. Other approaches like inverse modelling, which combines models and multiple satellite datasets, are promising to retrieve mineral dust sources (Dubovik et al. 2008; Wang et al. 2012; Chap. 10).

7.3.2 Transport

General Features

From a general point of view, the development of satellite technology has played a key role in improving our knowledge of transported dust. One of the first highlights is that desert dust is the species responsible for the largest and most persistent aerosol loads over the world's oceans as indicated by all global aerosol satellite maps (Husar et al. 1997; Herman et al. 1997). The first direct application of satellite observations has been to track long-range transport of desert dust. Satellites can provide spectacular imagery of major dust events, showing large plumes crossing the entire ocean basins, especially over the North Atlantic and Pacific (Husar et al. 2001; Hsu et al. 2006; Yu et al. 2013). One of the first studies of this kind has monitored the daily evolution of AOD during a dust event over the North Atlantic in March 1988 based on Meteosat observations (Jankowiak and Tanré 1992). Interestingly, some studies also attempted to go beyond simple detection with imagery to estimate columnar mass transport of desert dust (Dulac et al. 1992; Kaufman et al. 2005) or to derive more detailed characterization of transported dust (Kalashnikova and Kahn 2008). Generally the trans-Atlantic transport of dust has been well documented with satellite observations, while the trans-Pacific transport has been studied less. Other transport paths of dust would require more research efforts, particularly in the Southern Hemisphere where only a few observational studies are available (e.g. from the Patagonia desert; Gasso and Stein 2007; Li et al. 2010). Despite the dominance of dust mass emitted and transported from tropical and mid-latitude arid regions, dust events also occur in less explored areas at high latitudes such as Alaska, New Zealand or Iceland (Prospero et al. 2012), where the analysis of satellite imagery is of primary interest.

One main feature of dust transport revealed by ground- and space-based observations is high variability in space and time. Temporal variability is evident at timescales from the diurnal cycle to multiannual changes, including large seasonal variations. The main drivers are meteorological factors (see Chap. 6) that exert control on both emission and transport processes. As North Africa is the largest dust source, its transport over the surrounding marine regions has been investigated most in the past, with three major pathways identified, that is, (1) westwards and southwards to the North Atlantic Ocean, (2) towards the Mediterranean and Europe (Dulac et al. 1992; Israelevich et al. 2012) and (3) towards the eastern Mediterranean and the Middle East (Engelstaedter et al. 2006). Characteristics and seasonality of

this transport, especially to the northern tropical Atlantic, the dominant direction of export, have been the subject of many studies. Multiyear time series of dust concentrations recorded at different sites, including Barbados (Prospero and Lamb 2003), Miami (Prospero 1999), the Canary Islands and the Cape Verde Islands, have allowed assessing and understanding the large seasonal variability of the dust transport (Chiapello et al. 1995). Since the 1990s, the seasonal and monthly distributions of dust provided by satellite observations have allowed new insights into the spatial distribution associated to this seasonal variability of dust transported from North Africa and from other desert regions of emissions of the world (Swap et al. 1996; Herman et al. 1997; Husar et al. 1997; Cakmur et al. 2001). Table 4.7 of Goudie and Middleton (2006) summarizes current knowledge of seasons when maximum dust storm activity has been observed over the main affected areas of the globe.

AOD, Dust Discrimination and Dust Above Clouds

As indicated in Table 7.2, most of the algorithms applied to satellite sensors allow retrievals of AOD, defined as the vertically integrated aerosol extinction. AOD can be considered as an optical measure of the whole amount of aerosols (all types) with some wavelength dependence. The uncertainties on the retrieved AOD have been significantly reduced from the early sensors in operation in the 1980s and 1990s (AVHRR, GOES, Meteosat) to the current satellite missions dedicated to aerosol research, especially those of the A-Train (MODIS, MISR, POLDER). The accuracy varies between sensors and also depends on the underlying surface (land or ocean), but has been estimated to be on order of 20 % or ± 0.05 (Yu et al. 2013). Some of the most recent sensors allow partitions of AOD into fine and coarse modes, the latter being dominated by mineral dust and sea salt. POLDER measurements of spectral and angular polarization provide additional partition into the spherical and non-spherical components within the coarse mode (Herman et al. 2005). This product, available only over oceans under optimal geometric conditions, is expected to represent the desert dust component (Tanré et al. 2011; Peyridieu et al. 2010). Figure 7.4 illustrates seasonal distributions of the nonspherical coarse component of AOD derived from POLDER-3 over global oceans for the year 2009. The most widespread and intense transported dust plumes occur in summer (from Arabia and the Sahara) and spring (from Asia) with lowest dust loads generally occurring in autumn.

Other studies have attempted to separate the dust component from other aerosol types (i.e. marine, fine mode particles from pollution and smoke) by combining parameters derived from the satellite measurements (Angström exponent, size fraction, absorption), especially with MODIS (Kaufman et al. 2005; Ginoux et al. 2012). Because these approaches require assumptions, the unambiguous identification of dust is still challenging. Nevertheless, most of the current satellite sensors attempt to discern dust from the total aerosol signal, with an improved accuracy compared to early sensors. Figure 7.5 shows an illustration of dust AOD retrieved from MODIS, MISR and PARASOL over the North Atlantic. Although

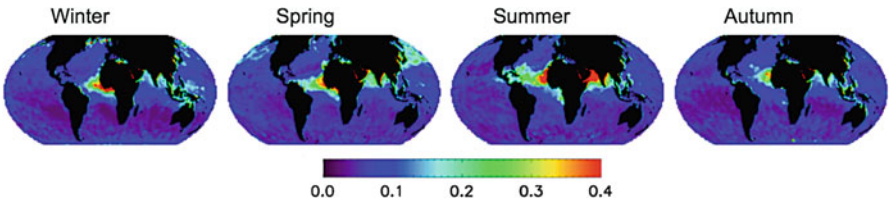

Fig. 7.4 Seasonal distribution of POLDER-3 AOD of the nonspherical coarse mode at 550 nm over oceans for the year 2009. Seasons are ordered from the *left* to the *right* (winter, spring, summer, autumn, respectively) (From Tanré et al. 2011)

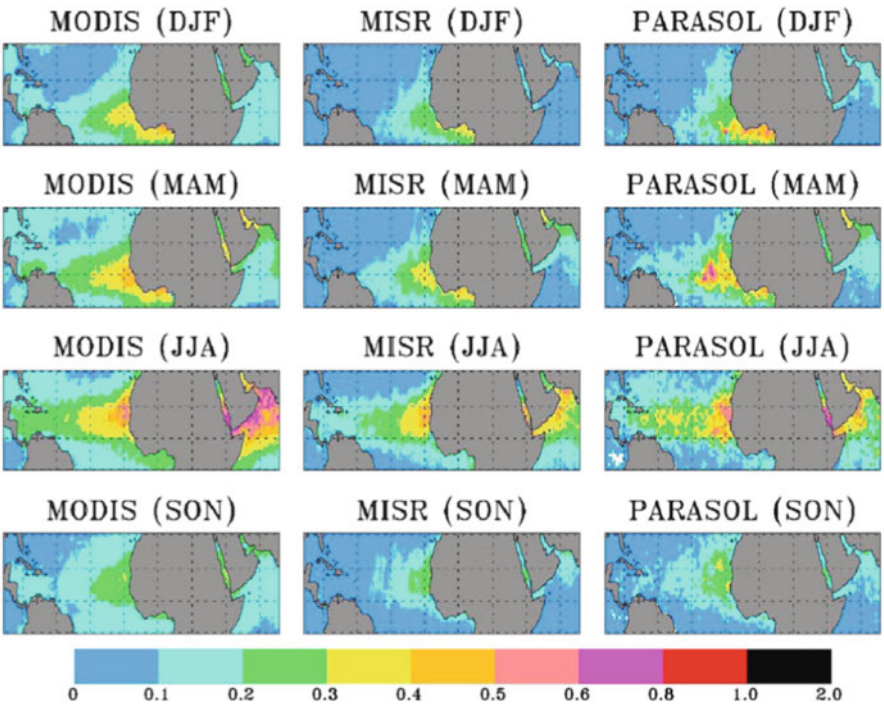

Fig. 7.5 Seasonal variations of trans-Atlantic dust transport. Shown are season-mean dust AODs as seen by MODIS, MISR and PARASOL. Each sensor applies a specific algorithm or methodology to discern dust from the total aerosol signal (From Yu et al. 2013)

the general seasonal patterns of dust distribution are consistent, notable differences exist, especially in magnitude of DOD. This illustrates current issues with satellite dust identification and quantification. Especially for cases of complex mixtures of dust and smoke in winter, MODIS and PARASOL DOD are higher than those derived from MISR. Sampling differences may also contribute to the variable DOD

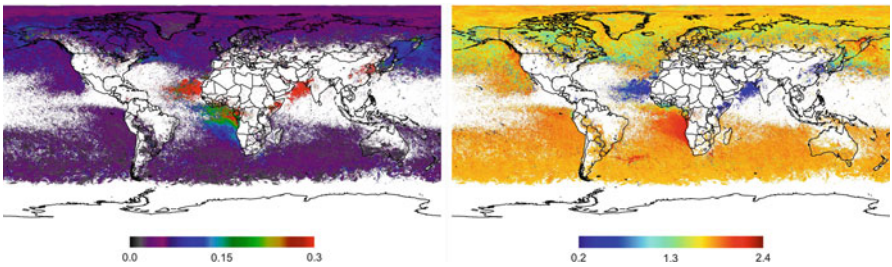

Fig. 7.6 Global mean AOD at 865 nm (*left*), mean Angström exponent (*right*) retrieved over clouds from POLDER-3 in summer 2009 (Courtesy of Peers and Waquet)

values retrieved by each sensor, as, for example, MODIS provides more extensive coverage than MISR.

As shown by Kalashnikova and Kahn (2008), the approach combining information from different satellite sensors such as MODIS and MISR is valuable to better analyse the evolution of dust properties during transport and to increase coverage. Studies based on daytime polar-orbiting satellites can be complemented by measurements from the new generation of high-resolution IR spectrometers and interferometers, which allow for dust characterization at night. Klüser et al. (2011) present an algorithm for retrieval of DOD from IASI on the Metop satellite, allowing for dust observation at day and night. Several recent studies (Pierangelo et al. 2004; DeSouza-Machado et al. 2010; Peyridieu et al. 2010) have shown that some information on dust altitude and effective particle size can be retrieved from AIRS data. Additionally, as highlighted by Yu et al. (2013), geostationary measurements have been underused up to now. Thieuleux et al. (2005) have shown, based on SEVIRI/MSG data, that finer temporal resolutions during the day not only allow monitoring of dust properties at higher frequencies but also remarkably increase spatial coverage compared to what is produced by polar-orbiting sensors.

Another important aspect in terms of dust observation is the limitation of satellite passive remote sensing to cloud-free conditions. Thus, until very recently and the advancement of lidar techniques (see Sect. 7.3.4), most of the satellite dust observations were limited to clear sky conditions. Today, new satellite algorithms are being explored to retrieve natural and man-made aerosols above clouds from passive sensors like OMI and POLDER (Waquet et al. 2013a, b). Figure 7.6 shows an example of new insight provided by POLDER-3 measurements in the A-Train, with aerosol above cloud properties at a global scale in summer 2009 (Waquet et al. 2013b). Mineral dust or mineral dust aerosols, associated with low Angström exponents and high AOD values, are detected for this season within the "dust belt" region of the Northern Hemisphere. The computed mean POLDER-3 aerosol optical thickness at 865 nm is 0.456 for summer dust in 2009, a value that may be considered as a minimum con-

sidering some limitations of the approach (optically thick cloud). Such new developments highlight that dust transported above clouds is significant at a global scale and has to be added to previous cloud-free satellite retrievals of dust.

7.3.3 Interannual Variability and Trends

Although visibility data collected at meteorological stations present potential biases that require careful uses to properly evaluate dustiness, they represent the longest time series available (Mahowald et al. 2007). Several studies have used them for analysis of long-term variability of dust events, that is, over periods of 30–40 years (Sun et al. 2001; Mahowald et al. 2007), especially in regions where no other continuous long-term dust observations are available. As an example in Asia, Shao and Dong (2006) examine the evolution of the total number of dust days since 1961, as recorded at 175 meteorological stations located in dust-affected areas of China. Their analysis (Fig. 7.7) shows that a marked decrease occurred in the late 1970s and the 1980s, with a clear negative trend until 1997. In contrast, this trend is not observed in annual variations of dust-event days in transport-affected regions such as Japan (Kurosaki and Mikami 2003) over the period 1971–2002. These discrepancies are not well understood and require further study (Shao and Dong 2006).

In the northern tropical Atlantic, the Barbados station in operation since 1965 has highlighted large interannual changes in African dust transport (Prospero and Lamb 2003). In the last 15 years, thanks to the availability of multiyear satellite observations of dust, substantial progress has been made in our understanding of dust variability on relatively long timescales, that is, over periods on the order of 10 years or more (Hsu et al. 2012). Indeed, certain satellite sensors in operation since the late 1970s (TOMS/Nimbus 7) or early 1980s (Meteosat, AVHRR) and some more recent products cover periods long enough to support analyses of dust variability at interannual timescales with attempts to identify their controlling factors (Engelstaedter et al. 2006). Most of these studies focus on the export of North African dust. Based on Meteosat observations, Moulin et al. (1997) analyse 11 years of dust transport out of North Africa and reveal the control of the North Atlantic Oscillation (NAO) on interannual variations of dust recorded over the North Atlantic Ocean and Mediterranean Sea.

Chiapello et al. (2005) analyse long-term measurements of surface concentrations of dust from Barbados (1966–2000) together with a 22-year satellite dust record combining TOMS and Meteosat observations over the tropical North Atlantic (1979–2000; Fig. 7.8). Their analysis shows a large regional impact of Sahel drought conditions on interannual variations of dust transport over the Atlantic, in both summer and winter seasons. The NAO influence appears to be restricted to interannual variability in winter. Focusing on the winter season and using a 23-year

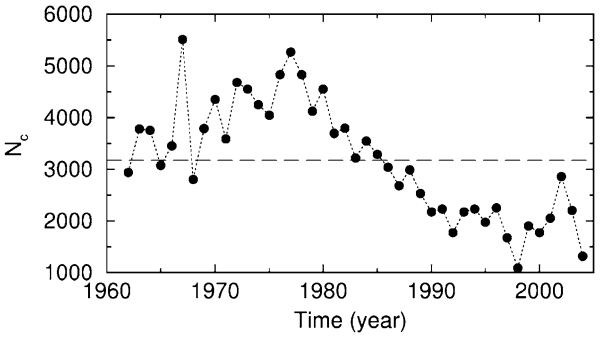

Fig. 7.7 Annual total number of dust days recorded at 175 meteorological stations of China for 1961–2003. The *dashed line* represents the long-term mean (From Shao and Dong 2006)

TOMS dataset, Riemer et al. (2006) demonstrate that the position of the Azores High is the most important single factor. Doherty et al. (2008) combine TOMS/Nimbus 7 (1979–1992) and TOMS/Earth Probe (1998–2000) to analyse summer interannual variability of North African dust over the Caribbean and conclude that both the quantity of dust and the length of the dust season were increased during the 1980s and then plateaued into the 1990s.

Both long-term satellite dust datasets over the Atlantic and ground-based dust concentrations from Barbados strongly suggest that years of increased dustiness are associated with reduced rainfall conditions in the Sahel in the previous year (Prospero and Lamb 2003; Moulin and Chiapello 2004; Chiapello et al. 2005). Furthermore, the year-to-year evolution of summer surface dust concentrations at Barbados and satellite-derived DOD over the tropical North Atlantic and the Sahel show similar variability during the period 1979–2000 and correlate significantly with drought conditions in the Sahel (Fig. 7.8).

From these observational studies, it remains difficult to demonstrate direct causal relationships between atmospheric indices (NAO, rainfall conditions in the Sahel) and multiannual evolution of dust transport. Furthermore the mechanisms by which those influences play out are not yet fully understood. Evan and Mukhopadhyay (2010) employed historical satellite aerosol retrievals from AVHRR over the period 1982–2008 to estimate DOD over the tropical North Atlantic. Combining this satellite dataset with an in situ proxy of atmospheric dust from the Cape Verde Islands, they reconstruct the annual evolution of DOD over the period 1955–2008. Their analysis suggests that during the 1950s and 2000s, DOD over the tropical North Atlantic was at a minimum and peaked during the early 1980s. Thus, a decreasing trend in Atlantic dustiness is observed over the period 1984–2008, in agreement with other independent satellite datasets, especially TOMS AOD during 1980–2006 (Foltz and McPhaden 2008). The most likely explanation of this negative trend is a significant increase of rainfall over the Sahel since the mid-1980s. A recent analysis from Cowie et al. (2013) suggests a reduction in dust emission over the Sahel, associated with reduced peak winds caused by the "greening" in the Sahel.

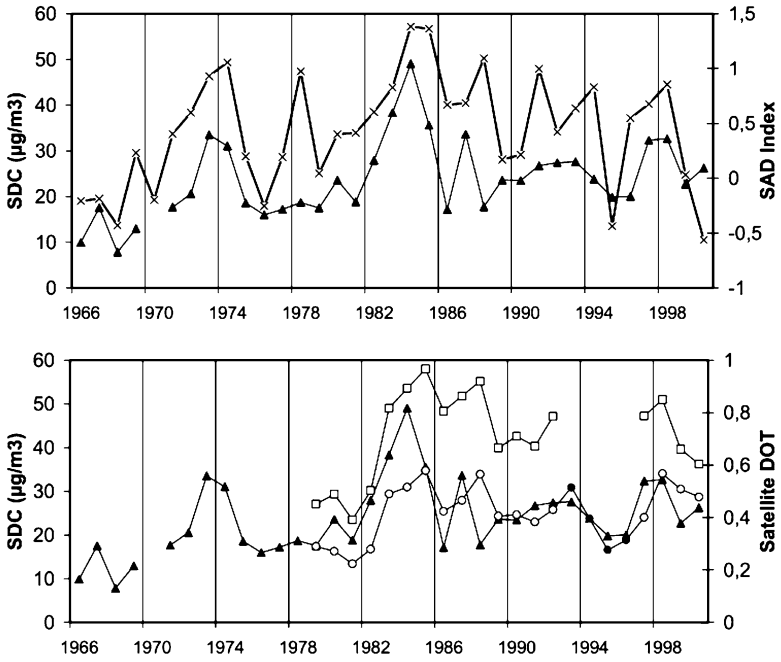

Fig. 7.8 *Top*: time series of summer mean Barbados surface dust concentrations (*solid triangles*) along with the Sahelian Annual Drought Index (*crosses*) from 1966 to 2000. *Bottom*: time series of summer mean Barbados surface dust concentrations (*solid triangles*) and summer mean satellite DOD over the tropical North Atlantic (15–30°N, *open circles* from TOMS, *shaded circles* from Meteosat/VIS) and over the Sahel (15–17°N, *squares*) (From Chiapello et al. 2005)

7.3.4 Vertical Structure

In recent years, the development and advancements of lidar (light detection and ranging) techniques, either ground-based or from space (Table 7.2), have been providing an unprecedented view of the vertical structure of the mineral dust distribution. The earliest investigations of dust vertical repartition were performed in the 1970s through limited aircraft measurements, especially during field campaigns in the North Atlantic region (Prospero and Carlson 1972). The first lidar observations of dust from space were provided by the Lidar In-Space Technology Experiment (LITE) and the Geoscience Laser Altimeter System (GLAS, on the ICEsat), but only for limited time periods (Karyampudi et al. 1999; Hart et al. 2005). Today an increasing number of lidar measurements are available from both field campaigns (AMMA, Léon et al. 2009; Cavalieri et al. 2010) and ground-based networks (Papayannis et al. 2008) and from the CALIPSO mission, the first satellite involving a lidar specifically designed to study aerosols and clouds (Winker et al. 2010). The CALIOP lidar on board the CALIPSO, thanks to depolarization measurements, enables aerosol classification, including identification of nonspherical particles such

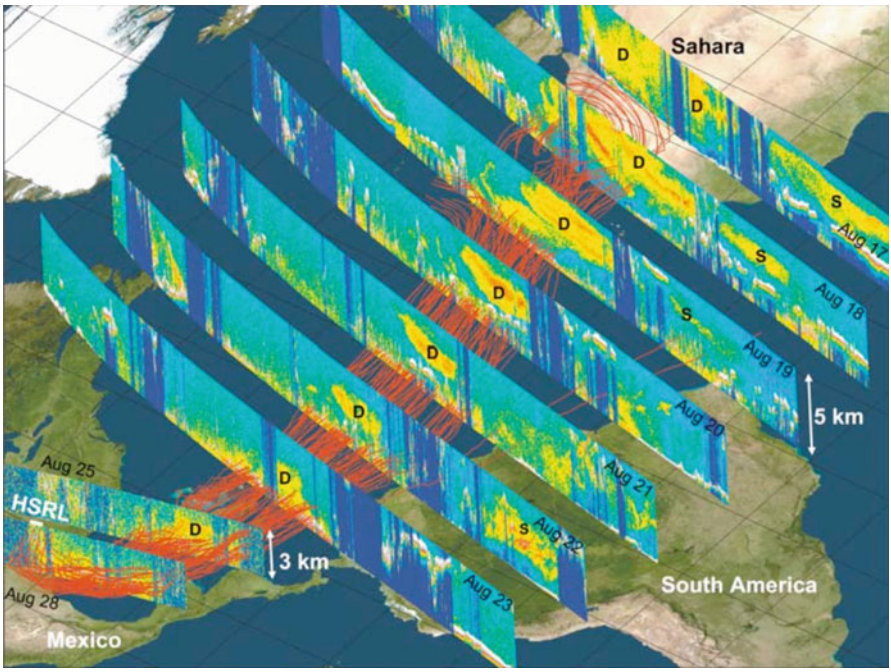

Fig. 7.9 An example demonstrating the capability of CALIOP to track dust long-range transport during a dust event that originated in the Sahara desert on 17 August 2007 and was transported to the Gulf of Mexico. Vertical images are 532-nm attenuated backscatter coefficients measured by CALIOP when passing over the dust transport track (From Liu et al. 2008a)

as dust (Omar et al. 2009). CALIOP started in spring 2006 measuring aerosol profiles with a 30-m vertical resolution and 70-m horizontal resolution. CALIPSO has acquired the largest amount of global dust vertical profiles so far (Mona et al. 2012, Fig. 7.9). The validation studies performed using ground-based lidar stations as a reference have shown a good quality of the CALIOP dataset (Pappalardo et al. 2010). Based on CALIOP measurements, a number of dust studies have been performed recently, especially for the characterization of North African dust transport over the Atlantic (Liu et al. 2008a; Ben-Ami et al. 2009; Generoso et al. 2008) and analysis of 3D structure of Asian dust (Huang et al. 2007; Uno et al. 2008). In parallel, Peyridieu et al. (2010) have shown the ability of infrared sounders like AIRS to retrieve the dust layer mean altitude quite accurately by comparing their results with the CALIOP-altitude product over the Atlantic. Figure 7.10 shows an illustration of a monthly climatology of dust mean altitude derived from AIRS data. This climatology allows observations of the spatial and seasonal variations of mean altitude of dust transport over the Atlantic, characterized by maximum heights in summer months and minimum heights in winter.

The CALIPSO mission offers considerable improvement in determining the vertical distribution of dust properties, also in situations where passive sensors do

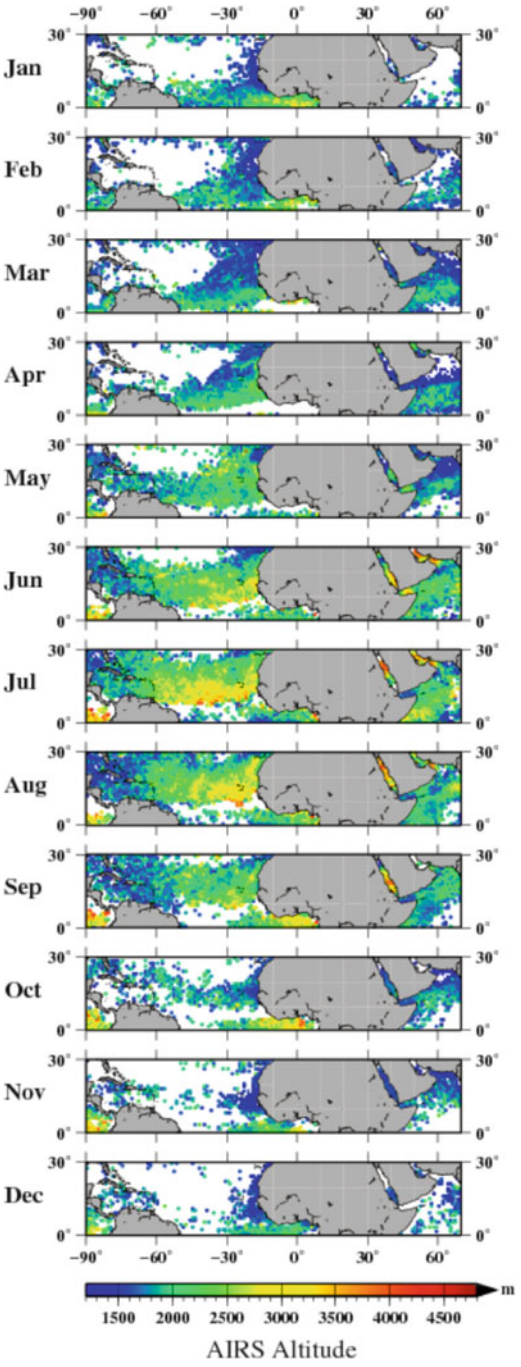

Fig. 7.10 Monthly climatology (1° × 1° resolution) of the aerosol layer mean altitude retrieved by AIRS over the period 2003–2008 (From Peyridieu et al. 2010)

not work, such as over snow and in cloudy situations (Winker et al. 2010). More generally the information about the vertical layering of aerosols provided by lidar instruments is crucial for aerosol-cloud interaction studies.

Systematic ground-based desert dust observations by lidar through networks are mainly located over two regions of interest: the Mediterranean Europe and Asia (Mona et al. 2012). Some recent studies have investigated dust vertical distributions over other less explored regions like Iran, but only in the form of case studies analysis (Abdi Vishkaee et al. 2011). The European Aerosol Research Lidar Network, EARLINET, was established in 2000 and provides systematic observations of Saharan dust events over several stations of the European continent (27 in 2012; Mona et al. 2012). Based on EARLINET data, Papayannis et al. (2008) showed that more than 130 days of Saharan dust outbreaks were monitored over Europe in 3 years, with the largest number of cases from late spring until early autumn months, and a much higher number of dust episodes observed in the southern parts of Europe. Continuous observations of vertical distribution and optical properties of Asian dust in East Asia (China, Korea, Japan and Mongolia) are made by depolarization and backscatter lidars with AD-Net (Mona et al. 2012). Müller et al. (2010) have shown that one of the important characteristics of Asian dust is the mixing of mineral dust with anthropogenic pollution.

7.4 Conclusion

For many remote areas of the globe, the only approach for quantitative and continuous dust observations is via satellites. With the advances in remote sensing measurements, a revolution in aerosol and dust monitoring has been taking place in recent years (Laj et al. 2009; Shao et al. 2011; Yu et al. 2013). Thanks to progress in both technology and algorithm development from active and passive sensors, the number and quality of observations of AOD and the optical properties of dust have considerably increased during the last decades (Redmond et al. 2010). Our current knowledge of the global distribution of mineral dust is for a good part based on satellite observations with passive remote sensors like AVHRR, MODIS, TOMS, Meteosat, MISR, POLDER and SeaWiFS. Since the launch of the CALIPSO mission in 2006, a global view of height-resolved dust distribution has become possible (Liu et al. 2008b). Moreover, the emerging satellite observations of above-cloud aerosols, from both spaceborne lidar and passive sensors, especially from the A-Train, certainly constitute a major advancement of the very recent years (Yu and Zhang 2013).

Compared to early sensors in operation in the 1990s, the last generation of satellites has better observing capabilities for dust, especially SEVIRI/MSG, MODIS, MISR, POLDER and CALIOP, allowing deeper understanding of aerosol processes in terms of emission and transport. Furthermore, with the most recent satellite algorithms from MODIS (Ginoux et al. 2012), POLDER (Herman et al. 2005) and

MISR (Kalashnikova and Kahn 2006), it has become possible to distinguish mineral dust from other aerosol species with an improved accuracy.

No single satellite instrument, associated algorithm and retrieval are without limitation. Uncertainties have manifold causes including cloud contamination, assumptions on optical properties and variability in surface properties, as, for example, land surface albedo and emissivity. Specificities in resolution, sampling and coverage of satellite sensors also cause significant differences in the dust observations provided by space measurements. Generally, different aerosol algorithms and retrievals agree better over ocean than over land, where the absolute uncertainties on AOD remain relatively high. Recently Carboni et al. (2012) have demonstrated discrepancies between different satellite aerosol products, especially during intense dust events.

Despite progress, especially with the Deep Blue algorithm, passive remote sensing from space of dust loads over arid continental surfaces has remained more challenging. New algorithms are currently being developed to continue the advances on satellite retrievals of aerosol over arid surfaces, as from POLDER polarized multidirectional spectral measurements (Dubovik et al. 2011). The performance of this kind of algorithm is promising, as it is expected to provide retrievals of an extended set of aerosol physical and optical properties along with surface properties with better accuracy.

Finally, progressing towards more accurate global estimates of desert dust loads and key properties, radiative effects and impacts on air quality will necessarily rely on integrated approaches based on multiple satellite observation analysis, verified with ground-truth measurements from reference networks, as AERONET, and combined to multi-scale models (Yu et al. 2006).

References

Abdi Vishkaee F, Flamant C, Cuesta J, Flamant P, Khalesifard HR (2011) Multiplatform observations of dust vertical distribution during transport over northwest Iran in the summertime. J Geophys Res 116, D05206. doi:10.1029/2010JD014573

Alonso-Pérez S, Cuevas E, Querol X, Viana M, Guerra JC (2007) Impact of the Saharan dust outbreaks on the ambient levels of total suspended particles (TSP) in the marine boundary layer (MBL) of the Subtropical Eastern North Atlantic Ocean. Atmos Environ 41:9468–9480

Ansmann A, Petzold A, Kandler K, Tegen I, Wendish M, Möller D, Weinzierl B, Müller T, Heintzenberg J (2011) Saharan mineral dust experiments SAMUM-1 and SAMUM-2: what have we learned? Tellus 63B:403–429

Arimoto R, Duce RA, Ray BJ, Ellis WG Jr, Cullen JD, Merrill JT (1995) Trace elements in the atmosphere over the North Atlantic. J Geophys Res 100:1199–1213

Banks JR, Brindley HE (2013) Evaluation of MSG-SEVIRI mineral dust retrieval products over North Africa and the Middle East. Remote Sens Environ 128:58–73

Ben-Ami Y, Koren I, Altaratz O (2009) Patterns of North African dust transport over the Atlantic: winter vs. summer, based on CALIPSO first year data. Atmos Chem Phys 9:7867–7875

Brooks N, Legrand M (2000) Dust variability over northern Africa and rainfall in the Sahel. In: McLaren SJ, Kniveton D (eds) Linking climate change to land surface change. Kluwer, Dordrecht, pp 1–25

Cakmur RV, Miller RL, Tegen I (2001) A comparison of seasonal and interannual variability of soil dust aerosols over the Atlantic Ocean as inferred by the TOMS AI and AVHRR AOT retrievals. J Geophys Res 106(D16):18287–18303

Carboni E, Thomas G, Sayer A, Poulsen C, Grainger D, Siddans R, Ahn C, Antoine D, Bevan S, Braak R, Brindley H, DeSouza-Machado S, Deuzé JL, Diner D, Ducos F, Grey W, Hsu C, Kalashnikova OV, Kahn R, North PRJ, Salustro C, Smith A, Tanré D, Torres O, Eihelmann BV (2012) Intercomparison of desert dust optical depth from satellite measurements. Atmos Meas Tech 5:1973–2002

Cavalieri O, Cairo F, Fierli F, Di Donfrancesco G, Snels M, Viterbini M, Cardillo F, Chatenet B, Formenti P, Marticorena B, Rajot JL (2010) Variability of aerosol vertical distribution in the Sahel. Atmos Chem Phys 10:12005–12023

Chiapello I, Bergametti G, Gomes L, Chatenet B, Dulac F, Pimenta J, Santos Soares E (1995) An additional low layer transport of Sahelian and Saharan dust over the North-Eastern Tropical Atlantic. Geophys Res Lett 22:3191–3194

Chiapello I, Bergametti G, Chatenet B, Bousquet P, Dulac F, Santos Soares E (1997) Origins of African dust transported over the northeastern tropical Atlantic. J Geophys Res 102:13701–13709

Chiapello I, Moulin C, Prospero JM (2005) Understanding the long-term variability of African dust transport across the Atlantic as recorded in both Barbados surface concentrations and large-scale TOMS optical thickness. J Geophys Res 110, D18S10. doi:10.1029/2004JD005132

Cowie SM, Knippertz P, Marsham JH (2013) Are vegetation-related roughness changes the cause of the recent decrease in dust emission from the Sahel? Geophys Res Lett 40:1868–1872. doi:10.1002/grl.50273

Cuesta J et al (2008) Multiplatform observations of the seasonal evolution of the Saharan atmospheric boundary layer in Tamanrasset, Algeria, in the framework of the African Monsoon Multidisciplinary Analysis field campaign conducted in 2006. J Geophys Res 113, D00C07. doi:10.1029/2007JD009417

Darwin C (1846) An account of the fine dust which often falls on vessels in the Atlantic Ocean. Q J Geol Soc Lond 2:26–30

Derimian Y, Karnieli A, Kaufman YJ, Andreae MO, Andreae TW, Dubovik O, Maenhaut W, Koren I, Holben BN (2006) Dust and pollution aerosols over Negev desert, Israel: properties, transport, and radiative effect. J Geophys Res 111, D05205. doi:10.1029/2005JD006549

DeSouza-Machado SG et al (2010) Infrared retrievals of dust using AIRS: comparisons of optical depths and heights derived for a North African dust storm to other collocated EOS A-Train and surface observations. J Geophys Res 115, D15201. doi:10.1029/2009JD012842

Di Iorio T, di Sarra A, Sferlazzo DM, Cacciani M, Meloni D, Monteleone F, Fua' D, Fiocco G (2009) Seasonal evolution of the tropospheric aerosol vertical profile in the central Mediterranean and role of desert dust. J Geophys Res 114, D02201. doi:10.1029/2008JD010593

Doherty OM, Riemer N, Hameed S (2008) Saharan mineral dust transport into the Caribbean: observed atmospheric controls and trends. J Geophys Res 113, D07211. doi:10.1029/2007JD009171

Dubovik O, Holben B, Eck TF, Smirnov A, Kaufman Y, King M, Tanré D, Slutsker I (2002) Variability of absorption and optical properties of key aerosol types observed in worldwide locations. J Atmos Sci 59(3):590–608

Dubovik O, Lapyonok T, Kaufman YJ, Chin M, Ginoux P, Kahn RA, Sinyuk A (2008) Retrieving global aerosol sources from satellites using inverse modeling. Atmos Chem Phys 8:209–250

Dubovik O, Herman M, Holdak A, Lapyonok T, Tanré D, Deuzé JL, Ducos F, Sinyuk A, Lopatin A (2011) Statistically optimized inversion algorithm for enhanced retrieval of aerosol properties from spectral multi-angle polarimetric satellite observations. Atmos Meas Tech 4:975–1018. doi:10.5194/amt-4-975-2011

Dulac F, Tanré D, Bergametti G, Buat-Ménard P, Desbois M, Sutton D (1992) Assessment of the African airborne dust mass over the western Mediterranean Sea using Meteosat data. J Geophys Res 97(D2):2489–2506

Engelstaedter S, Washington R, Tegen I (2006) North African dust emissions and transport. Earth Sci Rev 79:73–100

Escudero M, Querol X, Pey J, Alastuey A, Pérez N, Ferreira F, Alonso S, Rodriguez S, Cuevas E (2007) A methodology for the quantification of the net African dust load in air quality monitoring networks. Atmos Environ 41:5516–5524

Evan AT, Mukhopadhyay S (2010) African dust over the northern tropical Atlantic: 1955–2008. J Appl Meteorol Climatol 49:2213–2229. doi:10.1175/2010JAMC2485.1

Foltz GR, McPhaden MJ (2008) Trends in Saharan dust and tropical Atlantic climate during 1980–2006. Geophys Res Lett 35, L20706. doi:10.1029/2008GL035042

Gasso S, Stein AF (2007) Does dust from Patagonia reach the sub-Antarctic Atlantic Ocean? Geophys Res Lett 34, L01801. doi:10.1029/2006GL027693

Generoso S, Bey I, Labonne M, Breon F-M (2008) Aerosol vertical distribution in dust outflow over the Atlantic: comparisons between GEOS-Chem and Cloud-Aerosol Lidar and Infrared Pathfinder Satellite Observation (CALIPSO). J Geophys Res 113, D24209. doi:10.1029/2008JD010154

Ginoux P, Prospero JM, Gill TE, Hsu NC, Zhao M (2012) Global-scale attribution of anthropogenic and natural dust sources and their emission rates based on MODIS Deep Blue aerosol products. Rev Geophys 50, RG3005. doi:10.1029/2012RG000388

Goudie AS, Middleton NJ (1992) The changing frequency of dust storms through time. Clim Change 20:197–225

Goudie AS, Middleton NJ (2006) Desert dust in the global system. Springer, Berlin, Heidelberg, New York

Hart WD, Spinhirne JD, Palm SP, Hlavka DL (2005) Height distribution between cloud and aerosol layers from the GLAS spaceborne lidar in the Indian Ocean region. Geophys Res Lett 32, L22S06. doi:10.1029/2005GL023671

Haywood JM et al (2008) Overview of the dust and biomass-burning experiment and African monsoon multidisciplinary analysis special observing period-0. J Geophys Res 113, D00C17. doi:10.1029/2008JD010077

Herman JR, Bhartia PK, Torres O, Hsu C, Seftor C, Celarier E (1997) Global distribution of UV-absorbing aerosols from Nimbus 7/TOMS data. J Geophys Res 102:16911–16922

Herman M, Deuzé J-L, Marchant A, Roger B, Lallart P (2005) Aerosol remote sensing from POLDER/ADEOS over the ocean: improved retrieval using a nonspherical particle model. J Geophys Res 110, D10S02. doi:10.1029/2004JD004798

Holben BN, Tanré D, Smirnov A, Eck TF, Slutsker I, Chatenet B, Lavenu F, Kaufman YJ, Van de Castle J, Setzer A, Markham B, Clark D, Frouin R, Karneli NA, O'Neill N, Pietras C, Pinker VK, Zibordi G (2001) An emerging ground-based aerosol climatology: aerosol optical depth from AERONET. J Geophys Res 106:12067–12097

Hsu NC, Tsay SC, King MD, Herman JR (2004) Aerosol properties over bright-reflecting source regions. IEEE Trans Geosci Remote Sens 42(3):557–569

Hsu NC, Tsay S-C, King MD, Herman JR (2006) Deep Blue retrievals of Asian aerosol properties during ACE-Asia. IEEE Trans Geosci Remote Sens 44(11):3180–3195

Hsu NC, Gautam R, Sayer AM, Bettenhausen C, Li C, Jeong MJ, Tsay SC, Holben BN (2012) Global and regional trends of aerosol optical depth over land and ocean using SeaWiFS measurements from 1997 to 2010. Atmos Chem Phys 12:8037–8053

Huang J, Minnis P, Yi Y, Tang Q, Wang X, Hu Y, Liu Z, Ayers K, Trepte C, Winker D (2007) Summer dust aerosols detected from CALIPSO over the Tibetan Plateau. Geophys Res Lett 34, L18805. doi:10.1029/2007GL029938

Huneeus N, Chevallier F, Boucher O (2012) Estimating aerosol emissions by assimilating observed aerosol optical depth in a global aerosol model. Atmos Chem Phys 12:4585–4606

Husar RB, Prospero JM, Stowe LL (1997) Characterization of tropospheric aerosols over the oceans with the NOAA AVHRR optical thickness product. J Geophys Res 102:16889–16909

Husar RB et al (2001) The Asian dust events of April, 1998. J Geophys Res 106:18317–18330

Israelevich P, Ganor E, Alpert P, Kishcha P, Stupp A (2012) Predominant transport paths of Saharan dust over the Mediterranean Sea to Europe. J Geophys Res 117, D02205. doi:10.1029/2011JD016482

Jankowiak I, Tanré D (1992) Satellite climatology of Saharan dust outbreaks: method and preliminary results. J Clim 5:646–656

Kalashnikova OV, Kahn R (2006) Ability of multiangle remote sensing observations to identify and distinguish mineral dust types: 2. Sensitivity over dark water. J Geophys Res 111, D11207. doi:10.1029/2005JD006756

Kalashnikova OV, Kahn RA (2008) Mineral dust plume evolution over the Atlantic from MISR and MODIS aerosol retrievals. J Geophys Res 113, D24204. doi:10.1029/2008JD010083

Kalivitis N, Gerasopoulos E, Vrekoussis M, Kouvarakis G, Kubilay N, Hatzianastassiou N, Vardavas I, Mihalopulos N (2007) Dust transport over the eastern Mediterranean derived from Total Ozone Mapping Spectrometer, Aerosol Robotic Network, and surface measurements. J Geophys Res 112, D03202. doi:10.1029/2006JD007510

Karyampudi VM, Palm SP, Reagen JA, Fang H, Grant WB, Hoff RM, Moulin C, Pierce HF, Torres O, Browell EV, Melfi SH (1999) Validation of the Saharan dust plume conceptual model using lidar, Meteosat and ECMWF. Bull Am Meteorol Soc 80:1045–1075

Kaufman YJ, Koren I, Remer LA, Tanré D, Ginoux P, Fan S (2005) Dust transport and deposition observed from the Terra-Moderate Resolution Imaging Spectroradiometer (MODIS) spacecraft over the Atlantic Ocean. J Geophys Res 110, D10S12. doi:10.1029/2003JD004436

Kim D, Chin M, Yu H, Eck TF, Sinyuk A, Smirnov A, Holben BN (2011) Dust optical properties over North Africa and Arabian peninsula derived from the AERONET dataset. Atmos Chem Phys 11:10733–10741

Klose M, Shao Y, Karremann MK, Fink AH (2010) Sahel dust zone and synoptic background. Geophys Res Lett 37, L09802. doi:10.1029/2010GL042816

Klüser L, Marynenko D, Holzer-Popp T (2011) Thermal infrared remote sensing of mineral dust over land and ocean: a spectral SVD based retrieval approach for IASI. Atmos Meas Tech 4:757–773. doi:10.5194/amt-4-757-2011

Knippertz P, Todd MC (2012) Mineral dust aerosols over the Sahara: meteorological controls on emission and transport and implications for modeling. Rev Geophys 50, RG1007. doi:10.1029/2011RG000362

Kocha C, Tulet P, Lafore J-P, Flamant C (2013) The importance of the diurnal cycle of Aerosol Optical Depth in West Africa. Geophys Res Lett 40:785–790. doi:10.1002/grl.50143

Kurosaki Y, Mikami M (2003) Recent frequent dust events and their relation to surface wind in East Asia. Geophys Res Lett 30(14):1736. doi:10.1029/2003GL017261

Laj P et al (2009) Measuring atmospheric composition change. Atmos Environ 43:5351–5414

Legrand M, Plana-Fattori A, N'Doumé C (2001) Satellite detection of dust using the IR Imagery of Meteosat 1. Infrared difference dust index. J Geophys Res 106(D16):18251–18274

Lenoble J, Remer L, Tanré D (2013) Aerosol remote sensing. Springer, Heidelberg

Léon J-F, Legrand M (2003) Mineral dust sources in the surroundings of the north Indian Ocean. Geophys Res Lett 30(6):1309. doi:10.1029/2002GL016690

Léon J-F, Derimian Y, Chiapello I, Tanré D, Podvin T, Chatenet B, Diallo A, Deroo C (2009) Aerosol vertical distribution and optical properties over M'Bour (16.96W; 14.39 N), Senegal from 2006 to 2008. Atmos Chem Phys 9:9249–9261

Li F, Ginoux P, Ramaswamy V (2010) Transport of Patagonian dust to Antartica. J Geophys Res 115, D18217. doi:10.1029/2009JD012356

Liu Z et al (2008a) CALIPSO lidar observations of the optical properties of Saharan dust: a case study of long-range transport. J Geophys Res 113, D07207. doi:10.1029/2007JD008878

Liu D, Wang Z, Liu Z, Winker D, Trepte C (2008b) A height resolved global view of dust aerosols from the first year CALIPSO lidar measurements. J Geophys Res 113, D16214. doi:10.1029/2007JD009776

Mahowald NM, Dufresne J-L (2004) Sensitivity of TOMS aerosol index to boundary layer height: implications for detection of mineral aerosol sources. Geophys Res Lett 31, L03103. doi:10.1029/2003GL018865

Mahowald NM, Ballantine JA, Feddema J, Ramankutty N (2007) Global trends in visibility: implications for dust sources. Atmos Chem Phys 7:3309–3339

Mangold A, De Backer H, De Paepe B, Dewitte S, Chiapello I, Derimian Y, Kacenelenbogen M, Léon JF, Huneeus N, Schulz M, Ceburnis D, Dowd CO, Flentje H, Kinne S, Benedetti A, Morcrette JJ, Boucher O (2011) Aerosol analysis and forecast in the European Centre for Medium Range Weather Forecasts Integrated Forecast System: 3. Evaluation by means of case studies. J Geophys Res 116, D03302. doi:10.1029/2010JD014864

Marticorena B, Chatenet B, Rajot JL, Traoré S, Coulibaly M, Diallo A, Koné I, Maman A, NDiaye T, Zakou A (2010) Temporal variability of mineral dust concentrations over West Africa: analyses of a pluriannual monitoring from the AMMA Sahelian Dust Transect. Atmos Chem Phys 10:8899–8915

Martiny N, Chiapello I (2013) Assessments for the impact of mineral dust on the meningitis incidence in West Africa. Atmos Environ 70:245–253

Martonchik JV, Diner DJ, Kahn R, Gaitley B, Holben BN (2004) Comparison of MISR and AERONET aerosol optical depths over desert sites. Geophys Res Lett 31, L16102. doi:10.1029/2004GL019807

Meloni D, di Sarra A, Biavati G, DeLuisi JJ, Monteleone F, Pace G, Piacentino S, Sferlazzo DM (2007) Seasonal behavior of Saharan dust events at the Mediterranean island of Lampedusa in the period 1999–2005. Atmos Environ 41:3041–3056

Mona L, Liu Z, Müller D, Omar A, Papayannis A, Pappalardo G, Sugimoto N, Vaughan M (2012) Lidar measurements for desert dust characterization: an overview. Adv Meteorol 2012. doi:10.1155/2012/356265

Moulin C, Chiapello I (2004) Evidence of the control of summer atmospheric transport of African dust over the Atlantic by Sahel sources from TOMS satellites (1979–2000). Geophys Res Lett 31, L02107. doi:10.1029/2003GL018931

Moulin C, Lambert CE, Dulac F, Dayan U (1997) Control of atmospheric export of dust from North Africa by the North Atlantic oscillation. Nature 387:691–694

Müller D, Mattis I, Tatarov B, Noh YM, Shin DH, Shin SK, Lee KH, Kim YJ, Sugimoto N (2010) Mineral quartz concentration measurements of mixed mineral dust/urban haze pollution plumes over Korea with multi wavelength aerosol Raman-quartz lidar. Geophys Res Lett 37, L20810. doi:10.1029/2010GL044633

N'tchayi Mbourou GN, Bertrand JJ, Nicholson SE (1997) The diurnal and seasonal cycles of wind-borne dust over Africa north of the equator. J Appl Meteorol 36(7):868–882

Omar AH et al (2009) The CALIPSO automated aerosol classification and lidar ratio selection algorithm. J Atmos Oceanic Tech 26:1994–2014

Papayannis A et al (2008) Systematic lidar observations of Saharan dust over Europe in the frame of EARLINET (2000–2002). J Geophys Res 113, D10204. doi:10.1029/2007JD009028

Pappalardo G et al (2010) EARLINET correlative measurements for CALIPSO: first intercomparison results. J Geophys Res 115, D00H19. doi:10.1029/2009JD012147

Peyridieu S, Chedin A, Tanre D, Capelle V, Pierangelo C, Lamquin N, Armante R (2010) Saharan dust infrared optical depth and altitude retrieved from AIRS: a focus over North Atlantic – comparisons to MODIS and CALIPSO. Atmos Chem Phys 10:1953–1967

Pierangelo C, Chédin A, Heilliette S, Jacquinet-Husson N, Armante R (2004) Dust altitude and infrared optical depth from AIRS. Atmos Chem Phys 4:1813–1822. Res. 104 (D2), 2213–2222

Prospero JM (1999) Long-term measurements of the transport of African mineral dust to the south-eastern United States: implications for regional air quality. J Geophys Res 114(D13):15917–15927

Prospero JM, Carlson TN (1972) Vertical and areal distribution of Saharan dust over the western equatorial north Atlantic Ocean. J Geophys Res 77(27):5255–5265

Prospero JM, Lamb PJ (2003) African droughts and dust transport to the Caribbean: climate change implications. Science 302:1024–1027

Prospero JM, Ginoux P, Torres O, Nicholson SE, Gill TE (2002) Environmental characterization of global sources of atmospheric soil dust identified with the Nimbus 7 Total Ozone Mapping Spectrometer (TOMS) absorbing aerosol product. Rev Geophys 40(1):1002. doi:10.1029/2000RG000095

Prospero JM, Bullard JE, Hodgkins R (2012) High-latitude dust over the North Atlantic: inputs from Icelandic proglacial dust storms. Science 335:1078–1082

Querol X, Pey J, Pandolfi M, Alastuey A, Cusack M, Pérez N, Moreno T, Viana M, Mihalopoulos N, Kallos G, Kleanthous S (2009) African dust contributions to mean ambient PM10 mass-levels across the Mediterranean Basin. Atmos Environ 43:4266–4277

Rajot JL et al (2008) AMMA dust experiment: an overview of measurements performed during the dry season special observation period (SOP0) at the Banizoumbou (Niger) supersite. J Geophys Res 113, D00C14. doi:10.1029/2008JD009906

Redmond HE, Dial KD, Thompson JE (2010) Light scattering and absorption by wind blown dust: theory, measurement, and recent data. Aeolian Res 2:5–26. doi:10.1016/j;aeolia.2009.09.002

Riemer N, Doherty OM, Hameed S (2006) On the variability of African dust transport across the Atlantic. Geophys Res Lett 33, L13814. doi:10.1029/2006GL026163

Rodriguez S, Alastuey A, Querol X (2012) A review of methods for long term in situ characterization of aerosol dust. Aeolian Res 6:55–74

Schepanski K, Tegen I, Laurent B, Heinold B, Macke A (2007) A new Saharan dust source activation frequency map derived from MSG-SEVIRI IR-channels. Geophys Res Lett 34, L18803. doi:10.1029/2007GL030168

Schepanski K, Tegen I, Todd MC, Heinold B, Bönisch G, Laurent B, Macke A (2009) Meteorological processes forcing Saharan dust emission inferred from MSG-SEVIRI observations of subdaily dust source activation and numerical models. J Geophys Res 114, D10201. doi:10.1029/2008JD010325

Schepanski K, Tegen I, Macke A (2012) Comparison of satellite based observations of Saharan dust source areas. Remote Sens Environ 123:90–97. doi:10.1016/j.rse.2012.03.019

Schulz M et al (2012) Atmospheric transport and deposition of mineral dust to the ocean: implications for research needs. Environ Sci Technol 46:10390–10404

Shao Y, Dong CH (2006) A review on East Asian dust storm climate, modeling and monitoring. Global Planet Change 52:1–22

Shao Y, Wyrwoll K-H, Chappell A, Huang J, Lin Z, McTainsh GH, Mikami M, Tanaka TY, Wang X, Yoon S (2011) Dust cycle: an emerging core theme in Earth system science. Aeolian Res 2(4):181–204. doi:10.1016/j.aeolia.2011

Sun J, Zhang M, Liu T (2001) Spatial and temporal characteristics of dust storms in China and its surrounding regions, 1960–1999: relations to source area and climate. J Geophys Res 106(D10):10325–10333

Swap R, Ulanski S, Cobbett M, Garstang M (1996) Temporal and spatial characteristics of Saharan dust outbreaks. J Geophys Res 101(D2):4205–4220

Tanré D, Bréon FM, Deuzé JL, Dubovik O, Ducos F, François P, Goloub P, Herman M, Liferman A, Waquet F (2011) Remote sensing of aerosols by using polarized, directional and spectral measurements within the A-Train: the PARASOL mission. Atmos Meas Tech 4:1383–1395

Thieuleux F, Moulin C, Bréon FM, Maignan F, Poitou J, Tanré D (2005) Remote sensing of aerosols over the oceans using MSG/SEVIRI imagery. Ann Geophys 23:1–8

Todd MC et al (2013) Meteorological and dust aerosol conditions over the western Saharan region observed at Fennec Supersite-2 during the intensive observation period in June 2011. J Geophys Res Atmos 118:8426–8447. doi:10.1002/jgrd.50470

Torres O, Tanskanen A, Veihelmann B, Ahn C, Braak R, Bhartia PK, Veefkind P, Levelt P (2007) Aerosols and surface UV products from Ozone Monitoring Instrument observations: an overview. J Geophys Res 112, D24S47. doi:10.1029/2007JD008809

Uno I, Yumimoto K, Shimizu A, Hara Y, Sugimoto N, Wang Z, Liu Z, Winker DM (2008) 3D structure of Asian dust transport revealed by CALIPSO lidar and a 4DVAR dust model. Geophys Res Lett 35, L06803. doi:10.1029/2007GL032329

Vergé-Dépré G, Legrand M, Moulin C, Alias A, François P (2006) Improvement of the detection of desert dust over the Sahel using METEOSAT IR imagery. Ann Geophys 24:1–9

Wang X, Dong Z, Zhang J, Liu L (2004) Modern dust storms in China: an overview. J Arid Environ 58:559–574

Wang J, Xu X, Henze DK, Zeng J, Ji Q, Tsay S-C, Huang J (2012) Top-down estimate of dust emissions through integration of MODIS and MISR aerosol retrievals with the GEOS-Chem adjoint model. Geophys Res Lett 39, L08802. doi:10.1029/2012GL051136

Waquet F, Cornet C, Deuzé J-L, Dubovik O, Ducos F, Goloub P, Herman M, Lapyonok T, Labonnote LC, Riedi J, Tanré D, Thieuleux F, Vanbauce C (2013a) Retrieval of aerosol microphysical and optical properties above liquid clouds from POLDER/PARASOL polarization measurements. Atmos Meas Tech 6:991–1016. doi:10.5194/amt-6-991-2013

Waquet F, Peers F, Ducos F, Goloub P, Platnick SE, Riedi J, Tanré D, Thieuleux F (2013b) Global analysis of aerosol properties above clouds. Geophys Res Lett 40:5809–5814. doi:10.1002/2013GL057482

Winker DM, Pelon J, Coakley JA Jr, Ackerman SA, Charlson RJ, Colarco PR, Flamant P, Fu Q, Hoff RM, Kittaka C, Kubar TL, Le Treut H, McCormick MP, Mégie G, Poole l, Powell K, Trepte C, Vaughan MA, Wielicki BA (2010) The CALIPSO mission A global 3D view of aerosols and clouds. Bull Am Meteorol Soc 91:1211–1229

Yu H, Zhang Z (2013) New directions: emerging satellite observations of above-cloud aerosols and direct radiative forcing. Atmos Environ 72:36–40

Yu H et al (2006) A review of measurement-based assessments of the aerosol direct radiative effect and forcing. Atmos Chem Phys 6:613–666

Yu H, Remer LA, Kahn RA, Chin M, Zhang Y (2013) Satellite perspective of aerosol intercontinental transport: from qualitative tracking to quantitative characterization. Atmos Res 124:73–100

Chapter 8
Dust Deposition

Gilles Bergametti and Gilles Forêt

Abstract During transport, dust particles experience deposition processes that strongly affect their atmospheric lifetime and their radiative and geochemical impacts. Dust particles are removed either by dry deposition mainly controlled by gravity, impaction, and diffusion or by wet removal in or below clouds, all processes being strongly size dependent. Theoretical models have been developed to describe these processes, and parameterizations have been derived in order to represent as precisely as possible the deposition of dust in 3D models. However, direct measurements, especially for dry deposition, are difficult to perform and consequently data are sparse, limiting our capability to test the accuracy of the simulations of the dust deposition and thus to effectively constrain the dust mass budget simulated by these models.

Keywords Dust deposition • Particle size • Wet deposition • Dry deposition • Dust models • Advection • Precipitation • Scavenging • Washout • Rainout • Collision

8.1 Introduction

The assessment of the impacts that desert dust has on the behavior of the Earth system requires a reliable estimation of the dust concentration in the atmosphere and of its variability in space and time. It also requires information on the dust size distribution (see Chap. 2) and on the dust composition, since these characteristics control both radiative (see Chap. 11) and biogeochemical (see Chap. 14) impacts and deposition patterns. To do that, atmospheric dust models have to represent the

G. Bergametti (✉) • G. Forêt
LISA, UMR CNRS 7583 – Université Paris Est Créteil – Université Paris Diderot, Paris, France
e-mail: Gilles.Bergametti@lisa.univ-paris12.fr; Gilles.Foret@lisa.univ-paris12.fr

P. Knippertz and J.-B.W. Stuut (eds.), *Mineral Dust: A Key Player in the Earth System*, DOI 10.1007/978-94-017-8978-3_8,

three steps of the dust cycle: dust emissions, mainly from the arid and semiarid regions of the Earth; transport through the atmosphere depending strongly on the meteorological situations; and finally deposition of dust along their atmospheric path by wet or dry processes. The global atmospheric dust burden at any one moment is the result of the balance between the sources and sinks. Thus, a complete closure of the dust budget at the global scale needs to quantify precisely the amount of emitted dust, the atmospheric dust load, and the deposited dust mass (dry and wet). However, this budget is sufficiently constrained if, at least, two of these three terms are quantified with a good confidence level.

During the 1990s, dust emissions have been considered to be the main source of errors in dust models (Joussaume 1990; Genthon 1992; Marticorena and Bergametti 1995) (see Chap. 9). Large uncertainties were attached to (1) the representation of the involved processes and/or their parameterization, (2) the quality of the input data required by these dust emission models to characterize the main surface properties of the desert areas, and (3) the localization of the dust source regions (see Chap. 3). During the last twenty years, significant progress has been made on dust emission modelling (Shao et al. 1993; Marticorena and Bergametti 1995; Alfaro and Gomes 2001; Shao 2004; Marticorena 2014) and on the dust source monitoring, especially by using satellite observations (Prospero et al. 2002; Washington et al. 2003). However, quantitative estimates of dust emissions in 3D models are still affected by large uncertainties (Textor et al. 2006; Huneeus et al. 2011), mainly because a quantitative validation of dust emissions at a large scale is presently not possible.

The description of the atmospheric dust content in terms of both spatial distribution and temporal variability has also been significantly improved through the development of aerosol products from remote-sensing instruments. Despite some limitations of these techniques (see Chap. 7), the atmospheric dust content is clearly the term of the dust mass budget for which the quantitative estimates are most precise today (Textor et al. 2007). As a consequence, most of the dust cycle simulations are mainly compared to large datasets of aerosol optical depth (AOD) or dust concentrations measured during specific intensive campaigns.

Dry and wet depositions are the processes by which atmospheric dust particles are removed from the atmosphere (see, e.g., Duce et al. (1991); Schulz et al. (2012)). In the vicinity of source regions, dry deposition is generally the dominant process, due both to the presence of large dust particles and to the dry climate prevailing in deserts. Far from source regions, since the larger particles have already been deposited, the dust size spectrum is narrower with a typical mass median diameter close to 2 μm (e.g., Schütz (1980)). Thus, wet deposition is usually the dominant removal process for dust particles far from the source regions (e.g., Bergametti et al. (1989)). These two sinks, which counterbalance dust emissions on the global scale, control the atmospheric lifetime of dust particles and their biogeochemical impact by defining how much, when, and where dust is deposited onto continental or oceanic surfaces.

However, rather little attention has been paid to dust deposition. It was generally assumed that the existing schemes were sufficiently efficient for representing dust deposition in models. As a consequence, few experiments were dedicated to test

dust deposition schemes against in situ data. Moreover, direct dust deposition measurements are difficult to perform, especially dry, and suffer from a lack of standard and qualified procedure despite the fact that the existence of such reference methods should strongly help in combining different measurements in order to evaluate dust deposition simulations. In fact, networks monitoring dust deposition remain rare and most of the existing measurements are performed relatively far from source regions, although a large part of the dust mass is deposited during the first 1,000 km of transport (Schütz 1980). Finally, dust deposition, especially after long-range transport, is significantly affected by wet deposition, meaning that models dealing with dust (and more generally aerosol) simulations need more accurate precipitation fields (at least in terms of localization and frequency).

In conclusion, there is an urgent need for further research and measurements of dust deposition. Dust models are mainly validated against proxies for the atmospheric dust load, e.g., AOD, concentrations, dust vertical profiles, or combinations of these. However, because of various deficiencies in these datasets, they do not serve as a sufficient constraint to close the dust mass budget.

In this chapter, we will address the theoretical concepts allowing to describe the removal processes of dust (i.e., the dry and wet deposition pathways) and will discuss the importance of the representation of the size distribution into models to correctly simulate the dust deposition (Sect. 8.2). In Sect. 8.3, we will report and discuss the few measurements of dust deposition that have been performed in the past. Finally, we will illustrate how the lack of constraints on the deposition term limits the ability of dust models to precisely assess the mass budget of dust (Sect. 8.4) and we conclude with some final remarks (Sect. 8.5).

8.2 Deposition Processes

In the atmosphere, the vertical mass or number flux, F_z (respectively, in g m^{-2} s^{-1} and m^{-2} s^{-1}), of a given species at a given height z is linked to the mass or number concentration (respectively, in g m^{-3} or m^{-3}) of this species at z, C_z, by a parameter V having the dimension of a velocity (m s^{-1}):

$$F_z = V.C_z \tag{8.1}$$

By convention, F_z is negative when the flux is downward (i.e., from the atmosphere to the surface) and in this case, V is called the deposition velocity, V_d. When V_d is only controlled by dry deposition processes, V_d is named the dry deposition velocity.

Figure 8.1 shows the number and mass size distributions of dust deduced from wind-tunnel measurements (Alfaro et al. 1998). These distributions are assumed to be representative of dust size distributions in the vicinity of source regions. It demonstrates the efficiency of the removal processes for dust particles (i.e., the dry deposition velocity and the scavenging coefficient of dust by precipitation) versus the dust particle diameter. It can be noted that similarities exist between the size

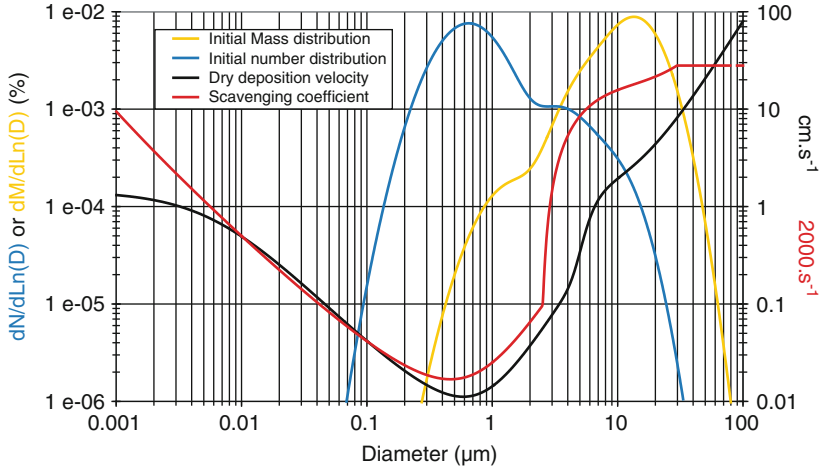

Fig. 8.1 Aerosol number distribution (*blue curve*) and mass distribution (*yellow curve*) representative of the dust size distribution in source regions as proposed by Alfaro and Gomes (2001) for the case of dust emission from an aluminosilicate silt soil type. For these two distributions, units (on the left axis) are relative units (normalized, respectively, by the total aerosol number and mass). Dry deposition velocity (*black curve*) and below-cloud scavenging coefficient (*red curve*) are also displayed with units indicated on the right axis, respectively, in cm.s^{-1} for dry deposition and in aerosol number.s^{-1} for the scavenging coefficient (multiplied by 2,000 to have a common scale). Computations are performed for a wind friction velocity of 0.3 m s^{-1}, which corresponds to a 10-m wind speed of about 7 m s^{-1} for a surface roughness length of 0.001 m. Neutral conditions are assumed. The below-cloud scavenging coefficient is computed by using the formulation proposed by Slinn (1984) (Adapted from Forêt et al. 2006)

dependency of dry and wet removal processes with, in both cases, a minimum and rather constant efficiency of removal for particles having diameters ranging from 0.1 and 2 μm and larger values and stronger size dependence of dry and wet deposition processes for particles having both smaller and larger diameters.

8.2.1 Dry Deposition

Due to the existence of large size modes in the dust size distribution, dry deposition is a major sink for dust particles. Three main removal processes, depending on the size domain we consider, control the dry deposition of particles: (1) for particles with diameters smaller than 0.1 μm, the deposition velocity V_d is controlled by the Brownian diffusion process and V_d can reach values as high as 1 cm s^{-1} for particles of 0.001 μm; (2) high V_d (some cm s^{-1}) are observed for particles with a diameter larger than 5 μm, mainly due to gravitational settling; (3) for particles in the intermediate size range (between 0.1 μm and 5 μm), the deposition velocity is at a minimum and controlled by turbulent processes (interception and impaction), which are less efficient to remove particles.

For a given particle, the relative importance of each of these physical processes depends on how close the particle approaches the surface. Generally two atmospheric layers are distinguished to describe dry deposition processes: a first layer close to the surface, with a thickness on the order of centimeters, where Brownian diffusion and gravitational settling are the main deposition processes, and a second layer, above the previous one, called the constant flux layer, where turbulent processes and gravitational settling are dominant (e.g., Slinn and Slinn 1980; Giorgi 1986, 1988).

Conceptually, diffusive (turbulent and Brownian) and gravitational processes are considered to act in parallel while the two layers operate in series. On a practical point of view, the derivation of such a formulation requires to neglect the influence of gravity in transport. Thus, the steady-state gravitational settling velocity of particles (also called terminal velocity, V_s) is added a posteriori to the calculated deposition rate from diffusive processes. The dry deposition of a particle with a given aerodynamic diameter is then considered as a set of associated pseudo resistances (Wesely 1989): one is the aerodynamic resistance, R_a (s m^{-1}), operating in the constant flux layer, and the other, the quasi-laminar resistance, R_b (s m^{-1}), operating in the layer closest to the surface. The dry deposition velocity of the system is the inverse of the total equivalent resistance:

$$V_d = V_s + (R_a + R_b + R_a R_b V_s)^{-1} \tag{8.2}$$

Gravitational Settling Velocity

V_s can be expressed according to the modified Stokes law:

$$V_s = \frac{D_p^2 \rho_p g C_c}{18 \mu_{air}} \tag{8.3}$$

with D_p the particle diameter (if particles are assumed spherical, the geometric diameter equals the aerodynamic diameter), ρ_p the particle density (generally taken as 2.6 g m^{-3} for dust particles), μ_{air} the dynamic viscosity of air (1.789 10^{-5} Pa s at 288 K, 1013.25 hPa), and g the gravitational acceleration (9.81 m s^{-2}).

For small particles (i.e., with sizes comparable to that of the mean free path of the molecules), the drag force onto settling particles must be corrected (reduced) since the considered fluid becomes more a discontinuous medium than a "dense" continuum. This is the purpose of the Cunningham (slip) correction factor, C_c. This correction factor, which can affect the deposition velocity for mineral particles smaller than about 1 μm in diameter by almost 10 %, is expressed as (Seinfeld and Pandis 1998)

$$C_c = 1 + \frac{2\lambda}{D_p}\left[1.257 + 0.4 \exp\left(-\frac{1.1 D_p}{2\lambda}\right)\right] \tag{8.4}$$

with λ, the mean free path of gas molecules in air (6.6 10^{-6} cm).

Aerodynamic and Quasi-laminar Resistances

In Eq. 8.2, the aerodynamic resistance, R_a, represents the effects of diffusion by turbulent processes in the surface layer. It mainly depends on the atmospheric stability and surface roughness. For neutral atmospheric conditions, the expression of R_a is

$$R_a = \frac{1}{(k u_*)} \left[\ln \left({}^{z}\!/_{z_0} \right) - \psi_h \right] \tag{8.5}$$

with k the von Karman constant (0.4); u_* the wind friction velocity; and z the reference height for wind velocity, z_0 the aerodynamic roughness length of the surface, and ψ_h the stability function.

The quasi-laminar resistance, R_b, describes the transfer of particles through the viscous layer taking into account both the Brownian diffusion of particles having small diameters (<0.5 μm) and the inertial impaction, more efficient for particles with large diameters (>2 μm):

$$R_b = \frac{1}{\left[u_* \left(\mathrm{Sc}^{-2/3} + 10^{-3/\mathrm{St}} \right) \right]} \tag{8.6}$$

The resistance to particle diffusion across the quasi-laminar layer to a solid surface is proportional to the Schmidt number, Sc, to the power of −2/3, at least for viscous flow at high Reynolds numbers, Re, over a fixed, smooth surface and is depending on the Stokes number, St (Slinn et al. 1978). However, a nonrigid surface (e.g., the ocean surface) will tend to slip in the direction of the mean wind so that the characteristic air velocity in the diffusion layer is somewhat larger and the resulting transfer coefficient for particles across the quasi-laminar layer to a free surface should be proportional to $\mathrm{Sc}^{0.5}$ (Slinn and Slinn 1980).

Sc is the ratio between viscous and diffusion forces associated with the Brownian diffusion:

$$\mathrm{Sc} = \upsilon_{\mathrm{air}} D_g^{-1} \tag{8.7}$$

with υ_{air} the kinematic viscosity of air ($1.461\ 10^{-5}$ m^2 s^{-1}) and D_g the Brownian diffusivity expressed according to Davies (1966):

$$D_g = \left(2.38 \times 10^{-7} / D_p \right) \left(1 + 0.163 / D_p + 0.0548 \exp\left(-6.66 D_p \right) / D_p \right) \tag{8.8}$$

In Eq. 8.6, St represents the particle susceptibility to inertial impaction. Indeed, the large particles, due to their high inertia, are less able to follow the flow when it changes direction to avoid obstacles on the surface (rocks, bushes, trees, etc.). It is expressed as

$$\mathrm{St} = \frac{(u_*)^2 V_s}{g \nu_{\mathrm{air}}} \tag{8.9}$$

In this approach, the deposition surface is considered as perfectly "sticky," since no bounce-off or remobilization of particles on the surface is considered. When turbulence increases, the thickness of the quasi-laminar layer decreases, while the wind friction velocity increases; as a consequence, V_d increases when u_* increases.

It is worth noting that theoretical developments have been relatively rare during the past twenty years. Some efforts have been made to better reproduce dry deposition of aerosols over vegetated surface (e.g., Zhang et al. 2001; Petroff et al. 2008, 2009) or to add additional effects (such as phoretic effects) to the actual formulation of the dry deposition (Petroff and Zhang 2010). The same authors also propose a new formulation of the Brownian diffusion more efficient to estimate dry deposition over smooth and water surfaces.

8.2.2 Wet Deposition

The term wet deposition includes all depositional processes by which aerosols are removed from the atmosphere due to the presence of water, i.e., mainly cloud, snow, and fog.

If, as already mentioned, dry deposition is by far the dominant removal process of atmospheric mineral particles in the vicinity of dust source areas, the relative importance of wet scavenging processes increases with the distance from the source regions (Tegen and Fung 1994; Zhao et al. 2003).

For atmospheric particles, there are two distinct ways of wet removal:

- Rainout or in-cloud scavenging corresponds to the scavenging of aerosol particles acting as condensation or freezing nuclei or to collision with preexisting cloud droplets or ice crystals inside the cloud.
- Washout or below-cloud scavenging corresponds to the impaction of aerosol particles by the falling droplets.

The below-cloud scavenging process is much more efficient for the removal of particles in the coarse mode (Fig. 8.1), while the in-cloud scavenging process is important for the removal of submicron particles. Moreover, in their initial composition (see Chap. 2), dust particles are generally assumed to be hydrophobic (Fan et al. 2004), reducing the in-cloud scavenging efficiency and suggesting that below-cloud scavenging is the dominant wet deposition process for pure dust particles. Nevertheless, recent work of Twohy et al. (2009) suggests that pure dust particles could act as condensation nuclei. Dust particles are also known to be efficient ice nuclei and Atkinson et al. (2013) demonstrate that it is strongly dependent on the aerosol mineralogy. Once more, the processes involved are, at the moment, too poorly known to be included in dust models.

During transport, dust particles may undergo transformations, aggregating more hydroscopic compounds like sulfates on their surface (Levin et al. 1996; Würzler et al. 2000; Perry et al. 2004; see also Chaps. 4 and 12). This coating could allow

dust particles to act more efficiently as cloud condensation nuclei (Fan et al. 2004). In-cloud processes, especially for dust particles, remain poorly understood and their representation in models is very crude (see Chap. 12). In models, dust particles are represented either as purely hydrophobic aerosols, and no in-cloud scavenging is considered (Genthon 1992; Tegen and Fung 1994) or in-cloud scavenging is considered and the scavenging efficiency of dust is assumed to be that of sulfate aerosols (Chin et al. 2000; Zender et al. 2003; Grini et al. 2005).

The below-cloud scavenging size dependency is better understood (Dana and Hales 1976; Slinn 1984; Garcia Nieto et al. 1994). Following Seinfeld and Pandis (1998), the removal of particles by washout can be computed as

$$C_i\,(t+1) = C_i(t) - \Lambda_i \times C_i(t) \times \Delta t \tag{8.10}$$

where i refers to a given particle diameter D_p and C_i is the mass or number concentration of particles, Δt the time step, and Λ_i the scavenging coefficient (s^{-1}). The scavenging coefficient is linked to the collision efficiency by

$$\Lambda_i = (3/2) \times E_i\,(D_\mathrm{d}) \times (p_0/D_\mathrm{d}) \tag{8.11}$$

with E the collision efficiency; p_0 the rainfall intensity, i.e., the amount of rain that falls over time (cm s^{-1}); and D_d, the droplet diameter (cm).

E is the key parameter since it represents the capacity of falling droplets to catch aerosols. It is computed as the ratio between the number of collisions between droplets and particles and the number of particles in the column swept by a falling droplet. Collision efficiency equal to 1 means that all particles of an air column swept by one droplet are removed by this droplet. Thus, E is the sum of the collision efficiencies due to Brownian diffusion, interception, and inertial impaction as explained in the following.

Brownian Diffusion

The collision efficiency due to Brownian diffusion results from the thermal motion of particles and thus is primarily important for submicron particles. Slinn (1984) proposes the following expression to describe the collision efficiency due to Brownian diffusion:

$$E_\mathrm{B} = \frac{4}{\mathrm{Re_d Sc}}\left[1 + 0.4\mathrm{Re_d}^{1/2}\mathrm{Sc}^{1/3} + 0.16\mathrm{Re_d}^{1/2}\mathrm{Sc}^{1/2}\right] \tag{8.12}$$

In this expression $\mathrm{Re_d}$ and Sc refer to different objects: $\mathrm{Re_d}$ is the Reynolds number of the droplet while Sc is the Schmidt number of the aerosol.

Interception

The collision efficiency for interception, E_I, indicates the proportion of particles remaining in the streamline when the distance of the streamline of fluid flow to an approaching raindrop is smaller than their radius. Obviously, this phenomenon is mainly of interest for the largest particles. According to Slinn (1984), E_i can be expressed as

$$E_i = 4\frac{D_p}{D_d}\left[\frac{\mu_{air}}{\mu_{H_2O}} + \frac{D_p}{D_d}\left(1 + 2\sqrt{Re_d}\right)\right] \tag{8.13}$$

where μ_{air} is the dynamic dry viscosity of air and μ_{H_2O} is the water viscosity.

Inertial Impaction

The collision efficiency due to impaction, E_{imp}, concerns large particles, i.e., those for which inertia does not allow them to follow the streamlines of the air when a raindrop is approaching; thus, the collision occurs and the droplet catches the particle.

A critical Stokes number St* can be defined as the maximum S_t of the relative flow a particle can have without impacting, when it is directly in the path of the approaching droplet:

$$St^* = \frac{\frac{12}{10} + \frac{1}{12}\ln(1 + Re_d)}{1 + \ln Re_d} \tag{8.14}$$

According to Slinn (1982), for St > St*, E_{imp} can be expressed as

$$E_{imp} = \left(\frac{\rho_d}{\rho_p}\right)^{1/2}\left(\frac{St - St^*}{St - St^* + \frac{2}{3}}\right)^{3/2} \tag{8.15}$$

When looking at collision processes, it appears that the number of collisions between a droplet of a given size falling in an atmospheric column and the particles contained in this column is highly dependent on the particles size. This efficiency is minimum for particles having a diameter around 0.5 μm (Greenfield 1957) (Fig. 8.1). When the particle size decreases, E increases due to Brownian diffusion. When the particle size increases, the collision efficiency increases due first to the effect of interception and then to the effect of inertial impaction.

Slinn (1982) emphasizes the point that although the collision processes discussed above are reasonably well known, other processes such as particle growth, thermophoresis (i.e., the effect of the force induced by the existence of a temperature gradient) or electrophoresis (i.e., the effect of the force resulting from

the presence of a charged interface between the particle surface and the air) may cause E predictions to differ significantly from what happens in reality (Wang et al 2010).

8.2.3 Particle Size Distribution and Deposition in Dust Models

Since deposition is highly size dependent, the knowledge of the dust size distribution is a prerequisite to estimate dust deposition fluxes (dry or/and wet). Then, in addition to dust emission fluxes, the dust size distribution in source region must be documented. However, direct measurements of the size distribution of dust particles in or in the vicinity of dust source regions are rare (see Chap. 5). Thus, most of the knowledge on dust size distributions representative of source regions is derived from wind-tunnel experiments (e.g., Alfaro and Gomes 2001). Only recently, measurements of the dust size distributions have been performed over the Sahara (Sow et al. 2009) and the Australian desert (Shao et al. 2011).

Early global dust aerosol models only used a unique aerosol particle size (e.g., Joussaume 1990, 1993) to represent the dust size distribution. Later, a limited number of modes have been used. A "mode" is characterized by a mean or median diameter, a predefined mathematical "shape" (often a log-normal function in the case of aerosols) and a constant geometric standard deviation for each mode. For example, Tegen and Fung (1994) use four constant log-normal modes, while Guelle et al. (2000) uses three log-normal semi-constant modes (e.g., median diameter is changing during transport but having constant geometric standard deviations).

To represent the dust size distributions during transport with a better accuracy, models now commonly use a binning of the particle size distribution. The advantage of this approach is that it does not need an assumption on the conservation of the particle size modes (e.g., Ginoux et al. 2001; Gao et al. 2003; Gong et al. 2003; Zhao et al. 2003; Meskhidze et al. 2005). Because the number of the particle size bins directly controls the computing time, the particle size range or the number of size bins (or both) is limited in models. For instance, Ginoux et al. (2001) and Meskhidze et al. (2005), respectively, use 7 and 5 bins between 0.2 and 12 μm in diameter, Zender et al. (2003) use 4 bins below 10 μm, Gao et al. (2003) 4 bins below 12 μm, while the model developed by Lu and Shao (2001) had 6 bins between less than 2 and 125 μm. One of the most sophisticated representations of the dust size distribution in a 3D dust transport model is that by Zhao et al. (2003), who use 12 size bins over a large size range (0.01–40.96 μm).

In 3D models, these size bins are often defined to have equal ranges in log D_p (e.g., Dulac et al. 1989; Schulz et al. 1998; Gong et al. 2003; Zhao et al. 2003). This splitting is thus called iso-log and each size bin is generally characterized by its geometric mean diameter. This approach leads to uncertainties, which depend on the number of bins used to represent the whole particle size distribution. Indeed, Gong et al. (2003) and Forêt et al. (2006) show that the number of bins directly

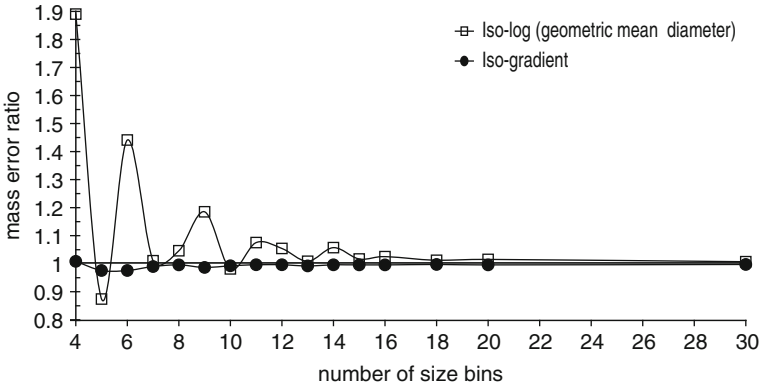

Fig. 8.2 Mass error ratios using an iso-log size bin scheme (*open squares*) and an iso-gradient scheme (*filled circles*) plotted against the number of size bins used. The error ratio in each case is the ratio of the mass of airborne dust aerosol remaining after two days of dry deposition calculated using 1,000 size bins (reference) or a reduced number of size bins (from 4 to 30 here). This is a measure of the error made when using a limited number of bins for representing the dust size distribution and the subsequent dry deposition. The initial mass size distribution is that shown in Fig. 8.1 (Adapted from Forêt et al. 2006)

controls the model accuracy and concludes that a minimum of 12 iso-log bins are necessary to correctly simulate both the number and the mass size distributions of tropospheric aerosols.

To limit the number of bins but keeping a good accuracy, Forêt et al. (2006) proposed a new approach for binning the size distribution into a limited number of size intervals. Their method, called iso-gradient scheme, assumes that it is more efficient to have more size bins for the size domain where the removal processes are strongly size dependent rather than having size bins equally distributed over the whole domain. Thus, they split the size distribution into bins having an equal range in V_d, i.e., following the size dependence in dry deposition velocity by satisfying an "iso-gradient" condition in V_d. Figure 8.2 shows a comparison of the accuracy of both approaches when compared to a highly size resolved simulation using 1,000 size bins. The new approach largely reduces the discretization errors for low bin numbers (Fig. 8.2). This has also been confirmed in case of full 3D dust simulations (Menut et al. 2007).

8.3 Dust Deposition Measurements

Measurements of dry deposition fluxes are hard to perform, since it is difficult to develop a sampler that correctly mimics natural surfaces (Fowler et al. 2009). As the deposition in the surface layer is highly dependent on the properties of that surface, such differences between the sampler and the surface generate significant

errors in the estimation of the dry deposition fluxes. Goossens (2005) tested many experimental systems (water surface, glass surface, metal surface, vertical array of metal plates, and an inverted frisbee filled with glass marbles) to collect dry deposited dust particles and showed that none of these surrogate systems are really efficient to collect quantitatively the dry deposition. This is especially critical for particles in the size range 0.1–10 μm, for which the dominating removal process is associated to the turbulent flux and which are most sensitive to surface properties (see Sect. 8.2.1). On the opposite, the dry deposition of larger particles is controlled by sedimentation and is therefore less sensitive to surface properties. Due to the lack of instruments able to perform measurements of dust concentration at high frequency, experimental determination of the dry deposition velocity of dust can only be performed using the classical "gradient method" (Gillette and Dobrowolski 1993), which defines the turbulent flux of a scalar in the vertical direction as

$$F = -K \, \mathrm{d}C/\mathrm{d}z \tag{8.16}$$

where K is the eddy diffusivity or turbulent transfer coefficient ($m^2\ s^{-1}$) and dC/dz is the scalar concentration gradient (expressed, e.g., for dust in $\mu g\ m^{-3}\ m^{-1}$).

Integration of (8.18) between two heights (z_1 and z_2) assuming a constant flux with height and neutral stability results in

$$F = \frac{u_* \Delta z \, k}{\ln (z_2 - z_1)} \frac{\Delta C}{\Delta z} \tag{8.17}$$

where ΔC is the scalar concentration difference between heights.

In practice, this method requires measurements of wind velocity and temperature profiles (since frequently corrections for non-neutral stability conditions are needed to precisely compute the wind friction velocity) and is often limited by the precision of the measurements of the scalar concentration difference between heights.

Wet (or total, when wet deposition strongly dominates the deposition) deposition measurements of dust are easier to perform. For example, long-time series of total deposition measurements were conducted in an area close to Barcelona in Spain (Avila 1996), which allow monitoring the intensity and frequency of red rains (i.e., precipitation associated with Saharan dust events). These records suggest that the deposition of Saharan dust is very discontinuous over the western Mediterranean region (about 10–20 events a year) and that a large part of the annual deposition flux of dust (up to 30 %) can occur in only two or three days. The deposition flux of Saharan dust in Miami (Florida, USA) was estimated from measurements of aluminum in precipitation to be around 1.26 g m^{-2} $year^{-1}$ (Prospero et al. 1987). More recently, measurements performed during three years at nine stations in Florida confirmed this value for Saharan dust deposition (deposition fluxes on the order of 2 g m^{-2} $year^{-1}$; Prospero et al. 2010). Dust deposition measurements are very scarce in and around the Sahara and Sahel regions, which are probably the most important dust sources of the world (see Chap. 3). Figure 8.3 shows most of

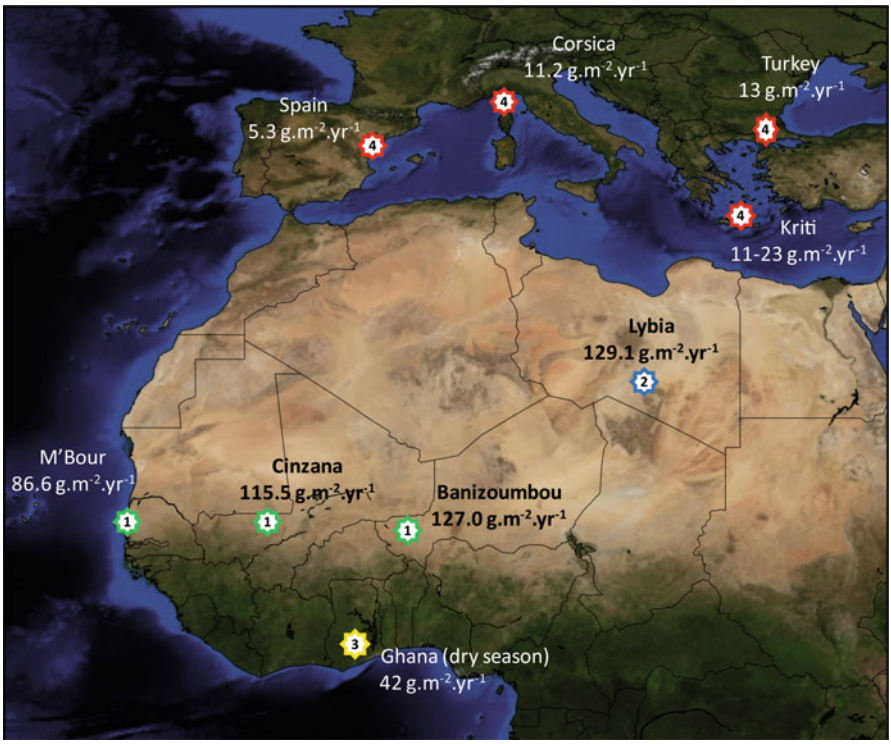

Fig. 8.3 Annual dust deposition fluxes measured over North Africa and in the Mediterranean basin. The data from Banizoumbou, Cinzana, and M'Bour (1) are unpublished data provided by LISA (B. Chatenet, B. Marticorena, J.L. Rajot) from measurements performed in the framework of the Sahelian Dust Transect, (2) O'Hara et al. (2006), (3) Breuning-Madsen and Awadzi (2005), and (4) Avila (1996), Bergametti et al. (1989), Kubilay et al. (2000), and Mattsson and Nihlen (1996)

the existing measurements in this region. These measurements show that the annual dust deposition fluxes measured in or close to the source regions (Banizoumbou (Niger), Cinzana (Mali), M'Bour (Senegal), in Libya) are very high with values on the order of 100 g m^{-2} $year^{-1}$. They also show a clear decrease of the deposition flux as a function of the distance from the Saharan dust source regions. In the Sahel, the dust deposition decreases only slowly along the main transport pathways of Saharan dust (see Chap. 7): from east (Banizoumbou) to west (M'Bour) and from north (Banizoumbou and Cinzana) to south (Ghana). On the opposite, the annual dust deposition fluxes measured in the Mediterranean Sea are lower by about one order of magnitude than those measured in the Sahara and Sahel, showing that a large part of the dust mass is deposited before reaching the Mediterranean basin.

Total deposition of atmospheric mineral particles (wet plus dry) has also been measured during consecutive two-week sampling intervals from January 1981 to March 1982 at four island stations (Midway, Oahu, Enewetak, and Fanning) of the

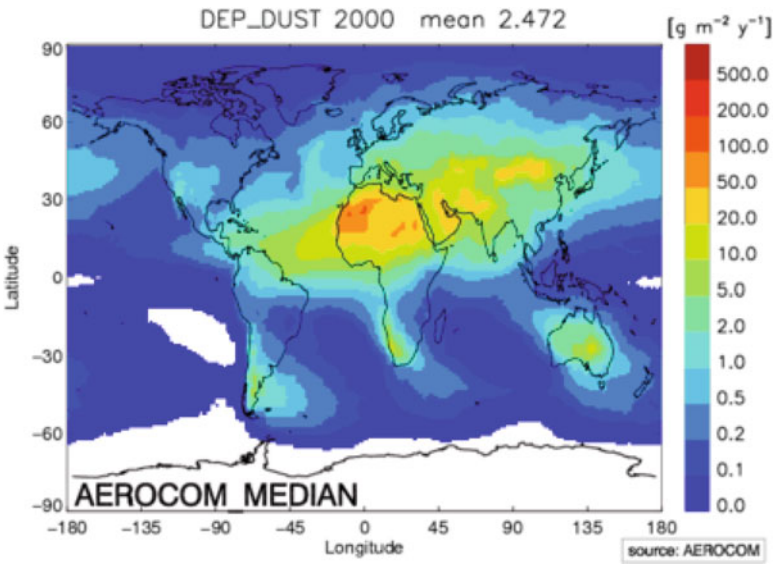

Fig. 8.4 Spatial distribution of dust deposition fluxes for the year 2000 as resulting of the median of the models participating to the AeroCom project (http://nansen.ipsl.jussieu.fr/AEROCOM)

SEAREX (Sea-Air Exchange Program) Asian Dust Study Network in the North Pacific (Arimoto et al. 1985; Uematsu et al. 1985). The annual dust deposition to the ocean appears to be dominated by sporadic dust events of short duration. The total deposition of atmospheric mineral material to the central North Pacific was estimated to be ∼0.2 g m^{-2} $year^{-1}$ (Uematsu et al. 1985). More recently, direct measurements of dust deposition (Heimburger et al. 2012; Heimburger et al. 2013) were performed in the Southern Ocean, one of the regions where dust deposition is expected to have the strongest biogeochemical impact (see Chap. 14). Total atmospheric deposition and crustal aerosol concentrations were monitored at Kerguelen Islands (49°18′S, 70°07′E) during a short campaign in early 2005 and then continuously for about 2 years (2009–2010). Results show very low atmospheric dust deposition fluxes compared to those reported in Fig. 8.3 but higher than those computed for the same oceanic region when applying deposition velocities to aerosol measurements (Wagener et al. 2008).

Figure 8.4 shows the mean deposition fluxes for the year 2000 obtained from the AeroCom project (Textor et al. 2006, 2007). It provides a synthetic vision of the spatial distribution of our knowledge of deposition fluxes. Spatial gradients are well marked with higher values near the source regions. Thus, highest deposition fluxes are simulated over the Sahara with values of 50–100 g m^{-2} $year^{-1}$, consistent with available observations (Fig. 8.3). Lower values are simulated over smaller deserts (China, Australia, Namibia, Patagonia). Over oceanic regions, located downwind source regions, deposition fluxes range from 2 to 50 g m^{-2} $year^{-1}$.

8.4 The Uncertainties in the Simulated Dust Mass Budget

An illustration of the impact of the weak constraints in dust modelling has been provided by the AeroCom model intercomparison exercise (Textor et al. 2006, 2007; Huneeus et al. 2011; see also Chap. 9). The aim of AeroCom is to analyze current global aerosol simulations based on harmonized diagnostics and to provide an evaluation of various models based on a model intercomparison and a comparison of these models to selected observations of aerosol properties (Textor et al. 2006). Among other aerosol species, comparisons for dust modelling are included. Most of the models participating in this intercomparison exercise used parameterization for deposition similar to those presented in the previous sections. The output of this intercomparison exercise are freely distributed (http://nansen.ipsl.jussieu.fr/AEROCOM) and used in the following to illustrate the present state of the uncertainties remaining in global dust models.

Fourteen research groups provided dust simulations to AeroCom. In the so-called Experiment A (Textor et al. 2006), each model worked in its nominal conditions, i.e., with its own parameterizations for emissions, transport, deposition, size distribution, etc. However, for some of these simulations, no information was provided on the size distribution prescribed in the simulations, while for some other models, the size distribution does not account for a supermicron mode. Since size distribution is a key factor for dust deposition, the set of models for the intercomparison is restricted to the seven models with a relatively similar size distribution. Figure 8.5a shows the simulated emissions in Mt/year for these models. It confirms that in global dust models, simulated dust emissions have large uncertainties as indicated by a ratio of $\approx$4.1 between the lowest ($\approx$975 Mt/year) and the highest emissions ($\approx$4000 Mt/year).

Surprisingly, despite such a large difference in dust emissions, the models are more or less in agreement in terms of dust load (Fig. 8.5b), since the ratio between the lowest ($\approx$17 Mt) and the highest atmospheric dust load ($\approx$29 Mt) is only 1.7, i.e., significantly lower than that for dust emissions. This low uncertainty in the simulated atmospheric dust load can be explained by the best observational constraints on this parameter (see Sect. 8.1), against which dust models are usually tuned. The adjustment of dust models with respect to the atmospheric dust load induces compensative effects: the simulated dust life time exhibits a similar range of variation between models than that observed for dust emissions (4.1) and models having the highest (lowest) emissions have the shortest (longest) lifetime (Fig. 8.5c).

To go further in the model evaluation, the AeroCom group proposed an additional Experiment B, for which the emission strength, the initial dust size distribution and the injection height were imposed to be the same for all models. Figure 8.6 reports the simulated annual dry and wet deposited mass (in Mt year^{-1}) for the six models that ran both experiments A and B (note that two models that had performed Experiment A but were omitted from the comparison because of their dust size distribution are reintroduced here, the size distribution now being identical for all models). For Experiment B, the differences (expressed in terms of ratio)

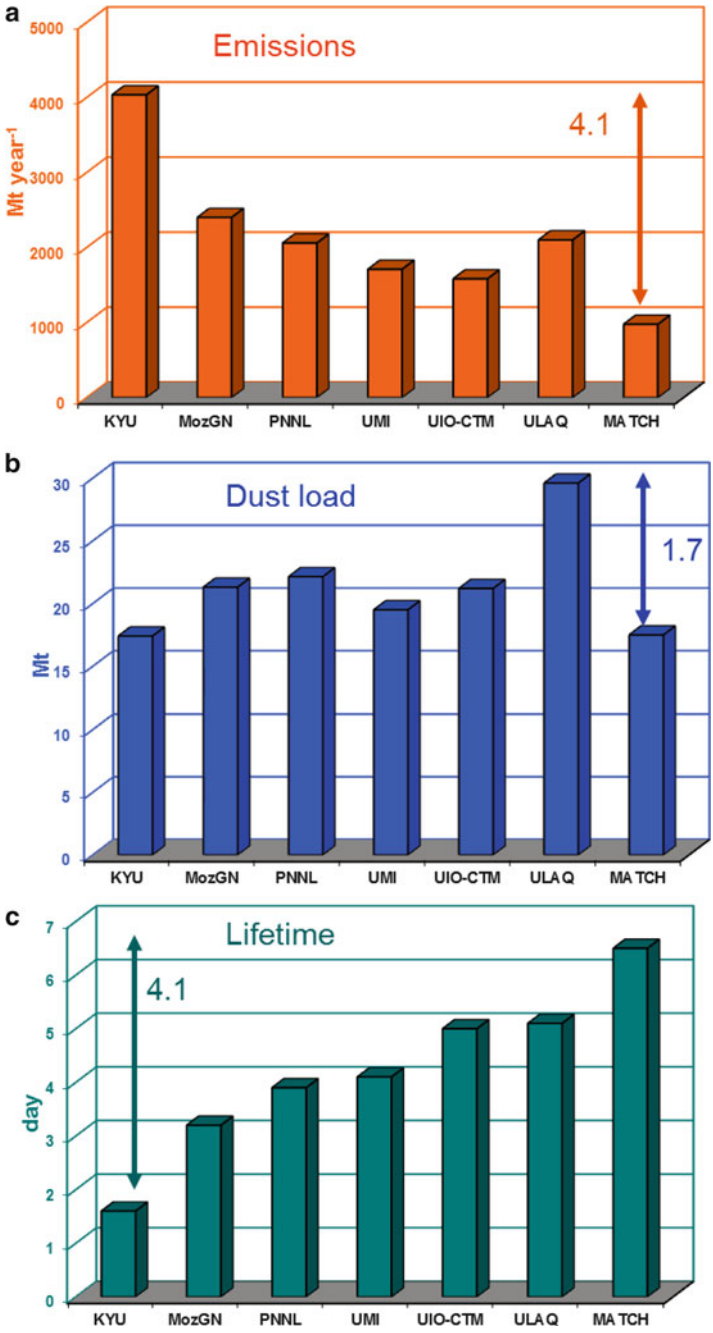

Fig. 8.5 Emission strength (**a**), dust load, (**b**) and lifetime (**c**) of dust as simulated by seven global dust models in the framework of the Experiment A of the AeroCom comparison exercise (derived from the AeroCom data base at http://nansen.ipsl.jussieu.fr/AEROCOM). *Arrows* and *associated numbers* indicate the ratio between highest and lowest model values for each parameter of interest

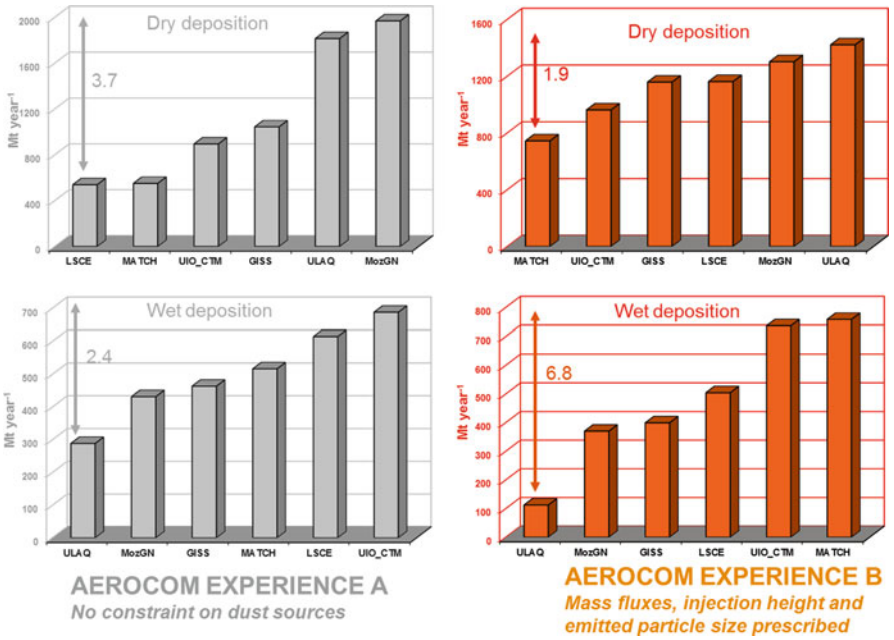

Fig. 8.6 Intercomparison of annual dry and wet deposition masses for mineral dust as simulated by different global dust models. Experiment A shows simulations performed in the nominal conditions for each model. Experiment B shows results for simulations performed by the same models but forced with identical dust emissions, size distribution, and injection height (derived from the AeroCom data base at http://nansen.ipsl.jussieu.fr/AEROCOM). *Arrows* and *associated numbers* indicate the ratio between highest and lowest model values for each parameter of interest

in the annual dry deposition mass between the two extreme models are reduced to a factor of 1.9 compared to Experiment A (3.7). This suggests that part of the differences between models in Experiment A could be due to differences in the dust size distributions. However, when looking at the annual wet deposition masses, the situation is reverse: the maximum difference between the simulated annual wet deposition masses is only a factor of 2.4 in Experiment A and almost tripled in Experiment B (6.8).

These results from the AeroCom dust model intercomparison exercise clearly suggest that the terms of the dust cycle are not sufficiently constrained to provide accurate estimates of the dust mass budget. As a general trend, the tested models simulate the climatology of vertically integrated parameters (AOD and Angström exponent) within a factor of two, whereas the total deposition and surface concentrations are reproduced within a factor of 10 (Huneeus et al. 2011). This points to large uncertainties in dust emissions, size distribution, and wet and dry deposition. Nevertheless, it should be recalled that AOD and Angström exponent are largely determined by the submicrometer fraction of aerosol and, therefore, model differences in AOD do not reflect discrepancies in the supra

micrometer aerosol size distribution. Based on the bias of the models, Huneeus et al. (2011) suggest that the range of possible emissions for North Africa is 400–2,200 Mt year^{-1} and 26–526 Mt year^{-1} for the Middle East, i.e., a factor of 5 and 20, respectively.

In conclusion, the relatively "good agreement" between simulated and observed atmospheric dust load appears to be the result of the compensation of the uncertainties associated with the different terms of the atmospheric dust cycle (as illustrated by the huge differences in the simulated life times). This results mainly from the fact that the dust load remains the only term of the mass budget reasonably constrained by observations. Thus, one of the main conclusions of this intercomparison exercise is the critical need for additional measurements to better constrain the mass budget in dust models. Since at this time no quantitative techniques allow measurements of dust emissions on a large scale, improving dust deposition modelling and measurements should be a good way to better constrain the dust mass budget (see, e.g., Han et al. 2008; Mahowald et al. 2005).

8.5 Conclusion

The dust mass budget is underconstrained in atmospheric dust models, leading to large uncertainties in both dust emission and deposition. These uncertainties strongly limit our capabilities to fully assess the radiative or biogeochemical impacts of dust. A promising way to improve simulations of the dust cycle is to reinforce research on deposition, both in terms of theoretical and numerical representation of dry and wet processes in models and by developing a dense and standardized dust deposition network in the vicinity of and far from source regions. This network should operate continuously throughout the year since annual dust deposition can be dominated by the sporadicity of dust events and the discontinuity of precipitation involved in wet removal.

References

Alfaro SC, Gomes L (2001) Modeling mineral aerosol production by wind erosion: emission intensities and aerosol distributions in source areas. J Geophys Res 106:18075–18084

Alfaro SC, Gaudichet A, Gomes L, Maillé M (1998) Mineral aerosol production by wind erosion: aerosol particle sizes and binding energies. Geophys Res Lett 25:991–994

Arimoto R, Duce RA, Ray BJ, Unni CK (1985) Atmospheric trace elements at Enewetak Atoll: 2. Transport to the ocean by wet and dry deposition. J Geophys Res 90:2391–2408

Atkinson JD, Murray BJ, Woodhouse MT, Carslaw KS, Whale TF, Baustian KJ, Dobbie S, O'Sullivan D, Malkin TL (2013) The importance of feldspar for ice nucleation by mineral dust in mixed-phase clouds. Nature 498:355–358. doi:10.1038/nature12278

Avila A (1996) Time trends in the precipitation chemistry at a mountain site in northeastern Spain for the period 1983–1994. Atmos Environ 30:1363–1373

Bergametti G, Gomes L, Remoudaki E, Desbois M, Martin D, Buat-Ménard P (1989) Present transport and deposition patterns of African dusts to the North-Western Mediterranean. In: Leinen M, Sarnthein M (eds) Paleoclimatology and paleometeorology: modern and past patterns of global atmospheric transport. Springer, New York, pp 227–252

Breuning-Madsen H, Awadzi TW (2005) Harmattan dust deposition and particle size in Ghana. Catena 63:23–38

Chin M, Rood RB, Lin S-J, Müller J-F, Thompson A (2000) Atmospheric sulfur cycle simulated in the global model GOCART: model description and global properties. J Geophys Res 105:24671–24687

Dana MT, Hales JM (1976) Statistical aspects of the washout of polydisperse aerosols. Atmos Environ 10:45–50

Davies CN (1966) Aerosol science. Academic, New York, p 33

Duce R et al (1991) The atmospheric input of trace species to the world ocean. Global Biogeochem Cycles 5:193–259

Dulac F, Buat-Ménard P, Ezat U, Melki S, Bergametti G (1989) Atmospheric input of trace metals to the western Mediterranean: uncertainties in modelling dry deposition from cascade impactor data. Tellus 41B:362–378

Fan S-M, Horowitz LW, Levy H II, Moxim WJ (2004) Impact of air pollution on wet deposition of mineral dust aerosols. Geophys Res Lett 31, L02104. doi:10.1029/2003GL0118501

Forêt G, Bergametti G, Dulac F (2006) An optimized particle size bin scheme for modeling mineral dust aerosols. J Geophys Res 111, D17310. doi:10.1029/2005JD 006797

Fowler D et al (2009) Atmospheric composition change: ecosystems–atmosphere interactions. Atmos Environ 43:5193–5267

Gao Y, Fan S-M, Sarmiento JL (2003) Aeolian iron input to the ocean through precipitation scavenging: a modeling perspective and its implication for natural iron fertilization in the ocean. J Geophys Res 108:4221. doi:10.1029/2002JD002420

Garcia Nieto PJ, Arganza Garcia B, Fernandez Diaz JM, Rodriguez Brana MA (1994) Parametric study of selective removal of atmospheric aerosol by below-cloud scavenging. Atmos Environ 28:2235–2342

Genthon C (1992) Simulations of desert dust and sea salt aerosols in Antarctica with a general circulation model of the atmosphere. Tellus 44:371–389

Gillette DA, Dobrowolski JP (1993) Soil crust formation by dust deposition at Shaartus, Tadzhik, U.S.S.R. Atmos Environ 27A:2519–2525

Ginoux P, Chin M, Tegen I, Prospero J, Holben BN, Dubovik O, Lin S-J (2001) Sources and distributions of dust aerosols simulated with the GOCART model. J Geophys Res 106:20255–20274

Giorgi F (1986) A particle dry-deposition parameterization scheme for use in tracer transport models. J Geophys Res 91:9794–9806

Giorgi F (1988) Dry deposition velocities of atmospheric aerosols as inferred by applying a particle dry deposition parameterization to a general circulation model. Tellus 40B:23–41

Gong SL, Barrie LA, Blanchet JP, von Salzen K, Lohmann U, Lesins G, Spacek L, Zhang LM, Girard E, Lin H, Leaitch R, Leighton H, Chylek P, Huang P (2003) Canadian Aerosol Module: a size-segregated simulation of atmospheric aerosol processes for climate and air quality models, 1. Module development. J Geophys Res 108:4007. doi:10.1029/2001JD002002

Goossens D (2005) Quantification of the dry aeolian deposition of dust on horizontal surfaces: an experimental comparison of theory and measurements. Sedimentology 52:859–873

Greenfield S (1957) Rain scavenging of radioactive particulate matter from the atmosphere. J Meteorol 14:115–125

Grini A, Myhre G, Zender CS, Isaksen ISA (2005) Model simulations of dust sources and transport in the global atmosphere: effects of soil erodibility and wind speed variability. J Geophys Res 110, D02205. doi:10.1029/2004JD005037

Guelle W, Balkanski Y, Schulz M, Marticorena B, Bergametti G, Moulin C, Arimoto R, Perry KD (2000) Modeling the atmospheric distribution of mineral aerosol: comparison with ground measurements and satellite observations for yearly and synoptic time scales over the North Atlantic. J Geophys Res 105:1997–2012

Han Q, Moore JK, Zender C, Measures C, Hydes D (2008) Constraining oceanic dust deposition using surface ocean dissolved Al. Global Biogeochem Cycles 22, GB2003. doi:10.1029/2007GB002975

Heimburger A, Losno R, Triquet S, Dulac F, Mahowald N (2012) Direct measurements of atmospheric iron, cobalt and aluminium-derived dust deposition at Kerguelen Islands. Global Biogeochem Cycles 26, GB4016. doi:10.1029/2012GB004301

Heimburger A, Losno R, Triquet S, Bon Nguyen E (2013) Atmospheric deposition fluxes of 26 elements over the Southern Indian Ocean: time series on Kerguelen and Crozet Islands. Global Biogeochem Cycles 27:440–449

Huneeus N, Schulz M, Balkanski Y, Griesfeller J, Prospero JM et al (2011) Global dust model intercomparison in AeroCom phase I. Atmos Chem Phys 11:7781–7811

Joussaume S (1990) Three-dimensional simulations of the atmosphere cycle of desert dust particles using a general circulation model. J Geophys Res 95:1909–1941

Joussaume S (1993) Paleoclimatic tracers: an investigation using an atmospheric general circulation model under Ice Age conditions. 1. Desert dust. J Geophys Res 98:2767–2805

Kubilay N, Nickovic S, Moulin C, Dulac F (2000) An illustration of the transport and deposition of mineral dust onto the eastern Mediterranean. Atmos Environ 34:1293–1303

Levin Z, Ganor E, Gladstein V (1996) The effects of desert particles coated with sulphate on rain formation in the eastern Mediterranean. J Appl Meteorol 35:1511–1523

Lu H, Shao Y (2001) Toward quantitative prediction of dust storms: an integrated wind erosion modelling system and its applications. Environ Model Software 16:233–249

Mahowald NM, Baker AR, Bergametti G, Brooks N, Duce RA, Jickells TD, Kubilay N, Prospero JM, Tegen I (2005) Atmospheric global dust cycle and iron inputs to the ocean. Global Biogeochem Cycles 19, GB4025. doi:10.1029/2004GB 002402

Marticorena B (2014) Dust production mechanisms. In: Knippertz P, Stuut J-B (eds) Mineral dust: a key player in the Earth System. Springer Sciences+ Business Media, Dordrecht. doi 10.1007/978-94-017-8978-3

Marticorena B, Bergametti G (1995) Modelling the atmospheric dust cycle: 1-Design of a soil-derived dust emission scheme. J Geophys Res 100:16415–16430

Mattsson JO, Nihlen T (1996) The transport of Saharan dust to southern Europe: a scenario. J Arid Environ 32:111–119

Menut L, Forêt G, Dulac F (2007) Sensitivity of mineral dust concentrations to the model size distribution accuracy. J Geophys Res 112, D10210. doi:10.129/2006JD007766

Meskhidze M, Chameides WL, Nenes A (2005) Dust and pollution: a recipe for enhanced ocean fertilization? J Geophys Res 110, D03301. doi:10.1029/2004JD005082

O'Hara SL, Clarke ML, Elatrash MS (2006) Field measurement of desert dust in Libya. Atmos Environ 40:3881–3897

Perry KD, Cliff SS, Jimenez-Cruz MP (2004) Evidence for hygroscopic mineral dust particles from the Intercontinental Transport and Chemical Transformation Experiment. J Geophys Res 109, D23S28. doi:10.1029/2004JD004979

Petroff A, Zhang L (2010) Development and validation of a size-resolved particle dry deposition scheme for application in aerosol transport models. Geosci Model Dev 3:753–769. doi:10.5194/gmd-3-753-2010

Petroff A, Mailliat A, Amielh M, Anselmet F (2008) Aerosol dry deposition on vegetative canopies. Part II: a new modelling approach and applications. Atmos Environ 42:3654–3683. doi:10.1016/j.atmosenv.2007.12.060

Petroff A, Zhang L, Pryor SC, Belot Y (2009) An extended dry deposition model for aerosols onto broadleaf canopies. J Aerosol Sci 40:218–240. doi:10.1016/j.jaerosci.2008.11.006

Prospero JM, Nees RT, Uematsu M (1987) Deposition rate of particulate and dissolved aluminum derived from Saharan dust in precipitation at Miami, Florida. J Geophys Res 92:14723–14731

Prospero JM, Ginoux P, Torres O, Nicholson SE, Gill TE (2002) Environmental characterization of global sources of atmospheric soil dust identified by the NIMBUS-7 Total Ozone mapping Spectrometer (TOMS)absorbing aerosol products. Rev Geophys 40(1):1002. doi:10.1029/2000RG000095

Prospero JM, Landing WM, Schulz M (2010) African dust deposition to Florida: temporal and spatial variability and comparisons to models. J Geophys Res 115, D13304. doi:10.1029/2009JD012773

Schulz M, Balkanski YJ, Guelle W, Dulac F (1998) Role of the aerosol size distribution and source location in a three-dimensional simulation of a Saharan dust episode tested against satellite-derived optical thickness. J Geophys Res 103(10):10579–10592

Schulz M, Prospero JM, Baker AR, Dentener F, Ickes L, Liss PS, Mahowald NM, Nickovic S, Pérez García-Pando C, Rodríguez S, Sarin M, Tegen I, Duce RA (2012) Atmospheric transport and deposition of mineral dust to the ocean: implications for research needs. Environ Sci Technol 46:10390–10404. doi:10.1021/es300073u

Schütz L (1980) Long-range transport of desert dust with special emphasis on the Sahara. Ann NY Acad Sci 338:515–532

Seinfeld JH, Pandis SN (1998) Atmospheric chemistry and physics. Wiley, New York

Shao Y (2004) Simplification of a dust emission scheme and comparison with data. J Geophys Res 109, D10202. doi:10.1029/2003JD004372

Shao Y, Raupach MR, Flindlater PA (1993) Effect of saltation on the entrainment of dust by wind. J Geophys Res 98:12719–12726

Shao Y, Ishizuka M, Mikami M, Leys JF (2011) Parameterization of size resolved dust emission and validation with measurements. J Geophys Res 116, D08203. doi:10.1029/2010JD014527

Slinn WGN (1982) Air-to-sea transfer of particles. In: Liss PS, Slinn WGN (eds) Air-sea exchange of gases and particles, NATO ASI series 108. D. Reidel Publishing Company, Boston, pp 299–405

Slinn WGN (1984) Precipitation scavenging. In: Randerson D (ed) Atmospheric sciences and power production, chapter 11, no. DOE/TIC-27601 (DE84005177). Office of Health and Environmental Research, Division of Biomedical Environmental Research, U.S. Dept. of Energy, Washington, DC, pp 466–532

Slinn SA, Slinn WGN (1980) Prediction for particle deposition on natural waters. Atmos Environ 14:1013–1016

Slinn WGN, Hasse L, Hicks BB, Hogan AW, Lal D, Liss PS, Munnich KO, Sehmel GA, Vittori O (1978) Some aspects of the transfer of atmospheric trace constituents past the air-sea interface. Atmos Environ 12:2055–2087

Sow M, Alfaro SC, Rajot JL, Marticorena B (2009) Size resolved dust emission fluxes measured in Niger during 3 dust storms of the AMMA experiment. Atmos Chem Phys 9(12):3881–3891

Tegen I, Fung I (1994) Modeling of mineral dust in the atmosphere: sources, transport and optical thickness. J Geophys Res 99:22897–22914

Textor C, Schulz M, Guibert S, Kinne S et al (2006) Analysis and quantification of the diversities of aerosol life cycles within AeroCom. Atmos Chem Phys 6:1777–1813

Textor C, Schulz M, Guibert S, Kinne S et al (2007) The effect of harmonized emissions on aerosol properties in global models – an AeroCom experiment. Atmos Chem Phys 7:4489–4501

Twohy CH, Kreidenweis SM, Eidhammer T, Browell EV, Heymsfield AJ, Bansemer AR, Anderson BE, Chen G, Ismail S, DeMott PJ, Van den Heever SC (2009) Saharan dust particles nucleate droplets in eastern Atlantic clouds. Geophys Res Lett 36. doi: 10.1029/2008GL035846

Uematsu M, Duce RA, Prospero JM (1985) Deposition of atmospheric mineral particles in the North Pacific Ocean. J Atmos Chem 3:123–138

Wagener T, Guieu C, Losno R, Bonnet S, Mahowald N (2008) Revisiting atmospheric dust export to the southern hemisphere ocean: biogeochemical implications. Global Biogeochem Cycles 22, GB2006. doi:10.1029/2007GB002984

Wang X, Zhang L, Moran MD (2010) Uncertainty assessment of current size-resolved parameterizations for below-cloud particle scavenging by rain. Atmos Chem Phys 10:5685–5705

Washington R, Todd M, Nicholson NJ, Goudie AS (2003) Dust-storm source areas determined by the Total Ozone Monitoring Spectrometer and surface observations. Ann Assoc Am Geogr 93:297–313

Wesely ML (1989) Parameterizations of surface resistance to gaseous dry deposition in regional-scale numerical models. Atmos Environ 23:1293–1304

Würzler S, Reisin TG, Levin Z (2000) Modification of mineral dust particles by cloud processing and subsequent effects on drop size distributions. J Geophys Res 105:4501–4512

Zender CS, Bian H, Newman D (2003) The mineral dust entrainment and deposition (DEAD) model: description and 1990's dust climatology. J Geophys Res 108:4416. doi:10.1029/2002JD002775

Zhang L, Gong S-L, Padro J, Barrie L (2001) A size-segregated particle dry deposition scheme for an atmospheric aerosol module. Atmos Environ 35:549–560

Zhao TL, Gong SL, Zhang XY, McKendry IG (2003) Modeled size-segregated wet and dry deposition budgets of soil dust aerosol during ACE – Asia 2001: implications for trans-Pacific transport. J Geophys Res 108:8665. doi:10.1029/2002JD003363

Chapter 9
Numerical Dust Models

Ina Tegen and Michael Schulz

Abstract Models of dust emission, transport and deposition are used as a tool to understand the various aspects that control distributions and impacts of dust. While global models of the dust cycle are used to investigate dust at large scales and long-term changes, regional dust models are the ideal tool to study in detail the processes that influence dust distribution as well as individual dust events. Simulating dust emissions, which depend non-linearly on surface wind speed, is a critical issue in dust transport models. Surface wind fields used to compute emission fluxes must be available at appropriate resolution to resolve the processes responsible for dust emissions. A major problem in model-based assessments of dust effects is that atmospheric models are often unable to reproduce the small-scale wind events that are responsible for a large part of dust emission. Recent satellite-retrieved surface roughness data for desert regions considerably improve dust emission computations. Model intercomparison studies highlight that the averages and seasonal variability of vertically integrated mineral dust parameters like optical thickness and Ångstrom exponent agree within a factor of two with observations. Less agreement is found for surface concentration and deposition fields of mineral dust particles.

Keywords Dust models • Emission • Surface parameters • Dust sources • Meteorology • Dust transport • Deposition • Optical properties • Regional dust models • Global dust models

I. Tegen (✉)
Leibniz Institute for Tropospheric Research, Permoserstr. 15, 04318 Leipzig, Germany
e-mail: itegen@tropos.de

M. Schulz
Norwegian Meteorological Institute, O313 Oslo, Norway
e-mail: Michael.Schulz@met.no

P. Knippertz and J.-B.W. Stuut (eds.), *Mineral Dust: A Key Player in the Earth System*, DOI 10.1007/978-94-017-8978-3_9,

9.1 Introduction

Dust aerosol particles influence the Earth's radiation balance, atmospheric dynamics, biogeochemical processes and atmospheric chemistry (see Chaps. 4, 11, 12, 13 and 14). These effects are only partly understood and remain largely unquantified to date. In turn, emission, transport and deposition of dust are influenced by meteorological and climate parameters, such as surface winds and the vegetation cover of soils (see Chaps. 5, 6, 7 and 8).

An assessment of the various effects and interactions of dust and climate requires a quantification of global atmospheric dust loads and their optical and microphysical properties (see Chaps. 11 and 12). Dust distributions that are used in assessments of dust effects on climate usually rely on results of large-scale numerical models that include dust as a tracer (e.g. Shao et al. 2011). One option for performing dust simulations are the so-called offline models, in which dust emission, transport and deposition processes are computed using meteorological fields from reanalyses or climate model simulations as meteorological drivers. Those fields are read into the model at regular time intervals (e.g. Mahowald et al. 1999). This approach allows multiple model studies of dust processes with identical meteorology, but the need of large data storage can be problematic. Also, this type of model setup does not allow taking into account feedbacks of dust radiative forcing on atmospheric dynamics and climate processes.

Alternatively, dust processes can be computed online by implementing dust as a tracer in regional or global models, that is, dust processes are computed utilizing the simulated wind fields, mixing processes and precipitation. To understand the interactions between dust and climate, dust needs to be described as a radiatively active tracer in general circulation models (GCMs) (Perlwitz et al. 2001; Woodward 2001; Stier et al. 2005; Miller et al. 2006; Mahowald et al. 2006; Colarco et al. 2010; see also Chap. 13, this book). In such models the changes of the radiative heating of dust-containing air layers and the cooling of the underlying surface are computed online, taking into account relevant model fields such as surface albedo and cloud cover.

In an early study, Coakley and Cess (1985) estimated the effect of dust aerosol on temperature and precipitation within the National Center for Atmospheric Research (NCAR) Atmospheric General Circulation Model (AGCM) through perturbing the incoming solar radiation above desert regions by a climatologically fixed amount under perpetual July conditions. Models of the three-dimensional dust transport first focused on simulating individual dust events (Westphal et al. 1988). Joussaume (1990) developed the first model of dust emission and transport at a global scale by implementing dust as a tracer in the Laboratoire de Météorologie Dynamique (LMD) AGCM. Dust emissions were prescribed in relative units as a function of wind speed in areas with low soil moisture for perpetual February and August conditions. Tegen and Fung (1994, 1995) included dust as a tracer in the offline Goddard Institute for Space Studies (GISS) tracer transport model, using the European Centre for Medium-Range Weather Forecasts (ECMWF) assimilated

10-m wind product to compute dust emissions. Subsequently developed global dust emission and transport models (e.g. Mahowald et al. 1999; Ginoux et al. 2001; Zender et al. 2003; Tanaka and Chiba 2005) improved the simulation of dust emissions by specifying the way in which land-surface conditions influence dust sources (see also Chap. 3). These specifications include prescribed vegetation cover from satellite remote sensing or vegetation models to determine potential dust source regions. In addition, the locations of preferential sources of dust aerosol are prescribed in several recent models.

The simulated dust concentrations and optical thickness distributions, resulting from such models, are validated with in situ observations and/or remotely sensed aerosol products (e.g. Mahowald et al. 2005; Huneeus et al. 2011). State-of-the-art global models reproduce the large-scale regional and seasonal patterns of the atmospheric dust loads (e.g. the Saharan dust plume over the North Atlantic, the transport of Asian dust to the Pacific and the Arabian dust plume in the northern hemisphere summer) (see also Chap. 7). However, uncertainties in description of source areas and processes controlling dust emission and deposition in global-scale models result in a wide range of simulated dust fluxes. The complex refractive indices of dust particles depend on the mineral composition of soils in the source areas. Since the refractive indices influence the optical properties of dust (Chap. 11), uncertainties in the location of sources lead also to uncertainties in simulated dust radiative effects in models. The radiative heating by mineral dust particles is parameterized in the radiative transfer scheme of the global models according to prescribed dust optical properties, which can depend on particle size, but normally constant complex refractive indices are prescribed globally when computing dust radiative effects. That implies that the varying mineral composition of dust from different source areas is usually not taken into account (e.g. Balkanski et al. 2007).

The performance of many global aerosol models was evaluated in the global aerosol model intercomparison study AeroCom (Textor et al. 2006). Within AeroCom, the simulated distribution and radiative effects of natural and anthropogenic aerosol components, including dust and sea salt particles, sulphate, organic carbon and black carbon, were compared. Textor et al. (2006) describe the results of the individual components of the aerosol cycles for 16 global models. While the AeroCom study shows that the averages and seasonal variability of vertically integrated mineral dust parameters like optical thicknesses and Ångstrom exponents agree within a factor of two with observations, less agreement is found for surface concentration and deposition fields of mineral dust particles.

Global models are of limited use for the investigation of regional-scale processes, but they are useful to study large-scale dust transport and to provide the global dust distribution. Some global models are designed to provide forecasts and boundary conditions for regional models. The latter are of more use in investigating processes close to dust source regions, since the typical horizontal grid resolution of several degrees and simplified emission and deposition parameterizations are too crude to accurately reproduce smaller-scale dust processes. Regional models are therefore used for simulations of individual dust storm events as well as for providing

operational dust forecasts (Chap. 10). Such models are also better suited for comparisons and interpretation of in situ observations made during intensive field experiments.

This chapter provides first an overview of the parameterization of the dust source regions, emission and deposition processes (that are described in detail in Chaps. 3, 4, 5, 6, 7 and 8 of this book) in regional- and global-scale dust models. Some aspects of regional dust models are briefly addressed (for more details, see Chap. 10). The last part of this chapter describes relevant results of the intercomparison of global dust models from the AeroCom project.

9.2 Dust Emission Modelling

The computation of a realistic distribution of dust emission fluxes is a central part of the model-based description of the dust aerosol cycle, as the emissions depend on both surface properties and surface wind speeds, and cannot be prescribed externally as, for example, many anthropogenic emissions. Dust emission processes are described in detail in Chap. 5. Parameterization of dust emission in transport models must take into account that dust emission processes are highly variable in space and time and can occur at small local scales that may not be resolvable in the regional- or global-scale dust models.

As described in Chap. 5, dust emission fluxes from bare soils depend strongly on the surface friction velocity u_*, which in turn depends on the surface wind speed at a reference height, aerodynamic surface roughness and atmospheric stability. The emission of dust particles from the soil surface is initiated when the surface wind friction velocity exceeds a threshold $u_{*\mathrm{tr}}$, which in turn depends on surface properties such as the soil particle size distribution, surface roughness and soil moisture. Dust emission is predominantly initiated by saltating soil particles, which dislocate smaller clay-sized dust particles that can be transported over large distances by a sandblasting process. In many models the computation of dust emission fluxes is realized by first computing saltation discharge G (Hagen et al. 1999), which in the literature is often referred to as horizontal dust flux. Based on observations and theoretical considerations of the momentum balance of the saltation layer, the magnitude of the saltation discharge depends on the cube of friction velocity above $u_{*\mathrm{tr}}$ (Bagnold 1941). Dust models use predictive flux equations generally of the form

$$G = c\frac{\rho_\mathrm{a}}{g}u_*^3\Phi\left(\frac{u_*}{u_{*\mathrm{tr}}}\right)$$

with ρ_a being the air density, g the gravitational constant and c a dimensionless adjustment factor, which depends on aerodynamic, surface and soil properties.

For the dimensionless function $\Phi(u_*/u_{*\mathrm{tr}})$, different expressions exist, for example, the semi-empirically derived formulation by White (1979):

$$\Phi = \left(1 - \frac{u_{*\mathrm{tr}}}{u_*}\right)\left(1 + \frac{u_{*\mathrm{tr}}^2}{u_*^2}\right)$$

The vertical dust flux is then derived from the horizontal saltation flux. As example, Marticorena and Bergametti (1995) use an empirical expression for relating the dust emission flux to saltation discharge by multiplying the saltation discharge by a proportionality constant that depends on the clay content of the soil.

While this approach has been applied in various dust models, more physically based descriptions of the emission processes during saltation and sandblasting have been developed by, for example, Shao (2000) and Alfaro and Gomes (2001). In those approaches the kinetic energy of saltating grains and the binding energy of dust particles determine the emission factor α. In wind tunnel experiments, Alfaro et al. (1998) were able to directly relate the kinetic energy of saltating particles on a kaolinite clay bed to the size of released dust particles. According to these wind tunnel experiments, the importance of disaggregation into smaller particles due to saltating sand increased for increasing wind speeds (Alfaro et al. 1997). Observational evidence by Washington et al. (2006) confirms the coincidence of saltation and strong dust emission for 2-m winds exceeding 10 m s^{-1} (Washington et al. 2006). In contrast, Kok (2011) found in a more recent analysis that the size distribution of emitted dust particles would not depend on the surface wind speed.

In addition to knowledge of the surface wind speeds in the dust source region, information on both surface roughness and soil particle size distributions in soils are required to compute dust emission fluxes. While surface roughness data in unvegetated regions can be derived from satellite remote sensing data (Laurent et al. 2005; Marticorena et al. 2004; Prigent et al. 2005), the information on soil particle size distributions relies on limited samples in dust regions.

9.3 Model Representation of Dust Source Properties

The particle size distribution in soils determines both $u_{*\mathrm{tr}}$ and the size distribution of emitted particles. Global estimates of soil size distributions that can be used in global- or regional-scale dust models are, for example, derived from the standard textural triangle, utilizing soil texture class data given in global soil property maps such as the FAO/UNESCO Soil Map of the World (Zobler 1986). However, there is a general lack of samples from dust source regions, and the wet sieving method used to determine soil texture breaks up soil aggregates during the treatment, which is therefore not appropriate for determining soil particle size distribution relevant for dust emission processes. Thus for the purpose of dust emission modelling in some regional studies, soil size distributions are taken from dry sieve techniques that avoid the breaking of aggregates in the soils (Alfaro and Gomes 2001; Laurent et al. 2006).

The aerodynamic surface roughness length z_0 plays a significant role in computing the dependence of dust emissions on surface wind speeds. This surface parameter is needed for the computation of surface friction velocity from surface wind speed and influences the threshold friction velocity necessary to initiate dust emission. Marticorena et al. (1997) developed a map of the distribution of z_0 in the northwestern Sahara based on a detailed geomorphological analysis. The z_0 values used in global and regional models to compute large-scale atmospheric dynamics contain information about vegetation and subgrid-scale topography in order to simulate realistic grid-scale wind fields. These do not reflect the roughness of the ground for the usually subgrid-scale dust sources and are not appropriate for modelling dust emissions. Global models of the dust cycle often compute dust emissions as a function of surface wind speed directly, implicitly assuming constant surface roughness and neutral stability. Alternatively, for global and regional models of dust emissions, datasets of satellite-derived z_0 are used. For use in global-scale models, estimates of z_0 in arid and semi-arid regions are provided at 25-km resolution from European remote sensing (ERS) scatterometer observations (Prigent et al. 2005). For regional model application in the Sahara, a surface roughness dataset with a 10-km resolution was retrieved from surface bidirectional reflectance products provided by passive multidirectional measurements in the solar spectrum of the Polarization and Directionality of the Earth Reflectance (POLDER-1) sensor, which has been used in several regional models of Saharan dust (e.g. Laurent et al. 2005).

Not all surfaces in deserts or semi-deserts are effective sources of dust aerosol particles (see Chap. 5). The absorbing aerosol index (AI) derived from the total ozone mapping spectrometer (TOMS) satellite instrument (Herman et al. 1997) has been widely used in order to evaluate large-scale patterns of atmospheric dust loading and the extent of source areas (see Chap. 7). From observations of the TOMS AI, enclosed topographic depressions were suspected to be particularly active sources of dust, the so-called hot spots of dust emission (Prospero et al. 2002). Such preferential dust sources have been prescribed in global dust emission models in different ways (Ginoux et al. 2001; Tegen et al. 2002; Zender et al. 2003). Figure 9.1 shows two examples of widely used parameterizations of such enclosed depressions. The first parameterization by Ginoux et al. (2001) derived the distribution of topographic depression from a $1^\circ \times 1^\circ$ topography dataset, and dust emissions were only allowed to occur in these areas. Tegen et al. (2002) prescribed the global distribution of the potential extent of paleolakes (Fig. 9.1) as preferential dust sources by using results from a water routing and storage model (Coe 1998). The use of this parameterization was based on the assumption that climate variations during the Quaternary have been sufficiently large to have allowed lakes to form in closed basins at some time in the past, like the paleolake Mega-Chad that covered the Bodélé Depression in Chad about 6,000 years ago (Leblanc et al. 2006). Possible errors of this parameterization include the misrepresentation of a preferential source that does not contain deflatable sediments and thus does not act as a dust source. It may also miss preferential source areas that contain fine deflatable dust particles from riverine transport, which are not located within an enclosed depression.

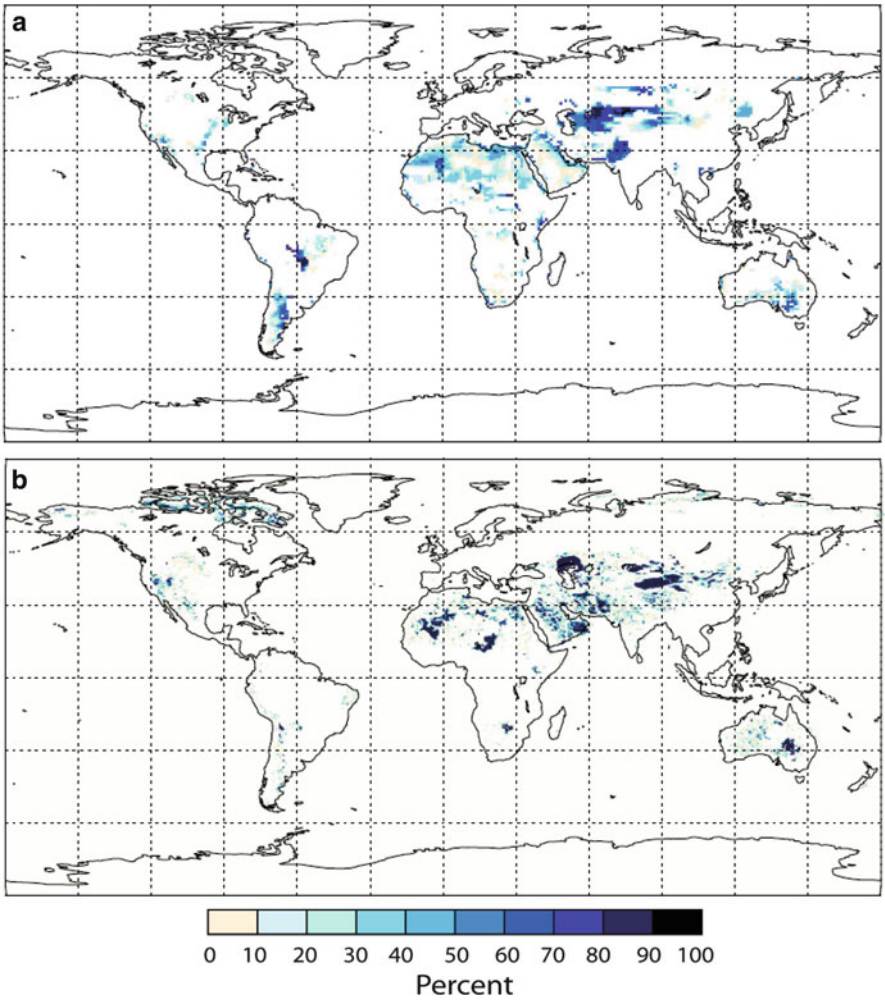

Fig. 9.1 Prescription of enclosed topographic depressions as preferential sources for dust emission based on a $1^\circ \times 1^\circ$ topography map used by Ginoux et al. (2001) (**a**) and based on a water routing and storage scheme (Coe 1998) used by Tegen et al. (2002) (**b**). The *colour scale* indicates the percentage of the grid cell acting as a preferential dust source

Due to the difficulties in determining the location of dust sources in particular for the Saharan desert, satellite retrievals from polar-orbiting satellite instruments (including the A-Train instruments Moderate Resolution Scanning Radiometer (MODIS), Multi-angle Imaging Spectroradiometer (MISR) and Ozone Monitoring Instrument (OMI)) or instruments on geostationary satellites (e.g. Spinning Enhanced Visible Infrared Imager (SEVIRI) on the Meteosat Second Generation satellite) are often used to identify dust source areas (Schepanski et al. 2007; Draxler

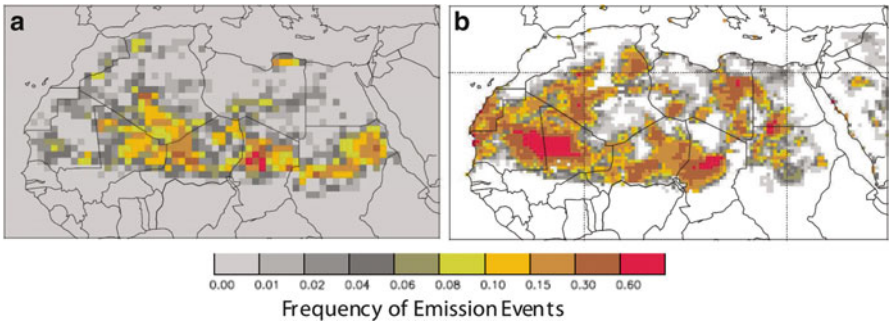

Fig. 9.2 Comparison of annual Saharan dust emission frequencies from geostationary Meteosat satellite data (**a**; Schepanski et al. 2007) and a global offline model (Tegen et al. 2004) (**b**)

et al. 2010). Alternatively to determining dust source areas from such remote sensing products by assigning high frequencies of large dust loadings to potential source regions, they can also be derived by tracking observed individual dust plumes back to their source location. The spatial distribution of such dust source areas derived by the different methods can differ considerably (Schepanski et al. 2012). This may be partly due to problems of quantifying the dust signal above bright land surfaces by remote sensing (see also Chap. 7).

As an example the Saharan dust source activation frequency computed with the model of Tegen et al. (2004) that uses topographic depressions as preferential dust sources is compared to the activation frequencies derived by the backtracking from Meteosat satellite data (Schepanski et al. 2007) (Fig. 9.2). The evident differences in the simulated source regions compared to the satellite-derived product may be due either to a misrepresentation of dust source areas or meteorology in the model or also to a smaller extent due to limitations of the satellite product (Brindley et al. 2012).

Dust emission can only occur when the soil surface is bare or only sparsely vegetated. Not only the vegetation cover but also the type of vegetation determines its capacity to protect soil surfaces, particularly in semi-arid areas at desert fringes. Non-forest biomes can be potential dust sources, that is, dust emissions can occur when other criteria (including sparse vegetation cover, soil dryness and absence of snow cover) are satisfied. To obtain an estimate of the monthly vegetation cover per model grid cell, seasonal changes in vegetation cover can be derived from satellite observations, for example, utilizing the fraction of absorbed photosynthetically active radiation derived from monthly retrievals of the Normalized Difference Vegetation Index results. Alternatively, results of vegetation models can be used to provide information on vegetation cover and type as input information for dust emission computations (e.g. Mahowald et al. 1999). Using output from vegetation models to mask dust sources for computing dust emissions is useful for computations of past dust concentrations or projections of future changes.

Dust emission fluxes are reduced when the soil is wet, as the soil water increases the cohesive forces between soil particles. However, in the field the strong winds required for dust emission increase evaporation and typically cause rapid drying of the thin soil top layer. It has been observed that dust emission can start shortly after a precipitation event (Gillette 1999), when the uppermost part of the soil has dried up, even though the lower layers of the soil may still be wet. Fécan et al. (1999) derived an empirical relationship for the dependency of $u_{*\mathrm{tr}}$ for dust emission on soil moisture from wind tunnel experiments, which is used in many regional and global dust emission models to describe the influence of soil moisture on dust emission fluxes (see Chap. 5).

9.4 Role of Meteorology in Dust Emission and Transport

A prerequisite for realistic modelling of dust emissions is the correct simulation of the meteorological processes that initiate dust emission and mix dust aerosol within the atmosphere. The activation of dust sources and prediction of dust emission fluxes resulting from model simulations can only be realistic with accurate representation of the meteorology in dust source regions.

Strong surface winds are required to initiate and sustain dust emission from soils. As described in detail in Chap. 6, typical meteorological phenomena that may cause dust emission are: (1) large-scale monsoon-type flows, (2) synoptic-scale systems, (3) gust fronts from moist convective storms and (4) dry convection events like dust devils and dust plumes. Models at sufficient spatial resolution can well resolve the synoptic-scale meteorological events such as cyclones and frontal passages and associated high surface winds leading to dust emissions.

Dry convective events like dust devils are mainly of local importance (Balme et al. 2003). So far the dust emissions from such events are not taken into account in dust emission models. Thunderstorms forming in unstable conditions may cause vigorous surface winds causing dust emission, but these are generally difficult to reproduce (e.g. Marsham et al. 2011). A case study of an observed dust mobilization event in southern Morocco caused by cold outflow from convection originating over the Atlas Mountains (Knippertz et al. 2007) shows the dependence of dust mobilization on model parameterization of convection (Fig. 9.3). Evidently the model using parameterized convection cannot reproduce the dust emission event, while the higher-resolution run simulates much more realistic emission fields. The model resolution that can be used for computing dust emissions is usually limited by the available computational resources and is typically much coarser than the example shown in Fig. 9.3.

Another important meteorological mechanism for dust emission is the morning breakdown of low-level jets that frequently form above the stable nocturnal boundary layer in arid areas (see Chap. 6). A prominent example for a strong low-level jet influence on dust emission is the Bodélé Depression in Chad, where the jet formation is locally enhanced through orographic channelling (Washington

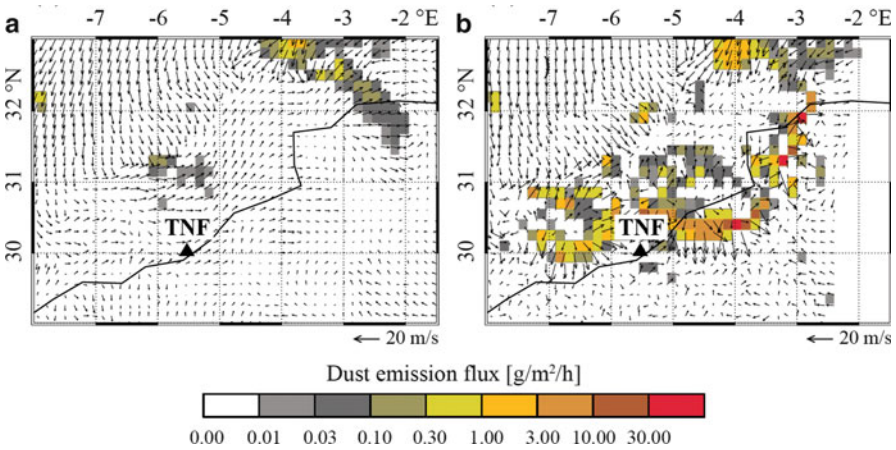

Fig. 9.3 Wind field on the first model level (*arrows*) and calculated dust emission (*colour bar*) at 18 UTC on June 3, 2006 near Tinfou, Morocco (*marked TNF*). Results are from a regional dust model experiment using the COSMO model over the Sahara desert with 14-km horizontal grid resolution with parameterized convection (**a**) and 2.8-km grid resolution without convection parameterization (**b**) (From Reinfried et al. 2009)

et al. 2006). The occurrence of such low-level jets, as well as their degradation through turbulent downward mixing of momentum in the morning hours, must be reproduced by the boundary layer scheme of the models in order to compute the dust emission events from those processes correctly.

9.5 Deposition

Dust can be removed from the atmosphere by dry and wet deposition (for details see Chap. 8). Dry deposition of dust particles is always parameterized in models as gravitational settling, which is the predominant removal mechanism for supermicron dust particles, and turbulent mixing to the surface from the first atmospheric layer. The dust deposition parameterization depends on particle size and density as well as on relevant meteorological quantities.

Wet deposition of aerosol particles occurs by in-cloud ('rainout') and sub-cloud ('washout') removal. In some models dust is assumed to be non-hygroscopic and therefore does not serve as cloud condensation nuclei. Rainout can be effective during deep convective events, since cloud formation can occur through the ice phase and dust particles are important ice nuclei (Chap. 12). Model description of wet deposition of particles by in-cloud removal of particles and sub-cloud removal often follow the form of a first-order decay:

$$\frac{\partial c(z)}{\partial t} = -\Lambda c(z)$$

where $c(z)$ is the particle concentration at height level z and Λ is the removal rate for either 'rainout' or 'washout' (see Chap. 8, this book).

Since dust deposition velocities strongly depend on particle sizes, the dust aerosol size distribution shifts to smaller sizes during transport from the source areas to remote regions due to the fast removal of large particles. Close to dust source regions, gravitational sedimentation is responsible for most of the dry dust deposition, while wet deposition is responsible for a large part of the removal of far-travelled dust over remote ocean areas (Jickells et al. 2005). Atmospheric lifetimes of dust particles depend on their size and may range from few hours for particles larger than 20 μm, which are quickly removed by gravitational settling, to some weeks for submicron particles that are mostly removed by wet deposition (Seinfeld and Pandis 1998).

9.6 Optical Properties of Dust Used in Dust Models

In large-scale models that compute the effect of radiative heating by mineral dust aerosol, the absorption and scattering by dust particles is parameterized as part of the radiative transfer schemes (see Chap. 11). Dust optical properties depend on particle sizes, which are modified during transport, since larger particles are removed more quickly (see Sect. 9.5). Atmospheric dust size distributions (Chap. 2) are represented either by assigning dust aerosol particles to the coarse mode in modal schemes (e.g. Stier et al. 2005) or as 5–10 bins in sectional schemes (e.g. Ginoux et al. 2001), considering particle size ranges from 0.1 to 10 μm or in some cases up to 50 μm. The size distributions of dust transported away from the sources are mostly well reproduced by such models (e.g. Haustein et al. 2012). However, for dust near the source areas, information on size distribution is sparse. In emission models the treatment of dust size distribution can vary considerably; large dust particles may be strongly underestimated near the source areas, which causes uncertainties in simulations of their optical properties and radiative forcing. Field measurements during the Fennec 2011 field campaign show large contributions of coarse mode dust particles downwind of Saharan dust source regions (Ryder et al. 2013). Models that neglect such large particles underestimate absorption of solar radiation by airborne dust. In addition to size, dust optical properties depend on the particles' complex refractive indices, which are prescribed as constant in most models. Possible differences in mineral composition of dust particles (Chap. 2) are not taken into account in current dust models when computing their radiative effects (e.g. Balkanski et al. 2007). Particle properties like single scattering albedo that may relate to mineral composition remain unrelated to the mineral composition at source areas in the models.

9.7 Regional Dust Models

Several regional (or mesoscale) models of the full cycle of dust emission, transport and deposition exist for key regions, including the Sahara (e.g. Nickovic and Dobricic 1996; Pérez et al. 2006; Heinold et al. 2007; Menut et al. 2009) and Asia (e.g. Shao and Wang 2003; Uno et al. 2006). Such regional-scale models that operate with horizontal grid resolutions of 10–50 km were mostly developed for the purpose of providing operational dust forecasts and are suited for simulation of individual dust storm events (see Chap. 10). Regional models are also useful for comparisons and interpretation of in situ dust observations, made during intensive field experiments. While the topography, soil conditions and small-scale extreme wind events are described with more detail in regional compared to global models, there are still uncertainties in describing the dust source area, surface conditions in the source area and changes in size distribution and chemical composition during transport.

A main purpose of regional dust models is the prediction of dust storms. For East Asia and the Mediterranean region, such forecasts are compiled in the World Meteorological Organization's Sand and Dust Storm Warning Advisory and Assessment System (SDS-WAS; http://www.wmo.int/pages/prog/arep/wwrp/new/Sand_and_Dust_Storm.html; see also Chap. 10). There, daily dust forecasts are provided by more than 15 organizations in different geographic regions, integrating research and user communities and including regional as well as global forecast models. Such regional dust forecast models are also utilized in the context of field experiments (like Fennec 2011 or the Saharan Mineral Dust Experiment (SAMUM) 2006–2011), as they are designed to simulate specific dust events and provide results for simulated dust concentration, deposition fluxes and aerosol optical thickness at scales that are suitable for comparison with in situ field observations. In turn, such dust models provide necessary information for planning measurements (e.g. research flights) during such field studies.

Differences in dust emission fluxes between different models can be due to the use of different soil datasets as input data (Laurent et al. 2010) or the use of different emission schemes (Kang et al. 2011). In addition, even at model grid resolutions of 10–50 km, meteorological features that impact on dust emission still need to be parameterized, which leads to discrepancies due to the parameterization choices. Darmenova and Sokolik (2007) point out that the choice of the planetary boundary layer scheme considerably influences the computed emission fluxes and vertical transport of dust. Intercomparison studies of regional-scale Asian dust models (Dust Model Intercomparison study (DMIP); Uno et al. 2006) and an intercomparison of models simulating a dust event in the Bodélé Depression (Todd et al. 2008) highlight considerable differences in the modelled dust distributions. In Todd et al. (2008), the performance of five regional-scale dust models was compared for a 3-day dust event over the Bodélé Depression in Chad simulating dust distributions during the BoDEX field experiment in 2005. While the models reproduce the diurnal cycle in surface winds, the peak wind speeds are often too low in the models leading to

underestimated dust emission fluxes. The spread of model results for the surface concentration, mass load and optical thickness is about one order of magnitude, leading to differences in model estimates of exported dust mass of a factor of 30. Similarly, Uno et al. (2006) find a range of an order of magnitude differences for modelled dust concentration from nine regional models comparing two East Asian dust events.

In general, dust events that are controlled by large-scale meteorological features that are well represented by meteorological models, for example, frontal passages or Sharav cyclones passing through northern Africa in spring (see Chap. 6), are well represented in regional-scale dust models. In contrast, these regional models have problems to represent dust emission, transport and deposition events that are controlled by small-scale atmospheric features like moist convective events, which are usually parameterized in regional models. Microscale events like dust devils causing dust emissions cannot be represented directly in such models, and therefore their contribution to the atmospheric dust load remains unclear.

In spite of the problems in the accurate determination of dust emission areas and reproducing the meteorological processes responsible for dust emission, model studies of individual dust events have been successful in simulating the spatio-temporal distribution of dust transported far downwind, for example, in cases of transport from the Sahara towards Europe (e.g. Pérez et al. 2006). For regional dust forecast models, an accurate simulation of the meteorology may be more important than a precise placement of active dust source areas.

9.8 Global Dust Models

Global dust models are used to investigate the role of dust in the climate system. While such models reproduce the large-scale regional and seasonal patterns of the atmospheric dust loads, the results of such models may deviate considerably from observations at individual locations (Huneeus et al. 2011). The global aerosol model intercomparison study AeroCom (Textor et al. 2006) was developed as a platform to evaluate the performance of global aerosol models. In the first AeroCom phase, aerosols computed with either offline transport models and GCMs were considered. Within AeroCom, the simulated distribution and radiative effects of dust as part of natural and anthropogenic aerosol components (dust and sea salt particles, sulphate, organic carbon and black carbon) were compared for 16 global models. In one series of experiments, each model used their own individual aerosol emissions (Experiment A), while in Experiment B the models computed the aerosol cycles using harmonized emission fields (Textor et al. 2007). The results were compared and evaluated with observational data, including concentrations of individual species at the surface, as well as optical thickness data from the global AERONET sun photometer network and derived satellite products (see Chap. 7). Kinne et al. (2006) evaluated differences in optical properties that lead to diversities in aerosol radiative forcing by the AeroCom models. With respect to dust, the multi-model median for

Experiment A, as reported by Textor et al. (2006), is 1,640 Tg/a for global annual dust emissions, 20.5 Tg for global dust burden and 4.04 days for lifetime, with large variations for the individual models. A revised analysis of AeroCom dust including CAM and ECMWF model results, but excluding models with fixed dust emission fields, suggests slightly lower median emissions of 1,123 Tg/a and 4.6 days lifetime (Table 9.1). Large variations are documented not only for emissions but also for lifetime and mass extinction efficiencies, making it difficult to attribute performance differences to differences in emission process modelling only.

In Textor et al. (2006), the model diversities δ are defined as the standard deviation of the model results normalized with the average of all models, expressed in percentage. The authors find that for dust emissions in Experiment A, the model diversity δ is 49 %, which is considerably higher than for the other aerosol types except sea salt aerosol. Similarly, the model diversities are 40 % and 43 % for burden and residence time, respectively. These are lower than the emission diversity, probably because global dust burdens are dominated by fine particles. Transported dust clouds, with larger fractions of fine dust particles, can be better constrained due to numerous observations of optical depth by satellite. By contrast, few observations exist to constrain the simulation of coarse dust, which may dominate emission fluxes.

The results for Experiment B with harmonized emissions, though distributed in particle size differently, cannot be compared directly to these results, since a lower number of models contributed. However, the diversities from the model results for Experiment B were at a similar level as in Experiment A for the atmospheric burdens and residence times (Textor et al. 2007), even though (almost) identical emission fields were used for dust mass. This confirms the crucial role of dust size but also that of wet deposition fluxes computed by the different models. The latter may be due to a lack of understanding of the hygroscopic behaviour of dust, which in turn influences the washout and rainout efficiencies of the dust particles. The globally averaged split between wet and dry deposition for the different models is shown in Fig. 9.4. While dry deposition is very important in all models, wet deposition contributes up to 65 % in some models.

The emitted dust mass fluxes are divided into different size fractions, which are then further transported and deposited in the models. Unfortunately, the diagnostics of the models collected at the time were not very precise with respect to the actual size distribution used. An average redistribution of the aggregated size bins for dust aerosol is shown in Fig. 9.5 for the models that contributed to AeroCom Experiment B. The differences in the size distribution lead to high diversities in the modelled deposition rates and atmospheric lifetimes, even for Experiment B, which uses the same emission mass fluxes for all models.

Focussing on dust aerosol simulations, Huneeus et al. (2011) evaluated the results of 14 different models that contributed to the AeroCom project with detailed comparisons of observations for aerosol optical thicknesses, near-surface concentrations and deposition fluxes (Fig. 9.6 shows the median dust aerosol optical thickness distribution for the AeroCom model ensemble). The authors find that the averages and seasonal variability of vertically integrated mineral dust parameters

Table 9.1 Annual dust budget from global AeroCom models, as reported in Huneeus et al. (2011)

Model	Emission (Tg year^{-1})	Load (Tg)	Deposition (Tg year^{-1})	Wet deposition (Tg year^{-1})	Dry depo. (Tg year^{-1})	Sedim. (Tg year^{-1})	OD550 dust	MEE (m^2 g^{-1})	Lifetime (days)
CAM	4,313	25.7	4,359	1,382	2,300	675	0.035	0.69	4.6
GISS	1,507	29.0	1,488	456	352	680	0.034	0.60	7.1
GOCART	3,157	29.5	3,178	583	120	2,475	0.035	0.60	3.5
SPRINTARS	3,995	17.2	3,984	628	2,791	565	0.024	0.72	1.6
MATCH	981	17.3	1,070	517	431	122	0.033	0.96	5.9
MOZGN	2,371	21.1	2,368	425	1,943	NaN	0.22	0.52	3.3
UMI	1,688	19.3	1,691	619	1,073	NaN	0.021	0.56	4.2
ECMWF	514	6.8	750	406	322	22	0.027	0.25	3.3
LOA	1,276	13.7	1,275	417	521	336	0.034	1.28	3.9
UIO-CTM	1,572	21.7	1,571	681	890	NaN	0.026	0.61	5.1
LSCE	1,158	20.3	1,156	616	310	231	0.031	0.77	6.4
ECHAM5-HAM	664	8.2	676	374	37	265	0.010	0.60	4.4
MIRAGE	2,066	22.0	2,048	1,361	687	NaN	0.053	1.22	3.9
TM5	1,683	9.3	1,682	295	592	794	0.013	0.68	2.0
Median	1,123	15.8	1,257	357	396	314	0.023	0.72	4.6

Column explanations: *Size* indication of range covered and scheme used to represent the size distribution, *Dry depo.* dry deposition due to processes other than sedimentation, *Sedim.* sedimentation, *OD550* aerosol optical depth at 550 nm, *MEE* mass extinction efficiency at 550 nm wavelength

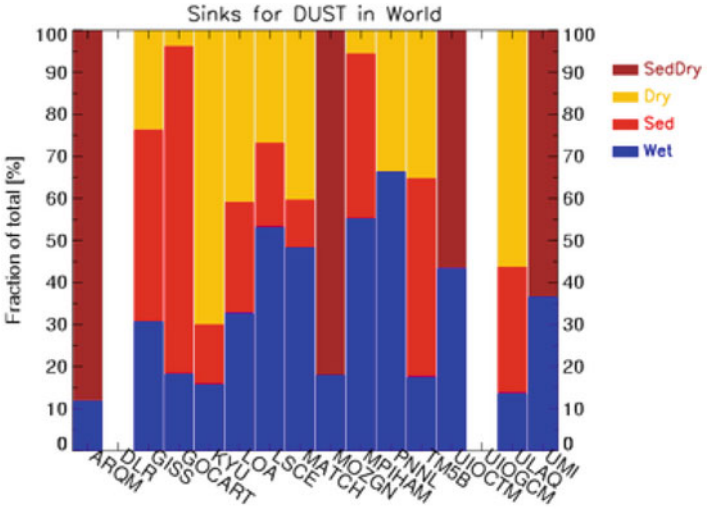

Fig. 9.4 Fraction of individual removal processes to total dust deposition (*Wet* wet deposition, *Sed* sedimentation, *Tur* turbulent dry deposition to the surface, *SedTur* sum of sedimentation and turbulent dry deposition) in the AeroCom Experiment A model versions (using results reported in Textor et al. 2006)

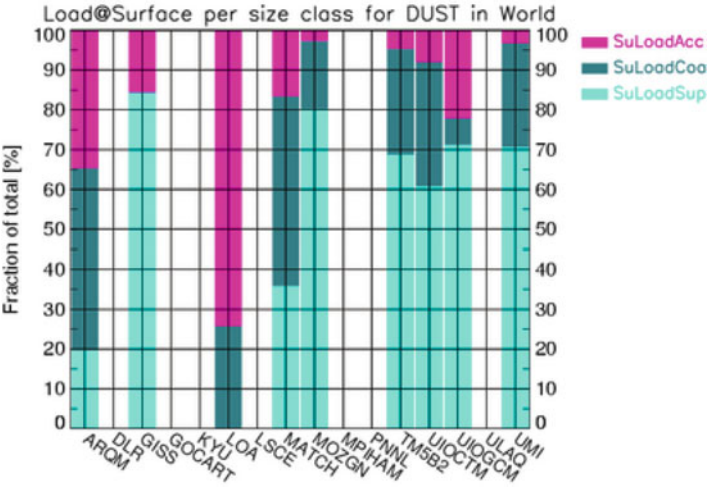

Fig. 9.5 Fractional distribution of surface level load in three dust size bins (approximate classification to accumulation mode (SuLoadAcc), coarse mode (SuLoadCoa) and super coarse mode dust (SuLoadSup)). Shown are global average values for AeroCom Experiment B models (using model results reported in Textor et al. 2007)

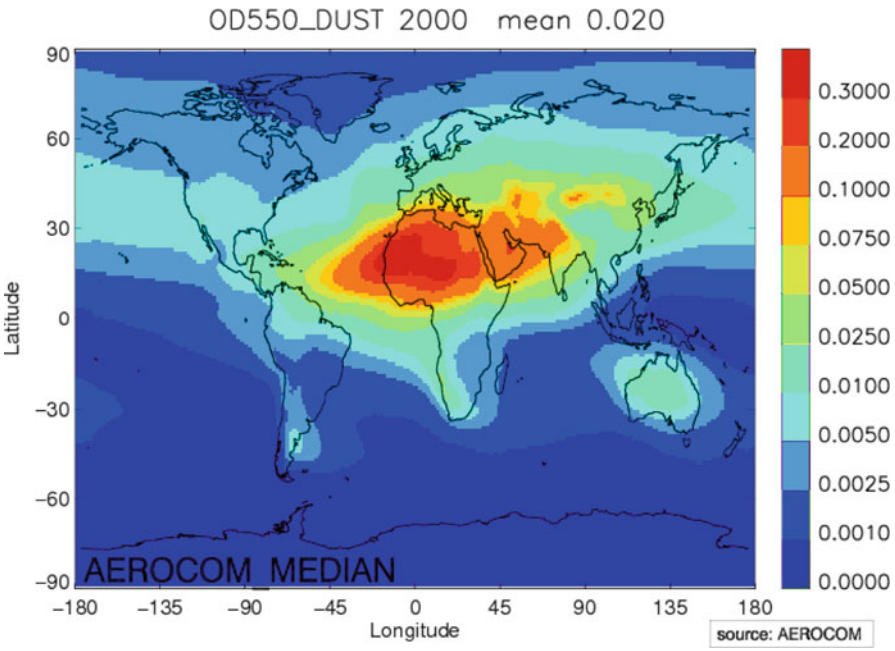

Fig. 9.6 Median dust optical thickness from the results of the AeroCom Experiment A models

like optical thicknesses and Ångstrom exponents agree within a factor of two with observations. However, much less agreement is found for surface concentration and deposition fields of mineral dust particles in comparison with measurements. Also, the dust model results show large variations in dust concentrations for particular regions. The averaged dust optical thickness values reported in the study by Huneeus et al. also vary considerably resulting in global annual average values between 0.01 and 0.05. This indicates that uncertainties in the description of source areas and processes controlling dust emission and deposition result in a wide range of simulated dust fluxes and atmospheric dust optical properties. Uncertainties in the descriptions of the initial size distribution of dust during emission are thus not only a major uncertainty factor in determining the global dust budget but also an addition to the uncertainties in the determination of dust optical properties and thus its radiative effect.

It should be noted that the results discussed above represent global dust model simulations that were completed before the year 2006. It is to be expected that ongoing model developments lead to improvements of model performance and parameterizations. However, dust observations near dust source regions are still sparse, such that the diversities in the model-based description of the distribution of dust properties near source regions remain a cause of considerable diversity in the models.

9.9 Conclusion

Model simulations of dust emission, transport and deposition processes that are performed to assess the spatio-temporal distribution of dust properties and study interactions of dust and atmospheric processes can be carried out by either offline models or computing dust processes online at regional or global scales. If dust is embedded in the tracer routines of a global climate model or a regional weather model, the dust processes are simultaneously computed with the atmospheric dynamics. This approach allows considering atmospheric processes that operate on short time scales. It also allows the simulation of feedback processes of dust and dynamic processes. While models that simulate the atmospheric cycle of dust particles as well as their influence on radiative fluxes at regional and global scales are useful to quantify the direct radiative forcing of dust, the effect of changes in meteorological parameters on dust emission is still not clear. As part of the global aerosol model intercomparison study AeroCom, the results of 14 different global-scale dust models were evaluated. It was found that the averages and seasonal variability of vertically integrated mineral dust parameters like optical thicknesses and Ångstrom exponents agree within a factor of two with observations. Less agreement is found for surface concentration and deposition fields of mineral dust particles. Also, the dust model results show large variations in dust concentrations for particular regions.

A critical issue in dust models is the simulation of dust emission fluxes. While the physical processes involved in dust emissions are well known and underpinned by wind tunnel measurements, those processes depend on soil surface properties like surface roughness and sediment availability that are not well documented for most dust emission regions. As those regions lie in remote desert areas that are difficult to access, methods will need to be developed to obtain the necessary information on soil properties by remote sensing. Dust emission depends not only on surface properties but also on surface meteorology that is usually provided by the regional or global models used. A major problem in model-based assessments of dust effects is that atmospheric models are often unable to reproduce the small-scale wind events that are responsible for a large part of dust emission events. For example, small-scale dry convective phenomena like dust devils and convective plumes that are frequently observed in desert regions cannot be resolved even in regional-scale models. While dust transport models usually perform well for long-range transport, the simulated dust concentrations near dust sources for individual events can vary by up to an order of magnitude for different models. This suggests that the modelled dust distribution in the long-range transport may, at least in some cases, be accurately reproduced for the wrong reasons. With only few anthropogenic sources, dust effects are part of the natural climate system, but their role may considerably change under changed climate conditions, even though the direction is yet unclear. Subgrid-scale parameterizations of dust emission events must be based on the actual wind processes that occur for the different regions at different times of the year in order to be able to correctly predict changes in dust emission

under changed climate scenarios. Fully coupled GCM experiments with interactive climate-vegetation and dust forcing will be useful to clarify possible feedback processes, but such developments are just now in the beginning stages.

References

Alfaro SC, Gomes L (2001) Modeling mineral aerosol production by wind erosion: emission intensities and aerosol size distributions in source areas. J Geophys Res 106(D16):18075–18084

Alfaro SC, Gaudichet A, Gomes L, Maillé M (1997) Modeling the size distribution of a soil aerosol produced by sandblasting. J Geophys Res 102(D10):11239–11249

Alfaro SC, Gaudichet A, Gomes L, Maillé M (1998) Mineral aerosol production by wind erosion: aerosol particle sizes and binding energies. Geophys Res Lett 25(7):991–994

Bagnold RA (1941) The physics of blown sand and desert dunes. Methuen, London, 265 pp

Balkanski Y, Schulz M, Claquin T, Guibert S (2007) Reevaluation of mineral aerosol radiative forcings suggests a better agreement with satellite and AERONET data. Atmos Chem Phys 7:81–95

Balme M, Metzger S, Towner M, Ringrose T, Greeley R, Iversen J (2003) Friction wind speeds in dust devils: a field study. Geophys Res Lett 30(16), 1830. doi:10.1029/2003GL017493

Brindley H, Knippertz P, Ryder C, Ashpole I (2012) A critical evaluation of the ability of the Spinning Enhanced Visible and Infrared Imager (SEVIRI) thermal infrared red-green-blue rendering to identify dust events: theoretical analysis. J Geophys Res 117, D07201. doi:10.1029/2011JD017326

Coakley JA Jr, Cess RD (1985) Response of the NCAR community climate model to the radiative forcing by the naturally occurring tropospheric aerosol. J Atmos Sci 42:1677–1692

Coe MT (1998) A linked global model of terrestrial hydrologic processes: simulation of modern rivers, lakes, and wetlands. J Geophys Res 103(D8):8885–8899

Colarco P, da Silva A, Chin M, Diehl T (2010) Online simulations of global aerosol distributions in the NASA GEOS-4 model and comparisons to satellite and ground-based aerosol optical depth. J Geophys Res 115, D14207. doi:10.1029/2009JD012820

Darmenova K, Sokolik IN (2007) Assessing uncertainties in dust emission in the Aral Sea region caused by meteorological fields predicted with a mesoscale model. Global Planet Change 56(3–4):297–310

Draxler RR, Ginoux P, Stein AF (2010) An empirically derived emission algorithm for wind-blown dust. J Geophys Res 115, D16212. doi:10.1029/2009JD013167

Fécan F, Marticorena B, Bergametti G (1999) Parametrization of the increase of the aeolian erosion threshold wind friction velocity due to soil moisture for arid and semi-arid areas. Ann Geophys Atmos Hydrosph Space Sci 17(1):149–157

Gillette DA (1999) A qualitative geophysical explanation for “hot spot” dust emitting source regions. Contrib Atmos Phys 72:67–77

Ginoux P, Chin M, Tegen I, Prospero JM, Holben B, Dubovik O, Lin S-J (2001) Sources and distributions of dust aerosols simulated with the GOCART model. J Geophys Res 106(D17):20255–20273

Hagen LJ, Wagner LE, Skidmore EL (1999) Analytical solutions and sensitivity analyses for sediment transport in WEPS. Trans ASAE 42(6):1715–1721

Haustein K, Pérez C, Baldasano JM, Jorba O, Basart S, Miller RL, Janjic Z, Black T, Nickovic S, Todd MC, Washington R, Müller D, Tesche M, Weinzierl B, Esselborn M, Schladitz A (2012) Atmospheric dust modeling from meso to global scales with the online NMMB/BSC-Dust model – Part 2: experimental campaigns in Northern Africa. Atmos Chem Phys 12:2933–2958. doi:10.5194/acp-12-2933-2012

Heinold B, Helmert J, Hellmuth O, Wolke R, Ansmann A, Marticorena B, Laurent B, Tegen I (2007) Regional modeling of Saharan dust events using LM-MUSCAT: model description and case studies. J Geophys Res 112, D11204. doi:10.1029/2006JD007443

Herman JR, Barthia PK, Torres O, Hsu C, Seftor C, Celarier E (1997) Global distribution of UV-absorbing aerosols from Nimbus 7/TOMS data. J Geophys Res 102(D14):16911–16922

Huneeus N, Schulz M, Balkanski Y, Griesfeller J, Kinne S, Prospero J, Bauer S, Boucher O, Chin M, Dentener F, Diehl T, Easter R, Fillmore D, Ghan S, Ginoux P, Grini A, Horowitz L, Koch D, Krol MC, Landing W, Liu X, Mahowald N, Miller RL, Morcrette J-J, Myhre G, Penner JE, Perlwitz JP, Stier P, Takemura T, Zender C (2011) Global dust model intercomparison in AeroCom phase I. Atmos Chem Phys 11:7781–7816. doi:10.5194/acp-11-7781-2011

Jickells TD, An ZS, Andersen KK, Baker AR, Bergametti G, Brooks N, Cao JJ, Boyd PW, Duce RA, Hunter KA, Kawahata H, Kubilay N, laRoche J, Liss PS, Mahowald N, Prospero JM, Ridgwell AJ, Tegen I, Torres R (2005) Global iron connections between desert dust, ocean biogeochemistry, and climate. Science 308(5718):67–71

Joussaume S (1990) Three-dimensional simulations of the atmospheric cycle of desert dust particles using a general circulation model. J Geophys Res 95:1909–1941

Kang J-Y, Yoon S-C, Shao Y, Kim S-W (2011) Comparison of vertical dust flux by implementing three dust emission schemes in WRF/Chem. J Geophys Res 116, D09202. doi:10.1029/2010JD014649

Kinne S, Schulz M, Textor C, Guibert S, Balkanski Y, Bauer S, Berntsen T, Berglen T, Boucher O, Chin M, Collins W, Dentener F, Diehl T, Easter R, Feichter J, Fillmore D, Ghan S, Ginoux P, Gong S, Grini A, Hendricks J, Herzog M, Horowitz L, Isaksen I, Iversen T, Kirkevåg A, Kloster S, Koch D, Kristjansson JE, Krol M, Lauer A, Lamarque JF, Lesins G, Liu X, Lohmann U, Montanaro V, Myhre G, Penner J, Pitari G, Reddy S, Seland O, Stier P, Takemura T, Tie X (2006) An AeroCom initial assessment – optical properties in aerosol component modules of global models. Atmos Chem Phys 6:1815–1834. doi:10.5194/acp-6-1815-2006

Knippertz P, Deutscher C, Kandler K, Müller T, Schulz O, Schütz L (2007) Dust mobilization due to density currents in the Atlas region: observations from the SAMUM 2006 field campaign. J Geophys Res 112, D21109. doi:10.1029/2007JD008774

Kok JF (2011) Does the size distribution of mineral dust aerosols depend on the wind speed at emission? Atmos Chem Phys 11:10149–10156

Laurent B, Marticorena B, Bergametti G, Chazette P, Maignan F, Schmechtig C (2005). Simulation of the mineral dust emission frequencies from desert areas of China and Mongolia using an aerodynamic roughness length map derived from the POLDER/ADEOS 1 surface products. J Geophys Res 110, D18S04. doi:10.1029/2004JD005013

Laurent B, Marticorena B, Bergametti G, Mei F (2006) Modeling mineral dust emissions from Chinese and Mongolian deserts. Global Planet Change 52(1–4):121–141

Laurent B, Tegen I, Heinold B, Schepanski K, Weinzierl B, Esselborn M (2010) A model study of Saharan dust emissions and distributions during the SAMUM-1 campaign. J Geophys Res 115, D21210. doi:10.1029/2009JD012995

Leblanc M, Favreau G, Maley J, Nazoumou Y, Leduc C, Stagnitti F, van Oevelen PJ, Delclaux F, Lemoalle J (2006) Reconstruction of Megalake Chad using Shuttle Radar Topographic Mission data. Paleogeogr Paleoclimatol Paleoecol 239(1–2):16–27

Mahowald N, Kohfeld KE, Hansson M, Balkanski Y, Harrison SP, Prentice IC, Schulz M, Rohde H (1999) Dust sources and deposition during the last glacial maximum and current climate: a comparison of model results with paleodata from ice cores and marine sediments. J Geophys Res 104:15895–16436

Mahowald NM, Baker AR, Bergametti G, Brooks N, Duce RA, Jickells TD, Kubilay N, Prospero JM, Tegen I (2005) Atmospheric global dust cycle and iron inputs to the ocean. Global Biogeochem Cycles 19(4), GB4025. doi:10.1029/2004GB002402

Mahowald NM, Muhs DR, Levis S, Rasch PJ, Yoshioka M, Zender CS, Luo C (2006) Change in atmospheric mineral aerosols in response to climate: last glacial period, preindustrial, modern, and doubled carbon dioxide climates. J Geophys Res 111, D10202. doi:10.1029/2005JD006653

Marsham JH, Knippert P, Dixon N, Parker D, Lister D (2011) The importance of the representation of deep convection for modeled dust-generating winds over West Africa during summer. Geophys Res Lett 38. doi:10.1029/2011GL048368

Marticorena B, Bergametti G (1995) Modeling the atmospheric dust cycle 1. Design of a soil-derived dust production scheme. J Geophys Res 100:16415

Marticorena B, Bergametti G, Aumont B, Callot Y, N'Doumé C, Legrand M (1997) Modeling the atmospheric dust cycle 2. Simulation of Saharan dust sources. J Geophys Res 102(D4):4387–4404

Marticorena B, Chazette P, Bergametti G, Dulac F, Legrand M (2004) Mapping the aerodynamic roughness length of desert surfaces from the POLDER/ADEOS bi-directional reflectance product. Int J Remote Sens 25(3):603–626

Menut L, Masson O, Bessagnet B (2009) Contribution of Saharan dust on radionuclides aerosols activity levels in Europe? The 21–22 February 2004 case study. J Geophys Res 114, D16202. doi:10.1029/2009JD011767

Miller RL, Cakmur RV, Perlwitz JP, Geogdzhayev IV, Ginoux P, Kohfeld KE, Koch D, Prigent C, Ruedy R, Schmidt GA, Tegen I (2006) Mineral dust aerosols in the NASA Goddard Institute for Space Sciences ModelE atmospheric general circulation model. J Geophys Res 111, D06208. doi:10.1029/2005JD005796

Nickovic S, Dobricic S (1996) A model for long-range transport of desert dust. Mon Weather Rev 124(11):2537–2544

Pérez C, Nickovic S, Pejanovic G, Baldasano JM, Ozsoy E (2006) Interactive dust-radiation modeling: a step to improve weather forecasts. J Geophys Res 111(D16), D16206

Perlwitz J, Tegen I, Miller RL (2001) Interactive soil dust aerosol model in the GISS GCM 1. Sensitivity of the soil dust cycle to radiative properties of soil dust aerosols. J Geophys Res 106(D16):18167–18192

Prigent C, Tegen I, Aires F, Marticorena B, Zribi M (2005) Estimation of the aerodynamic roughness length in arid and semi-arid regions over the globe with the ERS scatterometer. J Geophys Res 110, D09205. doi:10.1029/2004JD005370

Prospero JM, Ginoux P, Torres O, Nicholson SE, Gill TE (2002) Environmental characterization of global sources of atmospheric soil dust identified with the Nimbus 7 Total Ozone Mapping Spectrometer (TOMS) absorbing aerosol product. Rev Geophys 40(1):2-1–2-31

Reinfried F, Tegen I, Heinold B, Hellmuth O, Schepanski K, Cubasch U, Huebener H, Knippertz P (2009) Simulations of convectively-driven density currents in the Atlas region using a regional model: impacts on dust emission and sensitivity to horizontal resolution and convection schemes. J Geophys Res 114. doi:10.1029/2008JD010844

Ryder CL, Highwood EJ, Rosenberg PD, Trembath J, Brooke JK, Bart M, Dean A, Crosier J, Dorsey J, Brindley H, Banks J, Marsham JH, McQuaid JB, Sodemann H, Washington R (2013) Optical properties of Saharan dust aerosol and contribution from the coarse mode as measured during the Fennec 2011 aircraft campaign. Atmos Chem Phys 13:303–325. doi:10.5194/acp-13-303-2013

Schepanski K, Tegen I, Laurent B, Heinold B, Macke A (2007) A new Saharan dust source activation frequency map derived from MSG-SEVIRI IR-channels. Geophys Res Lett 34. doi:10.1029/2007GL030168

Schepanski K, Tegen I, Macke A (2012) Comparison of satellite based observations of Saharan dust source areas. Remote Sens Environ 123:90–97. doi:10.1016/j.rse.2012.03.019

Seinfeld JH, Pandis SN (1998) Atmospheric chemistry and physics. Wiley, New York, 1326 pp

Shao YP (2000) Physics and modelling of wind erosion. Kluwer, Dordrecht

Shao YP, Wang JJ (2003) A climatology of northeast Asian dust storms. Meteorol Z 12(4):187–196

Shao Y, Wyrwoll K-H, Chappell A, Huang JP, Lin ZH, McTainsh GH, Mikami M, Tanaka TY, Wang XL, Yoon S-C (2011) Dust cycle: an emerging core subject in Earth system science. Aeolian Res 2:181–204

Stier P, Feichter J, Kinne S, Kloster S, Vignati E, Wilson J, Ganzeveld L, Tegen I, Werner M, Balkanski Y, Schulz M, Boucher O, Minikin A, Petzold A (2005) The aerosol-climate model ECHAM5-HAM. Atmos Chem Phys 5:1125–1156

Tanaka TY, Chiba M (2005) Global simulation of dust aerosol with a chemical transport model, MASINGAR. J Met Soc Jpn 83A:255–278

Tegen I, Fung I (1994) Modeling of mineral dust in the atmosphere: sources, transport and optical thickness. J Geophys Res 99(D11):22897–22914

Tegen I, Fung I (1995) Contribution to the atmospheric mineral aerosol load from land surface modification. J Geophys Res 100(D9):18707–18726

Tegen I, Harrison SP, Kohfeld K, Prentice IC, Coe M, Heimann M (2002) Impact of vegetation and preferential source areas on global dust aerosol: results from a model study. J Geophys Res 107(D21), 4576. doi:10.1029/2001JD000963

Tegen I, Werner M, Harrison SP, Kohfeld KE (2004) Relative importance of climate and land use in determining present and future global soil dust emission. Geophys Res Lett 31:L05105. doi:10.1029/2003GL019216, 012004

Textor C, Schulz M, Guibert S, Kinne S, Balkanski Y, Bauer S, Berntsen T, Berglen T, Boucher O, Chin M, Dentener F, Diehl T, Easter R, Feichter H, Fillmore D, Ghan S, Ginoux P, Gong S, Kristjansson JE, Krol M, Lauer A, Lamarque JF, Liu X, Montanaro V, Myhre G, Penner J, Pitari G, Reddy S, Seland O, Stier P, Takemura T, Tie X (2006) Analysis and quantification of the diversities of aerosol life cycles within AeroCom. Atmos Chem Phys 6:1777–1813

Textor C, Schulz M, Guibert S, Kinne S, Balkanski Y, Bauer S, Berntsen T, Berglen T, Boucher O, Chin M, Dentener F, Diehl T, Feichter J, Fillmore D, Ginoux P, Gong S, Grini A, Hendricks J, Horowitz L, Huang P, Isaksen ISA, Iversen T, Kloster S, Koch D, Kirkevåg A, Kristjansson M, Krol A, Lauer JF, Lamarque X, Liu V, Montanaro G, Myhre G, Penner JE, Pitari G, Reddy MS, Seland Ø, Stier P, Takemura T, Tie X (2007) The effect of harmonized emissions on aerosol properties in global models – an AeroCom experiment. Atmos Chem Phys 7:4489–4501. doi:10.5194/acp-7-4489-2007

Todd MC, Bou Karam D, Cavazos C, Bouet C, Heinold B, Baldasano JM, Cautenet G, Koren I, Pérez C, Solmon F, Tegen I, Tulet P, Washington R, Zakey A (2008) Quantifying uncertainty in estimates of mineral dust flux: an intercomparison of model performance over the Bodélé Depression, northern Chad. J Geophys Res 113, D24107. doi:10.1029/2008JD010476

Uno I, Wang Z, Chiba M, Chun YS, Gong SL, Hara Y, Jung E, Lee SS, Liu M, Mikami M, Music S, Nickovic S, Satake S, Shao Y, Song Z, Sugimoto N, Tanaka T, Westphal DL (2006) Dust model intercomparison (DMIP) study over Asia: overview. J Geophys Res 111(D12), D12213

Washington R, Todd MC, Engelstaedter S, Mbainayel S, Mitchell F (2006) Dust and the low-level circulation over the Bodélé Depression, Chad: observations from BoDEx 2005. J Geophys Res 111, D03201. doi:10.1029/2005JD006502

Westphal DL, Toon OB, Carlson TN (1988) A case study of mobilization and transport of Saharan dust. J Atmos Sci 45:2145–2175

White BR (1979) Soil transport by wind on Mars. J Geophys Res 84(NB9):4643–4651

Woodward S (2001) Modeling the atmospheric life cycle and radiative impact of mineral dust in the Hadley Centre climate model. J Geophys Res 106(D16):18155–18166

Zender CS, Newman D, Torres O (2003) Spatial heterogeneity in aeolian erodibility: uniform, topographic, geomorphic, and hydrologic hypotheses. J Geophys Res 108(D17), 4543. doi:10.1029/2002JD003039

Zobler L (1986) A world soil file for global climate modeling, Technical report NASA TM- 87802. NASA, Washington, DC, 32 pp

Chapter 10
Operational Dust Prediction

Angela Benedetti, José Maria Baldasano, Sara Basart, Francesco Benincasa, Olivier Boucher, Malcolm E. Brooks, Jen-Ping Chen, Peter R. Colarco, Sunlin Gong, Nicolas Huneeus, Luke Jones, Sarah Lu, Laurent Menut, Jean-Jacques Morcrette, Jane Mulcahy, Slobodan Nickovic, Carlos Pérez García-Pando, Jeffrey S. Reid, Thomas T. Sekiyama, Taichu Y. Tanaka, Enric Terradellas, Douglas L. Westphal, Xiao-Ye Zhang, and Chun-Hong Zhou

Abstract Over the last few years, numerical prediction of dust aerosol concentration has become prominent at several research and operational weather centres due to growing interest from diverse stakeholders, such as solar energy plant managers, health professionals, aviation and military authorities and policymakers. Dust prediction in numerical weather prediction-type models faces a number of

A. Benedetti (✉) • L. Jones • J.-J. Morcrette
European Centre for Medium-Range Weather Forecasts, Reading, UK
e-mail: Angela.Benedetti@ecmwf.int; Luke.Jones@ecmwf.int; Jean-Jacques.Morcrette@ecmwf.int

J.M. Baldasano • S. Basart • F. Benincasa
Barcelona Supercomputer Center-Centro Nacional de Supercomputación (BSC-CNS), Barcelona, Spain
e-mail: Jose.Baldasano@bsc.es; Sara.Basart@bsc.es; Francesco.Benincasa@bsc.es

O. Boucher • L. Menut
Laboratoire de Météorologie Dynamique, Paris, France
e-mail: Olivier.Boucher@lmd.jussieu.fr; Menut@lmd.polytechnique.fr

M.E. Brooks • J. Mulcahy
Met Office, Exeter, UK
e-mail: Malcolm.E.Brooks@metoffice.gov.uk; Jane.Mulcahy@metoffice.gov.uk

J.-P. Chen
Department of Atmospheric Science, National Taiwan University, Taipei, Taiwan
e-mail: jpchen@as.ntu.edu.tw

P.R. Colarco
NASA Goddard Space Flight Center, Greenbelt, MD, USA
e-mail: Peter.R.Colarco@nasa.gov

P. Knippertz and J.-B.W. Stuut (eds.), *Mineral Dust: A Key Player in the Earth System*, DOI 10.1007/978-94-017-8978-3_10,

challenges owing to the complexity of the system. At the centre of the problem is the vast range of scales required to fully account for all of the physical processes related to dust. Another limiting factor is the paucity of suitable dust observations available for model, evaluation and assimilation. This chapter discusses in detail numerical prediction of dust with examples from systems that are currently providing dust forecasts in near real-time or are part of international efforts to establish daily provision of dust forecasts based on multi-model ensembles. The various models are introduced and described along with an overview on the importance of dust prediction activities and a historical perspective. Assimilation and evaluation aspects in dust prediction are also discussed.

Keywords Dust models • Prediction • Observations • Forecast • Data assimilation • Aerosol analysis • Multi-model ensembles • Verification metrics • Real-time evaluation

S. Gong • X.-Y. Zhang • C.-H. Zhou
Chinese Academy of Meteorological Sciences, Beijing, China
e-mail: sungling@cams.cma.gov.cn; xiaoye@cams.cma.gov.cn; zhouch@cma.gov.cn

N. Huneeus
Department of Geophysics and Center for Climate and Resilience Research,
University of Chile, Santiago, Chile
e-mail: nhuneeus@dgf.uchile.cl

S. Lu
National Centers for Environmental Prediction, College Park, MD, USA
e-mail: Sarah.Lu@noaa.gov

S. Nickovic
Institute of Physics Belgrade, Serbia and University of Arizona, Tucson, AZ, USA
e-mail: Nickovic@gmail.com

C. Pérez García-Pando
Department of Applied Physics and Applied Maths, NASA Goddard Institute for Space Studies,
Columbia University, New York, NY, USA
e-mail: Carlos.Perezga@nasa.gov

J.S. Reid • D.L. Westphal
Naval Research Laboratory, Monterey, CA, USA
e-mail: Reid@nrlmry.navy.mil; Westphal@nrlmry.navy.mil

T.T. Sekiyama • T.Y. Tanaka
Japan Meteorological Agency/Meteorological Research Institute, Tsukuba, Japan
e-mail: Tsekiyam@mri-jma.go.jp; yatanaka@mri-jma.go.jp

E. Terradellas
Spanish Meteorological Agency, AEMET, Barcelona, Spain
e-mail: eterradellasj@aemet.es

10.1 Introduction

10.1.1 Motivation for Dust Forecasting

While the importance of airborne dust for visibility, air quality and climate has been recognised for a long time, it was only in the past decade that development of operational forecasting capabilities for atmospheric aerosols in general and dust in particular has intensified. Several reasons motivated the development of dust monitoring and forecasting capabilities:

1. Decision-makers have long desired the ability to forecast severe dust events in order to mitigate their impacts on transportation, military operations, energy and health. In some regions of the world, people's livelihoods are threatened by severe dust storms that can force the closing of roads and airports due to poor visibility. Health advisories to susceptible populations require dust information as input (Chap. 15). Commercial solar energy production systems require forecasts of solar insolation to help predict their contribution to the power grid, especially those that rely on direct solar radiation (Schroedter-Homscheidt et al. 2013). Dust also affects the semiconductor industry, which requires a clean atmosphere to manufacture electronic chips.
2. Dust interacts with atmospheric radiation and can significantly modify the Earth's radiative budget (Chap. 11). While the importance of dust–climate interactions has long been recognised (Chap. 13), it is only recently that the importance of dust for weather forecasting itself has been appreciated (Pérez et al. 2006a). Haywood et al. (2005) showed that the UK Met Office numerical weather prediction (NWP) model had a bias of -35 Wm^{-2} in its top-of-the-atmosphere radiative budget over the Saharan region because it neglected the effects of dust on radiation. Such systematic biases in NWP models can be addressed by prescribing better aerosol climatologies (e.g. Rodwell and Jung 2008), but interactive aerosols in NWP models are increasingly being exploited to improve the skill of weather forecasts.
3. Dust's infrared (IR) signature causes interference in satellite retrievals and subsequent assimilation of temperature, humidity and sea surface temperature (SST). For example, Weaver et al. (2003) show how TOVS (see Table 10.1 for a list of acronyms) temperature profiles can be contaminated by dust. Ruescas et al. (2011) demonstrated the impact on SST retrievals, which are used operationally as a boundary condition in models. Maddy et al. (2012) demonstrated significant dust impacts of up to 4 K on AIRS retrievals of the atmospheric temperature profile. Given the extreme loadings of some dust events from Africa and Asia, dust must be accounted for in models that utilise data assimilation based on IR wavelengths.
4. There is a pressing need to monitor the Earth's environment to better understand changes and adapt to them, especially in the context of climate. Since the dust cycle is closely related to meteorological conditions, the benefit of combining

Table 10.1 Acronyms of models, satellite sensors, organisations and networks

AD-Net	Asian Dust Network
AERONET	Aerosol Robotic Network
AIRS	Atmospheric Infrared Sounder
AMMA	African Monsoon Multidisciplinary Analysis
BSC-CNS	Barcelona Supercomputing Center- Centro Nacional de Supercomputación
CALIOP	Cloud-Aerosol Lidar with Orthogonal Polarization
CALIPSO	Cloud-Aerosol Lidar and Infrared Pathfinder Satellite Observations
CMA	China Meteorological Administration
CMAQ-KOSA	CMAQ coupled with dust deflation module
COAMPS	Coupled Ocean–Atmosphere Mesoscale Prediction System
CUACE/Dust	Chinese Unified Atmospheric Chemistry Environment for Dust
DREAM	Dust Regional Atmospheric Model
ECMWF	European Centre for Medium-Range Weather Forecasts
FNMOC	Fleet Numerical Meteorology and Oceanography Center
GCM	General Circulation Model
GEMS	Global Earth-system Monitoring using Space and in-situ data
GEOS-5	Goddard Earth Observing System Model, Version 5
GFS	Global Forecast System
GMAO	Global Modeling and Assimilation Office
GMES	Global Monitoring for Environment and Security (now Copernicus)
GOCART	Goddard Chemistry Aerosol Radiation and Transport
GSFC	Goddard Space Flight Center
IASI	Infrared Atmospheric Sounding Interferometer
ICAP	International Cooperative for Aerosol Prediction
IRI	International Research Institute for Climate and Society
JMA	Japan Meteorological Agency
LMD	Laboratoire de Météorologie Dynamique
LOA	Laboratoire d'Optique Atmosphérique
LSCE	Laboratoire des Sciences du Climat et l'Environnement
MACC	Monitoring Atmospheric Composition and Climate
MACC-II	Monitoring Atmospheric Composition and Climate- Interim Implementation
MASINGAR	Model of Aerosol Species in the Global Atmosphere
MEDUSE	MEditerranean DUSt Experiment
MISR	Multi-angle Imaging SpectroRadiometer
MODIS	Moderate Resolution Imaging Spectroradiometer
MRI	Meteorological Research Institute
MSG	Meteosat Second Generation
NAAPS	Navy Aerosol Analysis and Prediction System
NCEP	National Centers for Environmental Prediction
NEMS	NCEP Environmental Modeling System
NESDIS	National Environmental Satellite Data and Information Service
NGAC	NEMS GFS Aerosol Component
NMMB	Non-hydrostatic Multiscale Model
NMME	National Multi-Model Ensemble

(continued)

Table 10.1 (continued)

NOGAPS	Navy Operational Global Atmospheric Prediction System
NRL	Naval Research Laboratory
NTU	National Taiwan University
OMI	Ozone Monitoring Instrument
SEVIRI	Spinning Enhanced Visible and Infrared Imager
SEEVCCC	South East European Virtual Climate Change Center
TAQM	Taiwan Air Quality Model
TAQM-KOSA	TAQM coupled with dust deflation module
TEPA	Taiwan Environmental Protection Administration
TIROS	Television InfraRed Observation Satellite
TOMS	Total Ozone Mapping Spectrometer
TOVS	TIROS Operational Vertical Sounder
USGS	US Geological Survey
WMO	World Meteorological Organization
SDS-WAS	Sand and Dust Storm Warning Advisory and Assessment System
NA-ME-E	North Africa-Middle East-Europe
WRF	Weather Research and Forecasting
WRF-CHEM	Weather Research and Forecasting model coupled with Chemistry

the monitoring of the atmosphere with the monitoring of atmospheric species became clear very early in the planning of the Global Monitoring of the Environment and Security (GMES, now renamed Copernicus), which was the first European attempt at establishing an integrated analysis and forecasting system for atmospheric composition. As such, it was natural to extend the capability of NWP models to aerosol and chemical species (Hollingsworth et al. 2008).

10.1.2 A Brief History of Dust Forecasting

Westphal et al. (1987, 1988) is the first study to use a multidimensional, size-resolving, full physics numerical dust transport model, which demonstrated the practicality of numerical simulations of dust storms. In the following years, this concept was developed into capabilities for operational dust forecasting. Between 1991 and 1993, the predecessor version of the current DREAM dust model (Nickovic 1996; Nickovic and Dobricic 1996) was the first regional model in which dust concentration was built into the prognostic equations of the atmospheric model driver. This system was implemented at the Tunisian Meteorological Service and was run on an experimental daily basis in the period March–May 1995. Experimental daily dust forecasts were also performed during 1996–1997 within the EU-funded project "MEDUSE" when the model was driven by the atmospheric SKIRON system (Nickovic et al. 1997). The US Navy has invested in aerosol and dust forecasting since the mid-1990s through the development of the Navy Aerosol

Analysis and Prediction System (NAAPS) to address military needs. NAAPS was developed to include dust, smoke and sea salt, allowing predictions of aerosol concentrations, extinction and visibility starting from a prescribed meteorology. It began running in near real-time in 1999 and became the first fully operational aerosol model through transition to the Fleet Numerical Meteorology and Oceanography Center (FNMOC) in 2005, making 6-day forecasts twice daily. Since dust storms are a significant weather phenomenon in the Iraq region in winter and spring, Liu et al. (2007) modified the Coupled Ocean–Atmosphere Mesoscale Prediction System (COAMPS) to include a dust aerosol module fully integrated in the forecast model for use during Operation Iraqi Freedom in March and April 2003. Verification showed that COAMPS predicted the arrival and retreat of the major dust events and predicted the reduction in visibility (a measure of dust storm intensity) with an error of less than 1 km. These forecasts are still produced on an operational basis.

Operational forecasts have since become available from a number of NWP and research centres around the world (see Sect. 10.2). Many of these forecasts are now delivered through the regional nodes of the WMO Sand and Dust Storm Warning Advisory and Assessment System programme (WMO SDS-WAS; http://www.wmo.int/sdswas). Other forecasts are delivered through dedicated web interfaces to serve the purposes of the individual operational centres.

10.1.3 Specific Challenges in Dust Prediction

Numerical prediction of dust in NWP-type models faces a number of challenges. At the centre of the problem are the vast dimensions of scale required to fully account for all of the physical processes related to dust. Dust production is a function of surface wind stress and soil conditions (Chap. 5). Wind alone can range from synoptic-scale generation to mesoscale phenomena such as those produced by mountain passes or thunderstorms and micro-scale phenomena related to boundary-layer mixing (see Chap. 6). In addition to meteorology, one must consider the heterogeneity of the soil properties and emissions physics. Typically in global models, the functional form of the emission parameterisation is that of a power law in surface wind speed, making emissions highly sensitive to modelled wind fields. As a result, size-dependent emissions and transport are a major factor of uncertainty (Chap. 9). While the average size of dust particles which undergo long-range transport is surprisingly static (Dubovik et al. 2002; Maring et al. 2003; Reid et al. 2003, 2008), with a volume median diameter of ∼4–7 μm, short-lived giant mode particles (15–100 μm) are an important but largely unstudied component of dust that contributes to degraded air quality and IR radiative effects near source regions.

The sensitivity of dust emissions to scale has led to recognition of the importance of model resolution (Liu and Westphal 2001; Gläser et al. 2012; Takemi 2012). The quality of the modelled winds is dictated by characteristics such as horizontal resolution and numerical solver, and this quality is also limited by the relatively

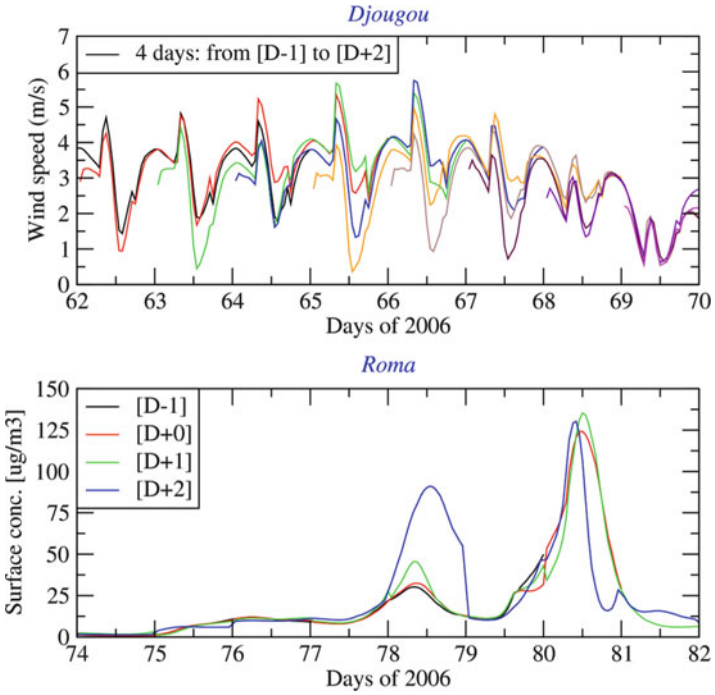

Fig. 10.1 Time series of modelled 10M winds in Djougou, 9.7 N, 1.6E (*top*), and corresponding dust surface concentrations in Rome, 41.9 N, 12.5E (*bottom*). Each coloured line represents successive forecasts of a single day starting 4 days in advance (*top*); and a forecast lead time (*bottom*), respectively

low amount of wind observations available to constrain the meteorological analysis driving the simulation. Moreover, nearly all large-scale models and regional models do not have the capability to resolve convective-scale phenomena (e.g. Reinfried et al. 2009) and are therefore missing potentially important emission sources (see Chap. 6 for more details). In the last few years, a good degree of accuracy in the prediction of dust at the synoptic scale and in some cases at the regional scale has been achieved, thanks to model improvements and in some cases data assimilation to the point that the information can be offered to forecasters as guidance.

The issue of predictability is illustrated with an example in Fig. 10.1, which presents time series of modelled 10 m wind speed and dust surface concentrations. For the wind speed, here presented for Djougou and modelled with WRF (Menut et al. 2009), each coloured line represents a forecast of 4 days. The corresponding days are superimposed and show the spread from one forecast to the following. The wind speed values range from 1 to 6 m/s, and the differences between each forecast do not exceed 1 m/s. This small variability is not important to those interested in the weather forecast. However, this variation becomes important when this wind speed is used to calculate dust emission and transport. The dust concentrations over Rome after long-range transport from Africa, modelled with CHIMERE, are presented in

the same figure. The variability in the dust surface concentrations at the various forecast ranges can be very large, especially compared to variations closer to the source at Djougou. Variations in dust can be of the same order of magnitude as the maximum concentrations of aerosols regulated by air quality policies.

Compounding predictability issues are challenges in dust observability. Both satellite- and ground-based observations are needed for nowcasting, data assimilation and evaluation tools. From satellite, a host of dust enhancement products is available to identify major dust features (see Chap. 7). However, many of these are qualitative in nature and as such cannot be readily used for assimilation in models. More quantitatively, aerosol optical depth (AOD) retrievals can be assimilated with corrections (e.g. Zhang and Reid 2006) but are commonly available only over water or dark surfaces. Over bright desert surfaces, where the aerosol signal cannot be so easily distinguished from the surface reflectance, "dark target" retrieval techniques (e.g. Kaufman et al. 1997) fail, and retrievals must exploit either different wavelengths like the Deep Blue algorithm (Hsu et al. 2004), multi-angle viewing such as with the MISR instrument (Martonchik et al. 2004) or polarimetric observations (e.g. Deuzé et al. 2001). But even in these circumstances, large errors exist, which can prohibit assimilation, and for the largest events, AODs are so high that the retrievals fail. This leaves models without reliable data for assimilation near source regions. Furthermore, while AOD is a common model benchmark, models carry mass, and there is virtually no reliable or representative data sets for mass evaluation in major dust source regions, where data is most needed. The little mass data that is available tends to come from short, episodic field missions. Lidar data of aerosol extinction and backscatter show promising potential towards constraining vertical profiles of aerosol fields and the height of the aerosol layers (Winker et al. 2007). Moreover, lidar depolarisation observations can be used to discriminate dust from other aerosol species.

The chapter is structured as follows. In Sect. 10.2, several operational and quasi-operational dust prediction models are described. Section 10.3 describes examples of regional and global multi-model ensembles for dust prediction that have been established in recent years to offer better information and products to the users. Key aspects of data assimilation for dust prediction are discussed in Sect. 10.4, while related technical details are given in Appendix A. Section 10.5 offers an overview of the type of verification and evaluation procedures these systems are subject to. Finally, Sect. 10.6 presents a summary and a future outlook on dust prediction activities.

10.2 Dust Prediction Models

This section summarises the characteristics of some of the current aerosol prediction models that are run in an operational or quasi-operational manner at various centres around the world. This compilation is not intended to be exhaustive. In an effort to be as inclusive as possible, both global and regional systems are described.

Further information regarding the model characteristics such as horizontal and vertical resolution and dust emission and deposition parameterisations is provided in Tables 10.2 and 10.3 together with references for each model.

10.2.1 Global Models

ECMWF/MACC Aerosol Prediction System

Starting in 2008, ECMWF has been providing daily aerosol forecasts including dust as part of the EU-funded projects GEMS, MACC and MACC-II (see Table 10.1 for acronyms). All data are publicly available online at http://www.copernicus-atmosphere.eu. A detailed description of the ECMWF forecast and analysis model including aerosol processes is given in Morcrette et al. (2009) and Benedetti et al. (2009). The initial package of ECMWF physical parameterisations dedicated to aerosol processes mainly follows the aerosol treatment in the LOA/LMD-Z model (Boucher et al. 2002; Reddy et al. 2005). Five types of tropospheric aerosols are considered: sea salt, dust, organic and black carbon and sulphate aerosols. Prognostic aerosols of natural origin, such as mineral dust, are described using three size bins. Emissions of dust depend on the 10 m wind, the soil moisture, the UV-visible component of the surface albedo and the fraction of land covered by vegetation when the surface is snow-free. A correction to the 10 m wind to account for gustiness is also included (Morcrette et al. 2008). MODIS AOD data are routinely assimilated in a 4D-Var framework. The global modelling system of MACC-II is also used to provide the boundary conditions for an ensemble of more detailed regional air quality models that are used to zoom in on the European domain and produce 4-day forecasts of air quality.

FNMOC Navy Aerosol Analysis and Prediction System

Based on the Danish Eulerian Hemispheric Model (Christensen 1997; Westphal et al. 2009), NAAPS is an offline chemical transport model currently running with single-size bin dust, smoke, sulphate and sea salt at $1/3 \times 1/3°$ and 30 levels driven by the 0.5° Navy Operational Global Atmospheric Prediction System (NOGAPS; Hogan and Rosmond 1991). Operational NAAPS has MODIS data assimilation via a 2D-Var framework (Zhang et al. 2008), with 3D-Var and ensemble Kalman filter (EnKF) systems in development (e.g. Zhang et al. 2011). Next generation models, such as an ensemble version of NAAPS run from the ensemble NOGAPS forecast, are run quasi-operationally NRL at 1° resolution. Dust emission in NAAPS is based on modelled friction velocity to the fourth power coupled to a source map which was empirically derived from TOMS Aerosol Index products. A transition is in place to adopt the recently expanded 1 km high-resolution database of Walker et al. (2009). Data products with verification tools can be found at http://www.nrlmry.navy.mil/aerosol/ with data archives at http://www.usgodae.org/.

Table 10.2 Global model synopsis

Model	GEOS-5	MACC-II	MASINGAR	MetUM	NAAPS	NGAC	NMMB/BSC-Dust
Institution	NASA	ECMWF	JMA/MRI	UK Met Office	FNMOC/NRL	NCEP	BSC-CNS
Meteorological driver	GEOS-5	IFS	MRI/JMA98 AGCM	MetUM	NOGAPS	NEMS GFS	NMMB/NCEP
Source mask	Ginoux et al. (2001)	Morcrette et al. (2009)		HWSD, FAO (2009)	USGS, TOMS-AI, Walker et al. (2009)	Ginoux et al. (2001)	USGS-FAO with Ginoux et al. (2001) and NESDIS vegetation fraction climatology (Ignatov and Gutman 1998)
Emission scheme	Based on Ginoux et al (2001)	Uplifting (Ginoux et al. 2001; Morcrette et al. 2008, 2009)	Uplifting with threshold wind velocity = 6.5 m/s (Gillette 1978; Tegen and Fung 1994)	Gillette (1978), Marticorena and Bergametti (1995), Woodward (2001, 2011)	Westphal et al. (1988)	Dust uplifting following Ginoux et al (2001)	Saltation and sandblasting (White 1979; Marticorena and Bergametti 1995; Marticorena et al. 1997; Janjic 1994; Nickovic et al. 2001)
Deposition schemes	Colarco et al. (2010)	Wet/dry deposition, in-cloud and below-cloud scavenging (Morcrette et al. 2009)	Tanaka et al. (2003)	Wet/Dry deposition (Woodward 2001)	Walcek et al. (1986), Iversen (1989)	Colarco et al. (2010)	Dry deposition (Zhang et al. 2001) and wet deposition (Ferrier et al. 2002; Betts 1986; Janjic, 1994)
Sedimentation scheme	Colarco et al. (2010)	Morcrette et al. (2009)	Tanaka et al. (2003)	Woodward (2001)	Hinds (1982)	Colarco et al. (2010)	Zhang et al. (2001)
Horizontal resolution	0.25° × 0.3125°	0.8° × 0.8°	1.125° × 1.125°	0.3516° × 0.2344°	1/3° operational 1° research	T126 (∼1°)	1.40625° × 1.0°

Vertical resolution	72 sigma-pressure hybrid layers. Top: 0.01 hPa	60 σ-layers	20 σ-p hybrid layers	70 levels. Charney–Phillips grid	25 layers	64 sigma-pressure hybrid layers, top at 0.2 hPa	24 σ-hybrid layers
Height first layer		10 m (above the surface)	40 m	20 m	20 m	20 m	60 m (above surface)
Radiation interactions	Direct effects fully included	Yes (not activated)	No	Yes (not activated)	No	Yes (not activated)	Yes (not activated)
Transport size bins	5 bins centred at 0.73 μm, 1.4 μm, 2.4 μm, 4.5 μm, and 8.0 μm	3 bins (0.03–0.55 μm, 0.55–0.9 μm and 0.9–20 μm)	10 bins (0.1–10 μm)	2 (0.1–2 μm and 2–10 μm)	1	5 bins centred at 0.73 μm, 1.4 μm, 2.4 μm, 4.5 μm, and 8.0 μm	8 bins (0.1–10 μm) Tegen and Lacis (1996)
Data assimilation	Yes	Yes AOD550/ MODIS	No	Yes AOD550/ MODIS	MODIS AOD (Zhang and Reid 2006; Zhang et al. 2008)	No	No

Table 10.3 Regional models synopsis

Model	BSC-DREAM8b	CHIMERE	CMAQ-KOSA	COAMPS	CUACE/Dust	DREAM8-NMME-MACC	NMMB/BSC-Dust	TAQM-KOSA
Institution	BSC-CNS	LMD	NTU/TEPA	FNMOC/NRL	CMA/CAMS	SEEVCCC	BSC-CNS	NTU/TEPA
Meteorological driver	Eta/NCEP	WRF	MM5/WRF	COAMPS	MM5 and GRAPES	NMME/NCEP	NMMB/NCEP	MM5/WRF
Meteorological initial fields	NCEP/GFS	NCEP/GFS	NCEP/GFS	COAMPS		ECMWF	NCEP/GFS	NCEP/GFS
Source mask	USGS-FAO with Ginoux et al. (2001)		Wang et al. (2000) + MODIS land type	Walker et al. (2009)	Gong et al. (2003a, b), Zhang et al. (2003)	USGS-FAO with Ginoux et al. (2001)	USGS-FAO with Ginoux et al. (2001) and NESDIS	Wang et al. (2000)
Emission scheme	Uplifting (Shao et al. 1993; Janjic 1994; Nickovic et al. 2001)	Saltation and sandblasting (Marticorena and Bergametti 1995; Alfaro and Gomes 2001; Menut et al. 2005)	Uplifting (Wang et al. 2000)	Lifting (Liu and Westphal 2001)	Marticorena and Bergametti (1995), Alfaro et al. (1997), Alfaro and Gomes (2001)	Uplifting (Shao et al. 1993; Janjic 1994; Nickovic et al. 2001)	Saltation and sandblasting (White 1979; Marticorena and Bergametti 1995; Janjic 1994; Nickovic et al. 2001)	Uplifting (Wang et al. 2000)
Deposition schemes	Dry deposition (Zhang et al. 2001) and below-cloud scavenging (Nickovic et al. 2001)	Dry deposition (Venkatram and Pleim, 1999) and wet deposition	Dry deposition and below-cloud scavenging (CMAQ; Byun and Schere 2006)	Dry and wet deposition and below-cloud scavenging (Liu et al. 2001)		Dry deposition (Zhang et al. 2001) and below-cloud scavenging (Nickovic et al. 2001).	Dry deposition (Zhang et al. 2001) and wet deposition (Ferrier et al. 2002; Betts 1986; Janjic 1994)	Dry deposition and below-cloud scavenging (RADM2; Stockwell et al. 1990)

Sedimentation scheme	Gravitational settling (Zhang et al. 2001)		Gravitational settling (CMAQ; Byun and Schere 2006)	Gravitational settling		Gravitational settling (Zhang et al. 2001)	Gravitational settling (Zhang et al. 2001)	Gravitational settling (RADM2; Stockwell et al. 1990)
Horizontal resolution	1/3° × 1/3°	Variable (1° × 1° for dust)	81 and 57 km	1–81 km		0.25° × 0.25°	1/3° × 1/3°	81 and 57 km (3 km for local dust)
Vertical resolution	24 Eta-layers	30 σ-layers	15 σ-layers	48 layers		24 σ-hybrid layers	40 σ-hybrid layers	15/19 σ-layers
Height first layer	86 m (above sea level)	40 m (above the surface)	40 m (above the surface)	20 m		86 m (above sea level)	100 m (above surface)	40 m (above surface)
Radiation interactions	Yes	No	No	No		No	Yes (not activated)	No
Transport size bins	8 bins (0.1–10 μm) Tegen and Lacis (1996)	9 bins (0.039–20 μm)	12 bins (0.1–24.6 μm)	1–10 bins 0.04–36 μm	12 bins (0.005–20.48 μm) Tegen and Lacis (1996)	8 bins (0.1–10 μm)	8 bins (0.1–10 μm)	12 bins (0.1–24.6 μm)
Data assimilation	No	No	No	No	Yes	Yes, using the MODIS-MACC initial fields	No	No

JMA Operational Dust Forecast Model

The Japan Meteorological Agency (JMA) has been providing the "Aeolian Dust Information" to the general public via its website (http://www.jma.go.jp/en/kosa/) since January 2004. The operational numerical dust forecast in JMA is based on the Model of Aerosol Species in the Global Atmosphere (MASINGAR) (Tanaka et al. 2003), which is coupled with the MRI/JMA98 AGCM. Dust particles are logarithmically divided into 10 discrete size bins from 0.1 to 10 μm in radius. The operational version of MASINGAR calculates the emission flux of dust as a function of the third power of 10 m wind velocity, soil moisture, soil type, snow cover and vegetation cover. Snow cover by JMA surface analysis and monthly mean MODIS-retrieved leaf area index are used to constrain the erodible surface. JMA is planning to update the operational dust forecast model to be based on the latest global climate model MRI-CGCM3 (Yukimoto et al. 2012).

Met Office Dust Prediction System

The publicly available dust forecasts from the UK Met Office are produced by the global NWP configuration of the Met Office Unified Model (MetUM^{TM}). The dust scheme is essentially that of Woodward (2001) with modifications as described in Woodward (2011) and Collins et al. (2011). The dust emission scheme is represents an initial horizontal/saltation flux in a number of size bins with a subsequent vertical flux of bare soil particles from the surface into the atmosphere. The global NWP model uses only two of the original nine size bins. The magnitude of the emission is a cubic function of the exceedance of the friction velocity over bare soil with respect to a threshold value, determined from the model wind field and boundary-layer structure. The horizontal flux is converted to the vertical flux by first limiting it using the clay fraction in the soil texture data set and then partitioning into the new bins with a prescribed emitted size distribution. Johnson et al. (2011) gives an in-depth description and evaluation of the Met Office dust forecasts in a limited area model over North Africa.

NASA GEOS-5 Aerosol Forecasting System

The Goddard Earth Observing System (GEOS-5; Rienecker et al. 2008) is an Earth system model maintained at the NASA Global Modeling and Assimilation Office (GMAO) to support NASA missions and climate studies. Aerosols are carried online and radiatively coupled to the GEOS-5 AGCM using a version of the Goddard Chemistry Aerosol Radiation and Transport module (GOCART, Chin et al. 2002). GOCART treats the sources, sinks, transport and optical properties of dust, sea salt, black and organic carbon and sulphate. For dust, GOCART employs a

topographic source function and uses a wind speed threshold for dust emissions. The dust particle-size distribution is discretised into five bins. Further description of the aerosol module, its implementation in the GEOS modelling system and its performance is provided in Colarco et al. (2010). The current version of the GEOS-5 forecasting system performs twice daily 5-day forecasts at $0.25° \times 0.3125°$ latitude/longitude horizontal resolution in a quasi-operational framework. AOD based on MODIS observations are assimilated in a 3D-Var framework.

NCEP/NGAC Global Aerosol Forecasting System

Since September 2012, NOAA NCEP has provided 5-day global dust forecasts once per day (at 00 UTC cycle) from the NEMS GFS Aerosol Component (NGAC) system. The forecast model is the Global Forecast System (GFS) within the NOAA Environmental Modeling System (NEMS), and the aerosol component is GOCART. The development of NGAC is part of NCEP's modelling efforts towards a unified modelling framework. The GOCART parameterisations, developed and implemented within GMAO's GEOS-5 Earth system model (Colarco et al. 2010), were coupled with NCEP's NEMS GFS to establish the first interactive atmospheric aerosol forecasting system at NCEP (Lu et al. 2010, 2013). While the ultimate goal at NCEP is a complete Earth system model with the inclusion of aerosol-radiation feedback and aerosol–cloud interaction, the current operational configuration is to maintain a low-resolution forecast-only system for aerosol prediction and a high-resolution forecasting and analysis system for medium-range NWP.

NMMB/BSC-Dust Model

The NMMB/BSC-Dust model (Pérez et al. 2011) is the global and regional dust forecast operational system developed and maintained at the Barcelona Supercomputing Center–Centro Nacional de Supercomputación (BSC-CNS). It is an online multi-scale atmospheric dust model designed and developed at BSC-CNS in collaboration with NOAA NCEP, NASA Goddard Institute for Space Studies and the International Research Institute for Climate and Society (IRI). The dust model is fully embedded into the Non-hydrostatic Multiscale Model (NMMB) developed at NCEP (Janjic et al. 2011 and references therein) and is intended to provide short- to medium-range dust forecasts for both regional and global domains. The NMMB/BSC-Dust model includes a physically based dust emission scheme, which explicitly takes into account saltation and sandblasting processes. It includes an 8-bin size distribution and radiative interactions. The NMMB/BSC-Dust model has been evaluated at regional and global scales (Pérez et al. 2011; Haustein et al. 2012). These developments represent the first step towards a unified multiscale chemical-weather prediction system at BSC-CNS (NMMB/BSC-CTM; Jorba et al. 2012).

10.2.2 Regional Models

CHIMERE Model

The CHIMERE model is dedicated to the transport and chemistry of numerous gaseous and aerosols species. It has been in development for more than 15 years and is intended to be a modular framework available for community use. The dust emission fluxes take into account physical processes such as saltation and sandblasting. A complete description of the dust calculation is presented in Menut et al. (2007). For long-range transport simulations, the model domain includes Africa and Europe requiring a coarse horizontal grid spacing of $1 \times 1°$. In order to take into account the subgrid-scale variability of winds, dust emissions are estimated using a Weibull distribution for the wind speed (Menut 2008). In Menut et al. (2009), an intensive observation period of the African Monsoon Multidisciplinary Analysis (AMMA) programme was modelled in forecast mode to study the variability of modelled surface dust concentrations. It was shown that most of this variability comes from model uncertainties in emissions, transport and deposition as well as from variations in the meteorological fields (see Fig. 10.1).

CUACE/Dust

CUACE/Dust is an integrated atmospheric chemistry modelling system applied for dust (see special issue at http://www.atmos-chem-phys.net/special_issue81.html), which has been operationally run for dust forecasts in China Meteorological Administration (CMA) since 2004 and for the WMO SDS-WAS Asia Node-Regional Centre since 2007. CUACE has been designed as a unified chemistry module to be easily coupled with atmospheric models through a common interface. Its aerosol module utilises a size-segregated multi-component algorithm for different types of aerosols including dust, sea salt, black and organic carbon, nitrate and sulphate (Gong et al. 2003a; Zhou et al. 2008, 2012). A detailed desert distribution with soil texture data base and dust particle-size distributions measurements from nine major deserts for China was adopted (Gong et al. 2003b; Zhang et al. 2003). One of the unique features of the CUACE/Dust is the implementation of a 3D-Var data assimilation system using both satellite and surface observations in near real-time to improve the initial conditions and hence the forecast results (Niu et al. 2008). A scoring system has been developed where observations from various sources concerning dust aerosol, i.e. surface observations of sand and dust storms and satellite retrieved Infrared Difference Dust Index (IDDI; Hu et al. 2008), are integrated into a geographic information system (Wang et al. 2008).

The DREAM/BSC-DREAM8b Models

The Dust Regional Atmospheric Model (DREAM; Nickovic et al. 2001) is based on the Euler-type partial differential nonlinear equation for dust mass continuity and is driven by NCEP/Eta. The model was developed at the Euro-Mediterranean Centre of Insular Coastal Dynamics (ICoD). In May 2005, the operational version of DREAM was transferred to the Environmental Modelling Laboratory of the Technical University of Catalonia (UPC) and in September 2006 to the BSC-CNS. A set of updates during 2002–2005 (Nickovic 2002, 2003, 2005; Nickovic et al. 2004) included a source function based on the 1 km USGS land use data, eight particle-size bins and an initial version of the dust-radiation feedback scheme in cooperation with the Oceanographic Institute (Erdemli, Turkey). In addition to these developments, the updated BSC-DREAM8b v2 model (Pérez et al. 2006a, b; Basart et al. 2012a) includes an improved source mask and updated wet and dry deposition scheme. The BSC-DREAM8b v2 model provides daily dust forecasts at BSC-CNS website (http://www.bsc.es/projects/earthscience/BSC-DREAM/) which are evaluated in near real-time against satellite- and ground-based observations. The model has been extensively evaluated against observations (see, e.g. Basart et al. 2012b).

Since recently, DREAM8-NMME-MACC, which is driven by the NCEP/NMME non-hydrostatic model and includes assimilation of MODIS AOD (Pejanovic et al. 2010; Nickovic et al. 2012), provides daily dust forecasts available at the South East European Virtual Climate Change Center (SEEVCCC; http://www.seevccc.rs/).

FNMOC Coupled Ocean–Atmosphere Mesoscale Prediction System (COAMPS)

NRL has developed an online, multi-bin dust module inside COAMPS, simulating the evolution of the spatial and size distributions of mineral dust particles and passive volcanic ash. Beginning with operational transition to FNMOC in 2001 for Operation Iraqi Freedom (Liu and Westphal 2001; Liu et al. 2007), COAMPS dust simulations are now run on multiple domains over the world daily, with forecasts out to 3 days at resolutions of up to 1 km. The aerosol physical processes of sedimentation, dry deposition and wet removal are calculated using the dynamics and cloud fields of COAMPS. The dust source is based on the 1 km high-resolution dust source database of Walker et al. (2009) that has been developed based on empirical relationships between satellite observed dust and static land cover information.

Regional Mineral Dust Forecast Model in Taiwan

Taiwan's Environment Protection Administration (TEPA) has conducted East Asian dust storm forecasts since 2002 in collaboration with the Department of Atmospheric Sciences, National Taiwan University (NTU). They incorporated the dust deflation module of Wang et al. (2000) into the Taiwan Air Quality Model (TAQM) in 2002 and into the CMAQ model in 2010. Some of the model details can be found in Chen et al. (2004) and Table 10.3. The dust-coupled TAQM (or TAQM-KOSA) is run twice a day for 57 and 81 km horizontal grid spacing, each providing a 5-day forecast. TAQM-KOSA has also been used as a research tool to study dust effects on cloud microphysics and marine phytoplankton bloom by the NTU group. Studies of dust produced from dry riverbeds and agricultural lands using 3 km grid spacing showed that these local sources may raise regional PM concentration more than dust from long-range transport. Local daily dust forecasts have been included in routine operation since 2010. The dust scheme is being improved and incorporated into WRF and WRF-CHEM models and coupled with the cloud microphysical scheme to provide better calculation of in-cloud and below-cloud scavenging of dust as well as dust-radiation feedback. These versions will be gradually incorporated into daily operation after extensive tests.

10.3 Multi-model Ensembles

Ensemble prediction aims to describe the future state of the atmosphere from a probabilistic point of view. Multiple simulations are run to account for the uncertainty of the initial state and/or for the inaccuracy of the model and the mathematical methods used to solve its equations. Multi-model forecasting intends to alleviate the shortcomings of individual models while offering an insight on the uncertainties associated with a single-model forecast. Use of ensemble forecast is especially encouraged in situation associated to unstable weather patterns or in extreme conditions. Ensemble approaches are also known to have more skills at longer ranges (>6 days) where the probabilistic approach provides more reliable information than a single model run due to the model error increasing over time. Moreover, an exhaustive comparison of different models with each other and against multi-model products as well as observations can reveal weaknesses of individual models and provide an assessment of model uncertainties in simulating the dust cycle. Multi-model ensembles also represent a paradigm shift in which offering the best product to the users as a collective scientific community becomes more important than competing for achieving the best forecast as individual centres. This new paradigm fosters collaboration and interaction and ultimately results in improvements in the individual models and in better final products. Two examples of multi-model ensembles for dust prediction are shown below.

10.3.1 The International Cooperative for Aerosol Prediction (ICAP) Multi-model Ensemble

As a result of the maturity of an international community of global aerosol forecast model developers (Reid et al. 2011; Benedetti et al. 2011), the creation of broadly acceptable norms, benchmarks and scorecards to evaluate aerosol forecast skill has become an important issue. At the same time, the NWP community has recognised the value in multi-model ensembles in developing probabilistic forecast tools. Similarly, ensembles of global aerosol analyses are becoming an important tool for climate studies (Huneeus et al. 2011). In response to community needs and views, member developers of the International Cooperative for Aerosol Prediction (ICAP) created a developmental global multi-model ensemble (MME) (Sessions et al. 2014) to allow exploration of relative differences between models and devise tools for probabilistic prediction. Current models in the ICAP-MME dust component include (1) NMMB/BSC-CTM, (2) ECMWF MACC, (3) JMA MASINGAR, (4) NASA GEOS-5, (5) NOAA NGAC, (6) NRL developmental NAAPS and (7) NRL 20-member ensemble mean E-NAAPS (see Sect. 10.2.1). To allow for the inclusion of quasi-operational models, the ICAP-MME is run 24 h behind actual time, which reduces the forecast range from 5 to 4 days. Daily products include a host of maps, mean-spread plots, verification plots and threat scores. As an example of available products, Fig. 10.2 shows the 24 h dust forecasts of aerosol optical depth at 550 nm wavelength valid for 2 January 2013, from the participating models. The maps of AOD show a high degree of consistency of the dust forecasts among the various models. However, there are differences in the magnitude of the AOD field and also in some features, such as the plume being transported towards the North Atlantic which is not present in all models. While currently ICAP-MME data is only available to participating member centres, it is expected to be made public on a quasi-operational basis by the end of 2014.

10.3.2 WMO SDS Regional Dust Prediction Multi-model Ensemble

The Sand and Dust Storm Warning Advisory and Assessment System (SDS-WAS) is a programme of the World Meteorological Organization (WMO) with the mission to enhance the ability of countries to produce and deliver to end users timely and precise sand and dust storm forecasts (Terradellas et al. 2011). The WMO SDS-WAS Regional Centre for Northern Africa, Middle East and Europe (NA-ME-E) coordinates the exchange of forecast products generated by different dust models (BSC-DREAM8b v2, MACC, DREAM8-NMME-MACC, CHIMERE, NMMB/BSC-Dust, MetUM, GEOS-5 and NGAC) and conducts a model inter-comparison and evaluation within its geographic scope (Terradellas et al. 2012). Two products describing centrality (multi-model median and mean) and two

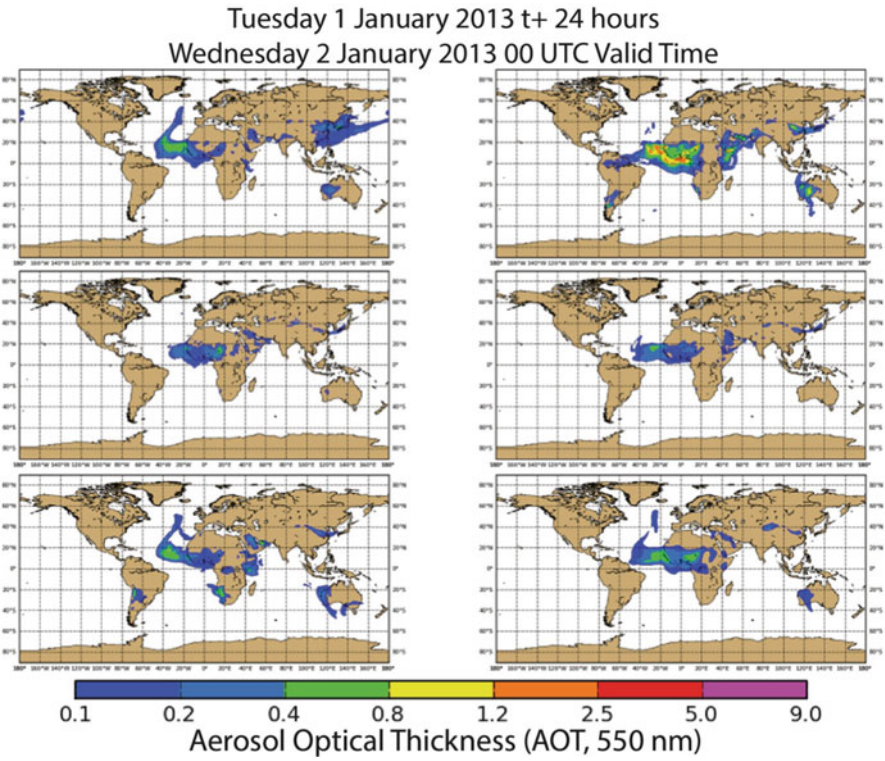

Fig. 10.2 Example of ICAP-MME 24 h dust forecasts of aerosol optical depth at 550 nm wavelength valid for 2 January 2013. Models are ordered as follows: NAAPS (*top left*), GEOS-5 (*middle left*), MASINGAR (*bottom left*), NMMB/BSC-CTM (*top right*), MACC/ECMWF (*middle right*) and NCEP NGAC (*bottom right*)

products describing spread (standard deviation and range of variation) are calculated and are available daily at http://sds-was.aemet.es/. An example of products is shown in Fig. 10.3. In order to generate them, the model outputs are bilinearly interpolated to a common grid mesh of $0.5° \times 0.5°$. The daily SDS-WAS NA-ME-E multi-model median (together with the individual models) is continuously evaluated against data from the Aerosol Robotic Network (AERONET; see also Chap. 7).

10.4 Data Assimilation for Dust Prediction

10.4.1 Introduction

Data assimilation offers a mathematical framework to incorporate observational information into models. When dust prediction was started at various operational

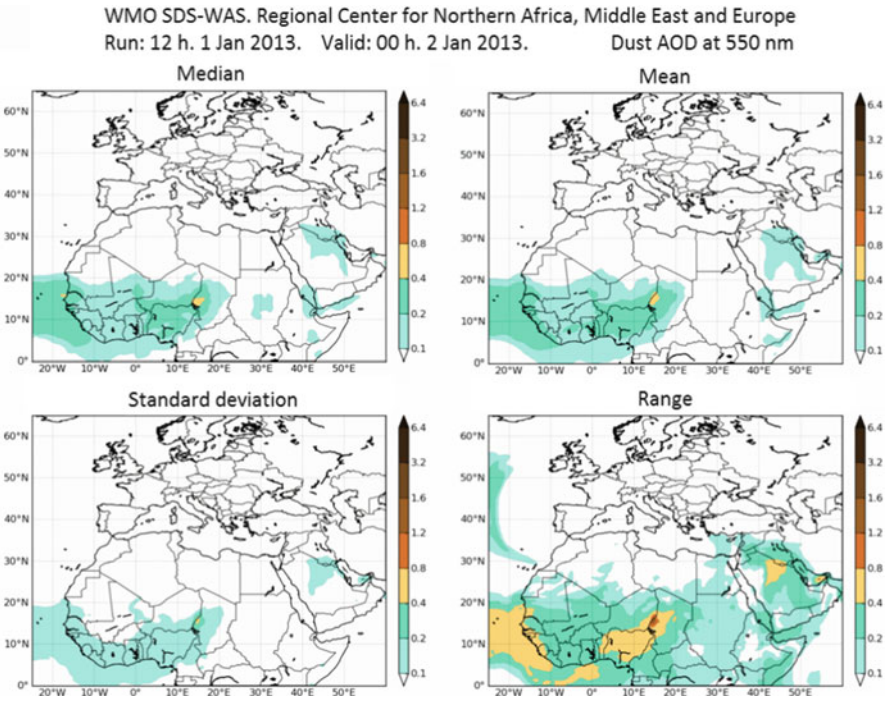

Fig. 10.3 Example of multi-model products issued by the WMO SDS-WAS Regional Center NAME-E: dust optical depth at 550 nm wavelength forecast for 2 January 2013. The *top two panels* describe centrality (multi-model median and mean), and the *bottom two panels* describe spread (standard deviation and range of variation)

centres with multi-annual experience in assimilation, it was a natural development to extend the system to include observations relevant to dust, and aerosols in general, in an effort to initialise the model also for these additional variables. Nowadays, most operational centres with aerosol forecasting capabilities run systems which include an aerosol analysis. While the general assimilation tools can be ported in a straightforward manner to any variable, there are some specific challenges in dust/aerosol assimilation which are mainly related to the paucity of suitable dust observations available for assimilation and the complexity of extracting specific dust signals from satellite radiances which are affected by all aerosol species and other atmospheric quantities. Moreover, due to the complex radiative transfer calculations needed to model aerosol-affected radiances from the visible channels of the current generation of imagers (see Chap. 12), most centres assimilate retrieved products (e.g. aerosol optical depth, AOD) rather than the raw observations. Even this approach has its limitations as AOD observations from sensors with visible channels are not available over bright surfaces such as deserts. This is, for example, the case for the standard AOD data from the MODIS sensor on board of the NASA Terra and Aqua satellites (see Chap. 7), which represent the most important source of near real-time information for the systems with assimilation capabilities.

MODIS data are assimilated in the ECMWF, NRL and NASA forecasting system, although each centre adopts individual strategies for filtering and bias correcting the MODIS observations. As mentioned, the standard MODIS product provides no information on dust over the sources, but it does, for example, over the Atlantic Ocean where dust outflow from the Sahara is the main contributor to the aerosol load. In regions that are not observed, therefore, the model plays a large role in generating that information. Recently, enhanced efforts have been made at several centres to include other observations, for example, the land AOD product from the SEVIRI instrument on board of the MSG payload at the UK Met Office, MODIS Deep Blue at NRL, OMI data at NASA and lidar backscatter at ECMWF, NRL and JMA. JMA/MRI has been pioneering the possibility of assimilating lidar data, with proven benefits on the dust prediction with their offline assimilation and forecasting system (Sekiyama et al. 2010, 2011). In what follows, the main concepts of data assimilation are briefly discussed with focus on some specific aspects related to dust/aerosol assimilation. Technical details are provided in Appendix A.

10.4.2 Main Concepts

Data assimilation is the process of finding the most likely estimation of the true system state via the combination of observations and any available a priori information. In the particular case of forecasts, this a priori information corresponds to the output of model simulations. In other words, data assimilation is an objective way of filling in information gaps and finding the optimal estimate of the true state by minimising the variance of the a posteriori probability distribution function describing the state. This approximation of the true state is the *analysis*. The method most commonly used to obtain an analysis is the least-squares method, which is based on minimising the variance of the a posteriori distribution according to a weighted-mean calculation. One of the simplest forms of analysis is, for example, the interpolation of the differences between model and observations from the locations where the observations have been taken back to the model grid points in order to correct the prior model state (*first guess*). Usually, the weights assigned are inversely proportional to the errors in the observations and the errors in the model first guess. No matter how complicated the schemes and systems involved are, the basic concepts of data assimilation can always be illustrated by this weighted-mean calculation.

Most of the current dust prediction systems rely on assimilation developments already in place for the meteorological models: for example, ECMWF uses the incremental 4D-Var formulation with augmented control vector to include an aerosol total mixing ratio variable (Benedetti et al. 2009). At the Met Office, 4D-Var assimilation of dust observations follows a similar approach, using total dust concentration as the analysis variable to be optimised (control variable). NRL and NASA GMAO use 2D- and 3D-Var approaches. In the case of the regional NMME-DREAM8 dust model (Pejanovic et al. 2010), an assimilation method based on Newtonian relaxation is applied using background dust concentrations from the DREAM dust model and the ECMWF dust analysis.

It is important to remember that most of these aerosol analysis systems solve an initial condition problem: the analysis is used to obtain the initial conditions in the aerosol fields, so that the subsequent forecast matches the observations. In some cases, finding the optimal initial conditions for the atmospheric aerosol concentrations is not sufficient as the actual aerosol amounts may be due to sources that are not accounted for. Studies which include direct estimation of emissions have been promising both for dust (Sekiyama et al. 2011) and other aerosol types (Huneeus et al. 2012), and it is likely that future aerosol analysis systems will include emission parameters in their control variables.

The other aspect which is peculiar to aerosol assimilation is that the problem is severely under-constrained due to the fact that several aerosol species have to be constrained with a total column-integrated observation for radiometric measurements or a profile of backscattering for lidar measurements. This implies that there is no one-to-one correspondence between the observations and the control variable. There are various approaches to get around this problem using sensible assumptions. For example, ECMWF formulates the control variable in terms of a total aerosol mixing ratio and distributes the increments from this variable into the single species mixing ratios in order to avoid defining the error statistics for all species, which would be heavily reliant on the model. Other centres, for example, MRI/JMA, use a method where the emission intensity is treated as a poorly known model parameter defined at each model surface grid point and estimated in the analysis. The control vector then consists of the dust emission parameters and model variables such as aerosol concentrations and meteorological components. In the end, it has to be accepted that no matter how complex and sophisticated the aerosol assimilation system is, a lot of the information comes from the *model* rather than the *observations*. This is a special limitation for dust because retrieval is often impossible over the bright deserts that are dust sources.

Even with its limitations, dust forecasts from systems with aerosol analysis have been shown to have reduced bias and improved correlations with respect to independent observations, when compared to forecasts from the same systems with no aerosol analysis, in particular for dust events (Benedetti et al 2009; Zhang et al. 2008). Moreover, aerosol reanalyses, in particular of dust and biomass burning aerosols, are becoming increasingly valued to assess annual and seasonal anomalies and to monitor the state of climate (Benedetti et al. 2013).

10.5 Evaluation of Atmospheric Dust Prediction Models

10.5.1 General Concepts

An important step in forecasting is the evaluation of the results that have been generated. This process consists of the comparison of the model results to observations on different temporal and spatial scales. In this framework, there are three primary objectives in forecast evaluation:

1. Assessing the value of the forecast variables. The main goal of the evaluation exercise is to evaluate quantitatively and qualitatively whether the modelling system is successfully predicting the temporal and spatial evolution of a particular process.
2. Determining the suitability of a specific application and configuration. Explore the adequacy and correctness of the science represented in the model for the purposes for which the model is applied. Comparison with other models in addition to the observations can be helpful in identifying the strength and weakness of the system.
3. Guiding improvement. Evaluation results should lead to new directions in model development and improvement

A forecast system is judged by its ability to simulate the spatial and temporal evolution of chosen forecast variables. In this regard, the metric is what drives model development and optimisation. Hence, the evaluation metrics must be chosen carefully.

The first evaluation is done right after the forecast period and depends on observations that are made available shortly after they were taken. This type of evaluation, sometimes referred to as verification, is generally part of the operational forecasting process and is therefore done on a regular basis in near real-time. The end result is the quantification of confidence and predictive accuracy of the model products. An additional and different type of evaluation is where the model's performance to simulate a given event or an annual cycle is examined in depth. This case study evaluation can be made any time after the forecast period, and observations that were not available for the near real-time evaluation can be included. The purpose is to identify potential sources of error in order to improve the model. In both cases, the evaluation process will depend on the intended use of the forecast product.

10.5.2 Observational Data for Evaluation

The first problem in identifying appropriate routine measurements for evaluation of dust models is the scarcity of observations of dust events. The location of the main dust sources in unpopulated areas complicates the establishment of observing networks.

Thus, the first option to address the evaluation of dust models has been the use of satellite products. They have the advantage of a large spatial coverage (regional to global), they are made regularly, and their observations are made available to weather centres and other institutions in near real-time. Shortcomings include satellite measurements' highly integrated nature, not only over the atmospheric column but also over all aerosol components. Therefore, applications involving a particular aerosol type (like dust) might be limited in some cases to seasons and regions, when or where that type dominates the aerosol composition (Basart et al.

2012a). Another limitation is the low aerosol detectability over bright surfaces, which affects instruments operating in the visible part of the spectrum. The new generation of high-resolution IR spectrometers and interferometers on polar orbiting satellite platforms (e.g. AIRS, IASI) has the potential to provide good quality dust information (Hilton et al. 2012). Algorithms are currently being developed and validated (Peyridieu et al. 2010; Klüser et al. 2011), and it is likely that these products will become prominent both for evaluation and assimilation.

Regions with air quality monitoring networks are the main surface data source for point evaluation of dust concentrations predicted by dust models. As with the satellites, air quality measurements integrate the contribution of the different types of atmospheric aerosol. Furthermore, observational values are usually limited to the concentration of particulate matter with an aerodynamic diameter less than 10 μm (PM10), which does not always encompass the full size range of dust particles suspended in the atmosphere. Finally, it is important to consider the selection of stations, since many of them are located in cities, industrial parks or roads, where local human activity is the main source of particles, obscuring the contribution of dust to measured quantities.

Visibility data included in meteorological observations have sometimes been used as an alternative source of information (Shao et al. 2003). Visibility is mainly affected by the presence of aerosol and humidity in the atmosphere. If visibility is recorded manually, illumination is also important for intermediate visibilities. Therefore, the use of visibility data must be complemented with information on present weather to discard those cases where visibility is reduced by the presence of hydrometeors (fog, rain, etc.). Several empirical relationships between visibility and dust surface concentration can be found in the literature (d'Almeida 1986; Ben Mohamed et al. 1992; Shao et al. 2003). However, the validity of these relationships is very limited because the visibility reduction depends not only on the dust mass concentration but also on the size spectrum of particles, as well as their density, chemical and mineralogical composition and atmospheric humidity.

Direct-sun photometric measurements are a powerful remote sensing tool that provides retrieval of column-integrated aerosol microphysical and optical properties. In particular, AERONET is a comprehensive set of continental and coastal sites complemented with several sparsely distributed oceanic stations that provides large and refined data sets in near real-time (Holben et al. 1998; Dubovik and King 2000). AERONET measurements are by far the most commonly used in dust model evaluation. Integral parameters such as AOD are complemented with spectral information, which permit retrieval of aerosol microphysical and composition properties (Dubovik et al. 2002). A major shortcoming of these measurements is their unavailability under cloudy skies and during night-time.

Finally, lidar and the most recent generation of ceilometers permit routine measurement of aerosol vertical profiles. However, continuous measurements in ground-based stations are only performed in a few stations that are, in general, far from the main dust sources. On the other hand, space-borne lidars (e.g. CALIOP) provide global spatial coverage, but their temporal coverage is limited.

Table 10.4 Definitions of common model validation metrics. o_i and m_i are respectively observed and modelled values at time and location i, n is the number of data pairs and ($^-$) denotes the mean value

Validation metrics	Formula	Range	Ideal score
Mean bias error (MBE)	$\mathrm{MBE} = \frac{1}{n}\sum_{i=1}^{n}(m_i - o_i)$	$-\infty$ to $+\infty$	0
Root-mean-square error (RMSE)	$\mathrm{RMSE} = \sqrt{\frac{1}{n}\sum_{i-1}^{n}(m_i - o_i)^2}$	0 to $+\infty$	0
Correlation coefficient (r)	$r = \frac{\sum_{i=1}^{n}(m_i - \overline{m})\ (o_i - \overline{o})}{\sqrt{\sum_{i=1}^{n}(m_i - \overline{m})^2} \cdot \sqrt{\sum_{i=1}^{N}(o_i - \overline{o})^2}}$	-1 to 1	1
Fractional gross error (FGE)	$\mathrm{FGE} = \frac{2}{n}\sum_{i=1}^{n}\left\lvert\frac{m_i - o_i}{m_i + o_i}\right\rvert$	0–2	0
Normalised mean bias error (NMBE)	$\mathrm{NMBE} = \frac{1}{n}\sum_{i=1}^{n}\left(\frac{m_i - o_i}{o_i}\right)$	-1 to $+\infty$ for non-negative variables	0
Normalised root-mean-square error (NRMSE)	$\mathrm{NRMSE} = \sqrt{\frac{1}{n}\sum_{i=1}^{n}\left(\frac{m_i - o_i}{o_i}\right)^2}$	0 to $+\infty$	0

10.5.3 Metrics

The evaluation typically starts with an analysis of the plots of the forecast values against observations for a particular location. This method, implemented for near real-time monitoring, is very valuable in detecting outliers and identifying jumps in performance. Then, the core of the evaluation process is the computation of metrics defined to provide a quantitative characterisation of the agreement between model results and observations over specific geographic regions and time periods. The most common metrics used to quantify the departure between modelled and observed quantities are described in Table 10.4.

- The BE captures the average deviations between two data sets with negative values indicating underestimation and positive overestimation of the model.
- The RMSE combines both the bias and the standard deviation. It is strongly dominated by the largest values due to squaring. Especially in cases where prominent outliers occur, the usefulness of RMSE is questionable, and the interpretation becomes difficult.
- r indicates the extent to which temporal and spatial patterns in the model match those in the observations.

– The FGE is a measure of the overall model error. It behaves symmetrically with respect to under- and overestimation, without overemphasising outliers.
– The NMBE and NRMSE are dimensionless versions of MBE and RMSE, built to facilitate comparison between the behaviour of different variables.

10.5.4 Examples of Near Real-Time Evaluation

The evaluations of dust forecasts are mainly conducted by the weather centres generating the forecasts or institutions working in collaboration with them. Evaluating the model forecasts against satellite- and ground-based observations is used to detect problems early on and also to provide a first indication of the accuracy of the products to the users. The evaluation systems developed in the framework of the WMO SDS-WAS NAMEE Regional Centre and MACC-II project are presented here.

The WMO SDS-WAS Dust Model Evaluation Initiative

For the evaluation of the WMO SDS-WAS multi-model ensemble, the dust optical depth (DOD) forecast by the models is first drawn together with the AERONET AOD observations in monthly charts for selected dust-prone stations. Then, different evaluation metrics (see Table 10.4) are computed in order to quantify the agreement between predictions and observations for individual stations and different regions (Sahara-Sahel, Middle East and Mediterranean) as well as different temporal scales (monthly, seasonal and annual basis). Comparison statistics are restricted to observations with low Ångström exponent (AE) values (<0.6) to ensure that forecast and observations are only compared during episodes where dust is the largest contributor. However, there will always be a small portion of particles from other sources, so a small negative bias can be expected. Figure 10.4 shows an example of routine verification of the multi-model ensemble products over the AERONET station of Santa Cruz, Tenerife. In this specific example, all models tend to overestimate the DOD for at the beginning of the month, while the dust episodes in mid-August and at the end of the month are better represented with various degrees of skills.

The MACC-II Evaluation

In the evaluation of the MACC-II forecasts, the DOD at 550 nm wavelength forecast by the MACC model are drawn together with the AERONET and MODIS retrievals of AOD in monthly charts for selected stations, as well as the contributions of other aerosol types. However, the scoring metrics that are calculated on a monthly averaged time frame for different regions or stations are always calculated for the

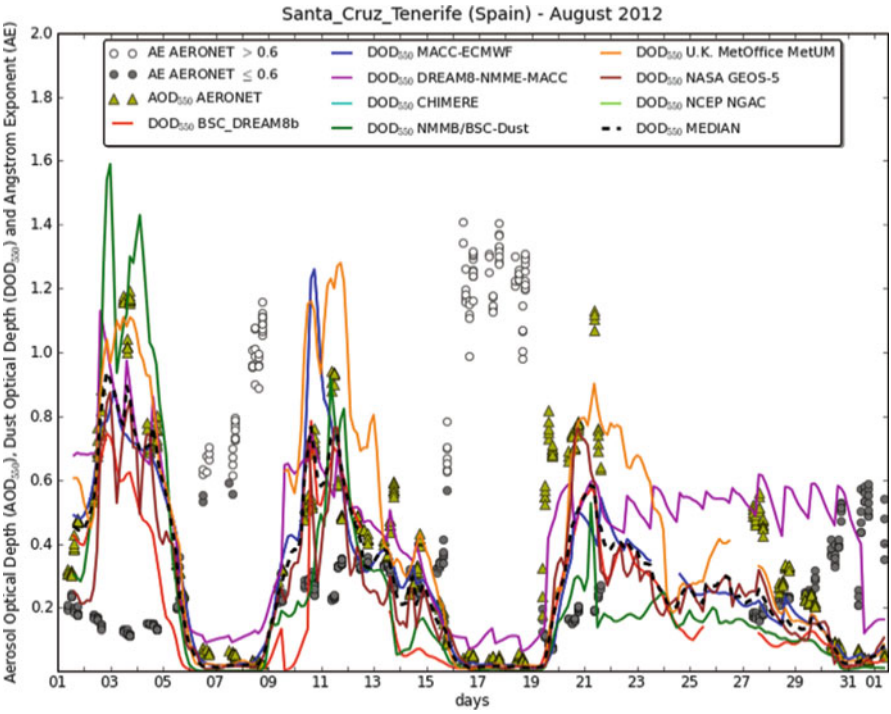

Fig. 10.4 Time series of aerosol optical depth at Santa Cruz de Tenerife (28.5 N, 16.2 W) for August 2012. The plot shows the DOD forecast by the different models (*solid lines*), the median value (*dashed black line*) and direct-sun AERONET observations (*yellow triangles*). An Ångström exponent (*AE*) lower than <0.6 (*dark grey dots*) indicates that the observed AOD is associated with the presence of desert dust

total atmospheric aerosol, without any distinction of the species. This evaluation is complemented with regular reports describing the model performance to forecast major and recent events (available online at www.copernicus-atmosphere.eu).

The calculation of scores is complicated by the geographic inhomogeneity of the observation sites. AERONET sites are not spread evenly over the globe, but are far more concentrated in developed parts of the world such as Europe and the USA. The sites in use are also time-varying, with new sites appearing and old sites disappearing. Taking simple means over the sites therefore leads to scores which reflect the geographic spread of the sites at the time and which are strongly biased towards certain regions.

In order to reduce geographic bias and increase long-term stability, model-versus-AERONET scores are computed using weights for each observation that reflect the local observation density at the observation time. This is done through the calculation of "Voronoi polygons". For a given set of points in space, the Voronoi polygon around a given point is the region closer to that point than any other. At each observation time, the polygons are calculated on the sphere for all available

sites, and the polygon areas are used as the observation weights. Since the polygons will naturally be smaller in data-dense areas, observations in these areas receive lower weights than those in data-sparse areas. To prevent observations in very data-sparse areas receiving higher than reasonable weights, the polygon edges are limited to a maximum radius. This is currently set to a value which results in a maximum polygon area of 1 % of the total area being scored.

Case Study Evaluation

An exhaustive comparison of model outputs against other models and observations can reveal weaknesses of individual models, provide an assessment of uncertainties in simulating the dust cycle and give additional information on sources for potential model improvement. For this kind of study, multiple and different observations are combined to deliver a detailed idea of the structure and evolution of the dust cloud and the state of the atmosphere at the different stages of the event. Observations detailed in Sect. 10.5.2 are usually complemented with strictly meteorological observations such as wind speed and direction at the surface and wind profile within the atmospheric boundary layer.

Multiple case studies concerning a single model can be found in the literature (e.g. Pérez et al. 2006b; Heinold et al. 2007; Cavazos et al. 2009). On the other hand, inter-comparisons of multiple models simulating the same event are described by Uno et al. (2006) and Todd et al. (2008). Both studies reveal the ability of models to reproduce the onset and duration, but not the magnitude of a given dust event. Furthermore, even though the models were able to reproduce surface measurements, large differences existed among them in processes such as emission, transport and deposition. Shao et al. (2003) evaluated not only the model performance to simulate a specific dust event but also the model capacity to predict the event for different lead times. The authors found that the predicted quantities agreed well with the observations. Many global aerosol models have also been evaluated over extended time periods as part of the AeroCom project (see Chap. 9).

10.6 Conclusion

Dust numerical prediction is a growing area of research with many operational applications. In the last few years, many centres have started activities to provide dust forecasts to interested stakeholders, who range from solar energy plant managers to health and aviation authorities, from policymakers to climate scientists. There is also a growing interest in understanding how dust impacts the general circulation of the atmosphere through its radiative effects which could help in improving numerical weather prediction and projections of climate change. Dust forecast models have reached a high degree of complexity and can provide useful information to forecasters. Some factors limiting the accuracy of the models are

related to the complex emission sources and the heterogeneous characteristics of the emitting surfaces, including texture, composition, vegetation type and topography. Dust prediction is also limited by the paucity of observations available for data assimilation, model initialisation and verification. A significant current limitation is that satellite instruments do not precisely distinguish the presence of dust from that of other aerosol species. As more products from satellite- and ground-based stations become available, it is foreseeable that dust prediction will improve. In order to provide the best dust forecasts possible, along with improving the dust models, there are currently international efforts to bring together several operational and quasi-operational models to form multi-model ensembles. The merit of these ensembles is to bring together the strengths of the various state-of-the-art models while offering the possibility to approach the dust prediction from a probabilistic perspective, thus enhancing the range of applications. The development of these multi-model ensembles is at an early stage, and exploitation of their potential is still limited, also because of the relatively small number of participating models. However, it is anticipated that the probabilistic approach to dust prediction both at level of the individual centres and within the context of the multi-model ensembles will become more important in the future.

Appendix A: Technical Aspects of Data Assimilation for Dust Prediction

A10.1 Assimilation Techniques

Variational Methods (CMA, ECMWF, FNMOC/NRL, Met Office, NASA GMAO)

The variational method is a well-established approach that combines model background information with observations to obtain the "best" initial conditions possible. In the 2D- and 3D-Var versions, the fields are adjusted at the analysis time whereas in 4D-Var, a short-term forecast is run over the selected time window (usually 12 h) to provide a so-called first guess. In 4D-Var, the dynamical model is then used as a strong constraint to minimise the difference between the model background and the observations. This approach is widely used in many NWP centres. The fundamental idea of the variational methods is based on minimisation of a cost function which measures the distance between observations and their model equivalent, subject to a background constraint usually provided by the model itself. Optimisation of this cost function is performed with respect to selected control variables (e.g. the initial conditions). Adjustments to these control variables allow for the updated model trajectory to match the observations more closely. Assuming the update to the initial condition is small, an incremental formulation can be adopted to ensure a good compromise between operational feasibility and physical

consistency in the analysis (Courtier et al. 1994). This so-called "incremental" approach is employed at ECMWF. Another key aspect of the variational methods is the use of the *adjoint* model to calculate the gradient of the cost function needed in the minimisation. Coding an adjoint of highly nonlinear parameterisations can be involved, and the parameterisations may need to be linearised before an adjoint can be constructed.

Kalman Filter and Ensemble Kalman Filter Methods (MRI/JMA, NRL)

Another data assimilation method, the Kalman filter (KF), has been well known since the 1960s (Kalman 1960). KF, which is based on the linear minimum variance estimation approach, evolves the error covariance matrix temporally. The KF calculation requires neither tangent linear models nor adjoint models. Despite these advantages, KF requires the inverse calculation of the matrices with the dimensions of the model state space. The size of the model state space in geosciences is often of the order of millions: for such large systems, KF cannot be adopted. In order to exploit the advantages of KF and reduce the computational burden, the ensemble Kalman filter (EnKF) was developed (Evensen 1994, 2007). The basic concept of EnKF is that the ensemble of the forward model forecasts is able to represent the probability distribution function (PDF) of the system state and approximate the error covariance distribution. The EnKF is mathematically equivalent to the original Kalman filter, under the ideal conditions where the simulation model is linear, and the EnKF employs an infinite ensemble size. In the MRI/JMA aerosol assimilation system, a 4D expansion of the EnKF (4D-EnKF) is adopted to assimilate asynchronous observations at the appropriate times. Using the 4D-EnKF aerosol assimilation system, the surface emission intensity distribution of dust aerosol is estimated (Sekiyama et al. 2010, 2011). The vector augmentation mentioned above enables EnKF to estimate the parameters through the background error covariance between dust emissions and observations. Consequently, EnKF simultaneously estimated the aerosol concentrations (as model variables) together with the dust aerosol emission intensity (as model parameters). The MRI/JMA aerosol assimilation system employs the local ensemble transform Kalman filter (LETKF), which is one of the EnKF implementation schemes (Hunt et al. 2007). The LETKF uses the ensemble transform approach (Bishop et al. 2001) to obtain the analysis ensemble as a linear combination of the background ensemble forecasts. The LETKF handles observations locally in space, where all the observations are assimilated simultaneously.

It is important to note that 4D-Var and ensemble Kalman filter methods approximately converge, when 4D-Var is run over a long assimilation window (e.g. 24 h) and model error is included, as they are both based on the Bayes theorem which postulates that the probability distribution of the analysis errors is a linear combination of the probability distribution of the observations and background errors (Fisher et al. 2005).

A10.2 Observations Used for the Dust Analyses

Main Products

The MODIS AOD product is used most widely due to its reliability and availability in near real-time (Kaufman et al. 1997; Remer et al. 2005). Two separate retrievals with different accuracies are applied over land and ocean. The former suffers from higher uncertainties due to the impact of the surface reflectance. Several other factors affect the accuracy of the retrievals both over land and ocean: cloud contamination, assumptions about the aerosol types and size distribution, near-surface wind speed, radiative transfer model biases and instrumental uncertainties (Zhang and Reid 2006). The MODIS product provides the total AOD, such that the partitioning between dust and other aerosol species is driven by the particular analysis system and its underlying model. However, the standard MODIS Dark Target method does not deliver data over bright surfaces where there is not enough contrast between the surface and overlying aerosol layer. However, iron in desert soils absorbs at blue wavelengths, and albedo in the blue part of the solar spectrum is considerably darker than the mid-visible and red. This allowed the development of the MODIS Deep Blue product (Hsu et al. 2004, 2006). Deep Blue is not currently assimilated at NRL, NASA or ECMWF, but it is expected to be incorporated into their systems now that an error matrix has been established (Shi et al. 2012).

At the Met Office, the standard MODIS and MODIS Deep Blue (Hsu et al. 2004, 2006; Ginoux et al. 2010) products are being assimilated, and the AOD products at 550 nm wavelength from SEVIRI from Brindley and Ignatov (2006) and Brindley and Russell (2009) are being monitored prior to being assimilated in the near future. However, only a subset of observations can be used, as the forecast model contains only dust rather than a full suite of aerosols. This restriction is achieved by geographic filtering of the SEVIRI AOD and by using the MODIS standard product aerosol-type flags over land and preferentially using the MODIS Deep Blue product over bright desert surfaces. The presence of other aerosols in these regions of high dust loading introduces uncertainty into the assimilation process.

CALIPSO (e.g. Winker et al. 2007) is the first satellite mission to have made aerosol lidar observations routinely available from space. At MRI/JMA, the CALIPSO Level 1B data have been successfully assimilated into the JMA dust forecast model with a positive impact on the prediction of aeolian dust. A derived CALIPSO product is also assimilated at NRL (Campbell et al. 2010; Zhang et al. 2011). In particular, Zhang et al. (2011) found that assimilation of lidar data had a beneficial impact on the 48 h forecast. The same product is under study for assimilation at ECMWF.

Data Quality Aspects and Bias Correction

Perhaps the most pressing issue for satellite data assimilation is the development of appropriate satellite error models. Indeed, a key assumption in data assimilation is that the observation errors are uncorrelated spatially. For satellite aerosol products, and dust products in particular, there is considerable spatially correlated bias. Such bias is formed from a number of factors, including biases in the algorithm's lower boundary condition/surface reflectance, microphysical bias in the assumed optical model of the aerosol particles and the cloud mask. These biases can lead to unphysical analysis fields, which in turn can lead to positive or negative perturbation "plumes" in forecast fields. Currently, satellite data providers do not generate prognostic error models, and it has fallen on the data assimilation community to modify the products for their own purposes. Debiasing data products and developing reliable point-by-point uncertainties are time-consuming. Further, aerosol product algorithms update frequently, leaving previous error analyses obsolete.

Each centre's development team has approached satellite data quality and bias correction differently. Development for FNMOC systems at NRL and the University of North Dakota has favoured extensive error analysis at the expense of sophistication in the data assimilation technology. MODIS over ocean, land and Deep Blue products have had extensive debiasing based on comparison with AERONET observations and error modelling applied (Zhang and Reid 2006; Shi et al. 2011a, 2012; Hyer et al. 2011). In addition, the spatial covariance of the MODIS and MISR products has also been undertaken (Shi et al. 2011b). Internal studies at NRL have shown that, overall, the assimilation of raw satellite aerosol products boosts model verification scores. After a set of quality assurance steps were taken with the satellite products, NAAPS root-mean-square error (RMSE) improved by more than 40 %. Lidar assimilation has taken a similar method, with considerable quality assurance (QA) checks (Campbell et al. 2010).

At ECMWF, a variational bias correction is implemented based on the operational set-up for assimilated radiances following the developments by Dee and Uppala (2009). The bias model for the MODIS data consists of a global constant that is adjusted variationally in the minimisation based on the first-guess departures. Although simple, this bias correction works well in the sense that the MACC analysis is not biased with respect to MODIS observations. Moreover, this approach has the advantage of being tied to the optimisation of the cost function, and as such it is estimated online, not requiring previous preprocessing of the observations. The bias error model allows more complex treatment with the addition of other bias predictors that are relevant for AOD, for example, instrument geometry, viewing angle, cloud cover, wind speed, etc. Improvements to the bias model are currently being undertaken.

A10.3 Definitions of Background and Observational Errors

Since the relative weight between the background and the observations is decided by the error statistics prescribed for both, in areas that are data-limited such as the deserts, the aerosol analysis is severely under-constrained relative to the observations and relies almost entirely on the background. Also, the background matrix is responsible for the redistribution of the aerosol information from the observations to the model fields. This is again especially true for dust due to the already-mentioned paucity of observations over bright surfaces.

Background Error Covariance Matrices

The aerosol background error covariance matrix used for aerosol analyses at ECMWF was derived using the Parrish and Derber method (also known as NMC method; Parrish and Derber 1992) as detailed by Benedetti and Fisher (2007). This method was long used for the definition of the background error statistics for the meteorological variables and is based on the assumption that the forecast differences between the 48 h and the 24 h forecasts are a good statistical proxy to estimate the model background errors. The advantage in using the model to define the errors is the grid-point availability of the statistics over a long period. This leads to a satisfactory background error covariance matrix without the need to prescribe the vertical and horizontal correlation length as shown in Kahnert (2008). However, a shortcoming of this method consists in the static definition of the background error covariance matrix, which can lead to suboptimal analysis in the case of unusual situations such as intense storms. This is addressed by the ensemble methods with flow-dependent error estimates which suit the specific situation ("errors of the day").

For the FNMOC/NRL NAAPS global model, background error covariances were estimated in a number of methods, all converging to the same number for the error covariance length (250 km, the same as is commonly assumed for water vapour). This length was determined from experiments from the MODIS data set. As a check, error covariances were also estimated from a 3-month simulation from the 20-member NAAPS ensemble driven purely from the NOGAPS meteorological ensemble.

Flow-Dependent Background Error Covariance Matrix

"Errors of the day" can be estimated in the context of the ensemble methods, where at each analysis time, a series of forecasts is run starting from perturbed conditions, and these forecasts provide an estimate of the model errors. However, the EnKF tends to be easily influenced by sampling errors at long distances because the available ensemble size is too small to estimate the background error covariance of the atmospheric system. Therefore, a covariance localisation must be applied

for all the EnKF implementation schemes to reduce the spurious impact of distant observations. The LETKF permits a flexible choice of observations to be assimilated at each grid point. For example, the MRI/JMA system employs the covariance localisation with a Gaussian weighting function that depends on the physical distance between the grid location and the observation. The limited ensemble size causes both sampling errors at long distances and filter divergence. To compensate for the error underestimation and avoid the filter divergence, it is necessary to increase the ensemble spread every data assimilation cycle. This technique is called covariance inflation. The MRI/JMA system utilises a multiplicative inflation method, in which the ensemble spread is uniformly multiplied by a constant value larger than one; it is common to tune this inflation factor empirically. Furthermore, adding random perturbations to the initial state of each ensemble member is sometimes necessary to maintain the diversity of the ensemble members and not to lose the error covariance among the model variables. In the MRI/JMA system, random perturbations are added to dust emission intensity. This type of flow-dependent background error definition is very promising, and it has also been progressively adopted for standard meteorological applications in variational systems through the so-called hybrid approach (Buehner et al. 2010a, b; Clayton et al. 2012), in which the assimilation framework is variational, but the background errors of the day are defined through ensemble methods. This approach should work well for dust initialisation, where the errors on the dust prediction are both associated to emission uncertainties and transport.

Observation Errors

The problem of defining appropriate errors for the observations when those are *retrieval products* is very complex. Observation errors for these products are comprised of measurements errors that depend on instrument calibration and characteristics and a priori and representativeness errors that depend on the retrieval assumptions regarding the parameters that are not directly observed but that affect the retrieval output, such as the optical properties assumed for the aerosols, as well as on the overall quality of the forward model used in the retrieval. Most satellite data providers do not provide errors at the pixel level, but rather provide regression parameters derived from comparison of the satellite products with ground-based equivalent products like AERONET retrievals of AOD which are deemed to have high accuracy. This type of regression-based error estimate does not faithfully represent the accuracy of the retrieved product at the level of individual pixels, which is what is needed in data assimilation. Often the developers end up assigning their own errors to the observations to be able to fit the needs of their system. For example, at ECMWF, the observation error covariance matrix is assumed to be diagonal, to simplify the problem. The errors are also chosen ad hoc and prescribed as fixed values over land and ocean for the assimilated observations (MODIS AOD at 550 nm). This was decided after investigation revealed that biases were introduced in the analysis due to the observation error assumptions when those were specified

as *relative* rather than absolute errors. While this might be a specific characteristic of the ECMWF system, the problem of a correct specification of the pixel-level errors on aerosol-retrieved products is a topic of ongoing research (Kolmonen et al. 2013).

References

Alfaro SC, Gomes L (2001) Modeling mineral aerosol production by wind erosion: emission intensities and aerosol size distribution in source areas. J Geophys Res 106:18075–18084

Alfaro SC, Gaudichet A, Gomes L, Maillé M (1997) Modeling the size distribution of a soil aerosol produced by sandblasting. J Geophys Res 102:11239–11249

Basart S, Pérez C, Nickovic S, Cuevas E, Baldasano JM (2012a) Development and evaluation of the BSC-DREAM8b dust regional model over Northern Africa, the Mediterranean and the Middle East. Tellus B 64. http://dx.doi.org/10.3402/tellusb.v64i0.18539

Basart S, Pay MT, Jorba O, Pérez C, Jiménez-Guerrero P, Schulz M, Baldasano JM (2012b) Aerosols in the CALIOPE air quality modelling system: evaluation and analysis of PM levels, optical depths and chemical composition over Europe. Atmos Chem Phys 12:3363–3392. doi:10.5194/acp-12-3363-2012

Ben Mohamed A, Frangi JP, Fontan J, Druilhet A (1992) Spatial and temporal variations of atmospheric turbidity and related parameters in Niger. J Appl Meteorol 31:1286–1294

Benedetti A, Fisher M (2007) Background error statistics for aerosols. Q J R Meteorol Soc 133:391–405

Benedetti A et al (2009) Aerosol analysis and forecast in the European Centre for Medium-Range Weather Forecasts Integrated Forecast System: 2. Data assimilation. J Geophys Res 114, D13205. doi:10.1029/2008JD011115

Benedetti A, Reid JS, Colarco PR (2011) International Cooperative for Aerosol Prediction (ICAP) workshop on aerosol forecast verification. Bull Am Meteorol Soc. doi:10.1175/BAMS-D-11-00105.I

Benedetti A, Jones LT, Inness A, Kaiser JW, Morcrette J-J (2013) [Global climate] Aerosols [in "State of the Climate in 2012"]. Bull Am Meteorol Soc 94(8):S34–S36

Betts AK (1986) A new convective adjustment scheme. Part 1, 1986: Observational and theoretical basis. Q J R Meteorol Soc 112:677–691. doi:10.1002/qj.49711247307

Bishop CH, Etherton BJ, Majumdar SJ (2001) Adaptive sampling with the ensemble transform Kalman filter. Part I: Theoretical aspects. Mon Weather Rev 129:420–436

Boucher O, Pham M, Venkataraman C (2002) Simulation of the atmospheric sulfur cycle in the LMD GCM: model description, model evaluation, and global and European budgets, Note 23, 26 pp. Institut Pierre-Simon Laplace, Paris. http://www.ipsl.jussieu.fr/poles/Modelisation/NotesSciences.htm

Brindley H, Ignatov A (2006) Retrieval of mineral aerosol optical depth and size information from Meteosat Second Generation SEVIRI solar reflectance bands. Remote Sens Environ 102:344–363

Brindley H, Russell J (2009) An assessment of Saharan dust loading and the corresponding cloud-free longwave direct radiative effect from geostationary satellite observation. J Geophys Res. doi:10.1029/2008JD011635

Buehner M, Houtekamer PL, Charette C, Mitchell HL, He B (2010a) Intercomparison of variational data assimilation and the ensemble Kalman filter for global deterministic NWP. Part I: Description and Single-Observation Experiments. Mon Weather Rev 138:1550–1566

Buehner M, Houtekamer PL, Charette C, Mitchell HL, He B (2010b) Intercomparison of variational data assimilation and the ensemble Kalman filter for global deterministic NWP. Part II: One-month experiments with real observations. Mon Weather Rev 138:1550–1566

Byun DW, Schere KL (2006) Review of the governing equations, computational algorithms, and other components of the models-3 Community Multiscale Air Quality (CMAQ) modeling system. Appl Mech Rev 59:51–77

Campbell JR, Reid JS, Westphal DL, Zhang J, Hyer EJ, Welton EJ (2010) CALIOP aerosol subset processing for global aerosol transport model data assimilation. J Sel Top Appl Earth Observ Remote Sens 3:203–214. doi:10.1109/JSTARS.2010.2044868

Cavazos C, Todd MC, Schepanski K (2009) Numerical model simulation of the Saharan dust event of 6–11 March 2006 using the Regional Climate Model version 3 (RegCM3). J Geophys Res 114, D12109. doi:10.1029/2008JD011078

Chen J-P, Wang Z, Young C-Y, Tsai F, Tsai I-C, Wang G-J, Shieh W-C, Lin HW, Huang J-Y, Lu M-J (2004) Simulations of Asian yellow dust incursion over Taiwan for the spring of 2002 and 2003. Terr Atmos Oceanic Sci 15(5):949–981

Chin M, Ginoux P, Kinne S, Torres O, Holben BN, Duncan BN, Martin RV, Logan JA, Higurashi A, Nakajima T (2002) Tropospheric optical thickness from the Gocart model and comparisons with satellite and sun photometer measurements. J Atmos Sci 59:461–483

Christensen JH (1997) The Danish Eulerian hemispheric model – a three-dimensional air pollution model used for the Arctic. Atmos Environ 31(24):4169–4191

Clayton A, Lorenc A, Barker DM (2012) Operational implementation of a hybrid ensemble/4D-Var global data assimilation system at the Met Office. Q J R Meteorol Soc. doi:10.1002/qj.2054

Colarco P, da Silva A, Chin M, Diehl T (2010) Online simulations of global aerosol distributions in the NASA GEOS-4 model and comparisons to satellite and ground-based aerosol optical depth. J Geophys Res 115, D14207. doi:10.1029/2009JD012820

Collins W, Bellouin N, Doutriaux-Boucher M, Gedney N, Halloran P, Hinton T, Hughes J, Jones C, Joshi M, Liddicoat S, Martin G, O'Connor F, Rae J, Senior C, Sitch S, Totterdell I, Wiltshire A, Woodward S (2011) Development and evaluation of an earth-system model – HadGEM2. Geosci Model Dev 4:1051–1075. doi:10.5194/gmd-4-1051-2011

Courtier P, The´paut J-N, Hollingsworth A (1994) A strategy for operational implementation of 4D-Var, using an incremental approach. Q J R Meteorol Soc 120:1367–1387

d'Almeida GA (1986) A model for Saharan dust transport. J Clim Appl Meteorol 25:903–916

Dee DP, Uppala S (2009) Variational bias correction of satellite radiance data in the ERA-Interim reanalysis. Q J R Meteorol Soc 135(644):1830–1841

Deuzé J, Breon F, Devaux C, Goloub P, Herman M, Lafrance B, Maignan F, Marchand A, Nadal F, Perry G, Tanre D (2001) Remote sensing of aerosols over land surfaces from POLDER-ADEOS-1 polarized measurements. J Geophys Res-Atmos 106(D5):4913–4926

Dubovik O, King MD (2000) A flexible inversion algorithm for retrieval of aerosol optical properties from sun and sky radiance measurements. J Geophys Res 105:20673–20696

Dubovik O, Holben B, Eck TF, Smirnov A, Kaufman YJ, King MD, Tanré D, Slutsker I (2002) Variability of absorption and optical properties of key aerosol types observed in worldwide locations. J Atmos Sci 59:590–608

Evensen G (1994) Sequential data assimilation with a nonlinear quasi-geostrophic model using Monte Carlo methods to forecast error statistics. J Geophys Res 99(C5):10143–10162

Evensen G (2007) Data assimilation the ensemble Kalman filter. Springer, Berlin, 279 pp

FAO/IIASA/ISRIC/ISSCAS/JRC (2009) Harmonized world soil database (version 1.1). FAO/IIASA, Rome/Laxenburg

Ferrier BS, Jin Y, Lin Y, Black T, Rogers E, DiMego G (2002) Implementation of a new grid-scale cloud and precipitation scheme in the NCEP Eta Model. In: Proceedings of 15th Conference on numerical weather prediction, American Meteorological Society, San Antonio, 12–16 Aug 2002, pp 280–283

Fisher M, Leutbecher M, Kelly GA (2005) On the equivalence between Kalman smoothing and weak-constraint four-dimensional variational data assimilation. Q J R Meteorol Soc 131:3235–3246. doi:10.1256/qj.04.142

Gillette D (1978) A wind tunnel simulation of the erosion of soil: effect of soil texture, sandblasting, wind speed, and soil consolidation on dust production. Atmos Environ 12:1735–1743

Ginoux P, Chin M, Tegen I, Prospero JM, Holben B, Dubovik O, Lin S-J (2001) Sources and distributions of dust aerosols simulated with the GOCART model. J Geophys Res 106:20255–20274. doi:10.1029/2000JD000053

Ginoux P, Garbuzov D, Hsu NC (2010) Identification of anthropogenic and natural dust sources using Moderate Resolution Imaging Spectroradiometer (MODIS) deep blue level 2 data. J Geophys Res 115, D05204. doi:10.1029/2009JD012398

Gläser G, Kerkweg A, Wernli H (2012) The mineral dust cycle in EMAC 2.40: sensitivity to the spectral resolution and the dust emission scheme. Atmos Chem Phys 12:1611–1627. doi:10.5194/acp-12-1611-2012

Gong SL, Barrie LA, Blanchet J-P, Salzen K, Lohmann U, Lesins G, Spacek L, Zhang LM, Girard E, Lin H, Leaitch R, Leighton H, Chylek P, Huang P (2003a) Canadian Aerosol Module: a size-segregated simulation of atmospheric aerosol processes for climate and air quality models 1. Module development. J Geophys Res 108:4007. doi:10.1029/2001JD002002

Gong SL, Zhang XY, Zhao TL, McKendry IG, Jaffe DA, Lu NM (2003b) Characterization of soil dust distributions in China and its transport during ACE-ASIA 2. Model simulation and validation. J Geophys Res 108:4262. doi:10.1029/2002JD002633

Haustein K, Pérez C, Baldasano JM, Jorba O, Basart S, Miller RL, Janjic Z, Black T, Nickovic S, Todd MC, Washington R, Müller D, Tesche M, Weinzierl B, Esselborn M, Schladitz A (2012) Atmospheric dust modeling from meso to global scales with the online NMMB/BSC-Dust model–part 2: Experimental campaigns in Northern Africa. Atmos Chem Phys 12:2933–2958. doi:10.5194/acp-12-2933-2012

Haywood JM, Allan RP, Culverwell I, Slingo T, Milton S, Edwards J, Clerbaux N (2005) Can desert dust explain the outgoing longwave radiation anomaly over the Sahara during July 2003? J Geophys Res 110, D05105. doi:10.1029/2004JD005232

Heinold B, Helmert J, Hellmuth O, Wolke R, Ansmann A, Marticorena B, Laurent B, Tegen I (2007) Regional modeling of Saharan dust events using LM-MUSCAT: model description and case studies. J Geophys Res 112, D11204. doi:10.1029/2006JD007443

Hilton F et al (2012) Hyperspectral earth observation from IASI: five years of accomplishments. Bull Am Meteorol Soc 93:347–370, http://dx.doi.org/10.1175/BAMS-D-11-00027.1

Hinds WC (1982) Aerosol technology: properties, behavior, and measurement of airborne particles. Wiley, New York, 424 p

Hogan TF, Rosmond TE (1991) The description of the Navy operational global atmospheric prediction system. Mon Weather Rev 119:1786–1815. doi:10.1175/1520-0493(1991)119

Holben BN, Eck TF, Slutsker I, Tanré D, Buis JP, Setzer A, Vermote E, Reagan JA, Kaufman Y, Nakajima T, Lavenu F, Jankowiak I, Smirnov A (1998) AERONET – a federated instrument network and data archive for aerosol characterization. Remote Sens Environ 66:1–16

Hollingsworth A, Textor C, Benedetti A, Boucher O, Chevallier F, Dethof A, Elbern H, Engelen R, Eskes H, Granier C, Morcrette J-J, Rayner P, Peuch V-H, Schultz M, Serrar S, Simmons A, GEMS consortium (2008) Open access toward a monitoring and forecasting system for atmospheric composition: The GEMS project. Bull Am Meteorol Soc 89:1147–1164

Hsu NC, Tsay SC, King MD, Herman JR (2004) Aerosol properties over bright-reflecting source regions. IEEE Trans Geosci Remote Sens 43:557–569

Hsu NC, Tsay S-C, King MD, Herman JR (2006) Deep blue retrievals of Asian aerosol properties during ACE Asia. IEEE Trans Geosci Remote Sens 44:3180–3195. doi:10.1109/TGRS.2006.879540

Hu XQ, Lu NM, Niu T, Zhang P (2008) Operational retrieval of Asian sand and dust storm from FY-2C geostationary meteorological satellite and its application to real time forecast in Asia. Atmos Chem Phys 8:1649–1659

Huneeus N, Schulz M, Balkanski Y, Griesfeller J, Prospero J, Kinne S, Bauer S, Boucher O, Chin M, Dentener F, Diehl T, Easter R, Fillmore D, Ghan S, Ginoux P, Grini A, Horowitz L, Koch D, Krol MC, Landing W, Liu X, Mahowald N, Miller R, Morcrette J-J, Myhre G, Penner J, Perlwitz J, Stier P, Takemura T, Zender CS (2011) Global dust model intercomparison in AeroCom phase I. Atmos Chem Phys 11:7781–7816. doi:10.5194/acp-11-7781-2011

Huneeus N, Chevallier F, Boucher O (2012) Estimating aerosol emissions by assimilating observed aerosol optical depth in a global aerosol model. Atmos Chem Phys 12:4585–4606

Hunt BR, Kostelich EJ, Szunyogh I (2007) Efficient data assimilation for spatiotemporal chaos: a local ensemble transform Kalman filter. Physica D 230:112–126

Hyer EJ, Reid JS, Zhang J (2011) An over-land aerosol optical depth data set for data assimilation by filtering, correction, and aggregation of MODIS Collection 5 optical depth retrievals. Atmos Meas Tech 4:379–408. doi:10.5194/amt-4-379-2011

Ignatov A, Gutman G (1998) The derivation of the green vegetation fraction from NOAA/AVHRR data for use in numerical weather prediction models. Int J Remote Sens 19:1533–1543. doi:10.1080/014311698215333

Iversen T (1989) Numerical modeling of the long range atmospheric transport of sulphur dioxide and particulate sulphate to the arctic. Atmos Environ 23:2571–2595

Janjic ZI (1994) The step-mountain eta coordinate model: further developments of the convection, viscous sublayer and turbulence closure schemes. Mon Weather Rev 122:927–945

Janjic Z, Janjic T, Vasic R (2011) A class of conservative fourth order advection schemes and impact of enhanced formal accuracy on extended range forecasts. Mon Weather Rev. doi:10.1175/2010MWR3448.1

Johnson BT, Brooks ME, Walters D, Christopher S, Schepanski K (2011) Assessment of the met office dust forecast model using observations from the GERBILS campaign. Q J R Meteorol Soc 137:1131–1148. doi:10.1002/qj.736

Jorba O, Dabdub D, Blaszczak-Boxe C, Pérez C, Janjic Z, Baldasano JM, Spada M, Badia A, Gonçalves M (2012) Potential significance of photoexcited NO2 on global air quality with the NMMB/BSC chemical transport model. J Geophys Res. doi:10.1029/2012JD017730

Kahnert M (2008) Variational data analysis of aerosol species in a regional CTM: background error covariance constraint and aerosol optical observation operators. Tellus B 60:753–770. doi:10.1111/j.1600-0889.2008.00377

Kalman RE (1960) A new approach to linear filter and prediction problems. J Basic Eng 82:35–45

Kaufman Y, Tanré D, Remer L, Vermote E, Chu A, Holben B (1997) Operational remote sensing of tropospheric aerosol over land from EOS moderate resolution imaging Spectroradiometer. J Geophys Res 102:51–67. doi:10.1029/96JD03988

Klüser L, Martynenko D, Holzer-Popp T (2011) Thermal infrared remote sensing of mineral dust over land and ocean: a spectral SVD based retrieval approach for IASI. Atmos Meas Tech Discuss 4:461–509. doi:10.5194/amtd-4-461-2011

Kolmonen P, Sundström A-M, Sogacheva L, Rodriguez E, Virtanen T, de Leeuw G (2013) Uncertainty characterization of AOD for the AATSR dual and single view retrieval algorithm. Atmos Meas Tech Discuss 6:4039–4075. doi:10.5194/amtd-6-4039-2013

Liu H, Jacob DJ, Bey I, Yantosca RM (2001) Constraints from ^{210}Pb and ^{7}Be on wet deposition and transport in a global three-dimensional chemical tracer model driven by assimilated meteorological fields. J Geophys Res 106(12):12109–12128

Liu M, Westphal DL (2001) A study of the sensitivity of simulated mineral dust production to model resolution. J Geophys Res Atmos 106(D16):18099–18112, Published: Aug 27, 2001

Liu M, Westphal DL, Walker AL, Holt TR, Richardson KA, Miller SD (2007) COAMPS real-time dust storm forecasting during operation Iraqi freedom. Weather Forecast 22:192–206, http://dx.doi.org/10.1175/WAF971.1

Lu S, Huang H-C, Hou Y-T, Tang Y, McQueen J, da Silva A, Chin M, Joseph E, Stockwell W (2010) Development of NCEP global aerosol forecasting system: an overview and its application for improving weather and air quality forecasts, NATO science for peace and security series: Air pollution modeling and its application XX, pp 451–454, Springer Science. doi:10.1007/978-90-481-3812-8

Lu S, da Silva A, Chin M, Wang J, Moorthi S, Juang H, Chuang H-Y, Tang Y, Jones L, Iredell M, McQueen J (2013) The NEMS GFS aerosol component: NCEP's global aerosol forecast system. NCEP Office Note 472

Maddy ES et al (2012) On the effect of dust aerosols on AIRS and IASI operational level 2 products. Geophys Res Lett 39, L10809. doi:10.1029/2012GL052070

Maring H, Savoie DL, Izaguirre MA, Custals L, Reid JS (2003) Mineral dust aerosol size distribution change during atmospheric transport. J Geophys Res 108(D19):8592. doi:10.1029/2002JD002536

Marticorena B, Bergametti G (1995) Modeling the atmospheric dust cycle: 1. Design of a soil derived dust emission scheme. J Geophys Res 100. doi:10.1029/95JD00690

Marticorena B, Bergametti G, Aumont B, Callot Y, N'Doume C, Legrand M (1997) Modeling the atmospheric dust cycle: 2. Simulation of Saharan dust sources. J Geophys Res 102:4387–4404

Martonchik JV, Diner DJ, Kahn R, Gaitley B, Holben BN (2004) Comparison of MISR and AERONET aerosol optical depths over desert sites. Geophys Res Lett 31:L16102. doi:10.1029/2004GL019807

Menut L (2008) Sensitivity of hourly Saharan dust emissions to NCEP and ECMWF modeled wind speed. J Geophys Res Atmos 113, D16201. doi:10.1029/2007JD009522

Menut L, Schmechtig C, Marticorena B (2005) Sensitivity of the sandblasting fluxes calculations to the soil size distribution accuracy. J Atmos Oceanic Tech 22(12):1875–1884

Menut L, Forêt G, Bergametti G (2007) Sensitivity of mineral dust concentrations to the model size distribution accuracy. J Geophys Res Atmos 112, D10210. doi:10.1029/2006JD007766

Menut L, Chiapello I, Moulin C (2009) Previsibility of mineral dust concentrations: the CHIMERE-DUST forecast during the first AMMA experiment dry season. J Geophys Res Atmos 114, D07202. doi:10.1029/2008JD010523

Morcrette J-J, Beljaars A, Benedetti A, Jones L, Boucher O (2008) Sea-salt and dust aerosols in the ECMWF IFS model. Geophys Res Lett 35, L24813. doi:10.1029/2008GL036041

Morcrette J-J et al (2009) Aerosol analysis and forecast in the European centre for medium-range weather forecasts integrated forecast system: forward modeling. J Geophys Res 114, D06206. doi:10.1029/2008JD011235

Nickovic S (1996) Modelling of dust process for the Saharan and Mediterranean area. In: Guerzoni S, Chester R (eds) The impact of African dust across the Mediterranean. Kluwer Academic Publishers, Dordrecht, pp 15–23

Nickovic S (2002) Dust aerosol modeling: step toward integrated environmental forecasting (invited paper). Eos. Trans. AGU, 83(47), Fall Meet. Suppl., Abstract A71E-04

Nickovic S (2003) Saharan dust outbreaks: modelling. In: First EARLINET symposium on the structure and use of the data base derived from systematic Lidar observations, 11–12 Feb 2003, Hamburg

Nickovic S (2005) Distribution of dust mass over particle sizes: impacts on atmospheric optics. In: Fourth ADEC workshop – Aeolian dust experiment on climate impact, 26–28 Jan, Nagasaki, pp 357–360

Nickovic S, Dobricic S (1996) A model for long-range transport of desert dust. Mon Weather Rev 124:2537–2544

Nickovic S, Jovic D, Kakaliagou O, Kallos G (1997) Production and long-range transport of desert dust in the Mediterranean region: Eta model simulations. In: 22nd NATO/CCMS international technical meeting on air pollution modelling and its applications, Clermont-Ferrand, 2–6 June 1997, pp 190–197

Nickovic S, Kallos G, Papadopoulos A, Kakaliagou O (2001) A model for prediction of desert dust cycle in the atmosphere. J Geophys Res 106:18113–18130. doi:10.1029/2000JD900794

Nickovic S, Pejanovic G, Ozsoy E, Pérez C, Baldasano JM (2004) Interactive radiation-dust model: a step to further improve weather forecasts. In: International symposium on sand and dust storm, 12–14 Sept 2004, Beijing

Nickovic S et al (2012) Dust operational forecast system with assimilation of MODIS satellite data. In: The regional conference on dust and dust storms, 20–22 Nov 2012, Kuwait

Niu T, Gong SL, Zhu GF, Liu HL, Hu XQ, Zhou CH, Wang YQ (2008) Data assimilation of dust aerosol observations for the CUACE/dust forecasting system. Atmos Chem Phys 8:3473–3482

Parrish DF, Derber JC (1992) The National Meteorological Center's spectral statistical-interpolation analysis system. Mon Weather Rev 120:1747–1763

Pejanovic G, Vukovic A, Vujadinovic M, Dacic M (2010) Assimilation of satellite information on mineral dust using dynamic relaxation approach. Geophys Res Abstr 12, EGU2010-7353

Pérez C, Nickovic S, Pejanovic G, Baldasano JM, Ozsoy E (2006a) Interactive dust-radiation modeling: a step to improve weather forecasts. J Geophys Res 11. doi:10.1029/2005JD006717

Pérez C, Nickovic S, Baldasano JM, Sicard M, Rocadenbosch F, Cachorro VE (2006b) A long Saharan dust event over the western Mediterranean: Lidar, sun photometer observations, and regional dust modeling. J Geophys Res 111. doi:10.1029/2005JD006579

Pérez C, Haustein K, Janjic Z, Jorba O, Huneeus N, Baldasano JM, Black T, Basart S, Nickovic S, Miller RL, Perlwitz J, Schulz M, Thomson M (2011) An online mineral dust aerosol model for meso to global scales: model description, annual simulations and evaluation. Atmos Chem Phys 11:13001–13027. doi:10.5194/acp-11-13001-2011

Peyridieu S, Chédin A, Tanré D, Capelle V, Pierangelo C, Lamquin N, Armante R (2010) Saharan dust infrared optical depth and altitude retrieved from AIRS: a focus over North Atlantic – comparison to MODIS and CALIPSO. Atmos Chem Phys 10:1953–1967. doi:10.5194/acp-10-1953-2010

Reddy MS, Boucher O, Bellouin N, Schulz M, Balkanski Y, Dufresne J-L, Pham M (2005) Estimates of global multi-component aerosol optical depth and direct radiative perturbation in the Laboratoire de Météorologie Dynamique general circulation model. J Geophys Res 110, D10S16. doi:10.1029/2004JD004757

Reid JS et al (2003) Comparison of size and morphological measurements of coarse mode dust particles from Africa. J Geophys Res 108(D19):8593. doi:10.1029/2002JD002485

Reid JS, Reid EA, Walker A, Piketh S, Cliff S, Al Mandoos A, Tsay S-C, Eck TF (2008) Dynamics of southwest Asian dust particle size characteristics with implications for global dust research. J Geophys Res 113, D14212. doi:10.1029/2007JD009752

Reid JS, Benedetti A, Colarco PR, Hansen JA (2011) International operational aerosol observability workshop. Bull Am Meteorol Soc 92:ES21–ES24, http://dx.doi.org/10.1175/2010BAMS3183.1

Reinfried F, Tegen I, Heinold B, Hellmuth O, Schepanski K, Cubasch U, Huebener H, Knippertz P (2009) Simulations of convectively-driven density currents in the Atlas region using a regional model: impacts on dust emission and sensitivity to horizontal resolution and convection schemes. J Geophys Res 114, D08127. doi:10.1029/2008JD010844

Remer LA et al (2005) The MODIS aerosol algorithm, products and validation. J Atmos Sci 62:947–973

Rienecker MM et al (2008) The GEOS-5 data assimilation system –documentation of versions 5.0.1 and 5.1.0, and 5.2.0. NASA technical report series on global modeling and data assimilation, NASA/TM-2008-104606, vol 27, 92 pp

Rodwell MJ, Jung T (2008) Understanding the local and global impacts of model physics changes: an aerosol example. Q J R Meteorol Soc 134:1479–1497. doi:10.1002/qj.298

Ruescas AB, Arbelo M, Sobrino JA, Mattar C (2011) Examining the effects of dust aerosols on satellite sea surface temperatures in the Mediterranean sea using the medspiration matchup database. J Atmos Oceanic Tech 28:684–697

Schroedter-Homscheidt M, Oumbe A, Benedetti A, Morcrette J-J (2013) Aerosols for concentrating solar electricity production forecasts: requirement quantification and ECMWF/MACC aerosol forecast assessment. Bull Am Meteorol Soc 94:903–914

Sekiyama TT, Tanaka TY, Shimizu A, Miyoshi T (2010) Data assimilation of CALIPSO aerosol observations. Atmos Chem Phys 10:39–49. doi:10.5194/acp-10-39-2010

Sekiyama TT, Tanaka TY, Maki T, Mikami M (2011) The effects of snow cover and soil moisture on Asian dust: II. Emission estimation by lidar data assimilation. SOLA 7A:40–43

Sessions W et al (2014) Development toward a global operational consensus: basic climatological characteristics of the ICAP-MME. Atmos Chem Phys Discuss 14:1–65. doi:10.519/acpd-14-1-2014

Shao Y, Raupach MR, Findlater PA (1993) Effect of saltation bombardment on the entrainment of dust by wind. J Geophys Res 98:12719–12726

Shao Y, Yang Y, Wang J, Song Z, Leslie LM, Dong C, Zhang Z, Lin Z, Kanai Y, Yabuki S, Chun Y (2003) Northeast Asian dust storms: real-time numerical prediction and validation. J Geophys Res 108(D22):4691. doi:10.1029/2003JD003667

Shi Y, Zhang J, Reid JS, Hyer EJ, Eck TF, Holben BN, Kahn RA (2011a) A critical examination of spatial biases between MODIS and MISR aerosol products – application for potential AERONET deployment. Atmos Meas Tech 4:2823–2836. doi:10.5194/amt-4-2823-2011

Shi Y, Zhang J, Reid JS, Holben B, Hyer EJ, Curtis C (2011b) An analysis of the collection 5 MODIS over-ocean aerosol optical depth product for its implication in aerosol assimilation. Atmos Chem Phys 11:557–565

Shi Y, Zhang J, Reid JS, Hyer EJ, Hsu NC (2012) Critical evaluation of the MODIS Deep Blue aerosol optical depth product for data assimilation over North Africa. Atmos Meas Tech Discuss 5:7815–7865. www.atmos-meas-tech-discuss.net/5/7815/2012/, doi:10.5194/amtd-5-7815-2012

Stockwell WR, Middleton P, Chang JS, Tang X (1990) The second generation regional acid deposition model chemical mechanism for regional air quality modeling. J Geophys Res 95:16343–16367

Takemi T (2012) Importance of the numerical representation of shallow and deep convection for simulations of dust transport over desert regions. Adv Meteorol 201:413584, 13 pp. doi:10.1155/2012/413584

Tanaka TY, Orito K, Sekiyama TT, Shibata K, Chiba M, Tanaka H (2003) MASINGAR, a global tropospheric aerosol chemical transport model coupled with MRI/JMA98 GCM: model description. Pap Meteorol Geophys 53:119–138

Tegen I, Fung I (1994) Modeling of mineral dust in the atmosphere: sources, transport, and optical thickness. J Geophys Res 99:22897–22914

Tegen I, Lacis AA (1996) Modeling of particle size distribution and its influence on the radiative properties of mineral dust aerosol. J Geophys Res 101:19237–19244. doi:10.1029/95JD03610

Terradellas E, Baldasano JM, Cuevas E (2011) The "WMO Sand and Dust Warning Advisory and Assessment System" Program. In: The 5th Spanish conference on aerosol science and technology, Madrid, June 2011

Terradellas E, Basart S, Schulz M, Baldasano JM, Morcrette J-J, Pejanovic G, Menut L, Benedetti A, Jorba O, Nickovic S, Benincasa F (2012) Intercomparison of dust prediction models in the framework of the WMO SDS-WAS programme, European aerosol conference, Sept 2012, Granada

Todd MC, Karam DB, Cavazos C, Bouet C, Heinold B, Baldasano JM, Cautenet G, Koren I, Pérez C, Solmon F, Tegen I, Tulet P, Washington R, Zakey A (2008) Quantifying uncertainty in estimates of mineral dust flux: an intercomparison of model performance over the Bodélé Depression, northern Chad. J Geophys Res 113, D24107. doi:10.1029/2008JD010476

Uno I, Wang Z, Chiba M, Chun YS, Gong SL, Hara Y, Jung E, Lee SS, Liu M, Mikami M, Music S, Nickovic S, Satake S, Shao Y, Song Z, Sugimoto N, Tanaka T, Westphal DL (2006) Dust model intercomparison (DMIP) study over Asia: overview. J Geophys Res Atmos 111(D12), D12213. doi:10.1029/2005JD006575

Venkatram A, Pleim J (1999) The electrical analogy does not apply to modeling dry deposition of particles. Atmos Environ 33(18):3075–3076. doi:10.1016/S1352-2310(99)00094-1

Walcek CJ, Brost RA, Chang JS, Wesely ML (1986) SO_2, sulfate and HNO_3 deposition velocities computed using regional landuse and meteorological data. Atmos Environ 20:949–964

Walker AL, Liu M, Miller SD, Richardson KA, Westphal DL (2009) Development of a dust source database for mesoscale forecasting in southwest Asia. J Geophys Res 114, D18207. doi:10.1029/2008JD011541

Wang Z, Ueda H, Huang M (2000) A deflation module for use in modeling long-range transport of yellow sand over East Asia. J Geophys Res 105:26947–26959

Wang YQ, Zhang XY, Gong SL, Zhou CH, Hu XQ, Liu HL, Niu T, Yang YQ (2008) Surface observation of sand and dust storm in East Asia and its application in CUACE/Dust. Atmos Chem Phys 8:545–553

Weaver C, Joiner J, Ginoux P (2003) Mineral aerosol contamination of TIROS Operational Vertical Sounder (TOVS) temperature and moisture retrievals. J Geophys Res Atmos 108(D8):4246. doi:10.1029/2002JD002571

Westphal DL, Toon OB, Carlson TN (1987) A two-dimensional numerical investigation of the dynamics and microphysics of Saharan dust stroms. J Geophys Res Atoms 92(D3):3027–3049
Westphal DL, Toon OB, Carlson TN (1988) A case study of mobilization and transport of Saharan dust. J Atmos Sci 45:2145–2175
Westphal DL, Curtis CA, Liu M, Walker AL (2009) Operational aerosol and dust storm forecasting. In: WMO/GEO expert meeting on an international sand and dust storm warning system, IOP conference series: Earth and Environmental Science, 7. doi:10.1088/1755-1307/7/1/012007
White BR (1979) Soil transport by winds on Mars. J Geophys Res 84:4643–4651
Winker DM, Hunt HH, McGill MJ (2007) Initial performance assessment of CALIOP. Geophys Res Lett 34, L19803. doi:10.1029/2007GL030135
Woodward S (2001) Modeling the atmospheric life cycle and radiative impact of mineral dust in the Hadley centre climate model. J Geophys Res 106:18155–18166. doi:10.1029/2000JD900795
Woodward S (2011) Mineral dust in HadGEM2, Technical report 87. Met Office Hadley Centre for Climate Change, Exeter. http://www.metoffice.gov.uk/archive/science/climate-science/hctn87
Yukimoto S et al (2012) A new global climate model of the Meteorological Research Institute: MRI CGCM3 model description and basic performance. J Meterol Soc Japan 90A:23–64. doi:10.2151/jmsj.2012-A02
Zhang J, Reid JS (2006) MODIS aerosol product analysis for data assimilation: assessment of over ocean level 2 aerosol optical thickness retrievals. J Geophys Res 111, D22207. doi:10.1029/2005JD006898
Zhang L, Gong S, Padro J, Barrie L (2001) A size-segregated particle dry deposition scheme for an atmospheric aerosol module. Atmos Environ 35:549–560
Zhang XY, Gong SL, Shen ZX, Mei FM, Xi XX, Liu LC, Zhou ZJ, Wang D, Wang YQ, Cheng Y (2003) Characterization of soil dust aerosol in China and its transport and distribution during 2001 ACE-Asia: 1. Network observations. J Geophys Res 108:8032–8039
Zhang J, Reid JS, Westphal DL, Baker N, Hyer EJ (2008) A system for operational aerosol optical depth data assimilation over global oceans. J Geophys Res 113, D10208. doi:10.1029/2007JD009065
Zhang J, Campbell JR, Reid JS, Westphal DL, Baker NL, Campbell WF, Hyer EJ (2011) Evaluating the impact of assimilating CALIOP-derived aerosol extinction profiles on a global mass transport model. Geophys Res Lett 38, L14801. doi:10.1029/2011GL047737
Zhou CH, Gong SL, Zhang XY, Wang YQ, Niu T, Liu HL, Zhao TL, Yang YQ, Hou Q (2008) Development and evaluation of an operational SDS forecasting system for East Asia: CUACE/Dust. Atmos Chem Phys 8:787–798
Zhou C, Gong S, Zhang XY, Liu HL, Xue M, Cao GL, An XQ, Che HZ, Zhang YM, Niu T (2012) Towards the improvements of simulating the chemical and optical properties of Chinese aerosols using an online coupled model CUACE/Aero. Tellus B 64:18965, http://dx.doi.org/10.3402/tellusb.v64i0.18965

Chapter 11
Radiative Effects of Dust

Eleanor J. Highwood and Claire L. Ryder

Abstract Dust is a major component of atmospheric aerosols, and aerosols in general are a major uncertainty in predicting climate change. Aerosols are crucial too in cloud formation processes and therefore in the hydrologic cycle. As a first step to understanding and quantifying the impact of dust on weather and climate, we must be able to characterise the impact of dust on radiative transfer processes in the atmosphere. In this chapter we consider the impact of dust on the reflection and absorption of both long-wave and short-wave radiation and illustrate the sensitivity of this effect to the size and composition of dust particles. We also consider the impact of dust on satellite retrievals of aerosol and other quantities.

Keywords Optical properties • Single-scattering albedo • Radiative effect • Satellite retrievals • Radiation • Scattering • Refractive index • Particle size • Extinction • Visibility • Dust models

11.1 Introduction

Dust affects weather and climate in two main ways – via modifying the capture or redirection of radiation by the atmosphere and by modification of cloud properties (see Chap. 12). Dust also deposits nutrients to oceanic and terrestrial ecosystems, which affects the global carbon cycle (see Chap. 14). This chapter will address the so-called "direct" impact of dust on radiation in both the short- and long-wave parts of the radiation spectrum. The interaction of dust with radiation also has impacts for satellite retrievals of surface temperature and other quantities, and this will also be discussed briefly in this chapter.

E.J. Highwood (✉) • C.L. Ryder
Department of Meteorology, University of Reading, Reading, UK
e-mail: E.J.Highwood@reading.ac.uk; C.L.Ryder@reading.ac.uk

P. Knippertz and J.-B.W. Stuut (eds.), *Mineral Dust: A Key Player in the Earth System*, DOI 10.1007/978-94-017-8978-3_11,

In the short-wave (SW) part of the spectrum (also called "solar" wavelengths), dust is mainly a scattering aerosol – an increase of dust therefore normally results in an increase in solar radiation scattered back to space and a decrease in the direct beam reaching the surface. However, there is also some absorption of SW by the dust which offsets to some extent the increased scattering at the top of the atmosphere. This effect is modified by the underlying surface, for example, more additional SW is scattered back to space by dust blowing over the ocean compared to dust over the desert surface itself that already scatters a fair proportion of SW back to space. In the long-wave (LW) part of the spectrum, dust can absorb infrared (IR) radiation being emitted by the warm surface and re-emit this radiation in all directions, including back towards the surface. Thus, the LW flux leaving the top of the atmosphere (TOA) is decreased and the LW flux arriving at the surface is increased – similar to the greenhouse effect of increased carbon dioxide. The TOA effect is enhanced and the surface effect is reduced if the dust layer is elevated and cold.

In order to quantify the radiative impacts of dust, it is necessary to know several things about both the dust itself and the surrounding environment. Firstly, we must be able to describe the so-called optical properties as a function of wavelength (these are the extinction coefficient, the single-scattering albedo and phase function, all defined below) – these are dependent on the size, shape and composition of the dust, which are in turn dependent on the dust source and transport processes (see Chap. 2). Secondly, the vertical profile of dust is crucial for assessing the impact on heating rates through the atmospheric column; it is this that determines the impact on, for example, stability and convection. Finally, the radiative impact of the dust does not solely depend on the properties of the dust itself, but also strongly on the underlying surface. For example, highly scattering dust present over a dark ocean will have a big impact on radiation balance at the TOA, whereas the same dust over the highly reflective sand seas of the Sahara will have a much smaller effect in the SW.

In this chapter we will first define and discuss the optical properties of dust and illustrate their sensitivity to key physical properties of the dust itself like particle size or shape (Sect. 11.2). We will then review recent measurements of dust optical properties and the corresponding perturbation to the radiative flux efficiency (Sect. 11.3). To conclude we will discuss the implications of our knowledge of dust radiative impact for satellite retrievals (Sect. 11.4) and its inclusion in weather and climate models (Sect. 11.5).

11.2 Optical Properties of Dust

11.2.1 Definition of Optical Properties

Mineral dust (and other atmospheric aerosols) is able to interact with both solar and terrestrial electromagnetic radiation. Particles can both scatter radiation in different directions and absorb it, re-emitting it as thermal energy. The sum of scattering and absorption of energy at a particular wavelength is known as *extinction* and can be expressed by

$$Q_{\text{ext}} = \frac{C_{\text{ext}}}{\pi r^2} \tag{11.1}$$

Here, C_{ext} is the single-particle extinction cross section in m^2, which is analogous to the shadow the aerosol particle casts on incident radiation. r is the radius of the particle and Q_{ext} is the non-dimensional extinction efficiency, which relates how efficiently the particle extinguishes radiation relative to its size. Scattering and absorption efficiencies can be defined in similar ways. Other metrics for extinction can be derived from C_{ext}. The mass-specific extinction coefficient (MEC), measured in m^2g^{-1}, is a commonly cited property of aerosols (can be derived from measurements of mass and extinction), representing how efficient a given particle is at extinguishing radiation per unit mass. It is defined as

$$\text{MEC} = \frac{3Q_{\text{ext}}}{4r\rho_{\text{aer}}}, \tag{11.2}$$

where ρ_{aer} is the density of the aerosol particle (note that the MEC is also simply the C_{ext} divided by the product of the parcel density and volume). A similar property, the aerosol extinction coefficient, σ_{ext}, is defined as

$$\sigma_{\text{ext}} = NC_{\text{ext}}, \tag{11.3}$$

where N is the number of particles per cubic metre of air and σ_{ext} is measured in m^{-1}. The vertically integrated value of the extinction coefficient is equal to the commonly used non-dimensional aerosol optical depth (AOD or τ),

$$\tau = \int \sigma_{\text{ext}} \mathrm{d}z \tag{11.4}$$

which represents the total amount of radiation extinguished by aerosol in an atmospheric column. AOD is commonly measured by ground-based sun photometers, retrieved by satellite products and calculated by aerosol models. (Note that the dust load can also be indicated by visibility measurements, but the correlation with AOD is only moderate – see Sect. 11.5 for more details.) All of the above properties (C_{ext}, Q_{ext}, σ_{ext}, MEC and τ) are typically reported at certain values of λ – usually around 550 nm for solar wavelengths since this is close to the wavelength of peak intensity of the solar spectrum and many instruments measure extinction in this range. However, we emphasise that these properties can vary markedly over the range of incident wavelengths, λ.

An important diagnostic of scattering and absorption measurements is the *single-scattering albedo* (*SSA*), ω_0, the ratio of scattering to extinction at a particular wavelength, defined as

$$\omega_0 = \frac{\sigma_{\text{sca}}}{\sigma_{\text{ext}}}. \tag{11.5}$$

This is useful as it tells us about what fraction of the extinguished radiation is scattered by aerosol; conversely, the *co-albedo* $(1-\omega_0)$ tells us what fraction is absorbed and therefore heats the aerosol-laden air. This can be important in determining the sign of radiative forcing due to the aerosol at the TOA and for affecting atmospheric circulation changes (see Chap. 13). Dust is notable for having a relatively low SSA compared to many aerosols, such as sulphate, which are more scattering.

The direction in which radiation is scattered when it interacts with a particle is also important in determining the magnitude of the radiative impact. This can be described in a number of ways. The *phase function*, $P(\theta)$, where θ is the angle of scatter relative to the incident beam, is the angular distribution of light intensity scattered by the particle – this is the most complete description of the scattering pattern and is important for satellite measurements of radiance at the TOA and subsequent retrievals of dust and other quantities. The radiative transfer parts of climate models are increasingly able to use the phase function (thanks to greater computational power allowing codes to represent radiation transfer as more than just up versus down). Knowledge of the phase function is also of critical importance for satellite applications. Several more commonly reported parameters can be derived from the phase function, including the *asymmetry parameter*, g, defined as the intensity-weighted average of the cosine of the scattering angle. A value of $g = 1$ denotes purely forward scattering, whilst a value of $g = -1$ denotes light scattered completely in the backward direction. Many simplified models of radiative forcing and climate (where radiation is limited to an upward and downward flux) use the asymmetry parameter, but to define it requires knowledge or calculation of the entire phase function. Finally, the *hemispheric backscatter ratio*, b, is the fraction of the scattered intensity that is redirected into the backward hemisphere of the scattering particle. The backscattering ratio can be measured directly by a nephelometer and can be related in some cases directly to g.

11.2.2 Methods of Characterising Dust Optical Properties

Many of the dust optical properties defined above can be measured directly (e.g. scattering and extinction – and subsequently SSA, hemispherical backscatter), whilst others must be calculated, or at least some model is required to retrieve their values from measurements. The instruments most commonly used to measure dust optical properties or integrated quantities such as optical depth include nephelometers (scattering at one or multiple wavelengths, e.g. McConnell et al. 2008; Osborne et al. 2008), sun photometers (AOD and via retrieval size distribution, refractive index and single-scattering albedo; e.g. Dubovik et al. 2002) and lidar (e.g. Mona et al. 2012).

The calculation of scattering and absorption properties of dust from radiances requires knowledge or assumptions about particle size, shape and refractive index. In many studies, dust particles are assumed to be spherical, and the scattering is

described by Mie theory (Bohren and Huffman 1983). Key governing parameters include λ, r and the complex refractive index of the particle, m, ($m = n + k_i$), where the real part n represents the amount of scattering and the imaginary part k represents the amount of absorption, both of which vary with λ. Thus, for a given particle size (or size distribution) and refractive index that varies with wavelength, spectral properties of scattering, absorption and extinction can be calculated. These can then be applied in a radiative transfer model to calculate irradiances and/or radiances throughout an atmospheric column, subsequently determining the radiative effect (RE) of the dust.

Observations of dust particles increasingly show that the assumption of sphericity is unrealistic, even at small sizes. Optical properties for non-spherical dust can be calculated using a range of other techniques (e.g. Otto et al. 2009; Yang et al. 2007). Oblate spheroids with an effective axis ratio of 1.16 were indicated by lidar measurements during the Saharan Mineral Dust Experiment (SAMUM) campaign. However, the simulated optical properties differed by only 1 % in SSA and 4 % in asymmetry parameter from those calculated using a spherical particle (Otto et al. 2009). The extinction optical depth was within 3.5 % of the spherical assumption case, but the backscattering towards the TOA was substantially enhanced (and therefore the dust is more cooling when non-spherical properties are used). Haapanala et al. (2012) consider several approaches to compare dust of different shapes and conclude that there is no simple relationship between particle shape and modification of the direct RE in comparison with spheres. They also acknowledge that any uncertainty introduced here is likely to be substantially smaller than other sources of uncertainty concerning dust in climate models, for example, spatial variability or differences in optical properties due to source region. However, non-sphericity is likely to be much more important for applications that measure the impact of dust on a beam oriented along a single direction, such as upwardly scattered radiation measured by aircraft or satellites, and particularly for lidar measurements where backscatter at 180° is crucial. Non-spherical scattering codes are considerably more expensive than Mie code, and many single non-spherical codes do not cover the whole size and wavelength ranges required for use with dust.

11.2.3 Sensitivity of Optical Properties to Size and Composition: An Illustrative Example

Dust optical properties are highly variable due to the sensitivity to particle size and composition. An overview of dust size distributions is given in Chap. 2. Figure 11.1 shows two contrasting examples of dust size distributions. The red line shows a size distribution retrieved from AErosol RObotic NETwork (AERONET; see also Chap. 7) ground-based sun photometer measurements at Cape Verde in the Atlantic Ocean over 8 years (Dubovik et al. 2002), representative of transported dust. Contrastingly, the black line shows a size distribution from recent aircraft measurements (Ryder et al. 2013) over the remote Sahara, much closer to dust

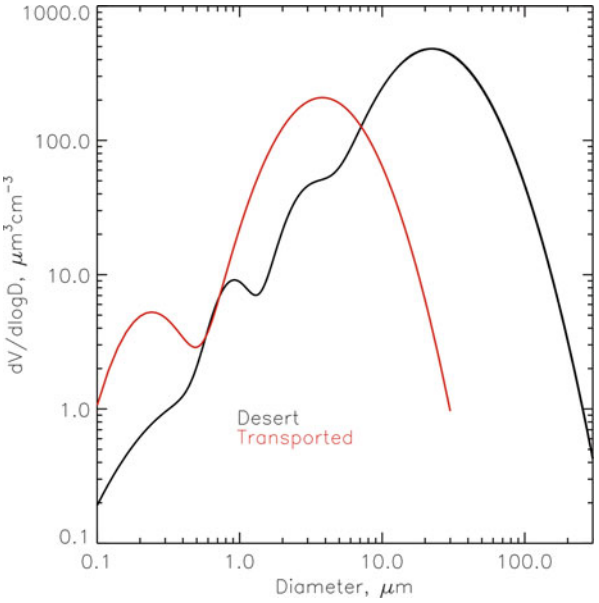

Fig. 11.1 Two contrasting dust volume size distributions. Data in *red* are from AERONET retrievals at Cape Verde (Dubovik et al. 2002) representing transported dust, whilst data in *black* are from aircraft measurements over the Sahara (Ryder et al. 2013), representing dust closer to sources

sources, with a larger coarse mode present, with a peak volume distribution at 20–30 μm diameter. It is possible that the different measurement platforms contribute to the different size distributions (Müller et al. 2010), but equally likely that the coarse mode is depleted through deposition during transport. Either way, these different size distributions will be used here to illustrate the impact of the coarse mode on dust optical properties.

Figure 11.2 shows typical spectral refractive indices in the SW spectrum. The black line shows data from Otto et al. (2007), which is a smoothed average of values from the literature. At 550 nm, this produces an imaginary value of 0.006, which has been shown to be high compared to recent work (e.g. Kandler et al. (2009); McConnell et al. (2010); Balkanski et al. (2007)), although variations in the index are expected due to variations in the mineral content of the dust source region (Sokolik and Toon 1999). Therefore, a less absorbing adjusted refractive index is also shown (red line). The higher imaginary values in the ultraviolet are typically caused by the presence of hematite (see Chap. 2).

The different combinations of refractive index and size distribution can be applied in a Mie scattering code to generate optical properties for dust, and these are shown in Fig. 11.3. The spectral dependence of the mass-specific extinction coefficient is mainly affected by the size distribution, with the spectral signature of extinction being fairly flat for both cases. This is because of the presence of particles across much of the size range. However, extinction decreases substantially at even longer wavelengths than shown here for the transported case (but not in the desert case), because fewer coarse particles are present resulting in lower MECs at longer wavelengths. MECs are higher for the transported case because a larger

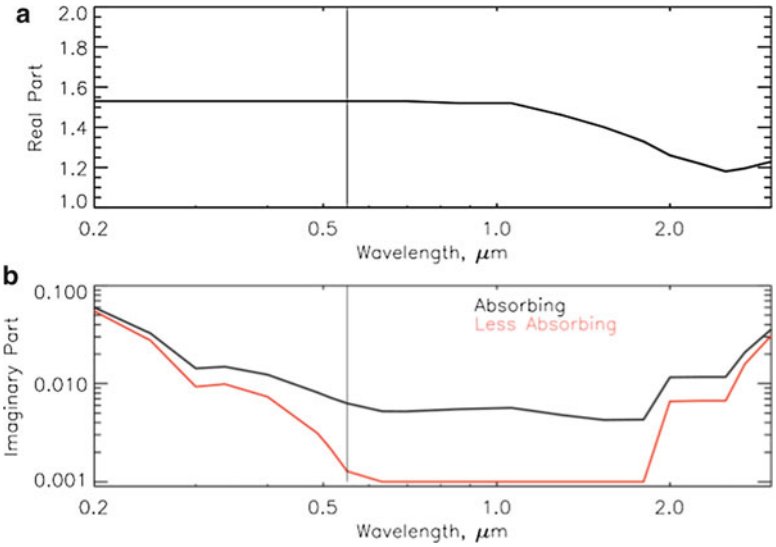

Fig. 11.2 Refractive indices of dust ((**a**) real part, (**b**) imaginary part) from Otto et al. (2007) (*black lines*). Values are averaged from data in the literature. *Red line* shows imaginary part with 0.005 subtracted to create a less absorbing dust type

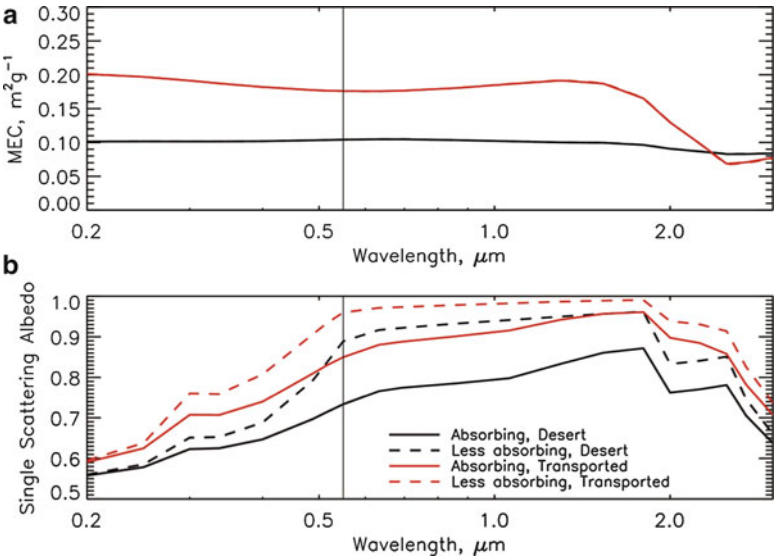

Fig. 11.3 Optical properties of dust for refractive indices and size distributions shown in Figs. 11.1 and 11.2. (**a**) Spectral mass-specific extinction coefficient (*MEC*). (**b**) Spectral single-scattering albedo. *Black lines* represent size distributions close to sources; *red lines* represent transported dust size distributions. *Solid lines* are for an absorbing refractive index; *dashed lines* are for a less absorbing refractive index

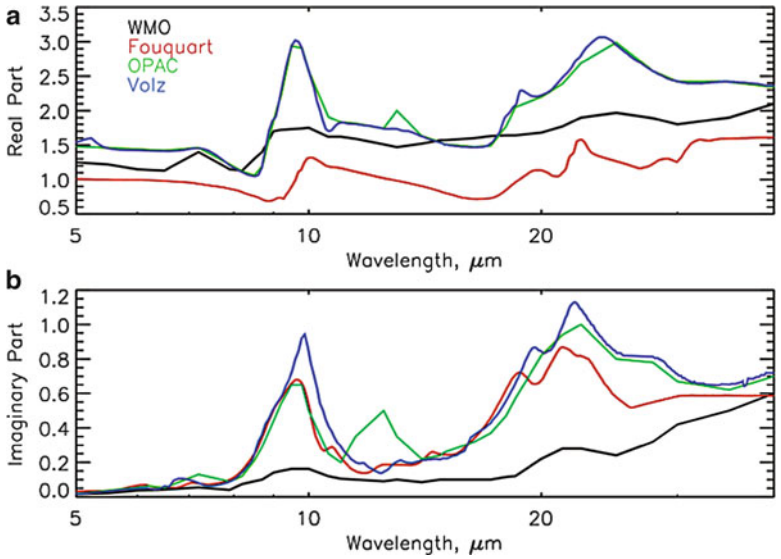

Fig. 11.4 Dust refractive indices in the terrestrial spectrum from WMO (WCP 1986) (*black*), Fouquart et al. (1987) (*red*), OPAC Hess et al. (1998) (*green*) and Volz (1973) (*blue*)

number of smaller particles are present, which interact more with the incident solar wavelengths. Changing the imaginary part of the refractive index does not affect the extinction significantly.

The SSA is notably lower towards the smaller wavelengths in the UV (indicating greater absorption), due to the higher imaginary refractive indices here. It is also sensitive to the size that also affects the amount of absorption. The more absorbing refractive index results in lower SSA values (solid lines). The size distribution with a greater number concentration of larger particles also results in lower SSA values (black lines). Therefore, the absorption properties of dust are sensitive to both the dust composition, and hence dust source region (via the imaginary part of the refractive index; see Chap. 3), and the size distribution, which is related to several factors including dust grain size at the source, uplift mechanism and strength and ageing processes such as deposition, dispersion and coagulation (see Chap. 4). Values shown in Fig. 11.3 at 550 nm wavelength range from 0.73 to 0.96, but higher values up to 0.99 have also been measured (Johnson and Osborne 2011) (see also Sect. 11.2.4).

Due to the large particle sizes present in mineral dust aerosol, dust also interacts effectively with LW radiation. As with SW radiation, the characteristics of dust optical properties in the IR are a function of the composition, the size distribution and the particle shape. Composition can be characterised shown by the complex refractive index, as in Fig. 11.4. Here, refractive indices from a number of different studies are shown, including Volz (1973) (Saharan dust transported to Barbados) and Fouquart et al. (1987) (sand in Niger), based on chemical analysis of samples.

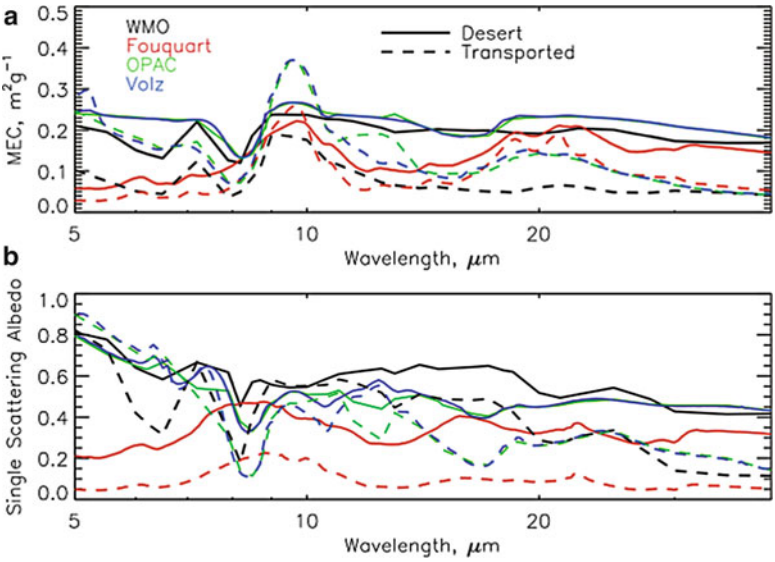

Fig. 11.5 Dust optical properties ((**a**) mass-specific extinction coefficient, MEC. (**b**) Single-scattering albedo) in the terrestrial spectrum for different refractive indices (*colours*) and size distributions, as shown in Fig. 11.1 for desert dust (*solid lines*) and transported dust (*dashed lines*)

Also shown are refractive indices from the Optical Properties of Aerosols and Clouds (OPAC) database (Hess et al. 1998), intended to represent a mixture of clay and quartz, and from the World Meteorological Organization (WMO) (WCP 1986) as these are frequently used in numerical prediction and climate models. All four representations show different values across the spectrum. This is likely to be due to differing compositions of dust, for example, the peak in absorption between 9 and 10 μm is caused by the absorption properties of various minerals with high absorption here, such as quartz, silicates, gypsum and calcite (e.g. Hansell et al. 2011), whilst the peak displayed in the OPAC refractive indices (green, Fig. 14b) from 12 to 13 μm is dominated by quartz.

As with the SW spectrum, LW spectral optical properties can be calculated using a Mie scattering code, assuming the dust particles are spheres, for the two different size distributions shown in Fig. 11.1 and the four refractive indices shown in Fig. 11.4. Figure 11.5 shows the contrasting optical properties that result. Some features can be traced back to the shape of the real part of the refractive index, such as peak extinction at 9.5 μm. Differences in SSA are related to the imaginary part of the refractive index that controls absorption. The lower WMO (black) values cause notably higher SSA values across the spectrum, whilst the reverse is true of the Fouquart data (red), though here the lower real part of the refractive index also contributes. The low real part of the Fouquart refractive index also creates lower mass-specific extinction coefficients compared to the other refractive indices. The transported size distribution containing fewer coarse particles (dashed line) results

in lower SSA values for each refractive index tested and lower MEC values across the spectrum, except around 9.5 μm. The spectral locations of the peaks in MEC and SSA can be important for remote sensing applications, which measure radiances across specific wavelength bands (e.g. Brindley et al. 2012), and in determining the magnitude of the LW direct aerosol effect, including effects on land and sea surface temperatures.

11.2.4 Measurements of Single-Scattering Albedo

As discussed earlier in this chapter, the SSA is crucial for determining the sign of radiative forcing due to aerosol. In contrast to most other aerosol types, the SSA for dust increases, or is almost constant, with wavelength due to the contribution from large particles. This spectral contrast can be used to distinguish dust from other types of aerosol. However, it is a troublesome quantity to measure. Table 11.1 shows the range of SSA found for dust in the existing literature, and it is not trivial to account for this wide range. Many factors, including source of dust, age since uplift, size distribution and measurement technique, can contribute. SSA calculated using scattering theory and the full size distribution, including the coarse mode, tend to be considerably lower than those reported as derived from airborne nephelometer measurements. In our experience, much of this difference can be accounted for, if it is assumed that the coarse mode particles do not enter the measurement apparatus and therefore that the scattering measured by most airborne nephelometers at least is only due to the sub-micron component of dust (Ryder et al. 2013). Sokolik and Toon (1999) demonstrate that the SSAs for a variety of mineral particles with radius 0.7 μm are up to 0.15 lower than the values for particles with radius 0.5 μm and up to 0.25 lower than those for particles with radius 0.25 μm. The SSAs reported from sun photometers such as AERONET tend to be lower than those from the other methods, although the reason for this is unclear.

Regardless of the absolute accuracy of one method compared to another, when the same methods are used, the SSA of dust can be seen to vary between locations. For example, Su and Toon (2011) show higher SSA close to sources in the Gobi Desert compared to source regions in the Sahara, whilst Koven and Fung (2006) show SSA variations within the latter region. Mineral composition of dust is discussed in detail in Chap. 2, but of particular interest here is the study by Moosmüller et al. (2012). Considering dust from a range of locations in the Middle East and Africa, they showed that the SSA of the accumulation mode at 405 nm was substantially lower than that at 870 nm and, at both wavelengths, is linearly correlated with the iron content. However, particularly in Asia, the dust is often mixed with other aerosol, and since this usually has an absorbing component (contributed by soot particles), this too can lead to a reduction in SSA.

Table 11.1 Single-scattering albedo of mineral dust from recent campaigns and literature

Location/campaign	SSA (uncertainty)	Reference	Notes
Sahara/North Africa			
Morocco (SAMUM)	0.8	Otto et al. (2009)	Full size distribution
SAMUM-1	0.82	Müller et al. (2010)	Full size distribution
SAMUM-1	0.9–0.95	Müller et al. (2012)	AERONET and other, peak of frequency distribution
SAMUM-2 Cape Verde	0.96	Müller et al. (2011)	Cape Verde
Mauritania (FENNEC 2011)	0.86–0.97	Ryder et al. (2013)	Full size distribution
Saharan dust plume	0.75–0.96	Otto et al. (2007)	Full size distribution
Mauritania (FENNEC 2011)	0.95–0.98	Ryder et al. (2013)	Nephelometer, airborne
Niger (DABEX)	0.99 (0.02)	Osborne et al. (2008)	Nephelometer, airborne
Senegal and Mauritania (DODO1)	0.99 (0.004)	McConnell et al. (2008)	Nephelometer, airborne
SHADE	0.97 (0.02)	Osborne et al. (2008)	Nephelometer, airborne
Eastern Atlantic (NAMMA)	0.97 (0.02)	Chen et al. (2011)	Nephelometer, airborne
North Africa and Arabian peninsula	0.9444 (0.005)	Kim et al. (2011)	AERONET
Mediterranean	0.85	Meloni et al. (2006)	Shadowband radiometer
Sahara (5 stations) + solar village	0.915[1]	Giles et al. (2012)	AERONET and remote sensing clustering
Sahara (GERBILS)	0.92–0.99	Johnson and Osborne (2011)	Nephelometer, airborne
Sahara (close to source)	0.92	Su and Toon (2011)	AERONET
Cape Verde	0.98[2] (0.01)	Dubovik et al. (2002)	AERONET
Middle East			
Iran, dust storm from Tigris/Euphrates	0.95[2]	Masoumi et al. (2013)	Sun photometer

(continued)

Table 11.1 (continued)

Location/campaign	SSA (uncertainty)	Reference	Notes
Middle East	0.96	Moosmüller et al. (2012)	Nephelometer and similar instrumentation
Bahrain-Persian Gulf	0.95[2] (0.03)	Dubovik et al. (2002)	AERONET
Solar Village (Saudi Arabia)	0.96[2] (0.02)	Dubovik et al. (2002)	AERONET
Asia			
Asia – long-range transport 0.85–0.975	0.935–0.955	Jung et al. (2010)	From nephelometer, mixed aerosol
China – dust days	0.92–0.955[3]	Yu et al. (2011)	AERONET, likely mixed aerosol
Gobi Desert	0.96	Su and Toon (2011)	AERONET, close to source

All values reported at 550 nm wavelength unless otherwise specified. (1) at 440 nm, (2) at 870 nm and (3) at 670 nm. Note that values of single-scattering albedo at solar wavelengths for individual minerals contained in desert dust and at a variety of sizes can be found in Sokolik and Toon (1999)

11.3 Measurements and Estimates of Radiative Effect

The assessments of the RE of mineral dust can be made either from observations or from models. Some of the challenges in estimating the radiative forcing due to dust are discussed in Weaver et al. (2002). Here, we define the RE as the instantaneous change in radiative flux due to the presence of dust compared to a no-dust atmosphere. It can be defined at the TOA, at the surface and for the atmosphere itself. Table 11.2 gives some recent estimates of dust RE in both the SW and LW from both model estimates and observations.

There are many more observations of RE and efficiency in the SW available than in the LW, and most of the LW observations are of Saharan dust. The SW effect depends crucially on whether the dust is over land or ocean – the efficiency being greater over the dark surface of the ocean. Several of the studies included in Table 11.2 compare the SW and LW radiative effects. However, it is important to note that the balance between different parts of the spectrum varies over the day, and this diurnal averaging must be done with care. It is also apparent from Table 11.2 that radiative efficiency in plumes of dust can be considerably larger than that measured over longer temporal timescales. Thus, comparing different studies is challenging. In the LW at least there does seem to be some consistency across measurements in that the LW efficiency at the TOA is between about 10 and 20 Wm^{-2} per unit AOD.

It is interesting to note that there are very few measurements of dust radiative efficiency, particularly in the LW, in Asia and Australia. We would benefit from further measurements in these regions in particular. Although the Sahara is the largest dust source, Australia is a significant source of dust for the southern

Table 11.2 Measurements of LW and SW radiative efficiency of dust

Location/campaign/method	SW efficiency			LW efficiency			Reference
	TOA	Surface	Atm	TOA	Surface	Atm	
North Africa							
Sahara (observed RE from CERES)	−35	−65					Li et al. (2004)
Sahara (RE from composition measurements, modelled distribution)	−45 to −39						Balkanski et al. (2007)
Saharan plume (observed optical properties SHADE)	−24						Anderson et al. (2005)
Saharan plume (observed optical properties and RE from SHADE)		−38					Haywood et al. (2003)
Saharan plume (observed optical properties and RE from SHADE)					11		Highwood et al. (2003)
Saharan dust (retrieved AOD from NAMMA)				13	2–10		Hansell et al. (2010)
SAMUM – sea (observed optical properties)		−81					Ansmann et al. (2011)
SAMUM – land (observed optical properties)		−10					Ansmann et al. (2011)
Mediterranean plume (2 days, observed RE)	−78	−140	62	11.5	28	−15	Di Sarra et al. (2011)
Sahara (observed optical properties, GERBILS)				17			Osborne et al. (2011)
Sahara (satellite obs)				16–20			Brindley and Russell (2009)
Middle East							
Cairo – April (observed RE)	−60 (20)	−180 (50)	122 (45)				El-Metwally et al. (2011)
Asia							
China – near source (observed optical properties and AOD)		−60		17–21	31–35		Hansell et al. (2012)
China – dust event (observed RE)		−80	50				Liu et al. (2011)
ACE-ASIA (observed RE)					0–10		Vogelmann et al. (2003)
India (observed optical properties)	−14	−66					Sharma et al. (2012)

Radiative efficiencies are in Wm^{-2} (per unit AOD). Studies use a range of methodologies, including observing the radiative effect (RE), observing the optical properties and AOD and then calculating RE or observing the optical properties and using these in global models

hemisphere, and one where in the past it has been a challenge for models to represent dust uplift and transport correctly. The problem in Asia is that pure mineral dust is almost never observed except very close to source; the numerous anthropogenic sources of aerosol result in a mixture in the fine mode at most times of year. However, the dust is a dominant contributor to the coarse mode even when mixed with anthropogenic aerosol.

11.4 Implications of Dust-Radiation Interactions for Satellite Retrievals

Satellites observe radiation at the TOA and apply radiative transfer models and estimates of aerosol properties to retrieve aerosol properties and, for example surface temperature. Thus, inadequate modelling or identification of the presence of dust which alters radiation in both the short-wave and the long-wave can lead to biases. For example, Highwood et al. (2003) demonstrated a likely effect of greater than 3 K consistent with dust outbreaks on eastern Atlantic sea surface temperatures retrieved by AVHRR, whilst Weaver et al. (2002) showed that the effect of dust in producing a systematic bias between assimilation temperatures and actual surface temperatures can lead to problems with long-wave radiation in model simulations that are nudged towards observations.

However, there are also issues with determining from satellites how much dust is in the atmosphere in the first place. Particularly over land, there remain some significant differences in the AOD retrieved from different instruments (e.g. Carboni et al. 2012). The accuracy of the quantity retrieved in regions affected by airborne dust can be affected by the optical properties assumed chosen for the dust, in particular the phase function. Figure 11.6 shows the impact of differing refractive indices (such as might be produced by differing dust composition) on the widely used SEVIRI RGB Dust product. In this product, the degree of "pinkness" represents the amount of dust in the atmosphere (as atmospheric dust load increases, the signal in the 10.8 μm channel that is used in the RGB Dust product tends to be suppressed more rapidly than the blue and red channels, and thus, the RGB Dust product becomes pink in colour). The "pinkness" of the RGB Dust product, which is related to dust load, is reproduced here as a function of temperature differences between different channels. For specific cases of dust and atmospheric conditions and for several different commonly used refractive indices, the expected temperatures are calculated and plotted on the coloured picture. As dust AOD increases (towards the most pink part of Fig. 11.6), if the retrieval uses the optical model of Fouquart et al. (1987) (crosses), the scene is much more likely to be described as dusty than if the OPAC model (Hess et al. 1998) is used. The effect of size distribution is less significant. A more comprehensive treatment of this subject can be found in studies such as Brindley et al. (2012) and Bulgin et al. (2011).

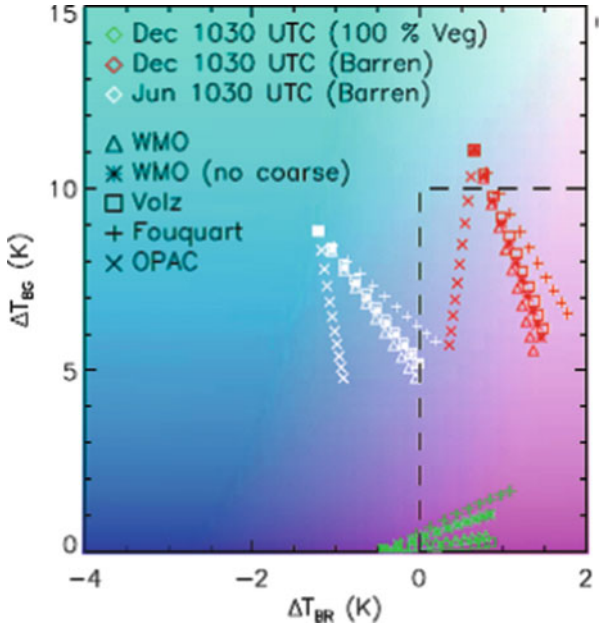

Fig. 11.6 Two-dimensional graphic depiction of RGB rendering showing colours as functions of the difference in brightness temperature between the 12 and 10.8 μm channel ($T_{B120} - T_{B108}$ (ΔT_{BR})) and a similar difference between the 10.8 and 8.7 μm channels ($T_{B108} - T_{B087}$ (ΔT_{BG})) with simulations using varying aerosol optical properties (*symbols*) for specific atmospheric conditions (*colours*). The different colours represent three different sets of land surface and atmospheric conditions, whilst the different symbols represent different refractive indices being used in the retrieval (Reproduced from Figure 6b of Brindley et al. 2012)

11.5 Dust and Visibility

Up to this point, we have considered the radiative effect of dust in scattering radiation in the framework of the Earth's energy balance. However, another way in which the interaction of dust and radiation manifests itself in the Earth's system is through the substantial reduction of visibility at ground level. Not only does this have impact on activities at the surface, but monitoring of visibility provides an alternative measurement of dust. However, although there are links between the column AOD measured from the ground or space and visibility, Mahowald et al. (2007) showed that AERONET AOD and visibility data are only moderately correlated in dusty regions. If the dust is elevated, a high AOD does not always mean low visibility at the ground. Conversely, we can imagine a case where there is very localised surface dust event that significantly reduces visibility on the ground, but does not give a substantial AOD.

11.6 Implications for Including the Radiative Impact of Dust in Models

It is important that we have confidence in our ability to model the interaction of dust with radiation, since dust responds to climate change induced by other forcings and is therefore an important feedback mechanism on a wide range of spatial and temporal scales (Chaps. 13, 16, 17 and 18). Changes in soil moisture, vegetation cover, source areas and circulation patterns could result in significant changes in dust concentrations. Recent assessments of the anthropogenic contribution to dust lie around 25 % globally (Ginoux et al. 2012). 8 % of this comes from the Sahel, and 13 % from Australia (although 75 % of Australia's total dust is anthropogenic). Dust sources created by cultivation may increase in the future as the need for food rises with the growing population. Thus, dust forcing may increase due to higher dust burden in the atmosphere. Additionally, anthropogenic aerosol emissions are projected to decrease in the future (Lamarque et al. 2011), although the extent to which these projections will be realised is a matter of some debate.

The current approach taken to include the radiative impact of dust in models depends on the application and the level of complexity of the dust scheme in the radiation, climate or NWP model concerned (see Chaps. 9 and 10 for the latter two). In general, all models require some specification of scattering and absorption efficiency and phase function or asymmetry parameter. Since these properties are a function of size, many climate models with interactive dust schemes use size-based pre-computed look-up tables of optical properties. Thus, the optical properties of dust can to some extent evolve within the model in so far as the size distribution changes. However, most models use only a limited number (or even one) of assumption of refractive index, which implies a uniform dust composition. Studies such as Su and Toon (2011) and Moosmüller et al. (2012) suggest that this is likely to be inappropriate globally or even regionally, but to do otherwise is likely to be computationally expensive as models will need to track the transport of individual minerals or at least the hematite fraction. Current research can more realistically assess the sensitivity of radiative effects, temperature changes, heating rate changes and other climate variables to the assumptions made concerning optical properties. Once this has been examined systematically in both weather and climate models and the results evaluated against observations, we will have a clearer idea of the properties and processes that need further observation or understanding.

The increasing numbers of in situ observations of dust radiative properties such as highlighted in this chapter and the size distribution and composition understanding discussed elsewhere in this volume clearly go some way to providing data for model evaluation (e.g. Greed et al. 2008). However, for many areas of the globe, the best prospect for enhanced observations is via satellites, not least because many of the regions where dust is the primary aerosol are logistically and physically challenging places to work. This approach will have its own challenges, not least the inconvenient fact that dust sources tend to be located within unvegetated desert regions where the surface is bright and satellite retrievals are difficult.

The appropriate choice of wavelength-dependent dust optical properties is itself crucial in making these remotely sensed observations, and thus, our work is far from done.

References

Anderson TL, Charlson RJ, Bellouin N, Boucher O, Chin M, Christopher SA, Haywood J, Kaufman YJ, Kinne S, Ogren JA, Remer LA, Takemura T, Tanre D, Torres O, Trepte CR, Wielicki BA, Winker DM, Yu AH (2005) An "A-Train" strategy for quantifying direct climate forcing by anthropogenic aerosols. Bull Am Meteorol Soc 86(12):1795–1809. doi:10.1175/BAMS-86-12-1795

Ansmann A, Petzold A, Kandler K, Tegen I, Wendisch M, Muller D, Weinzierl B, Mueller T, Heintzenberg J (2011) Saharan mineral dust experiments SAMUM-1 and SAMUM-2: what have we learned? Tellus Ser B Chem Phys Meteorol 63(4):403–429. doi:10.1111/j.1600-0889.2011.00555.x

Balkanski Y, Schulz M, Claquin T, Guibert S (2007) Reevaluation of mineral aerosol radiative forcings suggests a better agreement with satellite and AERONET data. Atmos Chem Phys 7:81–95

Bohren CF, Huffman DR (1983) Absorption and scattering of light by small particles. Wiley, New York

Brindley HE, Russell JE (2009) An assessment of Saharan dust loading and the corresponding cloud-free longwave direct radiative effect from geostationary satellite observations. J Geophys Res-Atmos 114, ISSN:2169-897X

Brindley H, Knippertz P, Ryder C, Ashpole I (2012) A critical evaluation of the ability of the Spinning Enhanced Visible and Infrared Imager (SEVIRI) thermal infrared red-green-blue rendering to identify dust events: theoretical analysis. J Geophys Res Atmos 117, D07201. doi:10.1029/2011JD017326

Bulgin CE, Palmer PI, Merchant CJ, Siddans R, Gonzi S, Poulsen CA, Thomas GE, Sayer AM, Carboni E, Granger RG, Highwood E, Ryder CL (2011) Quantifying the response of the ORAC aerosol optical depth retrieval for MSG SEVIRI to aerosol model assumptions. J Geophys Res Atmos 116, D05208. ISSN 0148-0227, doi:10.1029/2010JD014483

Carboni E, Thomas GE, Sayer AM, Siddans R, Poulsen CA, Grainger RG, Ahn C, Antoine D, Bevan S, Braak R, Brindley H, Desouza-Machado S, Deuze JL, Diner D, Ducos F, Grey W, Hsu C, Kalashnikova OV, Kahn R, North PRJ, Salustro C, Smith A, Tanre D, Torres O, Veihelmann B (2012) Intercomparison of desert dust optical depth from satellite measurements. Atmos Meas Tech 5:1973–2002. doi:10.5194/amt-5-1973-2012

Chen G, Ziemba LD, Chu DA, Thornhill KL, Schuster GL, Winstead EL, Diskin GS, Ferrare RA, Burton SP, Ismail S, Kooi SA, Omar AH, Slusher DL, Kleb MM, Reid JS, Twohy CH, Zhang H, Anderson BE (2011) Observations of Saharan dust microphysical and optical properties from the Eastern Atlantic during NAMMA airborne field campaign. Atmos Chem Phys 11:723–740. doi:10.5194/acp-11-723-201

Di Sarra A, Di Biagio C, Meloni D, Monteleone F, Pace G, Pugnaghi S, Sferlazzo D (2011) Shortwave and longwave radiative effects of the intense Saharan dust event of 25–26 March 2010 at Lampedusa (Mediterranean Sea). J Geophys Res 116, D23209. doi:10.1029/2011JD016238

Dubovik O, Holben B, Eck TF, Smirnov A, Kaufman YJ, King MD, Tanre D, Slutsker I (2002) Variability of absorption and optical properties of key aerosol types observed in worldwide locations. J Atmos Sci 59:590–608

El-Metwally M, Alfaro SC, Wahab MMA, Favez O, Mohamed Z, Chatenet B (2011) Aerosol properties and associated radiative effects over Cairo (Egypt). Atmos Res 99:263–276. doi:10.1016/j.atmosres.2010.10.017

Fouquart Y, Bonnel B, Brogniez G, Buriez JC, Smith L, Morcrette JJ, Cerf A (1987) Observations of Saharan aerosols – results of Eclats field experiment. 2. Broad-band radiative characteristics of the aerosols and vertical radiative flux divergence. J Clim Appl Meteorol 26:38–52

Giles DM, Holben BN, Eck TF, Sinyuk A, Smirnov A, Slutsker I, Dickerson RR, Thompson AM, Schafer JS (2012) An analysis of AERONET aerosol absorption properties and classifications representative of aerosol source regions. J Geophys Res 117, D17203. doi:10.1029/2012JD018127

Ginoux P, Prospero JM, Gill TE, Hsu NC, Zhao M (2012) Global-scale attribution of anthropogenic and natural dust sources and their emission rates based on MODIS Deep Blue aerosol products. Rev Geophys 50, RG3005. doi:10.1029/2012RG000388

Greed G, Haywood JM, Milton S, Keil A, Christopher S, Gupta P, Highwood EJ (2008) Aerosol optical depths over North Africa: 2. Modeling and model validation. J Geophys Res 113:D00C05. doi:10.1029/2007JD009457

Haapanala P, Räisänen P, Kahnert M, Nousiainen T (2012) Sensitivity of the shortwave radiative effect of dust on particle shape: comparison of spheres and spheroids. J Geophys Res 117, D08201. doi:10.1029/2011JD017216

Hansell RA, Reid JS, Tsay SC, Roush TL, Kalashnikova OV (2011) A sensitivity study on the effects of particle chemistry, asphericity and size on the mass extinction efficiency of mineral dust in the earth's atmosphere: from the near to thermal IR. Atmos Chem Phys 11:1527–1547

Hansell RA, Tsay SC, Ji Q, Hsu NC, Jeong MJ, Wang SH, Reid JS, Liou KN, Ou SC (2010) An assessment of the surface longwave direct radiative effect of airborne Saharan dust during the NAMMA field campaign. J Atmos Sci 67:1048–1065. doi:10.1175/2009JAS3257.1

Hansell RA, Tsay S-C, Hsu NC, Ji Q, Bell SW, Holben BN, Welton EJ, Roush TL, Zhang W, Huang J, Li Z, Chen H (2012) An assessment of the surface longwave direct radiative effect of airborne dust in Zhangye, China, during the Asian Monsoon Years field experiment (2008). J Geophys Res 117

Haywood JM, Francis P, Osborne S, Glew M, Loeb N, Highwood EJ, Tanre D, Myhre G, Formenti P (2003) Radiative properties and direct effect of Saharan dust measured by C-130 aircraft during SHADE. 1. Solar spectrum. J Geophys Res Atmos 108 (art. no.-8). doi:10.1029/2002JD002687

Hess M, Koepke P, Schult I (1998) Optical properties of aerosols and clouds: the software package OPAC. Bull Am Meteorol Soc 79:831–844

Highwood EJ, Haywood JM, Silverstone MD, Newman SM, Taylor JP (2003) Radiative properties and direct effect of Saharan dust measured by the C-130 aircraft during Saharan Dust Experiment (SHADE): 2. Terrestrial spectrum. J Geophys Res Atmos 108 (art. no.-8). doi:10.1029/2002JD002552

Johnson BT, Osborne SR (2011) Physical and optical properties of mineral dust aerosol measured by aircraft during the GERBILS campaign. Q J Roy Meteorol Soc 137:1117–1130

Jung J, Kim YJ, Lee KY, Cayetano MG, Batmunkh T, Koo J-H, Kim J (2010) Spectral optical properties of long-range transport Asian dust and pollution aerosols over Northeast Asia in 2007 and 2008. Atmos Chem Phys 10:5391–5408

Kandler K, Schutz L, Deutscher C, Ebert M, Hofmann H, Jäckel S, Jaenicke R, Knippertz P, Lieke K, Massling A, Petzold A, Schladitz A, Weinzierl B, Wiedensohler A, Zorn S, Weinbruch S (2009) Size distribution, mass concentration, chemical and mineralogical composition and derived optical parameters of the boundary layer aerosol at Tinfou, Morocco, during SAMUM 2006. Tellus Ser B Chem Phys Meteorol 61:32–50

Kim D, Chin M, Yu H, Eck TF, Sinyuk A, Smirnov A, Holben BN (2011) Dust optical properties over North Africa and Arabian Peninsula derived from the AERONET dataset. Atmos Chem Phys 11:10733–10741

Koven CD, Fung I (2006) Inferring dust composition from wavelength-dependent absorption in Aerosol Robotic Network (AERONET) data. J Geophys Res 111, D14205. doi:10.1029/2005JD006678

Lamarque J-F, Page Kyle G, Meinshausen M, Riahi K, Smith S, van Vuuren DP, Conley AJ, Vitt F (2011) Global and regional evolution of short-lived radiatively-active gases and aerosols in the representative concentration pathways. Clim Change 109(1–2):191–212

Li F, Vogelmann AM, Ramanathan V (2004) Saharan dust aerosol radiative forcing measured from space. J Clim 17:2558–2571

Liu Y, Huang J, Shi G, Takamura T, Khatri P, Bi J, Shi J, Wang T, Wang X, Zhang B (2011) Aerosol optical properties and radiative effect determined from sky-radiometer over Loess Plateau of Northwest China. Atmos Chem Phys 11:11455–11463. doi:10.5194/acp-11-11455-2011

Mahowald NM, Ballntine JA, Feddema J, Ramankutty N (2007) Global trends in visibility: implications for dust sources. Atmos Chem Phys 7:3309–3339

Masoumi A, Khalesifard HR, Bayat A, Moradhaseli R (2013) Retrieval of aerosol optical and physical properties from ground-based measurements for Zanjan, a city in Northwest Iran. Atmos Res 120–121:343–355

Mcconnell CL, Highwood EJ, Coe H, Formenti P, Anderson B, Osborne S, Nava S, Desboeufs K, Chen G, Harrison MAJ (2008) Seasonal variations of the physical and optical characteristics of Saharan dust: results from the Dust outflow and Deposition to the Ocean (DODO) experiment. J Geophys Res 113, D14S05. ISSN 0148-0227, doi: 10.1029/2007JD009606

Mcconnell CL, Formenti P, Highwood EJ, Harrison MAJ (2010) Using aircraft measurements to determine the refractive index of Saharan dust during the DODO experiments. Atmos Chem Phys 10:3081–3098

Meloni D, Di Sarra A, Pace G, Monteleone F (2006) Aerosol optical properties at Lampedusa (Central Mediterranean). 2. Determination of single scattering albedo at two wavelengths for different aerosol types. Atmos Chem Phys 6:715–727

Mona L, Liu Z, Muller D, Omar A, Papayannis A, Pappalardo G, Sugimoto N, Vaughan M (2012) Lidar measurements for desert dust characterization: an overview. Adv Meteorol, Article ID 356265, 36 p. doi:10.1155/2012/356265

Moosmüller H, Engelbrecht JP, Skiba M, Frey G, Chakrabarty RK, Arnott WP (2012) Single scattering albedo of fine mineral dust aerosols controlled by iron concentration. J Geophys Res 117, D11210. doi:10.1029/2011JD016909

Müller T, Schladitz A, Kandler K, Wiedensohler A (2011) Spectral particle absorption coefficients, single scattering albedos, and imaginary parts of refractive indices from ground based in-situ measurements at Cape Verde Island during SAMUM-2. Tellus 63B:573–588. doi:10.1111/j.1600-0889.2011.00572.x

Müller D, Weinzierl B, Petzold A, Kandler K, Ansmann A, Müller T, Tesche M, Freudenthaler V, Esselborn M, Heese B, Althausen D, Schladitz A, Otto S, Knippertz P (2010) Mineral dust observed with AERONET Sun photometer, Raman lidar, and in situ instruments during SAMUM 2006: shape-independent particle properties. J Geophys Res Atmos 115, D07202. doi:10.1029/2009JD012520

Müller D et al (2012) Comparison of optical and microphysical properties of pure Saharan mineral dust observed with AERONET Sun photometer, Raman lidar, and in situ instruments during SAMUM 2006. J Geophys Res 117, D07211. doi:10.1029/2011JD016825

Osborne SR, Baran AJ, Johnson BT, Haywood JM, Hesse E, Newman S (2011) Short-wave and long-wave radiative properties of Saharan dust aerosol. Q J R Meteorol Soc 137:1149–1167. doi:10.1002/qj.771

Osborne SR, Johnson BT, Haywood JM, Baran AJ, Harrison MAJ, Mcconnell CL (2008) Physical and optical properties of mineral dust aerosol during the dust and biomass-burning experiment. J Geophys Res 113, D00C03. doi:10.1029/2007JD009551

Otto S, De Reus M, Trautmann T, Thomas A, Wendisch M, Borrmann S (2007) Atmospheric radiative effects of an in situ measured Saharan dust plume and the role of large particles. Atmos Chem Phys 7:4887–4903

Otto S, Bierwirth E, Weinzierl B, Kandler K, Esselborn M, Tesche M, Schladitz A, Wendisch M, Trautmann T (2009) Solar radiative effects of a Saharan dust plume observed during SAMUM assuming spheroidal model particles. Tellus 61B:270–296

Ryder CL, Highwood EJ, Rosenberg P, Trembath J, Brooke J, Bart M, Dean A, Crosier J, Dorsey J, Brindley H, Banks JR, Marsham JH, Mcquaid JB, Sodemann H, Washington R (2013) Optical properties of Saharan dust aerosol and contribution from teh coarse mode as measured during the Fennec 2011 aircraft campaign. Atmos Chem Phys 13:303–325

Sharma D, Singh D, Kaskaoutis DG (2012) Impact of two intense dust storms on aerosol characteristics and radiative forcing over Patiala, Northwestern India. Adv Meteorol. Article Number: 956814. doi:10.1155/2012/956814

Sokolik IN, Toon OB (1999) Incorporation of mineralogical composition into models of the radiative properties of mineral aerosol from UV to IR wavelengths. J Geophys Res 104(d8):9423–9444

Su L, Toon OB (2011) Saharan and Asian dust: similarities and differences determined by CALIPSO, AERONET, and a coupled climate-aerosol microphysical model. Atmos Chem Phys 11:3263–3280

Vogelmann AM, Flatau PJ, Szczodrak M, Markowicz KM, Minnett PJ (2003) Observations of large aerosol infrared forcing at the surface. Geophys Res Lett 30(12):1655. doi:10.1029/2002GL016829

Volz FE (1973) Infrared optical-constants of ammonium sulfate, Sahara dust, volcanic pumice, and flyash. Appl Optics 12:564–568

Weaver CJ, Ginoux P, Hsu NC, Chou M-D, Joiner J (2002) Radiative forcing of Saharan dust: GOCART model simulations compared with ERBE data. J Atmos Sci 59:736–747

World Climate Program (WCP) (1986) A preliminary cloudless standard atmosphere for radiation computation. World Meteorological Organisation, Geneva

Yang P, Feng Q, Hong G, Kattawar GW, Wiscombe WJ, Mishchenko MI, Dubovik O, Laszlo I, Sokolik IN (2007) Modelling of the scattering and radiative properties of nonspherical dust-like aerosols. Aerosol Sci 38:995–1014

Yu XN, Zhu B, Yin Y, Yang J, Li YW, Bu XL (2011) A comparative analysis of aerosol properties in dust and haze-fog days in a Chinese urban region. Atmos Res 99:241–247. doi:10.1016/j.atmosres.2010.10.015

Chapter 12
Mineral Dust and its Microphysical Interactions with Clouds

Athanasios Nenes, Benjamin Murray, and Aikaterini Bougiatioti

Abstract Our understanding of the interactions of aerosols and clouds has a strong heritage in laboratory experiments, field measurements, and process modeling. We present a review on the state of knowledge for mineral dust emitted from major global dust source regions. Laboratory studies and field measurements have given insights on processes and mechanisms taking place when mineral dust is released into the atmosphere and reacts with the atmospheric constituents. Furthermore, theoretical approaches and parameterizations have been established to interpret the observations and quantitatively express the mechanisms by which dust can act as cloud condensation nuclei (CCN) and ice nuclei (IN). Finally, model simulations have been used in order to study the effects of dust particles to different aerosol-cloud-climate interactions. Dust can act as efficient CCN in clouds solely based on their relatively large size combined with the hydrophilicity from the adsorption of water vapor on their insoluble core. When mixed with even small fractions of hygroscopic material from emission or atmospheric processing, their hygroscopicity and

A. Nenes (✉)
School of Earth and Atmospheric Sciences, Georgia Institute of Technology, Atlanta, GA, USA

School of Chemical and Biomolecular Engineering, Georgia Institute of Technology, Atlanta, GA, USA

Institute of Chemical Engineering Sciences (ICE-HT), FORTH, Patras, Greece
e-mail: Athanasios.Nenes@gatech.edu

B. Murray
Institute for Climate and Atmospheric Science, School of Earth and Environment, University of Leeds, Leeds LS2 9JT, UK
e-mail: B.J.Murray@leeds.ac.uk

A. Bougiatioti
School of Earth and Atmospheric Sciences, Georgia Institute of Technology, Atlanta, GA, USA

Laser Remote Sensing Laboratory, National Technical University of Athens, Athens, Greece
e-mail: katerina.bougiatioti@eas.gatech.edu

P. Knippertz and J.-B.W. Stuut (eds.), *Mineral Dust: A Key Player in the Earth System*, DOI 10.1007/978-94-017-8978-3_12,

CCN activity are significantly enhanced. The theoretical frameworks of adsorption activation and Köhler theory are presented to explain dust CCN activity, together with a summary on the potential contributions of dust to cloud droplet number concentration (CDNC), and its role in regulating supersaturation. Mineral dust aerosol is an effective IN and, combined with their concentration, can dominate ice production in cirrus and mixed-phase clouds even at great distances from source regions. The pathways to nucleation of ice are different for different cloud types and have distinct effects in those clouds. Our fundamental understanding of ice nucleation lags behind that for CCN activation, and a key challenge is that we cannot predict a priori which aerosol materials will make effective IN. Nevertheless, numerous field and laboratory studies have shown that mineral dust from deserts is one of the most important ice-nucleating aerosol types around the globe.

Keywords Cloud condensation nuclei • Ice nuclei • Water • Clouds • Hydrological cycle • Particles • Droplets • Cloud formation • Hygroscopicity • Warm clouds • Ice clouds • Laboratory experiments • Observations

12.1 CCN, IN, and Their Impacts on Clouds, the Hydrological Cycle, and Climate

Atmospheric aerosol particles originate from different sources with a wide compositional range, including soil and desert dust (see Chaps. 2 and 3), sea salt, volcanoes, biogenic activity, biomass burning, resource extraction activities, and burning of fossil fuels. Aerosol composition and size distribution are continuously modified in the atmosphere by the mixing of aerosol particles and their aging through interactions with clouds (see Chap. 4). The interactions of aerosols with clouds, radiation, and the hydrological cycle, referred to as "aerosol-cloud interactions," constitute the largest source of uncertainty in assessments of climate sensitivity and anthropogenic climate change (Boucher et al. 2013; Carslaw et al. 2013). Cloud feedbacks and the resulting buffered response of clouds and cloud systems pose a grand challenge in understanding the sign and magnitude of aerosol impacts on clouds (Stevens and Feingold 2009). Nevertheless, considerable progress in understanding the links between aerosol and clouds has been established and constitutes the physical basis upon which aerosol-cloud-climate interaction studies are carried out with.

Increasing concentrations of cloud condensation nuclei (CCN) in low-level stratus results in higher droplet concentrations and smaller droplet sizes relative to pristine clouds (Twomey 1977). These microphysical changes increase shortwave albedo and longwave emissivity (Penner et al. 2006; Lohmann et al. 2007; Kirkevag et al. 2008; Takemura et al. 2005; Ghan et al. 2001, 2012; Menon et al. 2002; Topping et al. 2013) and are less likely to form precipitation-size drops (Albrecht 1989), delay the onset of freezing, and decrease riming efficiency (Lohmann and Feichter 2005; Lance et al. 2011). Ice latent heating will increase the buoyancy

and vertical velocity strengths of updraft parcels (Andreae et al. 2004). Enhanced aerosol concentration may also increase the lifetime and vertical extent of clouds with important feedbacks on the hydrological cycle (Penner et al. 2006; Lohmann et al. 2007; Kirkevag et al. 2008; Menon et al. 2002; Andreae et al. 2004; Rosenfeld 2006; Rosenfeld et al. 2008). Increased concentration of large aerosol, termed giant CCN (GCCN), may act as efficient collector drops and promote the formation of precipitation (e.g., Woodcock 1950; Levin and Cotton 2008; Cheng et al. 2009). GCCN may also deplete supersaturation (the relative humidity exceeding 100 %) in the early stages of cloud formation and reduce the concentration of droplets that eventually form (Ghan et al. 1998), and strongly impact the sensitivity of droplets to submicron aerosol variations (Morales Betancourt and Nenes 2013). There is no strict size definition for what constitutes a GCCN, with sizes ranging between 1 and 10 μm radius (Mechem and Kogan 2008; Cheng et al. 2009). Increased aerosol may also enhance evaporation rates of droplets at cloud fringes, which may result in a negative buoyancy feedback from evaporative entrainment and reduce cloudiness (Xue and Feingold 2006).

Besides influencing cloud properties through nucleation of cloud droplets, some aerosol particles are capable of nucleating ice crystals. These ice-nucleating (IN) aerosol particles are rare in comparison with CCN with around one aerosol particle in a million capable of nucleating ice. This rarity has important implications for clouds. For example, in a supercooled liquid stratus cloud, only a small fraction of cloud droplets will or can freeze, but these ice crystals will then grow at the expense of the supercooled water droplets. Hence, the introduction of ice nuclei to a supercooled cloud therefore increases the hydrometeor size, reduces hydrometeor concentration, increases precipitation rates, reduces cloud lifetime, and decreases cloud shortwave reflectivity and longwave emissivity (Lohmann and Feichter 2005; Andreae et al. 2004; Rosenfeld 2006; Rosenfeld et al. 2008). Increases of IN can profoundly impact cirrus clouds, as IN form ice before the more populous supercooled haze droplets. As a consequence, the ice from IN strongly competes for water vapor with the supercooled drops, potentially reducing or completely inhibiting their freezing, with profound impacts on ice crystal number and size and hence cloud lifetime and longwave emissivity (e.g., Lohmann and Feichter 2005; Barahona and Nenes 2007, 2009; Barahona et al. 2010; Liu et al. 2012; Murray et al. 2010; Karcher and Lohmann 2003; Ren and Mackenzie 2005; Jensen et al. 2010; Gettelman et al. 2012). However, our quantitative understanding of ice formation in clouds remains poor. Apart from the technical difficulties in making accurate measurements of ice nuclei in the atmosphere, we lack a fundamental understanding of what makes an effective ice-nucleating particle; as a result, a general and practical theoretical framework in which to place laboratory and field measurements of ice nuclei is currently lacking and severely limits our predictive ability in aerosol-ice cloud studies. Nevertheless, several approaches to describing ice nucleation have been put forward (e.g., Barahona 2012; Khvorostyanov and Curry 2005; Hoose et al. 2010; Niedermeier et al. 2011b; Broadley et al. 2012; Connolly et al. 2009; Vali 1994; Herbert et al. 2014). A number of materials have been identified as ice nuclei including mineral dust, soot, bacteria, fungal spores, pollen, crystalline

soluble salts, glassy aqueous materials, and volcanic ash (Hoose and Möhler 2012; Murray et al. 2012). Of these, mineral dusts have been identified as one of the most important ice-nucleating aerosol types around the globe and in clouds ranging from mixed-phase wave clouds and stratus to cirrus clouds (Cziczo et al. 2013; Pratt et al. 2009; Baustian et al. 2012; Kamphus et al. 2010; DeMott et al. 2003b; Creamean et al. 2013).

Mineral dust is one of the most abundant components of particulate matter in the atmosphere, accounting for more than 50 % of the global aerosol mass load (Yin et al. 2002; Cakmur et al. 2006). Large amounts are annually emitted into the atmosphere by wind-driven erosion over arid and semiarid areas (Chap. 5), and it is observed even at the most remote regions of the world (Chap. 7). Source regions are found close to coastal regions, for example, the Atlantic Ocean and Mediterranean Sea neighboring northern Africa and the Arabian Peninsula, the Indian Ocean surrounding Australia, the Yellow Sea, and East China Sea located leeward to Eastern China (Chap. 3). Dust is also emitted close to anthropogenically influenced areas such as near industrial and/or highly populated cities. During their atmospheric transport, mineral dust particles form internally mixed particles through coagulation with other types of aerosol, heterogeneous reactions of gas species, and processing through clouds (Yamashita et al. 2011; Chap. 4). Due to this internal mixing, particles undergo profound changes in their size, shape, surface, and physical-chemical and optical properties, which affect atmospheric lifetime, radiative properties (Chap. 11), as well as their CCN and IN activity (e.g., Dentener et al. 1996; Sokolik et al. 2001; Kelly et al. 2007; Crumeyrolle et al. 2008; Cheng et al. 2009).

In this chapter, we discuss the role mineral dust plays in cloud microphysical processes. We first concentrate on the fundamentals of mineral dust CCN and IN and how to describe their activity. For CCN activity we discuss the role of condensable material versus water uptake on bare uncoated dusts, while for IN we address the various pathways of nucleation and how these pathways are relevant in different parts of the atmosphere. We then summarize field and laboratory studies of mineral dust CCN and IN before briefly discussing modeling studies of mineral dust interactions with clouds.

12.2 The CCN Activity of Mineral Dust

Cloud droplet formation depends on the condensation of water vapor on ambient aerosols under conditions that favor the formation of a liquid phase. The main physical-chemical principles involved in the transformation (“activation”) of CCN into cloud droplets depend on whether the particle can experience unconstrained water uptake from the vapor phase. For this to occur, the ambient water vapor pressure has to persistently exceed the equilibrium water vapor pressure over the dust particle throughout most of its residence in cloud. The level of water vapor available in clouds for condensation is however affected also by the amount of CCN

present as it is determined by a delicate balance between water vapor availability from cooling (through, e.g., expansion or radiative cooling; Pruppacher and Klett 1997) and condensation of water vapor upon existing droplets. Treatments of this process of droplet formation in models vary significantly, but invariably consider the strong coupling between water vapor availability and condensation onto CCN that have activated into droplets (Ghan et al. 2011 and references therein). Particle size and chemical affinity for water (termed "hygroscopicity" if the affinity is related to bulk absorption of water and "hydrophilicity" if it involves the adsorption of water molecules upon the particle surface) eventually determine the particle equilibrium vapor pressure and its ability to act as a CCN.

Mineral dust close to source region comprises a broad and variable mixture of minerals, which include insoluble aluminosilicate clays (e.g., kaolinite, montmorillonite, illite), tectosilicates (feldspars, quartz), metal oxides (e.g., hematite, goethite), carbonates (e.g., calcite, dolomite), and sparingly soluble gypsum, as well as soluble halite salts (Sullivan et al. 2009a; Murray et al. 2012; Chap. 2). Many field observations have shown that almost 50 % of mineral particles contain sulfate or nitrate which are formed during their transport in the troposphere by heterogeneous reactions involving sulfur dioxide and nitrogen oxides (Trochkine et al. 2003; Levin et al. 2005; Li and Shao 2009a, b; Matsuki et al. 2010). Formation of sulfate and nitrate is closely related to the mineral composition, as laboratory experiments and in situ measurements both have revealed that carbonate minerals are preferentially associated with nitrates, whereas aluminum silicates (i.e., clay minerals and feldspars) are preferentially associated with sulfates (Gibson et al. 2007; Li et al. 2006). Calcium sulfate (the reaction product of sulfur on carbonates) is sparingly soluble in water and, once formed upon dust, can act as a barrier preventing further uptake of water and other gaseous species. Consequently, the transformation of sulfur dioxide to sulfate is suppressed in these particles. In contrast, the major product of nitrate formation on carbonate particles is highly hydrophilic and hygroscopic (Gibson et al. 2006; Vlasenko et al. 2006; Sullivan et al. 2009b).

Cloud processing of aerosol particles and the coating of mineral dust particles with sulfate may influence cloud microphysics and cloud development (Yin et al. 2002). Insoluble mineral dust particles become increasingly effective CCN after processing through cloud, owing to layers of soluble material (e.g., sulfate) that form upon their surface. The introduction of such aerosol into warm or cold clouds may have two competing effects on precipitation: firstly, a suppression by providing large concentrations of CCN that compete for the available water, which leads to the formation of clouds dominated by small droplets with low coalescence efficiencies (Rosenfeld et al. 2001). Secondly, the large mineral particles may act as GCCN, producing large collector drops that collect small drops in their swath downward, thus accelerating and enhancing precipitation (Kelly et al. 2007). Such changes in the number concentration of droplets in clouds and their size distribution are thought to alter the brightness, lifetime, and extent of a cloud.

The ability of particles to act as CCN and form droplets in clouds involves the effects of surface curvature and depression of water activity from soluble solutes

and water adsorption on hydrophilic insoluble enclosures within the aerosol particle. When the size of a droplet decreases, its curvature is enhanced; this promotes the equilibrium vapor pressure of water at the surface, as there are fewer molecules available for interaction in the condensed phase (this is known as the "Kelvin effect"; Pruppacher and Klett 1997). Furthermore, water equilibrium vapor pressure may be depressed from the dissolution of solutes in the aqueous phase that forms on the CCN. This depression is known as the "Raoult effect" (Pruppacher and Klett 1997). The solutes can preexist in the particle phase (e.g., ammonium sulfate, sea salt, organics) or partition from the gas phase (e.g., HNO_3, NH_3, volatile organic acids; Laaksonen et al. 1998; Nenes et al. 2002; Topping et al. 2013). Combination of the Kelvin and Raoult effects yields the total equilibrium vapor pressure of a wet aerosol particle, and how it varies as its wet size changes due to fluctuations in environmental conditions. When the ambient relative humidity (the ratio of ambient water vapor pressure over the equilibrium vapor pressure of pure water over a flat surface) approaches 100 %, the CCN continuously absorbs water vapor but remains in stable equilibrium with the environment. Even when the system becomes supersaturated, the water tends to condense from the gas phase onto the particle, but remains in stable equilibrium owing to the Kelvin effect. However, once the supersaturation exceeds a characteristic (or "critical") value, the wet aerosol particle cannot remain in stable equilibrium with its environment and experiences unconstrained growth. It is this point and on where the particle is said to act as a CCN and activates into a cloud droplet.

The above theory was first introduced by Köhler in the early twentieth century (Köhler 1936) to describe the activation of soluble (such as sea salt) aerosol particles into cloud droplets. With appropriate extensions to account for the multicomponent nature of global aerosol, Köhler theory (KT) remains the theoretical framework used in models to link aerosol with CCN and cloud droplet formation. The theory determines the lowest-level (or "critical") ambient water vapor supersaturation, S_c, required for particles to activate into cloud droplets (Pruppacher and Klett 1997). The chemical complexity of ambient aerosol can be addressed by parameterizing the solute effects in terms of a hygroscopicity parameter, κ (Petters and Kreidenweis 2007). κ can be thought as an "equivalent volume fraction" of solute with hygroscopicity similar to sea salt (Lance 2007) and allows a direct comparison of the water uptake properties of aerosol over a wide composition range; $\kappa \to 0$ represents completely insoluble, wettable material, while $\kappa \to 1.4$ for NaCl (effectively, the most hygroscopic of all atmospheric aerosol species). For dust-relevant range of κ (i.e., $\kappa < 0.05$; Kumar et al. 2009a, b), the critical supersaturation of a particle with dry diameter D_{dry} is computed from the maximum of the following equation:

$$S = \frac{4\sigma_W M_W}{RT\rho_W D_P} - \frac{D_{dry}^3 \kappa}{D_p^3 - D_{dry}^3 (1-\kappa)} \tag{12.1}$$

where S is the particle equilibrium supersaturation (equal to the fractional relative humidity minus one), D_p is the droplet diameter, σ_w is the CCN surface tension at

the point of activation, ρ_w is the water density, M_w is the molar mass of water, R is the universal gas constant, and T is the ambient temperature. It can be shown that S_c scales with ${D_{dry}}^{-3/2}$ for hygroscopic aerosol; as the soluble fraction decreases to zero, S_c approaches the Kelvin limit, where it scales as ${D_{dry}}^{-3/2}$ (Pruppacher and Klett 1997; Petters and Kreidenweis 2007; Khvorostyanov and Curry 2007; Kumar et al. 2009a, b).

KT implies that dust particles devoid of any solute would require very high ambient supersaturations (dictated by the Kelvin equation) to act as CCN (Kumar et al. 2009a, b). However, for particles containing a large fraction of insoluble material (such as dust), physisorption of water onto the insoluble surface may also depress water activity. In fact, when the insoluble surface contains significant amounts of hydrophilic material (such as clays), the adsorption process may be strong enough to yield significant CCN activity to the particle, without the need for any soluble material at all (Henson 2007; Sorjamaa and Laaksonen 2007; Kumar et al. 2009a, b, 2011a, b; Navea et al. 2010; Lathem et al. 2011). To describe the effects of adsorption on CCN activity, Sorjamaa and Laaksonen (2007) and Kumar et al. (2009a) suggested the combination of the Frenkel-Halsey-Hill (FHH) adsorption isotherm together with particle curvature to express the CCN activity of completely insoluble particles that exhibit hydrophilicity. The resulting FHH activation theory (FHH-AT) contains two adjustable parameters, A_{FHH} and B_{FHH}, which describe the intensity and range of adsorption, respectively. Similar to KT, the critical supersaturation of a particle following FHH-AT with dry diameter D_{dry} is computed from the maximum of the following equation:

$$S = \frac{4\sigma_W M_W}{RT\rho_W D_P} - A_{FHH}\left(\frac{D_P - D_{dry}}{2D_{H_2O}}\right)^{-B_{FHH}} \tag{12.2}$$

The value of B_{FHH} is the key measure of the particle hydrophilicity, with lower B_{FHH} values corresponding to a more hydrophilic particle. As B_{FHH} increases, particles become less hydrophilic and resemble to insoluble (but wettable) particles (Kumar et al. 2011b). The maxima of Eq. 12.2 can then be expressed in the form $S_c = C{D_{dry}}^x$, where both C and x depend on A_{FHH} and B_{FHH} (Kumar et al. 2009a). As the intensity of water adsorption goes to zero, it can be shown that S_c approaches the Kelvin limit, where it scales as ${D_{dry}}^{-1}$ (Kumar et al. 2009a).

Depending on the theory (KT, FHH-AT), S_c scales with ${D_{dry}}^x$, where x is an exponent that ranges between -1.5 for KT and -0.8 for FHH-AT (Kumar et al. 2009b). Based on the discussion of Kumar et al. (2009b), from laboratory experiments of size-resolved CCN activity of particles, one can experimentally determine the relationship of S_c and D_{dry}; a power law fit between the data can then determine the "experimental" exponent, x_{exp}, $S_c = C{D_{dry}}^{x_{exp}}$ (Kumar et al. 2009b). Comparing x_{exp} against theoretical predictions of the exponent can then be used to infer the mechanism that dominates particle-water interaction, with $x_{exp} \sim -1.5$ indicating that the solute effect dominates (hence, KT applies), while

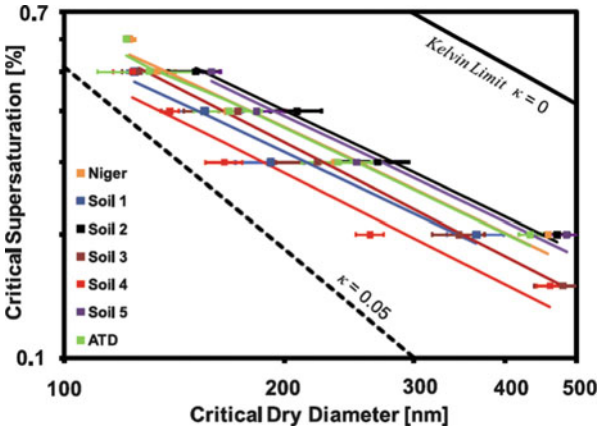

Fig. 12.1 CCN activation curves for different dust types as presented in Kumar et al. (2011a). CCN activation curves for different dust types presented in Table 1 of Kumar et al. (2011a). Symbols show experimentally determined CCN activity and lines show FHH adsorption activation fits. *Error bars* represent measurement uncertainty in the dry diameter measurement. Also shown in *black thick line* is the $\kappa = 0$, Kelvin curve. *Black dashed line* corresponds to $\kappa = 0.05$

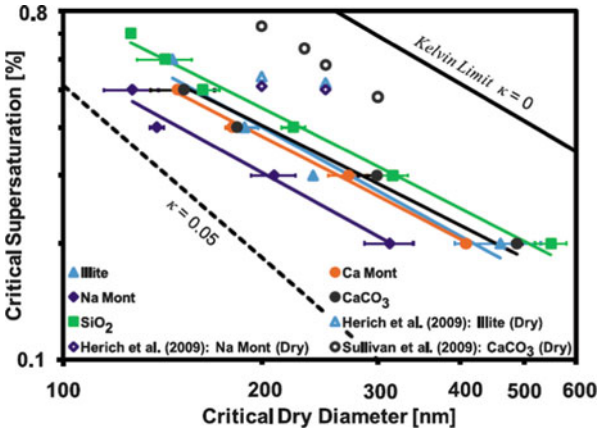

Fig. 12.2 Similar to Fig. 12.1, but for dry-generated minerals from the Kumar et al. (2011a) study. Also shown are data from the Herich et al. (2009) and Sullivan et al. (2009a) studies

$-0.8 < x_{\text{exp}} < -1.2$ indicates the dominance of the water vapor adsorption effect (hence, FHH-AT applies) (Kumar et al. 2011b).

Using this approach, Kumar et al. (2011a) showed that dry-generated dusts from a wide variety of soils tend to follow FHH-AT, and not κ-KT (Fig. 12.1); the same study also showed that aerosol generated from pure minerals also followed the same trend (Fig. 12.2). Kumar et al. (2011a) also suggest that one set of FHH-AT parameters ($A_{\text{FHH}} = 2.25$ and $B_{\text{FHH}} = 1.20$) could, to first order, be applied to global dust in aerosol-cloud interaction studies. Lathem et al. (2011) also demonstrated that volcanic ash displayed CCN activity that was consistent with FHH-AT, but with less hydrophilicity overall compared to dust. The latter was attributed to differences

in water adsorption capacity arising from differences in molecular structure of the minerals between the two particle types. Similar to dust, one set of adsorption parameters ($A_{FHH} = 2.41 \pm 0.93$ and $B_{FHH} = 1.31 \pm 0.12$) was found to describe the CCN activity of all volcanic ash samples considered, except for one (Mt. Redoubt ash). The latter displayed comparable hydrophilicity to inorganic aerosol CCN, but with x_{exp} consistent with FHH-AT. The highly porous nature of Mt. Redoubt ash particles, which increases their surface-to-volume ratio considerably, is postulated to cause the observed high level of hydrophilicity; the lack of any considerable soluble fraction upon these particles is consistent with this hypothesis. Lathem et al. (2011) also noted that the combination of CCN activity and subsaturated hygroscopicity growth measurements can also be used as proof of adsorption, as the water uptake characteristics vary considerably between FHH-AT and KT in each relative humidity regime. Hatch et al. (2014) directly measured water vapor adsorption upon Na-montmorillonite and illite clay; FHH parameters derived differed slightly from those reported by Kumar et al. (2011a), although the CCN activity inferred from the adsorption measurements is in excellent agreement with wet-generated mineral particles.

Considerable work remains however to better constrain the values of the adsorption parameters and the effect of chemical aging and presence of soluble materials. To account for the CCN activity of dust containing soluble salt fraction, Kumar et al. (2011b) proposed a new framework of CCN activation that accounts for concurrent effects of solute as well as water vapor adsorption, based on a core-and-shell model with the core representing insoluble dust and shell consisting of a layer of soluble salt. The model describes equilibrium supersaturation as a function of adsorption parameters, hygroscopicity parameter of the soluble fraction, size of the dry particle, and insoluble and soluble volume fractions as follows:

$$S = \frac{4\sigma_W M_W}{RT\rho_W D_P} - \frac{\varepsilon_s {D^3}_{dry}\kappa}{\left(D_P^3 - \varepsilon_i D_{dry}^3\right)} - A_{FHH}\left(\frac{D_P - {\varepsilon_i}^{1/3} D_{dry}}{2D_{H_2O}}\right)^{-B_{FHH}} \tag{12.3}$$

where ε_i represents the insoluble volume fraction and ε_s the soluble volume fraction, given by $\varepsilon_s = 1 - \varepsilon_i$. The new framework, referred to as the unified dust activation framework, predicts that as ε_i decreases, x_{exp} changes from -0.85 (FHH-AT limit) to -1.5 (KT limit) and predicts values of x_{exp} consistent with published CCN activity of playa salts that tend to contain a substantial soluble fraction (Fig. 12.3).

KT (and especially the κ-KT formulation) is the standard approach to describe CCN activity; one might consider adopting an "effective" hygroscopicity parameter for dust instead of invoking FHH-AT. Indeed all studies on dust CCN activity before Kumar et al. (2009a, b) and many after adopted this approach (see Table 12.2). While using an effective hygroscopicity can certainly be used for predicting CCN number, the consequences of adopting fundamentally different activation physics for mineral dust in calculations of cloud droplet number (CDNC) are important. FHH-AT particles require less water uptake to reach their critical diameter, compared to KT particles with the same critical supersaturation (Kumar et al. 2009a, b).

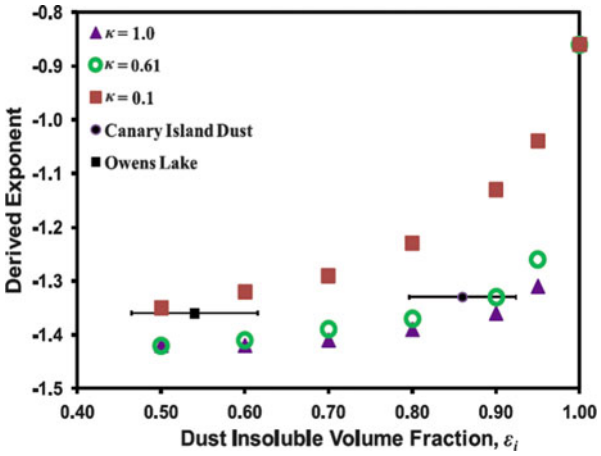

Fig. 12.3 Derived theoretical exponent, x, in the critical supersaturation relationship $S_c = CD_{dry}^{x}$ for dust coated with material of hygroscopicity characteristic of organic aerosol ($\kappa = 0.1$), ammonium sulfate ($\kappa = 0.61$), and sea salt ($\kappa = 1$). Results computed for an aerosol with FHH-AT parameters $A_{FHH} = 2.25$ and $B_{FHH} = 1.20$. Also shown are data points for Canary Islands dust and Owens Lake dust that are known to contain a large fraction of soluble salts (figure obtained from Kumar et al. 2011b). Aging of dust corresponds to going from right to left (i.e., in the direction of decreasing insoluble fraction)

This means KT particles can deplete considerably more water vapor than FHH-AT particles in cloudy updrafts (even if both theories are applied so that the CCN spectra computed are identical). This can affect the maximum supersaturation that develops, which would affect both the droplet number that forms and its sensitivity to aerosol variations. The latter point was demonstrated by Kumar et al. 2009b with parcel simulations and by Karydis et al. (2011) in a global modeling study; the latter showed that droplet number in regions of dust emissions can be affected by up to 60 % when dust hygroscopicity transitions from an FHH-type to KT-type behavior. Recently, Morales Betancourt and Nenes (2013) showed that large particles (following KT) had a disproportionately strong impact on CDN, its sensitivity to aerosol variations, and cloud forcing; such supersaturation depletion is largely mitigated when FHH-AT is used instead.

12.3 The IN Activity of Mineral Dust

The nucleation of ice crystals in the atmosphere can occur though a number of distinct pathways, only some of which are likely to be important in any one cloud type. For mineral dust there are two distinct temperature ranges where the nucleation behavior is distinct. These ranges approximately correspond to the conditions of mixed-phase and cirrus-type clouds and are illustrated in Fig. 12.4.

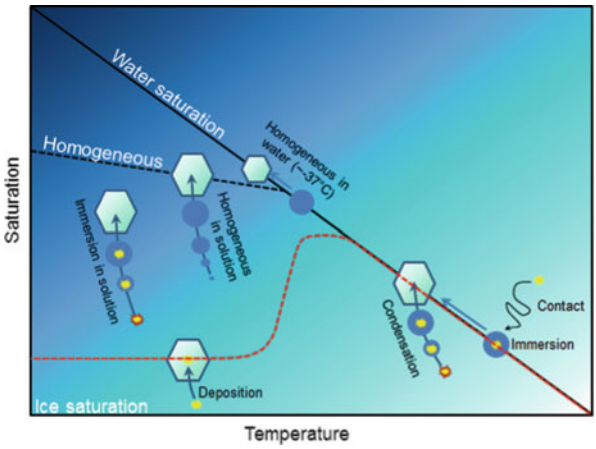

Fig. 12.4 Pathways of ice nucleation

The definitions of the various pathways of ice nucleation are not uniform throughout the literature, but in general we use those of the International Commission on Cloud Physics (Vali 1985) which contrast with those of Pruppacher and Klett (1997) in some respects. These pathways are *immersion freezing* that occurs when the IN is immersed within a supercooled liquid droplet, *contact freezing* through the collision between an IN and the air-liquid interface of a supercooled droplet, *deposition nucleation* that occurs via deposition of water vapor directly onto the IN surface, and *condensation freezing* that involves the condensation of water vapor onto the IN prior to freezing. In addition to these standard modes of nucleation, an "inside-out" nucleation process has been identified in which solid particles immersed within a droplet come into contact with the air-water interface and only then initiate freezing (Durant and Shaw 2005; Shaw et al. 2005; Fornea et al. 2009). It has been proposed that this may occur while a droplet evaporates (Durant and Shaw 2005).

At temperatures above about −25 °C, where supercooled water commonly exists in mid- or low-altitude clouds (Kanitz et al. 2011; Choi et al. 2010; Morrison et al. 2012), ice nucleation tends to only occur at around water saturation (i.e., under conditions where liquid water can exist). A number of field studies of ice formation in mixed-phase clouds show that nucleation below water saturation does not occur to a significant extent and instead liquid water is a prerequisite for ice formation (Ansmann et al. 2009; de Boer et al. 2011; Field et al. 2012; Westbrook and Illingworth 2013). Contact nucleation is not thought to be significant in deep convective clouds (Cui et al. 2006; Phillips et al. 2007), but may be important in some situations, particularly where droplets are evaporating (Ansmann et al. 2005; Ladino Moreno et al. 2013). In contrast, immersion freezing is thought to play a key role in cloud glaciation throughout the development of mixed-phase clouds generally.

Cirrus- and cirrostratus-type clouds are composed entirely of ice and form in the upper troposphere below the homogeneous freezing temperature (∼−37 °C). Some of these clouds form in situ, whereas others are formed from the outflow of deep

convection; we focus here on ice clouds which form in situ. In the absence of ice-nucleating particles, haze particles become sufficiently dilute and sufficiently cold that ice nucleates homogeneously within them at an RH below water saturation (Koop et al. 2000). Hence, in the upper troposphere, ice crystals tend to form well below water saturation. If heterogeneous ice nuclei are present, nucleation can occur at much lower ice supersaturation. Mineral dust particles free of any coatings are thought to initiate ice formation through deposition nucleation at low supersaturations ($RH_i \approx 110$–120 %). Recently, it has been suggested that what is observed as the direct deposition of ice onto a solid material is in fact a result of condensation of water into cracks or pores which then freezes (Marcolli 2013). When mineral dusts become coated with chemically inert (or reactive) soluble materials, the pathway of nucleation changes and nucleation tends to occur at a higher supersaturation. Instead of nucleation occurring on a mineral surface in contact with air, nucleation occurs in an aqueous solution which Hoose and Möhler (2012) term "immersion freezing of solution droplets."

The complexity and range of nucleation pathways which are possible in the atmosphere means that it is critical to discuss IN concentrations in connection to a particular pathway under a set of specific conditions pertinent for a particular cloud type. As mentioned earlier we have no underpinning fundamental understanding of ice nucleation, and in fact, different materials may nucleate ice for different reasons. However, there have been some advances, for example, Knopf and Alpert (2013) suggest a means of describing immersion mode nucleation in both solution droplets and pure water using a water activity-based approach. In the following paragraphs, we review several methods for quantifying ice nucleation by mineral dust particles.

In the past, it was common to quote the conditions under which an observable amount of ice formed in an experiment (e.g., Pruppacher and Klett 1997). These threshold ice nucleation conditions (temperature or RH) are experiment-specific values and difficult to translate to the atmosphere. For example, reported freezing temperatures in recent work on feldspar mineral dust immersed in water droplets ranged from -5 to -25 °C depending on the surface area available for nucleation (Atkinson et al. 2013). Since the surface area available and the sensitivity of ice particle detection vary between different instruments, the threshold freezing temperature will be different for different instruments. Hence, it is necessary to parameterize the freezing probability in a form which is then transferable to atmospheric conditions. This task remains a challenge, but a number of parameterizations/models/descriptions have been put forward.

Nucleation is a probabilistic, stochastic, process and the probability of nucleation increases with a greater surface area of IN and for longer times (Kashchiev 2000; Mullin 2001). For an idealized uniform ice-nucleating material where each particle of the same size has the same probability of nucleating ice as the next particle, the probability of droplets remaining liquid is

$$\frac{N_2}{N_1} = \exp\left(-J_{\text{het}} s \Delta t\right) \tag{12.4}$$

where N_1 and N_2 are the number of liquid droplets at the beginning and end of the time step, Δt, respectively. J_{het} is the heterogeneous nucleation rate coefficient and s is the surface area of nucleant per droplet. Traditionally, J_{het} has been described with classical nucleation theory where a contact angle parameter is used as an independent measure of how efficiently a material will nucleate ice. If this equation holds, then we would expect a first-order decay of droplets at constant temperature and also values of J_{het} from experiments with different cooling rates to be the same. The only known IN sample which is consistent with this model is kaolinite (KGa-1b) from the clay mineral society (Herbert et al. 2014; Murray et al. 2011). Unfortunately, the assumption of particle uniformity does not hold for other atmospherically relevant aerosol types; instead, their ice-nucleating ability exhibits diversity with some particles having a greater propensity to nucleate ice than others (Herbert et al. 2014; Broadley et al. 2012; Wheeler and Bertram 2012; Niedermeier et al. 2011b; Lüönd et al. 2010; Barahona 2012).

In order to account for the diverse nature of ice-nucleating particles, a number of authors introduced models in which a distribution of ice-nucleating abilities was incorporated into a stochastic model (Broadley et al. 2012; Niedermeier et al. 2011b; Wright and Petters 2013; Marcolli et al. 2007; Stoyanova et al. 1994; Barahona 2012). In these models, the effects of many different ice-nucleating particles are summed; however, these models are complex. Barahona (2012) reinforces the view that IN tend to be diverse, commenting that inferring the aerosol heterogeneous nucleation properties from measurements of onset conditions may have significant error.

An alternative approach to dealing with the diverse nature of atmospheric ice nuclei is to make the assumption that the time dependence of nucleation is of secondary importance compared to the particle-to-particle variability of ice nuclei. It has been shown that individual droplets freeze over a wide range of temperatures, whereas the variability in freezing temperature on repeated freezing cycles is much smaller (Vali 2008; Wright et al. 2013). This shows that in many samples it is the nature of the IN in the droplets which primarily determines freezing temperature and the stochastic effects are second order, at least under some conditions. Observations such as these have given rise to the singular approximation in which the time dependence of nucleation is neglected. In the singular description, nucleation occurs instantaneously on an active site once a characteristic temperature is reached. The fraction of droplets frozen as a function of temperature and saturation (S) can be expressed as (Connolly et al. 2009; Murray et al. 2012; Demott 1995)

$$f_{ice}(T, S) = \frac{n_{ice}(T, S)}{N_{tot}} = 1 - \exp\left(-n_s(T, S)\, s\right) \tag{12.5}$$

where n_{ice} is the number of frozen droplets, N_{tot} is the total number of frozen and unfrozen droplets, and n_s is the active site density. n_s is the cumulative number of nucleation sites per surface area that become active on decreasing T and increasing S. When IN are immersed in pure water, S is defined by water saturation; hence, n_s is then reported as a function of T only.

While n_s has become widely used for mineral dust and other IN species, it is important to bear in mind its inherent limitations. A key limitation is that if the measurement timescale is very different to the timescale available for nucleation in the atmosphere, n_s values (or time-independent IN concentrations) must be used with caution. In convective cloud systems, the singular description most likely captures the key features of the IN spectrum, whereas in stratus clouds, it has been suggested that slow stochastic nucleation could account for prolonged production of ice crystals (Westbrook and Illingworth 2013). Recently, Herbert et al. (2014) proposed a means of representing the time dependence of nucleation using the singular description through the recognition that the quantity $\ln J_{het}/T$, where J_{het} is for each component in an IN population, defines the time-dependent nature of ice nucleation.

12.4 Field Observations of Dust CCN Activity/Hygroscopicity

During the last decade, several field measurements have been dedicated to the physicochemical properties of mineral dust, such as the Saharan Dust Experiment (SHADE), the Aerosol Characterization Experiment – Asia (ACE-Asia), the African Monsoon Multidisciplinary Analysis (AMMA), the Mediterranean Israeli Dust Experiment (MEIDEX), the Dust and Biomass-burning Experiment (DABEX), and the Saharan Mineral Dust Experiment (SAMUM) (Manktelow et al. 2010; Formenti et al. 2011 and references within). The foci in these campaigns were the study of dust composition, the impacts of atmospheric aging thereon, and in some the hygroscopic and CCN properties of the dust samples; a list of studies and major findings is shown in Table 12.1.

From these observations, it is often found that dust particles are internally mixed with sulfate and/or nitrate, as a result of their atmospheric processing. The production of the different aged dust particles depending on their transport pathways has important implications on their different effects on cloud formation, radiation balance, and health (see Chaps. 4, 11 and 16). Of all the studies cited above, few studies directly measure the CCN activity of dust in situ. Given the wide range of soluble fraction, combined with the importance of both adsorption (FHH) and absorption (Raoult) of water on the equilibrium vapor pressure above dust, necessitates more field measurements directly addressing the origin of dust aerosol hygroscopicity.

Table 12.1 List of major field campaigns involving the study of dust and its hygroscopicity

Campaign	Focus	Major findings
AMMA, Matsuki et al. (2010)	Characteristics of mineral dust incorporated in cloud droplets and related cloud processing	Secondary sulfate, nitrate, and chlorate found on many dust particles; enhanced in clouds Strong differences between calcium-rich and silicate particles; carbonates containing secondary species in significantly larger frequency and amount
NASA portion of AMMA, Twohy et al. (2009)	Hygroscopicity of sampled aerosol and effect of Saharan dust on clouds in the area	Saharan dust particles do commonly act as CCN in the eastern North Atlantic Due to slightly hygroscopic nature, even submicron dust can be important as CCN Due to its dual nature to act as both CCN and IN, dust can impact not only droplet size in small clouds but ice formation in deep convective clouds
MEIDEX, Levin et al. (2005)	Size distribution and chemical composition of aerosol particles during a dust storm	Approximately 35 % of the coarse particles up to about 1 km in height were internal mixtures of dust and sea salt Depending on whether dust particles are active as GCCN and/or effective IN, droplet concentration, diameter, lifetime, area cover, and amount of rain may differ
Beijing, Li and Shao (2009b)	Study of the sizes, morphologies, and composition of samples collected during brown haze and dust episodes	In haze events, almost 90 % of the mineral particles were covered by visible coating, whereas only 5 % in the dust events were coated The majority of coatings were Ca-, Mg-, and Na-rich, containing oxygen and nitrogen (possibly nitrates) and minor amounts of sulfur
SAMUM-2, Schladitz et al. (2011)	Particle number size distributions, mixing state, and hygroscopicity of aerosol in Cape Verde	The sampled Saharan dust aerosol was an external mixture of nearly hygrophobic and hygroscopic particles with κ values ranging from 0.3 to 1

(continued)

Table 12.1 (continued)

Campaign	Focus	Major findings
ACE-Asia, Trochkine et al. (2003)	Examination of the composition of mineral particles in source region and comparing them with those after long-range transport	The main difference between particles collected in China and Japan was that 40–45 % of mineral particles in Japan were internally mixed with sulfate
Data from MODIS, AMSR-E, and CERES, Li et al. (2010)	Mineral dust impacts on warm clouds	Clouds are affected strongly by the dust aerosols coming from the Saharan region Statistically significant impacts on clouds for only some of the segregated cloud classes
Gwangju, Korea, Kim and Park (2012)	Hygroscopicity and volatility of dust particles originating from the Gobi Desert	Particles were aged, internally mixed with hygroscopic and volatile species characteristic transport pathway "Less polluted" dust particles attributed to interaction with sea salt and/or cloud processing, while "highly polluted" particles linked to interaction with anthropogenic pollutants and heterogeneous reactions

12.5 Field Observations of Mineral Dust as IN

Mineral dusts were identified as IN in the early years of ice nucleation research. For example, Kumai (1961) identified the particles often found at the center of snowflakes as mineral dust using electron microscopy. These results were consistent with fog chamber studies where various mineral dusts were found to be effective at triggering glaciation in a supercooled fog (Pruppacher and Klett 1997; Mason 1971). This early picture is reinforced by contemporary measurements of ice crystal residues in a range of environments.

As part of the CRYSTAL-FACE (Cirrus Regional Study of Tropical Anvils and Cirrus Layers-Florida Area Cirrus Experiment), DeMott et al. (2003b) used an airborne continuous flow diffusion chamber (CFDC) to expose ambient aerosol to a supersaturated environment (the processing conditions were 36.5 °C and 123 % RH_i). They showed that the highest IN concentrations in the measurements over Florida occurred within plumes of mineral dust from the Sahara. This was clear evidence that mineral dust could significantly contribute to IN populations at great distances from source. More direct evidence that mineral dust makes up a significant proportion of heterogeneous IN came from the mountain top atmospheric observatory at Storm Peak in Colorado. DeMott et al. (2003a) used a CFDC to activate IN in ambient air under conditions pertinent to cirrus; these ice crystals were

then isolated using a counterflow virtual impactor and then probed with an aerosol mass spectrometer. They found that 33 % of the ice crystal residues contained either mineral dust or fly ash (these materials could not be distinguished with the mass spectra), whereas this category only made up 1 % of the background aerosol. On the basis of electron microscopy analysis, they suggest that 80 % of these particles were mineral dust. Later, Baustian et al. (2012) sampled from the same site using a comparable technique and showed that more than 50 % of the fine mode IN were mineral dust under conditions relevant for cirrus clouds.

Measurements have also been performed where ice crystals in natural cirrus clouds were isolated, the ice sublimed away, and analyzed by mass spectrometry or offline with electron microscopy. Cziczo et al. (2013) summarize the results from several campaigns where the composition of the ice crystal residues was determined. They show that mineral dust/metallic particles were enhanced in most cirrus clouds sampled. Of notable exception is cirrus which forms in the tropical tropopause where nucleation may occur on glassy aerosol or crystalline solid salts (Cziczo et al. 2013; Murray et al. 2010; Wise et al. 2012) and mineral dusts are not enhanced in ice crystal residues (Froyd et al. 2010). Nevertheless, these studies in combination reveal that mineral dust is one of the most important ice nuclei for cirrus-type clouds.

In addition to cirrus, ice crystal residues have been examined in mixed-phase cloud types. Pratt et al. (2009) used a counterflow virtual impactor to separate ice crystals from supercooled cloud droplets in a wave cloud during ICE-L (Ice in Clouds Experiment – Layer clouds). They found that 50 % of the ice crystals contained mineral dust particles. Mineral dust was also found to be the dominant ice crystal residue in mixed-phase clouds at the high alpine observatory at Jungfraujoch in the Swiss Alps (Kamphus et al. 2010). Ebert et al. (2011) used electron microscopy to characterize ice crystal residues sampled at the same site and found that aerosols with silicates or metal oxides as a major component were enhanced by a factor of 11, but also commented that mixing state may play a very important role in determining ice nucleation behavior.

These studies of ice crystal residues from both natural ice crystals and ice crystals nucleated from ambient aerosol in a CFDC collectively show that mineral dust is one of the most important IN species in both mixed-phase and cirrus clouds. Despite it being dominantly emitted in the African and Asian dust belts, it is transported in sufficient concentrations that it contributes to IN concentrations on a global basis. However, it is unclear if mineral dust is also the dominant IN aerosol type in regions very remote from dust sources, such as the Southern Ocean or the Arctic (Burrows et al. 2013); hence, more measurements are needed.

12.6 Laboratory Experiments on Mineral Dust CCN

The hygroscopic growth and CCN activity of various, mostly calcium, mineral dust particles have been extensively studied in several laboratory experiments. Dust aerosols are generated from either aqueous solution or dry; wet generation

comprises the atomization of a suspension of dust powder in water, drying of the aerosol, subsequent size selection of generated aerosol by a differential mobility analyzer (DMA), and a hygroscopic growth, CCN, or IN measurement. Dry generation varies between studies but mainly involves the resuspension of dust powder using a jet of gas, soft saltation, or fluidized bed followed by a similar instrumentation as for the wet generation. The generation technique has been shown to influence both cases of CCN activity as well as ice nucleation experiments. The corresponding studies along with their major findings are listed in Table 12.2. These experimental studies demonstrate the fact that the ability of dust particles to act as CCN is closely dependent on both the mineralogical composition of the dust particles and their mixing state with other atmospheric components. Therefore, different activities are accordingly expected for different parts of the globe.

A number of studies (e.g., Sullivan et al. 2009a, b; Kumar et al. 2011a, b; Garimella et al. 2013) point to the importance of carefully characterizing the effects of multiple particle charging and the shape factor of particles; both are particularly strong effects given the large size and highly irregular geometry of the particles. The same studies (and references therein) point out that wet generation of dust leads to considerable biases in hygroscopicity and should be avoided. Kumar et al. (2011b) showed that wet-generated particles tend to be bimodal with the smaller size mode displaying considerable hygroscopicity and following a KT-type dependence of S_c vs. D_{dry}; the larger-mode particles display a FHH-type CCN activity with characteristics that resembled dry-generated dust.

12.7 Laboratory Experiments on Mineral Dust IN

There have been two recent reviews of ice nucleation that extensively cover the ice-nucleating properties of mineral dust (Murray et al. 2012; Hoose and Möhler 2012). However, since these reviews were published, there have been some advances in the field which help us to interpret the information summarized in those reviews. For many years it was thought that the clay minerals were the most important ice-nucleating component of mineral dust, but this view was recently challenged for ice nucleation in the immersion mode (Atkinson et al. 2013) and deposition mode (Yakobi-Hancock et al. 2013). Atkinson et al. (2013) performed droplet freezing experiments with minerals common in mineral dust from the world's arid regions. The purity of the mineral samples was quantified using X-ray diffraction. The results are shown in Fig. 12.5 and show that the feldspars, in particular the K-feldspar (microcline), are the most efficient ice-nucleating minerals in mineral dusts. This result conflicted with the prevailing view that the clay minerals are the most active component of mineral dust. Atkinson et al. (2013) examined the mineral composition of several clay samples which had been used in previous studies and found that many of them contain a significant amount of feldspar. They suggested that the ice-nucleating ability of these clay samples was in fact determined by the feldspar content, highlighting the importance of quantifying the composition

Table 12.2 List of major laboratory experiments involving the study of dust and its interactions with water vapor

Experiment	Major findings	Reference
Study of the carbonate component of mineral dust and its reaction products	$Ca(NO_3)_2$ particles from aqueous solution showed orders of magnitude greater growth and CCN activity than $CaCO_3$ but also reflected a greater amount of near-infrared radiation at higher relative humidities	Gibson et al. (2006)
Mixed insoluble and soluble aerosol particles to investigate atmospheric aging and heterogeneous processing on CCN activity	The critical supersaturation of calcite was reduced by 46 % when mixed with $Ca(NO_3)_2$, while S_c of kaolinite was reduced by half when mixed with ammonium sulfate. For a given supersaturation, the mixing with a soluble component may decrease the critical diameter by as much as 42 % relative to pure mineral dust	Gibson et al. (2007)
Hygroscopicity and CCN activity of different actual mineral dust samples	Only the sample from the Canary Islands showed appreciable hygroscopic growth at subsaturated conditions. All particles with diameters >200 nm activated as cloud droplets at low supersaturations (0.2–0.3 %)	Koehler et al. (2009)
Water uptake of clay and desert dust samples at sub- and supersaturated water vapor conditions	All dust particles activated at higher saturations than typical atmospheric aerosol, with wet-generated mineral dust particles in all cases activating at significantly lower supersaturations than the corresponding dry-generated ones	Herich et al. (2009)
Reaction of calcite with nitric acid vapor over a wide range of relative humidities	Calcite rapidly converts into hygroscopic particles within 4 h for low nitric acid mixing ratios (10 ppt) and less than 3 min for 1,000 ppt	Sullivan et al. (2009a)
Effect of chemical mixing state on hygroscopicity and CCN properties of calcium mineral dust particles	$CaCO_3$ and $CaSO_4$ exhibited low solubility and hygroscopicity similar to that of an insoluble component, but small amounts of sufficiently soluble contaminants increased the measured hygroscopicity	Sullivan et al. (2009b)

(continued)

Table 12.2 (continued)

Experiment	Major findings	Reference
Impact of generation method on measured hygroscopicity	Particles from atomization of aqueous solutions displayed hygroscopicities 100 times greater than the ones obtained for dry-generated calcite mineral dust particles. Using wet-generation methods to suspend mineral dust will not produce particles with the correct physicochemical properties in laboratory studies	Sullivan et al. (2010a, b)
Novel method to produce calcite	Calcite produced by spraying $Ca(HCO_3)_2$ solution in a tube furnace. Dried $Ca(HCO_3)_2$ particles were somewhat more hygroscopic than calcite, but during humidification a restructuring takes place and 2/3 is transformed to calcite	Zhao et al. (2010)
CCN activity and droplet activation kinetics of fresh unprocessed regional dust samples	Dust aerosols are CCN at atmospherically relevant supersaturations, with dry diameters much larger than pure salt. The CCN activity is controlled by the adsorption of water onto the clay and the mineral components in the samples	Kumar et al. (2011a)
CCN activity and size distribution of wet processed regional dust samples	Wet-generated clays and minerals produce a bimodal size distribution with the CCN activity of the smaller mode following the Köhler approach (KA), while the larger mode which is less hygrophilic follows the water adsorption approach. Wet-generated regional dust samples, on the other hand, produced unimodal size distributions with small particle sizes, CCN activation consistent with the KA, and exhibit hygroscopicity similar to inorganic salts	Kumar et al. (2011b)

(continued)

Table 12.2 (continued)

Experiment	Major findings	Reference
CCN ability of Asian mineral dust and its effect on cloud droplet formation	The activation fractions (CCN/CN) were 0.7 at 0.2 % supersaturation and 0.8 at SS = 0.4 %, suggesting that Asian mineral dust particles, by themselves, may effectively act as CCN. The hygroscopicity of the mineral dust particles was considerably enhanced, and droplets activated on them grew much larger when internally mixed with sea salt particles	Yamashita et al. (2011)
Effect of oxalic acid on CCN activity of mineral dust aerosol	Oxalate/calcite aerosols had identical CCN activity with the original ones, whereas polystyrene latex spheres (PSL)/oxalate aerosols showed much greater CCN activity. The increased CCN activity by incorporation of oxalic acid is only expected for unreactive, insoluble dust particles that form a soluble coating around the core	Gierlus et al. (2012)

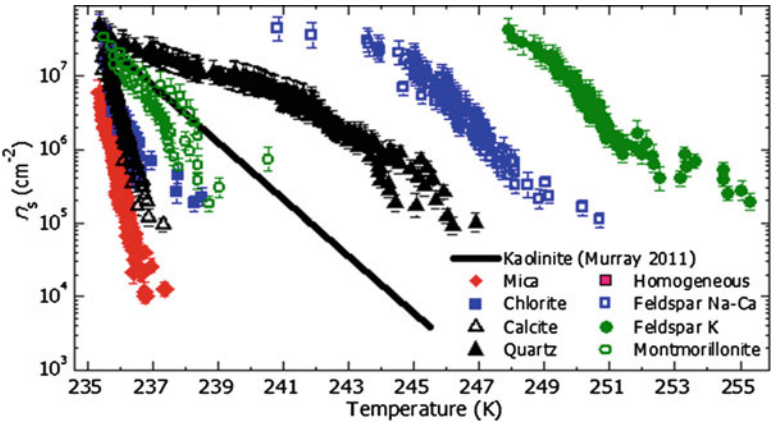

Fig. 12.5 Ice-active site densities (n_s) for a range of minerals common in mineral dust which were immersed in water droplets. These results are from Atkinson et al. (2013) and show that feldspars, in particular K-feldspar, are the most active ice-nucleating components of mineral dust

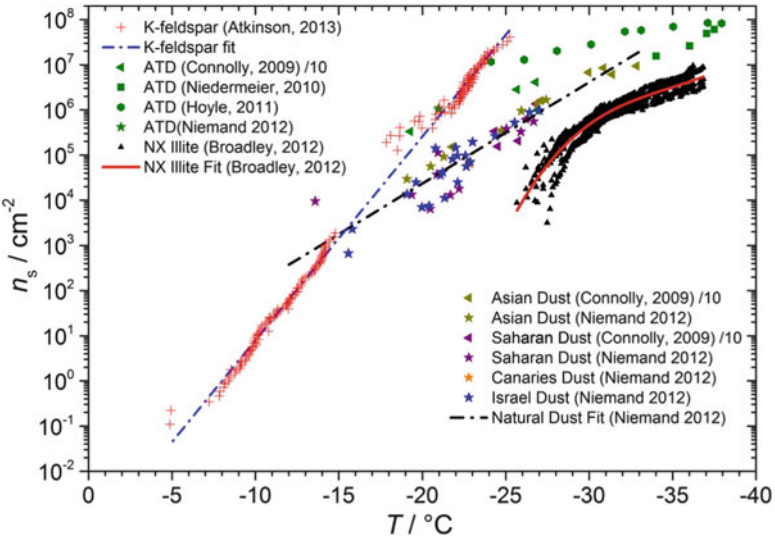

Fig. 12.6 Ice-active site density (n_s) derived from experimentally data for mineral dust particles immersed in water droplets. This figure is similar to Fig. 19 of Murray et al. (2012), where the derivation of n_s is detailed, but in addition the data of Atkinson et al. (2013) is also shown

of the dust samples used in ice nucleation studies. Yakobi-Hancock et al. (2013) examined ice nucleation by 24 mineral dusts using a CFDC in the deposition mode at −40 °C, that is, under conditions pertinent for cirrus. They found that the feldspars were some of the most efficient IN they examined, although they note that their feldspar samples nucleated ice at a similar supersaturation to kaolinite from the clay mineral society. In the immersion pathway, kaolinite was clearly much less active than feldspar, which suggests that there are differences between the pathways in the relative importance of the different minerals.

Ice-active surface site densities for a range of natural desert dust samples and proxies for natural dust and K-feldspar, determined using a number of techniques, are shown in Fig. 12.6. These results for natural dusts are from the two studies using a large cloud simulation chamber (AIDA, Aerosol Interaction and Dynamics in the Atmosphere) in which dust was aerosolized and then exposed to a supersaturation sufficient to condense water onto the particles. On further expansive cooling, the mineral dust particles were observed to act as IN and the fraction of aerosol which activated to ice was determined. Combining this information with the size distribution of the mineral dust aerosol, using measurements of the aerodynamic and mobility sizes, they were able to determine $n_s(T)$ (Connolly et al. 2009; Niemand et al. 2012). A striking result of these measurements is that samples from Asia, the Sahara (near Cairo), the Canary Islands, and Israel all produced very similar values of $n_s(T)$ which is consistent with a common minor component causing ice nucleation. Atkinson et al. (2013) suggested this common component is K-feldspar, which is ubiquitous to soil dusts around the world (Nickovic et al. 2012).

Also shown in Fig. 12.6 are results for two commercially available proxies for natural mineral dust: Arizona Test Dust (ATD) and NX-illite. ATD has been the subject of numerous studies and is made of material which has been milled to produce particles with a specific range of sizes. It is sold on a commercial basis for testing the efficiency of filters. It is attractive for ice nucleation experiments because of its well-defined particle size, it is available in large quantities, and its mineralogical composition has been reported (Broadley et al. 2012). In Fig. 12.6, we summarize and compare ice-active site densities for a number of experiments performed in the immersion mode with ATD. Its ice-nucleating ability has been explored in the AIDA cloud chamber during experiments similar to those described above for natural dusts (Connolly et al. 2009; Niemand et al. 2012). Niedermeier et al. (2010) report n_s values for ATD determined with the LACIS (Leipzig Aerosol Cloud Interaction Simulator) chamber which is a temperature-controlled laminar flow tube, allowing the activated fraction of aerosol particles to be determined under specific conditions. Using a CFDC, Hoyle et al. (2011) activated individual size-selected ATD particles to droplets in order to measure the ice-nucleating fraction from which Murray et al. (2012) determined n_s values. Inspection of the results for ATD in Fig. 12.6 shows that n_s values from these diverse experiments are in good agreement with one another. This suggests that ATD is a very useful material for benchmarking instrumentation. However, it appears to be roughly an order of magnitude more efficient at nucleating ice than the natural dusts based on the information summarized in Fig. 12.6. One explanation is that ATD has significantly more feldspar in it than average natural dusts (see Figure 13 of Murray et al. 2012) but may also be related to the intense milling process used in the production of ATD.

On the basis of mineralogical makeup, it has been argued that NX-illite is a better proxy for natural dusts (Broadley et al. 2012; Murray et al. 2012). The n_s values reported for NX-illite by Broadley et al. (2012), and shown in Fig. 12.6, are clearly much lower than any of the other values. However, it must be noted that there are significant differences in experimental approach and in particular the measure of surface area. All other measurements discussed above employed instruments which yield equivalent spherical diameters based on aerodynamic or mobility size measurements from which surface area was determined, whereas for NX-illite a gas adsorption technique was used. The measured size distribution in the AIDA experiments, for example, peaked at around 1 μm diameter, but for clays the primary grains are on the order of just 10s nanometers. Hence, a micron-scaled particle will be made up of numerous smaller grains (see, e.g., Fig. 12.7) and therefore has a substantial internal surface area. Gas adsorption techniques report the total surface area of all grains, whereas determining surface area from a spherical approximation does not. Accounting for the internal surface area would bring the various results in Fig. 12.6 into closer agreement.

When using n_s values to estimate the production of ice crystals in the atmosphere, it is essential to consider how surface area was determined. If a spherical approximation was made in the laboratory, then this assumption should also be made for atmospheric aerosol if they are of a similar size. If a specific surface area (gas adsorption) has been used, then a similar estimate should be made for

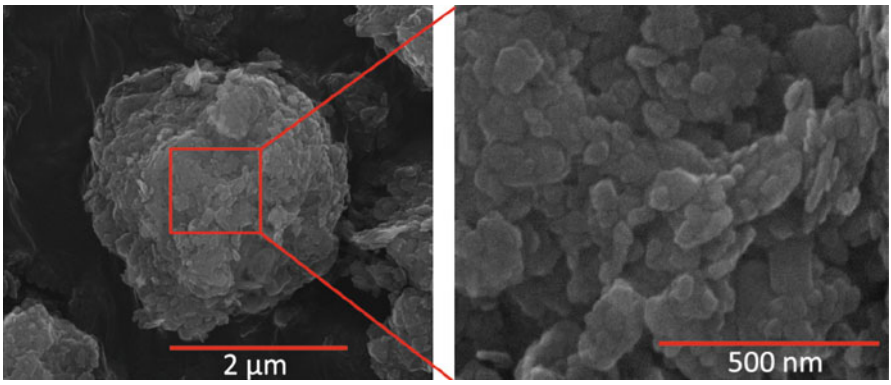

Fig. 12.7 Electron microscope images of a typical NX-illite particle showing that a micron-scaled particle is made up of many smaller primary grains (Image from Broadley et al. (2012))

the atmospheric counterpart. This issue is most acute when the primary grain size is small in comparison to the overall size of the aggregate particle and is a particular problem for materials which contain clay minerals (which tend to be made up of nanometer-scaled primary particles). For feldspars and quartz, the primary grain sizes tend to be much larger which means the surface area determined from a spherical approximation and gas adsorption techniques is in reasonable agreement (Atkinson et al. 2013).

Finally, also shown in Fig. 12.6 are n_s values for K-feldspar discussed above (Atkinson et al. 2013). It was argued above that K-feldspar is the most efficient single mineral in mineral dusts; hence, one would expect n_s values for K-feldspar to exceed those of the natural dusts. Below −18 °C this is the case, but there are three data points at around −15 °C for the natural desert dust sampled near Cairo which has similar n_s values to K-feldspar in our study. This might suggest that there is another component of this dust which becomes more important than K-feldspar at these warmer temperatures. One candidate might be ice-nucleating biological residues which have been observed to nucleate in fertile soils (Conen et al. 2011; O'Sullivan et al. 2014). Further work at temperatures of −15 °C and above is clearly required.

A selection of data for ice nucleation by natural desert dusts and ATD is shown in Fig. 12.8 for conditions pertinent for both mixed-phase and cirrus clouds (Hoose and Möhler 2012). As was discussed in Sect. 12.3, mineral dusts tend not to nucleate below water saturation at above about −30 °C, and this is consistent with field observations where ice only forms after the development of a liquid cloud. Under conditions pertinent for cirrus clouds, mineral dusts can nucleate ice well below water saturation. Interestingly, ATD tends to nucleate ice at lower threshold saturations than dusts sampled from arid regions (Fig. 12.8). This echoes the findings in the immersion mode shown in Fig. 12.6 where ATD tended to have a greater n_s than natural desert dusts. One possible explanation for this difference,

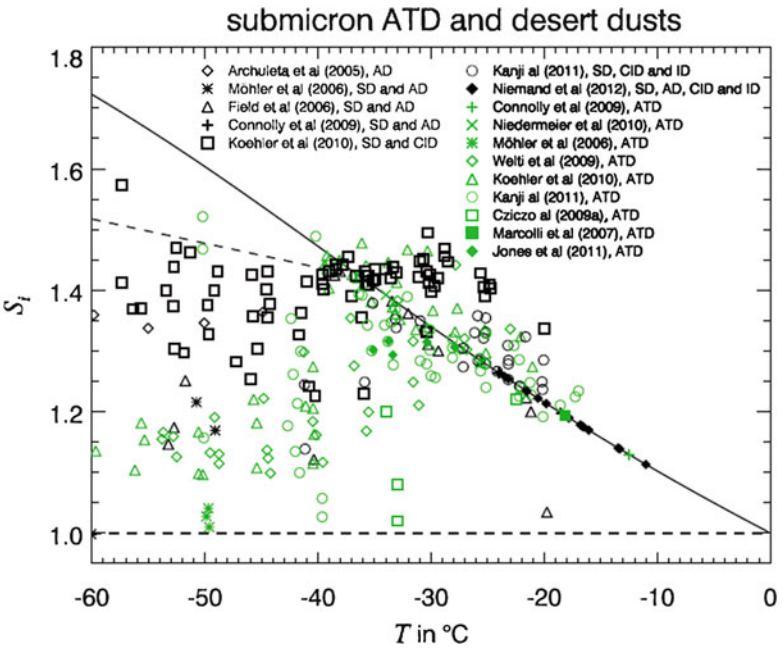

Fig. 12.8 Experimentally derived ice nucleation onset temperatures and saturation ratios for natural and surrogate for natural dusts, Arizona Test Dust (*ATD*) as presented in the review of Hoose and Möhler (2012). *SD* Saharan dust, *AD* Asian dust, *CID* Canary Islands dust, *ID* Israeli dust

apart from differences in mineralogy discussed above, could be that the surfaces of natural dusts are chemically aged or coated, whereas for ATD the grinding process reveals fresh mineral surfaces on which ice can nucleate more effectively. In fact, the role of coatings on mineral dusts has been explored in the laboratory in the past.

It has been shown in a number of experimental studies that exposure of mineral dusts to inorganic and organic coatings can reduce their ice-nucleating ability (Hoose and Möhler 2012). Reaction with sulfuric acid has received significant attention and studies have focused on both ice nucleation below water saturation, which is most relevant for cirrus clouds (Chernoff and Bertram 2010; Cziczo et al. 2009; Knopf and Koop 2006; Archuleta et al. 2005; Eastwood et al. 2009), and also with particles suspended inside water droplets at temperatures pertinent for mixed-phase clouds (Niedermeier et al. 2011a; Sullivan et al. 2010a, b; Wex et al. 2013). It has become apparent that the effect of the coating depends on the nucleation pathway and the nature of the coating material. Tobo et al. (2012) showed that both chemically inert levoglucosan and reactive sulfuric acid coatings reduced the ice-nucleating ability of kaolinite particles below water saturation, whereas at water saturation, only sulfuric acid-treated particles were less active. This shows that below water saturation, the pathway of nucleation changes from deposition on bare mineral to nucleation of ice by particles immersed in solution droplets and that this

generally increases the threshold nucleation saturation. However, at water saturation when particles are immersed in very dilute solutions, chemically inert, then soluble coatings have no impact on ice nucleation (Koehler et al. 2010; Tobo et al. 2012). In contrast, sulfuric acid irreversibly reduced the ice-nucleating behavior of the dust which is consistent with the surface modifications observed by Reitz et al. (2011) when dust was exposed to sulfuric acid. More recently Wex et al. (2013) showed that only a kaolinite sample with feldspar impurities was susceptible to sulfuric acid, whereas a sample with no detectable feldspar was not. Feldspars are known to be converted to clay minerals and amorphous silica by acids (Zhu et al. 2006), and these reactions are therefore consistent with the observations of Wex et al. (2013).

12.8 Modeling Studies on the Interaction of Dust with Clouds

A thorough treatment of all studies focused on dust interactions with clouds and climate is beyond the scope of this section; we however present representative examples of studies on aspects of dust impacts and their major conclusions.

Mineral dust, sea salt aerosol, and their mixtures have been simulated in an attempt to quantify their effect on precipitation development and rain amounts. Based on the chemical and physical properties of particles obtained during MEIDEX, Levin et al. (2005) concluded that allowing the soluble component of the mixed aerosol to act as efficient GCCN enhances the development of the warm rain process in continental clouds with higher rain amounts by as much as 37 % compared to the case without GCCN. Introducing similar coarse particles into maritime-type clouds on the other hand does not have a significant effect on neither cloud nor amount of rainfall. When dust particles are active as both GCCN and effective ice nuclei (IN), continental clouds become wider, there are higher concentrations of droplets, and the cloud lifetime is longer, while once more the effects on more maritime clouds is very uncertain. Smoydzin et al. (2012) also arrived at the conclusion that the contribution of dust to the CCN population is potentially significant only over land. They investigate the impact of the coarse mode hygroscopicity on aerosol activation and the largest impact was found for warm phase clouds. Precipitation was not influenced by changing the hygroscopicity, except when dust entered into an area of orographic ascent, causing glaciations of the clouds and leading to local enhancement of rainfall.

The effect of GCCN on global climate, warm clouds, and precipitation was also simulated within the ECHAM5 General Circulation Model (GCM) (Posselt and Lohmann 2008). It was found that measured distributions agree much better with GCCN concentrations when considering an upper size limit of 10 μm particles, than concentrations for chosen cutoff radii of 5 μm. The incorporation of GCCN in the results does not affect precipitation globally as regions with increasing precipitation rates alternate with regions with decreasing precipitation rates so that the zonal average does not change. Nonetheless, depending on the amount of added GCCN,

the reduction of total water and cloud drops account for up to 20 % compared to a control run without GCCN. Therefore, the incorporation of the GCCN accelerates the hydrological cycle so that clouds precipitate faster (but not more).

Van den Heever et al. (2006) highlight the fact that the impacts of varying GCCN and IN concentration are just as significant as those associated with CCN in convective storms and their subsequent anvil development. With varying CCN, GCCN, and IN concentrations, they found that all three nucleating aerosols affect the depth, microphysical characteristics, water mass, and organization of the anvil. Updrafts are consistently stronger as the concentrations of cloud-nucleating aerosol are increased, with CCN having the greatest impact on updraft during the initial stages and GCCN and IN concentrations having a greater impact on updraft strength during the mature and dissipating storm stages. Cloud water increases with increasing aerosol concentrations, with increases in GCCN concentrations producing the most cloud water on average. Increasing either the GCCN or IN concentrations produces the most rainfall at the surface, whereas enhanced CCN concentrations reduce surface rainfall. The same model (RAMS) was also used by Zhang et al. (2009) to investigate the mechanisms by which Saharan dust acting as CCN can impact a tropical cyclone evolution. They showed that by adding CCN within the initial environment, CCN directly affected the early eyewall evolution by varying distributions of latent heat, therefore triggering variations in dynamic and thermodynamic processes that ultimately modify eyewall intensity. Furthermore, CCN indirectly affected the eyewall by modulating rainband development but in a way that did not systematically depend on input CCN. Finally, Karydis et al. (2011) used the NASA Global Modeling Initiative (GMI), modular 3-D chemistry, and transport model to assess the contribution of insoluble dust to global CCN and CDNC. The predicted annual average contribution of insoluble mineral dust to CDNC in cloud-forming areas was found to be up to 40 and 24 %, respectively, with the results being sensitive to the level of hygroscopicity as well as the dust size distribution. Coating of dust by hygroscopic salts during atmospheric aging can substantially deplete in-cloud supersaturation during the initial stages of cloud formation and therefore eventually reduce CDNC.

As mentioned earlier, IN in mixed-phase clouds tend to counteract the effect of increased CCN. Lohmann and Diehl (2006) found that mineral dust in mixed-phase stratiform clouds can have a significant impact on the liquid water path, cloud lifetime, precipitation rate, and top of the atmosphere radiation on a global scale. Although they based their IN parameterizations on laboratory data which has been superseded, they show that stratus clouds are very sensitive to the parameterization of ice nucleation. They show that precipitation is enhanced which reduces lifetime of clouds, resulting in a warming due to reduced cloud cover. The decrease in net radiation at the top of the atmosphere was up to 2.1 W m^{-2}, which is of a similar magnitude but opposite direction to the anthropogenic CCN impacts on cloud albedo. Storelvmo et al. (2011) modeled the impact of increased ice particle concentrations on the radiative properties of clouds and showed that the greater reflectivity largely counteracted the increased reflectivity from decreased cloud lifetime.

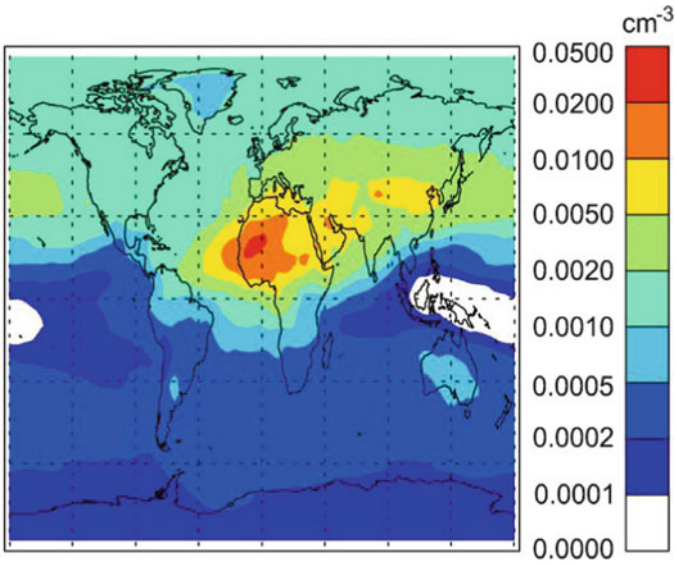

Fig. 12.9 Annual average mineral dust IN concentrations at 600 hPa active at −20 °C. The IN concentration is based on the modeled K-feldspar content of airborne mineral dust (This figure is reproduced from Atkinson et al. (2013))

A limitation in these modeling studies was the lack of fundamental quantitative understanding of what causes ice nucleation and how efficiently it does so. Recently, Atkinson et al. (2013) published the global distribution of IN from mineral dust aerosol based on the laboratory discovery that K-feldspar is the most efficient mineral IN in mineral dust. They used the laboratory-derived ice-active site densities together with a global aerosol model (GLOMAP) to predict the mineral dust IN concentration globally. In GLOMAP, the dust emissions were based on AeroCom recommendations (Dentener et al. 2006), together with the dust mineralogy of Nickovic et al. (2012). Figure 12.9 shows the resulting IN concentrations at 600 hPa which are active at −20 °C and at water saturation. This figure shows a clear peak in IN concentrations near in vicinity of the dust belt with less dust in remote locations. It should be borne in mind that aging and all scavenging processes were not represented; hence, the IN concentrations far from source were probably overestimated. Another general feature is the strong hemispheric divide, with dust IN concentrations much lower in the Southern Hemisphere.

We now turn our attention to the much colder upper troposphere where heterogeneous IN have a profound impact on the properties of cirrus clouds (DeMott et al. 1997; Krämer et al. 2009; Cziczo et al. 2013; Barahona et al. 2010). In the absence of heterogeneous IN, in situ cirrus (not including anvil outflow cirrus) forms via the homogeneous nucleation of ice in aqueous haze particles. The number of ice crystals which form is, in part, determined by the competition between the rate of increase in saturation driven by adiabatic expansion and ice crystal

growth which eventually quenches the supersaturation. Homogeneous nucleation of haze particles occurs around 155–160 % RH_i depending on temperature, but independently of solute composition (Koop et al. 2000). Since the nucleation rate for homogeneous nucleation increases rapidly with increasing saturation, many of these droplets freeze before the supersaturation is quenched by the growth of the nucleated ice crystals. In the presence of heterogeneous IN capable of nucleating ice at lower supersaturations, far fewer ice crystals typically form (Gettelman et al. 2012; Lohmann and Feichter 2005; Barahona and Nenes 2007, 2009; Barahona et al. 2010; Murray et al. 2010; Karcher and Lohmann 2003; Ren and Mackenzie 2005; Jensen et al. 2010). Several studies have shown that nucleation by dusts, and other materials, below water saturation results in a much more gradual nucleation of ice crystals on increasing saturation than in the case of homogeneous nucleation (Koehler et al. 2010; Möhler et al. 2006). Wheeler and Bertram (2012) reach a similar conclusion through showing that nucleation by mineral dust cannot be represented with classical nucleation theory assuming a single contact angle. Models show that the growth of heterogeneously nucleated ice crystals can result in a peak saturation below that required for homogeneous nucleation with the result that a small number of ice crystals nucleate, but these crystals grow to larger sizes (Murray et al. 2010; Barahona and Nenes 2007, 2009; Barahona et al. 2010).

12.9 Conclusion

In this chapter, we discuss the role of mineral dust as CCN and IN as well as the subsequent influence on cloud microphysics and climate. Field observations have shown that on numerous occasions, secondary sulfate and nitrate are heterogeneously formed on many dust particles and aerosol particles appear to be internally mixed, especially during long-range transport. It has been found that carbonate minerals are preferentially associated with nitrates, whereas aluminum silicates are preferentially associated with sulfates. Apart from internal mixtures, nearly hygrophobic mineral particles can also be found as external mixtures with hygroscopic particles. In all cases of either internal or external mixtures, the presence of hygroscopic components can substantially alter the hygroscopic growth and CCN activity, as well as the IN ability and nucleation pathway, of mineral dust particles.

For the majority of studies, the CCN activity of mineral dust particles is solely described by Köhler theory, which is based only on the contribution of the solute and curvature effects upon water equilibrium vapor pressure using the hygroscopicity parameter κ introduced by Petters and Kreidenweis (2007). Kumar et al. (2011b) proposed a new framework of CCN activation that takes into account not only the effects of solute but also water vapor adsorption, based on a core-and-shell model with the core representing insoluble dust and shell consisting of a layer of soluble salt. These attempts to parameterize better the activity of mineral dust aerosols are crucial in order to better comprehend the aerosol-cloud-climate interactions.

Considerable work still remains to constrain the importance of adsorption on the CCN activity of dust particles and determine the appropriate set of adsorption parameters for freshly emitted and aged dust. Work toward understanding the role of individual minerals on the overall observed CCN activity is also important for understanding the global distribution of dust hygroscopicity. Direct water adsorption measurements (Hatch et al. 2014) and measurement of subsaturated water uptake (Lathem et al. 2011) can provide crucial information toward resolving these outstanding questions.

It has become apparent from field and laboratory studies that mineral dusts are one of the most important IN types in the atmosphere. Other materials, such as some bacteria or fungal materials, can nucleate ice at much higher temperatures (Hoose and Möhler 2012; Murray et al. 2012). However, mineral dust tends to have a greater abundance in the atmosphere and therefore contributes far more IN than bacteria, pollen, or fungal spores below −15 °C (Murray et al. 2012) and in cirrus clouds (Cziczo et al. 2013), although the situation in tropical cyclones may be different (DeLeon-Rodriguez et al. 2013). The impact of IN on clouds depends on the cloud type and the pathways of ice nucleation that are relevant for that cloud. For example, nucleation below water saturation on dry mineral dust or by mineral dust particles immersed in concentrated solution droplets is thought to be most important in the upper troposphere where cirrus clouds form. In contrast, ice nucleation by particles immersed in water droplets is thought to be most important in mixed-phase clouds.

In the past it was thought that the clay minerals were the component of mineral dust which nucleated ice, but recent work suggests that feldspars are in fact the most important minerals in mineral dust for ice nucleation (Atkinson et al. 2013; Yakobi-Hancock et al. 2013). This provided the basis for estimating the global distribution of IN using a global aerosol model with a description of desert dust mineralogy (Atkinson et al. 2013). There remain many aspects of mineral dust IN that are poorly understood. The atmospheric aging of mineral dusts is an open issue. Experimental studies show that mineral dust can be passivized (or deactivated) with acid coatings (Wex et al. 2013; Sullivan et al. 2010a, b), but it has also been argued that there is a significant population of mineral dust that remain active even after transport in the atmosphere (Cziczo et al. 2013). Some work shows that mineral dusts, especially those from fertile soils, contain significant amounts of biological IN associated with mineral dusts which may enhance ice nucleation (O'Sullivan et al. 2014; Conen et al. 2011; Creamean et al. 2013). The role of this biological-derived material also needs to be investigated further in order to determine its global impact.

References

Albrecht B (1989) Aerosols, cloud microphysics, and fractional cloudiness. Science 245:1227–1230

Andreae MO, Rosenfeld D, Artaxo P, Costa AA, Frank GP, Longo KM, Silva-Dias MAF (2004) Smoking rain clouds over the Amazon. Science 303:1337–1342

Ansmann A, Mattis I, Müller D, Wandinger U, Radlach M, Althausen D, Damoah R (2005) Ice formation in Saharan dust over central Europe observed with temperature/humidity/aerosol Raman lidar. J Geophys Res Atmos 110(D18), D18S12. doi:10.1029/2004jd005000

Ansmann A, Tesche M, Seifert P, Althausen D, Engelmann R, Fruntke J, Wandinger U, Mattis I, Mueller D (2009) Evolution of the ice phase in tropical altocumulus: SAMUM lidar observations over Cape Verde. J Geophys Res 114, D17208. doi:10.1029/2008jd011659

Archuleta CM, DeMott PJ, Kreidenweis SM (2005) Ice nucleation by surrogates for atmospheric mineral dust and mineral dust/sulfate particles at cirrus temperatures. Atmos Chem Phys 5:2617–2634

Atkinson JD, Murray BJ, Woodhouse MT, Whale TF, Baustian KJ, Carslaw KS, Dobbie S, O'Sullivan D, Malkin TL (2013) The importance of feldspar for ice nucleation by mineral dust in mixed-phase clouds. Nature 498(7454):355–358. doi:10.1038/nature12278

Barahona D (2012) On the ice nucleation spectrum. Atmos Chem Phys 12(8):3733–3752. doi:10.5194/acp-12-3733-2012

Barahona D, Nenes A (2007) Parameterization of cloud droplet formation in large scale models: including effects of entrainment. J Geophys Res 112:D16026. doi:10.1029/16207JD008473

Barahona D, Nenes A (2009) Parameterizing the competition between homogeneous and heterogeneous freezing in ice cloud formation-polydisperse ice nuclei. Atmos Chem Phys 9:5933–5948. http://www.atmos-chem-phys.net/9/5933/2009/

Barahona D, Rodriguez J, Nenes A (2010) Sensitivity of the global distribution of cirrus ice crystal concentration to heterogeneous freezing. J Geophys Res 115, D23213. doi:10.1029/2010JD014273

Baustian KJ, Cziczo DJ, Wise ME, Pratt KA, Kulkarni G, Hallar AG, Tolbert MA (2012) Importance of aerosol composition, mixing state, and morphology for heterogeneous ice nucleation: a combined field and laboratory approach. J Geophys Res 117, D06217. doi:10.1029/2011jd016784

Boucher O, Randall D, Artaxo P, Bretherton C, Feingold G, Forster P, Kerminen V-M, Kondo Y, Liao H, Lohmann U, Rasch P, Satheesh SK, Sherwood S, Stevens B, Zhang XY (2013) Clouds and aerosols. In: Stocker TF, Qin D, Plattner G-K, Tignor M, Allen SK, Boschung J, Nauels A, Xia Y, Bex V, Midgley PM (eds) Climate change 2013: the physical science basis. Contribution of working group I to the fifth assessment report of the Intergovernmental Panel on Climate Change. Cambridge University Press, Cambridge/New York

Broadley SL, Murray BJ, Herbert RJ, Atkinson JD, Dobbie S, Malkin TL, Condliffe E, Neve L (2012) Immersion mode heterogeneous ice nucleation by an illite rich powder representative of atmospheric mineral dust. Atmos Chem Phys 12(1):287–307. doi:10.5194/acp-12-287-2012

Burrows SM, Hoose C, Pöschl U, Lawrence MG (2013) Ice nuclei in marine air: biogenic particles or dust? Atmos Chem Phys 13(1):245–267. doi:10.5194/acp-13-245-2013

Cakmur RV, Miller RL, Perlwitz J, Geogdzhayev IV, Ginoux P, Koch D, Kohfeld KE, Tegen I, Zender CS (2006) Constraining the magnitude of the global dust cycle by minimizing the difference between a model and observations. J Geophys Res 111, D06207. doi:10.1029/2005JD005791

Carslaw KS, Lee LA, Reddington CL, Pringle KJ, Rap A, Forster PM, Mann GW, Spracklen DV, Woodhouse MT, Regayre LA (2013) Large contribution of natural aerosols to uncertainty in indirect forcing. Nature 503. doi: 10.1038/nature12674

Cheng WYY, Carrió GG, Cotton WR, Saleeby SM (2009) Influence of cloud condensation and giant cloud condensation nuclei on the development of precipitating trade wind cumuli in a large eddy simulation. J Geophys Res 114, D08201. doi:10.1029/2008JD011011

Chernoff DI, Bertram AK (2010) Effects of sulfate coatings on the ice nucleation properties of a biological ice nucleus and several types of minerals. J Geophys Res 115. doi:10.1029/2010jd014254

Choi YS, Lindzen RS, Ho CH, Kim J (2010) Space observations of cold-cloud phase change. Proc Natl Acad Sci U S A 107(25):11211–11216. doi:10.1073/pnas.1006241107

Conen F, Morris CE, Leifeld J, Yakutin MV, Alewell C (2011) Biological residues define the ice nucleation properties of soil dust. Atmos Chem Phys 11(18):9643–9648. doi:10.5194/acp-11-9643-2011

Connolly PJ, Mohler O, Field PR, Saathoff H, Burgess R, Choularton T, Gallagher M (2009) Studies of heterogeneous freezing by three different desert dust samples. Atmos Chem Phys 9(8):2805–2824. doi:10.5194/acp-9-2805-2009

Creamean JM, Suski KJ, Rosenfeld D, Cazorla A, DeMott PJ, Sullivan RC, White AB, Ralph FM, Minnis P, Comstock JM, Tomlinson JM, Prather KA (2013) Dust and biological aerosols from the Sahara and Asia influence precipitation in the Western U.S. Science 339(6127):1572–1578. doi:10.1126/science.1227279

Crumeyrolle S, Gomes L, Tulet P, Matsuki A, Schwarzenboeck A, Crahan K (2008) Increase of the aerosol hygroscopicity by cloud processing in a mesoscale system: a case study from the AMMA campaign. Atmos Chem Phys 8:6907–6924

Cui ZQ, Carslaw KS, Yin Y, Davies S (2006) A numerical study of aerosol effects on the dynamics and microphysics of a deep convective cloud in a continental environment. J Geophys Res 111, D05201. doi:10.1029/2005JD005981

Cziczo DJ, Froyd KD, Gallavardin SJ, Moehler O, Benz S, Saathoff H, Murphy DM (2009) Deactivation of ice nuclei due to atmospherically relevant surface coatings. Environ Res Lett 4(4). doi:10.1088/1748-9326/4/4/044013

Cziczo DJ, Froyd KD, Hoose C, Jensen EJ, Diao M, Zondlo MA, Smith JB, Twohy CH, Murphy DM (2013) Clarifying the dominant sources and mechanisms of cirrus cloud formation. Science 340(6138):1320–1324. doi:10.1126/science.1234145

de Boer G, Morrison H, Shupe MD, Hildner R (2011) Evidence of liquid dependent ice nucleation in high-latitude stratiform clouds from surface remote sensors. Geophys Res Lett 38, L01803. doi:10.1029/2010gl046016

DeLeon-Rodriguez N, Lathem TL, Rodriguez LM, Barazesh JM, Anderson BE, Beyersdorf AJ, Ziemba LD, Bergin M, Nenes A, Konstantinidis KT (2013) The microbiome of the upper troposphere: species composition and prevalence, effects of tropical storms, and atmospheric implications. Proc Natl Acad Sci U S A. doi:10.1073/pnas.1212089110

DeMott PJ (1995) Quantitative descriptions of ice formation mechanisms of silver iodide-type aerosols. Atmos Res 38(1–4):63–99

DeMott PJ, Rogers DC, Kreidenweis SM (1997) The susceptibility of ice formation in upper tropospheric clouds to insoluble aerosol components. J Geophys Res 102(D16):19575–19584

DeMott PJ, Cziczo DJ, Prenni AJ, Murphy DM, Kreidenweis SM, Thomson DS, Borys R, Rogers DC (2003a) Measurements of the concentration and composition of nuclei for cirrus formation. Proc Natl Acad Sci U S A 100(25):14655–14660

DeMott PJ, Sassen K, Poellot MR, Baumgardner D, Rogers DC, Brooks SD, Prenni AJ, Kreidenweis SM (2003b) African dust aerosols as atmospheric ice nuclei. Geophys Res Lett 30(14),1732. doi:10.1029/2003GL017410

Dentener FJ, Carmichael GR, Zhang Y, Lelieveld J, Crutzen PJ (1996) Role of mineral aerosol as a reactive surface in the global troposphere. J Geophys Res 101(D17):22869–22889

Dentener F, Kinne S, Bond T, Boucher O, Cofala J, Generoso S, Ginoux P, Gong S, Hoelzemann JJ, Ito A, Marelli L, Penner JE, Putaud JP, Textor C, Schulz M, van der Werf GR, Wilson J (2006) Emissions of primary aerosol and precursor gases in the years 2000 and 1750 prescribed datasets for AeroCom. Atmos Chem Phys 6(12):4321–4344. doi:10.5194/acp-6-4321-2006

Durant AJ, Shaw RA (2005) Evaporation freezing by contact nucleation inside-out. Geophys Res Lett 32, L20814. doi:10.1029/2005GL024175

Eastwood ML, Cremel S, Wheeler M, Murray BJ, Girard E, Bertram AK (2009) The effects of sulfuric acid and ammonium sulfate coatings on the ice nucleation properties of kaolinite particles. Geophys Res Lett 36, L02811. doi:10.1029/2008GL035997

Ebert M, Worringen A, Benker N, Mertes S, Weingartner E, Weinbruch S (2011) Chemical composition and mixing-state of ice residuals sampled within mixed phase clouds. Atmos Chem Phys 11(6):2805–2816. doi:10.5194/acp-11-2805-2011

Field PR, Heymsfield AJ, Shipway BJ, DeMott PJ, Pratt KA, Rogers DC, Stith J, Prather KA (2012) Ice in clouds experiment-layer clouds. Part II: testing characteristics of heterogeneous ice formation in Lee wave clouds. J Atmos Sci 69(3):1066–1079. doi:10.1175/jas-d-11-026.1

Formenti P, Schütz L, Ballanski Y, Desboeufs K, Ebert M, Kandler K, Petzold A, Scheuvens D, Weinbruch S, Zhang D (2011) Recent progress in understanding physical and chemical properties of African and Asian mineral dust. Atmos Chem Phys 11:8231–8256

Fornea AP, Brooks SD, Dooley JB, Saha A (2009) Heterogeneous freezing of ice on atmospheric aerosols containing ash, soot and soil. J Geophys Res 114, D13201. doi:10.1029/2009JD011958

Froyd KD, Murphy DM, Lawson P, Baumgardner D, Herman RL (2010) Aerosols that form subvisible cirrus at the tropical tropopause. Atmos Chem Phys 10(1):209–218. doi:10.5194/acp-10-209-2010

Garimella S, Huang Y-w, Seewald JS, Cziczo DJ (2013) Cloud condensation nucleus activity comparison of dry- and wet-generated mineral dust aerosol: the significance of soluble material. Atmos Chem Phys Discuss 13:31041–31078. doi:10.5194/acpd-13-31041-2013

Gettelman A, Liu X, Barahona D, Lohmann U, Chen C (2012) Climate impacts of ice nucleation. J Geophys Res 117. doi:10.1029/2012jd017950

Ghan S, Guzman G, Abdul-Razzak H (1998) Competition between sea-salt and sulfate particles as cloud condensation nuclei. J Atmos Sci 55:3340–3347

Ghan S, Easter R, Hudson J, Breon FM (2001) Evaluation of aerosol indirect radiative forcing in MIRAGE. J Geophys Res 106(D6):5317–5334

Ghan SJ, Abdul-Razzak H, Nenes A, Ming Y, Liu X, Ovchinnikov M, Shipway B, Meskhidze N, Xu J, Shi X (2011) Droplet nucleation: physically-based parameterization and comparative evaluation. J Adv Model Earth Syst 3:M10001. doi:10.1029/2011MS000074

Ghan SJ, Liu X, Easter RC, Zaveri R, Rasch PJ, Yoon J-H, Eaton B (2012) Toward a minimal representation of aerosols in climate models: comparative decomposition of aerosol direct, semidirect, and indirect radiative forcing. J Clim 25:6461–6476

Gibson ER, Hudson PK, Grassian VH (2006) Aerosol chemistry and climate: laboratory studies of the carbonate component of mineral dust and its reaction products. Geophys Res Lett 33, L13811. doi:10.1029/2006GL026386

Gibson ER, Gierlus KM, Hudson PK, Grassian VH (2007) Generation of internally mixed insoluble and soluble aerosol particles to investigate the impact of atmospheric aging and heterogeneous processing on the CCN activity of mineral dust aerosol. Aerosol Sci Technol 41(10):914–924

Gierlus KM, Laskina O, Abernathy TL, Grassian VH (2012) Laboratory study of the effect of oxalic acid on the cloud condensation nuclei activity of mineral dust aerosol. Atmos Environ 46:125–130

Hatch CD, Greenaway AL, Christie MJ, Baltrusaitis J (2014) Water adsorption constrained Frenkel-Halsey-Hill adsorption activation theory: montmorillonite and illite. Atmos Environ 87:26–33

Henson BF (2007) An adsorption model of insoluble particle activation: application to black carbon. J Geophys Res 112, D24S16. doi:10.1029/2007JD008549

Herbert RJ, Murray BJ, Whale TF, Dobbie SJ, Atkinson JD (2014) Representing time-dependent freezing behaviour in immersion mode ice nucleation. Atmos Chem Phys Discuss 14(2):1399–1442. doi:10.5194/acpd-14-1399-2014

Herich H, Tritscher T, Wiacek A, Gysel M, Weingartner E, Lohmann U, Baltensperger U, Cziczo DJ (2009) Water uptake of clay and desert dust aerosol particles at sub- and supersaturated water vapor conditions. Phys Chem Chem Phys 11:7804–7809. doi:10.1039/b901585j

Herich H, Tritscher T, Wiacek A, Gysel M, Weingartner E, Lohmann U, Baltensperger U, Cziczo DJ (2011) Water uptake of clay and desert dust aerosol particles at sub- and supersaturated water vapor conditions. Phys Chem Chem Phys 11:7804–7809

Hoose C, Möhler O (2012) Heterogeneous ice nucleation on atmospheric aerosols: a review of results from laboratory experiments. Atmos Chem Phys 12:9817–9854

Hoose C, Kristjánsson JE, Chen JP, Hazra A (2010) A classical-theory-based parameterization of heterogeneous ice nucleation by mineral dust, soot, and biological particles in a global climate model. J Atmos Sci 67(8):2483–2503. doi:10.1175/2010jas3425.1

Hoyle CR, Pinti V, Welti A, Zobrist B, Marcolli C, Luo B, Höskuldsson Á, Mattsson HB, Stetzer O, Thorsteinsson T, Larsen G, Peter T (2011) Ice nucleation properties of volcanic ash from Eyjafjallajökull. Atmos Chem Phys 11(18):9911–9926. doi:10.5194/acp-11-9911-2011

Jensen EJ, Pfister L, Bui TP, Lawson P, Baumgardner D (2010) Ice nucleation and cloud microphysical properties in tropical tropopause layer cirrus. Atmos Chem Phys 10(3):1369–1384. doi:10.5194/acp-10-1369-2010

Kamphus M, Ettner-Mahl M, Klimach T, Drewnick F, Keller L, Cziczo DJ, Mertes S, Borrmann S, Curtius J (2010) Chemical composition of ambient aerosol, ice residues and cloud droplet residues in mixed-phase clouds: single particle analysis during the Cloud and Aerosol Characterization Experiment (CLACE 6). Atmos Chem Phys 10(16):8077–8095. doi:10.5194/acp-10-8077-2010

Kanitz T, Seifert P, Ansmann A, Engelmann R, Althausen D, Casiccia C, Rohwer EG (2011) Contrasting the impact of aerosols at northern and southern midlatitudes on heterogeneous ice formation. Geophys Res Lett 38, L17802. doi:10.1029/2011gl048532

Karcher B, Lohmann U (2003) A parameterization of cirrus cloud formation: heterogeneous freezing. J Geophys Res 108(D14),4402. doi:10.1029/2002JD003220

Karydis VA, Kumar P, Barahona D, Sokolik IN, Nenes A (2011) On the effect of dust particles on global cloud condensation nuclei and cloud droplet number. J Geophys Res 116, D23204. doi:10.1029/2011JD016283

Kashchiev D (2000) Nucleation: basic theory with applications. Butterworth-Heinemann, Oxford

Kelly JT, Chuang CC, Wexler AS (2007) Influence of dust composition on cloud droplet formation. Atmos Environ 41:2904–2916

Khvorostyanov VI, Curry JA (2005) The theory of ice nucleation by heterogeneous freezing of deliquescent mixed CCN. Part II: parcel model simulation. J Atmos Sci 62(2):261–285

Khvorostyanov VI, Curry JA (2007) Refinements to the Köhler's theory of aerosol equilibrium radii, size spectra, and droplet activation: effects of humidity and insoluble fraction. J Geophys Res 112, D05206. doi:10.1029/2006JD007672

Kim J-S, Park K (2012) Atmospheric aging of Asian dust particles during long range transport. Aerosol Sci Technol 46(8):913–924

Kirkevag A, Iversen T, Seland O, Debernard JB, Storelvmo T, Kristjansson JE (2008) Aerosol-cloud-climate interactions in the climate model CAM-Oslo. Tellus 60(3):492–512

Knopf DA, Alpert PA (2013) A water activity based model of heterogeneous ice nucleation kinetics for freezing of water and aqueous solution droplets. Faraday Discuss 165:513–534. doi:10.1039/c3fd00035d

Knopf DA, Koop T (2006) Heterogeneous nucleation of ice on surrogates of mineral dust. J Geophys Res 111(D12):D12201. doi:10.1029/2005JD006894

Koehler KA, Kreidenweis SM, DeMott PJ, Petters MD, Prenni AJ, Carrico CM (2009) Hygroscopicity and cloud droplet activation of mineral dust aerosol. Geophys Res Lett 36, L08805. doi:10.1029/2009GL037348

Koehler KA, Kreidenweis SM, DeMott PJ, Petters MD, Prenni AJ, Möhler O (2010) Laboratory investigations of the impact of mineral dust aerosol on cold cloud formation. Atmos Chem Phys 10(23):11955–11968. doi:10.5194/acp-10-11955-2010

Köhler H (1936) The nucleus in the growth of hygroscopic droplets. Trans Faraday Soc 32:1152

Koop T, Luo BP, Tsias A, Peter T (2000) Water activity as the determinant for homogeneous ice nucleation in aqueous solutions. Nature 406(6796):611–614

Krämer M, Schiller C, Afchine A, Bauer R, Gensch I, Mangold A, Schlicht S, Spelten N, Sitnikov N, Borrmann S, de Reus M, Spichtinger P (2009) Ice supersaturations and cirrus cloud crystal numbers. Atmos Chem Phys 9(11):3505–3522. doi:10.5194/acp-9-3505-2009

Kumai M (1961) Snow crystals and the identification of the nuclei in the Northern United-States of America. J Meteorol 18(2):139–150

Kumar P, Sokolik IN, Nenes A (2009a) Parameterization of cloud droplet formation for global and regional models: including adsorption activation from insoluble CCN. Atmos Chem Phys 9:2517–2532

Kumar P, Nenes A, Sokolik I (2009b) The importance of adsorption for CCN activity and hygroscopic properties of mineral dust aerosol. Geophys Res Lett 36, L24804. doi:10.1029/2009GL040827

Kumar P, Sokolik IN, Nenes A (2011a) Measurements of cloud condensation nuclei activity and droplet activation kinetics of fresh unprocessed regional dust samples and minerals. Atmos Chem Phys 11:3527–3541

Kumar P, Sokolik IN, Nenes A (2011b) Cloud condensation nuclei activity and droplet activation kinetics of wet processed regional dust samples and minerals. Atmos Chem Phys 11:8661–8676

Laaksonen A, Korhonen P, Kulmala M, Charlson RJ (1998) Modification of the Kohler equation to include soluble trace gases and slightly soluble substances. J Atmos Sci 55:853–862

Ladino Moreno LA, Stetzer O, Lohmann U (2013) Contact freezing: a review of experimental studies. Atmos Chem Phys 13(19):9745–9769. doi:10.5194/acp-13-9745-2013

Lance, S. (2007) Quantifying compositional impacts of ambient aerosol on cloud droplet formation. Doctoral thesis, Georgia Institute of Technology. https://smartech.gatech.edu/handle/1853/26700

Lance S, Shupe M, Feingold G, Brock C, Cozic J, Holloway J, Moore RH, Nenes A, Schwarz J, Spackman R, Froyd KD, Murphy DM, Brioude J, Cooper O, Stohl A, Burkhart JF (2011) CCN as a modulator for ice processes in arctic mixed-phase clouds. Atmos Chem Phys 11:8003–8015

Lathem TL, Kumar P, Nenes A, Dufek J, Sokolik IN, Trail M, Russell A (2011) Hygroscopic properties of volcanic ash. Geophys Res Lett 38, L11802. doi:10.1029/2011GL047298

Levin Z, Cotton WR (2008) Aerosol pollution impact on precipitation: a scientific review. Springer, New York, p 382. ISBN: 978-1-4020-8689-2

Levin Z, Teller A, Ganor E (2005) On the interactions of mineral dust, sea-salt particles, and clouds: a measurement and modeling study from the Mediterranean Israeli Dust Experiment campaign. J Geophys Res 110, D20202. doi:10.1029/2005JD005810

Li W, Shao LY (2009a) Transmission electron microscopy study of aerosol particles from the brown hazes in northern China. J Geophys Res 114, D09302. doi:10.1029/2008JD011285

Li WJ, Shao LY (2009b) Observation of nitrate coatings on atmospheric mineral dust particles. Atmos Chem Phys 9:1863–1871

Li L, Chen ZM, Zhang YH, Zhu T, Li JL, Ding J (2006) Kinetics and mechanism of heterogeneous oxidation of sulfur by ozone on surface of calcium carbonate. Atmos Chem Phys 6:2453–2464

Li R, Min Q-L, Harrison LC (2010) A case study: the indirect aerosol effects of mineral dust on warm clouds. J Atmos Sci 67:805–816. doi:10.1175/2009JAS3235.1

Liu X, Shi X, Zhang K, Jensen EJ, Gettelman A, Barahona D, Nenes A, Lawson P (2012) Sensitivity studies of dust ice nuclei effect on cirrus clouds with the community atmosphere model CAM5. Atmos Chem Phys 12:12061–12079

Lohmann U, Diehl K (2006) Sensitivity studies of the importance of dust ice nuclei for the indirect aerosol effect on stratiform mixed-phase clouds. J Atmos Sci 63:968–981

Lohmann U, Feichter J (2005) Global indirect aerosol effects: a review. Atmos Chem Phys 5:715–737

Lohmann U, Stier P, Hoose C, Ferrachat S, Kloster S, Roeckner E, Zhang J (2007) Cloud microphysics and aerosol indirect effects in the global climate model ECHAM5-HAM. Atmos Chem Phys 7(13):3425–3446

Lüönd F, Stetzer O, Welti A, Lohmann U (2010) Experimental study on the ice nucleation ability of size selected kaolinite particles in the immersion mode. J Geophys Res 115(D14), D14201. doi:10.1029/2009jd012959

Manktelow PT, Carslaw KS, Mann GW, Spracklen DV (2010) The impact of dust on sulfate aerosol, CN, and CCN during an East Asian dust storm. Atmos Chem Phys 10:365–382

Marcolli C (2013) Deposition nucleation viewed as homogeneous or immersion freezing in pores and cavities. Atmos Chem Phys Discuss 13(6):16367–16456. doi:10.5194/acpd-13-16367-2013

Marcolli S, Gedamke S, Peter T, Zobrist B (2007) Efficiency of immersion mode ice nucleation on surrogates of mineral dust. Atmos Chem Phys 7:5081–5091

Mason BJ (1971) The Physics of clouds. Clarendon Press, Oxford

Matsuki A, Schwarzenboeck A, Venzac H, Laj P, Crumeyrolle S, Gomes L (2010) Cloud processing of mineral dust: direct comparison of cloud residual and clear sky particles during AMMA aircraft campaign in summer 2006. Atmos Chem Phys 10:1057–1069

Mechem DB, Kogan YL (2008) A bulk parameterization of giant CCN. J Atmos Sci 65:2458–2466

Menon S, Del Genio AD, Koch D, Tselioudis G (2002) GCM simulations of the aerosol indirect effect: sensitivity to cloud parameterization and aerosol burden. J Atmos Sci 59:692–713

Möhler O, Field PR, Connolly P, Benz S, Saathoff H, Schnaiter M, Wagner R, Cotton R, Kramer M, Mangold A, Heymsfield AJ (2006) Efficiency of the deposition mode ice nucleation on mineral dust particles. Atmos Chem Phys 6:3007–3021

Morales Betancourt R, Nenes A (2013) Understanding the contributions of aerosol properties and parameterization discrepancies to droplet number variability in a Global Climate Model. Atmos Chem Phys Discuss 13:31479–31526. doi:10.5194/acpd-13-31479-2013

Morrison H, de Boer G, Feingold G, Harrington J, Shupe MD, Sulia K (2012) Resilience of persistent Arctic mixed-phase clouds. Nat Geosci 5(1):11–17. doi:10.1038/ngeo1332

Mullin JW (2001) Crystallization, 4th edn. Elsevier Butterworth-Heinemann, Oxford

Murray BJ, Wilson TW, Dobbie S, Cui ZQ, Al-Jumur S, Mohler O, Schnaiter M, Wagner R, Benz S, Niemand M, Saathoff H, Ebert V, Wagner S, Karcher B (2010) Heterogeneous nucleation of ice particles on glassy aerosols under cirrus conditions. Nat Geosci 3(4):233–237. doi:10.1038/NGEO817

Murray BJ, Broadley SL, Wilson TW, Atkinson JD, Wills RH (2011) Heterogeneous freezing of water droplets containing kaolinite particles. Atmos Chem Phys 11(9):4191–4207. doi:10.5194/acp-11-4191-2011

Murray BJ, O'Sullivan D, Atkinson JD, Webb ME (2012) Ice nucleation by particles immersed in supercooled cloud droplets. Chem Soc Rev 41(19):6519–6554. doi:10.1039/c2cs35200a

Navea JG, Chen H, Huang M, Carmichael GR, Grassian VH (2010) A comparative evaluation of water uptake on several mineral dust sources. Environ Chem 7(2):162–170

Nenes A, Charlson RJ, Facchini MC, Kulmala M, Laaksonen A, Seinfeld JH (2002) Can chemical effects on cloud droplet number rival the first indirect effect? Geophys Res Lett 29(17):1848. doi:10.1029/2002GL015295

Nickovic S, Vukovic A, Vujadinovic M, Djurdjevic V, Pejanovic G (2012) Technical note: high-resolution mineralogical database of dust-productive soils for atmospheric dust modeling. Atmos Chem Phys 12(2):845–855. doi:10.5194/acp-12-845-2012

Niedermeier D, Hartmann S, Shaw RA, Covert D, Mentel TF, Schneider J, Poulain L, Reitz P, Spindler C, Clauss T, Kiselev A, Hallbauer E, Wex H, Mildenberger K, Stratmann F (2010) Heterogeneous freezing of droplets with immersed mineral dust particles – measurements and parameterization. Atmos Chem Phys 10(8):3601–3614. doi:10.5194/acp-10-3601-2010

Niedermeier D, Hartmann S, Clauss T, Wex H, Kiselev A, Sullivan RC, DeMott PJ, Petters MD, Reitz P, Schneider J, Mikhailov E, Sierau B, Stetzer O, Reimann B, Bundke U, Shaw RA, Buchholz A, Mentel TF, Stratmann F (2011a) Experimental study of the role of physicochemical surface processing on the IN ability of mineral dust particles. Atmos Chem Phys 11(21):11131–11144. doi:10.5194/acp-11-11131-2011

Niedermeier D, Shaw RA, Hartmann S, Wex H, Clauss T, Voigtländer J, Stratmann F (2011b) Heterogeneous ice nucleation: exploring the transition from stochastic to singular freezing behavior. Atmos Chem Phys 11(16):8767–8775. doi:10.5194/acp-11-8767-2011

Niemand M, Möhler O, Vogel B, Vogel H, Hoose C, Connolly P, Klein H, Bingemer H, DeMott P, Skrotzki J, Leisner T (2012) A particle-surface-area-based parameterization of immersion freezing on desert dust particles. J Atmos Sci. doi:10.1175/jas-d-11-0249.1

O'Sullivan D, Murray BJ, Malkin TL, Whale TF, Umo NS, Atkinson JD, Price HC, Baustian KJ, Browse J, Webb ME (2014) Ice nucleation by fertile soil dusts: relative importance of mineral and biogenic components. Atmos Chem Phys 14(4):1853–1867. doi:10.5194/acp-14-1853-2014

Penner JE, Quaas J, Storelvmo T, Takemura T, Boucher O, Guo H, Kirkevag A, Kristjansson JE, Seland O (2006) Model intercomparison of indirect aerosol effects. Atmos Chem Phys 6:3391–3405

Petters MD, Kreidenweis SM (2007) A single parameter representation of hygroscopic growth and cloud condensation nucleus activity. Atmos Chem Phys 7:1961–1971

Phillips VTJ, Donner LJ, Garner ST (2007) Nucleation processes in deep convection simulated by a cloud-system-resolving model with double-moment bulk microphysics. J Atmos Sci 64(3):738–761. doi:10.1175/jas3869.1

Posselt R, Lohmann U (2008) Influence of Giant CCN on warm rain processes in the ECHAM5 GCM. Atmos Chem Phys 8:3769–3788

Pratt KA, DeMott PJ, French JR, Wang Z, Westphal DL, Heymsfield AJ, Twohy CH, Prenni AJ, Prather KA (2009) In situ detection of biological particles in cloud ice-crystals. Nat Geosci 2(6):397–400

Pruppacher HR, Klett JD (1997) Microphysics of clouds and precipitations, atmospheric and oceanographic sciences library. Kluwer Academic Publishers, Dordrecht

Reitz P, Spindler C, Mentel TF, Poulain L, Wex H, Mildenberger K, Niedermeier D, Hartmann S, Clauss T, Stratmann F, Sullivan RC, DeMott PJ, Petters MD, Sierau B, Schneider J (2011) Surface modification of mineral dust particles by sulphuric acid processing: implications for ice nucleation abilities. Atmos Chem Phys 11(15):7839–7858. doi:10.5194/acp-11-7839-2011

Ren C, Mackenzie AR (2005) Cirrus parametrization and the role of ice nuclei. Q J R Meteorol Soc 131(608):1585–1605. doi:10.1256/qj.04.126

Rosenfeld D (2006) Aerosols, clouds, and climate. Science 312:1323–1324

Rosenfeld D, Rudich Y, Lahav R (2001) Desert dust suppressing precipitation: a possible desertification feedback loop. Proc Natl Acad Sci U S A 98(11):5975–5980

Rosenfeld D, Lohmann U, Raga GB, O'Dowd CD, Kulmala M, Fuzzi S, Reissell A, Andreae MO (2008) Flood or drought: how do aerosols affect precipitation? Science 321:1309–1313

Schladitz A, Müller T, Nowak A, Kandler K, Lieke K, Massling A, Wiedensohler A (2011) In situ aerosol characterization of Cape Verde Part 1: particle number size distributions, hygroscopic growth and state of mixing of the marine and Saharan dust aerosol. Tellus B 63:531–548

Shaw RA, Durant AJ, Mi Y (2005) Heterogeneous surface crystallization observed in undercooled water. J Phys Chem B 109(20):9865–9868. doi:10.1021/jp0506336

Smoydzin L, Teller A, Tost H, Fnais M, Lelieveld J (2012) Impact of mineral dust on cloud formation in a Saharan outflow region. Atmos Chem Phys 12:11383–11393

Sokolik IN, Winker DM, Bergametti G, Gillette DA, Carmichael G, Kaufman YJ, Gomes L, Schuetz L, Penner JE (2001) Introduction to a special section: outstanding problems in quantifying the radiative impacts of mineral dust. J Geophys Res 106:18015–18027. doi:10.1029/2000JD900498

Sorjamaa R, Laaksonen A (2007) The effect of H2O adsorption on cloud drop activation of insoluble particles: a theoretical framework. Atmos Chem Phys 7:6175–6180

Stevens B, Feingold G (2009) Untangling aerosol effects on clouds and precipitation in a buffered system. Nature 461:607–613. doi:10.1038/nature08281

Storelvmo T, Hoose C, Eriksson P (2011) Global modeling of mixed-phase clouds: the albedo and lifetime effects of aerosols. J Geophys Res 116, D05207. doi:10.1029/2010jd014724

Stoyanova V, Kashchiev D, Kupenova T (1994) Freezing of water droplets seeded with atmospheric aerosols and ice nucleation activity of the aerosols. J Aerosol Sci 25:867–877

Sullivan RC, Moore MJK, Petters MD, Kreidenweis SM, Roberts GC, Prather KA (2009a) Effect of chemical mixing state on the hygroscopicity and cloud nucleation properties of calcium mineral dust particles. Atmos Chem Phys 9:3303–3316

Sullivan RC, Moore MJK, Petters MD, Kreidenweis SM, Roberts GC, Prather KA (2009b) Timescale for hygroscopic conversion of calcite mineral particles through heterogeneous reaction with nitric acid. Phys Chem Chem Phys 11:7826–7837

Sullivan RC, Moore MJK, Petters MD, Kreidenweis SM, Qafoku O, Laskin A, Roberts GC, Prather KA (2010a) Impact of particle generation method on the apparent hygroscopicity of insoluble particles. Aerosol Sci Technol 44(10):830–846

Sullivan RC, Petters MD, DeMott PJ, Kreidenweis SM, Wex H, Niedermeier D, Hartmann S, Clauss T, Stratmann F, Reitz P, Schneider J, Sierau B (2010b) Irreversible loss of ice nucleation active sites in mineral dust particles caused by sulphuric acid condensation. Atmos Chem Phys 10(23):11471–11487. doi:10.5194/acp-10-11471-2010

Takemura T, Nozawa T, Emori S, Nakajima TY, Nakajima T (2005) Simulation of climate response to aerosol direct and indirect effects with aerosol transport-radiation model. J Geophys Res 110, D02202

Tobo Y, DeMott PJ, Raddatz M, Niedermeier D, Hartmann S, Kreidenweis SM, Stratmann F, Wex H (2012) Impacts of chemical reactivity on ice nucleation of kaolinite particles: a case study of levoglucosan and sulfuric acid. Geophys Res Lett 39(19), L19803. doi:10.1029/2012gl053007

Topping D, Connolly P, McFiggans G (2013) Cloud droplet number enhanced by co-condensation of organic vapours. Nat Geosci 6:443–446. doi:10.1038/NGEO1809

Trochkine D, Iwasaka Y, Matsuki A, Yamada M, Kim Y-S, Nagatani T, Zhang D, Shi G-Y, Shen Z (2003) Mineral aerosol particles collected in Dunhuang, China, and their comparison to chemically modified particles collected over Japan. J Geophys Res 108(D23):8642. doi:10.1029/2002JD003268

Twohy CH, Kreidenweis SM, Eidhammer T, Browell EV, Heymsfield AJ, Bansemer AR, Anderson BE, Chen G, Ismail S, DeMott PJ, Van Den Heever SC (2009) Saharan dust particles nucleate droplets in eastern Atlantic clouds. Geophys Res Lett 36, L01807. doi:10.1029/2008GL035846

Twomey S (1977) The influence of pollution on the shortwave albedo of clouds. J Aerosol Sci 34:1149–1152

Vali G (1985) Nucleation terminology. Bull Am Meteorol Soc 66:1426

Vali G (1994) Freezing rate due to heterogeneous nucleation. J Atmos Sci 51:1843–1856

Vali G (2008) Repeatability and randomness in heterogeneous freezing nucleation. Atmos Chem Phys 8(16):5017–5031

Van den Heever SC, Carrió GG, Cotton WR, DeMott PJ, Prenni AJ (2006) Impacts of nucleating aerosol on Florida storms. Part I: mesoscale simulations. J Atmos Sci 63:1752–1775

Vlasenko A, Sjogren S, Weingartner E, Stemmler K, Gäggeler HW, Ammann M (2006) Effect of humidity on nitric acid uptake to mineral dust aerosol particles. Atmos Chem Phys 6:2147–2160

Westbrook CD, Illingworth AJ (2013) The formation of ice in a long-lived supercooled layer cloud. Q J R Meteorol Soc, n/a-n/a. doi:10.1002/qj.2096

Wex H, DeMott PJ, Tobo Y, Hartmann S, Rösch M, Clauss T, Tomsche L, Niedermeier D, Stratmann F (2013) Kaolinite particles as ice nuclei: learning from the use of different types of kaolinite and different coatings. Atmos Chem Phys Discuss 13(11):30311–30348. doi:10.5194/acpd-13-30311-2013

Wheeler MJ, Bertram AK (2012) Deposition nucleation on mineral dust particles: a case against classical nucleation theory with the assumption of a single contact angle. Atmos Chem Phys 12(2):1189–1201. doi:10.5194/acp-12-1189-2012

Wise ME, Baustian KJ, Koop T, Freedman MA, Jensen EJ, Tolbert MA (2012) Depositional ice nucleation onto crystalline hydrated NaCl particles: a new mechanism for ice formation in the troposphere. Atmos Chem Phys 12(2):1121–1134. doi:10.5194/acp-12-1121-2012

Woodcock AH (1950) Condensation nuclei and precipitation. J Meteorol 7:161–162

Wright TP, Petters MD (2013) The role of time in heterogeneous freezing nucleation. J Geophys Res Atmos 118(9):3731–3743. doi:10.1002/jgrd.50365

Wright TP, Petters MD, Hader JD, Morton T, Holder AL (2013) Minimal cooling rate dependence of ice nuclei activity in the immersion mode. J Geophys Res Atmos 118(18):10535–10543. doi:10.1002/jgrd.50810

Xue H, Feingold G (2006) Large eddy simulations of trade wind cumuli: investigation of aerosol indirect effects. J Atmos Sci 63:1605–1622

Yakobi-Hancock JD, Ladino LA, Abbatt JPD (2013) Feldspar minerals as efficient deposition ice nuclei. Atmos Chem Phys 13(22):11175–11185. doi:10.5194/acp-13-11175-2013

Yamashita K, Murakami M, Hashimoto A, Tajiri T (2011) CCN ability of Asian mineral dust particles and their effects on cloud droplet formation. J Meteorol Soc Jpn 89(5):581–587

Yin Y, Wurzler S, Levin Z, Reisin T (2002) Interactions of mineral dust particles and clouds: effects on precipitation and cloud optical properties. J Geophys Res 107(D23):4724. doi:10.1029/2001JD001544

Zhang H, McFarquhar GM, Cotton WR, Deng Y (2009) Direct and indirect impacts of Saharan dust acting as cloud condensation nuclei on tropical cyclone eyewall development. Geophys Res Lett 36, L06802. doi:10.1029/2009GL037276

Zhao DF, Buchholz A, Mantel TF, Müler K-P, Borchardt J, Kiendler-Scharr A, Spindler C, Tillmann R, Trimborn A, Zhu T, Wahner A (2010) Novel method of generation of Ca(HCO3)2 and CaCO3 aerosols and first determination of hygroscopic and cloud condensation nuclei activation properties. Atmos Chem Phys 10:8601–8616

Zhu C, Veblen DR, Blum AE, Chipera SJ (2006) Naturally weathered feldspar surfaces in the Navajo Sandstone aquifer, Black Mesa, Arizona: electron microscopic characterization. Geochim Cosmochim Acta 70(18):4600–4616. doi:10.1016/j.gca.2006.07.013

Chapter 13
Impact of Dust Radiative Forcing upon Climate

Ron L. Miller, Peter Knippertz, Carlos Pérez García-Pando, Jan P. Perlwitz, and Ina Tegen

Abstract Dust aerosols perturb the atmospheric radiative flux at both solar and thermal wavelengths, altering the energy and water cycles. The climate adjusts by redistributing energy and moisture, so that local temperature perturbations, for example, depend upon the forcing over the entire extent of the perturbed circulation. Within regions frequently mixed by deep convection, including the deep tropics, dust particles perturb the surface air temperature primarily through radiative forcing at the top of the atmosphere (TOA). Many models predict that dust reduces global precipitation. This reduction is typically attributed to the decrease of surface evaporation in response to dimming of the surface. A counterexample is presented, where greater shortwave absorption by dust increases evaporation and precipitation despite greater dimming of the surface. This is attributed to the dependence of surface evaporation upon TOA forcing through its influence upon surface temperature and humidity. Perturbations by dust to the surface wind speed and vegetation (through precipitation anomalies) feed back upon the dust aerosol concentration. The current uncertainty of radiative forcing attributed to dust and the

R.L. Miller (✉) • C. Pérez García-Pando • J.P. Perlwitz
NASA Goddard Institute for Space Studies, 2880 Broadway, New York, NY 10025, USA

Department of Applied Physics and Applied Mathematics, Columbia University, New York, NY, USA
e-mail: ron.l.miller@nasa.gov; Carlos.Perezga@nasa.gov; Jan.P.Perlwitz@nasa.gov

P. Knippertz
School of Earth and Environment, University of Leeds, Leeds, UK

Institute for Meteorology and Climate Research, Karlsruhe Institute of Technology, Karlsruhe, Germany
e-mail: peter.knippertz@kit.edu

I. Tegen
Leibniz Institute for Tropospheric Research, Permoserstr. 15, 04318 Leipzig, Germany
e-mail: itegen@tropos.de

P. Knippertz and J.-B.W. Stuut (eds.), *Mineral Dust: A Key Player in the Earth System*, DOI 10.1007/978-94-017-8978-3_13,

resulting range of climate perturbations calculated by models remain a useful test of our understanding of the mechanisms relating dust radiative forcing to the climate response.

Keywords Aerosol radiative forcing • Climate response • Precipitation response • Feedback upon dust mobilization

13.1 Introduction

Mineral dust from the Chinese deserts routinely shrouds western North America (Kavouras et al. 2009), extending as far downwind as the French Alps (Grousset et al. 2003), while African dust replenishes mineral nutrients within the Amazon (Swap et al. 1992). Dust perturbs the radiative flux within the atmosphere, changing transports of energy and moisture to alter temperature and precipitation thousands of kilometers beyond the dust layer (Miller and Tegen 1998). Deposition measurements suggest that the global mass of dust aerosols doubled during the twentieth century (Mahowald et al. 2010). This demonstrates the potential importance of dust radiative forcing to climate trends observed during the Anthropocene and the need to anticipate future changes in the dust load.

Mineral dust (also referred to as "soil" dust due to its origin through wind erosion of the land surface) alters climate through a number of mechanisms that are described in this volume. However, robust inferences of the effect of dust remain elusive, even in recent decades when the aerosol distribution is better observed due to multiple satellite retrievals and an expanding network of surface measurements. Scientists study dust aerosols because of their potential importance for climate, but much of the activity within this large interdisciplinary community is directed toward simply deriving more precise constraints upon the dust burden and its regional distribution, along with the particle radiative properties needed to compute the forcing. This remains a key unsolved problem as noted throughout this volume (e.g., Chaps. 7, 9, and 11).

During recent decades, large teams of scientists have built comprehensive Earth system models (ESMs) that have been tested against a widening range of observations (e.g., Randall et al. 2007). These models explicitly calculate the dust cycle and the mechanisms by which it perturbs climate. However, the climate response to direct radiative forcing by dust remains uncertain for several reasons. First, the ESMs show varying sensitivity to radiative forcing as a result of their different treatments of clouds, for example. Global average projections of the twenty-first century warming in response to rising concentrations of greenhouse gases vary by a factor of 2, and discrepancies among projections of regional climate are even larger (e.g., Meehl et al. 2007). This is especially relevant for dust where prolific sources are highly localized so that the aerosol concentration and forcing show strong regional contrasts. In practice, models calculate a variety of temperature and precipitation anomalies in response to dust radiative forcing. It is difficult to know what behavior exhibited by the models is robust and likely to be corroborated

by future studies. Here, mechanistic arguments relating the forcing to the response may provide guidance, although these arguments are typically based upon simple models lacking the complexity that may be necessary to simulate the regional climate anomalies resulting from dust.

In this chapter, we discuss the influence of dust radiative forcing upon climate. Our discussion of the climate response emphasizes variables like surface air temperature and precipitation that directly impact our society. The climate effect of dust through its influence upon clouds and the carbon cycle is discussed elsewhere in this volume (Chaps. 12 and 14, respectively). Our method is to summarize calculations by ESMs, attempting to identify robust behavior and turning to mechanistic arguments when available. In Sect. 13.2, we summarize the physical and environmental factors contributing to varying estimates of the forcing among models. We discuss the climate response to this forcing in Sect. 13.3. In Sect. 13.4, we consider the feedback of the climate perturbation upon the process by which dust enters the atmosphere. In particular, we discuss the relation of dust radiative forcing to surface wind speed and vegetation. Our concluding remarks are presented in Sect. 13.5, where we emphasize outstanding questions.

13.2 Radiative Forcing by Dust Aerosols

Direct radiative forcing is defined as the change in the radiative flux by dust particles prior to any response by the climate (e.g., Hansen et al. 2005). Forcing is typically calculated at the top of the atmosphere (TOA), but because the aerosol perturbation to the flux at the surface can be markedly different and modify the hydrologic cycle, the forcing is characterized at this level as well. Within a few months of the forcing onset, the stratosphere returns to approximate radiative equilibrium, and the radiative flux at TOA approaches the value at the tropopause. The initial tropopause forcing is often a better indicator of the radiative perturbation at TOA following stratospheric adjustment (Hansen et al. 1997). It is this adjusted flux at TOA that perturbs the climate within the troposphere, but here we neglect the distinction between the initial forcing at TOA and the tropopause that is small for dust (Miller et al. 2004b). Direct radiative forcing by dust is described more fully in Chap. 11. Here, we summarize the physical properties that contribute to differences in the forcing among the models because these differences ultimately result in uncertainties in the effect of dust radiative forcing upon climate.

Dust particles scatter and absorb both solar and thermal (or "longwave") radiation (Tegen and Lacis 1996). At TOA, net insolation is reduced by scattering but increased by absorption of sunlight that otherwise would be reflected back to space. The dust layer also acts like a greenhouse gas, reducing outgoing longwave radiation (OLR) at TOA, while increasing thermal emission toward the surface.

One model calculation of dust radiative forcing for boreal summer is shown in Fig. 13.1. The dust distribution is prescribed from Miller et al. (2006), while the forcing is calculated using a development version of the NASA Goddard Institute for Space Studies (GISS) ModelE: an ESM that is intermediary between the

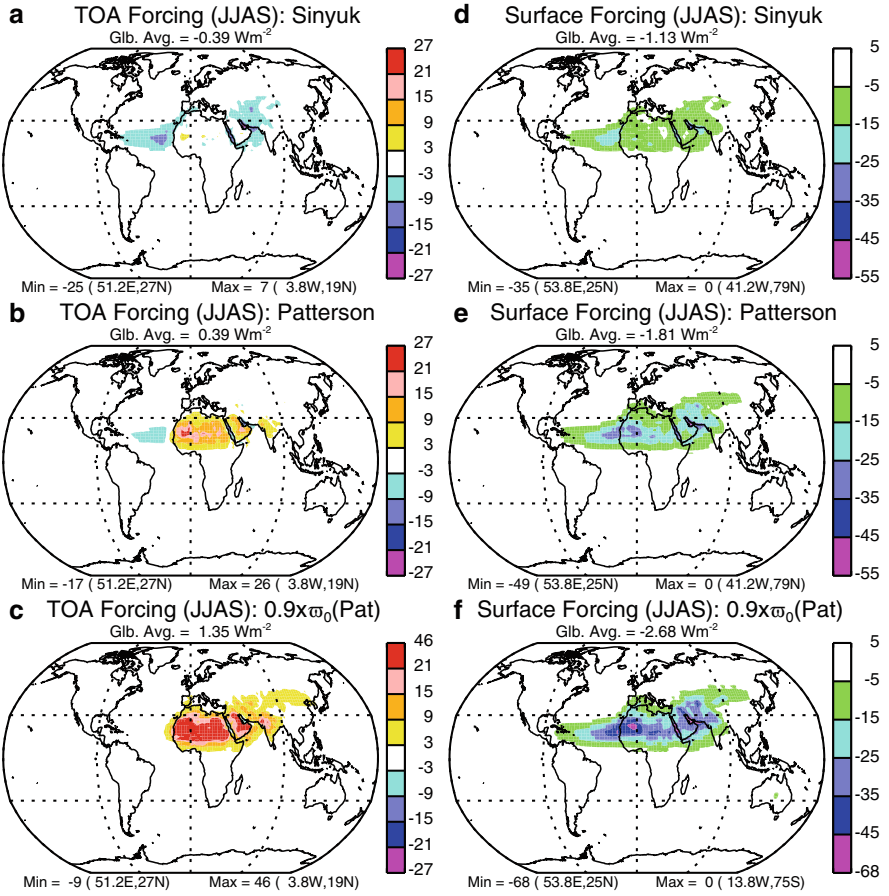

Fig. 13.1 Forcing calculated at TOA and the surface during Northern Hemisphere (NH) summer with the dust distribution prescribed from Miller et al. (2006). Shortwave absorption is prescribed using (**a**, **d**) the compilation of Sinyuk et al. (2003), (**b**, **e**) Patterson et al. (1977), and (**c**, **f**) Patterson et al. (1977) but with the particle single scattering albedo reduced by 10 %. The forcing is calculated using the "double-call" method, and represents an average during the initial 5 years of a simulation whose climate is perturbed by dust. Ocean temperature evolves according to a mixed-layer model (Miller et al. 1983). The forcing equals the contrast between radiative fluxes calculated with and without dust. Note that extreme values of the color scale may vary among panels

versions documented by Schmidt et al. (2006, 2014). Three different versions of the forcing are calculated using distinct prescriptions of the particle optical properties. The first prescription is taken from the compilation of shortwave absorption as a function of wavelength by Sinyuk et al. (2003) that includes values retrieved by Dubovik et al. (2002) and Colarco et al. (2002). The second is based upon measurements of far-travelled Saharan dust (Patterson et al. 1977). These two cases probably bracket the global solar absorption. For the third case, we arbitrarily reduce the single scattering albedo calculated from Patterson et al. (1977) by 10 %, which roughly doubles the solar absorption. This third case is intended to emphasize the

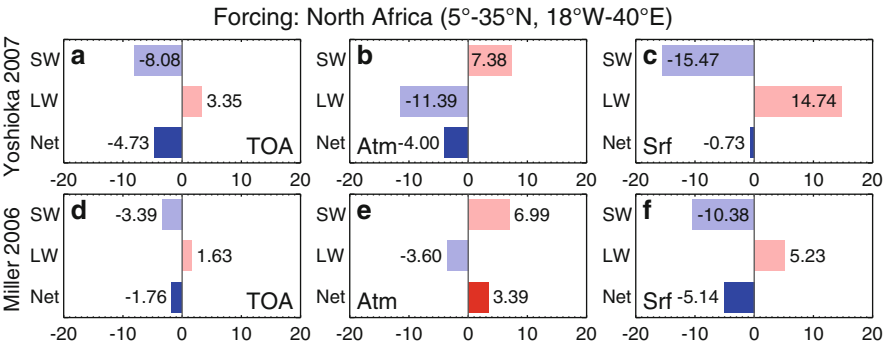

Fig. 13.2 Annual dust radiative forcing (Wm^{-2}) over North Africa at the (*left*) top of atmosphere (*TOA*) and (*right*) surface (*Srf*), with the atmospheric flux divergence (*Atm*) calculated as their difference (*center*). Forcing is calculated by Yoshioka et al. (2007) and using the dust concentration of Miller et al. (2006) with optical properties compiled by Sinyuk et al. (2003)

sensitivity of both the forcing and response to the particle optical properties, but may also be realistic in some regions due to the mineral composition of the dust source. Longwave absorption for all three cases is based upon measurements by Volz (1973).

Figure 13.1 illustrates the dependence of TOA forcing upon the surface albedo. Forcing is positive over the Sahara desert, where the bright surface reflects sunlight back into the dust plume, resulting in additional absorption (Liao and Seinfeld 1998). The region of positive forcing extends across the Sahel to the Guinea coast for the cases with greater solar absorption (Fig. 13.1b, c), presumably due to the presence of dust among the bright clouds that accompany the monsoon precipitation during this season. TOA forcing is negative where the dust plume extends downwind over the subtropical Atlantic Ocean and Arabian Sea, where the reflectivity of the aerosol particles is in contrast to the low albedo of the ocean surface, especially for the case of small solar absorption (Fig. 13.1a). At the surface, the forcing is negative and generally marks the region of high dust concentration (Fig. 13.1d–f). Both local and global dimming increase by roughly a factor of 2 for the range of shortwave absorption considered in the figure.

Figure 13.2 compares two calculations of annual forcing over North Africa, based upon either Yoshioka et al. (2007) or the Sinyuk et al. (2003) compilation illustrated in Fig. 13.1. The prescribed particle index of refraction is nearly identical in both calculations, so that forcing differences indicate the influence of contrasting particle size distributions and environmental factors including surface albedo, temperature, and humidity. In both cases, dust aerosols reduce the energy captured at TOA, resulting in net forcing that is negative but of different magnitude (Fig. 13.2a, d). The compensation between scattering of insolation on the one hand and solar absorption and reduced OLR on the other results in net TOA forcing that is the small residual of opposing effects, magnifying the contrast in net forcing between the two calculations that results from differences between the separate shortwave and longwave fluxes. The largest difference between the models occurs in

the surface longwave forcing (Fig. 13.2c, f). Yoshioka et al. (2007) calculate such a large longwave value that the *net* surface forcing is small and even positive when the regional average is restricted to the Sahara (not shown). In this region, dust increases the net radiative flux incident upon the ground (Figures 2b and c of Yoshioka et al. 2007). As a consequence of the longwave forcing, the atmospheric forcing (equal to the difference in forcing between TOA and the surface) has contrasting signs in the two models (Fig. 13.2b, e). The dust layer is heated according to Miller et al. (2006), while this layer is cooled in Yoshioka et al. (2007). The contrasting estimates of the sign of atmospheric forcing by dust have implications for the dynamical response, as described in the following sections.

Shortwave forcing at the surface is smaller in the GISS ESM (Fig. 13.2c, f), partly as a result of its brighter desert surface (Yoshioka et al. 2007). The net solar flux at this level is small due to reflection, so that any perturbation by aerosols is also small (Liao and Seinfeld 1998). The warm, dry climate of the Sahara exaggerates differences in surface longwave forcing between the models. The low humidity allows dust particles to absorb longwave radiation with reduced competition from water vapor, while high temperatures within the boundary layer increase downward longwave emission by dust (Liao and Seinfeld 1998).

Near dust sources, aerosol radiative forcing is intermittently much larger than the annual averages illustrated by Fig. 13.2. Dust was mobilized along a cold front over North Africa on March 8, 2006. Surface radiometers at Niamey, Niger, measured a dimming of 250 $\mathrm{W\,m^{-2}}$, compared to an unperturbed value near 1,000 $\mathrm{W\,m^{-2}}$ (Slingo et al. 2006). The sun was almost completely obscured, but the surface remained illuminated by diffuse radiation scattered within the dust layer. Such large episodic forcing results in an initial temperature response that is large compared to the seasonal average, as described in the next section.

13.3 Dust Radiative Impacts upon Climate

13.3.1 Temperature

A dust outbreak interrupts the daily cycle of solar heating by dimming the surface. Over land, the ground cools with the passage of the dust layer overhead, reducing the upward transfer of heat by the longwave and sensible fluxes, as documented by measurements in the Sahel (Miller et al. 2009). Measured temperature anomalies can be attributed to dust using models. Within the Bodélé Depression, a prolific dust source at the southern margin of the Sahara, midday temperature is reduced by a few degrees K during dust outbreaks, while warmer nights result from the inhibition of longwave cooling by the surface (Tegen et al. 2006).

Pérez et al. (2006) simulated the regional cooling accompanying a dust outbreak that extended across North Africa during April 2002. Figure 13.3a shows midday dimming of the surface as large as 700 $\mathrm{W\,m^{-2}}$ beneath the dust plume. Dust reduces

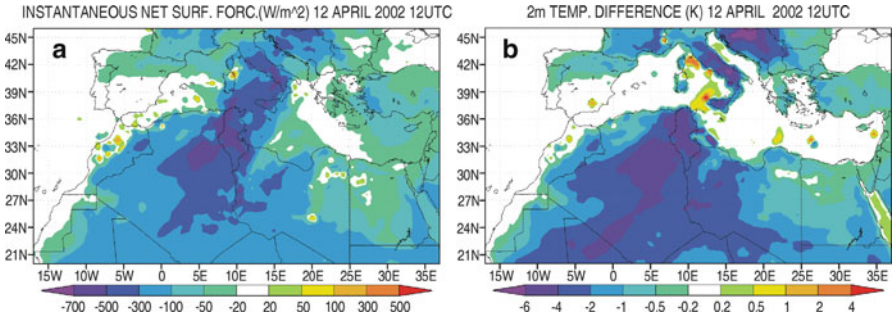

Fig. 13.3 Midday (**a**) forcing at the surface by a dust outbreak on April 12, 2002 (W m^{-2}), and (**b**) contemporaneous change in surface air temperature attributed to dust by contrasting experiments with radiatively active dust and no dust (Reproduced from Pérez et al. (2006). Copyright (2006) with permission from the American Geophysical Union)

surface air temperature by up to 6 K coincident with the surface forcing, compared to an experiment without dust radiative forcing (Fig. 13.3b). Behind the dust plume, the surface air temperature is quickly restored to its unperturbed value following the passage of the dust layer.

13.3.1.1 Temperature Adjustment in Convectively Mixed Regions

On time scales longer than a few days, the atmospheric temperature adjusts to the aerosol forcing at TOA and the perturbed energy exchange at the lateral margins of the dust layer. In regions of frequent vertical mixing, forcing at TOA is an especially strong constraint upon temperature at the surface.

Figure 13.4 shows the adjustment to a succession of weekly dust outbreaks in a simple single-column model of a coupled atmosphere and ocean (Miller 2012). During each outbreak, the prescribed radiative forcing peaks within a day, with gradual decay during the subsequent week. The atmospheric temperature anomaly is assumed to be identical at all levels as a result of vigorous vertical mixing by convection. Figure 13.4a shows that the atmosphere initially warms after each outbreak, while cooling of the ocean is smaller in magnitude due to its greater heat capacity. (Warming of the surface air in the simple model is in contrast to the continental cooling beneath the dust plume in Fig. 13.3b and is an artifact of the instantaneous coupling between the dust layer and surface that is assumed by the simple model.) In response to each dust outbreak, temperature anomalies in both the ocean and atmosphere diminish within a few days (Fig. 13.4a), but total restoration of the unperturbed state occurs over a time scale of several months, representing the time required for the ocean temperature to return to its original value through reduced longwave radiation to space from the upper troposphere (cf. Schopf 1983). Because the dust outbreaks are frequent compared to this slow restoration, the residual cooling accumulates with each additional outbreak,

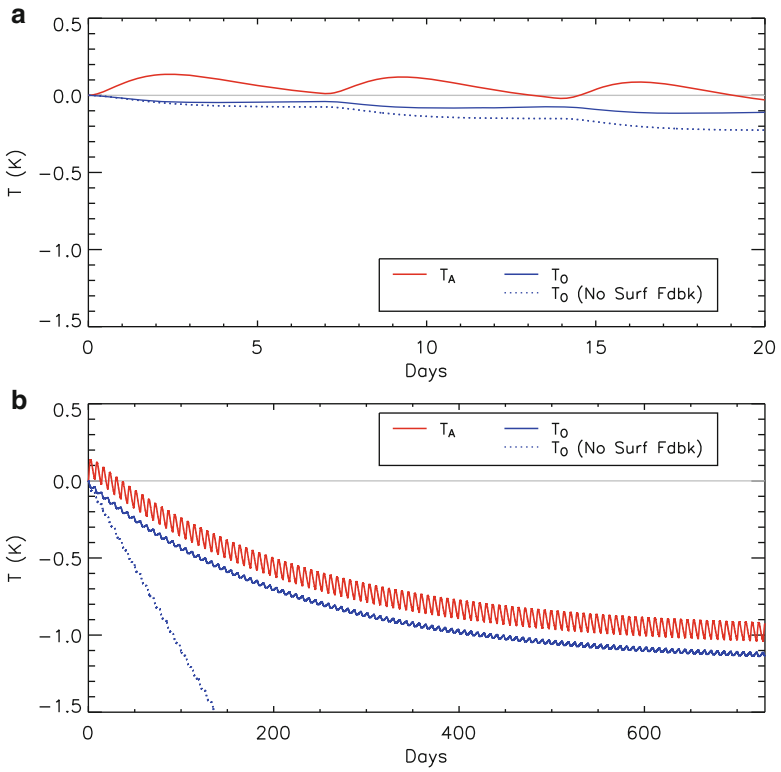

Fig. 13.4 Anomalous atmospheric (*red*) and ocean (*blue*) temperature during the first (**a**) 20 days and (**b**) 2 years after the onset of forcing in a simple single-column model. The forcing consists of a succession of weekly dust outbreaks where the magnitude of aerosol radiative forcing increases rapidly for a day before diminishing more gradually with a 1 day e-folding time. The time averaged forcing equals $-5\,\mathrm{W\,m^{-2}}$ at TOA and $-10\,\mathrm{W\,m^{-2}}$ at the surface. The *dotted line* shows the ocean temperature response in the absence of coupling by the surface turbulent and radiative fluxes, so that the ocean temperature responds only to the surface forcing (Reproduced from Miller (2012). Copyright (2012) with permission from the American Meteorological Society)

reaching equilibrium when the temperature increment due to a new outbreak is balanced by the recovery following an earlier outbreak (Fig. 13.4b). Although the atmosphere warms temporarily after each outbreak, it cools on a longer time scale due to the diminished heat import from the cooling ocean. The dotted line in Fig. 13.4b represents the ocean temperature change that would result solely from the surface forcing. Its divergence from the full response indicates the importance of coupling between the atmosphere and ocean. At equilibrium, the temperature perturbation is linearly proportional to the forcing at TOA, but is only weakly dependent upon the surface forcing, in contrast to the immediate continental response in Fig. 13.3b.

The surface forcing has limited influence upon the equilibrium air temperature because this forcing is balanced by surface radiative and turbulent fluxes that depend upon the contrast in temperature and moisture between the lower boundary and the air just above. Consequently, the surface forcing by itself is not sufficient to simultaneously constrain the temperature of both the lower boundary and the overlying air. An additional constraint is needed, relating the climate perturbation to any energy imbalance at TOA or the lateral boundary of the dust layer. This makes the climate perturbation by aerosols after the return to equilibrium more difficult to anticipate than the initial response because the final perturbation is not determined solely by the local forcing, but by a convolution of the forcing over the entire extent of the perturbed circulation. Regional adjustment occurs over the Rossby radius of deformation, which is inversely related to the Coriolis parameter. This distance of adjustment is especially large in the Tropics, as demonstrated by the observed tropic-wide response to warming of the eastern equatorial Pacific Ocean during El Niño events (Yulaeva and Wallace 1994). This suggests by analogy that the entire Tropics adjust in concert to dust radiative forcing, even if the largest aerosol concentration is restricted to the vicinity of the arid source regions. Temperature adjustment far beyond the regional extent of aerosol forcing has been demonstrated in a number of models (Shindell et al. 2010).

The equilibrium surface temperature is controlled primarily by the TOA forcing if two conditions are satisfied. First, the lower troposphere must be sufficiently humid and opaque to thermal wavelengths that most OLR originates in the upper troposphere. Then, the TOA forcing F_T is compensated by an OLR anomaly δOLR that is related to an anomaly of the upper tropospheric emitting temperature δT_E according to

$$a_F F_T = a_R \, \delta OLR = a_R 4\sigma T_E^3 \, \delta T_E, \tag{13.1}$$

where σ is the Stefan-Boltzmann constant and T_E is the unperturbed emitting temperature. Here, a_F and a_R refer to the areal extent of the forcing and response, respectively. As noted above, aerosol forcing is usually restricted to an area downwind of its source that is small compared to the extent of the response.

The second condition is that the column must be efficiently mixed by deep convection so that the temperatures of the upper troposphere and surface are coupled by a moist adiabat. Then

$$\delta h_S = \delta h_E^*, \tag{13.2}$$

where $h = C_P T + gz + Lq$ is the moist static energy that is constant along a moist adiabat; δh_S and δh_E^* are the anomalous moist static energy at the surface and saturated value at the emitting level, respectively. (C_p is the specific heat of air, g is gravity, z is height, L is the latent heat of vaporization, and q is the specific humidity.) If the height of the emitting level is unperturbed by dust, then $\delta h_E^* = C_P \, \delta T_E$, neglecting changes in upper tropospheric moisture. In addition, $\delta h_S = C_P \, \delta T_S + L \, \delta q_S$, where δT_S and δq_S are the anomalous surface air temperature and

Table 13.1 Forcing and response of surface air temperature T_S, precipitation P, and evaporation E (global and JJAS average) as a function of the shortwave absorptivity of the dust particles. The forcing is calculated using the dust distribution calculated by Miller et al. (2006). Particle optical properties are taken either from the compilation of Sinyuk et al. (2003) or Patterson et al. (1977), where the latter assumes greater shortwave absorption. As a third sensitivity experiment, even greater absorption is prescribed by reducing the single scatter albedo ϖ_0 by a factor of 0.9 compared to the case derived from Patterson et al. (1977)

	Sinyuk et al. (2003)	Patterson et al. (1977)	Patterson et al. (1977) $0.9 \times \varpi_0$
Forcing (W m^{-2})			
F_T (TOA)	−0.39	0.39	1.35
F_S (Surface)	−1.13	−1.81	−2.68
Surface temperature response (K)			
δT_S	−0.28	−0.07	0.30
Precipitation (and evaporation) response (mm day^{-1})			
δP $(= \delta E)$	−0.033	−0.026	−0.014

humidity, respectively. Thus, if relative humidity is constant (so that $C_P \delta T_S + L \delta q_S$ can be written as $\alpha C_P \delta T_S$), then (13.2) implies

$$\alpha \delta T_S = \delta T_E. \tag{13.3}$$

The parameter α is related to the surface relative humidity, and can be generalized to include the effects of feedbacks by upper tropospheric water vapor and the lapse rate, for example. Both of the conditions leading to (13.1) and (13.2) are generally satisfied within regions of tropical convection or the mid-latitude storm tracks, so that adjustment of the surface air temperature and humidity are related to the temperature anomaly at the emitting level, where anomalous OLR compensates the TOA forcing.

Table 13.1 shows that on a global scale, the anomalous surface air temperature calculated by an ESM increases with TOA forcing, even though forcing at the surface decreases. This is consistent with (13.1) and (13.2). As the prescribed particle absorption of solar radiation increases, the TOA forcing increases. OLR must increase in compensation, raising the emitting temperature and the surface value despite increased dimming of the surface. Similar behavior has been demonstrated in a single-column model (Cess et al. 1985).

Figure 13.5 shows the regional response of surface air temperature and moist static energy to the forcing shown in Fig. 13.1. (This particular model has a relatively large climate sensitivity of 4.2 K for a doubling of CO_2 that magnifies the climate response by about 50 % compared to the current CMIP5 model version: Schmidt et al. 2014.) An increase in TOA forcing is associated with a larger value of moist static energy at the surface, as expected from the combination of (13.1) and (13.2). (h_S is divided by C_p in Fig. 13.5 to have units of temperature.) Despite the increase of the global average surface air temperature with TOA forcing as shortwave absorption by the dust particles increases, the surface air cools in some

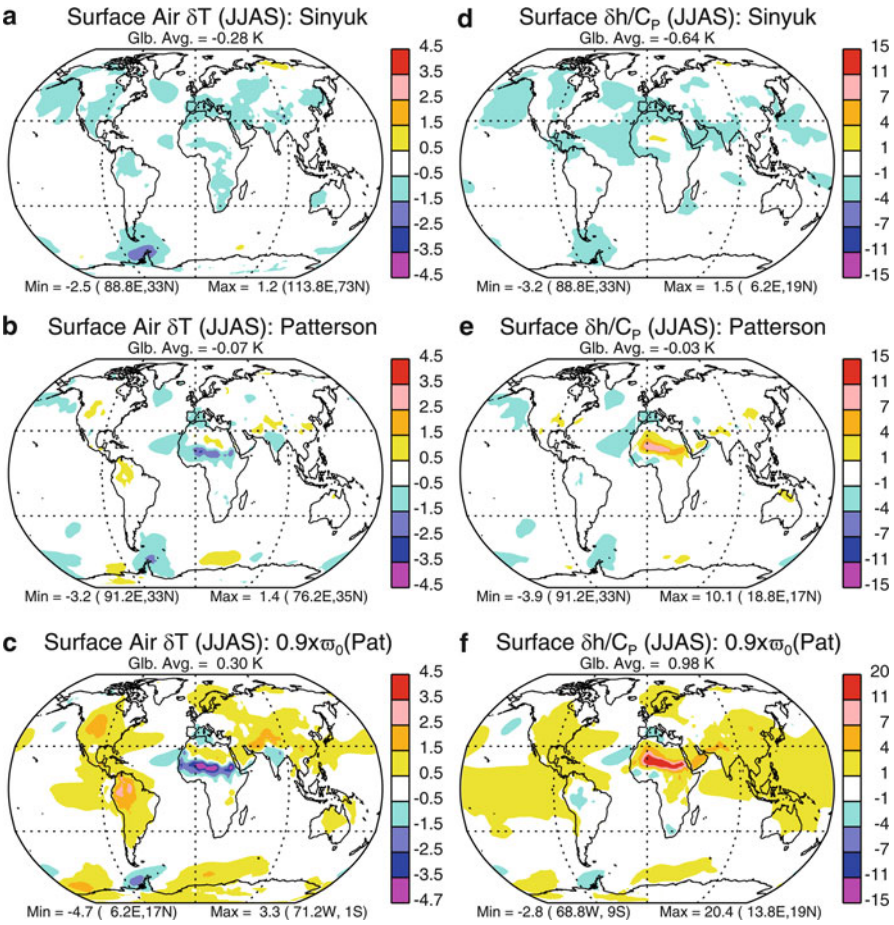

Fig. 13.5 (*Left*) Anomalous surface air temperature δT_S and (*right*) moist static energy δh_S (divided by C_p) in response to the forcing in Fig. 13.1. Extreme values of the color scale may vary among panels

regions of large aerosol forcing, including the Sahel (Fig. 13.5b, c). This cooling is attributed to the increase of Sahel precipitation with particle absorption (Fig. 13.7) and not the increasing magnitude of the surface forcing and dimming of the surface. As precipitation increases, the surface becomes more humid. The contribution of increasing humidity to δh_S (not shown) exceeds the increase of δh_S required by F_T, so that the near-surface air must cool (Fig. 13.5b, c). Similar compensation of surface temperature and humidity where dust increases precipitation is seen in the experiments of Miller et al. (2004b), as well as the simple model of Miller and Tegen (1999).

Coupling of surface air temperature to the TOA forcing is seen in the ESM experiments of Miller and Tegen (1998). In this model, the dust concentration is largest over the Arabian Sea during NH summer, due to the confluence of plumes

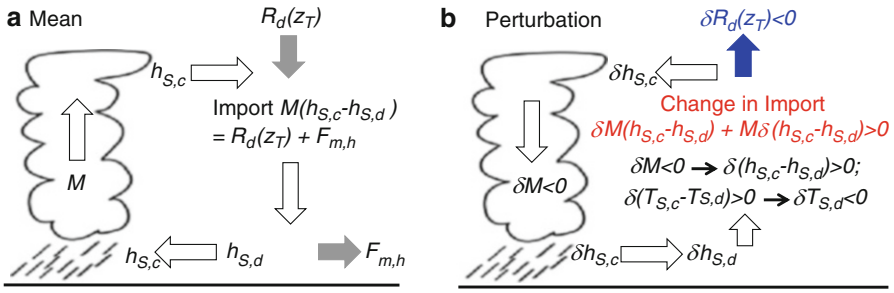

Fig. 13.6 Schematic showing how negative radiative forcing by dust within the descending branch of a direct circulation can cause cooling beneath the dust layer if aerosol forcing slows the rate of subsidence and mass exchange M with the convecting region. The moist static energy contrast between the convecting and descending regions, $h_{S,c} - h_{S,d}$, is approximately proportional to the surface temperature contrast $T_{S,c} - T_{S,d}$. $R_d(z_T)$ is the net downward radiation at the tropopause and $F_{m,h}$ is the dynamical export of moist static energy to mid-latitudes by extratropical eddies (For simplicity, $F_{m,h}$ is assumed to be unperturbed by dust) (**a**) Mean. (**b**) Perturbation

from Africa and the Arabian Peninsula. Seasonally averaged dimming of the surface beneath the dust layer is as large as $55\,\mathrm{W\,m^{-2}}$, but the surface air temperature is nearly unchanged, consistent with the relatively small TOA forcing and frequent deep convection calculated by the ESM.

13.3.1.2 Temperature Adjustment in Subsiding Regions

In regions of subsidence, mixing between the surface and emitting level is relatively weak, and radiative forcing at TOA is a weaker influence upon the surface temperature. While temperature is relatively unchanged beneath the dust layer in the ESM experiments of Miller and Tegen (1998), temperature is reduced at the margins of the layer, even though the forcing is smaller. In these marginal regions, deep convection is infrequent, and surface temperature is not directly coupled to the emitting value higher in the column. Instead, this cooling is attributed to the weakening of the tropical overturning circulation by dust (Miller and Tegen 1999), illustrated schematically in Fig. 13.6 where the change in overturning strength is represented by δM. The overturning slows so that reduced adiabatic warming associated with descent compensates the increased radiative heating within the dust layer. (This compensation between the overturning strength and the atmospheric forcing assumes that changes to the stratification by dust are of secondary importance to the anomalous adiabatic heating.) Because the TOA forcing is near zero, the export of energy from the precipitating region is unperturbed. This export is roughly proportional to the product of the overturning strength and the surface temperature contrast between the precipitating and subsiding regions (Miller and Tegen 1999). To compensate the reduction of the subsidence rate ($\delta M < 0$), the surface of the subsiding region must cool compared to the convecting region,

as illustrated by Fig. 13.6. This mechanism accounts not only for the cooling on the margins of the precipitating region but also the cooling over the Arabian Sea during NH winter. During this season, dust concentrations are lower, but subsidence occurs following the migration of precipitation across the equator into the Southern Hemisphere (Miller and Tegen 1998): cooling results as a consequence of the reduced overturning in response to dust atmospheric forcing. This mechanism is also consistent with cooling over the subtropical Atlantic, where the dust plume extends downwind from North Africa (Fig. 13.5a–c). The dependence of the surface temperature response upon the anomalous tropical overturning shows the importance of the atmospheric forcing by dust, the sign of which varies among current models according to Fig. 13.2b, e.

Over the Sahara Desert, surface air temperature increases as the prescribed shortwave absorption by dust is increased (Fig. 13.5), despite further dimming of the surface (Fig. 13.1). During NH summer, a deep boundary layer that is well mixed by dry convection is observed between the surface and the mid-troposphere (Carlson and Prospero 1972). The low humidity allows the ground to radiate directly to space, and the conditions leading to (13.1) and (13.2) are rarely satisfied. In this region, the sign of the anomalous surface air temperature calculated by models is not consistently related to the sign of the forcing (Table 13.2). For example, warming is calculated by Yoshioka et al. (2007) and Yue et al. (2011), despite forcing whose sign differs between the two models at both TOA and the surface. This is only possible if the perturbation to lateral energy transport varies among models, demonstrating that this transport must be considered when attributing temperature perturbations to dust forcing, especially in regions of weak vertical mixing.

13.3.2 Precipitation

13.3.2.1 The Global Anomaly

Aerosols alter precipitation by changing the regional distribution of diabatic heating along with surface evaporation that supplies moisture to the atmosphere. Evaporation is coupled to aerosol forcing through the surface energy balance, where dimming beneath the aerosol layer is compensated by a reduction in the net flux of heat from the surface into the atmosphere:

$$F_S = \delta R^{LW}(0) + \delta LE + \delta S_E. \tag{13.4}$$

Here, $\delta R^{LW}(0)$ is the anomalous net upward flux of longwave radiation, while δLE and δS_E are the anomalous turbulent fluxes of latent and sensible heat, respectively. Over most of the ocean, the net heat flux is dominated by the latent component, and dimming of the surface is primarily compensated by a reduction in evaporation (cf. Figure 12 from Perlwitz and Miller 2010). This is illustrated by the reduction of precipitation within the tropical Atlantic ITCZ (Fig. 13.7) that is associated with

Table 13.2 Qualitative summary of dust radiative forcing and the response of surface air temperature in the Sahara and precipitation in the Sahel. All averages are for NH summer (JJA or JJAS) unless noted. Figures used to describe the forcing and response in the cited article are also listed along with the identity of the experiment where there is more than one. All models calculate SST using a mixed-layer ocean model with fixed heat transport unless otherwise noted

Surface air temperature over the Sahara					
Study	F_T	F_S	Cited figure	δT_S	Cited figure
Miller and Tegen (1998)	+	–	2a, 1a	–	5a[1]
Miller et al. (2004b)	–	–	8	–	Unpublished[2]
Yoshioka et al. (2007)	–	+	2c	+	6b[3]
Yue et al. (2011)	+	–	2e,f	+	4b[6]
This study	+	–	13.1b	+	13.5b[8]
Precipitation within the West African and Atlantic ITCZ					
Study	F_T	F_S	Cited figure	δP	Cited figure
Miller and Tegen (1998)	–	–	2a, 1a	–	7a[1]
Miller et al. (2004b)	–	–	8	–	16[2]
Yoshioka et al. (2007)	–	–	2c	–/+	4b[3]
Solmon et al. (2008)	–/+	–	1a,b	–	2b, 3[4]
Perlwitz and Miller (2010)	+		2f		5f[5]
Yue et al. (2011)	+	–	2e,f	+	4h[6]
Solmon et al. (2012)	–/+		7c	–	6d[7]
This study	+	–	13.1b	+	13.7b[8]

[1]Dust concentration is largest over the Arabian Sea in this model and unrealistically low over the Sahara. Cooling occurs over most of Sahara, despite $F_T > 0$. A weak precipitation anomaly extends offshore over the Atlantic toward the ITCZ

[2]Forcing is listed for the $1.0 \times \varpi_0$ experiment whose shortwave absorption is taken from Patterson et al. (1977). $F_T < 0$ and $F_S < 0$ within the subtropical Atlantic and precipitation is reduced downwind within the Atlantic ITCZ. Only annual average precipitation is shown: the anomaly over the West African coast switches sign to positive as the solar absorption is increased by 10 %. Dust cools the Sahara (unpublished), in part due to moistening of the surface air by the precipitation anomaly

[3]Annual forcing from the SOM.SP experiment, JJAS response from the SOM.SP (precipitation) and SOM.SL (precipitation, temperature) experiments. Complicated precipitation response with reduction over the West Atlantic and increase along the Guinea coast. Warming over the Sahara, cooling over the Sahel

[4]Regional model, with prescribed SST. Precipitation is reduced within the Sahel, with an increase over the Atlantic that is an artifact of the prescribed SST according to Solmon et al. (2012)

[5]Forcing is from the $1.0 \times$ SSA experiment. Dust concentration peaks over the Arabian Sea, with comparatively low values over the Sahara. The regional distribution of high cloud cover is used as a proxy for the precipitation anomaly

[6]Annual forcing and response. Forcing from Yue et al. (2010). Response from MXLSST_FD experiment. Warming over the Sahara, cooling over the Sahel. Precipitation is reduced over the Atlantic, with a smaller reduction over the western Sahel and coastal region

[7]Forcing is from the standard case, but response is for the experiment where SST is reduced in proportion to dust optical thickness. Precipitation is reduced within the Sahel, with a larger reduction over the Atlantic when the ocean is cooled in proportion to the dust load

[8]JJAS averages of forcing and response. The simulation with solar absorption taken from Patterson et al. (1977) is tabulated here, but use of the absorption compiled by Sinyuk et al. (2003) results in nearly zero forcing at TOA, a correspondingly weak warming within the Sahara and virtually no rainfall anomaly within the Sahel

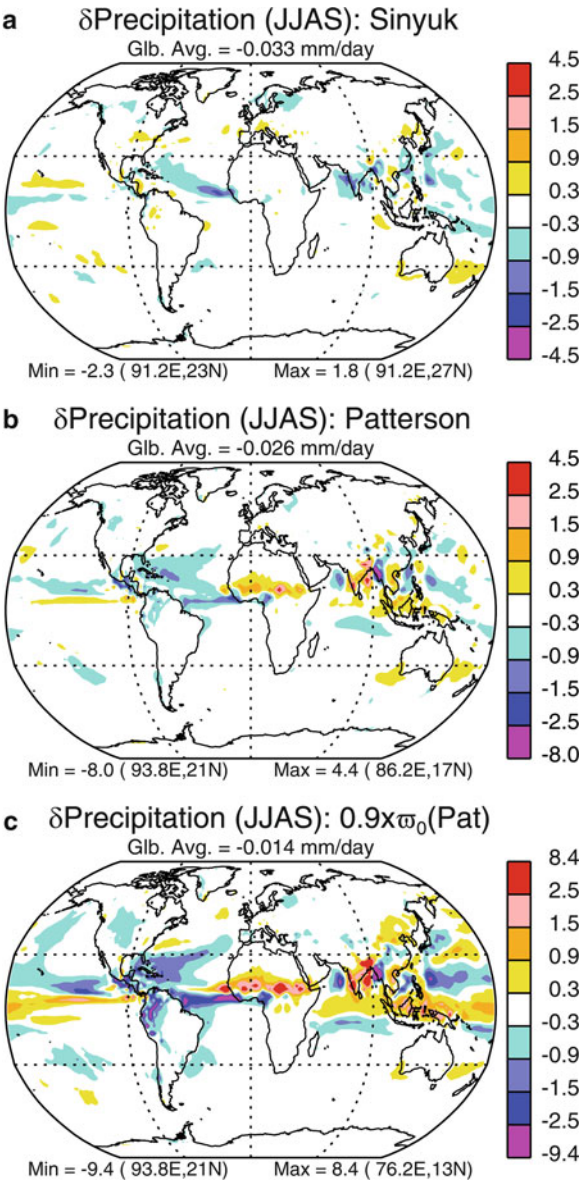

Fig. 13.7 As in Fig. 13.5 but for anomalous precipitation δP. Extreme values of the color scale may vary among panels

the reduction in upwind evaporation where the aerosol plume extends offshore from West Africa.

For each experiment in Table 13.1, global precipitation is reduced by dust radiative forcing, a decrease that has been noted previously (e.g., Coakley and Cess 1985; Miller and Tegen 1998; Miller et al. 2004b; Liepert et al. 2004). However, the relation of global evaporation and precipitation to surface forcing

is not straightforward. Table 13.1 shows that evaporation actually increases as increasing particle absorption causes further dimming of the surface, a dependence corroborated by a previous version of the climate model and dust distribution (Miller et al. 2004b).

Xian (2008) describes one mechanism by which evaporation can increase with shortwave absorption, noting that ocean evaporation depends upon forcing at TOA in addition to the surface value. The evaporative anomaly δE can be written using a bulk formula:

$$\begin{aligned}\delta E &= \rho C_D |u_0| \, \delta \left[q^*(\mathrm{SST}) - q_S \right] \\ &= \rho C_D |u_0| \left(\left. \frac{dq*}{dT} \right|_{\mathrm{SST}} \delta \mathrm{SST} - r \left. \frac{dq*}{dT} \right|_{T_S} \delta T_S \right) \\ &= \rho C_D |u_0| \left. \frac{dq*}{dT} \right|_{\mathrm{SST}} \delta \left(\mathrm{SST} - T_S \right) + \rho C_D |u_0| \left(\left. \frac{dq*}{dT} \right|_{\mathrm{SST}} - r \left. \frac{dq*}{dT} \right|_{T_S} \right) \delta T_S ,\end{aligned} \tag{13.5}$$

where ρ is the atmospheric density, C_D is a drag coefficient, and u_0 is the surface wind speed, all of which we assume constant for purposes of discussion. The quantities q_S and $q^*(\mathrm{SST})$ represent the surface specific humidity and the saturation specific humidity at the sea surface temperature SST, respectively. Equation 13.5 is derived by expressing each specific humidity in terms of the unperturbed temperature and linearizing. Xian (2008) notes that TOA forcing influences evaporation through its effect upon the anomalous surface air temperature, the final term in (13.5). In convecting regions, δT_S is directly related to the TOA forcing according to (13.1) and (13.3), so that positive F_T increases evaporation.

The sensible and longwave fluxes can be parameterized according to the difference in temperature between the surface and near-surface air (a representation that is conventional for the sensible flux but more approximate for longwave radiation). Then, from (13.5) it can be shown that

$$\delta(LE) = \delta(LP) = \epsilon F_T + \eta F_S , \tag{13.6}$$

where $\delta(LP)$ is the global precipitation anomaly multiplied by L. Both η and ϵ are positive (with $\epsilon \approx 0.5\eta$ for typical tropical values), so that evaporation is reduced by dimming of the surface ($F_S < 0$) but increased by positive TOA forcing.

Equation (13.6) applies only over the ocean or else vegetated regions with abundant reservoirs of soil moisture, where the evaporative anomaly can be represented by (13.5). However, ESMs show that evaporation in arid regions like the Sahel can also increase with shortwave absorption, given an increase in precipitation (Miller et al. 2004b). Soil moisture supplied by a precipitation anomaly allows the surface to respond to incident radiation with a greater proportion of evaporation. Thus, evaporation may increase beneath the aerosol layer, despite the reduction of the

incident radiative flux by dust that reduces the total flux of energy back into the atmosphere.

The increase of evaporation with dimming in Table 13.1 remains a provocative result that has yet to be explained quantitatively. Nonetheless, (13.6) opens the possibility that absorbing aerosols with sufficiently large F_T can *increase* surface evaporation and precipitation. (In this case, dimming of the surface must be compensated by reduced longwave and sensible fluxes.) The more general point is that the aerosol perturbation to the global hydrologic cycle and precipitation does not depend solely upon surface forcing but depends additionally upon forcing at TOA. Indeed, Ming et al. (2010) refer to the right side of (13.6) as "hydrologic forcing".

The influence of aerosol forcing upon the hydrologic cycle is mediated through the surface energy balance (13.4). Models that prescribe SST as a lower boundary condition lack this balance and fail to simulate the full influence of aerosol radiative forcing upon the hydrologic cycle. Models with prescribed SST generally underestimate the reduction in precipitation by dust forcing compared to companion experiments with calculated SST (e.g., Miller and Tegen 1998; Yoshioka et al. 2007; Yue et al. 2011). Mixed-layer ocean models, where heat transport by ocean currents is fixed (Miller et al. 1983), necessarily compensate the surface forcing with the various fluxes comprising the surface energy balance. Inclusion of an ocean general circulation model (OGCM) within an ESM allows the additional possibility of compensating surface dimming with anomalous ocean heat import. OGCMs allow for the most general response to aerosol forcing, but they have been used in only a few cases (e.g., Ramanathan et al. 2005; Bollasina et al. 2011).

13.3.2.2 Regional Anomalies

Regional anomalies of precipitation forced by aerosols are also sensitive to the implementation of a surface energy balance. Precipitation associated with the Asian monsoon is increased by dust radiative forcing when SST is prescribed, but reduced when a surface energy constraint is added as part of a mixed-layer ocean model (Miller et al. 2004a).

Only on shorter time scales of a few weeks after the onset of aerosol radiative forcing, before SST has time to adjust, can the neglect of a surface energy balance be justified. Stephens et al. (2004) consider the initial effect of radiative heating by a dust outbreak using a cloud-resolving model within a tropical ocean domain. Heating within the aerosol layer acts as an elevated "heat pump" (e.g., Schneider 1983; Lau and Kim 2006), driving ascent along with low-level convergence of moisture and precipitation.

At equilibrium (that is achieved by the upper ocean after several months), the transport of energy by the atmospheric circulation must compensate the loss (or gain) of energy within the region of aerosol forcing, equal to the difference of the total energy flux at TOA and the surface. Initially, this gain corresponds to the atmospheric forcing $F_T - F_S$, but as the circulation adjusts, the net flux imbalance

at the surface and TOA is altered. At the surface, the radiative and turbulent fluxes adjust until F_S is fully compensated. Only if heat transport by the ocean circulation adjusts to the aerosol forcing can the net energy flux across the surface remain nonzero.

At TOA, however, an imbalance between the forcing and anomalous OLR may persist even after the climate returns to equilibrium. Consider the example of negative forcing at TOA due to a layer of reflective aerosols. To balance this reduction of insolation, OLR and temperature decrease, and because of dynamical adjustment, this decrease generally extends beyond the forcing region. The net radiative anomaly at TOA is positive beyond the aerosol layer due to the decrease of OLR. Conversely, within the region of aerosol forcing, the net radiative anomaly at TOA is negative because this anomaly must be zero when summed over the extent of the response, as expressed by (13.1). Thus, above the aerosol layer, the reduction of OLR cannot fully compensate the forcing. The mismatch between the regional extent of the forcing and the equilibrium response creates a horizontal contrast in the TOA energy flux that must be balanced by the atmospheric transport of energy. In our example, the continual net radiative loss at TOA above the aerosol layer is balanced by anomalous energy import.

The coupling of TOA forcing and anomalous atmospheric energy transport can lead to regional anomalies of precipitation. Here, we discuss precipitation anomalies over the Sahel and their relation to TOA forcing in this region (Figs. 13.1 and 13.7). Following an argument by Chou et al. (2005), we consider the anomalous moisture budget for the convecting region:

$$\delta P_c = \delta E_c + \delta M(q_{S,d} - q_{T,c}) + M\,\delta(q_{S,d} - q_{T,c}), \tag{13.7}$$

where δP_c and δE_c are the anomalous precipitation and evaporation within the convecting region, respectively, and δM is the circulation anomaly linking the convecting region to the neighboring regions of subsidence. The quantity $q_{S,d} - q_{T,c}$ is the difference between the unperturbed specific humidity entering the convecting region from the surface of the subsiding region ($q_{S,d}$) and the upper tropospheric humidity $q_{T,c}$ where the rising air detrains (Fig. 13.8a). Equation (13.7) says that anomalous precipitation δP_c exceeds the local evaporative anomaly δE_c as a result of two contributions to the anomalous moisture flux. The first is the product of the anomalous overturning δM and the net inflow of unperturbed moisture ($q_{S,d} - q_{T,c}$) into the column. The second is the unperturbed circulation M multiplied by the anomalous net inflow $\delta(q_{S,d} - q_{T,c})$.

Negative TOA forcing within a region of climatological convection must be balanced by a decrease in energy export. Chou et al. (2005) assume that this decrease occurs due to weakening of the direct circulation ($\delta M < 0$), neglecting a possible contribution by a changing contrast in moist static energy between the convecting and subsiding regions. They also assume that the primary contribution to anomalous precipitation is by the anomalous moisture flux resulting from the weakened overturning (the penultimate term in Eq. 13.7). Thus, negative TOA

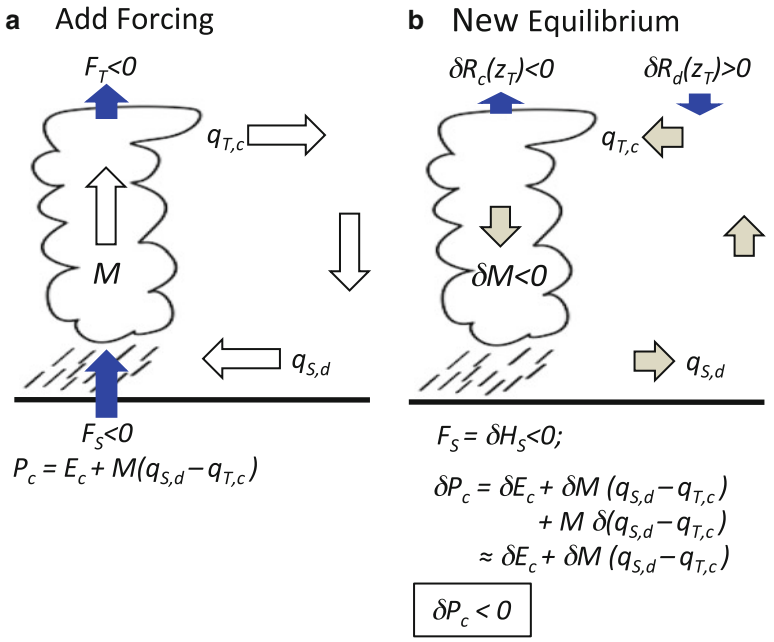

Fig. 13.8 (**a**) A direct circulation with overturning M is perturbed by aerosol radiative forcing at TOA ($F_T < 0$) and the surface ($F_S < 0$) with atmospheric absorption ($F_T - F_S > 0$). (**b**) At equilibrium, the surface forcing is balanced by the net heat flux anomaly ($F_S = \delta H_S < 0$), but the TOA forcing is incompletely compensated within the convecting region since some of the compensating OLR occurs within the descending branch of the circulation. Thus, the net radiative flux anomaly at the tropopause is negative within the convecting region [$\delta R_c(z_T) < 0$] and positive within the descending branch [$\delta R_d(z_T) > 0$], such that the sum of the flux anomalies is zero over the extent of the circulation. This regional contrast of the flux anomalies requires an anomalous convergence of energy into the convecting column, even though $F_T - F_S > 0$. Chou et al. (2005) assume that this convergence results from a slowing of the circulation ($\delta M < 0$). The weaker circulation ($\delta M < 0$) imports less moisture into the base of the convecting region, so precipitation is reduced ($\delta P_c < 0$). This analysis neglects changes in moisture import by the mean circulation transporting the specific humidity anomaly. The quantities $q_{S,d}$ and $q_{T,c}$ are the specific humidity of air entering the convecting region from the surface of the descending branch and air leaving at the tropopause, respectively

forcing reduces precipitation by decreasing the export of energy but also the import of moisture, as illustrated schematically by Fig. 13.8.

This argument accounts for gross differences among model precipitation anomalies within the Sahel during NH summer, as summarized in Table 13.2. Models with negative TOA forcing over West Africa generally show a reduction of precipitation (Yoshioka et al. 2007). In contrast, precipitation increases in models with positive F_T (cf. Fig. 13.7b, c along with Miller et al. 2004b; Yue et al. 2011).

However, the relation between model forcing and regional anomalies of precipitation illustrated by Fig. 13.8 depends upon certain simplifications that are not always appropriate for dust. First, significant TOA forcing during NH summer

extends over the Sahara Desert, upwind of the precipitation anomaly; in other seasons, the dust concentration and forcing are largest outside the region of convection. Thus, the overturning anomaly δM is not solely related to the TOA forcing within the convecting region, although this case can be accommodated by including forcing within the subsidence region when calculating the anomalous energy transport and overturning. Second, Fig. 13.8 assumes that anomalous energy transport occurs through adjustment of the overturning, but changes in the contrast of moist static energy between the convecting and subsiding regions can also contribute. In fact, the anomalous overturning is more closely related to atmospheric forcing $F_T - F_S$ within the subsiding region, so long as changes to the stratification by F_T are of secondary importance, as discussed in Sect. 13.3.1.2 (cf. Miller and Tegen 1998, 1999). (In this case, the regional contrast of moist static energy adjusts to allow the necessary anomaly of energy transport.) Third, the sensitivity of moisture import to the overturning anomaly requires that the inflow is humid and that perturbations to humidity by dust are small, allowing the neglect of the last term in (13.7). Where the inflow is from arid regions that are dust sources (so that $q_{S,d}$ is small), the moisture import will be relatively insensitive to changes in the circulation strength. Finally, where the dust layer extends offshore and evaporation is reduced to compensate the surface forcing, moisture export from the subsiding region may be sensitive to the anomalous humidity in addition to the anomalous circulation strength, so that the last term in Eq. 13.7 is not negligible. In summary, the mechanism illustrated by Fig. 13.8 is consistent with the relation between TOA forcing and modeled Sahel precipitation in Table 13.2, but several assumptions need further consideration.

The coupling of TOA forcing and precipitation illustrated by Fig. 13.8 has three consequences. First, ascent and precipitation can increase where $F_T > 0$ within a convecting region (Fig. 13.7b, c), despite strong negative forcing at the surface and intense heating within the aerosol layer. These latter conditions occasionally lead to claims of column "stabilization" by dust, but precipitation in fact increases; heating of the aerosol layer is nullified by adiabatic cooling associated with ascent related to the increased export of energy. This again illustrates that aerosol forcing is not automatically balanced by a local temperature anomaly because the circulation allows the forcing to be balanced nonlocally. The second consequence, as shown by Chou et al. (2005), is that the anomalous export of energy from the region of forcing is driven by F_T and not the aerosol forcing within the column $F_T - F_S$. That is, the "elevated heat pump" described by Lau and Kim (2006) drives ascent only in the initial period, before there is significant compensation of the surface forcing. Full compensation occurs within a few weeks over land, but takes several months over the ocean, where heat is stored over a deeper layer. Thus, the "heat pump" mechanism is not relevant for precipitation anomalies on interannual and longer time scales. Again, the exception is where ocean heat transport adjusts in response to aerosol forcing, allowing the net surface energy flux to remain nonzero in equilibrium. The third consequence is that negative forcing at TOA by reflective dust particles is equally effective at driving precipitation anomalies, compared to

positive TOA forcing by more absorbing minerals. A similar magnitude of the precipitation response occurs despite much smaller atmospheric heating (i.e., a weaker "heat pump") associated with reflective aerosols.

13.4 Feedback of Climate Anomalies upon the Dust Cycle

13.4.1 Surface Wind Speed and Dust Mobilization

The entrance of dust into the atmosphere is a sensitive function of surface wind speed (Chap. 5). The circulations raising dust are described in Chap. 6 and by Knippertz and Todd (2012). Here, we consider how dust perturbs the surface wind that feeds back upon dust mobilization.

Several studies have found that dust radiative forcing reduces the mobilization on the order of 10 % compared to a model where the dust distribution is calculated but has no radiative effect (e.g., Perlwitz et al. 2001; Yue et al. 2011). Miller et al. (2004a) and Pérez et al. (2006) related the decrease in emission to a reduction of eddy mixing within the boundary layer. Negative radiative forcing at the surface reduces the flux of sensible heat from the ground that powers eddy mixing in the arid regions that are dust sources. These eddies normally accelerate the surface wind each morning by mixing down fast air that accelerated above the stable stratification of the nocturnal boundary layer. The reduction of the surface wind speed by dust radiative forcing is largest at midmorning when the boundary layer deepens most rapidly, following warming of the surface. This is the time of day when dust events are most frequently initiated in North Africa (N'Tchayi Mbourou et al. 1997; Schepanski et al. 2009). Nocturnal warming of the surface by dust also contributes to the slowing of the surface winds the following morning by reducing stratification and the nocturnal acceleration of the winds aloft. The dependence of wind speed upon surface forcing predicts that dust emission should increase in models with positive forcing (Miller et al. 2004a). An increase in emission has been found by Woodage et al. (2010), although the precise mechanism has not been identified.

A few models calculate the intermittent increase of surface wind speed and mobilization by eddies whose amplitude is parameterized in terms of the surface flux of sensible heat (e.g., Lunt and Valdes 2002; Cakmur et al. 2004). A reduction of eddy wind speed by negative surface forcing has been shown to cause a reduction in dust emission that is comparable to the decrease by the explicitly resolved model surface wind (Miller, unpublished results). Other studies have shown that dust radiative forcing alters the regional distribution of surface pressure, increasing mobilization where the surface wind is augmented (Heinold et al. 2007; Ahn et al. 2007).

13.4.2 Vegetation and Dust Source Extent

The removal of vegetation exposes soil particles to a greater force by the wind, potentially increasing mobilization (Chap. 5). Conversely, increased vegetation within the Sahel during recent decades is correlated with the reduced occurrence of dust storms (Cowie et al. 2013). By changing precipitation, dust radiative forcing alters the regional distribution of vegetation, feeding back upon the mobilization of dust. The sign of this feedback and its quantitative importance remain unresolved. A positive feedback between dust radiative forcing and climate may contribute to observed climate anomalies including desertification within the Sahel (Yoshioka et al. 2007), the North American Dust Bowl during the 1930s (Koven 2006; Cook et al. 2008), and the multidecadal droughts within the Great Plains during the Medieval Climate Anomaly (Cook et al. 2013).

Devegetation is represented by several effects within models (Koven 2006). The area vulnerable to wind erosion is expanded, while surface roughness is decreased, reducing the wind stress that must be exceeded for soil mobilization (Chap. 5). In addition, the areal expansion of bare soil reduces transpiration of soil moisture into the atmosphere, increasing the turbulent flux of sensible heat at the expense of the latent heat flux. As noted above, the increased sensible heat flux increases the strength of wind gusts, leading to greater mobilization.

Understanding the feedback between dust aerosols and vegetation introduces the challenge of specifying the strength of a new dust source, defined as the mass of dust mobilized at a given wind speed. Source strength depends upon the availability of easily eroded particles. Some models assume that newly exposed sources are more prolific than existing sources because loosely bound soil particles that were protected by roots and leaves are now exposed to the force of the wind (e.g., Tegen et al. 1996). In contrast, existing sources may have been already stripped of their most easily erodible particles. In the absence of an increase to the strength of newly created sources, model dust loads seem unrealistically insensitive to large expansions of source extent related to the disappearance of vegetation (Yoshioka et al. 2007). African dust arriving at Barbados increases fourfold between wet and dry decades. In contrast, Yoshioka et al. (2007) find that removal of Sahel vegetation associated with an equatorward expansion of the Sahara by 2° latitude, meant to represent the probable change between a wet decade like the 1950s and the comparatively dry 1990s, increases dust emission from North Africa by only about one-third. This discrepancy with respect to observations suggests that the model underestimates the initial strength of the new sources by assuming that they are no stronger than the original sources. Inferring the strength of new sources from observations is complicated by concurrent changes to the wind threshold for mobilization. Some models assume that mechanical disturbance of the soil by cultivation reduces this threshold (e.g., Tegen et al. 2004). Other models raise the threshold to account for the prevalence of cultivated sources in soils dominated by clay, whose particles are subject to greater cohesion (Ginoux et al. 2012).

Constraining the strength of newly created sources will require untangling the full range of changes to the mobilization process by devegetation.

The historical record indicates the presence of new dust sources during dry climates like the Dust Bowl (e.g., Hansen and Libecap 2004). This drought was preceded by a La Niña event in the equatorial eastern Pacific that typically reduces precipitation during winter months over the southwestern United States. However, the Dust Bowl is unique among droughts in the historical record for its exaggerated amplitude and persistence compared to the unexceptional ocean forcing as well as the unusual northward displacement of the drought into the Great Plains. This is illustrated by contrasting the observed and SST-forced precipitation anomalies in Fig. 13.9 (left and center columns, respectively), reproduced from Cook et al. (2009). One hypothesis is that the modest drought induced by La Niña withered crops that had recently replaced more resilient natural grasses. Devegetation led to wind erosion and aerosol radiative forcing that amplified and sustained the drought over the new sources created by cultivation (Koven 2006). This amplification is supported by model experiments that show a reduction in precipitation in the vicinity of the new dust sources (Koven 2006; Cook et al. 2008). To constrain the strength of the new sources, Cook et al. (2008, 2009) used measurements of downwind deposition (Hansen and Libecap 2004) and showed that the source expansion brought the anomalies of temperature and precipitation into better agreement with observations compared to the effect of equatorial Pacific SST by itself (Fig. 13.9, right column).

Models suggest that the drought of the Dust Bowl was exacerbated by human disturbance, but natural "megadroughts" within the Great Plains of North America have been inferred from tree-ring measurements throughout the past millennium (Cook et al. 2007). During the Medieval Climate Anomaly (MCA), there is geologic evidence of expanding sand dunes within the Great Plains, implying increased dust mobilization (e.g., Jacobs and Mason 2007; Miao et al. 2007). Cook et al. (2013) show that new dust sources amplify the reduction of precipitation initiated by remote forcing from the equatorial Pacific, increasing not only the magnitude of the drought but its persistence, consistent with the tree-ring record.

These studies show that new dust sources can significantly amplify and prolong precipitation anomalies. What remains to be quantified is whether the regional extent and strength of the new dust sources assumed by these studies are realistic. Models of vegetation and its response to climate anomalies are needed to investigate the entire feedback loop. For the example of the MCA, a vegetation model is needed to demonstrate that mild forcing from the equatorial Pacific can lead to the areal expansion of bare soil that is vulnerable to wind erosion. This requires that vegetation models exhibit realistic sensitivity to climate perturbations. Some models show large sensitivity. For example, anthropogenic climate change simulated by one model converts the Amazon into a desert that triples the global dust load (Woodward et al. 2005). Vegetation models give source extent, but additional information about source strength is needed, which depends upon soil mechanics and soil conservation

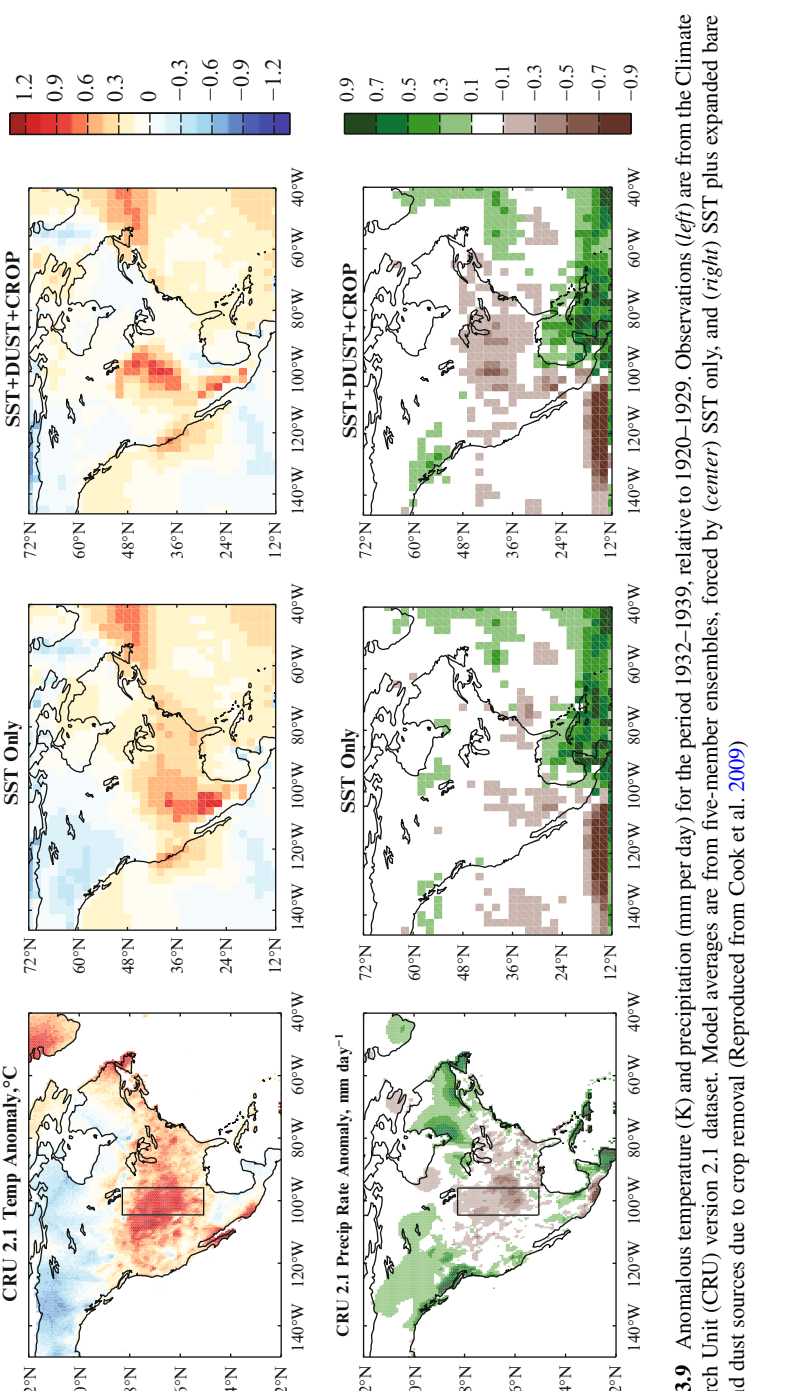

Fig. 13.9 Anomalous temperature (K) and precipitation (mm per day) for the period 1932–1939, relative to 1920–1929. Observations (*left*) are from the Climate Research Unit (CRU) version 2.1 dataset. Model averages are from five-member ensembles, forced by (*center*) SST only, and (*right*) SST plus expanded bare soil and dust sources due to crop removal (Reproduced from Cook et al. 2009)

practices. These might be constrained with deposition inferred from geological surveys. Only with both source extent and strength constrained can we quantify the complete feedback loop between dust, climate, and vegetation.

13.5 Conclusion

Radiative forcing by dust aerosols changes surface temperature and rainfall along with variables like wind speed and vegetation that feed back upon the dust concentration. ESMs demonstrate that adjustment to the forcing occurs over the extent of the perturbed circulation. As a result, the temperature perturbation at any location at equilibrium is not directly related to the local temperature tendency associated with the forcing. In regions of frequent vertical mixing by deep convection, the anomalous surface temperature is controlled primarily by the aerosol forcing at TOA rather than the surface. The strong coupling of surface air temperature to TOA forcing is implicitly recognized in the classic definition of climate sensitivity that is the ratio of these two variables (e.g., Forster et al. 2007). Outside of convecting regions, the influence of surface forcing is similarly limited. Many models calculate warming of the Sahara by dust, despite surface forcing of contrasting sign. The sign of TOA forcing also varies inconsistently among these models, indicating that lateral transports of energy need to be considered to interpret the temperature response. Surface temperature anomalies depend not only upon changes by dust to the energy budget but also changes to precipitation and humidity, as shown by the cooling within the Sahel as the TOA forcing becomes increasingly positive (Fig. 13.5). In general, transports of energy and moisture should be diagnosed along with the forcing to attribute the climate response calculated by ESMs.

Models generally predict a reduction of global precipitation by dust radiative forcing. This has been interpreted in the literature as a simple consequence of the negative surface forcing beneath the aerosol layer that leads to a compensating reduction in surface evaporation. However, while precipitation is reduced for all three prescriptions of particle shortwave absorption in Table 13.1, the reduction is not proportional to dimming of the surface. The decrease of global precipitation (and evaporation) is smallest for the most absorbing particles, even though the magnitude of the surface forcing is largest. Xian (2008) demonstrates how the influence of positive TOA forcing upon surface air temperature and humidity can increase surface evaporation and precipitation over the ocean. While the precise relation between global precipitation and forcing needs further investigation, the more general point is that precipitation depends upon forcing at both TOA and the surface (Ming et al. 2010).

Regional precipitation responds in a complicated way to dust radiative forcing. Dust generally reduces oceanic precipitation downwind of the aerosol layer, beneath which evaporation is reduced, as in the tropical Atlantic. Over the Sahel, however, the sign of the precipitation anomaly seems to follow the local TOA forcing (Table 13.2). Figure 13.7 shows that Sahel precipitation increases for positive TOA forcing, despite shortwave heating within the dust layer and reduced radiation

incident upon the surface: temperature tendencies that would seemingly inhibit convection by stabilizing the column. One resolution to this paradox is that positive TOA forcing increases the export of energy from the convecting region, resulting in anomalous convergence of moisture at the surface that makes the air conditionally unstable and likely to ascend (Chou et al. 2005). This argument makes certain assumptions that deserve further investigation. Most importantly, the climate is assumed to respond to dust through a direct circulation. In the Tropics, this circulation type dominates the transport of energy and moisture. Relatively little attention has been devoted to how dust changes precipitation in the middle latitudes. In general, extratropical cyclones have a complicated dependence upon the time-averaged flow, and anticipating how they are modified by dust radiative forcing is difficult. The precipitation response also depends upon the compensation of the surface forcing by evaporation as opposed to ocean heat transport. The latter has been calculated in only a few studies (Ramanathan et al. 2005; Bollasina et al. 2011).

While many studies emphasize the effect of dust forcing upon climatological precipitation, there is recent interest regarding the effect of dust upon tropical cyclones within the Atlantic, where dusty summers are associated with a reduction in cyclone activity. There has been extensive work untangling the radiative and microphysical effects of dust upon tropical cyclone development from other environmental factors like the low humidity that accompanies dusty air, along with broader climate variations that modulate both cyclones and dust. Understanding the observed relation remains a topic of active research and importance, given the destructive power of cyclones and their potential to amplify in the warming climate.

Several studies have shown how climate anomalies created by dust forcing feed back on the mobilization of additional soil particles. Surface wind speed responds to forcing through either a perturbation to surface pressure or the sensible heat flux that controls mixing within the boundary layer. Dust changes the strength of mixing that delivers momentum to the surface each morning from jets that form above the nocturnal boundary layer. In addition, a reduction of precipitation by dust can diminish the extent of vegetation, leading to the mobilization of additional particles and amplification of droughts like the Dust Bowl. What remains in characterizing this positive feedback is to model quantitatively the impact of the precipitation anomaly by dust upon vegetation. This in turn requires the development of dynamical vegetation models with realistic sensitivity.

The largest contribution to the uncertainty of forcing and the attendant climate response probably originates with the uncertain dust distribution. Estimates of the global dust aerosol mass by current models range between 20 and 35 Tg in most cases (Textor et al. 2006). To reduce the uncertainty of forcing and its impact upon climate, we need a more confident estimate of the dust distribution. The shortwave contribution to forcing is sensitive to the presence of absorbing minerals like hematite, and routine measurements of mineral content will help to document regional variations in the particle optical properties that are almost always neglected by current ESMs. Forcing also varies among models due to environmental factors like surface albedo. A more precise characterization of albedo remains a challenge

because radiation from the surface is absorbed at many wavelengths by clouds and aerosols before being measured by a satellite instrument. In the meantime, the forcing uncertainty and the resulting range of climate perturbations calculated by ESMs remain a useful test of our understanding of the mechanisms relating dust radiative forcing to the climate response.

References

Ahn H-J, Park S-U, Chang L-S (2007) Effect of direct radiative forcing of Asian dust on the meteorological fields in East Asia during an Asian dust event period. J Appl Meteorol Climatol 46:1655–1681. doi:10.1175/JAM2551.1

Bollasina MA, Ming Y, Ramaswamy V (2011) Anthropogenic aerosols and the weakening of the South Asian summer monsoon. Science 334:502–505. doi:10.1126/science.1204994

Cakmur R, Miller RL, Torres O (2004) Incorporating the effect of small-scale circulations upon dust emission in an atmospheric general circulation model. J Geophys Res 109:D07201. doi:10.1029/2003JD4067

Carlson TN, Prospero JM (1972) The large-scale movement of Saharan air outbreaks over the northern equatorial Atlantic. J Appl Meteorol 11:283–297

Cess RD, Potter GL, Ghan SJ, Gates WL (1985) The climatic effects of large injections of atmospheric smoke and dust: a study of climate feedback mechanisms with one- and three-dimensional climate models. J Geophys Res 90:12937–12950

Chou C, Neelin JD, Lohmann U, Feichter J (2005) Local and remote impacts of aerosol climate forcing on tropical precipitation. J Clim 18:4621–4636

Coakley JA, Cess RD (1985) Response of the NCAR community climate model to the radiative forcing by the naturally occurring tropospheric aerosol. J Atmos Sci 42:1677–1692

Colarco PR, Toon OB, Torres O, Rasch PJ (2002) Determining the UV imaginary index of refraction of Saharan dust particles from total ozone mapping spectrometer data using a three-dimensional model of dust transport. J Geophys Res 107(D16):4312. doi:10.1029/2001JD000903

Cook ER, Seager R, Cane MA, Stahle DW (2007) North American drought: reconstructions, causes, and consequences. Earth Sci Rev 81:93–134. doi:10.1016/j.earscirev.2006.12.002

Cook BI, Miller RL, Seager R (2008) Dust and sea surface temperature forcing of the 1930s "dust bowl" drought. Geophys Res Lett 35:L08710. doi:10.1029/2008GL033486

Cook BI, Miller RL, Seager R (2009) Amplification of the North American 'dust bowl' drought through human induced land degradation. Proc Natl Acad Sci USA 106(13):4997–5001. doi:10.1073/pnas.0810200106

Cook B, Seager R, Miller RL, Mason J (2013) Intensification of North American megadroughts through surface and dust aerosol forcing. J Clim 26:4414–4430. doi:10.1175/JCLI-D-12-00022.1

Cowie SM, Knippertz P, Marsham JH (2013) Are vegetation-related roughness changes the cause of the recent decrease in dust emission from the Sahel? Geophys Res Lett 40:1868–1872. doi:10.1002/grl.50273

Dubovik O, Holben BN, Eck TF, Smirnov A, Kaufman YJ, King MD, Tanré D, Slutsker I (2002) Variability of absorption and optical properties of key aerosol types observed in worldwide locations. J Atmos Sci 59:590–608

Forster P, Ramaswamy V, Artaxo P, Berntsen T, Betts R, Fahey D, Haywood J, Lean J, Lowe D, Myhre G, Nganga J, Prinn R, Raga G, Schulz M, Dorland RV (2007) Changes in atmospheric constituents and in radiative forcing (chap. 2). In: Solomon S, Qin D, Manning M, Chen Z, Marquis M, Averyt K, Tignor M, Miller H (eds) Climate change 2007: the physical science

basis. Contribution of working group I to the fourth assessment report of the intergovernmental panel on climate change. Cambridge University Press, Cambridge/New York

Ginoux P, Prospero JM, Gill TE, Hsu N, Zhao M (2012) Global scale attribution of anthropogenic and natural dust sources and their emission rates based on MODIS Deep Blue aerosol products. Rev Geophys 50:RG3005. doi:10.1029/2012RG000388

Grousset FE, Ginoux P, Bory A, Biscaye PE (2003) Case study of Chinese dust plume reaching the French Alps. Geophys Res Lett 30:1277–1280. doi:10.1029/2002GL016833

Hansen ZK, Libecap GD (2004) Small farms, externalities, and the dust bowl of the 1930s. J Pol Econ 112:665–694. doi:10.1086/383102

Hansen J, Sato M, Ruedy R (1997) Radiative forcing and climate response. J Geophys Res 102:6831–6864

Hansen J, Sato M, Ruedy R, Nazarenko L, Lacis A, Schmidt GA, Russell G, Aleinov I, Bauer M, Bauer S, Bell N, Cairns B, Canuto V, Chandler M, Cheng Y, Del Genio A, Faluvegi G, Fleming E, Friend A, Hall T, Jackman C, Kelley M, Kiang N, Koch D, Lean J, Lerner J, Lo K, Menon S, Miller R, Minnis P, Novakov T, Oinas V, Perlwitz J, Perlwitz J, Rind D, Romanou D, Shindell D, Stone P, Sun S, Tausnev N, Thresher D, Wielicki B, Wong T, Yao M, Zhang S (2005) Efficacy of climate forcings. J Geophys Res 110:D18104. doi:19.1029/2005JD005776

Heinold B, Helmert J, Hellmuth O, Wolke R, Ansmann A, Marticorena B, Laurent B, Tegen I (2007) Regional modeling of Saharan dust events using LM-MUSCAT: model description and case studies. J Geophys Res 112:D11204. doi:10.1029/2006JD007443

Jacobs PM, Mason JA (2007) Late quaternary climate change, loess sedimentation, and soil profile development in the central great plains: a pedosedimentary model. Geol Soc Am Bull 119:462475. doi:10.1130/B25868.1

Kavouras IG, Etyemezian V, DuBois DW, Xu J, Pitchford M (2009) Source reconciliation of atmospheric dust causing visibility impairment in class I areas of the Western United States. J Geophys Res 114:D02308. doi:10.1029/2008JD009923

Knippertz P, Todd MC (2012) Mineral dust aerosols over the Sahara: meteorological controls on emission and transport and implications for modeling. Rev Geophys 50:RG1007. doi:10.1029/2011RG000362

Koven CD (2006) On the sources, composition, and climatic effects of mineral dust in the atmosphere. PhD thesis, University of California at Berkeley, Berkeley

Lau K-M, Kim K-M (2006) Observational relationships between aerosol and asian monsoon rainfall, and circulation. Geophys Res Lett 33:L21810. doi:10.1029/2006GL027546

Liao H, Seinfeld JH (1998) Radiative forcing by mineral dust aerosols: sensitivity to key variables. J Geophys Res 103:31637–31645

Liepert BG, Feichter J, Lohmann U, Roeckner E (2004) Can aerosols spin down the water cycle in a warmer and moister world? Geophys Res Lett 31:L06207. doi:10.1029/2003GL019060

Lunt DJ, Valdes PJ (2002) The modern dust cycle: comparison of model results with observations and study of sensitivities. J Geophys Res 107(D23):4669. doi:10.1029/2002JD002316

Mahowald NM, Kloster S, Engelstaedter S, Moore JK, Mukhopadhyay S, McConnell JR, Albani S, Doney SC, Bhattacharya A, Curran MAJ, Flanner MG, Hoffman FM, Lawrence DM, Lindsay K, Mayewski PA, Neff J, Rothenberg D, Thomas E, Thornton PE, Zender CS (2010) Observed 20th century desert dust variability: impact on climate and biogeochemistry. Atmos Chem Phys 10:10875–10893. doi:10.5194/acp-10-10875-2010

Meehl G, Stocker T, Collins W, Friedlingstein P, Gaye A, Gregory J, Kitoh A, Knutti R, Murphy J, Noda A, Raper S, Watterson I, Weaver A, Zhao Z-C (2007) Global climate projections (chap. 10). In: Solomon S, Qin D, Manning M, Chen Z, Marquis M, Averyt K, Tignor M, Miller H (eds) Climate change 2007: the physical science basis. Contribution of working group I to the fourth assessment report of the intergovernmental panel on climate change. Cambridge University Press, Cambridge/New York

Miao X, Mason JA, Swinehart JB, Loope DB, Hanson PR, Goble RJ, Liu X (2007) A 10,000 year record of dune activity, dust storms, and severe drought in the central great plains. Geology 35:119–122. doi:10.1130/G23133A.1

Miller RL (2012) Adjustment to radiative forcing in a simple coupled ocean-atmosphere model. J Clim 25:7802–7821. doi:10.1175/JCLI-D-11-00119.1

Miller RL, Tegen I (1998) Climate response to soil dust aerosols. J Clim 11:3247–3267

Miller RL, Tegen I (1999) Radiative forcing of a tropical direct circulation by soil dust aerosols. J Atmos Sci 56:2403–2433

Miller JR, Russell GL, Tsang L-C (1983) Annual oceanic heat transports computed from an atmospheric model. Dyn Atmos Oceans 7:95–109

Miller RL, Perlwitz J, Tegen I (2004a) Modeling Arabian dust mobilization during the Asian summer monsoon: the effect of prescribed versus calculated SST. Geophys Res Lett 31(22):L22214. doi:10.1029/2004GL020669

Miller RL, Tegen I, Perlwitz J (2004b) Surface radiative forcing by soil dust aerosols and the hydrologic cycle. J Geophys Res 109:D04203. doi:10.1029/2003JD004085

Miller RL, Cakmur RV, Perlwitz J, Geogdzhayev IV, Ginoux P, Koch D, Kohfeld KE, Prigent C, Ruedy R, Schmidt GA, Tegen I (2006) Mineral dust aerosols in the NASA Goddard Institute for Space Studies ModelE AGCM. J Geophys Res 111:D06208. doi:10.1029/2005JD005796

Miller RL, Slingo A, Barnard JC, Kassianov E (2009) Seasonal contrast in the surface energy balance of the Sahel. J Geophys Res 114:D00E05. doi:10.1029/2008JD010521

Ming Y, Ramaswamy V, Persad G (2010) Two opposing effects of absorbing aerosols on global-mean precipitation. Geophys Res Lett 37, L13701. doi:10.1029/2010GL042895

N'Tchayi Mbourou G, Bertrand J, Nicholson S (1997) The diurnal and seasonal cycles of wind-borne dust over Africa North of the equator. J Appl Meteorol 36:868–882

Patterson EM, Gillette DA, Stockton BH (1977) Complex index of refraction between 300 and 700 nm for Saharan aerosols. J Geophys Res 82:3153–3160

Pérez C, Nickovic S, Pejanovic G, Baldasano JM, Özsoy E (2006) Interactive dust-radiation modeling: a step to improve weather forecasts. J Geophys Res 111:D16206. doi:10.1029/2005JD006717

Perlwitz J, Miller R (2010) Cloud cover increase with increasing aerosol absorptivity—a counterexample to the conventional semi-direct aerosol effect. J Geophys Res 115:D08203. doi:10.1029/2009JD012637

Perlwitz J, Tegen I, Miller RL (2001) Interactive soil dust aerosol model in the GISS GCM. Part I: sensitivity of the soil dust cycle to radiative properties of soil dust aerosols. J Geophys Res 106:18167–18192

Ramanathan V, Chung C, Kim D, Bettege T, Buja L, Kiehl JT, Washington WM, Fu Q, Sikka DR, Wild M (2005) Atmospheric brown clouds: impacts on South Asian climate and hydrological cycle. Proc Natl Acad Sci USA 5326–5333. doi:10.1073/pnas.0500656102

Randall D, Wood R, Bony S, Colman R, Fichefet T, Fyfe J, Kattsov V, Pitman A, Shukla J, Srinivasan J, Stouffer R, Sumi A, Taylor K (2007) Cilmate models and their evaluation (chap. 8). In: Solomon S, Qin D, Manning M, Chen Z, Marquis M, Averyt K, Tignor M, Miller H (eds) Climate change 2007: the physical science basis. Contribution of working group I to the fourth assessment report of the intergovernmental panel on climate change. Cambridge University Press, Cambridge/New York

Schepanski K, Tegen I, Todd MC, Heinold B, Boñisch G, Laurent B, Macke A (2009) Meteorological processes forcing Saharan dust emission inferred from msg-seviri observations of subdaily dust source activation and numerical models. J Geophys Res 114:D10201. doi:10.1029/2008JD010325

Schmidt GA, Ruedy R, Hansen JE, Aleinov I, Bell N, Bauer M, Bauer S, Cairns B, Cheng Y, DelGenio A, Faluvegi G, Friend AD, Hall TM, Hu Y, Kelley M, Kiang N, Koch D, Lacis AA, Lerner J, Lo KK, Miller RL, Nazarenko L, Oinas V, Perlwitz J, Perlwitz J, Rind D, Romanou A, Russell GL, Sato M, Shindell DT, Stone PH, Sun S, Tausnev N, Thresher D, Yao M-S (2006) Present day atmospheric simulations using GISS modelE: comparison to in-situ, satellite and reanalysis data. J Clim 19:153–192

Schmidt GA, Kelley M, Nazarenko L, Ruedy R, Russell GL, Aleinov I, Bauer M, Bauer S, Bhat MK, Bleck R, Canuto V, Chen Y, Cheng Y, Clune TL, DelGenio A, de Fainchtein R, Faluvegi G, Hansen JE, Healy RJ, Kiang NY, Koch D, Lacis AA, LeGrande AN, Lerner

J, Lo KK, Marshall J, Mathews EE, Menon S, Miller RL, Oinas V, Oloso A, Perlwitz J, Puma MJ, Putman WM, Rind D, Romanou A, Sato M, Shindell DT, Sun S, Syed R, Tausnev N, Tsigaridis K, Unger N, Voulgarakis A, Yao M-S, Zhang J (2014) Configuration and assessment of the GISS ModelE2 contributions to the CMIP5 archive. J Adv Model Earth Syst 6:141–184. doi:10.1002/2013MS000265

Schneider EK (1983) Martian dust storms: interpretive axially symmetric models. Icarus 55:302–331

Schopf PS (1983) On equatorial waves and El Niño. II: effects of air-sea thermal coupling. J Phys Oceanogr 13:1878–1893

Shindell D, Schulz M, Ming Y, Takemura T, Faluvegi G, Ramaswamy V (2010) Spatial scales of climate response to inhomogeneous radiative forcing. JGR 115:D19110. doi:10.1029/2010JD014108

Sinyuk A, Torres O, Dubovik O (2003) Combined use of satellite and surface observations to infer the imaginary part of the refractive index of Saharan dust. Geophys Res Lett 30. doi:10.1029/2002GL016189

Slingo A, Ackerman TP, Allan RP, Kassianov EI, McFarlane SA, Robinson GJ, Barnard JC, Miller MA, Harries JE, Russell JE, Dewitte S (2006) Observations of the impact of a major Saharan dust storm on the atmospheric radiation balance. Geophys Res Lett 33:L24817. doi:10.1029/2006GL027869

Solmon F, Mallet M, Elguindi N, Giorgi F, Zakey A, Konare A (2008) Dust aerosol impact on regional precipitation over Western Africa, mechanisms and sensitivity to absorption properties. Geophys Res Lett 35:L24705. doi:10.1029/2008GL035900

Solmon F, Elguindi N, Mallet M (2012) Radiative and climatic effects of dust over West Africa, as simulated by a regional climate model. Clim Res. doi:10.3354/cr01039

Stephens GL, Wood NB, Pakula LA (2004) On the radiative effects of dust on tropical convection. Geophys Res Lett 31:L23112. doi:10.1029/2004GL021342

Swap R, Garstang M, Greco S, Talbot R, Kållberg P (1992) Saharan dust in the Amazon basin. Tellus 44B:133–149

Tegen I, Lacis AA (1996) Modeling of particle influence on the radiative properties of mineral dust aerosol. J Geophys Res 101:19237–19244

Tegen I, Lacis AA, Fung I (1996) The influence on climate forcing of mineral aerosols from disturbed soils. Nature 380:419–422

Tegen I, Werner M, Harrison SP, Kohfeld KE (2004) Relative importance of climate and land use in determining present and future global soil dust emission. Geophys Res Lett 31:L05105. doi:10.1029/2003GL019216

Tegen I, Heinold B, Todd M, Helmert J, Washington R, Dubovik O (2006) Modelling soil dust aerosol in the bodéelé depression during the BoDEx campaign. Atmos Chem Phys 6:4345–4359

Textor C, Schulz M, Guibert S, Kinne S, Balkanski Y, Bauer S, Berntsen T, Berglen T, Boucher O, Chin M, Dentener F, Diehl T, Easter R, Feichter H, Fillmore D, Ghan S, Ginoux P, Gong S, Grini A, Hendricks J, Horowitz L, Huang P, Isaksen I, Iversen I, Kloster S, Koch D, Kirkevåg A, Kristjansson JE, Krol M, Lauer A, Lamarque JF, Liu X, Montanaro V, Myhre G, Penner J, Pitari G, Reddy S, Seland Ø, Stier P, Takemura T, Tie X (2006) Analysis and quantification of the diversities of aerosol life cycles within aerocom. Atmos Chem Phys 6(7):1777–1813. doi:10.5194/acp-6-1777-2006

Volz FE (1973) Infrared optical constants of ammonium sulfate, Sahara dust, volcanic pumice and flyash. Appl Opt 12:564–568

Woodage MJ, Slingo A, Woodward S, Comer RE (2010) U.K. HiGEM: simulations of desert dust and biomass burning aerosols with a high-resolution atmospheric GCM. J Clim 23:1636–1659. doi:10.1175/2009JCLI2994.1

Woodward S, Roberts DL, Betts RA (2005) A simulation of the effect of climate changeinduced desertification on mineral dust aerosol. Geophys Res Lett 32:L18810. doi:10.1029/2005GL023482

Xian P (2008) Seasonal migration of the ITCZ and implications for aerosol radiative impact. PhD thesis, Columbia University

Yoshioka M, Mahowald NM, Conley AJ, Collins WD, Fillmore DW, Zender CS, Coleman DB (2007) Impact of desert dust radiative forcing on Sahel precipitation: relative importance of dust compared to sea surface temperature variations, vegetation changes, and greenhouse gas warming. J Clim 20:1445–1467

Yue X, Wang H, Liao H, Fan K (2010) Simulation of dust aerosol radiative feedback using the GMOD: 2. Dust-climate interactions. J Geophys Res 115:D04201. doi:10.1029/2009JD012063

Yue X, Liao H, Wang HJ, Li SL, Tang JP (2011) Role of sea surface temperature responses in simulation of the climatic effect of mineral dust aerosol. Atmos Chem Phys 6049–6062. doi:10.5194/acp-11-6049-2011

Yulaeva E, Wallace JM (1994) The signature of ENSO in global temperature and precipitation fields derived from the microwave sounding unit. J Clim 7:1719–1736. doi:10.1175/1520-0442(1994)007<1719:TSOEIG>2.0.CO;2

Chapter 14
Biogeochemical Impacts of Dust on the Global Carbon Cycle

Tim Jickells, Philip Boyd, and Keith A. Hunter

Abstract Dust supply can directly affect primary production in terrestrial and marine ecosystems and thereby affect local and planetary biogeochemistry. The impact on land appears to be primarily in terms of dust providing a supply of phosphorus to phosphorus-limited ecosystems, thereby increasing primary production directly, and to also relieve phosphorus limitation of nitrogen fixation, which then also allows increased primary production. The impact of dust as a phosphorus source seems to have the biggest impacts in terrestrial tropical systems, reflecting both the global dust supply pattern as well as the fundamental biogeochemistry of soil development and biogeochemical cycling in these environments. Dust supply can also in some environments, particularly Caribbean islands, provide a significant part of the soil itself. In marine ecosystems, the most important role of dust appears to be a source of iron. This dust-derived iron supply acts to directly increase primary production in surface waters of high-nitrate low-chlorophyll regions where primary production is iron limited. These areas are predominantly at high latitudes and include the vast Southern Ocean. The dust-derived iron supply also plays an important role in relieving iron limitation of nitrogen fixation in tropical surface ocean waters and thereby increases primary production in these areas.

T. Jickells (✉)
School of Environmental Sciences, University of East Anglia, Norwich Research Park, Norwich NR47TJ, UK
e-mail: t.jickells@uea.ac.uk

P. Boyd
University of Tasmania, Hobart, Australia

Otago University, P.O. Box 56, Dunedin 9016, New Zealand
e-mail: Philip.Boyd@utas.edu.au

K.A. Hunter
Otago University, P.O. Box 56, Dunedin 9016, New Zealand
e-mail: Keith.Hunter@otago.ac.nz

P. Knippertz and J.-B.W. Stuut (eds.), *Mineral Dust: A Key Player in the Earth System*, DOI 10.1007/978-94-017-8978-3_14,

Keywords Biogeochemistry • Nutrients • Iron • Nitrogen • Carbon • Phosphorous • Deposition • Productivity • Oceans • Terrestrial environment • Soil formation • Marine environment • Ocean

14.1 Introduction

The sources (Chap. 3), transport (Chap. 7) and transformations (Chap. 4) of dust have been considered in previous chapters of this book. In this chapter on the biogeochemical impacts of dust, we focus on its impacts on photosynthetic fixation of carbon and the associated supply of key nutrients to sustain this fixation, which is the basis of the planetary ecosystem, the carbon cycle and global biogeochemistry. Mahowald et al. (2011) consider the overall impacts of aerosols (of which dust represents an important but only locally dominant part) on climate in terms of overall radiative forcing. She identifies the reasonably well-established "direct" and "indirect" effects of aerosols on radiative forcing and also the biogeochemical impacts from aerosol deposition on ocean productivity and terrestrial carbon storage. Mahowald et al. (2011) estimate that the overall biogeochemical aerosol effects are comparable to the aerosol direct effect and slightly smaller than the aerosol indirect effect, although the magnitudes of all three are rather uncertain. These biogeochemical impacts of dust are therefore substantial and are the subject of this chapter. The focus is on dust specifically, although many of the effects considered by Mahowald et al. (2011) apply to other components of the aerosol such as fertilisation of primary production by atmospheric deposition of nitrogen. Dust in the atmosphere also affects solar radiation (Chap. 11), supply to ecosystems (Chap. 8) and temperatures (Chap. 6) as discussed earlier in this book, and both light supply and temperature can potentially influence the biological carbon cycle. Climate change is therefore expected to have substantial impacts on terrestrial (Malhi et al. 1999; Mahowald et al. 2010; Cox et al. 2013) and marine (Moore et al. 2013) productivity and hence global biogeochemistry. The focus of this chapter is on biogeochemical impacts associated primarily with nutrients supplied by dust, rather than effects arising from changes in climate, although we recognise such changes are potentially very important.

On a long-term basis, the amounts of carbon fixed by the terrestrial and marine ecosystems (measured as annual carbon fluxes) are similar (Denman et al. 2007), but the character of the photosynthetic carbon fixation is very different in the two systems as discussed below. In the oceans primary production is dominated by microscopic and short-lived (days) algae, while terrestrial productivity is dominated by large plants, which are rooted in soil and can live for periods from weeks to centuries.

Marine algae live within an ocean water column that is generally well oxygenated with a pH $\sim$ 8. Ocean waters mix completely on timescales of about 1,000 years, but the geochemical residence times of different key plant nutrients within the ocean range from tens of years to millions of years (Moore et al. 2013). Sunlight only

penetrates about 100 m into the oceans, so photosynthesis is confined to a surface mixed layer of the oceans of about 100 m depth, within which the residence times of nutrients and carbon are estimated to be of the order of weeks to a few years. The internal mixing times of the oceans mean that they can be divided into very large biogeochemical provinces with length scales of many hundreds of kilometres, over which there is some coherence in the ecosystem structure (Longhurst 2007).

Terrestrial productivity is dominated by relatively long-lived (months to centuries) plants, which therefore invest biogeochemical effort in creating carbon-rich structural material (e.g. tree trunks). Plants grow from soil upwards and compete for light and nutrients. Terrestrial plants grow associated with soils that are generally centimetres to metres deep and developed over tens of thousands to millions of years. Within soils and the associated plant community, nutrient elements are recycled very efficiently, influenced by small-scale relatively large variations in pH and redox (or oxygen status) regions. The nutrient status of soils depends in large part on the supply of nutrients from the underlying rock and hence varies on length scales of the surface expressions of rock types, kilometres to perhaps hundreds of kilometres.

As discussed below, there are well-documented examples of dust transport having biogeochemical impacts in both terrestrial and marine systems, although the impacts are different in many ways in the two systems and considered separately here. There have also been suggestions that dust can also act as a vehicle for the transfer of bacteria and fungi through the atmosphere, although the biogeochemical significance of such transfer is uncertain and not discussed further here (Griffin et al. 2003, 2007).

14.2 Biogeochemical Impacts of Dust on Terrestrial Systems

14.2.1 Soil Formation

The existence of soil itself is fundamental to the functioning of most terrestrial ecosystems, and dust supply can contribute to soil formation, with an attendant impact on global biogeochemistry. In the areas of the world where the underlying sedimentary material is itself loess (fine-grained sediment deposited by wind), the soil is ultimately derived from this atmospherically transported dust. Such loess sediments are particularly abundant in Asia, Europe and North America, but are also known from South America (Muhs 2012). In other areas of the world, wind transport of dust has provided at least a part of the soil in a particular region, as reviewed by Muhs et al. (2012). The wind-blown material in a soil is identifiable by its morphology or chemical composition, and the proportion of wind-blown material in the overall soil varies from minor through to being a relatively large proportion in some regions. Examples of the latter situation are areas such as the Canary Island and Cape Verde downwind of large desert dust source regions, or areas where the

Table 14.1 Essential nutrient elements for plant growth

Macronutrient elements	C, O, N, Ca, Mg, K, P, S
Micronutrient elements	Co, Fe, Mn, Cu, Si, Zn, Mo, B, Cl, Ni and Na

Based on Ashman and Puri (2002) and Mengel and Kirkby (1978)

underlying rock provides very little soil components, such as on some oceanic limestone islands (e.g. Caribbean, Bahamas, Bermuda). In other areas where soils have developed under arid conditions and with very little available calcium from the underlying bedrocks, calcium delivered in association with atmospheric dust can lead to the formation of petrocalcic soil horizons, which can alter the soil structure. In all these cases where dust provides a major component of the soil itself, dust transport can be said to have a very important biogeochemical role (Muhs 2012; Muhs et al. 2012). While dust deposition is potentially a source of soil in these areas, it necessarily also must represent a loss of soil and associated carbon in dust source areas (Webb et al. 2012).

14.2.2 Nutrient Supply

In addition to the role of dust in providing the soil fabric, dust can potentially be an important source of nutrients for plants growing in soils. Mengel and Kirkby (1978) list 20 elements as essential nutrients for plant growth, although they suggest four of these (Co, Si, Ni and Na) are only essential for certain plants and hence will only limit species composition and not overall productivity. Fraústo da Silva and Williams (2001) produce a similar list although they also include V and Cr. Ashman and Puri (2002) further divide the nutrients into macronutrients and micronutrients as shown in Table 14.1. The C, N, S and H requirements of plants are readily met from the atmosphere as carbon (CO_2), oxygen (O_2 and H_2O), sulphur (sulphate aerosol) and hydrogen (H_2O) and hence are not relevant to the discussion of dust here. However, the atmospheric transport and transformation of atmospheric S (as sulphate and sulphuric acid) and N compounds (as nitric acid, nitrate, ammonia and ammonium) may be modified by reactions with dust in the atmosphere (e.g. Usher et al. 2003), and hence, the delivery of these nutrients may be coupled to that of dust. Atmospheric N deposition influences primary production and contributes significantly to the indirect biogeochemical impact discussed by Mahowald (2011). The nitrogen requirement of plant ecosystems can also be met, at least in part from the biological fixation of atmospheric nitrogen, and supplemented by atmospheric deposition. However, biological nitrogen fixation does require trace elements for the relevant enzymes and hence may be indirectly coupled to atmospheric dust supply of these trace elements as discussed later (Vitousek et al. 2010).

Epstein (1972) lists the relative nutrient requirements for various elements as ratios to the requirement for Mo (Fig. 14.1a). Although such estimates are of course

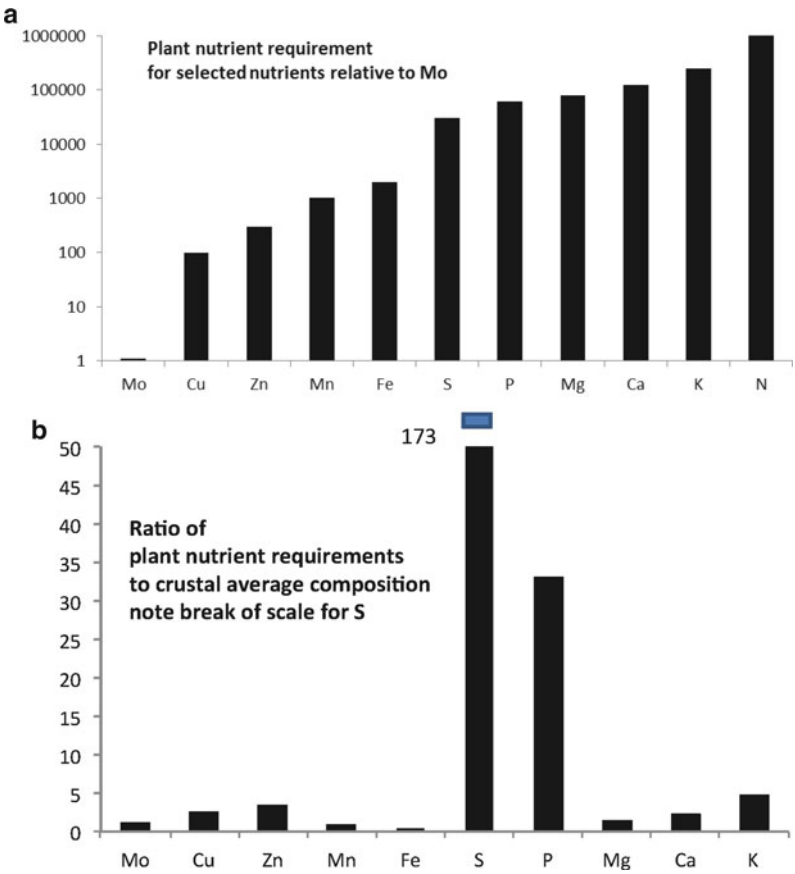

Fig. 14.1 (**a**) Terrestrial plant nutrient requirements for selected key nutrients relative to Mo (Epstein 1972). (**b**) Ratio of terrestrial plant nutrient requirements from 1a to average crustal rock abundance (Rudnick and Gao 2003); note break in scale for S

uncertain and variable with other factors such as the specific plant species involved, their growth phase and the availability of other nutrients, they can still be useful. Ignoring at this stage the bioavailability of elements within crustal material, this nutrient requirement can be compared to the average total abundance of elements within the crustal material (Rudnick and Gao 2003) from which soils are derived, recognising that this composition varies between different rock types. Such a comparison allows us to consider the relative scale of the potential supply of these elements from parent rock material to plant nutrient requirements and hence which elements are more likely to be limiting to primary production. This comparison is illustrated in Fig. 14.1b which emphasises that crustal material (including dust) is very deficient in S and P relative to plant requirements. Nitrogen and carbon are not illustrated because of their low and variable crustal composition and also because

they are readily available from the atmosphere. The plant requirement for S can be met in part from atmospheric deposition of S derived from marine or combustion sources. This argument therefore leads to the identification of a critical role for phosphorus supply in limiting terrestrial plant growth, as also discussed by Vitousek et al. (2010).

Sterner and Elser (2002) note the potential importance of a wide range of trace elements in growth but focus on C, N and P as the "three of the main constituents of biological structural material" which are also not particularly abundant in the Earth's crust. Similarly Aerts and Chapin (2000) argue that N and P are the main growth-limiting nutrients in natural environments, suggesting that generally N is limiting because of the high energy demands of nitrogen fixation along with the requirements for P, Mo and Fe for nitrogen fixation, but with P limitation frequently evident. Chapin and Eviner (2003) suggest that N is the most common limiting nutrient, although P may commonly limit productivity in wetlands and old soils, with K or other trace element limitation rare. Hedin (2004) suggests that there is a systematic global gradient in terrestrial ecosystems from P limitation at low latitudes to N limitation at high latitudes. Limitations by N and P are linked both through their common role in primary production and through the potential for P limitation of nitrogen fixation (e.g. Wang et al. 2010 and references therein) which may be common (Augusto et al. 2013).

Since nitrogen can be derived from atmospheric sources (nitrogen fixation and atmospheric deposition), it is clear that in the context of impacts of dust on terrestrial ecosystems, dust supply of phosphorus is potentially an important issue, even though the phosphorus content of dust (which is similar to that of average crustal rock) is low. The P supply from dust will influence both photosynthesis directly and nitrogen fixation, which can then relieve nitrogen limitation and thereby further influence photosynthesis. There is much less published information on the impacts of other trace nutrients although Kaspari et al. (2008) and Sayer et al. (2012) have demonstrated multiple nutrient limitation of different components of the productivity of a system (litter production, cellulose decomposition, leaf litter decomposition), including N, P, K and a mix of micronutrients (B, Ca, Cu, Fe, Mg, Mn, Mo, S and Zn). The subsequent discussion here therefore focusses on P and to a lesser extent other macronutrient cations (Ca, Mg, K, Na) because it is clear that the supply of these elements has been implicated in the limitation of primary productivity in at least some terrestrial systems. In the future we may discover that other metals supplied by dust are also important nutrients in regulating productivity. We will see later that iron plays an important role in limiting ocean primary production. However, in soils iron is always relatively abundant, although its low solubility means that specialist biogeochemical mechanisms, usually involving organic chelation, have developed to facilitate this access. Iron limitation can still occur in calcareous soils where high pH reduces iron solubility (e.g. Stevenson and Cole 1999).

In most environments, the soil is formed in situ from the degradation of bedrock on timescales of hundreds to millions of years (e.g. Okin et al. 2004). Vitousek et al. (2010), for instance, identify soils ranging in age from <40,000 years to four

million years. Many of the studies of the nutrient balance of soils in unperturbed ecosystems have focussed on forested systems, which represent a major component of the global carbon cycle, although the principles derived by such studies should be more widely applicable. Over the long term, the nutrient balance of a forest depends on the supply of nutrients from the atmosphere and from weathering and losses from the soil by leaching and volatilisation. The measurement of none of these fluxes is straightforward (Bruijnzeel 1991), particularly on the very long timescales that are relevant to soil development. This makes it difficult to construct nutrient budgets and evaluate the relative importance of atmospheric nutrient supply associated with dust. Bruijnzeel (1991) reviewed a number of budget studies and suggested that overall P is accumulating in forest soils, but that the balance of atmospheric supply to loss by run-off varies systematically with soil type. The balance for other major nutrients (Ca, Mg, K and N) between accumulation and loss was not clear. Sayer et al. (2012) and Vitousek et al. (2010) suggest that, on average, as soils age, they might be expected to evolve from nitrogen to phosphorus limitation as the supply of P from weathering declines, and nitrogen accumulates through nitrogen fixation, although testing this paradigm at the ecosystem scale is challenging (Vitousek et al. 2010). In an elegant study of soils developed on the Hawaiian Islands over different periods of time ranging from 300 years to 4.1 million years, Chadwick et al. (1999) concluded that over time, rock-derived nutrients are lost from soils during weathering. They suggest that cations such as calcium are renewed by atmospheric deposition of marine aerosols and that, over timescales of thousands of years, atmospheric dust deposition becomes the main source of P inputs to soils to replace that lost by leaching, despite the rather low dust deposition seen on these remote ocean islands. Looking to the future, Sayer et al. (2012) note that changes in atmospheric CO_2 concentrations, N deposition and possibly P deposition may alter forest productivity and the relative importance of different potential limiting nutrients, and Dezi et al. (2010) suggest that atmospheric N deposition has already significantly increased forest carbon storage.

We now focus on the role of P supply from dust deposition on terrestrial ecosystems. Mahowald et al. (2008) develop a global model of P deposition and argue that dust deposition dominates the total P deposition, with biomass burning, fossil fuel emissions, volcanoes and sea salt as secondary sources on a global basis, although the relative importance of the sources will obviously vary regionally. The readily soluble P component of atmospheric deposition is rather small, but on the long timescales of soil P cycling (thousands of years), it seems likely that all forms of P are potentially bioavailable. The global deposition of dust is illustrated in Fig. 14.2, which emphasises the importance of deserts as dust sources and the large gradients in global dust deposition, reflecting the short lifetime of atmospheric dust compared to global atmospheric mixing times (see Chap. 7).

In regions of higher dust deposition, the atmospheric P supply will be relatively large. Swap et al. (1992) have argued that dust deposition is an important source of nutrient P and K to the Amazon Basin in regions of ancient and highly weathered nutrient-poor soils. The atmospheric K supply will be partly directly from atmospheric dust deposition and partly from deposition of sea-salt aerosols.

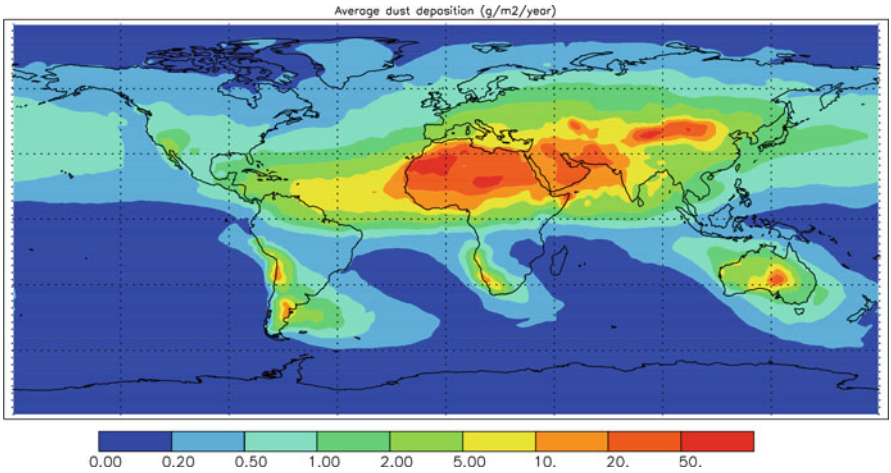

Fig. 14.2 Average global dust deposition flux based on Jickells et al. (2005)

Bristow et al. (2010) report the composition and mineralogy of dust from the Bodélé depression in the Sahara, a major dust source, and also conclude that this is an important source of P to the Amazon. Swap et al. suggest that atmospheric P inputs are equivalent to up to 3 % of the annual cycling of P by leaf fall in the Amazon. Hence, on an annual basis, most of the P cycling is driven by internal recycling within the ecosystem, but viewed from a different perspective, the atmosphere can supply the entire soil P reservoir over timescales of ~25,000 years (Okin et al. 2004). Phosphorus is usually considered as involatile and so is only lost from the soil by runoff, but Mahowald et al. (2008) suggest that emissions associated with biomass burning may now be of the same scale as atmospheric P deposition and result in a net P loss from parts of the Amazon Basin and an increase in atmospheric P deposition downwind of fires. As discussed by Okin et al. (2004) over timescales of thousands of years, the climate in the Sahara desert, the source region for dust over the Amazon, has changed dramatically; indeed, the Sahara desert was not truly a desert 5,000 years ago. The terrestrial Amazon ecosystem may still be responding to the increasing dust P input of the last few thousand years.

Pett-Ridge (2009) suggests that the atmospheric supply of phosphorus to the montane wet tropical forests of Puerto Rico is higher than the input to the Amazon and the soil P lower, suggesting that atmospheric P supply is quantitatively even more important in the Puerto Rican system than in the Amazon. Overall Pett-Ridge (2009) suggests that atmospheric P supply is the main source of phosphorus in this system which has a particularly high dust-associated P flux because it is directly downwind of the Sahara desert. Similar nutrient-poor ancient soils to those in parts of Puerto Rico and the Amazon underlie most of the tropical rainforests (Vitousek and Sanford 1986; Augusto et al. 2013), and these authors present data which, despite the uncertainties they note for it, do suggest that atmospheric deposition

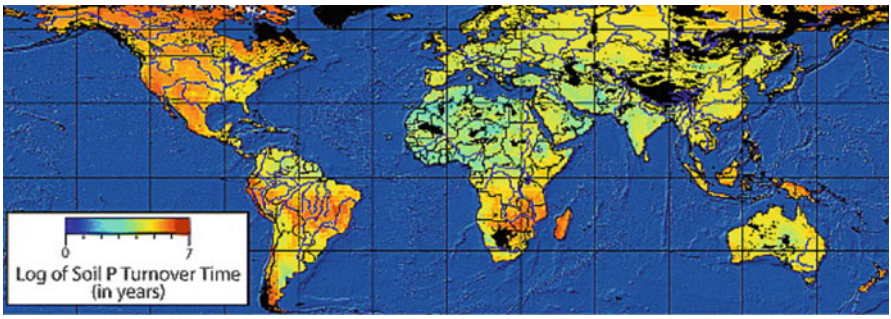

Fig. 14.3 Terrestrial soil phosphorus turnover times; shorter times mean a greater relative importance of atmospheric supply relative to soil reservoir note timescales to millions of years (Okin et al. 2004)

of P, K, Ca and Mg may be large compared to loss rates of these nutrients for many tropical rainforest systems, and hence, that dust inputs may be an important control on productivity and carbon cycling. Houlton et al. (2008) demonstrate that nitrogen fixation is very important in tropical forests and limited by phosphorus supply, while outside of the tropics, nitrogen fixation is limited by temperature.

As noted earlier, most analyses of nutrient budgets focus on forest systems, but Soderberg and Compton (2007) suggest that atmospheric deposition of dust is a very important source of Al, Si, Ca and P in the Fynbos ecosystem developed on nutrient-poor sandy spoils in the Cape region of South Africa, so the potential importance of atmospheric P deposition associated with dust is not limited to tropical rainforests.

Okin et al. (2004) attempted a global evaluation of the significance of atmospheric dust P supply based on an estimate of P associated with desert dust and the global pattern of soil P. They expressed the results as a pseudo turnover time for phosphorus, defined as the inventory of P in the top 20 cm of soil divided by the estimated atmospheric input. This pseudo turnover time ranged from 10^2 to 10^7 years in different regions of the world, and a shorter turnover time equates to increasing importance of atmospheric P supply in sustaining the soil P reservoir, which they note to be "an important nutrient that is often limiting in terrestrial environments". The results are shown in Fig. 14.3 and indicate that dust deposition of P is relatively more important for soil P supply in Europe, North and Central Africa and Southern Asia compared to other regions. Menge et al. (2012) developed an ecosystem model and use this to estimate that an atmospheric P supply associated with dust of 0.1 kg ha^{-1} $year^{-1}$ is sufficient to avoid P limitation. A comparison of this threshold to the global modelled P deposition (Mahowald et al. 2008) suggests that quite large areas of tropical forests receive atmospheric P supply below this threshold and so are potentially vulnerable to long-term P limitation.

Terrestrial carbon cycle models which include P have recently been developed (e.g. Wang et al. 2010; Goll et al. 2012) allowing the relative controls on productivity to be estimated, although none that we know of have currently attempted to directly quantify the impacts of atmospheric dust deposition. The results of one such

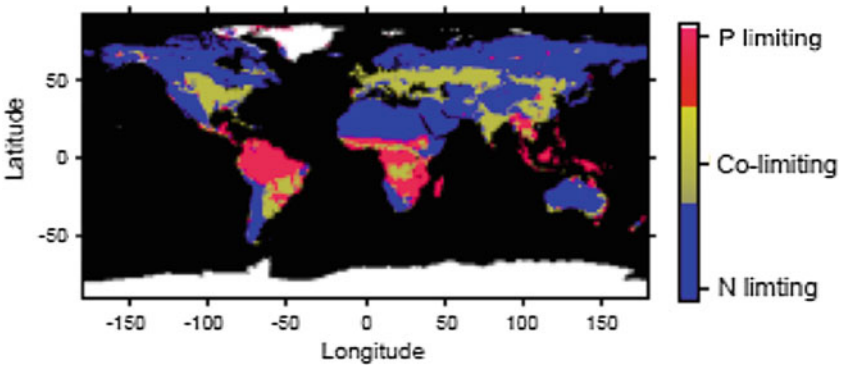

Fig. 14.4 Estimates of the terrestrial regions where net primary productivity is N limited, P limited or N and P co-limited (Wang et al. 2010)

model are shown in Fig. 14.4 suggesting that P limitation is relatively widespread particularly in the tropical forest and savannah regions, with other regions N limited or NP co-limited. The approximate scale of the effect of dust deposition on terrestrial ecosystems globally can be estimated from this model simulation.

Wang et al. (2010) have developed a global model of C, N and P cycling in the terrestrial biosphere which includes a spatially explicit representation of atmospheric P deposition. They suggest that P limitation of net primary productivity is particularly prevalent in tropical forest and savannah systems and this reduces overall productivity by about 20 %, an estimate consistent with a separate modelling study of Goll et al. (2012). Wang et al. use their model to estimate that globally atmospheric P inputs represent 4 % of total P supply to the terrestrial biosphere. Malhi et al. (1999) estimate global C sequestration in terrestrial systems to be 1.6 GtC year^{-1} (Gt is equivalent to 10^{15} g), and if 4 % is sustained by atmospheric dust supply of P, then the direct effect of dust deposition is about 0.06 GtC year^{-1}. This calculation is very crude and simplistic and probably an overestimate because it implies all the ecosystems respond to the P deposition, whereas only P limited areas will respond, although in some of these, the importance of P deposition may be higher. In the Amazon, Mahowald et al. (2005a) estimate that dust deposition supplies about 7 % of total atmospheric deposition (the remainder being primarily associated with deposition of biological material) but that the dust P input is only sufficient to sustain <1 % of net primary production. Hence, this estimate of the impact of dust on terrestrial C sequestration at 0.06 GtC year^{-1} seems likely to be an upper limit and can be compared later to the oceanic impacts of dust on the carbon cycle.

As noted earlier, P limitation appears to be particularly prevalent in tropical regions. Vitousek et al. (2010) and Okin et al. (2004) note that in high-latitude regions, glaciations have occurred repeatedly over the last few million years.

These serve to remove soils, but then allow the redevelopment of new soils with abundant rock sources of mineral nutrients. They therefore suggest that atmospheric deposition of nutrients is particularly important in tropical systems, where the long timescales of undisturbed soil development allow for P and other cation depletion to develop, and less important in high-latitude terrestrial ecosystems. However, there is evidence that atmospheric dust supply is important as a nutrient calcium source in temperate areas such as the boreal shield forest of Canada (Belanger and Holmden 2010). Input–output budgets for base cations along with nitrogen and sulphur have been constructed for forest soils at sites across the northern United States and Europe which suggest that atmospheric supply of cations is significant relative to loss rates from the system (Watmough et al. 2005). The motivation for the Watmough et al. (2005) budget studies is concern over loss of cations due to acid rain-driven soil acidification, and the budgets do not directly address the issue of nutrient limitation of productivity, although these authors note that calcium deficiency is evident within some of these temperate forest ecosystems. In these areas of northern Europe and America, atmospheric cation deposition is associated with dust material, but this dust is derived from combustion sources rather than from deserts (although both are compositionally similar), and this flux is declining due to improved emission controls (Hedin et al. 1994; Watmough et al. 2005).

In conclusion, it seems clear that dust supply for P, and possibly a few other major cations, may influence the long-term (hundreds to thousands of year time or longer timescales) fertility of tropical ecosystems developed on nutrient-poor soils. This P supply will also increase nitrogen fixation, emphasising the linkages between the nutrient cycles. In temperate regions subject to glaciations, the soils have been renewed on timescales of 10^3 years and hence generally have access to relatively strong source of nutrients from rock weathering. However, in some temperate and tropical regions with soils developed on rocks that are inherently poor in nutrients and not renewed by glaciation, there is evidence that atmospheric nutrient supply may be important. The net effect of atmospheric nutrient supply associated with dust is likely to be an increase in productivity of the temperate and tropical ecosystem, unless impacts such as biomass burning offset this supply, as may now be the case in the Amazon Basin (Mahowald et al. 2008). The long timescales of soil development and the efficiency of nutrient retention mean that soil nutrient balances are therefore sensitive to climate change and associated changes in dust deposition on relatively long timescales (Okin et al. 2004; Vitousek et al. 2010).

Although the impact of dust deposition seems likely to be an increase in nutrient supply and productivity in the receiving ecosystem, the overall effect on the global carbon cycle may be more complex. Soils represent a major component of the terrestrial carbon pool and the production of dust from soil in a particular region involves a net loss of organic carbon and associated nutrients from that region. This soil carbon may be transferred to another region or lost/modified by oxidation during atmospheric transport (Webb et al. 2012).

14.3 Biogeochemical Impacts of Dust Deposition on the Oceans

The differences between the oceans and the land surface profoundly alter the controls on primary production and the impacts of dust on both. We therefore begin this section with a short introduction to the broad patterns of ocean physics and biogeochemistry based on recent reviews (Boyd and Ellwood 2010; Chester and Jickells 2012; Moore et al. 2013) in order to provide a context within which to discuss the impacts of dust on this system.

Primary production is dominated by microscopic phytoplankton and is confined to the upper approximately 100 m (called the euphotic zone) of the oceans whose average depth overall is about 4 km. Ocean waters are almost exclusively well oxygenated and have a pH of about 8. In *tropical* waters surface heating produces a stable less dense surface mixed layer within which photosynthesis can take place, but losses of nutrients associated with sinking phytoplankton cells lead to very low nutrient concentrations, and rates of primary production controlled by rates of recycling within the euphotic zone, and rather inefficient and poorly understood inputs from below. Decomposition of sinking material at depth leads to increases in nutrient concentrations at depths below a few hundred metres in the water column. In *temperate* regions, cooling in winter reduces surface water density and allows mixing of the water column depths of many hundreds of metres below the surface, which effectively returns nutrients to the sunlit surface waters. This leads to relatively high surface water nutrient concentrations, but the low winter light levels limit productivity. As spring arrives, heating and reduced winds allow water column stratification, and this along with improved light levels allows a major seasonal burst of growth (the spring bloom) followed by a summer season of nutrient depletion with growth limited by nutrient recycling within the euphotic zone or supply from below, before winter mixing resets the seasonal system. Underlying this surface seasonal cycle is the massive global thermohaline circulation, which carries water at abyssal depths from the North Atlantic through the Pacific and Indian Oceans to ultimately return to the North Atlantic via a shallower circulation on timescales of a few thousand years. Although there are gradients in mixing and primary productivity across all the oceans, this simple description of the seasonality does allow us to broadly separate the oceans into biogeochemical provinces (Longhurst 2007) defined by the physical mixing cycles, which, at the coarsest level, divides the oceans into:

1. The warm tropical ocean gyres with low nutrients and relatively little seasonal variation in primary production which is sustained throughout the year
2. The temperate and polar waters subject to seasonal mixing and systematic seasonally variable primary production

Coastal waters cycle nutrients rather differently because loss to great ocean depths cannot occur, but since these coastal areas are relatively small compared to the open oceans and little impacted by atmospheric deposition compared to

riverine inputs, we will concentrate here on the open ocean waters and utilise this simple division into tropical and temperate waters. This large-scale pattern is evident in many ocean properties including the surface water distributions of nitrate and chlorophyll (Fig. 14.5). Chlorophyll provides an index of the amount of phytoplankton biomass, and nitrate represents the major deep ocean reservoir of available fixed nitrogen, although in surface waters there is a complex nutrient cycle involving several other nitrogen species. The tropical ocean gyres stand out in these figures as large areas of low surface water chlorophyll and nitrate while the temperate waters have generally higher and more variable concentrations of both.

Nitrogen and phosphorus are recognised as key macronutrients whose supply can limit ocean primary production, along with silicate which influences species composition because it is essential for one major group of phytoplankton, the diatoms. Iron is also a key nutrient and will be considered later. These three macronutrients are coupled via the large-scale ocean biogeochemical cycles with nitrate and phosphate present through the deep ocean in a constant ratio known as the Redfield ratio which also approximates to the proportions in which they are required by phytoplankton, although this varies with species and growth phase (Martiny et al. 2013). The residence times of nitrate, phosphate and silicate in the oceans are of the order of thousands of years. However, these nutrients spend most of this time in the deep ocean, away from the sunlit surface waters where primary production takes place, and the supply of these nutrients to sustain surface water primary productivity in the oceans is largely regulated by internal ocean supply by mixing between surface and deep waters.

It is now recognised that anthropogenic increases in atmospheric nitrogen supply can influence ocean productivity (Duce et al. 2008). As with atmospheric nitrogen inputs to terrestrial systems, the contemporary nitrogen inputs is influenced by atmospheric emissions from fuel combustion and agriculture and these emissions may interact with dust in the atmosphere, but we do not discuss these atmospheric nitrogen inputs in detail given the focus here on dust. Atmospheric P supply to the oceans is mainly associated with dust (Mahowald et al. 2008), but the fluxes of P are very small in comparison to those of Fe and N scaled against phytoplankton requirements (Baker et al. 2003, 2007; Moore et al. 2013). Increases in atmospheric inputs generally may therefore increase primary production, but not relieve P limitation overall. Hence, in contrast to terrestrial ecosystems, the impact of atmospheric P supply associated with atmospheric dust delivery is probably of limited biogeochemical significance for the oceans as is also the case for Si (Baker et al. 2003; Okin et al. 2011).

Phytoplankton requires a wide range of elements to sustain all their cellular functions. Moore et al. (2013) have elegantly summarised these requirements in comparison to ocean availability (Fig. 14.6), an analysis that illustrates that many of these nutrients are relatively abundant in seawater compared to their cellular requirements (e.g. S, Mo, Ca), while others, including N, P, Si and some trace metals such as Fe, Co, Mn and Cu, are deficient relative to cellular requirements and hence most likely to become limiting for primary production. In addition to N and P, there is clear evidence that iron supply limits productivity over large areas of the ocean

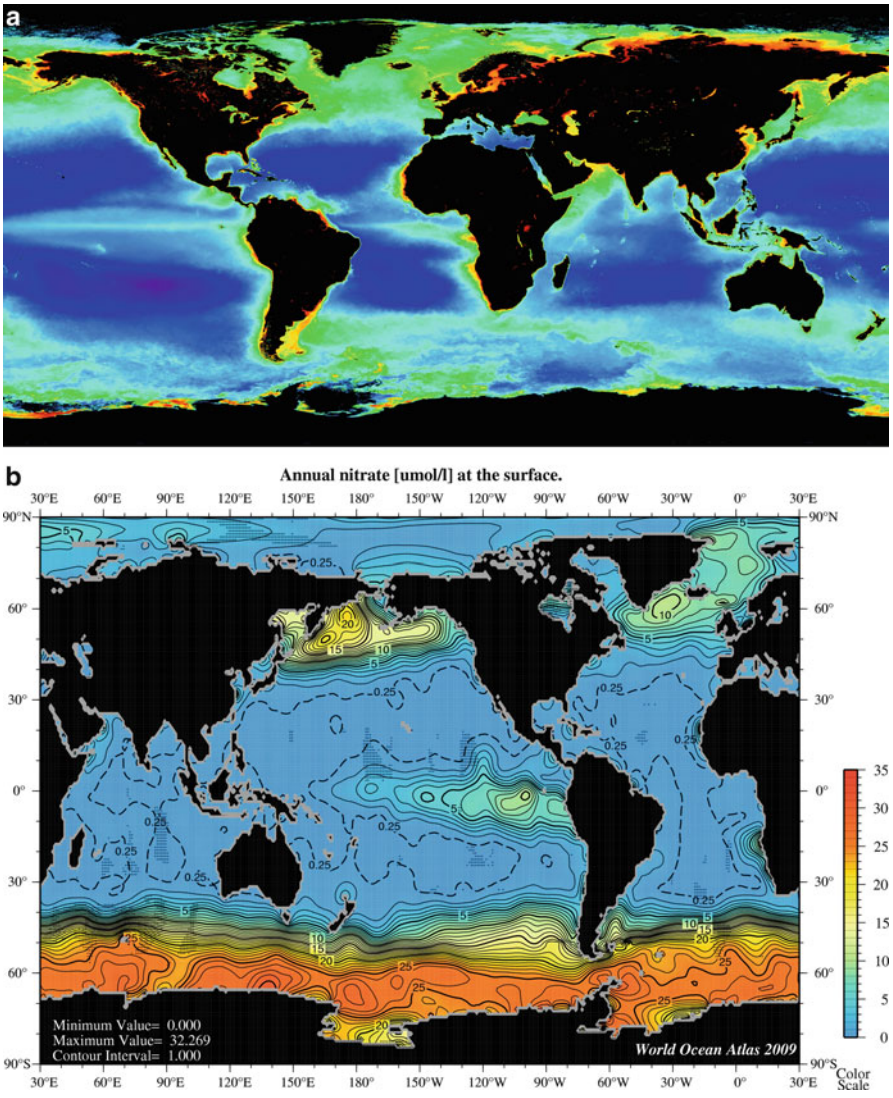

Fig. 14.5 (**a**) Satellite-derived map of average surface water chlorophyll distribution (NASA). This data visualisation comes from the MODIS instrument on NASA's AQUA spacecraft. Here we see a measure of global chlorophyll concentration derived from data collected between July 1, 2002 and December 31, 2004. This visualisation has a 4-km measure of resolution. (Credit: NASA. http://www.nasa.gov/vision/earth/lookingatearth/plankton.html). (**b**) Map of surface ocean nitrate concentrations from the Levitus atlas (NOAA) http://www.nodc.noaa.gov/OC5/WOA09F/pr_woa09f.html. All data are made available internationally without restriction consistent with the data policy of World Data System

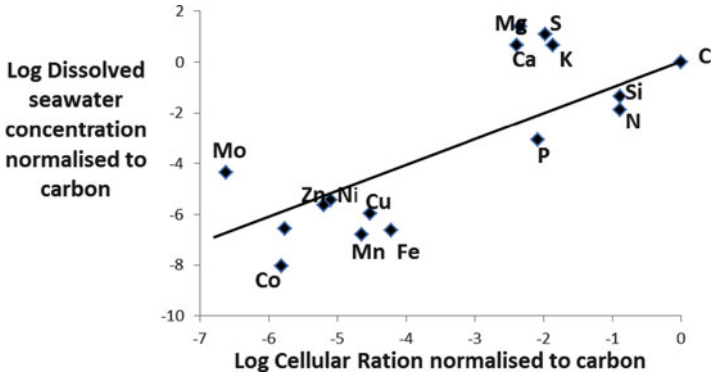

Fig. 14.6 Plot of the dissolved concentrations of selected elements against their cellular quota both normalised to carbon and plotted on a log–log basis, based on (Moore et al. 2013). Note that the requirements for some elements are variable and can be met by substitution with other metals. Elements lying above the line are at concentrations above cellular requirements while those below are deficient and hence may potentially be limiting primary production. To date there is good evidence for N, P and Fe limitation, but not for the other trace elements

(see below) but the evidence that the supply of these other trace metals plays a major role in the regulation of ocean productivity is currently limited, although it may influence species composition (Moore et al. 2013). Paytan et al. (2009) have suggested that atmospheric supply of other metals such as copper may induce toxic effects in regions of high dust deposition, although this conclusion has been questioned because they assumed a very high copper solubility (Sholkovitz et al. 2010) and also because effective organic complexation of metals such as copper in ocean waters generally acts to effectively detoxify the metal in the oceans (Chester and Jickells 2012).

The recognition of iron as a potential key limiting nutrient has prompted a great deal of research into iron cycling in the oceans over the last 20 years, summarised recently by Boyd and Ellwood (2010). The ocean biogeochemical cycle of iron is radically different from that of the macronutrients, due to the relative insolubility of inorganic Fe(III) and very low dissolved iron concentrations of the order of 1 nmol l^{-1}, about a thousand times less than N and P. The biogeochemistry of iron is complex with much of the iron organically complexed. This complexation of iron increases its solubility and residence time, but its ocean residence time is still only 100–200 years, hence much less than ocean mixing time, and so the relationship between concentrations and ocean circulation is less evident than for N and P. Relative to phytoplankton requirements, iron supply for photosynthesis from the deep ocean iron reservoir is relatively low compared to nitrate and phosphate supply and is supplemented in many areas by external inputs from shelf sediments, ice, rivers, anthropogenic emissions to the atmosphere and dust (Jickells et al. 2005). The relatively rapid removal of iron from seawater means that ocean margin inputs from sediments, rivers and ice dominate in coastal areas, where

Table 14.2 Atmospheric dust deposition to different ocean basins and total global dust emissions

Ocean basin	Dust deposition Mt (10^{12} g) year^{-1}
North Pacific	72
South Pacific	29
North Atlantic	202
South Atlantic	17
Indian Ocean	118
Global emissions	1,790

Mahowald et al. (2005b)

there is therefore generally an adequate supply of iron for phytoplankton growth. However, iron from these ocean margin sources is effectively trapped in coastal waters and does not efficiently reach open ocean waters, and hence, in open ocean regions, dust transport is therefore of particular interest as a supply of iron (Jickells et al. 2005). The absolute requirement of phytoplankton photosynthesis for iron when ocean concentrations are so low seems paradoxical, but probably reflects the evolution of photosynthesis at a time when the oceans were more reducing and iron concentrations much higher (Hunter and Boyd 2007).

Primary production is estimated to be limited by iron supply over about 30 % of the world oceans (see later), and these areas largely coincide with regions of low dust input. In many of these areas, the macronutrients such as nitrate are not efficiently removed even in summer, and these regions are often referred to as high-nitrate low-chlorophyll (HNLC) regions. In these regions, elegant oceanographic experiments have demonstrated iron limitation of photosynthesis by showing that addition of iron leads to increases in biomass on timescales of days (Boyd et al. 2007). Recent studies suggest that some additional areas of the ocean such as the high-latitude North Atlantic may become iron limited for part of the growing season after the main spring bloom has removed most of the available dissolved iron (Nielsdottir et al. 2009).

The global deposition of dust to the oceans is shown in Fig. 14.2. This emphasises the importance of desert sources, particularly the Saharan and Asian desert, and that dust deposition to the oceans of the Northern Hemisphere is much higher than to the Southern Hemisphere. Glacial deposits can also be dust sources (Schroth et al. 2011). This is further illustrated in Table 14.2 which also shows that about 24 % of all dust produced reaches the oceans. The regions of low dust deposition coincide with HNLC regions, implying a direct link between dust supply and HNLC status as discussed above.

In addition to dust deposition, iron can also be supplied to the oceans through the atmosphere, associated with anthropogenic emissions. Although these anthropogenic sources are much smaller source of total iron than desert dust, they do appear to be more soluble, and hence, this anthropogenic iron may be a quantitatively important source of iron downwind of large industrial emission regions (see Chap. 4, Sholkovitz et al. 2012) and possibly from emissions from ships (Ito 2013). Volcanic emissions of dust are generally smaller than desert dust emissions, but during eruptive episodes, these emissions can be large and can influence primary

production, as elegantly demonstrated by the impact of dust deposition from the eruption of the Kasatochi Volcano in the Aleutian arc in phytoplankton productivity in the Gulf of Alaska (Hamme et al. 2010).

Dust particles deposited to the oceans remain in the surface waters for a period of tens of days before sinking into the deep ocean usually associated with larger particles such as biological aggregates and faeces (Croot et al. 2004; Chester and Jickells 2012). These particles sink to the ocean floor on timescales of many tens of days (Chester and Jickells 2012). The residence time of dissolved iron in surface waters is a little longer (a few years) and may vary systematically and inversely with dust loading (Ussher et al. 2013). Thus, the timescales for interactions between dust and the surface water pelagic ocean biogeochemical system are of the order of 100 days to a few years, which can be compared to the timescales for soil process measured in thousands or even millions of years. Some iron will dissolve immediately from the dust (Chap. 4), although this is often only a few percent of the total, and more may dissolve during active cycling within the euphotic zone and possibly the deeper ocean biogeochemical community (e.g. Frew et al. 2006). Iron is regenerated at depth in the oceans along with N, P and Si as biological material is degraded, although the subsequent relatively rapid removal of iron from the oceans to sediments compared to N and P means that mixing of deep water into the surface will generally lead to water that is deficient in iron relative to N and P compared to phytoplankton requirements. Thus, while supply of iron from deeper waters is very important in sustaining ocean primary production, external inputs from atmospheric deposition or other sources are required to allow phytoplankton to utilise all of the available N and P. Hence, in region of low external iron inputs, primary production is iron limited and unable to utilise all of the available nitrogen and phosphorus, leading to the creation of the HNLC waters.

Iron supply to the oceans not only influences primary production; it also influences the phytoplankton ecosystem structure (Boyd and Ellwood 2010). Diatoms are an important group of phytoplankton characterised by their siliceous skeletons. Diatoms have a high iron requirement compared to other phytoplankton species, and addition of iron in HNLC waters, where N, P and Si are present at sufficient concentrations, favours their growth particularly relative to other species. This shift to larger diatoms compared to smaller phytoplankton species has implications for grazers and the higher food chain, and also for the export of carbon to deep waters, since larger diatoms may sink faster from the surface waters and hence export carbon to deep waters more efficiently (de Baar et al. 2005). This argument then suggests that increasing dust supply to the oceans increases both photosynthesis and the proportion of the fixed carbon exported to deep waters, although recent evidence suggests this conceptual model of carbon export may be too simplistic and that fluxes may depend on plankton community structure in a complex way (Buesseler and Boyd 2009). It has also been argued that the dust itself may contribute to the efficient sinking of material within the ocean by adding "ballast" to the sinking material and increasing its sinking rate. This hypothesis would therefore also imply that dust influences both the primary production and the subsequent export of the

associated organic carbon to the deep ocean, although recent studies suggest this ballast effect is of limited quantitative importance (e.g. Le Moigne et al. 2012 and references therein).

In ocean areas where nitrogen supply limits primary production, nitrogen fixation may become competitively advantageous, despite its high energy requirements (Mahaffey et al. 2005). Enzymes for nitrogen fixation have a relatively high iron content, and it is now evident that rates of nitrogen fixation in the oceans may be regulated at least in part by iron supply (Fig. 14.7) (Moore et al. 2004). Perhaps the most striking example of this is seen in data collected on north to south transects in the Atlantic Ocean passing from the high dust deposition regions in the tropical North Atlantic to the much lower dust deposition regions of the tropical South Atlantic (Fig. 14.8). Much higher dissolved iron concentrations are found in waters underlying the Saharan dust plume (Fig. 14.2), and these are associated with higher rates of nitrogen fixation. These higher rates of nitrogen fixation are also associated with exceptionally low levels of surface water phosphate, and this is believed to be due to phosphorus utilisation either by nitrogen-fixing organisms or another phytoplankton, for which nitrogen limitations are relieved by nitrogen release from nitrogen-fixing organisms (Moore et al. 2009). The waters of the eastern Mediterranean are severely phosphorus depleted, and so even under the very high dust deposition regime of this region, nitrogen fixation and primary production rates become phosphorus limited and very low (Krom et al. 2010).

Over the last 20 years, it has become clear that in addition to light and the macronutrients N, P and Si, iron also limits primary production over large areas of the oceans. Figure 14.7 shows the results from a recent modelling study calculating the limiting nutrient for ocean primary productivity in different regions of the oceans. Overall Moore and Braucher (2008) estimate that 30 % of global oceanic N fixation is limited by iron supply from dust. These model results suggest that in different areas of the oceans, either nitrogen or iron supply is generally the limiting factor for productivity (Moore et al. 2004), consistent with experimental evidence (Moore et al. 2013). There is little evidence of short-term limitation of ocean productivity by phosphorus supply, although this may be the ultimate long-term limitation on ocean productivity (Tyrrell 1999; Moore et al. 2004). Using a model it has been estimated that atmospheric dust deposition, and the associated iron supply, drives 5 % of ocean productivity and 18 % of the export of carbon to deep waters (Moore and Braucher 2008). Much of ocean productivity is driven by the internal cycling of nutrients within the euphotic zone, so the export to deep waters is of particular interest because it can potentially remove CO_2 from the atmosphere for periods of hundreds of years and hence influence climate. Export production is in this context comparable to the long-term carbon sequestration in terrestrial ecosystems. Moore and Braucher use their model to estimate that the dust supply to the oceans is responsible for the export to deep ocean waters of about 1 GtC year^{-1}. This model suggests that the dust supply is particularly important for sustaining nitrogen fixation, although the model also suggests that in terms of ocean carbon cycling, the biggest impact of dust is directly on primary production rather than via nitrogen fixation.

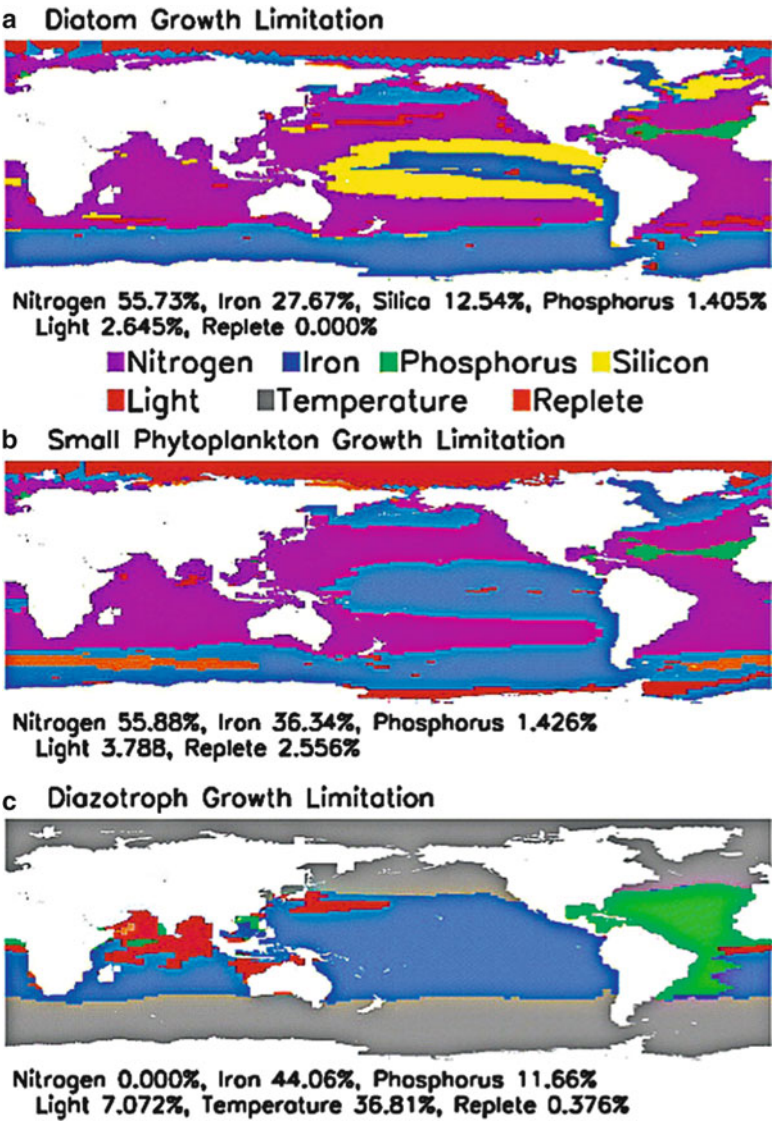

Fig. 14.7 Maps of factor most limiting phytoplankton growth rates for different phytoplankton groups during summer months in each hemisphere. Percentages refer to percent of total ocean area where limitation by each element is predicted (Moore et al. 2004)

The inputs of dust to the ocean were much higher during the last glacial maximum and the increased iron supply from that dust probably increased primary productivity and contributed to the lower CO_2 levels and associated colder climate, although it was probably not the main driver of the change in CO_2 concentrations (Jickells et al. 2005). Dust supply may change in the future due to climate change

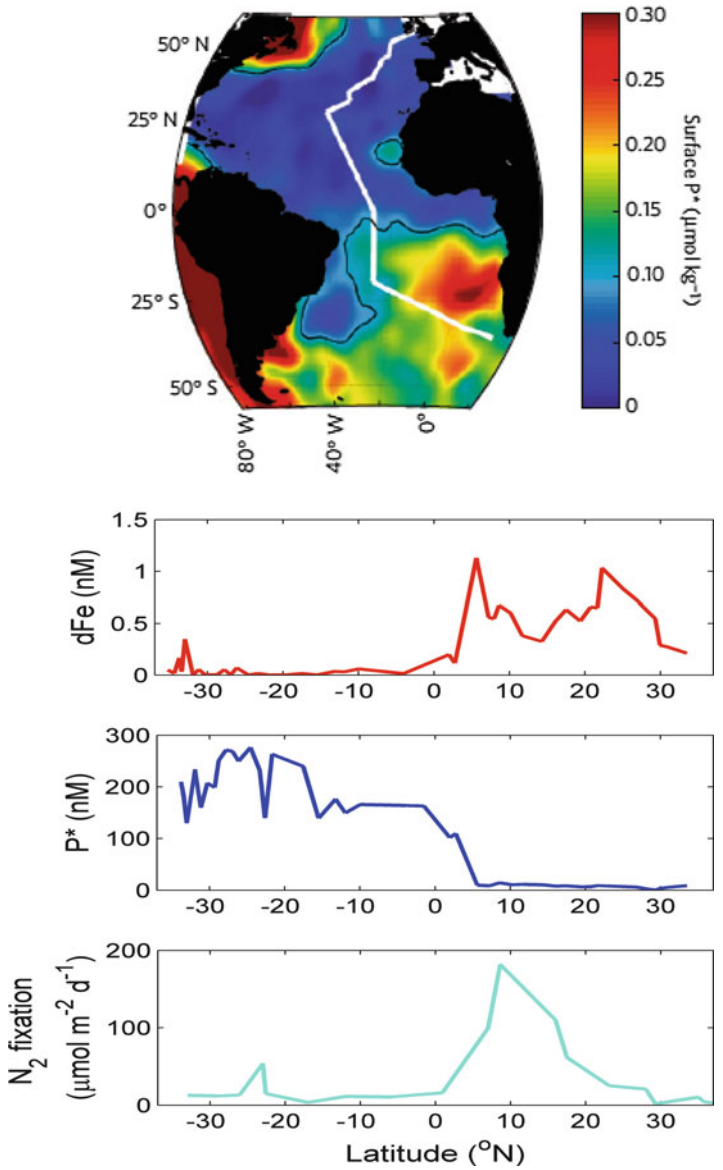

Fig. 14.8 Map indicates P* concentrations (P concentrations in excess of phytoplankton requirements) in Atlantic surface waters and the line on map indicates the sampling ship's transect. Graphs show dissolved iron and phosphate concentrations and nitrogen fixation rates in the Atlantic ocean surface waters (Moore et al. 2009); *y axis* on graphs is latitude with negative numbers being south of the equator

and other global change pressures, although the impacts of such changes on ocean productivity are very uncertain (Moore et al. 2013).

14.4 Conclusion

Atmospheric dust is transported from source regions (predominantly deserts) to terrestrial and marine ecosystems. There are strong global gradients in that deposition with highest deposition over the tropical North Atlantic and Central/South America downwind of the Sahara desert as well as over the North Indian Ocean and surrounding land area and the NW Pacific ocean and northwestern Asia. This dust can contribute to the formation of soils themselves in some regions, and more generally, this transport represents a net loss of organic carbon and nutrients from these regions and a net import to the receiving regions. The regions of soil loss are desert regions where primary production rates are low due to water limitation, so the impacts of the soil and nutrient loss from these regions on the global carbon cycle are small, although the impacts are locally important in the dust source regions. The deposition of these nutrients has been demonstrated to have biogeochemical impacts on receiving terrestrial and marine ecosystems, but the scale and the nature of these impacts vary geographically. This geographical pattern of impacts inevitably reflects, in part, the deposition pattern of dust and also the characteristics of the receiving ecosystems.

In the case of terrestrial ecosystems, the main impact appears to arise from inputs of phosphorus associated with dust, which can impact primary production both directly and also via encouragement of nitrogen fixation. Overall about 20 % of terrestrial ecosystems are P limited. This impact is greatest in tropical ecosystems developed on highly weathered soils and/or on nutrient-poor underlying rock and develops over timescales of thousands to millions of years as the soils evolve and ultimately lose nutrients derived from weathering of the underlying rock.

In the case of marine ecosystems, the main impact arises from the iron associated with dust. This iron input influences two important but distinctly different ocean biogeochemical processes.

The first biogeochemical process arises in situations where the iron is used to support photosynthesis. The supply of iron from dust and other ocean margin sources is sufficient to meet phytoplankton photosynthetic needs over about 70 % of the oceans. In the remaining regions of the oceans, HNLC systems develop where iron supply limits primary production either on its own or as a co-limiting factor. These essentially permanently iron-limited ocean regions are all regions remote from dust sources including areas of the Southern Ocean, the North Pacific and the tropical South East Pacific. Some other regions may become seasonally iron limited. The iron limitation of the Southern Ocean may be particularly important because of its size and because it is a region in which deep ocean waters form due to cooling, allowing the unutilised nutrients to be transported deep into the oceans and hence reducing overall ocean CO_2 uptake. Changes in productivity in this region,

such as those that may have occurred under higher dust fluxes during the last glacial period, have the potential to change ocean CO_2 uptake at a scale that may affect atmospheric CO_2 and climate.

The second biogeochemical impact of dust arises in ocean regions where the iron supply from the dust stimulates microbial nitrogen fixation. This process occurs predominantly in warm tropical nutrient-poor waters and appears to be limited by iron supply over most of the tropical Pacific, South Atlantic and Indian Ocean. Only in the tropical North Atlantic does it seem that the iron supply is sufficient to remove this limitation and induce phosphorus limitation of nitrogen fixation.

Thus, dust has a substantial biogeochemical impact on both terrestrial and marine ecosystems, but the mechanisms are different, as are the locations of impact. These can simplified and summarised as follows:

- Low-latitude tropical forests respond to phosphorus inputs from dust with increased rates of nitrogen fixation and primary production.
- Ocean gyre plankton communities respond to iron supply from dust with increasing rates of nitrogen fixation leading to increased primary production.
- HNLC ocean regions (predominantly at high latitudes) respond directly to iron inputs from dust via stimulation of primary productivity.

In the discussion above, we suggest the effects of dust on terrestrial productivity are of the order of 0.06 GTC year^{-1} net atmospheric CO_2 uptake and the impact on the oceans equivalent to 1 GTC year^{-1}. In terms of the global carbon cycle, therefore, the impact on primary productivity in HNLC waters appears to dominate. However, the ocean iron uptake represents a flux to the deep ocean where the carbon will be trapped for hundreds or a few thousand years, before returning to the atmosphere. Only a fraction of this carbon will be buried in ocean sediments and stored for even loner timescales. The soil uptake is over long timescales of thousands or even millions of years. Global and regional dust transport has changed considerably over glacial, interglacial and shorter timescales and is likely to change in the future. The timescales over which the terrestrial and marine systems respond to changes in dust inputs are very different reflecting the very different biogeochemical environments of soils and the oceans. We need to understand the nature and scale of ecosystem responses to changes and how these will feed back on global change pressures and processes, recognising that such changes will not occur in isolation, but will be coupled to changes in global and regional temperature, hydrology, CO_2 and nitrogen flows.

References

Aerts R, Chapin FS (2000) The mineral nutrition of wild plants revisited: a re-evaluation of processes and patterns. Adv Ecol Res 30:1–67

Ashman MR, Puri G (2002) Essential soil science: a clear and concise introduction to soil science. Blackwell, Oxford, 208pp

Augusto L, Delerue F, Gallet-Budynek A, Achat DL (2013) Global assessment of limitation to symbiotic nitrogen fixation by phosphorus availability in terrestrial ecosystems using a meta-analysis approach. Global Biogeochem Cycles 27:804–815

Baker AR, Kelly SD, Biswas KF, Witt M, Jickells TD (2003) Atmospheric deposition of nutrients to the Atlantic Ocean. Geophys Res Lett 30. doi:10.1029/2003GL018518

Baker AR, Weston K, Kelly SD, Voss M, Streu P, Cape JN (2007) Dry and wet deposition of nutrients from the tropical Atlantic atmosphere: links to primary productivity and nitrogen fixation. Deep-Sea Res Pt I-Oceanogr Res Pap 54:1704–1720

Belanger N, Holmden C (2010) Influence of landscape on the apportionment of Ca nutrition in a Boreal Shield forest of Saskatchewan (Canada) using Sr-87/Sr-86 as a tracer. Can J Soil Sci 90:267–288

Boyd PW, Ellwood MJ (2010) The biogeochemical cycle of iron in the ocean. Nat Geosci 3:675–682

Boyd PW, Jickells T, Law CS, Blain S, Boyle EA, Buesseler KO et al (2007) Mesoscale iron enrichment experiments 1993–2005: synthesis and future directions. Science 315:612–617

Bristow CS, Hudson-Edwards KA, Chappell A (2010) Fertilizing the Amazon and equatorial Atlantic with West African dust. Geophys Res Lett 37. doi:10.1029/210GL043486

Bruijnzeel LA (1991) Nutrient input output budgets of tropical forest ecosystems – a review. J Trop Ecol 7:1–24

Buesseler KO, Boyd PW (2009) Shedding light on processes that control particle export and flux attenuation in the twilight zone of the open ocean. Limnol Oceanogr 54:1210–1232

Chadwick OA, Derry LA, Vitousek PM, Huebert BJ, Hedin LO (1999) Changing sources of nutrients during four million years of ecosystem development. Nature 397:491–497

Chapin F III, Eviner V (2003) Biogeochemistry of terrestrial net primary production. Treatise Geochem 8:215–247

Chester R, Jickells TD (2012) Marine geochemistry, 3rd edn. Wiley-Blackwell, Chichester, 240pp

Cox PM, Pearson D, Booth BB, Friedlingstein P, Huntingford C, Jones CD et al (2013) Sensitivity of tropical carbon to climate change constrained by carbon dioxide variability. Nature 494:341–344

Croot PL, Streu P, Baker AR (2004) Short residence time for iron in surface seawater impacted by atmospheric dry deposition from Saharan dust events. Geophys Res Lett 31, L23S08. doi:10.1029/2004GL020153

de Baar HJW, Boyd PW, Coale KH, Landry MR, Tsuda A, Assmy P et al (2005) Synthesis of iron fertilization experiments: from the iron age in the age of enlightenment. J Geophys Res Oceans 110

Denman K, Brasseur G, Chidthaisong A, Ciais P, Cox PM, Dickinson RE et al (2007) Couplings between changes in the climate system and biogeochemistry. In: Solomon S, Qin D, Manning M, Chen Z, Marquis M, Averyt KB, Tignor M, Miller HL (eds) Climate change 2007: the physical science basis. Cambridge University Press, Cambridge, pp 544–547

Dezi S, Medlyn BE, Tonon G, Magnani F (2010) The effect of nitrogen deposition on forest carbon sequestration: a model-based analysis. Glob Chang Biol 16:1470–1486

Duce RA, LaRoche J, Altieri K, Arrigo KR, Baker AR, Capone DG et al (2008) Impacts of atmospheric anthropogenic nitrogen on the open ocean. Science 320:893–897

Epstein E (1972) Mineral nutrition of plants: principles and perspectives. Wiley, New York/ Chichester, 412pp

Fraústo da Silva JJR, Williams RJP (2001) The biological chemistry of the elements: the inorganic chemistry of life, 2nd edn. Oxford University Press, Oxford, 600pp

Frew RD, Hutchins DA, Nodder S, Sanudo-Wilhelmy S, Tovar-Sanchez A, Leblanc K et al (2006) Particulate iron dynamics during FeCycle in subantarctic waters southeast of New Zealand. Global Biogeochem Cycles 20. doi:10.1029/2005GB002558

Goll DS, Brovkin V, Parida BR, Reick CH, Kattge J, Reich PB et al (2012) Nutrient limitation reduces land carbon uptake in simulations with a model of combined carbon, nitrogen and phosphorus cycling. Biogeosciences 9:3547–3569

Griffin DW, Kellogg CA, Garrison VH, Lisle JT, Borden TC, Shinn EA (2003) Atmospheric microbiology in the northern Caribbean during African dust events. Aerobiologia 19:143–157
Griffin DW, Kubilay N, Kocak M, Gray MA, Borden TC, Shinn EA (2007) Airborne desert dust and aeromicrobiology over the Turkish Mediterranean coastline. Atmos Environ 41:4050–4062
Hamme RC, Webley PW, Crawford WR, Whitney FA, DeGrandpre MD, Emerson SR et al (2010) Volcanic ash fuels anomalous plankton bloom in subarctic northeast Pacific. Geophys Res Lett 37. doi:10.1029/2010GL044629
Hedin LO (2004) Global organization of terrestrial plant-nutrient interactions. Proc Natl Acad Sci U S A 101:10849–10850
Hedin LO, Granat L, Likens GE, Buishand TA, Galloway JN, Butler TJ et al (1994) Steep declines in atmospheric base cations in regions of Europe and North-America. Nature 367:351–354
Houlton BZ, Wang YP, Vitousek PM, Field CB (2008) A unifying framework for dinitrogen fixation in the terrestrial biosphere. Nature 454:327–330
Hunter KA, Boyd PW (2007) Iron-binding ligands and their role in the ocean biogeochemistry of iron. Environ Chem 4:221–232
Ito A (2013) Global modeling study of potentially bioavailable iron input from shipboard aerosol sources to the ocean. Global Biogeochem Cycles 27:1–10. doi:10.1029/2012GB004378
Jickells TD, An ZS, Andersen KK, Baker AR, Bergametti G, Brooks N et al (2005) Global iron connections between desert dust, ocean biogeochemistry, and climate. Science 308:67–71
Kaspari M, Garcia MN, Harms KE, Santana M, Wright SJ, Yavitt JB (2008) Multiple nutrients limit litterfall and decomposition in a tropical forest. Ecol Lett 11:35–43
Krom MD, Emeis KC, Van Cappellen P (2010) Why is the Eastern Mediterranean phosphorus limited? Prog Oceanogr 85:236–244
Le Moigne FAC, Sanders RJ, Villa-Alfageme M, Martin AP, Pabortsava K, Planquette H et al (2012) On the proportion of ballast versus non-ballast associated carbon export in the surface ocean. Geophys Res Lett 39. doi:10.1029/2012GL052980
Longhurst AR (2007) Ecological geography of the sea, 2nd edn. Academic Press, Burlington, 560pp
Mahaffey C, Michaels AF, Capone DG (2005) The conundrum of marine N-2 fixation. Am J Sci 305:546–595
Mahowald N (2011) Aerosol indirect effect on biogeochemical cycles and climate. Science 334:794–796
Mahowald NM, Artaxo P, Baker AR, Jickells TD, Okin GS, Randerson JT et al (2005a) Impacts of biomass burning emissions and land use change on Amazonian atmospheric phosphorus cycling and deposition. Global Biogeochem Cycles 19. doi:10.1029/2005GB002541
Mahowald NM, Baker AR, Bergametti G, Brooks N, Duce RA, Jickells TD et al (2005b) Atmospheric global dust cycle and iron inputs to the ocean. Global Biogeochem Cycles 19. doi:10.1029/2004GB002402
Mahowald N, Jickells TD, Baker AR, Artaxo P, Benitez-Nelson CR, Bergametti G et al (2008) Global distribution of atmospheric phosphorus sources, concentrations and deposition rates, and anthropogenic impacts. Global Biogeochem Cycles 22. doi:10.1029/2008GB003240
Mahowald NM, Kloster S, Engelstaedter S, Moore JK, Mukhopadhyay S, McConnell JR et al (2010) Observed 20th century desert dust variability: impact on climate and biogeochemistry. Atmos Chem Phys 10:10875–10893
Mahowald N, Lindsay K, Rothenberg D, Doney SC, Moore JK, Thornton P et al (2011) Desert dust and anthropogenic aerosol interactions in the community climate system model coupled-carbon-climate model. Biogeosciences 8:387–414
Malhi Y, Baldocchi DD, Jarvis PG (1999) The carbon balance of tropical, temperate and boreal forests. Plant Cell Environ 22:715–740
Martiny AC, Pham CT, Primeau FW, Vrugt JA, Moore JK, Levin SA et al (2013) Strong latitudinal patterns in the elemental ratios of marine plankton and organic matter. Nat Geosci 6:279–283
Menge DNL, Hedin LO, Pacala SW (2012) Nitrogen and phosphorus limitation over long-term ecosystem development in terrestrial ecosystems. Plos One 7:e42045

Mengel K, Kirkby EA (1978) Principles of plant nutrition, 2nd edn. International Potash Institute, Bern, 849pp
Moore JK, Braucher O (2008) Sedimentary and mineral dust sources of dissolved iron to the world ocean. Biogeosciences 5:631–656
Moore JK, Doney SC, Lindsay K (2004) Upper ocean ecosystem dynamics and iron cycling in a global three-dimensional model. Global Biogeochem Cycles 18. doi:10.1029/2004GB002220
Moore CM, Mills MM, Achterberg EP, Geider RJ, LaRoche J, Lucas MI et al (2009) Large-scale distribution of Atlantic nitrogen fixation controlled by iron availability. Nat Geosci 2:867–871
Moore CM, Mills MM, Arrigo KR, Berman-Frank I, Bopp L, Boyd PW et al (2013) Processes and patterns of oceanic nutrient limitation. Nat Geosci 6:701–710
Muhs DR (2012) The geological records of dust in the Quaternary. Aeolian Res 9:3–48
Muhs DR, Budahn JR, Prospero JM, Skipp G, Herwitz SR (2012) Soil genesis on the island of Bermuda in the Quaternary: the importance of African dust transport and deposition. J Geophys Res Earth Surf 117
Nielsdottir MC, Moore CM, Sanders R, Hinz DJ, Achterberg EP (2009) Iron limitation of the postbloom phytoplankton communities in the Iceland Basin. Global Biogeochem Cycles 23. doi:10.1029/2008GB003410
Okin GS, Mahowald N, Chadwick OA, Artaxo P (2004) Impact of desert dust on the biogeochemistry of phosphorus in terrestrial ecosystems. Global Biogeochem Cycles 18. doi:10.1029/2003GB002145
Okin GS, Baker AR, Tegen I, Mahowald NM, Dentener FJ, Duce RA et al (2011) Impacts of atmospheric nutrient deposition on marine productivity: roles of nitrogen, phosphorus, and iron. Global Biogeochem Cycles 25. doi:10.1029/2010GB003858048376
Paytan A, Mackey KRM, Chen Y, Lima ID, Doney SC, Mahowald N et al (2009) Toxicity of atmospheric aerosols on marine phytoplankton. Proc Natl Acad Sci U S A 106:4601–4605
Pett-Ridge JC (2009) Contributions of dust to phosphorus cycling in tropical forests of the Luquillo mountains, Puerto Rico. Biogeochemistry 94:63–80
Rudnick R, Gao S (2003) Composition of the continental crust. Treatise Geochem 3:1–64
Sayer EJ, Wright SJ, Tanner EVJ, Yavitt JB, Harms KE, Powers JS et al (2012) Variable responses of lowland tropical forest nutrient status to fertilization and litter manipulation. Ecosystems 15:387–400
Schroth AW, Crusius J, Chever F, Bostick BC, Rouxel OJ (2011) Glacial influence on the geochemistry of riverine iron fluxes to the Gulf of Alaska and effects of deglaciation. Geophys Res Lett 38. doi:10.1029/2011GL
Sholkovitz ER, Sedwick PN, Church TM (2010) On the fractional solubility of copper in marine aerosols: toxicity of aeolian copper revisited. Geophys Res Lett 37, L20601. doi:10.1029/2010GL044817
Sholkovitz ER, Sedwick PN, Church TM, Baker AR, Powell CF (2012) Fractional solubility of aerosol iron: synthesis of a global-scale data set. Geochim Cosmochim Acta 89:173–189
Soderberg K, Compton JS (2007) Dust as a nutrient source for fynbos ecosystems, South Africa. Ecosystems 10:550–561
Sterner RW, Elser JJ (2002) Ecological stoichiometry: the biology of elements from molecules to the biosphere. Princeton University Press, Princeton/Oxford, 584pp
Stevenson FJ, Cole MA (1999) Cycles of soil: carbon, nitrogen, phosphorus, sulfur, micronutrients, 2nd edn. Wiley, New York/Chichester, 448pp
Swap R, Garstang M, Greco S, Talbot R, Kallberg P (1992) Saharan dust in the Amazon Basin. Tellus Ser B Chem Phys Meteorol 44:133–149
Tyrrell T (1999) The relative influences of nitrogen and phosphorus on oceanic primary production. Nature 400:525–531
Usher CR, Michel AE, Grassian VH (2003) Reactions on mineral dust. Chem Rev 103:4883–4939
Ussher SJ, Achterberg EP, Powell C, Baker AR, Jickells TD, Torres R et al (2013) Impact of atmospheric deposition on the contrasting iron biogeochemistry of the North and South Atlantic Ocean. Global Biogeochem Cycles 27:1096–1107

Vitousek PM, Sanford RL (1986) Nutrient cycling in moist tropical forest. Ann Rev Ecol Syst 17:137–167

Vitousek PM, Porder S, Houlton BZ, Chadwick OA (2010) Terrestrial phosphorus limitation: mechanisms, implications, and nitrogen-phosphorus interactions. Ecol Appl 20:5–15

Wang YP, Law RM, Pak B (2010) A global model of carbon, nitrogen and phosphorus cycles for the terrestrial biosphere. Biogeosciences 7:2261–2282

Watmough SA, Aherne J, Alewell C, Arp P, Bailey S, Clair T et al (2005) Sulphate, nitrogen and base cation budgets at 21 forested catchments in Canada, the United States and Europe. Environ Monit Assess 109:1–36

Webb NP, Chappell A, Strong CL, Marx SK, McTainsh GH (2012) The significance of carbon-enriched dust for global carbon accounting. Glob Chang Biol 18:3275–3278

Chapter 15
Dust and Human Health

Suzette A. Morman and Geoffrey S. Plumlee

Abstract It is generally accepted that exposure to fine particulate matter may increase risk for human morbidity and mortality. Until recently, population health related studies examining the effects of particulate matter on human health generally examined anthropogenic (industry and combustion by-products) sources with few studies considering contributions from natural sources. This chapter provides an overview of naturally occurring inorganic mineral dust research and associated human health ailments and some of the challenges in elucidating the etiological mechanisms responsible.

Keywords Pollution • Exposure • Particle size • Composition • Microorganisms • Microbiology • Susceptibility • Respiratory system • Asthma • Ailments • Meningitis • Hospitalization • Mortality • Agricultural dust

15.1 Introduction

Potential increases in aerosols and emitted dust resulting from climate related changes such as drought and desertification have generated concern and interest in potential local and long-distance public health effects. Dust emissions can change greatly over time due to changes in climate and land use. In particular, studies are focusing on mineral dust which may be present at high concentrations over vast regions of the Earth and may be carried great distances by winds. Epidemiological studies have recently identified associations between far-traveled dusts and increased morbidity and mortality in Europe and Asia. Prior epidemiological studies

S.A. Morman (✉) • G.S. Plumlee
United States Geological Survey, Denver, CO 80225, USA
e-mail: SMorman@usgs.gov; GPlumlee@usgs.gov

P. Knippertz and J.-B.W. Stuut (eds.), *Mineral Dust: A Key Player in the Earth System*, DOI 10.1007/978-94-017-8978-3_15,

have demonstrated an association between fine particulate matter (PM) exposure and the exacerbation of cardiovascular disease (myocardial infarction and stroke), respiratory disease (asthma, bronchitis, chronic obstructive pulmonary disease), and resulting mortality in large urban areas (Dockery et al. 1993; Pope et al. 1995 and others); however, the etiological or causal factors are not well understood.

Over the years, most studies of PM health effects have focused on urban settings and anthropogenic (industry and combustion by-products) PM sources, but there are few studies of contributions from natural geological sources. Geogenic PM is produced from the Earth by natural processes (e.g., volcanic ash, windborne ash from wildfires, and mineral dusts). Geoanthropogenic PM is produced from natural sources by processes that are modified or enhanced by human activities (e.g., dusts from lakebeds dried by human removal of water, dusts produced from areas that have undergone desertification as a result of human practices, and dusts from agricultural fields). About 2,000 Mt of dust is emitted into the atmosphere every year (Chap. 5, Shao et al. 2011) from geogenic and geoanthropogenic sources such as the Sahara and Sahel in Africa.

Only recently have public health studies sought to elucidate links between the environmental exposure to airborne mineral dusts (MD) and population health. The prior lack of these studies may be related to the focus of early air pollution regulations that were aimed at limiting mobile and industrial sourced pollutants. Additionally, epidemiological study design requires amongst other criteria a large population sample size (such as those found in urban areas) to demonstrate association with health-related effects. Other factors that have hindered research on MD include the following: long-established emphasis on occupational health exposures, difficulty identifying etiological mechanisms responsible for disease secondary to a complex matrix (i.e., dust may contain multiple components), lack of sample and source characterization, and quantifying human exposures (Baxter et al. 2013).

This chapter provides an overview of the primary known or suspected adverse health effects of, and related research on, mineral dusts. Research related to anthropogenic and occupational exposures will also be discussed to provide perspective.

15.2 Review of Air Pollution Basics

Although interest and speculation regarding the potential health effects of exposure to airborne "pollution" dates back to the fifteenth century (Gallo 2008), the exposures examined were work related. Interest in community or population exposures to air pollution is a somewhat recent development and few studies occurred prior to the 1950s. Deterioration of air quality from centuries of industrial and urban development prompted researchers to begin developing methods to study the health effects of air pollution on communities. For example, to elucidate the scope and burden of air pollution in the United States, several regulations were enacted,

including the Air Pollution Control Act (1955) that provided funds for air pollution research and the Clean Air Act of 1963 that focused on air pollution control.

The term particulate matter (PM) is widely used and in the United States, for example, such usage was the result of the legislated requirements under the Clean Air Act (McClellan 2000). Regulations to limit emissions from mobile and stationary (industrial) sources were established with the Clean Air Act of 1970 through several programs such as the National Air Quality Standards (NAAQS) program. Standards for six principal pollutants (carbon monoxide, lead, nitrogen dioxide, ozone, particle pollution, and sulfur dioxide) were established, thus providing enforceable criteria for the protection of sensitive populations, decreased visibility, and damage to animals and crops. Many other nations have also established regulatory criteria for PM and other pollutants.

According to the World Health Organization (WHO), particulate matter affects more people than any other pollutant and is primarily composed of sulfates, nitrates, ammonia, sodium chloride, carbon, mineral dust, and water (WHO 2012a). Particulate matter sources may be natural (e.g., volcanic ash, forest fires, and dusts) or anthropogenic (e.g., fossil fuel combustion).

The classification used by WHO and the US EPA defines coarse particles as those less than or equal to 10 but greater than 2.5 micrometers (μm) in diameter (PM10); and fine particles are those less than 2.5 μm (PM2.5) (WHO 2011; USEPA 2012a). The definition of fine particles, in some schemes, is less than 2.5–0.1 μm and a category is added for ultrafine particles (those less than 0.1 μm). Coarse (PM10) particles may also be described as inhalable particles, or the fraction that enters the body but is generally trapped within the nose, mouth, and upper respiratory tract, whereas fine (PM2.5) particles may penetrate into the lower respiratory tract. It should be noted that particles contained in aerosols, sometimes also referred to as far-traveled dusts, fall within these guidelines in terms of size distribution (see Scheuvens and Kandler, Chap. 1—this volume). In the United States, PM monitoring is only required in areas with populations of 100,000 or more (USEPA 2012b). Thus, in areas where regional inorganic minerals dusts may provide greater exposures, such as close to rural dryland dust sources, PM concentrations are largely unavailable. Hence, large urban areas capable of providing sufficient hospitalization and PM data necessary for statistical analysis have long been the focus for epidemiological studies and data collection.

15.3 Human Exposure Pathways

A toxicant may enter the body by one of several exposure pathways: inhalation, passive ingestion (larger particles are swallowed), ingestion, and dermal or skin contact. Inhalation and ingestion are the primary routes of exposure for particulate matter. Particles are transported with inhaled air through the nose, or in some cases such as during exercise, the mouth.

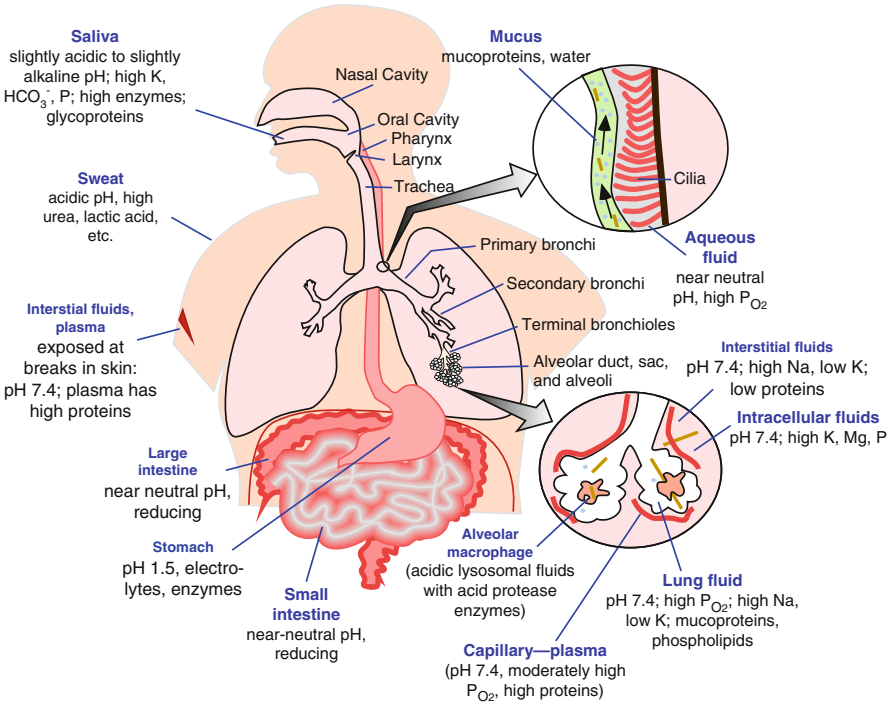

Fig. 15.1 A schematic diagram illustrating exposure pathways and the variability in the composition and pH of the body fluids encountered during exposure (After Plumlee et al. 2006)

The respiratory tract (Fig. 15.1) serves as a portal of entry, a deposition site, and target organ (McClellan 2000). The structure of the respiratory tract provides the first line of defense against the deposition of inhaled particles (Lehnert 1993). This is accomplished by its structural design creating a filtration system that supports deposition in the nasopharyngeal region (nose, mouth, and larynx) and consequently limits deposition in the lower pulmonary region. The efficiency of this system is dependent on many factors, including individuals' breathing patterns, the geometric structural configuration of the airways (airway diameter, branching, and bifurcation angles), and the physiochemical characteristics of the inhaled particle (Lehnert 1993). During exercise, heavy labor, or very dusty conditions, mouth breathing may occur that allows larger particles to enter the respiratory system. There is evidence that increases in the ventilation rate during exercise or exertion may increase the total deposition for all respirable particles (Schultz et al. 2000). Inhaled particles may then be exhaled or deposited by coming in contact with wet airspace surfaces.

The respiratory system may be divided into three components or regions and particle size deposition roughly correlates with these regions (Fig. 15.1). The nasopharyngeal region operates as an initial barrier to larger particles, generally PM10 or greater. The tracheobronchial compartment consists of conducting airways

that are lined with mucus-covered ciliated cells that provide two major clearance mechanisms for particles: absorption of dissolved material and particle transport to the larynx where they are swallowed or to the lymphatic system where they are disposed of (Kreyling and Scheuch 2000). Finally, the bronchioles, alveolar ducts, alveolar sacs, and alveoli make up the pulmonary region whose primary purpose is gas exchange. Particles may be deposited there by impaction, sedimentation, and Brownian diffusion. As airflow velocities are greater in the nasopharyngeal and upper portion of the tracheobronchial tree, impaction plays a greater role in these regions. In the midsize and smaller bronchioles and the alveolar region, gravitational settling prevails. Diffusional transport is important for particles less than 0.5 μm, as their likelihood of contacting the airway walls is governed by where collisions between gas molecules and particles cause small displacements of the particle (Schultz et al. 2000).

Inhaled particles that are deposited in the different parts of the respiratory tract can react chemically with the fluids and tissues (Plumlee and Ziegler 2007). Deposited particles that are soluble in the respiratory tract fluids or that contain loosely surface-bound material may dissociate or undergo dissolution upon deposition, and surface-bound components may react or interact with airway fluids or cells. Some constituents released from soluble particles may combine with fluid components to reprecipitate as other insoluble phases; an example is calcium released from dissolution of inhaled particles of calcium sulfate, which can reprecipitate as calcium phosphate phases (Plumlee et al. 2013a). Insoluble deposited particles are cleared by coughing, phagocytosis by alveolar macrophages, transport along the mucociliary escalator, or retention in the tissues with sequestration by collagen (Kreyling et al. 2007). Because they contain chemically aggressive, acidic lysosomal fluids, alveolar macrophages can digest some types of particles that escape dissolution in the lung fluids (Plumlee and Ziegler 2007). They then transport particles that they cannot digest to the lymph system.

15.4 Characteristics That Contribute to Observed Health Effects

Studies of occupational exposures throughout history have contributed significantly to our understanding of respiratory exposure and pulmonary toxicology. Agricola and Paracelsus, for example, documented the etiology and treatment of miner's disease in the fifteenth century (Gallo 2008). Epidemiological studies examining community risk have generally focused on anthropogenic sources of pollution and related events such as the 1948 Donora, Pennsylvania incident or the great smog of 1952 in London.

A number of factors have been identified as contributing to the adverse health effects of airborne dusts, other airborne Earth materials, and particulate matter including the following: intensity and duration of the exposure; physical and chemical characteristics of the material; microbial or other pathogens present in

the material; the bioaccessibility, biodurability, and bioreactivity of the material in the body fluids; the body's physiological processes; and individual factors such as genetics, personal habits (e.g., smoking), and nutritional status (Plumlee et al. 2006). Although numerous PM studies have been conducted in an effort to identify which components are responsible for the observed health effects (e.g., cardiovascular or respiratory), there is little agreement among studies. Study inconsistencies may be related to a number of factors including the following: PM sample and source characterization, model design and parameters, and individual susceptibility. Additionally, variation in the number of components to which people are exposed, their concentrations in and on the surface of particles, and the complexity of surface chemistry on small volume-to- high surface area particles magnifies the difficulty of identifying specific etiological mechanisms responsible for observed adverse effects. As the amount of literature on PM effects and toxicity is quite large and not specific to MD, we provide here an overview of select factors and related research likely to be associated with MD.

15.4.1 Particle Size and Composition

Early studies of "air pollution" often focused on particle size alone and ignored composition. Studies that focus on size-dependent effects and ignore chemistry address the concept of a "nonspecific" effect, meaning the effect is due only to the particle's presence (Schlesinger et al. 2006). Crustally derived materials such as MD are not often identified as components in many PM studies, though some studies have used surrogates such as Al or Si to represent all crustal materials that may be present in the sample (Schlesinger 2007). Results of studies designed to measure the influence of particle size on adverse health effects have been inconsistent. Some studies found no increase in health risk related to coarse PM exposure (Puett et al. 2009), while other studies have demonstrated an association (Brunekreef and Forsberg 2005; Malig and Ostro 2009). Also, as measures of PM concentration and size are obtained from established monitoring sites, not necessarily where people live or work, they may not provide representative exposures (Baxter et al. 2013).

Complicating the task of identifying the component or mechanism of action responsible for illness or death is the variation in the numbers of components that make up PM, their concentrations, and their chemical behaviors in the body. In occupational settings, some trace metals have been recognized as inhalation toxicants, such as iron, nickel, and hexavalent chromium. Studies indicate a variety of metals likely contribute to air pollution toxicity, although no single physiochemical property has emerged as a common etiological factor (Samet and Ghio 2007). Several studies have associated metals with a variety of toxicity effects, such as reactive oxygen species generation and oxidative stress (e.g., iron), production of inflammatory or fibrotic responses (e.g., zinc), and cancer (e.g., hexavalent chromium or nickel) (Adamson et al. 2000; Knaapen et al. 2002; Samet and Ghio 2007; Schaumann et al. 2004). Unfortunately, some studies assume that the metals

present in PM are all of anthropogenic origin (Schlesinger 2007), neglecting to note the observed natural variation of metals with known toxicities and different states of solubility present in soils and dusts. Examples of geogenic or geoanthropogenic dusts containing high levels of metal (loid) toxicants include hexavalent chromium-rich dusts derived from ultramafic rocks in Oman that are deposited to the east in the United Arab Emirates (Wood et al. 2010) and dusts from Owens dry lakebed in California, USA, that are enriched in arsenic, barium, antimony, lithium, and tungsten (Reheis et al. 2009).

Garrison et al. (2006) found that dusts from Mali, Africa, and downwind sites in the Caribbean contained metals, pesticides, polycyclic aromatic hydrocarbons, and polychlorinated biphenyls from various anthropogenic or geoanthropogenic sources and over 300 taxa of microorganisms. Additional studies of the collected dusts demonstrated that while total ppm concentrations for several metals (As, Cr, Cu, Fe, Mn, and V) decreased slightly at downwind sites, lung fluid bioaccessibility (solubility in a physiologically based simulated lung fluid) tended to increase (Morman et al. 2009; Garrison et al. 2010; Morman et al. 2014). As ferrous iron release from respirable PM (e.g., asbestos, coal fly ash, iron sulfides, iron-rich volcanic ash) has been implicated as a contributor to oxidative stress and toxicity in the lungs (e.g., Aust et al. 2011; Horwell et al. 2007), these results raise the possibility that intercontinental dusts may pose risks for chronic, low-level oxidative stress related to bioaccessible iron (see also Chap. 4). Gyan et al. (2005) speculated that the increased rates of asthma exacerbation they observed were caused by potential allergens and irritants in Saharan dust including plant-derived constituents such as pollens and the high iron content in the form of surface-complexed iron. More research is needed to elucidate how particle surface chemistry, occurring during atmospheric transport in chemically and physically extreme conditions (e.g., exposed to high levels of solar radiation, multiple freeze-thaw cycles, and relatively acidic conditions), alters the bioaccessibility of metals transported with dusts (see also Chap. 4).

15.4.2 Microorganisms in Dust

Dusts also serve as a vehicle to carry biological components such as bacteria, endotoxins, and fungi via atmospheric pathways (Griffin 2007; Kellogg and Griffin 2006; Prospero et al. 2005). Some microorganisms (pathogens) are acknowledged as precursors of disease (e.g., meningitis) and their ability to be transported by dust, wind, or vector has been established. Others, such as endotoxins, may contribute to asthma-related symptoms and inflammation (Kirkhorn and Garry 2000). Although dust events have occurred for millennia, there is concern that desertification and the frequency and volume of dusts produced will increase with climate change (Kuehn 2006). Evidence exists that the quantity (Mahowald et al. 2010; Prospero and Lamb 2003; Prospero and Nees 1986) and composition (Garrison et al. 2003) of dust emissions from some primary sources have changed. The implications for

public health in response to these changes are unclear, but rates of asthma especially in children are increasing (Braman 2006).

Although the production and transportation of dusts is covered elsewhere (see Chaps. 2, 3, 4, 5, 6 and 7), it is interesting to note that speculation about far-traveled dusts from primary sources, such as the Sahel, is not new. In the early 1800s, aeolian dusts were collected over the Atlantic Ocean and archived as part of the Ehrenberg collection housed in the Museum of Natural History (Gorbushina et al. 2007). Some of the archived samples were recently analyzed (Gorbushina et al. 2007) and found to contain numerous viable microorganisms.

Aerobiology is a rapidly developing research area focused on atmospheric transportation of microorganisms that has broad applications for human and ecosystem health (Kellogg and Griffin 2006). Scientists are currently examining the transportation, survival, and identification of microbes in conjunction with far-traveled dusts. Misconceptions that may have previously hampered research include the belief that desert soils are incapable of harboring a diverse microbial community and that microorganisms could not survive the conditions encountered during intercontinental transport (freezing, temperatures, desiccation, lack of nutrients, and UV radiation) (Kellogg and Griffin 2006). Several studies now document a correlation between dust events and increased concentrations of culturable bacteria and fungi (Wu et al. 2004; Prospero et al. 2005; Griffin 2007; Smith et al. 2012). How these microbial hitchhikers will affect human health is unclear. Favet et al. (2013) analyzed samples from various locations in the Republic of Chad, including the Bodélé depression, and dusts transported to Cape Verde and found only a few pathogenic strains though the samples contained a wide variety of microbes.

Examples of disease caused by vectors transported with regional dusts include meningitis, discussed in Sect. 5.2, and Valley Fever. Caused by inhalation of spores of the soil fungus *Coccidioides immitis*, cases of Valley Fever have more than doubled in some areas of the southwestern United States in the last two decades (CDC 2012). Climatic factors such as drought conditions are thought to be involved in the recent escalation of reported cases (Galgiani 1993; Bultman et al. 2005). Outbreaks often follow dust storms and were observed after the North Ridge, California earthquake triggered landslides in the area (Kirkland and Fierer 1996; Schneider et al. 1997).

15.4.3 Mechanisms of Action

Proposed biological mechanisms responsible for the observed health effects of PM exposures include oxidative stress and systemic inflammation (Mills et al. 2007). Although the inflammatory response to PM exposure plays a significant role in both respiratory and cardiovascular diseases, the exact physiological pathways have not been identified (Schwarze et al. 2006). Several studies have identified the role of fine PM (<2.5) in the production of inflammation (Adamson et al. 1999; Schaumann et al. 2004), though some studies suggest that coarser particles

may be equally involved in triggering the body's defense system to produce an inflammatory response. Shins et al. (2004) observed that coarse particles (PM10) from a rural setting produced greater inflammatory effects in rat lungs than fine (PM2.5) particles from an industrial area and attribute the response to endotoxins or related contaminants. There is some evidence that particle surface area may be a more accurate measure of particle concentration than the mass (Ovrevik et al. 2005). In a study to assess mineral dusts, Ovrevik et al. (2005) found that when cytokine release was related to equal surface areas of the particles, there was no difference in bioactivity between the two size fractions (i.e., PM10 and PM2.5).

The importance of a particle's biosolubility or biopersistence has also been examined with respect to its ability to promote inflammation and toxicity, especially for minerals associated with occupational exposures such as crystalline silica and asbestos. Researchers commonly measure the production of cytokines and other biomarkers following exposure of cell lines (i.e., cultures of physiologically appropriate cell types such as lung epithelial cells) to particulate matter (Hetland et al. 2001). Some of these studies indicate that biopersistent or poorly soluble particles are a primary factor in terms of promoting inflammation, possibly due to particle accumulation and/or overload, and longer retention times (Hetland et al. 2001; Muhle and Mangelsdorf 2003). Other studies indicate soluble components (e.g., metals), may be more important (Adamson et al. 1999; Costa and Dreher 1997). Veranth et al. (2006) found a wide range of potency when examining cytokine response to soil-derived particulate matter and suggested that it is the bioavailable (amount that the body absorbs) metal fraction not the total metal concentration that is the toxicologically relevant variable.

15.4.4 Exposure and Susceptibility

Other challenges relate to qualifying and quantifying environmental exposures and individual susceptibility. Exposures to PM (and MD) may exacerbate existing disease such as cardiovascular and respiratory ailments (Dockery et al. 1993; Pope et al. 1995) resulting in the need for additional medications (Chimonas and Gessner 2007), emergency room visits (Mahboub et al. 2012), and hospitalizations (Kanatani et al. 2010). Due to current scientific limitations, exposures are usually estimated (Baxter et al. 2013). Although low-level environmental exposures may contribute to common complex diseases, the relationship between exposure and health outcome requires the integration of a wide range of factors—extrinsic (e.g., environmental), intrinsic (e.g., genotype), and mechanistic (e.g., toxicological) (Hubal 2009).

Inhaled dusts, for example, that are cleared from the respiratory tract via the mucociliary escalator and then ingested can also be a source of metal toxicant uptake. Plumlee et al. (2013b) showed that such an exposure route contributed to a recent fatal outbreak of childhood lead poisoning associated with artisanal mining in northern Nigeria. While the predominant exposure route was hand-to-mouth transmission and inadvertent ingestion of particles from soils heavily contaminated

by processing dusts, ingestion of dusts cleared from the respiratory tract was also a likely but subordinate exposure pathway. In contrast, direct uptake of lead from the respiratory tract was likely negligible due to the generally low solubility of the respired lead minerals in the respiratory tract fluids and the likely reprecipitation of any solubilized lead as insoluble lead phosphates (Plumlee et al. 2013b).

A recent review by Sacks et al. (2011) identified population attributes that may increase health risk from PM exposures. In addition to individuals with preexisting disease (i.e., cardiovascular and respiratory), they identified life stage (i.e., children, older adults), genetic polymorphisms, low socioeconomic status, and obesity as additional factors. By reviewing epidemiological studies that presented stratified results (e.g., males vs. females or <65 vs. >65 years of age), their study was able to compare populations exposed to similar PM concentrations, thus providing a basis for characterizing susceptible populations.

15.5 Ailments Associated with Airborne Dusts

Chronic or repeated acute exposures such as those that might be encountered by communities in or near dryland areas where dust storms prevail have not received much scrutiny prior to the last decade. Few population health studies related to regionally produced dust exist, particularly for dusts differentiated as inorganic minerals dusts and not PM (e.g., a size fraction such as PM2.5). The consistent observation in the few studies that have been done is an increased incidence of some form of respiratory disease. Interestingly, a lag period has been identified in several studies, generally 2–3 days from exposure to illness, but the reason is unclear. In China, in addition to an increased relative risk (1.14 %) of hospitalization for respiratory and cardiovascular disease associated with dust events, a 3-day lag period between exposure and hospitalization was observed (Meng and Lu 2007). Other studies, particularly of respiratory disease associated with dust events, have observed a similar lag period (Lopez-Villarrubia et al. 2010; Grineski et al. 2011; Johnston et al. 2011).

15.5.1 Asthma

One common chronic disease associated with exposure to airborne MD is asthma. Asthma is characterized by airway inflammation, variable lung function, and airway responsiveness. However, epidemiological studies have been hampered because no clear definition of asthma or clinically acceptable method for measuring inflammation exists (Hartert and Peebles 2000). About 235 million people worldwide have asthma (WHO 2011), and estimates suggest that asthma prevalence increases globally by 50 % every decade with the highest increases seen among children (Braman 2006). Direct medical and indirect economic costs related to asthma in

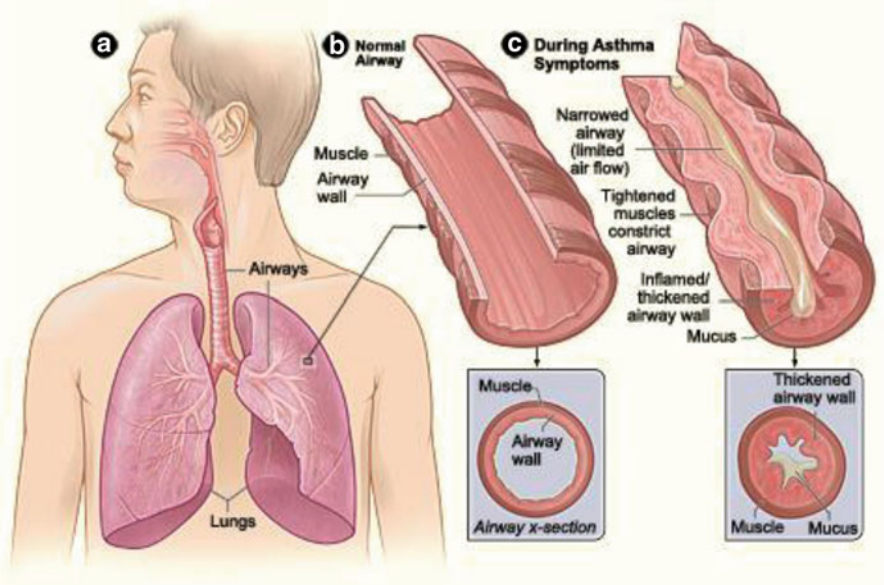

Fig. 15.2 (**a**) Shows the position of the lungs. (**b**) Depicts a cross section of a normal airway. (**c**) Shows a cross section of an airway during asthma symptoms (Source: National Heart, Lung, and Blood Institute; National Institutes of Health; U.S. Department of Health and Human Services. National Institutes of Health)

Europe average 21 billion dollars annually (Braman 2006). In 2007, costs related to asthma in the United States were 56 billion dollars (CDC 2011).

Asthma has been described as a complex inflammatory disease, characterized by episodes of wheezing, coughing, and shortness of breath secondary to reversible airflow limitations (Zervas et al. 2012; Fig. 15.2). Studies have demonstrated that childhood asthma actually begins in infancy (Hartert and Peebles 2000). Evidence suggests reduced lung function in children and adults, as well as adult lung disease, may be linked to events that occur during fetal development and postnatal (after birth to about 6 weeks) life (Soto-Martinez and Sly 2010). The importance of genetic factors in the development of asthma has also been established (Zervas et al. 2012). Epidemiological and genome-wide linkage studies have identified more than 100 genes associated with allergy and asthma in eleven different populations (Subbarao et al. 2009). Risk factors for childhood asthma include genetic predisposition, exposure to tobacco smoke or animals, and respiratory infections. Adult-onset asthma may occur as a relapse of childhood asthma or have environmental or occupational causes (Subbarao et al. 2009).

Environmental exposures are acknowledged as a factor in the exacerbation of existing asthma and to a lesser degree the development of asthma (Zervas et al. 2012). Gene-environment interactions support the observed increase of asthma cases over the last 50 years as genetic susceptibility factors within a population cannot

change over such a short time period (Hartert and Peebles 2000; Subbarao et al. 2009; Zervas et al. 2012). Until recently, few studies have sought to link MD and respiratory disease such as asthma though several studies have demonstrated an association between PM exposure and increased risk for respiratory disease exacerbation.

Few population health studies for regionally produced dust exist, particularly for dusts differentiated as MD and not as PM. Those that do support an association between exposure to MD and asthma. For example, Chimonas and Gessner (2007) reported a 9.3 % increase in the rate of outpatient visits for asthma and an 18 % increase in quick relief medication prescriptions (for asthma) following exposures to PM10 levels of 22–33 $\mu g/m^3$, which is substantially lower than the National Ambient Air Quality Standards (NAAQS) level of 150 $\mu g/m^3$. Their study examined PM exposures that the authors describe as being derived primarily from geological sources in Alaska. In El Paso, Texas, where dust events are common, Grineski et al. (2011) found that hospitalizations for asthma and acute bronchitis increased in all age groups (children, adults, and elderly) following dust events caused by relatively low winds. Study participants from the Cheyenne River Reservation in South Dakota identified dust as one of the top four asthma triggers (other top triggers were cold air, smoke, and exercise) for all seasons (O'Leary and Wallace 2012). Describing the composition of dusts in regional storms as particulates from nonindustrial sources, Hefflin et al. (1994) found an increase in daily emergency room visits for bronchitis for each 100 $\mu g/m^3$ increase in PM10 during a study of the effects of dust storms in Washington State. The authors relate that the dusts in these regional seasonal storms are volcanic in origin (Hefflin et al. 1994).

International studies demonstrate similar findings. Rutherford et al. (1999) analyzed rural dust events in Australia and observed that in spite of study design limitations, the potential for adverse health effects in predisposed individuals such as asthmatics was evident. A study in the United Arab Emirates indicates sudden heavy exposures to dust and sand storms may precipitate acute severe asthma in uncontrolled asthmatics and result in emergency room visits and hospitalizations (Mahboub et al. 2012). In Japan, using light detection and ranging (LIDAR) to distinguish between mineral dust particles ("nonspherical") and nonmineral dust particles ("spherical"), Kanatani et al. (2010) found mineral dust events originating in Asia were associated with increased risk of hospitalizations for asthma in pediatric patients. In Barbados, however, Prospero et al. (2008) found no substantial changes in clinic attendance for pediatric asthma cases related to short-term increases in dust concentrations that were transported substantial distances from Africa. Their study reports that although these dusts had not been extensively studied in terms of composition, the presence of commonly suspected pollutants, concentrations of major pollutant aerosol species, ozone and organic matter are low when compared to urban dusts (Prospero et al. 2008). Measurements of dust in the trade winds at Barbados and in the southeastern United States (Prospero et al. 2008) indicate that one third to one half of the transported African dust mass was below 2.5 μm, a fraction which is generally deemed respirable.

Fig. 15.3 Map identifying high prevalence areas of meningitis in Africa (Source: Center for Disease Control and Prevention)

15.5.2 Meningitis

Meningococcal meningitis is a serious infection of the meninges, the membrane lining that surrounds the brain and spinal cord. Caused by bacteria, it can result in brain damage or, if untreated, death in 50 % of cases (WHO 2012b). *Neisseria meningitidis* is the bacteria usually responsible for epidemics, though other bacteria (i.e., *Streptococcus pneumonia* and *Haemophilus influenzae*) may also cause meningitis (WHO 2012b). The bacteria, spread by respiratory secretions, can colonize the nasopharyngeal region of the respiratory system, cross the mucosa, and enter the bloodstream where they are carried to the meninges.

Outbreaks of meningitis may occur worldwide, yet the highest recorded incidence or rate of disease is found in the "meningitis belt" of sub-Saharan Africa (Fig. 15.3). The earliest recorded outbreak occurred in Algiers in 1841 and more than 425 epidemics have been documented since (Molesworth et al. 2003). The 2009 epidemic reported over 88,000 meningitis cases and 5,352 deaths. Of interest is the observation that these epidemics tend to occur at intervals of 7–14 years (WHO 2012b). Factors predisposing populations to meningitis epidemics are not well understood but are thought to include overcrowded housing, regional population displacement such as pilgrimages or markets (WHO 2012b), and environmental factors.

In the 1960s a correlation between meningitis outbreaks and dry, dusty weather was observed (Lapeyssonnie 1963). Recent studies have proposed a link between environmental conditions such as low humidity and dusty conditions and meningitis (Molesworth et al. 2003; Thomson et al. 2006). It has been suggested that the hot dry weather may damage the mucosa in the nose and throat, thus providing a portal of entry for the bacteria (Dukic et al. 2012; Agier et al. 2013). Several studies have modeled population and environmental variables in an attempt to understand and predict favorable conditions and locations for meningitis epidemics; these have identified dust as an important factor (Agier et al. 2013; Molesworth et al. 2003; Thomson et al. 2006). Dukic et al. (2012) modeled environmental variables in a study of meningitis outbreaks in Ghana and identified the current month maximum temperature, total number of days with dust, previous month average humidity at 3 pm, and burning biomass as the most significant predictors in their full model. As there is some indication that the decrease in rainfall and severe drought conditions may continue into the twenty-first century (Dukic et al. 2012), the ability to make such predictions would allow public health officials to focus resources such as personnel and supplies. Because an effective and inexpensive vaccine has been developed (Roberts 2010), such advanced notice of a potential epidemic could allow public health officials to target specific areas for vaccination, possibly saving hundreds of lives. However, there are inherent difficulties associated with modeling complex problems with numerous variables such as meningitis outbreaks. Two studies have cited challenges associated with the limited accuracy of data (i.e., population data), variables that may not reflect ground conditions (i.e., remote sensing or satellite data), a lack of exposure information, and understanding how environmental variables may interact with each other (Molesworth et al. 2003; Thomson et al. 2006).

Meningitis is not just endemic in Africa but disease estimates are not always available for many countries in Asia (Vyse et al. 2011) or some regions of the Middle East and North Africa (Ceyhan et al. 2012). Vyse et al. (2011) suggest that meningococcal cases in Asia may be underreported, as epidemiological information is lacking for several countries. This lack of information is in part due to healthcare barriers to reporting disease, poor bacterial detection methods, and an absence of surveillance methods (Vyse et al. 2011). In a review of epidemiological data for countries in northern Africa and the Middle East, Ceyhan et al. (2012) found a similar lack of surveillance and data collection. The implementation of standard methods for data collection and surveillance is needed in addition to research to understand the transmission and extent of this disease.

15.5.3 Hospitalization and Mortality Related to Intercontinental Dust

There is increasing concern that desertification and the frequency and volume of dusts produced will increase with climate change (Kuehn 2006). Recently, studies

have begun to focus on the potential health effects of dusts transported from large primary sources such as the Sahel/Sahara and Asia. In Europe, Perez et al. (2007) examined the relationship between coarse particles from Saharan dust and daily mortality in Barcelona, Spain. They observed that daily mortality increased by 8.4 % (per increase of 10 $\mu g/m^3$ PM10) on Saharan dust days in Barcelona, but no increased risk was observed with PM2.5 (Perez et al. 2007). Chemical analysis to examine potential compositional differences did not explain the differences (Perez et al. 2007). Similar results for far-traveled dusts were observed in studies elsewhere in Europe (Jimenez et al. 2010; Mallone et al. 2011).

Studies have also been done for areas that are closer to the source locations for major dust events. Lopez-Villarrubia et al. (2010) found increased rates of respiratory mortality, 4.9 % for each PM10 increase of 10 $\mu g/m^3$, in the Canary Islands linked to dust events sourced in nearby Africa. In Asia, similar associations between dust events and emergency room visits, hospitalizations, and deaths were observed. In Taiwan, emergency room visits for cardiovascular and respiratory illnesses were increased following dust storms from Asia (Chan et al. 2008). In Taipei, Chan and Ng (2011) found an increase in the number of nonaccidental and cardiovascular deaths on dust storm days over a 14-year period. Hashizume et al. (2010) found conflicting results in a review of Japanese literature for evidence of potential health problems related to Asian dust events. Their analysis indicated that some studies suggested an increase in mortality and hospital admissions related to dust exposure, while others did not demonstrate any statistically significant associations. A study of a far-traveled Gobi desert dust event, however, found no evidence of increased hospitalization in a retrospective examination of hospitalizations following the dust event in British Columbia (Bennett et al. 2006).

15.5.4 Exposures to Agricultural Dusts

We have included as part of this discussion occupational exposures to agricultural dusts, as results indicate respiratory disease may be a chronic condition among farmers. It is unclear if these exposures could be extended to nearby communities as we were unable to locate studies linking nonoccupational agricultural dust exposures to health risks for community members residing near farms. In the United States, many farm operations are small and do not fall under the jurisdiction of the Occupational Safety and Health Administration (OSHA), and the cause and extent of disease in farmworkers is difficult to determine (Kirkhorn and Garry 2000). In addition to field activities such as plowing, grain handling and harvesting may also expose workers to high concentrations of inorganic dusts such as crystalline silica (quartz) and noncrystalline silica (diatomite) (Kirkhorn and Garry 2000). Green et al. (1990) characterized mineral dusts associated with farm activities in rural Alberta, Canada, and found that the respirable mass fraction (particles with diameters <5 μm) was 50 % or greater and free silica content ranged from 1 to 17 %.

Autopsy reports have documented mineral grains in the lungs of farmworkers (Gylseth et al. 1984; Pinkerton et al. 2000 and Domingo-Neumann 2009), a finding that belies long-held assumptions that MD particles were too large to be respired. Pinkerton et al. (2000) examined lungs provided by the coroner's office of young individuals who had been primarily employed in agriculture, but who had died from unrelated causes; they found evidence of mineral dust retention and associated small airway disease (26 %), pneumoconiosis (10 %), lymph node fibrosis (38 %), and asthma (33 %) in lungs on autopsy. Schenker (2000) suggests the magnitude of the exposures to agricultural dusts may be a clinically significant etiological component. This is in agreement with the concept of biopersistence, which may lead to accumulation and/or overload and longer retention times.

15.5.5 Other Potential Risks Related to MD Exposures: Pneumoconioses

The inhalation of certain mineral dusts through occupational exposures has been recognized since the 1930s as a precursor to the development of pneumoconioses (McClellan 2000). This term which describes a group of interstitial lung diseases, such as silicosis, is still endemic in some areas of the world where dust control and protective measures are not adequately implemented, notably China (WHO 2013). As an occupational disorder, silicosis has been well studied and is associated with tuberculosis (teWaterNaude et al. 2006) and lung cancer (Attfield and Costello 2004).

Nonindustrial silicosis, or desert lung syndrome, has not received extensive scrutiny. It has been recognized in North Africa, the Middle East, China, and India (Policard and Collet 1952; Hirsch et al. 1974; Norboo et al. 1991; Xu et al. 1993; Mathur and Choudhary 1997; Derbyshire 2007). It is difficult to ascertain how widespread desert lung is, as cases may not be reported or diagnosed, depending in part on health services available. Further, in some areas of the world, large population-based studies would be problematic because diagnosis is made by radiographic findings of silicotic nodules in the lungs and history of exposure to airborne silica dust.

No current related research was identified; however, available studies found the incidence of nonindustrial silicosis to be greater in women than in men (Hirsch et al. 1974; Norboo et al. 1991) and identified an association between desert lung syndrome and cataracts (Hawass 1987). Xu et al. (1993) observed that the prevalence of siliceous pneumoconiosis in residents near a desert area in Gansu Province was 7.09 %, less than the rates for occupational exposures in South African gold miners (18–19 %, Churchyard et al. 2004) but comparable to that of surface coal miners in Pennsylvania (3.7–9.7 %, CDC 2000) (Fig. 15.4).

A related disease, Al Eskan, or desert storm pneumonitis, was recognized in troops deployed to the Persian Gulf in Operation Desert Storm in 1991

Fig. 15.4 Dust storm at Kandahar Airfield, 2006, Afghanistan. (Photograph courtesy of Jared Abraham, USGS)

(Korenyi-Both et al. 1992). Analysis of dust samples, after a high incidence of respiratory disease, revealed the presence of many fine-grained (<1 μm) sand particles, but most cultures for pathogens were negative. The abundance of respirable particles, the authors suggest, induced hyperergia or an increased sensitivity to allergens and overwhelmed pulmonary macrophages, thereby reducing their capacity to protect against infectious agents. Kelsall et al. (2004) found no increase in respiratory disease related to dust storms in a study of deployed military personnel. Studies are ongoing to understand exposures and related health effects for currently or recently deployed troops to Iraq and Afghanistan (Engelbrecht et al. 2008; Szema et al. 2010; King et al. 2011 and others).

The health effects from exposures to dusts of asbestos have been known for decades and include asbestosis, pleural plaques or pleural abnormalities, mesothelioma cancer, lung cancer, tracheal cancer, and plausibly cancers of some other organs (NIOSH 2011). These diseases have a long latency period (time from exposure until disease presentation), making them difficult to study. As a result, in spite of decades of research, considerable uncertainties remain regarding how asbestos and so-called respirable elongate mineral particles or REMPs cause toxicity (NIOSH 2011). Contributing factors are thought to include (1) their length, which inhibits engulfment and clearance by the alveolar macrophages, (2) their biodurability in the lungs, and (3) their ability to trigger inflammation and generate reactive oxygen species (the latter, e.g., via release of iron from the fiber surfaces) (Aust et al. 2011).

In the past, these diseases were largely thought to result from occupational exposures to high levels of the dusts, with lesser but still measureable impacts from lower-level environmental exposures to dusts from commercial asbestos. However, concerns have increased over the last several decades about potential health risks resulting from environmental and occupational exposures to dusts of these minerals that are liberated from their source rocks by natural processes (e.g., weathering, erosion, landslides) or anthropogenic activities (e.g., road building or excavation). For example, unusually high rates of malignant mesothelioma were linked to environmental exposures to erionite dusts released from tuffaceous lake sediments in three Turkish villages (Carbone et al. 2011; Baris et al. 1978). Concerns about the potential for similar environmental exposures to erionite in the western United States are increasing, such as in parts of North Dakota where erionite-bearing gravels were used to gravel hundreds of miles of dirt roads (Weissman and Keifer 2011; Carbone et al. 2011). A California study linked residential proximity to ultramafic rock units containing natural occurrences of asbestos (NOA) to an increased risk for mesothelioma (Pan et al. 2005); however, the study was unable to exclude with certainty other possible causes, such as the retirement of asbestos-exposed shipyard workers to areas with geologically elevated NOA. Baumann et al. (2011) linked high incidences of malignant mesothelioma in New Caledonia to environmental asbestos exposures, particularly to dusts from gravel roads.

More research is needed to understand the potential health risks posed by exposures to dusts from natural occurrences of asbestos, erionite, and other REMPs. One key step is to understand the spatial distribution of geological favorable host rocks from which dusts containing these minerals may be released. The US Geological Survey has completed a systematic inventory of known geological occurrences of asbestos, fibrous amphiboles, and erionite across the United States (Van Gosen et al. 2013; Van Gosen and Clinkenbeard 2011). These compilations provide public health and other local agencies (e.g., environment, land use and development) with important information that can be used for future planning, exposure mitigation, and reducing risks of disease (Van Gosen et al. 2013; Meeker and Miller 2012; Van Gosen 2007).

15.6 Conclusion

The National Research Council recently identified ten research priorities for airborne particulate matter. Two of these were the characterization of emission sources and the assessment of hazardous particulate matter components. The research summarized in this chapter indicates that MD exposures may play a role in human morbidity and mortality although in some cases the association is tentative and the biological mechanisms and components responsible remain unclear. It is apparent that additional research is needed to identify contributions made by MD and the resulting risks posed to human health. Several studies indicate an increase in exposure and/or particle concentration related to dust events may

be an important factor. Yet, as previously noted, few population health studies related to regionally produced dust exist, particularly for dusts differentiated as MD. For example, no work has been conducted to examine the health effects of dust on populations in West Africa (de Longueville et al. 2010). Additionally, more information regarding source and sample characterization for a wider range of MD sources including agricultural dusts is needed. Mass of emission from diverse dust sources, variation in particle size distribution, variation in dust mineralogy and geochemistry, and emission and transport rates under varied wind conditions would aid in understanding exposure and health risks. Where such information exists, its collection into a research database available to all would greatly benefit population health studies. The diversity of MD characteristics, sources, exposure pathways, and potential health outcomes outlined in this chapter clearly indicates that elucidating the role of MD in human and ecosystem health will benefit from an interdisciplinary approach involving scientists from the Earth, climate, atmospheric, agricultural, public health, and other science disciplines.

References

Adamson IY, Prieditis H, Vincent R (1999) Pulmonary toxicity of an atmospheric particulate sample is due to the soluble fraction. Toxicol Appl Pharmacol 157:43–50

Adamson IY, Prieditis H, Hedgecock C, Vincent R (2000) Zinc is the toxic factor in the lung response to an atmospheric particulate sample. Toxicol Appl Pharmacol 166:111–119

Agier L, Deroubaix A, Martiny N, Yaka P, Djibo A, Broutin H (2013) Seasonality of meningitis in Africa and climate forcing: aerosols stand out. J R Soc Interface 10:20120814

Attfield MD, Costello J (2004) Quantitative exposure-response for silica dust and lung cancer in Vermont granite workers. Am J Ind Med 45(2):129–138

Aust AE, Cook PM, Dodson RF (2011) Morphological and chemical mechanisms of elongated mineral particle toxicities. J Toxicol Environ Health B Crit Rev 14:40–75

Baris YI, Sahin AA, Ozesmi MM, Kerse II, Ozen EE, Kolcan BB (1978) An outbreak of pleural mesothelioma and chronic fibrosing pleurisy in the village of Karain/Urgüp in Anatolia. Thorax 33:181–192

Baumann F, Maurizot P, Mangeas M, Ambrosi JP, Douwes J, Robineau B (2011) Pleural Mesothelioma in New Caledonia: associations with environmental risk factors. Environ Health Perspect 119(5):695–700

Baxter LK, Burke J, Lunden M, Turpin BJ, Rich DQ, Thevenet-Morrison K, Hodas N, Ozkaynak H (2013) Influence of human activity patterns, particle composition, and residential air exchange rates on modeled distributions of exposure compared with central-site monitoring data. J Expo Sci Environ Epidemiol 23:241–247

Bennett CM, McKendry IG, Kelly S, Denike K, Koch T (2006) Impact of the 1998 Gobi dust event on hospital admissions in the lower Fraser Valley, British Columbia. Sci Total Environ 366:918–925

Braman SA (2006) The global burden of asthma. Chest 130:4S–12S

Brunekreef B, Forsberg B (2005) Epidemiological evidence of effects of coarse airborne particles on health. Eur Respir J 26:309–318

Bultman MW, Fisher FS, Pappagianis D (2005) Soil borne human pathogens. In: Selinus O, Alloway B, Centeno J, Finkelman R, Fuge R, Lindh U, Smedley P (eds) Essentials of medical geology. Elsevier, Amsterdam, pp 481–511

Carbone M, Baris I, Bertino P, Brass B, Comertpay S, Dogan AU, Gaudino G, Jube S, Kanodia S, Partridge CR, Pass HI, Rivera ZS, Steel I, Tuncer M, Way S, Yang H, Miller A (2011) Erionite exposure in North Dakota and Turkish villages with mesothelioma. Proc Natl Acad Sci U S A 108–133:13618–13623

Centers for Disease Control and Prevention (2000) Silicosis screening in surface coal miners – Pennsylvania, 1996–1997. MMWR 49(27):612–615

Centers for Disease Control and Prevention (2011) Asthma in the US Growing every year. http://www.cdc.gov/VitalSigns/Asthma/. Accessed 7 July 2012

Centers for Disease Control and Prevention (2012) Fungal pneumonia: a silent epidemic Coccidioidomycosis (valley fever). http://www.cdc.gov/fungal/pdf/cocci-fact-sheet-sw-us-508c.pdf. Accessed 3 Apr 2013.

Ceyhan M, Anis S, Htun-Myint L, Pawinski R, Soriano-Gabarro M, Vyse A (2012) Meningococcal disease in the Middle East and North Africa: an important public health consideration that requires further attention. Int J Infect Dis 16:e574–e582

Chan CC, Ng HC (2011) A case crossover analysis of Asian dust storms and mortality in the downwind areas using 14-year data in Taipei. Sci Total Environ. doi:10.1016/j.sciotenv.2011.09.031

Chan CC, Chuang KJ, Chen WJ, Chang WT, Lee CT, Peng CM (2008) Increasing cardiopulmonary emergency room visits by long range transported Asian dust storms in Taiwan. Environ Res 106:393–400

Chimonas MR, Gessner BD (2007) Airborne particulate matter from primarily geologic, non-industrial sources at levels below National Ambient Air Quality Standards is associated with outpatient visits for asthma and quick relief medication prescriptions among children less than 20 years old enrolled in Medicaid in Anchorage, Alaska. Environ Res 103:397–404

Churchyard GJ, Ehrkich R, teWaterNuade JM, Pemba L, Dekker K, Vermeijs M, White N, Myers J (2004) Silicosis prevalence and exposure-response relations in South African gold miner's. Occup Environ Med 61:811–816

Costa DL, Dreher KL (1997) Bioavailable transition metals in particulate matter mediate cardiopulmonary injury in health and compromised animal models. Environ Health Perspect 105(Suppl 5):1053–1060

de Longueville FP, Ozer S, Doumbia S, Henry S (2010) Desert dust impacts on human health: an alarming worldwide reality and a need for studies in West Africa. Int J Biometeorol 57(1):1–19

Derbyshire E (2007) Natural minerogenic dust and human health. Ambio 36:73–77

Dockery DW, Pope CA III, Xu X (1993) An association between air pollution and mortality in six US cities. N Engl J Med 329:1753–1759

Domingo-Neumann R (2009) Mineral dust retained in lung tissue of residents reflects ambient PM10 mineralogy in Fresno, California. Geol Soc Am 41(7), 90, Abstract with Program

Dukic V, Hayden M, Forgor AA, Hopson T, Akweongo P, Hodgson A, Monaghan A, Weidinmyer C, Yoksas T, Thomson M, Trzaska A, Pandya R (2012) The role of weather in meningitis outbreaks in Navrongo, Ghana: a generalized additive modeling approach. J Agric Biol Environ Stat 17(3):442–460

Engelbrecht JP, McDonald EV, Gillies JA, Gertler AW (2008) Department of Defense Enhanced Particulate Matter Surveillance Program (EPMSP) 2008. Desert Research Institute. http://phc.amedd.army.mil/PHC Resource Library/Final EPMSP Report without appx Feb08.pdf

Favet J, Lapanje A, Giongo A, Kennedy S, Aung Y, Cattaneo A et al (2013) Microbial hitchhikers on intercontinental dust: catching a lift in Chad. ISME J 7:850–876

Galgiani JN (1993) Coccidioidomycosis. West J Med 159:153–171

Gallo MA (2008) History and scope of toxicology. In: Klassen C (ed) Casarett and Doull's Toxicology the basic science of poisons, 7th edn. McGraw Hill, New York

Garrison VH, Shinn EA, Foreman WT, Griffin DW, Holmes CW, Kellogg CA et al (2003) African and Asian Dust: from Desert soils to Coral Reefs. BioScience 53(5):469–480

Garrison VH, Foreman WT, Genualdi S, Griffin DW, Kellogg CA, Majewski MS et al (2006) Saharan dust – a carrier of persistent organic pollutants, metals and microbes to the Caribbean? Rev Biol Trop 54(Suppl 3):9–21

Garrison V, Lamothe P, Morman S, Plumlee G (2010) Trace-metal concentrations in African dust: effects of long-distance transport and implications for human health. In: Proceedings of 19th world congress of soil science: soil solutions for a changing world. Division symposium 4.2; Soils and human health, IUSS, Brisbane, 1–6 Aug 2010, pp 33–36, ISBN 978-0-646-53783-2; published on DVD; http://www.iuss.org

Gorbushina AA, Kort R, Schulte A, Lazarus D, Schnetger B, Brumsack H et al (2007) Life in Darwin's dust: intercontinental transport and survival of microbes in the nineteenth century. Environ Microbiol 9(12):2911–2922

Green FHY, Yoshida K, Fick P, Hugh A, Green WF (1990) Characterization of airborne mineral dusts associated with farming activities in rural Alberta, Canada. Int Arch Occup Environ Health 62:423–430

Griffin DW (2007) Atmospheric movement of microorganisms in clouds of desert dust and implications for human health. Clin Microbiol Rev 20:459–477

Grineski SE, Staniswalis JG, Bulathsinhala P, Peng Y, Gill TE (2011) Hospital admission for asthma and acute bronchitis in El Paso, Texas: do age, sex, and insurance modify the effects of dust and low wind events? Environ Res 111(8):1148–1155

Gyan K, Henry W, Lacaille S, Laloo A, Lamsee-Ebanks C, McKay S et al (2005) African dust clouds are associated with increased paediatric asthma accident and emergency admissions on the Caribbean. Int J Biometeorol 49:371–376

Gylseth B, Stettler L, Mowe G, Skaud V, Lexow PA (1984) Striking deposition of mineral particles in the lungs of a farmer: a case report. Am J Ind Med 6:231–240

Hartert TV, Peebles RS (2000) Epidemiology of asthma: the year in review. Curr Opin Pulm Med 6:4–9

Hashizume M, Ueda K, Nishiwaki Y, Michikawa T, Onozuka D (2010) Health effects of Asian dust events: a review of the literature. Jpn J Hyg 65:413–421

Hawass N (1987) An association between 'desert lung' and cataract – a new syndrome. Br J Ophthalmol 71(9):694–697

Hefflin BJ, Jalaludin B, McClue E, Cobb N, Johnson CA, Jecha L, Etzel RA (1994) Surveillance for dust storms and respiratory diseases in Washington State. Arch Environ Health 49(3):170–174

Hetland RB, Myhre O, Lag M, Hongve D, Schwarze PE, Refsnes M (2001) Importance of soluble metals and reactive oxygen species for cytokine release induced by mineral particles. Toxicology 165:133–144

Hirsch M, Bar-Ziv J, Lehmann E, Goldberg GM (1974) Simple siliceous pneumoconiosis of Bedouin females in the Negev Desert. Clin Radiol 25:507–510

Horwell CJ, Fenoglio I, Fubini B (2007) Iron induced hydroxyl radical generation from basaltic volcanic ash. Earth Planet Sci Lett 2261:662–669

Hubal EC (2009) Biologically relevant exposure science for 21st Century toxicity testing. Toxicol Sci 111:226–232

Jimenez E, Linares C, Martinez D, Diaz J (2010) Role of Saharan dust in the relationship between particulate matter and short-term daily mortality among the elderly in Madrid (Spain). Sci Total Environ 408:5729–5736

Johnston F, Hanigan I, Henderson S, Morgan G, Bowman D (2011) Extreme air pollution events from bushfires and dust storms and their association with mortality in Sidney, Australia 1994–2007. Environ Res 111:811–816

Kanatani KT, Ito I, Al-Delaimy WK, Adachi Y, Mathews WC, Ramsdell JW (2010) Increased risk of asthma hospitalization in children. Am J Respir Crit Care Med 182:1475–1481

Kellogg GA, Griffin DW (2006) Aerobiology and the global transport of desert dust. Trends Ecol Evol 21:638–644

Kelsall HL, Sim MR, Forbes AB, McKenzie DP, Glass DC, Ikin JF et al (2004) Respiratory health status of Australian veterans of the 1991 Gulf War and the effects of exposure to oil fire and dust storms. Thorax 59:897–903

King MS, Eisenberg R, Newman JH, Tolle JJ, Harrell FE Jr, Nain H et al (2011) Constrictive bronchiolitis in soldiers returning from Iraq and Afghanistan. N Engl J Med 365(3):222–230

Kirkhorn SR, Garry VF (2000) Agricultural lung disease. Environ Health Perspect 108(S4):705–712

Kirkland TN, Fierer J (1996) Coccidioidomycosis: a reemerging infectious disease. Emerg Infect Dis 3:192–199

Knaapen AM, Shi T, Borm PJA, Schins RPF (2002) Soluble metals as well as insoluble particle fraction are involved in cellular DNA damage induced by particulate matter. Mol Cell Biochem 234–235:317–326

Korenyi-Both AL, Molnar AC, Fidelus-Gort R (1992) Al Eskan disease: desert storm pneumonitis. Mil Med 157:452–462

Kreyling WG, Scheuch G (2000) Clearance of particles deposited in the lungs. In: Gehr P, Heyder J (eds) Lung biology in health and disease. Particle-lung interactions, vol 143. Marcel Dekker, Inc., New York, pp 323–366

Kreyling WG, Moller W, Semmler-Behnke M, Oberdorster G (2007) Particle dosimetry: deposition and clearance from the respiratory tract and translocation towards extra-pulmonary sites. In: Donaldson K, Borm P (eds) Particle toxicology. CRC Press, Boca Raton, pp 48–69

Kuehn BM (2006) Desertification called global health threat. JAMA 295(21):2463–2465

Lapeyssonnie L (1963) Cerebrospinal meningitis in Africa. Bull WHO 28:1–114

Lehnert BE (1993) Defense mechanisms against inhaled particles and associated particle-cell interactions. In: Guthrie G, Mossman B (eds), Reviews in mineralogy, vol 28. Mineralogical Society of America, Washington, DC, pp 425–469

Lopez-Villarrubia E, Ballaster F, Iniguez C, Peral N (2010) Air pollution and mortality in the Canary Islands: a time series analysis. Environ Health 9:8

Mahboub B, Vats M, Afzal S, Sharif W, Iqbal MN (2012) Environmental exposure and nonadherence with medicines directly correlate with exacerbations and hospitalizations for asthma: a population –based survey from UAE. ISRN. Pulmonology. doi:10.5402/2012/831687

Mahowald NM, Kloster S, Engelstaeder S, Moore JK, Mukhopadhyay S, McConnell JR et al (2010) Observed 20th century desert dust variability: impact on climate and biogeochemistry. Atmos Chem Phys 10:10875–10893

Malig BJ, Ostro BD (2009) Coarse particles and mortality: evidence from a multi-city study in California. Occup Environ Med. doi:10.1136/oem.2008.045393

Mallone S, Stafoggia M, Faustini A, Gobbi GP, Marconi A, Forastiere F (2011) Saharan dust and associations between particulate matter and daily mortality in Rome, Italy. Environ Health Perspect. doi:10.1289/ehp.1003026

Mathur ML, Choudhary RC (1997) Desert lung syndrome in rural dwellers of the Thar desert, India. J Arid Environ 35:559–562

McClellan RO (2000) Particle interactions with the respiratory tract. In: Gehr P, Heyder J (eds) Particle-lung interactions. Lung biology in health and disease, vol 143. Marcel Dekker, Inc., New York, pp 3–56

Meeker GP, Miller AK (2012) The distribution of fibrous erionite in the United States and implications for human health. U.S. Geological Survey Powell Working Group Technical Abstract. http://powellcenter.usgs.gov/current_projects.php#DistributionAbstract. Accessed 20 Mar 2013

Meng Z, Lu B (2007) Dust events as a risk factor for daily hospitalization for respiratory and cardiovascular diseases in Minqin, China. Atmos Environ 41:7048–7058

Mills NL, Newby DE, MacNee W, Donaldson K (2007) Effects of particles on the cardiovascular system. In: Donaldson K, Borm P (eds) Particle toxicology. CRC Press, Boca Raton, pp 259–274

Molesworth AM, Cuevas LE, Connor SJ, Morse AP, Thomson MC (2003) Environmental risk and meningitis epidemics in Africa. Emerg Infect Dis 9:1287–1293

Morman SA, Garrison VG, Plumlee GS (2014) Trace metals in Saharan Dust: the use of in vitro bioaccessibility extractions to assess potential health risks in a dustier world. In: McConnell L, Dachs J, Hapeman C (eds) Occurrence, fate and impact of atmospheric pollutants on environmental and human health, vol 1149, ACS symposium series. American Chemical Society, Washington, DC

Morman SA, Garrison VH, Plumlee GS, Lowers HA, Bunnell JE (2009) Assessing concentration and bioaccessibility of potentially toxic elements in African dust. In: Proceedings of Geological Society of America, Portland, OR, USA, 41(7):544

Muhle H, Mangelsdorf I (2003) Inhalation toxicity of mineral particles: critical appraisal of endpoint and study design. Toxicol Lett 140:223–228

NIOSH (2011) Asbestos fibers and other elongate mineral particles: state of the science and roadmap for research, revised edition. National Institutes of Occupational Safety and Health. Curr Intell Bull 62:174

Norboo T, Angchuk PT, Yahya M, Kamat SR, Pooley FD, Corrin B et al (1991) Silicosis in a Himalayan village population: role of environmental dust. Thorax 46(5):341–343

O'Leary R, Wallace J (2012) Asthma triggers on the Cheyenne River Indian reservation in western south Dakota: the breathing relief education and tribal health empowerment (BREATHE) study. South Dakota Med 65(2):57–61

Ovrevik J, Myran T, Refsnes M, Lag M, Becher R, Hetland RB, Schwarze PE (2005) Mineral particles of varying compositions induce differential chemokine release from epithelial lung cells: importance of physico-chemical characteristics. Ann Occup Hyg 49:219–231

Pan X, Day H, Wang W, Beckett LA, Schnecker MB (2005) Residential proximity to naturally occurring asbestos and mesothelioma risk in California. Am J Respir Crit Care Med 172:1019–1025

Perez L, Tobias A, Querol X, Kunzli N, Pey J, Alastuey A et al (2007) Coarse particles from Saharan dust and daily mortality. Epidemiology 19:800–807

Pinkerton KE, Green FHY, Saiki C, Vallyathan V, Plopper CG, Gopal V et al (2000) Distribution of particulate matter and tissue remodeling in the human lung. Environ Health Perspect 108(11):1063–1069

Plumlee GS, Ziegler TL (2007) The medical geochemistry of dusts, soils, and other earth materials. In: Lollar BS (ed) Treatise on geochemistry, online update, vol 9, Chapter 7. Elsevier, pp 1–61. http://www.sciencedirect.com/science/referenceworks/9780080437514

Plumlee GS, Morman SA, Ziegler TL (2006) The toxicological geochemistry of earth materials: an overview of processes and the interdisciplinary methods used to understand them. In: Sahai N, Schoonen MAA (eds) Medical mineralogy and geochemistry. Reviews in mineralogy and geochemistry, vol 64. Mineralogical Society of America, VA, pp 2–57

Plumlee GS, Morman SA, Hoefen TM, Meeker GP, Wolf RE, Hageman PL (2013a) The environmental and medical geochemistry of potentially hazardous materials produced by disasters. In: Treatise on geochemistry, vol 11, pp 257–304. http://www.sciencedirect.com/science/article/pii/B9780080959757009074

Plumlee GS, Durant JT, Morman SA, Neri A, Wolf RE, Dooyema CA et al (2013b) Linking geological and health sciences to assess childhood lead poisoning from artisanal gold mining in Nigeria. Environ Health Perspect 121(6):744–750. doi:10.1289/ehp.1206051

Policard A, Collet A (1952) Deposition of siliceous dust in the lung of the inhabitants of the Saharan regions. Arch Ind Hyg Occup Med 5:527–534

Pope CA, Thun MJ, Namboodiri MM, Dockery DW, Evans JS, Speizer FE, Heath CW (1995) Particulate air pollution as a predictor of mortality in a prospective study of U.S. adults. Am J Respir Crit Care Med 151:669–674

Prospero JM, Lamb PJ (2003) African droughts and dust transport to the Caribbean: climate change implications. Science 302(5647):1024–1027

Prospero JM, Nees RT (1986) Impact of the North African drought and El-Nino on mineral dust in the Barbados trade winds. Nature 320(6064):735–738

Prospero JM, Blades E, Mathison G, Naidu R (2005) Interhemispheric transport of viable fungi and bacteria from Africa to the Caribbean with soil dust. Aerobiologia 21:1–19

Prospero JM, Blades E, Naidu R, Mathison G, Thani H, Lavoie MC (2008) Relationship between African dust carried in the Atlantic trade winds and surges in pediatric asthma attendances in the Caribbean. Int J Biometeorol 52:823–832

Puett RC, Hart JE, Yanosky JD, Paciorek C, Schwartz J, Suh H et al (2009) Chronic fine and coarse particle exposure, mortality and coronary heart disease in the Nurses' heart study. Environ Health Perspect 117:1697–1701

Reheis MC, Budahn JR, Lamothe PJ, Reynolds RL (2009) Compositions of modern dust and surface sediments in the Desert Southwest, United States. J Geophys Res 114, F01028. doi:10.1029/2008JF001009

Roberts L (2010) The beginning of the end for Africa's devastating meningitis outbreaks? Science 330:1446–1467

Rutherford S, Clark E, McTainsh G, Simpson R, Mitchell C (1999) Characteristics of rural dust events shown to impact on asthma severity in Brisbane, Australia. Int J Biometeorol 42:217–225

Sacks JD, Stanek LW, Luben TJ, Johns DO, Buckley BJ, Brown JS, Ross M (2011) Particulate matter-induced health effects: who is susceptible? Environ Health Perspect 119:446–454

Samet JM, Ghio AJ (2007) Particle-associated metals and oxidative stress in signaling. In: Donaldson K, Borm P (eds) Particle toxicology. CRC Press, Boca Raton, pp 161–181

Schaumann F, Borm PJA, Herbrich A, Knoch J, Pitz M, Schins RPF et al (2004) Metal-rich ambient particles (particulate matter 2.5) cause airway inflammation in health subjects. Am J Respir Crit Care Med 170:898–903

Schenker M (2000) Exposures and health effects from inorganic agricultural dusts. Environ Health Perspect 108(S4):661

Schlesinger RB (2007) The health impact of common inorganic components of fine particulate matter (PM2.5) in ambient air: a critical review. Inhal Toxicol 19:811–832

Schlesinger RB, Kunzli N, Hidy GM, Gotschi T, Jerret M (2006) The health relevance of ambient particulate matter characteristics: coherence of toxicological and epidemiological interferences. Inhal Toxicol 18:95–125

Schneider E, Hajjeh RA, Spiegel RA, Jibson RW, Harp EL, Marshall GA et al (1997) A coccidioidomycosis outbreak following the Northridge, Calif Earthquake. JAMA 277:904–908

Schultz H, Brand P, Heyder J (2000) Particle deposition in the respiratory tract. In: Gehr P, Heyder J (eds) Particle-lung interactions. Lung biology in health and disease, vol 143. Marcel Dekker, Inc., New York, pp 292–277

Schwarze PE, Ovrevik J, Lag M, Refsnes M, Nafstad P, Hetland RB, Dybing E (2006) Particulate matter properties and health effects: consistency of epidemiological and toxicological studies. Hum Exp Toxicol 25:559–579

Shao Y, Wyrwoll KH, Chappell A, Huang J, Lin Z, McTainish GH et al (2011) Dust cycle: an emerging core theme in Earth system science. Aeolian Res 2:181–204

Shins RPH, Lightbody JL, Borm PJA, Shi T, Donaldson K, Stone V (2004) Inflammatory effects of coarse and fine particulate matter in relation to chemical and biological constituents. Toxicol Appl Pharmacol 195:1–11

Smith DJ, Griffin DW, Schuerger AC (2012) Stratospheric microbiology at 20 km over the Pacific Ocean. Aerobiologia 26:35–46

Soto-Martinez M, Sly P (2010) Relationship between environmental exposures in children and adult lung disease: the case for outdoor exposures. Chron Respir Dis 7(3):173–186

Subbarao P, Mandhane PJ, Sears MR (2009) Asthma: epidemiology, etiology and risk factors. CMAJ 181. doi:10.1503/cmaj.080612

Szema AM, Peters A, Weissinger KM, Gagliano CA, Chen JJ (2010) New-onset asthma among soldiers serving in Iraq and Afghanistan. Allergy Asthma Proc 31(5):e67–e71

teWaterNaude JM, Ehrlich RI, Churchyard GJ, Pemba L, Dekker K, Vermeis M et al (2006) Tuberculosis and silica exposure in South African gold miners. Occup Environ Med 63:187–192

Thomson MC, Molesworth AN, Djingarey MH, Yameogo KR, Belanger F, Cuevas LE (2006) Potential of environmental models to predict meningitis epidemics in Africa. Trop Med Int Health 11:781–788

USEPA (2012a) Particulate matter. http://www.epa.gov/airquality/particlepollution/. Accessed 6/2012

USEPA (2012b) Coarse particulate Matter (PM10) standards and agriculture fact sheet. http://www.epa.gov/airquality/particulatepollution/agroculture.html. Accessed 6/2012

Van Gosen BS (2007) The geology of asbestos in the United States and its practical applications. Environ Eng Geosci 13:55–68

Van Gosen BS, Clinkenbeard JP (2011) Reported historic asbestos mines, historic asbestos prospects, and other natural occurrences of asbestos in California. U.S. Geological Survey Open-File Report 2011–1188. http://pubs.usgs.gov/of/2011/1188/

Van Gosen BS, Blitz T, Plumlee GS, Pierson MP (2013) Geological occurrences of the erionite in the United States: an emerging national public health concern for respiratory disease. Environ Geochem Health. doi:10.1007/s10653-012-9504-9

Veranth JM, Moss TA, Chow JC, Labban R, Nichols WK, Walton JC et al (2006) Correlation of in vitro cytokine responses with the chemical composition of soil-derived particulate matter. Environ Health Perspect 114:341–349

Vyse A, Wolter JM, Chen J, Ng T, Soriano-Gabarro M (2011) Meningococcal disease in Asia: an unrecognized public health burden. Epidemiol Infect 139(7):967–985

Weissman D, Keifer M (2011) Erionite – an emerging North American hazard. NIOSH Science Blog. National Institute for Occupational Safety and Health. http://blogs.cdc.gov/niosh-science-blog/2011/11/erionite/

Wood WW, Clark D, Imes JL, Councell TB (2010) Eolian transport of geogenic hexavalent chromium to groundwater. Ground Water. 48:19–29. doi:10.1111/j.1745-6584.2009.00592

World Health Organization (2011) http://www.who.int/mediacentre/factsheets/fs307/en/index.html

World Health Organization (2012a) Asthma. http://www.who.int/mediacentre/factsheets/fs313/en/index.html.

World Health Organization (2012b) http://www.who.int/mediacentre/factsheets/fs141/en/

World Health Organization (2013) http://www.who.int/collaboratingcentres/casestudies/en/index10.html

Wu PC, Tsai JC, Li FC, Lung SC, Su HJ (2004) Increased levels of ambient fungal spores in Taiwan are associated with dust events from China. Atmos Environ 38:4879–4886

Xu XZ, Cai XG, Men XS, Yang PY, Yang JF, Jing SL et al (1993) A study of siliceous pneumoconiosis in a desert area of Sudan County, Gansu Province, China. Biomed Environ Sci 6(3):217–222

Zervas E, Holloway JW, Kehagia V (2012) Gene-environment interactions in asthma: what we know today? Pneumon 25:83–98

Chapter 16
Loess Records

Daniel R. Muhs, Stephen R. Cattle, Onn Crouvi, Denis-Didier Rousseau, Jimin Sun, and Marcelo A. Zárate

Abstract Loess is aeolian sediment, dominated by silt-sized particles, that is identifiable in the field as a distinct sedimentary body. It covers a significant portion of the land surface of the Earth and as such constitutes one of the most important archives of long-term dust deposition. Large tracts of loess cover Europe, Asia, South America, and North America, and smaller loess bodies are found covering parts of Africa, the Middle East, New Zealand, and Australia. Loess thickness, particle size, and carbonate content decrease downwind from sources, trends that are powerful tools for reconstructing paleowinds. Many loess sections consist of

D.R. Muhs (✉)
U.S. Geological Survey, Federal Center, MS 980, Box 25046, Denver, CO 80225, USA
e-mail: dmuhs@usgs.gov

S.R. Cattle
Faculty of Agriculture and Environment, The University of Sydney, Sydney, NSW 2006, Australia
e-mail: Stephen.Cattle@sydney.edu.au

O. Crouvi
Geological Survey of Israel, 30 Malkhe Israel St., Jerusalem 95501, Israel
e-mail: Crouvi@gsi.gov.il

D.-D. Rousseau
Ecole Normale Supérieure, Laboratoire de Météorologie Dynamique, UMR CNRS-ENS 8539 & CERES-ERTI, 24 rue Lhomond, 75231 Paris Cedex 5, France

Lamont-Doherty Earth Observatory, Columbia University, Palisades, NY 10964, USA
e-mail: Denis.Rousseau@lmd.ens.fr

J. Sun
Institute of Geology and Geophysics, Chinese Academy of Sciences, Beijing, China
e-mail: jmsun@mail.igcas.ac.cn

M.A. Zárate
Instituto de Ciencias de la Tierra y Ambientales de la Pampa (INCITAP), Avenida Uruguay 151, 6300 Santa Rosa La Pampa, Argentina
e-mail: marcelozarate55@yahoo.com.ar

P. Knippertz and J.-B.W. Stuut (eds.), *Mineral Dust: A Key Player in the Earth System*, DOI 10.1007/978-94-017-8978-3_16,

relatively thick deposits of mostly unaltered sediment with intercalated paleosols. Paleosols represent periods of landscape stability when loess deposition ceased or at least slowed significantly. Studies from several continents show that loess in most regions was deposited during glacial periods and paleosols formed during interglacial and interstadial periods.

Keywords Loess • Glacial • Interglacial • Silt • Paleosol • Deposition • Mineralogy • Geomorphology • Sediment • Stratigraphy • Geochronology • Dispersal • Paleoclimate • Records • Archive • Aeolian • Quaternary

16.1 Introduction

Loess is aeolian (windblown) sediment and is one of the most extensive surficial deposits on the surface of the Earth. Loess has come to be regarded as one of the most important archives of long-term dust deposition and Quaternary climate change. Combined with intercalated paleosols (buried soils), loess provides one of the most complete terrestrial records of glacial–interglacial cycles. Loess is distinctive in that it is one of the few Quaternary sediments that provides a direct record of atmospheric circulation. Thus, given favorable circumstances, loess can be used to reconstruct synoptic-scale paleoclimatology over millennial timescales. Finally, loess is unusual in that it can be dated directly using methods, such as luminescence geochronology, that require only the sediment itself. Thus, the combination of loess deposits, fossil remains, and intercalated paleosols provides a highly valued source of information of Quaternary paleoclimate.

16.2 Definition of Loess

Loess can be defined as sediment, dominated by silt-sized particles, that has been entrained, transported, and deposited by the wind. It differs from other dust archives (deep-sea cores, ice cores; see Muhs (2013a) for a review) in that it is found on land and is identifiable in the field as a distinct sedimentary body (Figs. 16.1 and 16.2). Loess occupies an intermediate position in a continuum of aeolian sediments, with an average particle size that is smaller than windblown sand (2–0.05 mm) but coarser than long-range-transported (LRT) dust (typically <10 μm). Commonly, loess contains 60–90 % silt-sized (50–2 μm diameter) particles, with smaller amounts of sand (>50 μm) and clay (<2 μm). Some loess deposits are more sand rich and others are more clay rich, but all have a dominance of silt-sized particles. Loess is also much more poorly sorted than aeolian sand or LRT dust. The wide range of mean particle size and relatively poor sorting can be the result of (a) multiple sources, (b) clay-sized particles being transported as

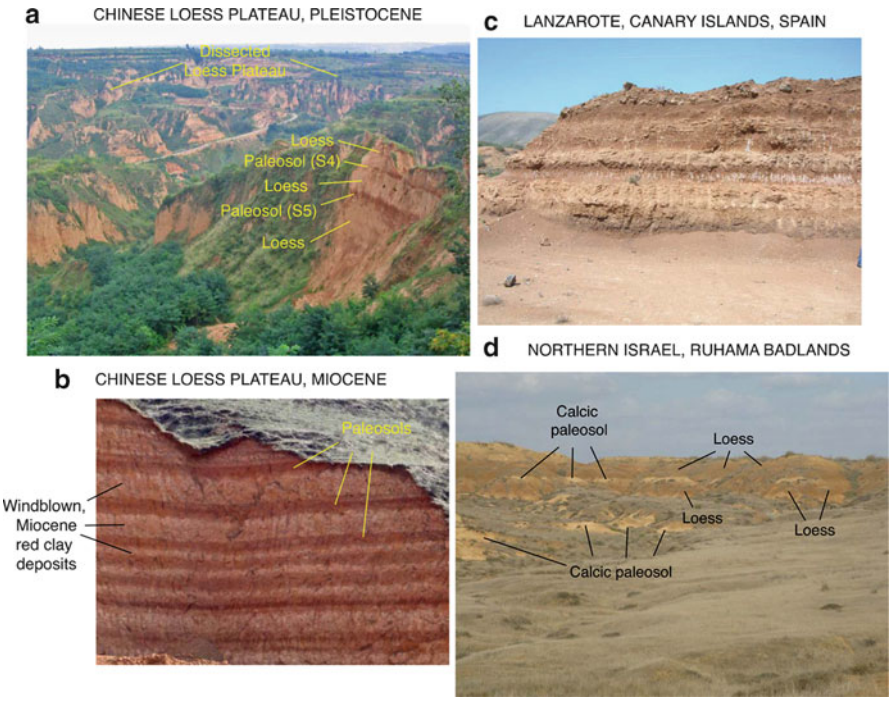

Fig. 16.1 Gallery of loess exposures from around the world, 1: (**a**) dissected loess plateau landscape and Pleistocene loess exposed at Luochuan, Chinese Loess Plateau – "L" prefix indicates loess units, and "S" prefix indicates paleosols; (**b**) Miocene Red Clay on the Chinese Loess Plateau (section is ∼10 m thick, light bands are aeolian clay, and dark bands are paleosols) (photo by Youbin Sun); (**c**) loess-like (fluvially and colluvially reworked) sediment exposed near Guatiza, Lanzarote, Canary Islands, Spain (see von Suchodoletz et al. (2009) for detailed study); (**d**) Pleistocene loess and paleosols exposed in the Ruhama badlands area, northern Negev Desert of Israel

silt-sized aggregates (see discussion by S. Cattle below), (c) loess bodies extending considerable distances from their sources, and/or (d) varying wind strengths over time.

Loess thickness is highly variable. It can range from a few centimeters to several hundred meters in thickness. Indeed, variability of loess thickness is one of its advantages as a paleoclimate indicator, as we discuss below. Loess deposits are commonly draped over preexisting landforms as a mantle, with thickest accumulations in protected, low-lying areas or broad, flat, stable upland divides and thinnest accumulations occurring on narrow, rounded hillcrests. Loess deposits can be intercalated with other sorts of sediments, such as tephras, where there is active volcanism, as is the case in Iceland, South America, Alaska, and New Zealand. Commonly, multiple loess units are apparent in outcrop, separated by paleosols that mark periods of cessation of loess deposition or at least periods when loess sedimentation rates were greatly diminished.

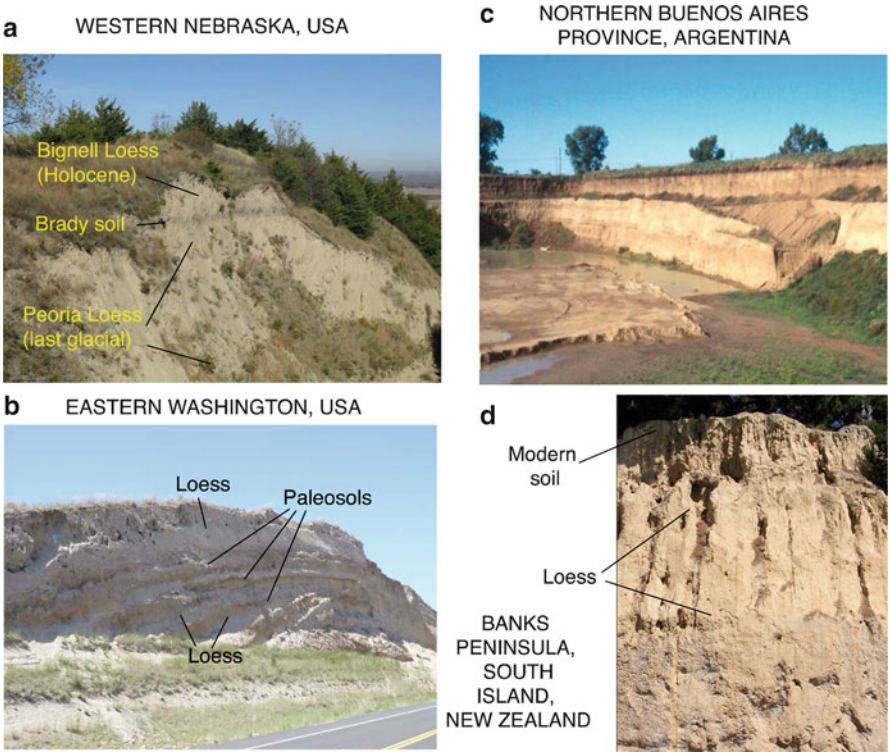

Fig. 16.2 Gallery of loess exposures from around the world, 2: (**a**) non-glacial Holocene and Pleistocene loess at Bignell Hill, Nebraska, Great Plains of the USA (see Muhs et al. (2008) for detailed study); (**b**) Pleistocene loess and paleosols exposed in a roadcut in the Palouse loess country of eastern Washington, USA; (**c**) Pleistocene loess exposed in the Pampas region, northern Buenos Aires province, Argentina; (**d**) Pleistocene loess and modern soil exposed on the Banks Peninsula, South Island, New Zealand

16.3 Mineralogy and Geochemistry of Loess

Loess typically has a mineralogy that reflects a mixture of sources, but most loess is derived from upper crustal source rocks. Exceptions to this include loesses derived from mafic volcanic rocks in Iceland, parts of New Zealand, and parts of South America. Elsewhere, on most continents, loess deposits typically include quartz, plagioclase, K-feldspar, mica, calcite (sometimes with dolomite), and phyllosilicate clay minerals (smectite, chlorite, mica, and kaolinite). Heavy minerals are usually present but commonly are found only in small amounts. Bulk geochemical studies show that the dominant constituent in loess is SiO_2, which ranges from ~45 to 75 % but is typically 55–65 %, reflecting a dominance of quartz. Lower concentrations of quartz, feldspars, and micas in glaciogenic loess from North

America are due to higher amounts of carbonate minerals (dolomite and calcite), derived from dolostones and limestones that were traversed by the Laurentide ice sheet (mid-continent) and valley glaciers (Alaska).

16.4 Genesis of Loess Deposits

Although few (if any) modern investigators doubt the aeolian origin of loess, there is still considerable debate about the specific processes whereby silt particles are generated before they are entrained by the wind. The issue is whether silt particles in loess can be produced only by glacial grinding or if they can be produced in sufficient quantities by other processes. Thus, the debate has been between advocates of "glacial loess" versus those of "desert loess" (see reviews in Pye 1995; Tsoar and Pye 1987; Smalley 1995; Livingstone and Warren 1996; Wright 2001a; Muhs and Bettis 2003; Muhs 2007, 2013b).

The "glacial loess model" proposes that silt-sized particles are produced mostly by glacial grinding of bedrock surfaces, deposition as till, reworking by fluvial processes as outwash, and finally entrainment, transportation, and deposition by wind. Glaciers are efficient producers of silt, and the close geographic association of loess with glacial terrain supports this model.

"Desert" loess is a term that has been applied to aeolian silt generated in and/or derived from arid or semiarid regions that were not glaciated. Silt-sized particles found in what has been called desert loess may be derived from a variety of non-glacial processes. These processes include frost shattering, chemical weathering, salt weathering, fluvial comminution, and aeolian abrasion and ballistic impacts (Wright 2001b). Examples of desert loess formed by these processes are given below.

An often overlooked source of silt is particle inheritance from sedimentary rocks, such as siltstones and shales. Silt is abundant in the geologic record. In fact, Blatt (1987) estimates that fully half of the detrital quartz in the world's sedimentary rocks is comprised of silt-sized particles. Furthermore, silt-sized volcanic ash particles form the major or at least a significant source for many of the loess deposits in South America, Iceland, Alaska, and New Zealand. We stress that the multiple pathways of loess particle origins are not mutually exclusive. It is likely that loess in many regions has origins from both glacial and non-glacial processes, as well as some silt-particle inheritance.

16.5 Loess Stratigraphy

Paleosols are common in loess sections (Figs. 16.1 and 16.2). In most regions, glacial periods are dominantly times of loess deposition, whereas interglacial and interstadial periods are dominantly times of soil formation. Thus, this alternation of

glacial times of loess deposition and interglacial times of soil formation has been correlated with the deep-sea oxygen isotope record of glacial–interglacial cycles. In general, this model has validity, but when loess records are examined in more detail, the stratigraphy is rarely simple. Perhaps a more realistic way to view the system is to consider loess sedimentation and soil formation as competing processes. When loess sedimentation rates are high, pedogenic processes cannot keep up, and relatively unaltered sediment accumulates (Verosub et al. 1993; Muhs et al. 2004). In contrast, when loess sedimentation rates are low, soil-forming processes extend deeper into previously deposited loess. Thus, whereas in deep-sea or lacustrine sediments, a case can be made for more or less continuous sedimentation, loess–paleosol sequences are more complex systems, and distinguishing between sediment and soil is not always an easy task. Examples of loess–paleosol sequences are provided below.

16.6 Loess Geochronology

Precisely because sedimentation is *not* continuous in loess–paleosol sequences, numerical dating is essential in loess stratigraphy. A particularly illuminating example of this is the study by Stevens et al. (2007), where an extensive suite of luminescence ages demonstrates that many loess sequences in China have been affected by nonconstant sedimentation rates, diagenesis, bioturbation, and erosion. Muhs et al. (2003), using a combination of radiocarbon ages, tephrochronology, and inventory ^{10}Be methods, show that loess sequences in Alaska contain numerous unconformities. Today, the most commonly used methods in dating loess are paleomagnetism, luminescence geochronology, radiocarbon dating, and magnetic susceptibility (see review in Muhs (2013b)).

16.7 Paleoclimatic and Paleoenvironmental Interpretation of Loess Deposits

Much valuable paleoenvironmental information can be obtained from loess–paleosol sequences, particularly because loess covers large areas of most continents (Figs. 16.3, 16.4, 16.5, and 16.6). Loess properties can change over a landscape, and these variations can yield important clues about the paleowinds that deposited the loess. Thickness of loess, particle size, and carbonate content, in general, decrease away from sources (Liu 1985; Porter 2001; Bettis et al. 2003; Muhs and Bettis 2003; Muhs et al. 2004, 2008, Muhs 2013b). Reduction in sediment load downwind from a source is inferred from decreases in loess thickness. Paleowinds can also be inferred from the decrease in mean particle size away from a source, reflecting a winnowing of the coarse load. With decreases in loess deposition rate away from a

source, there is often syndepositional leaching, reflected in a decrease in carbonate content. Thus, if a hypothesized loess source were a north-to-south-trending river valley, a decrease in loess thickness and mean particle size to the east of the river would imply northwesterly, westerly, or southwesterly paleowinds.

In contrast to unaltered loess itself, loess-hosted paleosols frequently yield valuable information about interglacial or interstadial periods. Measurement of magnetic susceptibility and other mineral magnetic properties has been one of the most common approaches to interpreting paleoclimate from loess-hosted paleosols (Verosub et al. 1993; Maher et al. 1994; Porter 2001; Porter et al. 2001; Singer and Verosub 2007). Unfortunately, one problem that arises is that magnetic susceptibility in modern, loess-derived soils in China is partly a function of particle size and sediment accumulation rate (as a dilution effect), as well as climate. Porter et al. (2001) show that both of these factors are spatially variable but highly correlated with one another (and climate) across the Chinese Loess Plateau. Another approach is to examine the degree of chemical weathering in loess-derived paleosols, as this reflects past climate and vegetation (Muhs 2007).

Loess lacks many of the Quaternary paleoecological indicators that are commonly used in lacustrine or marine sediments, such as pollen, diatoms, ostracodes, radiolaria, or foraminifera. Furthermore, it is rare for mammalian fossils to be preserved in loess, although Alaska (USA) is an important exception to this generalization (Péwé 1975). Fortunately, it is common for the shells of land snails to be preserved in loess, and they are abundant in China, Europe, and North America (see Liu 1985; Rousseau 1991; and Rossignol et al. 2004 for examples). Most or all of these snails are extant species, and their modern zoogeography is reasonably well established. Thus, it is possible to infer past climates during the times of loess deposition by identification of extralimital taxa, i.e., those species that do not presently live at a locality where they are found as fossils.

16.8 Global Loess Deposits

16.8.1 Europe

Loess is extensive over much of Europe (Fig. 16.3a; see also Haase et al. 2007; Rousseau et al. 2007a). Although there is no source for loess at present, during the last glacial period, potential sources included glaciogenic silt from the ice sheets on Ireland, the United Kingdom, and Scandinavia, plus smaller ice caps at lower latitudes on mountain ranges such as the Alps, the Pyrenees, and the Vosges. In addition, the continental shelf areas of the present English Channel, Celtic Sea, and the North Sea were subaerially exposed due to lowered sea level and were potential dust source areas.

European loess deposits are distributed over three main zones (Fig. 16.3a). Eastward to about longitude 15° east, loess is found mostly (and is thickest) in

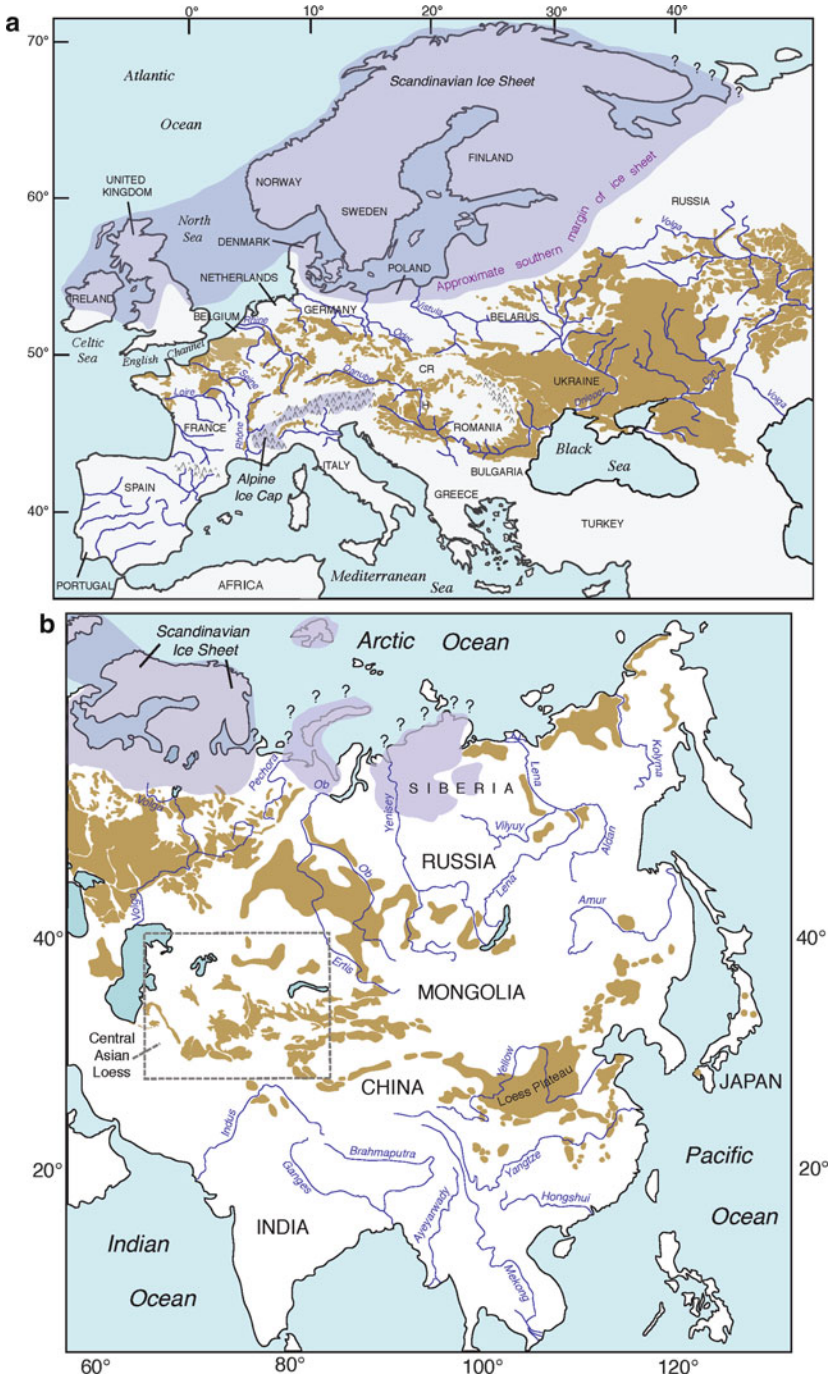
a
0°
10°
20°
30°
40°
70°
60°
50°
40°
Atlantic
Ocean
Scandinavian Ice Sheet
FINLAND
UNITED KINGDOM
NORWAY
SWEDEN
RUSSIA
North Sea
DENMARK
Approximate southern margin of ice sheet
Volga
NETHERLANDS
POLAND
IRELAND
BELGIUM
GERMANY
Vistula
BELARUS
Celtic Sea
English Channel
Seine
Oder
Elbe
CR
UKRAINE
Loire
Danube
Dniester
Dnieper
Volga
FRANCE
Rhone
ROMANIA
Black Sea
ITALY
Alpine Ice Cap
BULGARIA
SPAIN
GREECE
TURKEY
PORTUGAL
AFRICA
Mediterranean Sea
b
Scandinavian Ice Sheet
Arctic Ocean
Pechora
Ob
Yenisey
Lena
Kolyma
SIBERIA
Vilyuy
Aldan
RUSSIA
Volga
Ural
Ob
Lena
Amur
40°
Ertis
MONGOLIA
Central Asian Loess
Yellow
Loess Plateau
CHINA
JAPAN
Indus
Brahmaputra
Yangtze
Hongshui
Pacific
Ocean
20°
Ganges
Ayeyarwady
INDIA
Indian
Ocean
Mekong
60°
80°
100°
120°

a latitudinal band at about latitude 50 °N, between the continental ice sheets to the north and the Alpine glaciers in the south. Between longitudes 15° and 25° east, the thickest loess sequences are mostly located south of the Carpathian arch. Finally, eastward from 25° east, the loess deposits are distributed in a broader domain, corresponding to the wide Ukrainian and Russian plains. The loess deposits show a distribution in close proximity with the major European rivers such as the Seine, the Somme, the Rhine, the Danube, and the Dnieper.

Focusing on the past ~40 ka, the Nussloch loess section, south of Heidelberg, Germany, shows the most detailed and expanded record of this time interval (Fig. 16.7). The Nussloch quarry is located at N49°19′ and E8°43′ and is situated on the Odenwald Plateau, above the Rhine Valley (Antoine et al. 2001). The loess accumulated through elongated structures described as greda, the main dunelike morphology being built during the last glacial period, above the Arctic brown paleosol named Lohne Boden and dated between 34 ka and 40 ka by luminescence (Rousseau et al. 2007a, b).

The stratigraphy of the last glacial period at Nussloch shows that there are a minimum of eight tundra gley paleosols (Antoine et al. 2009a, b). The alternation of loess and tundra gley paleosols is interpreted as a series of loess–paleosol doublets (Rousseau et al. 2002), and such stratigraphic successions are observed from one dunelike landform to another (Antoine et al. 2009a, b; Rousseau et al. 2007a, b). The use of a combination of ^{14}C (Hatté et al. 1999) and luminescence (Lang et al. 2003) dating techniques demonstrates that the last glacial period interval, corresponding to the upper 13 m of the 18 m-thick last climate cycle sequence, lasted between ~40 and ~15 ka. Thus, the sequence at Nussloch shows a very high sedimentation rate over the last glacial period, although the tundra gley paleosols show that it was episodic. This succession of loess–paleosol doublets was correlated with the Greenland interstadial–stadial succession from DO events 8–2.

The upper Pleistocene record preserved in the Stayky (N50°05.65′, E30°53.92′) loess sequence, located 1,800 km westward from Nussloch, south of Kyiv, along the Dnieper River in Ukraine, shows a similar pattern, a succession of loess–paleosol doublets, corresponding to the same time interval (Fig. 16.7), with alternating dry-cold and wet-cool intervals (Rousseau et al. 2011). Moisture conditions are nevertheless lower than in Nussloch, as the paleosols are mostly expressed as embryonic soils, with only two tundra gleys being identified. Nevertheless, even though Nussloch and Stayky are distant from one another, grain size variations show similarities at both localities.

Fig. 16.3 (**a**) Distribution of loess in Europe (Redrawn in simplified form from Haase et al. (2007)). Also shown are major rivers (*solid blue lines*) and the approximate extent of the Scandinavian ice sheet (*light purple*) during the last glacial period (*thick dashed line*) (Simplified from Flint (1971)). *CR* Czech Republic, *H* Hungary. (**b**) Distribution of loess in Asia (Compiled from Velichko et al. (1984, 2006), Liu (1985), Dodonov (2007), and Frechen et al. (2009a)). Note: loess is also reported for Japan (Watanuki et al. 2005; Matsu'ura et al. 2011), but distribution maps are not shown in those reports. Ice sheet extents during the last glacial period (*light purple*) are approximate (Redrawn from Flint (1971))

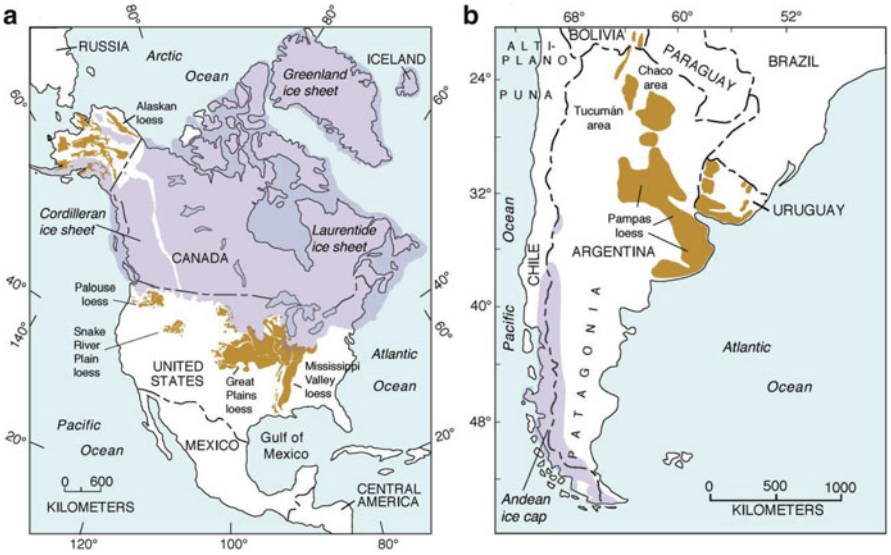

Fig. 16.4 (**a**) Distribution of loess in North America and the extent of ice sheets during the last glacial period (*light purple*) (Redrawn from Péwé (1975), Bettis et al. (2003), Busacca et al. (2004), and sources therein). (**b**) Loess distribution in South America and ice extent (*light purple*) during the last glacial period (Redrawn from Zárate (2003, 2007) and sources therein)

At lower latitudes in Europe, thick loess deposits have been described in the Carpathian basin along the Danube River, corresponding to the succession of several glacial–interglacial cycles (Markovic et al. 2006, 2009). The stratigraphy is much different than is typically observed elsewhere in Europe, with the appearance of a rather homogenous period of loess deposition (Antoine et al. 2009a), including an absence of the loess–paleosol doublets identified at localities in the 50 °N latitude loess belt. The environmental conditions appear to have been much drier during the whole last climate cycle, with conditions again allowing the occurrence and development of C_4 plants, indicative of vegetation living under severe moisture stress (Hatté et al. 2013).

16.8.2 Africa and the Middle East

Loess in Africa and the Middle East is not as extensive and thick as in Europe and in North America: it is patchy in nature (Fig. 16.6). Yet loess is the parent material for some of the most fertile soils in these regions. A few characteristics are common to all reported desert loess sites in Africa and the Middle East (following Crouvi et al. (2010)): (1) loess bodies are located in semiarid to subhumid climate

Fig. 16.5 (**a**) Map of Australia showing the approximate areas with widespread fine-grained loess (parna) deposits and patchy to isolated loess deposits (this study), localities where dust additions to soils are documented, and last glacial maximum dust additions to offshore areas ("LGM dust") (Compiled by Hesse and McTainsh (2003)). Also shown is the distribution of aeolian sand (stippled areas) in Australia, with inferred paleowind directions (All from Bowler et al. (2001)). (**b**) Distribution of loess in New Zealand (Redrawn from Eden and Hammond (2003))

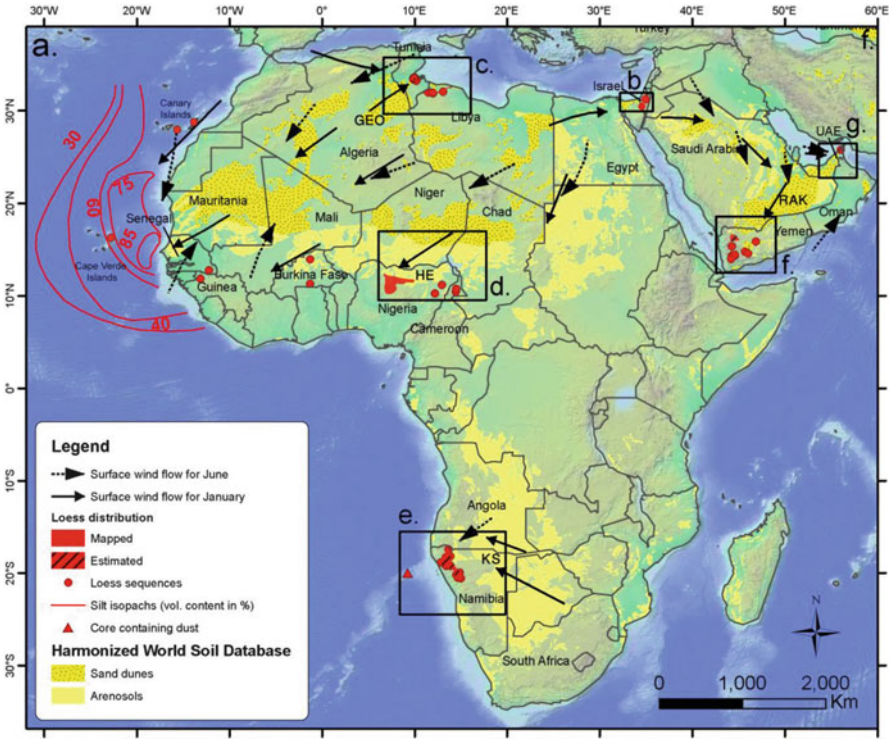

Fig. 16.6 (**a**) Spatial distribution of loess in Africa and the Middle East, active sand seas, and Arenosols (sandy soils) (From Crouvi et al. 2010 and references therein). Near-surface dominant wind directions for January and June are based on Breed et al. (1979). Red contours are content of silt (24 μm mode) in oceanic sediments off the West Africa coast deposited during the last glacial maximum (Sarnthein et al. 1981, see also Chap. 17). *Black rectangles* mark the location of well-studied loess sites in these regions mentioned in the text and in Crouvi et al. (2010): (**b**) Israel (Negev), (**c**) Tunisia and Libya, (**d**) Nigeria, (**e**) Namibia, (**f**) Yemen, and (**g**) the UAE. Abbreviations: *GEO* Grand Erg Oriental, *HE* Hausaland Erg, *KS* Kalahari Sands, *RAK* Rub' al Khali

regions; (2) at most sites, loess covers an area of 10^3–10^4 km^2; (3) loess sediments are dominated by coarse silt to very fine sand grains, with median grain size ranging from 50 to 80 μm; in some sites, the particle size distribution (PSD) is reported to be tri- or bimodal; (4) the loess bodies are generally characterized by calcic soils; (5) loess mineralogy is mostly quartz and feldspars, with various amounts of carbonate, depending on the degree of soil development in the loess; (6) in most sites, the underlying lithologies are inconsistent with the presence of quartz in the loess and suggest an external source for the silt; (7) the shapes of particles are reported as subangular to angular for most regions; and (8) most loess bodies were deposited during the last glacial period (~110–10 ka).

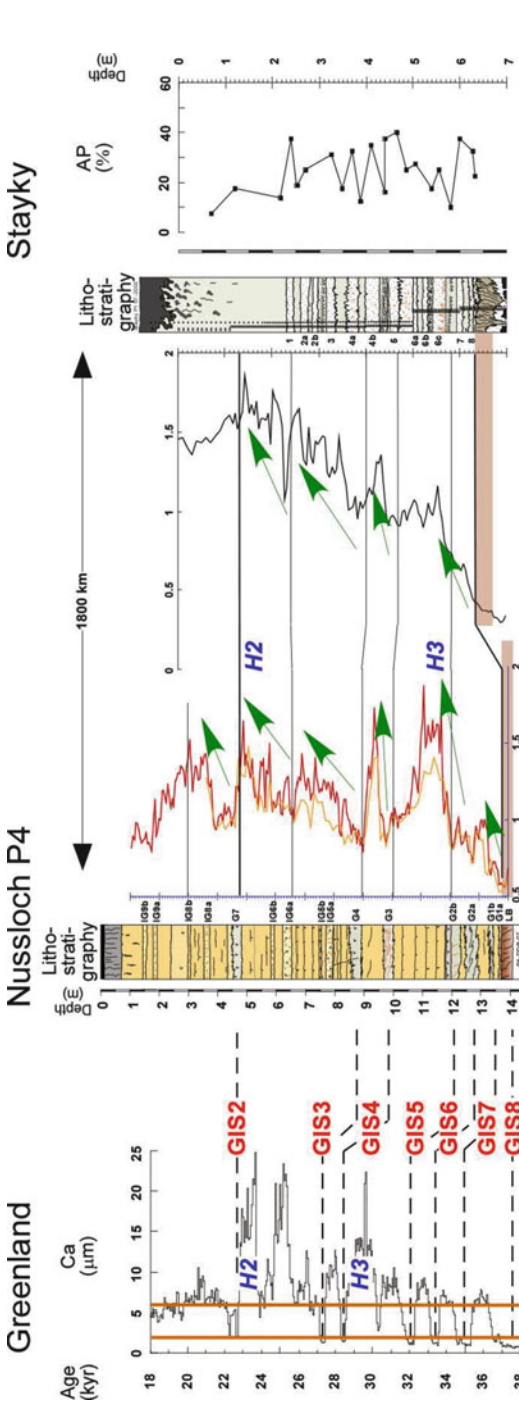

Fig. 16.7 Comparison between the grain size index (GSI) records in Nussloch (P3 and P4 sequences) (After Rousseau et al. 2007b) and in Stayky (Rousseau et al. 2011). Identification of similar cycles (marked by the *green arrows*) and proposed correlation between the two continental records, supported by IRSL dates, and pollen characteristics (arboreal pollen (AP) percentages) of the embryonic soils. Correlation between the Greenland GRIP dust record (Johnsen et al. 2001) and the Nussloch record according to Rousseau et al. (2007b), with GIS 8 correlated with the Nussloch Lohner Boden (LB). H3 and H2 correspond to marine Heinrich events 3 and 2 in the Greenland and European records. G1–7 and IG5–9 are the identified tundra gleys or oxidized horizons in Nussloch (From Rousseau et al. 2011)

The best-studied desert loess in northern Africa is located on the carbonate-rich Matmata Plateau in southern Tunisia (Coudé-Gaussen 1987; Coudé-Gaussen et al. 1987; Coudé-Gaussen and Rognon 1988; Coudé-Gaussen 1990; White et al. 2002; Dearing et al. 2001). The Tunisian loess covers an estimated area of ~4,000 km^2 and reaches thicknesses of up to 20 m. On the basis of radiocarbon ages, Coudé-Gaussen et al. (1987) showed that the age of the Tunisian loess ranges from >43 to 10 ka, whereas a chronology based on optically stimulated luminescence (OSL) (Dearing et al. 2001) suggests that the lower part of this loess is much older (250–100 ka). Loess deposits are also located on a carbonate-rich mountain range in northwestern Libya, between the Jefera Plain to the north and the Tripolitanian Plateau to the south. These deposits are considered to be a continuation of the Tunisian loess (Coudé-Gaussen 1987).

The best-known loess in the Sahel of Africa is the informally named Zaria loess, located on the Kano Plains in central-northern Nigeria (McTainsh 1984, 1987). This is probably one of the largest desert loess regions known in the world, covering an area of 41,000 km^2 and located today in a tropical climate zone. Loess PSD is mainly trimodal, with modes at 75 μm, 44 μm, and <2 μm (McTainsh 1984). OSL dating of the loess indicates an age of 37–10 ka (Stokes and Horrocks 1998). Scattered reports from other Sahelian countries suggest the presence of a noncontinuous loess belt, oriented west to east from southern Senegal through Guinea, Mali, Burkina Faso, Niger, and Nigeria to northern Cameroon; loess-like deposits are also found on the Canary Islands (Figs. 16.1c and 16.6).

Loess in southern Africa is found mainly in northwestern Namibia, where it is located on a vast area between the Great Escarpment to the coast, and it is characterized by variable underlying lithologies (Eitel et al. 2001, 2006; Brunotte et al. 2009). On the basis of the carbonate content and the heavy-mineral assemblage of the loess, Eitel et al. (2001) suggested that the source of the loess was a combination of exposed calcretes from the east and silt from local metamorphic and volcanic rocks. Crouvi et al. (2010) suggested that the main sources of quartz silt in the loess are the nearby quartz-rich Kalahari Sands that lie only a few tens to hundreds of kilometers to the east and southeast of the loess. Linear dunes in these sands are oriented east–west to east–southeast–west–northwest, suggesting an easterly wind regime when the dunes were formed; these easterly winds currently prevail in the region (Fig. 16.6). Similar to the Sahelian loess, the Namibian loess stretches westward into the Atlantic Ocean, as finer silt deposits from marine cores are reported off the Namibian coast (e.g., Stuut et al. 2002, see also Chap. 17). There is a good temporal correlation between the period of sand-dune activity, loess accumulation, and silt deposition off the Namibian coast (Crouvi et al. 2010).

The most prominent loess in the Middle East is located in the Negev desert, southern Israel, covering an area of ~5,500 km^2 (Figs. 16.1d and 16.6). It mantles most of the exposed carbonate bedrock in the northern Negev and fills depressions and valleys farther south in the central Negev highlands (Yaalon and Dan 1974). The PSD of the loess is bimodal (50–60 μm and 3–8 μm), with a general upward increase of the coarse mode versus the fine mode in all sequences that have been studied (Crouvi et al. 2008, 2009). Bulk mineralogy is quartz, calcite,

phyllosilicates, and feldspars, whereas the coarse mode is composed mostly of quartz and feldspars (Crouvi et al. 2008). Recent OSL ages suggest that the upper Pleistocene Negev loess started accumulating at 95 ka (Crouvi et al. 2008, 2009).

Crouvi et al. (2008, 2009) suggested that the main sources of the coarse silt grains in the loess are the adjacent sand dunes in western Negev and Sinai that advanced eastward during the late Pleistocene. These studies based their suggestion mainly on the observation that the increase of the PSD fraction of coarse silt grains in the loess (composed mainly of quartz) is temporally associated with the incursions of adjacent sand dunes upwind from the loess. Elsewhere in the Middle East, loess is found in northwestern Yemen (Fig. 16.6), on the volcanic plateau of Sana (Grolier and Overstreet 1978; Nettleton and Chadwick 1996; Wilkinson 1997), and in the United Arab Emirates (Goudie et al. 2000).

In a recent compilation, Crouvi et al. (2010) suggested that for all reported loess in Africa and the Middle East, sand seas supply the coarse silt for desert loess, based on the following observations: (1) all loess sites are spatially associated with adjacent sand seas (Fig. 16.6) and are located only a few tens of kilometers from sand dunes, within the range for aeolian transport of coarse silt grains (Tsoar and Pye 1987); (2) there is a good agreement between the mineralogical composition of the loess and that of the sand dunes; (3) according to the paleowind direction interpreted from the orientation of the sand dunes, all loess sites are located downwind of the adjacent sand seas; (4) there is evidence of decreases in grain size downwind from the sand dunes toward the loess in a few sites; and (5) the estimated ages of loess deposition and dune activity generally overlap, where, in most cases, sand-dune activity preceded loess deposition, and no data indicate loess deposition preceding sand-dune activity.

The identification of sand dunes as the source for coarse silt grains in downwind loess deposits can support or rebut different hypotheses for the generation of silt in deserts. Because, in most places, sand dunes are composed of well-sorted sand grains, with limited amounts of coarse silt grains, this observation strengthens the hypothesis raised in the past that aeolian abrasion of sand grains is one of the important mechanisms for generating silt grains in deserts (e.g., Whalley et al. 1982; Crouvi et al. 2010; Enzel et al. 2010). The reported angularity of desert loess grains supports this hypothesis. Laboratory experiments show that aeolian abrasion of sand grains produces both coarse and fine silt grains (e.g., Whalley et al. 1982; Bullard et al. 2004). Given the absence of glacial activity near most low-latitude deserts, even during the late Pleistocene, and the large sand seas there (Fig. 16.6), it is reasonable that spalling might be the dominant source of silt, at least locally.

16.8.3 Asia

Loess mantles extensive regions in Asia, especially in the largest midlatitude arid–semiarid zone in the Northern Hemisphere (Fig. 16.3b). The most widespread loess deposits in Asia occur in China, centered in the Loess Plateau, where the oldest loess

can be dated back to 22–25 Ma (Guo et al. 2002; Qiang et al. 2011), and loess can be hundreds of meters thick, as at Lanzhou in the western Loess Plateau (Burbank and Li 1985). Loess is also found in Central Asia including Tajikistan, Kyrgyzstan, Turkmenistan, Uzbekistan, and Kazakhstan. Regardless of where the loess is found in Asia, all loess bodies are bordered by or in the downwind areas of gobi (stony desert) and sand deserts.

Loess in China is widespread between latitudes 34–45 °N and longitudes 75–130 °E (Fig. 16.3b). Although the most continuous loess cover is in the central part of northern China, forming the Loess Plateau, loess deposits also occur on pediments in the forelands of high mountains in northeastern China. On the Loess Plateau, the thickness of loess varies from tens to hundreds of meters, found at elevations ranging from 1,000 to 1,500 m. In northwestern China, loess is found mainly blanketing mountain slopes, with thickness usually less than tens of meters, but the elevation where it is found can be up to 4,000 m.

In Central Asia, loess deposits are adjacent to mountain regions and dominantly cover piedmonts and hills (Dodonov 1991, 2007). In contrast to the Chinese Loess Plateau, loess in Central Asia mostly accumulates on the windward slopes of the Central Asian orogenic belt (including the Tian Shan, Kunlun, Hindu Kush, and Pamir Mountains), where loess can be found at elevations of up to 2,500–3,000 m (Dodonov 1991). Generally, loess deposits in Central Asia are several tens of meters thick, except in certain regions, such as Tajikistan, or in the vicinity of Tashkent, where the loess strata can be up to 100–200 m (Dodonov 1991; Ding et al. 2002a).

For Chinese loess, the basal age of the Quaternary loess–paleosol successions is near the Gauss/Matuyama (G/M) geomagnetic polarity boundary (Heller and Liu 1982; Liu 1985), with an age of about 2.58 Ma. More recently, the Neogene Red Clay (Fig. 16.1b), also on the Loess Plateau, has now been demonstrated to be aeolian. The latter deposits are discontinuously overlain by the Quaternary loess–soil successions, being usually younger than 8 Ma in most sites (Ding et al. 1998; Qiang et al. 2001), with the exception of the Qinan section that extends to 22 Ma (Guo et al. 2002). The most recent study in the Junggar basin of northwestern China reveals aeolian deposits of 24 Ma (Sun et al. 2010), whereas a long core taken on the western Loess Plateau reveals aeolian dust accumulation that can be dated back to 25 Ma (Qiang et al. 2011). In Central Asia, stratigraphic and chronological studies have previously shown that loess began to accumulate about 2–2.5 Ma ago and the loess–soil sequences at different sites can be correlated with each other (Dodonov 1991; Dodonov and Baiguzina 1995).

For the most extensive and thickest loess deposits on the Loess Plateau, a vast provenance of northwestern China had been proposed (Liu 1985). However, multiple isotopic, chemical, and mineralogical data demonstrate that the loess deposits on the Loess Plateau are mainly derived from the gobi deserts that lie to the north of the Loess Plateau, whereas aeolian dust entrained from the three inland arid basins (the Tarim, Junggar, and Qaidam basins) of northwestern China contributes very little to the loess deposits on the Loess Plateau. Dust from these basins accumulates mainly on the piedmont forelands of high mountains surrounding the basins (Sun et al. 2001; Sun 2002a, b). Moreover, although these gobi and sand

deserts are regarded as the main source regions, they serve as dust and silt holding areas rather than dominant producers. The mountain processes (including glacial grinding, frost weathering, salt weathering, tectonic processes, and some fluvial comminution) in the Gobi Altay Mountains, Hangayn Mountains, and the Qilian Mountains have played an important role in producing the vast amounts of loess-sized material for forming the Loess Plateau (Sun 2002a).

Sun et al. (2007) argued that fine silt- to clay-sized quartz in the northwestern deserts are heterogeneous and derived mainly from the nearby high-altitude mountains in East Asia, whereas the eastern deserts in China mainly have a local source. Based on the luminescence sensitivity variations of quartz grains from Chinese deserts, four regional groups of Chinese deserts can be distinguished including the eastern, central, western, and northwestern deserts. The different luminescence sensitivity signals are dominantly related to the rock types of mountains surrounding or adjacent to the deserts (Lü and Sun 2011).

Temporal variations of loess provenance have also been studied. Based on temporal variations in Sr, Nd, and Pb isotopes and trace element concentrations within airborne dust on the central Loess Plateau (Sun 2005; Sun and Zhu 2010), a distinct change in source occurred at about 2.6 Ma. This change in the source of aeolian dust at 2.6 Ma is considered to be coincident with the initiation of Quaternary glaciation in the Northern Hemisphere. The dramatic climatic cooling induced glacial grinding, which plays an important role in modifying the source material of the dust.

Loess accumulation in Central Asia is closely linked to the geographic and atmospheric conditions in the area. The great deserts such as Karakum, Kyzylkum, and Sary-Ishikotrau are situated directly to the west and northwest of the loess region, covering the windward piedmont forelands and river valleys of Tian Shan and the Pamir Plateau (e.g., Dodonov and Baiguzina 1995; Finaev 1995; Ding et al. 2002a). In addition, airborne dust can be also transported to Iran and accumulate as loess (Asadi et al. 2012). Paleowinds in northeastern Iran were dominated by northerly or northeasterly winds blowing from Central Asia, as suggested by the delineation of dune fields in the Karakum Desert, in Turkmenistan (Rozychi 1991; Letolle and Mainguet 1993), and by the spatial distribution of loess deposits along Kopeh Dagh (Kehl 2009).

Loess–paleosol sequences on the Loess Plateau of north-central China (Fig. 16.1a) have provided abundant information about regional and global climate changes during the Quaternary (Heller and Liu 1982; Kukla and An 1989). The most important studies of the orbital-scale paleoclimatic record on the Loess Plateau were completed by Ding's group (Ding et al. 1993, 1994, 2002b). Based on detailed pedostratigraphy and magnetostratigraphy of the Baoji section, thirty-seven pedostratigraphic units are identified, representing thirty-seven major cold-to-warm climatic cycles in the past 2.5 Ma (Ding et al. 1993).

For the Central Asia loess, the best long-term paleoclimatic record is the Chashmanigar loess section (Fig. 16.8) of southern Tajikistan (Ding et al. 2002a; Yang and Ding 2006; Yang et al. 2006). This section is about 200 m thick and consists of an alternation of loess and paleosol layers with a basal age of about 1.77 Ma (Ding et al. 2002a). The high-resolution magnetic susceptibility,

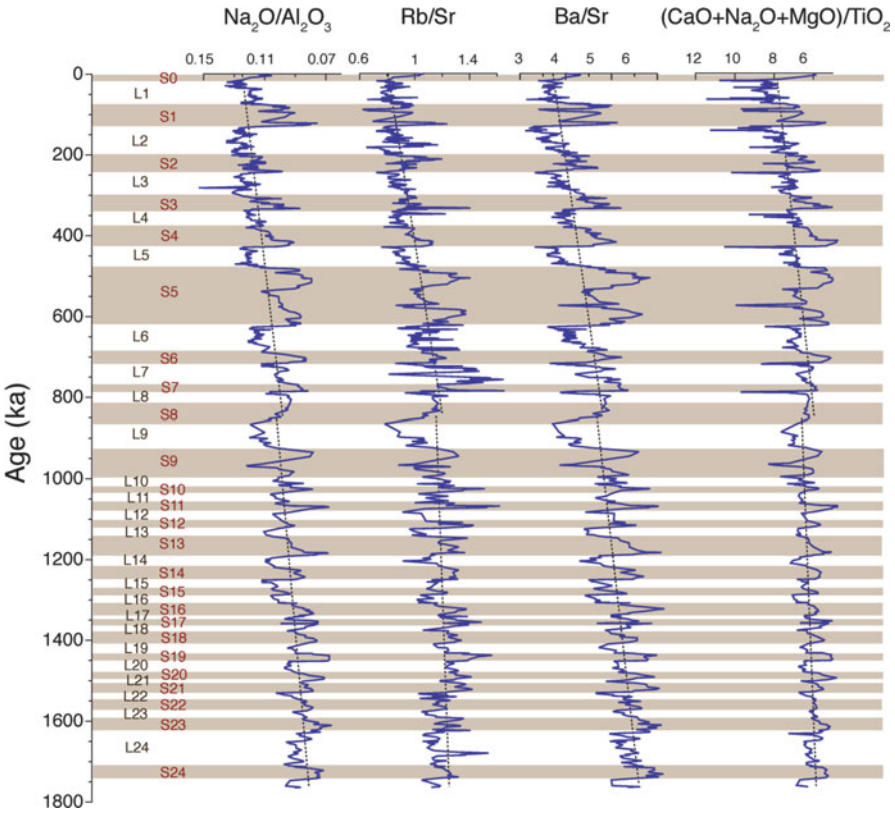

Fig. 16.8 Changes in Na_2O/Al_2O_3 (weight–percent ratio, not molar ratio), Rb/Sr, Ba/Sr, and $(CaO + Na_2O + MgO)/TiO_2$ (weight–percent ratio, not molar ratio) at loess–paleosol section at Chashmanigar, Tajikistan. The timescale is taken from Ding et al. (2002b). The *shaded zones* indicate interglacials, as represented by paleosols. Greater alteration of weatherable minerals in paleosols can be seen in these plots (note reversed horizontal scales on Na_2O/Al_2O_3 and $(CaO + Na_2O + MgO)/TiO_2$ plots). The *dashed lines* are linear fits of each curve for different time intervals (Redrawn from data in Yang et al. (2006))

grain size, and color reflectance time series all show astronomical periodicities during the Pleistocene. The mid-Pleistocene climate transition, characterized by a shift of dominant climatic periods from 41 to 100 kyr at about 1.0–0.8 Ma, is clearly documented in these proxy records (Ding et al. 2002a). It is suggested that alternations of loess and soil horizons in Central Asia were controlled by global ice volume variations. The long-term chemical weathering history of this section (Fig. 16.8) indicates a decreasing chemical weathering trend since 0.85 Ma (Yang et al. 2006). This event may be causally related to the expansion of Northern Hemisphere ice and/or the regional tectonic uplift of high mountains in Asia since the mid-Pleistocene.

16.8.4 Australia and New Zealand

Despite the proximity of the two countries, the understanding and characterization of loess in Australia and New Zealand are vastly different, due to differences in landscape processes, paleo- and contemporary climatic regimes, and sedimentological nomenclature. Whereas in the generally cooler, wetter New Zealand, loess is widespread and very well described, in Australia there is a scarcity of published work describing "loess" and a general view that soil derived from fine-grained aeolian sediment is quite restricted in distribution. Undoubtedly, the dominance of the cold-climate loess paradigm throughout the twentieth century entrenched the view that loess was largely absent from the Australian continent. But over the past two decades, a counterview has emerged that the hitherto described "parna" (Butler 1956) should be regarded as clayey, hot-climate loess (Dare-Edwards 1984; Hesse and McTainsh 2003; Haberlah 2007). In this chapter, parna will be regarded as fine-grained loess.

At present on the Australian continent, there are two major wind paths emanating from the arid interior. One of these extends in an east–southeasterly direction across the eastern states to the Tasman Sea, and the other extends in a northwesterly direction across Western Australia to the Indian Ocean (Fig. 16.5a). It is along the so-called southeastern dust path that the majority of the identified Australian loess deposits exist. In particular, southern New South Wales and northern Victoria have prominent areas of red, clayey, and often calcareous soil derived from clayey loess (parna) deposits.

The fine-grained material that dominates Australian loess deposits is characterized by a relatively high clay content; the presence of coarse, silt-sized quartz; a strong red to yellow color; and a variable presence of calcium carbonate. Indeed, it is the combination of these attributes in soil profiles over a variety of lithologies that first led Butler (1956) to identify and popularize the concept of "parna" on the Riverine Plain. Mineralogically, these clayey loess deposits are dominated by kaolinite, illite, and quartz (Beattie 1970), with inclusions of calcium carbonate being more prevalent at the arid–semiarid western end of the deposition zone.

The current understanding of the genesis of Australian parna is that during arid and windy glacial periods of the Quaternary, fine-grained materials were winnowed from the sand hills, playas, and floodplains of what are now western New South Wales, northwestern Victoria, and eastern South Australia and deposited 300–500 km downwind as a blanket of sediment. A central tenet of this model is that while the transported material contained considerable clay-sized particles, it was transported in the form of silt-sized pellets accompanied by quartz companion grains. Unfortunately, there is a dearth of reliable age estimates for loess deposits in eastern Australia.

In New Zealand, loess mantles are widely distributed across both the North and South Islands, with McCraw (1975) estimating that 10 % of the country's land mass ($\sim$26,000 km^2) is covered by loess at least a meter thick (Fig. 16.5b). The range of loess mantle thickness is 0.5–6.0 m (Eden and Hammond 2003), but

the thickest mantles are located in the southern parts of the North Island and the eastern and southern parts of the South Island (Fig. 16.5). On the North Island, loess deposits are most prominent in the Manawatu region, where old terraces of cold-climate floodplains have been mantled by dust from nearby braided streambeds (Molloy 1998), and in the inland basins of Hawke's Bay. On the South Island, loess deposits are most prominent on the high terraces of the Canterbury Plain, the North Canterbury and South Canterbury downlands, the Banks Peninsula, and the South Otago downlands and Southland Plains (Molloy 1998).

New Zealand loesses tend to exhibit more "classical loess" features: silty loam texture, pale colors, and weak/massive structure (Fig. 16.2d). In many localities, loess facies are characterized by multiple paleosol horizons and/or inclusions of tephric layers (Eden and Hammond 2003), while fragipans are a feature of some relatively unaltered loess deposits. Common minerals in New Zealand loess deposits and soil developed therein include quartz, feldspars, micas, vermiculite, kaolinite, and halloysite. Where volcanic ash has contributed significantly to the loess deposit, ferromagnesian minerals, allophane, and volcanic glass may be prominent (McCraw 1975; Molloy 1998; Eden and Hammond 2003).

Most loess in New Zealand has been produced by cold-climate processes, such as freeze/thaw action and glacial grinding, as well as river abrasion, comminution, and sorting (Eden and Hammond 2003). The North Island loess deposits are nearly all products of fluvial processes and the winnowing of dry streambeds, while in the South Island cold-climate loess processes operated in the Southern Alps during the Quaternary glacial periods, supplying silt-sized sediment to the rivers of the eastern half of the island for eventual winnowing and transport to adjacent plains and downlands. A further form of loess, tephric loess or volcanic loess, also occurs in and near the central volcanic region of the North Island (Eden and Hammond 2003), but the significance of this tephric parent material is perhaps greatest from a chronological standpoint. Volcanic ash conveniently identifies (and separates) the Ohakea loess, which was laid down across the Manawatu between 25,000 and 12,000 years ago and which acts as the parent material for the present-day soils (Molloy 1998). In the South Island of New Zealand, accretion rates and ages of loess deposits have been estimated through the identification of the Kawakawa Tephra (deposited ~26,0000 years before present), thermoluminescence techniques, and ^{14}C dating (Eden and Hammond 2003).

16.8.5 South America

South American loess presents a broad geographic distribution (Fig. 16.4b) extending across the Chaco–Pampean Plain of Argentina and neighboring areas of Uruguay, southern Brazil (Rio Grande do Sul), Paraguay, and the eastern Bolivia lowlands (Zárate 2003). Loess is extensive in the western Chaco (Iriondo 1997) and forms a wide belt in the eastern Pampas, grading into sand mantles and dune

fields toward the west and southwest. Thick loess deposits are located in the sub-Andean mountainous area of northwestern Argentina (Tucumán); they also occur in the highland plains of Sierras Pampeanas of Córdoba and San Luis. In addition, loess has been reported in Tierra del Fuego and the eastern Andean piedmont (Zárate 2003), while Holocene peridesert loess has been reported in the Atacama Desert of Peru (Eitel et al. 2005).

Much of the knowledge of South American loess comes from the Pampean Plain where the deposits consist of complex stratigraphic sequences composed of primary loess and loess-like (loessoid) deposits that are usually much more abundant (Fig. 16.2c; Zárate and Blasi 1993; Zárate et al. 2009). Loess deposits are commonly interlayered with fluvial gravels and/or colluvial deposits along the piedmonts of the southern Buenos Aires ranges (Ventania, Tandilia) and the Pampean ranges of Córdoba and San Luis provinces. Carbonate accumulations of variable morphology and genesis are common in the loess sequences. Fossil vertebrate remains are very common, together with abundant bioturbation features of both vertebrates and invertebrates (Zárate 2007).

The Pampean stratigraphic record dates back to the late Miocene (~12–10 Ma). The thickest (~40–50 m) Quaternary loess and loess-like deposits are located in the northern Pampas with only the uppermost 10–15 m exposed. The loess sedimentation process during the Neogene–Quaternary was characterized by the occurrence of several pulses of landscape reactivation marked by major erosional episodes (Folguera and Zárate 2011).

The chronology of the Pampean loess sequence traditionally has been estimated on the basis of their vertebrate fossil content, being subdivided into several biostratigraphic units (land mammal ages; see Marshall et al. 1983) later redefined as stage–ages (Cione and Tonni 1995). In recent years, numerous luminescence dates were obtained from several upper Quaternary sections of the northern and southern Pampas (e.g., Kemp et al. 2006; Frechen et al. 2009b; Kruck et al. 2011).

The loess–paleosol sequences in the mountains of the Tucumán region (Kemp et al. 2003) are situated at an altitude between 1,800 m and 2,500 m asl and west of the western Chaco Plain (Fig. 16.4b). This sequence, which exhibits a much higher stratigraphic resolution than the Pampean successions, consists of a thick (~40–50 m) record of loess and reworked loess. The deposits, rich in vertebrate fossil remains, are characterized by the occurrence of numerous (28–32) discrete paleosols (Zinck and Sayago 2001; Schellenberger and Veit 2006).

The Pampean loess deposits are chiefly of volcanoclastic composition, with particles made up of volcanic lithic fragments (basaltic, andesitic, and rhyolithic rocks), volcanic glass shards, feldspar (mainly orthoclase), plagioclase (albite to labradorite), and quartz, usually with percentages lower than 20 %. The mineralogical and geochemical compositions of loess and loess-like deposits (Teruggi 1957; Smith et al. 2003) suggest that the explosive, volcanic Andes Cordillera is the main loess source area, including the direct input of volcanic particles as well as discrete tephra layers. The mountain loess of Tucumán is thought to be derived from the northwestern Argentinian/southern Bolivian Andes and the Altiplano

(Schellenberger and Veit 2006). Secondary source areas of loess are present across the region that comprise the Pampean ranges of Córdoba and San Luis, the Paraná River basin, the southern Buenos Aires ranges (Ventania and Tandilia), the ranges and outcrops of Paleozoic and Mesozoic rocks of the south-central Pampas, and likely the igneous and metamorphic rocks of southern Uruguay (Zárate 2003, and references therein). The accumulation of loess has been explained through a combined mechanism of fluvial and aeolian transport from the Andes to the eastern lowlands.

The loess–paleosol pattern of South America, even back to the Pliocene, is interpreted to be the result of cyclic climatic conditions, with loess accumulating during glacial intervals and soils developing during periods of climatic amelioration, interglacials and interstadials (Kemp and Zárate 2000). Recently, Rabassa et al. (2011) reported late Pliocene glacial deposits in the northern Patagonian Andes, making more plausible the linkage between the loess accumulation and glacial conditions at this time interval. The mountain Loess Plateau of Tucumán and the northern Pampas of Buenos Aires province provide long and quasi-continuous records that have permitted inferences of the environmental history during a considerable time span of the Pleistocene.

The accumulation of loess deposits was widespread across different localities of the northern and southern Pampas between ~30 ka and ~10 ka. The significant aeolian activity during this interval is also suggested by OSL ages that indicate active dunes in the western sand-dune fields that fringe the eastern Pampean loess belt (Tripaldi and Forman 2007; Tripaldi et al. 2011). A major decrease of the loess accumulation rate occurred at the Pleistocene–Holocene transition (~12–9 ka) when soil formation began to dominate in several areas of the eastern Pampas, giving way to the development of modern soils. While the Holocene is basically documented by soil formation in the eastern Pampas, some settings of the southern Pampas (Tandilia range, Bahia Blanca) document loess accumulation between ~5 and 4 ka.

Southern South America has been proposed as the likely source area of the dust found in Antarctica (Delmonte et al. 2004, see Chap. 18). Patagonia, the Chaco–Pampean region, and the continental shelf are the specific areas considered to be potential dust sources. Gaiero (2007) and Gaiero et al. (2013) point out that isotopic data indicate that Patagonia and the Puna–Altiplano Plateau could represent the most important Southern Hemisphere provenance areas for glacial dust deposited in East Antarctica.

16.8.6 North America

In North America, loess is found mostly beyond the margins of where the Laurentide and Cordilleran ice sheets and mountain glaciers advanced during the last glacial period (Bettis et al. 2003; Roberts et al. 2007). In the northwestern part of North America, loess is found in Alaska and the adjacent western parts of Yukon Territory

of Canada (Muhs et al. 2003). There are also large tracts of loess in the Palouse area of eastern Washington and adjacent Oregon and the Snake River Plain and adjacent uplands of Idaho. By far, however, the greatest extent of loess is found in the mid-continent region, including the greater Mississippi River drainage basin and the Great Plains (Fig. 16.4a).

In the greater Mississippi River basin (including the Missouri and Ohio river drainage basins), south of the Laurentide ice sheet, loess is dominantly glaciogenic, although there are non-glacial contributions (Grimley 2000; Bettis et al. 2003). Thus, loess units represent glacial periods and paleosols represent interglacial or interstadial periods. To a great extent, therefore, loess deposition is a "turn-on/turn-off" process that differs from the more complex pattern seen in China. In this region, the three youngest loess units are the Loveland Loess of penultimate glacial age, the Roxana Silt of early last glacial age, and the Peoria Loess of late last glacial age. Dating of Peoria Loess to the last glacial period, about 25,000–12,000 radiocarbon years ago, is based on studies conducted at dozens of sections (Bettis et al. 2003). Peoria Loess can reach extraordinary thickness, up to ~40 m in some sections in western Iowa (Bettis et al. 2003).

Farther west, in the Great Plains region, studies by Aleinikoff et al. (2008) and Muhs et al. (2008) show that sedimentary rock (volcaniclastic siltstone) is the most important source of silt-sized particles in the Peoria Loess of last glacial age (Fig. 16.2a). Despite the different modes of origin of Great Plains loess, radiocarbon and OSL ages indicate that Peoria Loess in the Great Plains was deposited at about the same time as Peoria Loess farther east (Roberts et al. 2003; Muhs et al. 2008). Thus, even without glaciers, the Great Plains region experienced favorable conditions for loess formation during the last glacial period. Unlike the Mississippi River basin, however, the Great Plains region also has a younger Holocene loess called the Bignell Loess.

The loess deposits in the Columbia Plateau, or "Palouse" region (Fig. 16.4a), present a very different record than those of other parts of North America. In this area, loess records may extend as far back as 1–2 Ma (Busacca 1991). The loess deposits preserve many paleosols (Fig. 16.2b), reflecting periods of nondeposition and stability between times of more active loess deposition. The timing of the deposition of loess in the Palouse region of eastern Washington differs from that for other loess deposits of North America and, indeed, the world (Busacca et al. 2004). In this area, the principal source of the loess is believed to be flood sediments of proglacial Lake Missoula, exposed during glacial maxima at least six times in the Pleistocene (Busacca et al. 2004). Thus, the production of the loess deposits is believed to peak late in the glacial cycle.

Loess is widely distributed in Alaska and adjacent Canada and is geographically the most extensive surficial deposit in the region (Fig. 16.4a). In central Alaska, studies by Westgate et al. (1990) indicate that the Alaskan loess record may extend back to ~3.0 Ma. The thicknesses of the deposits range from a few centimeters in some areas to more than 60 m near Fairbanks. Throughout Alaska, loess deposits are thickest near rivers, with thicknesses decreasing rapidly with distance away

from the rivers and downwind of valley dust sources (Péwé 1975; Muhs et al. 2004). The transport and deposition of loess are processes that are still active today in Alaska, particularly along the Delta, Knik, Matanuska, and Copper Rivers, all of which drain mountain ranges with glaciers. Holocene loess is exposed in these valleys. Although there is indirect evidence for glacial-age loess in Alaska, there are surprisingly few ages that actually document last glacial-aged loess (see review in Muhs et al. 2003). Paleosols are common in central Alaskan loess, indicating that loess deposition here, like elsewhere, has been episodic.

16.9 Conclusion

Loess is aeolian sediment that is dominated by silt-sized particles. Unlike both coarser dune sand and finer-grained LRT dust, loess is relatively poorly sorted, reflecting a combination of transport processes, including saltation, low suspension, and high suspension. Loess can be readily identified in the field and has thicknesses ranging from a few centimeters to many tens of meters. It is found over large areas of Europe, Asia, South America, and North America, and smaller areas of New Zealand, Australia, Africa, and the Middle East. Most loess deposits have compositions that are similar to and reflect derivation from the upper continental crust. Loess can be derived from glacially ground rock and silt particles derived from "desert" (non-glacial) processes of rock breakup or simply inherited from silt-sized sedimentary rocks or silt-sized tephra.

Loess has distinct advantages over other Quaternary sediments for documenting climate change in that it provides a direct record of atmospheric circulation and can be dated directly by both luminescence and radiocarbon methods. Loess can be used to reconstruct paleowinds using spatial trends of thickness and particle size. Paleosols are common in loess and represent periods of little or no loess deposition. Paleosols and snails in loess can be used to reconstruct paleoclimates.

In most of Europe and many parts of North America and South America, much loess is clearly tied to glacial-sediment supplies. In both Europe and North America, however, rates of loess deposition varied within glacial periods. In many areas, the stratigraphic record is more complex than a simple correlation of loess with glacial periods and paleosols with interglacial periods. In China, neither loess deposition nor soil formation ever ceases completely, so sedimentation and pedogenesis are best portrayed as competing processes that are modulated by climate change. Still, glacial periods show higher rates of loess deposition than interglacial periods. In the Great Plains of North America, non-glacial sources of loess were available during both glacial and interglacial periods, but much greater rates of deposition occurred during glacial periods, indicating that a glacial-type climate is one that is most favorable to thick loess accumulation.

References

Aleinikoff JN, Muhs DR, Bettis EA III, Johnson WC, Fanning CM, Benton R (2008) Isotopic evidence for the diversity of late Quaternary loess in Nebraska: glaciogenic and non-glaciogenic sources. Geol Soc Am Bull 120:1362–1377

Antoine P, Rousseau D-D, Zöller L, Lang A, Munaut AV, Hatté C et al (2001) High-resolution record of the last interglacial-glacial cycle in the loess palaeosol sequences of Nussloch (Rhine Valley-Germany). Quatern Int 76(77):211–229

Antoine P, Rousseau D-D, Fuchs M, Hatté C, Gauthier C, Markovic SB et al (2009a) High-resolution record of the last climatic cycle in the southern Carpathian Basin (Surduk, Vojvodina, Serbia). Quatern Int 198:19–36

Antoine P, Rousseau D-D, Moine O, Kunesch S, Hatté C, Lang A et al (2009b) Rapid and cyclic aeolian deposition during the last glacial in European loess: a high-resolution record from Nussloch, Germany. Quatern Sci Rev 28:2955–2973

Asadi S, Moore F, Keshavarzi B (2012) The nature and provenance of Golestan loess deposits in northeast Iran. Geol J. doi:10.1002/gj.2466

Beattie JA (1970) Peculiar features of soil development in parna deposits in the eastern Riverina, NSW. Aust J Soil Res 8:145–156

Bettis EA III, Muhs DR, Roberts HM, Wintle AG (2003) Last glacial loess in the conterminous U.S.A. Quatern Sci Rev 22:1907–1946

Blatt H (1987) Oxygen isotopes and the origin of quartz. J Sediment Petrol 57:373–377

Bowler JM, Wyrwoll K-H, Lu Y (2001) Variations of the northwest Australian summer monsoon over the last 300,000 years: the paleohydrological record of the Gregory (Mulan) lakes system. Quatern Int 83–85:63–80

Breed CS, Fryberger SG, Andrews S, McCauley C, Lennartz F, Gebel D, Horstman K (1979) Regional studies of sand seas, using Landsat (ERTS) imagery. In: McKee ED (ed) A study of global sand seas. United States Geological Survey, Professional Paper 1052, Washington, pp 305–397

Brunotte E, Maurer B, Fischer P, Lomax J, Sander H (2009) A sequence of fluvial and aeolian deposits (desert loess) and palaeosoils covering the last 60 ka in the Opuwo basin (Kaokoland/Kunene Region, Namibia) based on luminescence dating. Quatern Int 196:71–85

Bullard JE, McTainsh G, Pudmenzky C (2004) Aeolian abrasion and modes of fine particle production from natural red dune sands: an experimental study. Sedimentology 51:1103–1125

Burbank DW, Li JJ (1985) Age and palaeoclimatic significance of the loess at Lanzhou, north China. Nature 316:429–431

Busacca AJ (1991) Loess deposits and soils of the Palouse and vicinity. In: Morrison RB (ed) The geology of North America vol. K-2, Quaternary nonglacial geology; conterminous U.S. Geological Society of America, Boulder, pp 216–228

Busacca AJ, Begét JE, Markewich HW, Muhs DR, Lancaster N, Sweeney MR (2004) Eolian sediments. In: Gillespie AR, Porter SC, Atwater BF (eds) The Quaternary period in the United States. Elsevier, Amsterdam, pp 275–309

Butler BE (1956) Parna – an aeolian clay. Aust J Sci 18:145–151

Cione AL, Tonni EP (1995) Chronostratigraphy and "land-mammal ages" in the Cenozoic of southern South America: principle, practices, and the "Uquian" problem. J Paleontol 69:135–159

Coudé-Gaussen G (1987) The perisaharan loess: Sedimentological characterization and paleoclimatical significance. GeoJournal 15:177–183

Coudé-Gaussen G (1990) The loess and loess-like deposits along the sides of the western Mediterranean Sea; genetic and palaeoclimatic significance. Quatern Int 5:1–8

Coudé-Gaussen G, Rognon P (1988) The upper Pleistocene loess of Southern Tunisia: a statement. Earth Surf Process Landf 13:137–151

Coudé-Gaussen G, Rognon P, Rapp A, Nihlen T (1987) Dating of peridesert loess in Matmata, south Tunisia, by radiocarbon and thermoluminescence methods. Z Geomorphol N F 31:129–144

Crouvi O, Amit R, Enzel Y, Porat N, Sandler A (2008) Sand dunes as a major proximal dust source for late Pleistocene loess in the Negev desert, Israel. Quatern Res 70:275–282

Crouvi O, Amit R, Porat N, Gillespie AR, McDonald EV, Enzel Y (2009) Significance of primary hilltop loess in reconstructing dust chronology, accretion rates, and sources: an example from the Negev desert, Israel. J Geophys Res 114, F02017

Crouvi O, Amit R, Enzel Y, Gillespie AR (2010) The role of active sand seas in the formation of desert loess. Quatern Sci Rev 29:2087–2098

Dare-Edwards AJ (1984) Aeolian clay deposits of south-eastern Australia: parna or loessic clay? Trans Inst Br Geogr NS 9:337–344

Dearing JA, Livingstone IP, Bateman MD, White K (2001) Palaeoclimate records from OIS 8.0-5.4 recorded in loess-palaeosol sequences on the Matmata Plateau, southern Tunisia, based on mineral magnetism and new luminescence dating. Quatern Int 76–77:43–56

Delmonte B, Basile-Doelsch I, Petit J-R, Maggi V, Revel-Rolland M, Michard A, Jagoutz E, Grousset F (2004) Comparing the Epica and Vostok dust records during the last 220,000 years: stratigraphical correlation and provenance in glacial periods. Earth Sci Rev 66:63–87

Ding ZL, Rutter NW, Liu TS (1993) Pedostratigraphy of China loess deposits and climatic cycle in the last 2.5 Myr. Catena 20:73–91

Ding ZL, Yu Z, Rutter NW, Liu T (1994) Towards an orbital time scale for Chinese loess deposits. Quatern Sci Rev 13:39–70

Ding ZL, Sun JM, Liu TS, Zhu RX, Yang SL, Guo B (1998) Wind-blown origin of the Pliocene red clay formation in the central Loess Plateau, China. Earth Planet Sci Lett 161:135–143

Ding ZL, Derbyshire E, Yang SL, Yu ZW, Xiong SF, Liu TS (2002a) Stacked 2.6-Ma grain size record from the Chinese loess based on five sections and correlation with the deep-sea $\delta^{18}O$ record. Paleoceanography 17:1033. doi:10.1029/2001PA000725

Ding ZL, Ranov V, Yang SL, Finaev A, Han JM, Wang GA (2002b) The loess record in southern Tajikistan and correlation with Chinese loess. Earth Planet Sci Lett 200:387–400

Dodonov AE (1991) Loess of Central Asia. GeoJournal 24:185–194

Dodonov AE (2007) Central Asia. In: Elias S (ed) The encyclopedia of Quaternary sciences. Elsevier, Amsterdam, pp 1418–1429

Dodonov AE, Baiguzina LL (1995) Loess stratigraphy of Central Asia: palaeoclimatic and palaeoenvironmental aspects. Quatern Sci Rev 14:707–720

Eden DN, Hammond AP (2003) Dust accumulation in the New Zealand region since the last glacial maximum. Quatern Sci Rev 22:2037–2052

Eitel B, Blumel WD, Huser K, Mauz B (2001) Dust and loessic alluvial deposits in Northwestern Namibia (Damaraland, Kaokoveld): sedimentology and palaeoclimatic evidence based on luminescence data. Quatern Int 76–77:57–65

Eitel B, Hecht S, Mächtle S, Schukraft G, Kadereit A, Wagner GA, Kromer B, Unkel I, Reindel M (2005) Geoarchaeological evidence from desert loess in the Nazca–Palpa region, southern Peru: palaeoenvironmental changes and their impact on pre-Columbian cultures. Archaeometry 47:137–158

Eitel B, Kadereit A, Blumel WD, Huser K, Lomax J, Hilgers A (2006) Environmental changes at the eastern Namib desert margin before and after the last glacial maximum: new evidence from fluvial deposits in the upper Hoanib river catchment, northwestern Namibia. Palaeogeogr Palaeoclimatol Palaeoecol 234:201–222

Enzel Y, Amit R, Crouvi O, Porat N (2010) Abrasion-derived sediments under intensified winds at the latest Pleistocene leading edge of the advancing Sinai-Negev erg. Quatern Res 74:121–131

Finaev A (1995) Processes of transportation and sedimentation of dust aerosol. In: Global analysis, interpretation, and modeling: first science conference, 25–29 Sept 1995, IGBP Secretariat of Germany in Berlin, Garmisch-Partenkirchen, p 22

Flint RF (1971) Glacial and Quaternary geology. Wiley, New York, 906 pp

Folguera A, Zárate M (2011) Neogene sedimentation in the foreland zone between 34°30´and 41°S and its relation to the Pampa Central block uplift and the tectonic Colorado basin. In: Salfity J, Marquillas R (eds) Cenozoic geology of central Andes of Argentina. Instituto del Cenozoico, Salta, pp 123–134

Frechen M, Kehl M, Rolf C, Sarvati R, Skowronek A (2009a) Loess chronology of the Caspian Lowland in northern Iran. Quatern Int 198:220–233

Frechen M, Seifert B, Sanabria JA, Argüello GL (2009b) Chronology of late Pleistocene Pampa loess from the Córdoba area in Argentina. J Quatern Sci 24:761–772

Gaiero DM (2007) Dust provenance in Antarctic ice during glacial periods: from where in southern South America? Geophys Res Lett 34, L17707

Gaiero DM, Simonella L, Gassó S, Gili S, Stein AF, Sosa P, Becchio R, Arce J, Marelli H (2013) Ground/satellite observations and atmospheric modeling of dust storms originating in the high Puna-Altiplano deserts (South America): implications for the interpretation of paleo-climatic archives. J Geophys Res Atmos 118:3817–3831

Goudie AS, Parker AG, Bull PA, White K, Al-Farraj A (2000) Desert loess in Ras Al Khaimah, United Arab Emirates. J Arid Environ 46:123–135

Grimley DA (2000) Glacial and nonglacial sediment contributions to Wisconsin episode loess in the central United States. Geol Soc Am Bull 112:1475–1495

Grolier MJ, Overstreet WC (1978) Geologic map of the Yemen Arab Republic (San'a'), United States Geological Survey, Miscellaneous Investigations Series, Map 1-1143-B, scale 1:500,000

Guo ZT, Ruddiman WF, Hao QZ, Wu HB, Qiao YS, Zhu RX, Peng SZ, Wei JJ, Yuan BY, Liu TS (2002) Onset of Asian desertification by 22 Myr ago inferred from loess deposits in China. Nature 416:159–163

Haase D, Fink J, Haase G, Ruske R, Pésci M, Richter H, Altermann M, Jäger K-D (2007) Loess in Europe – its spatial distribution based on a European loess map, scale 1:2,500,000. Quatern Sci Rev 26:1301–1312

Haberlah D (2007) A call for Australian loess. Area 39:224–229

Hatté C, Antoine P, Fontugne M, Rousseau D-D, Tisnérat-Laborde N, Zöller L (1999) New chronology and organic matter $\delta^{13}C$ paleoclimatic significance of Nussloch loess sequence (Rhine Valley, Germany). Quatern Int 62:85–91

Hatté C, Gauthier C, Rousseau D-D, Antoine P, Fuchs M, Lagroix F et al (2013) Excursions to C4 vegetation recorded in the upper Pleistocene loess of Surduk (Northern Serbia): an organic isotope geochemistry study. Clim Past Discuss 9:187–215

Heller F, Liu TS (1982) Magnetostratigraphic dating of loess deposits in China. Nature 300:431–433

Hesse PP, McTainsh GH (2003) Australian dust deposits: modern processes and the Quaternary record. Quatern Sci Rev 22:2007–2035

Iriondo MH (1997) Models of deposition of loess and loessoids in the upper Quaternary of South America. J South Am Earth Sci 10:71–79

Johnsen SJ, Dahl-Jensen D, Gundestrup N, Steffensen JP, Clausen HB, Miller H, Masson-Delmotte V, Sveinbjörnsdottir AE, White J (2001) Oxygen isotope and palaeotemperature records from six Greenland ice-core stations: Camp Century, Dye-3, GRIP, GISP2, Renland and NorthGRIP. J Quatern Sci 16:299–307

Kehl M (2009) Quaternary climate change in Iran–the state of knowledge. Erdkunde 63:1–17

Kemp RA, Zárate MA (2000) Pliocene pedosedimentary cycles in the southern Pampas, Argentina. Sedimentology 47:3–14

Kemp RA, Toms PS, Sayago JM, Derbyshire E, King M, Wagoner L (2003) Micromorphology and OSL dating of the basal part of the loess-paleosol sequence at La Mesada in Tucumán. Quatern Int 106–107:111–117

Kemp RA, Zárate MA, Toms P, King M, Sanabria J, Arguello G (2006) Late Quaternary paleosols, stratigraphy and landscape evolution in the Northern Pampas, Argentina. Quatern Res 66:119–132

Kruck W, Helms F, Geyh M, Suriano J, Marengo H, Pereyra F (2011) Late Pleistocene-Holocene history of Chaco-Pampa sediments in Argentina and Paraguay. Quatern Sci J 60:188–202

Kukla G, An Z (1989) Loess stratigraphy in central China. Palaeogeogr Palaeoclimatol Palaeoecol 72:203–225

Lang A, Hatté C, Rousseau DD, Antoine P, Fontugne M, Zöller L et al (2003) High-resolution chronologies for loess: comparing AMS^{14}C and optical dating results. Quatern Sci Rev 22:953–959

Letolle R, Mainguet M (1993) Aral. Springer, Paris, 357 pp

Liu T (1985) Loess in China, 2nd edn. China Ocean Press/Springer, Beijing/Berlin, 224 pp

Livingstone I, Warren A (1996) Aeolian geomorphology. Addison Wesley Longman Limited, Essex, 211 p

Lü TY, Sun JM (2011) Luminescence sensitivities of quartz grains from eolian deposits in northern China and their implications for provenance. Quatern Res 76:181–189

Maher BA, Thompson R, Zhou LP (1994) Spatial and temporal reconstructions of changes in the Asian palaeomonsoon: a new mineral magnetic approach. Earth Planet Sci Lett 125:461–471

Markovic SB, Oches E, Sumegi P, Jovanovic M, Gaudenyi T (2006) An introduction to the middle and upper Pleistocene loess-paleosol sequence at Ruma brickyard, Vojvodina, Serbia. Quatern Int 149:80–86

Markovic SB, Hambach U, Catto N, Jovanovic M, Buggle B, Machalett B et al (2009) Middle and late Pleistocene loess sequences at Batajnica, Vojvodina, Serbia. Quatern Int 198:255–266

Marshall LG, Hoffstetter R, Pascual R (1983) Geochronology of the continental mammal-bearing tertiary of South America. Palaeovertebrata, Montpellier, Mém. Extr. 1–93

Matsu'ura T, Miyagi I, Furusawa A (2011) Late Quaternary cryptotephra detection and correlation in loess in northeastern Japan using cummingtonite geochemistry. Quatern Res 75:624–635

McCraw JD (1975) Quaternary airfall deposits of New Zealand. In: Suggate RP, Cresswell MM (eds) Quaternary studies, vol 13. Bulletin of Royal Society of New Zealand, Wellington, pp 35–44

McTainsh G (1984) The nature and origin of the aeolian mantles of central northern Nigeria. Geoderma 33:13–37

McTainsh G (1987) Desert loess in Northern Nigeria. Z Geomorphol NF 31:145–165

Molloy L (1998) Soils in the New Zealand landscape: the living mantle, 2nd edn. New Zealand Society of Soil Science, Lincoln University, Canterbury

Muhs DR (2007) Loess deposits, origins, and properties. In: Elias S (ed) The encyclopedia of Quaternary sciences. Elsevier, Amsterdam, pp 1405–1418

Muhs DR (2013a) The geologic records of dust in the Quaternary. Aeolian Res 9:3–48

Muhs DR (2013b) Loess and its geomorphic, stratigraphic, and paleoclimatic significance in the Quaternary. In: Shroder JF (Editor-in-chief), Lancaster N, Sherman DJ, Baas ACW (volume eds) Treatise on geomorphology, vol. 11, Aeolian geomorphology. Academic, San Diego, pp 149–183

Muhs DR, Bettis EA III (2003) Quaternary loess-paleosol sequences as examples of climate-driven sedimentary extremes. Geol Soc Am Spec Pap 370:53–74

Muhs DR, Ager TA, Bettis EA III, McGeehin J, Been JM, Begét JE, Pavich MJ, Stafford TW Jr, Pinney D (2003) Stratigraphy and paleoclimatic significance of late Quaternary loess-paleosol sequences of the last interglacial-glacial cycle in central Alaska. Quatern Sci Rev 22:1947–1986

Muhs DR, McGeehin JP, Beann J, Fisher E (2004) Holocene loess deposition and soil formation as competing processes, Matanuska Valley, southern Alaska. Quatern Res 61:265–276

Muhs DR, Bettis EA III, Aleinikoff J, McGeehin JP, Beann J, Skipp G, Marshall BD, Roberts HM, Johnson WC, Benton R (2008) Origin and paleoclimatic significance of late Quaternary loess in Nebraska: evidence from stratigraphy, chronology, sedimentology, and geochemistry. Geol Soc Am Bull 120:1378–1407

Nettleton WD, Chadwick OA (1996) Late Quaternary redeposited loess-soil developmental sequences, South Yemen. Geoderma 70:21–36

Péwé TL (1975) Quaternary geology of Alaska, U.S. Geological Survey Professional Paper 835. U.S. Government Printing Office, Washington, DC, pp 1–145

Porter SC (2001) Chinese loess record of monsoon climate during the last glacial-interglacial cycle. Earth Sci Rev 54:115–128
Porter SC, Hallet B, Wu X, An Z (2001) Dependence of near-surface magnetic susceptibility on dust accumulation rate and precipitation on the Chinese Loess Plateau. Quatern Res 55:271–283
Pye K (1995) The nature, origin and accumulation of loess. Quatern Sci Rev 14:653–657
Qiang XK, Li ZX, Powell CM, Zheng HB (2001) Magnetostratigraphic record of the Late Miocene onset of the East Asian monsoon, and Pliocene uplift of northern Tibet. Earth Planet Sci Lett 187:83–93
Qiang XK, An ZS, Song YG, Chang H, Sun YB, Liu WG, Ao H, Dong JB, Fu CF, Wu F, Lu FY, Cai YJ, Zhou WJ, Cao JJ, Xu XW, Ai L (2011) New aeolian red clay sequence on the western Chinese Loess Plateau linked to onset of Asian desertification about 25 Ma ago. Sci China 54:136–144
Rabassa J, Coronato A, Ponce JF, Schlieder G, Martínez O (2011) Depósitos glacigénicos (Cenozoico tardío-Cuaternario) y geoformas asociadas. Relatorio del XVIII Congreso Geológico Argentino, Neuquén, pp 295–314
Roberts HM, Muhs DR, Wintle AG, Duller GAT, Bettis EA III (2003) Unprecedented last glacial mass accumulation rates determined by luminescence dating of loess from western Nebraska. Quatern Res 59:411–419
Roberts HM, Muhs DR, Bettis EA III (2007) North America. In: Elias S (ed) The encyclopedia of Quaternary sciences. Elsevier, Amsterdam, pp 1456–1466
Rossignol J, Moine O, Rousseau D-D (2004) The Buzzard's Roost and Eustis mollusc sequences: comparison between the paleoenvironments of two sites in the Wisconsinan loess of Nebraska, USA. Boreas 33:145–154
Rousseau D-D (1991) Climatic transfer function from Quaternary molluscs in European loess deposits. Quatern Res 36:195–209
Rousseau D-D, Antoine P, Hatté C, Lang A, Zöller L, Fontugne M, Ben Othman D, Luck JM, Moine O, Labonne M, Bentaleb I, Jolly D (2002) Abrupt millennial climatic changes from Nussloch (Germany) Upper Weichselian eolian records during the last glaciation. Quatern Sci Rev 21:1577–1582
Rousseau D-D, Derbyshire E, Antoine P, Hatté C (2007a) Europe. In: Elias S (ed) The encyclopedia of Quaternary sciences. Elsevier, Amsterdam, pp 1440–1456
Rousseau D-D, Sima A, Antoine P, Hatte C, Lang A, Zöller L (2007b) Link between European and North Atlantic abrupt climate changes over the last glaciation. Geophys Res Lett 34, L22713. doi:10.1029/2007gl031716
Rousseau D-D, Antoine P, Gerasimenko N, Sima A, Fuchs M, Hatté C, Moine O, Zoeller L (2011) North Atlantic abrupt climatic events of the last glacial period recorded in Ukrainian loess deposits. Clim Past 7:221–234
Rozychi SZ (1991) Loess and loess-like deposits. The Publishing House of the Polish Academy of Science. Ossolineum, Wroclaw, 187 pp
Sarnthein M, Tetzlaff G, Koopmann B, Wolter K, Pflaumann U (1981) Glacial and interglacial wind regimes over the eastern subtropical Atlantic and North-West Africa. Nature 293:193–196
Schellenberger A, Veit H (2006) Pedostratigraphy and pedological and geochemical characterization of Las Carreras loess–paleosol sequence, Valle de Tafí, NW-Argentina. Quatern Sci Rev 25:811–831
Singer MJ, Verosub KL (2007) Mineral magnetic analysis. In: Elias S (ed) The encyclopedia of Quaternary sciences. Elsevier, Amsterdam, pp 2096–2102
Smalley IJ (1995) Making the material: the formation of silt-sized primary mineral particles for loess deposits. Quatern Sci Rev 14:645–651
Smith J, Vance D, Kemp R, Archer C, Toms P, King M, Zárate M (2003) Isotopic constraints on the source of Argentinian loess-with implications for atmospheric circulation and the provenance of Antarctic dust during recent glacial maxima. Earth Planet Sci Lett 6682:1–16

Stevens T, Thomas DSG, Armitage SJ, Lunn HR, Lu H (2007) Reinterpreting climate proxy records from late Quaternary Chinese loess: a detailed OSL investigation. Earth Sci Rev 80:111–136

Stokes S, Horrocks J (1998) A reconnaissance survey of the linear dunes and loess plains of northwestern Nigeria: granulometry and geochronology. In: Alsharhan AS, Glennie KW, Whittle GL, Kendall CGSC (eds) Quaternary deserts and climatic change. Balkema, Rotterdam, pp 165–174

Stuut J-BW, Prins MA, Schneider RR, Weltje GJ, Jansen JHF, Postma G (2002) A 300-kyr record of aridity and wind strength in southwestern Africa: inferences from grain-size distributions of sediments on Walvis Ridge, SE Atlantic. Mar Geol 180:221–233

Sun J (2002a) Source regions and formation of the loess sediments on the high mountain regions of northwestern China. Quatern Res 58:341–351

Sun J (2002b) Provenance of loess material and formation of loess deposits on the Chinese Loess Plateau. Earth Planet Sci Lett 203:845–859

Sun J (2005) Nd and Sr isotopic variations in Chinese eolian deposits during the past 8 Ma: implications for provenance change. Earth Planet Sci Lett 240:454–466

Sun J, Zhu X (2010) Temporal variations in Pb isotopes and trace element concentrations within Chinese eolian deposits during the past 8 Ma: Implications for provenance change. Earth Planet Sci Lett 290:438–447

Sun J, Zhang M, Liu T (2001) Spatial and temporal characteristics of dust storms in China and its surrounding regions, 1960–1999: relations to source area and climate. J Geophys Res 106:10325–10333

Sun J, Yie J, Wu WY, Ni XJ, Bi SD, Zhang ZQ, Liu WM, Meng J (2010) Late Oligocene-Miocene mid-latitude aridification and wind patterns in the Asian interior. Geology 38:515–518

Sun YB, Tada R, Chen J, Chen HZ, Toyoda S, Tani A, Isozaki Y, Nagashima K, Hasegawa H, Ji JF (2007) Distinguishing the sources of Asian dust based on electron spin resonance signal intensity and crystallinity of quartz. Atmos Environ 41:8537–8548

Teruggi ME (1957) The nature and origin of Argentine loess. J Sediment Petrol 27:322–332

Tripaldi A, Forman SL (2007) Geomorphology and chronology of late Quaternary dune fields of western Argentina. Palaeogeogr Palaeoclimatol Palaeoecol 251:300–320

Tripaldi A, Zárate MA, Brook GA (2011) Late Quaternary paleoenvironments and paleoclimatic conditions in the distal Andean piedmont, southern Mendoza, Argentina. Quatern Res 76:181–294

Tsoar H, Pye K (1987) Dust transport and the question of desert loess formation. Sedimentology 34:139–153

Velichko AA, Bogucki AB, Morozova TD, Udartsev VP, Khalcheva TA, Tsatskin AI (1984) Periglacial landscapes of the East European Plain. In: Velichko AA, Wright HE Jr, Barnosky CW (eds) Late Quaternary environments of the Soviet Union. University of Minnesota Press, Minneapolis, pp 94–118

Velichko AA, Morozova TD, Nechaev VP, Rutter NW, Dlusskii KG, Little EC, Catto NR, Semenov VV, Evans ME (2006) Loess/paleosol/cryogenic formation and structure near the northern limit of loess deposition, East European Plain, Russia. Quatern Int 152–153:14–30

Verosub KL, Fine P, Singer MJ, TenPas J (1993) Pedogenesis and paleoclimate: interpretation of the magnetic susceptibility record of Chinese loess-paleosol sequences. Geology 21:1011–1014

von Suchodoletz H, Kühn P, Hambach U, Dietze M, Zöller L, Faust D (2009) Loess-like and palaeosol sediments from Lanzarote (Canary Islands/Spain) – indicators of palaeoenvironmental change during the late Quaternary. Palaeogeogr Palaeoclimatol Palaeoecol 278:71–87

Watanuki T, Murray AS, Tsukamoto S (2005) Quartz and polymineral luminescence dating of Japanese loess over the last 0.6 Ma: comparison with an independent chronology. Earth Planet Sci Lett 240:774–789

Westgate JA, Stemper BA, Péwé TL (1990) A 3 m.y. record of Pliocene-Pleistocene loess in interior Alaska. Geology 18:858–861

Whalley WB, Marshall JR, Smith BJ (1982) Origin of desert loess from some experimental observations. Nature 300:433–435

White K, Livingstone I, Gurney S, Dearing J, Bateman M (2002) Post-processing of mineral mixture maps for mapping surficial materials: the example of the Matmata loess, southern Tunisia. Int J Remote Sens 23:3091–3106

Wilkinson TJ (1997) Holocene environments of the high plateau, Yemen: recent geoarchaeological investigations. Geoarchaeology 12:833–864

Wright JS (2001a) "Desert" loess versus "glacial" loess: quartz silt formation, source areas and sediment pathways in the formation of loess deposits. Geomorphology 36:231–256

Wright JS (2001b) Making loess-sized quartz silt: data from laboratory simulations and implications for sediment transport pathways and the formation of 'desert' loess deposits associated with the Sahara. Quatern Int 76–77:7–19

Yaalon DH, Dan J (1974) Accumulation and distribution of loess-derived deposits in the semi-desert and desert fringe areas of Israel. Z Geomorphol Supplementband 20:91–105

Yang SL, Ding ZL (2006) Winter–spring precipitation as the principal control on predominance of C3 plants in Central Asia over the past 1.77 Myr: evidence from $\delta^{13}C$ of loess organic matter in Tajikistan. Palaeogeogr Palaeoclimatol Palaeoecol 235:330–339

Yang SL, Ding F, Ding ZL (2006) Pleistocene chemical weathering history of Asian arid and semi-arid regions recorded in loess deposits of China and Tajikistan. Geochim Cosmochim Acta 70:1695–1709

Zárate MA (2003) Loess of southern South America. Quatern Sci Rev 22:1987–2006

Zárate MA (2007) South America. In: Elias S (ed) The encyclopedia of Quaternary sciences. Elsevier, Amsterdam, pp 1466–1479

Zárate M, Blasi A (1993) Late Pleistocene-Holocene eolian deposits of the southern Buenos Aires Province, Argentina: a preliminary model. Quatern Int 17:15–20

Zárate MA, Kemp R, Toms P (2009) Late Quaternary landscape reconstruction and geochronology in the northern Pampas of Buenos Aires province, Argentina. J South Am Earth Sci 27:88–99

Zinck JA, Sayago JM (2001) Climatic periodicity during the late Pleistocene from a loess-paleosol sequence in northwest Argentina. Quatern Int 78:11–16

Chapter 17
Subaquatic Dust Deposits

Jan-Berend W. Stuut

Abstract Sedimentary deposits of dust found on lake and ocean floors are here considered subaquatic dust deposits. In this chapter, a state-of-the-art overview is given of these subaquatic dust deposits and their value as archives of environmental change. Examples are given of subaquatic dust deposits that register over millions of years fluctuations in dust fluxes that can be interpreted in terms of past environmental changes in the source area(s) of the dust particles. The tools (the so-called proxies) that have been used to read these records of environmental changes are also presented and discussed. Subaquatic dust deposits are usually continuous through time, relatively easy to date; they reflect both wet and dry deposition of mineral dust particles and are not biased by the altitude at which the particles are deposited. This set of properties makes them a very valuable archive of dust as recorder of palaeo-environmental change. Finally, it is discussed in this chapter how the ocean potentially plays a role in the process of dust as a player of environmental change.

Keywords Marine • Lacustrine • Archive • Palaeo-environments • Reconstruction • Proxies • Particle size • Sink • Nutrients • Fertilization • CO_2 sequestration

J.-B.W. Stuut (✉)
NIOZ – Royal Netherlands Institute for Sea Research, Department of Marine Geology and Chemical Oceanography, Texel, The Netherlands

MARUM – Center for Marine Environmental Sciences, Department of Marine Sedimentology, University of Bremen, Bremen, Germany
e-mail: jbstuut@nioz.nl

P. Knippertz and J.-B.W. Stuut (eds.), *Mineral Dust: A Key Player in the Earth System*, DOI 10.1007/978-94-017-8978-3_17,

17.1 Introduction

Another archive of dust deposits, next to the well-studied on-land – loess – deposits (Chap. 16), is dust archives that are found in lacustrine and marine settings. In this chapter, the great potential of these "underwater" dust deposits as an archive for past environmental conditions is explored.

Through geologic time, rivers, icebergs and winds transport sediments from land to the ocean floor as well as to lake floors. On these lake and ocean floors, there are places where sedimentary archives can be found that record continuous accumulation of these land-derived sediments and which are undisturbed by syndepositional changes (e.g. lobe switching in delta fans) and post-depositional changes (e.g. bottom-current winnowing and re-deposition in gravity flows and bioturbation). Usually, these undisturbed deposits are in the distal (several hundred kilometres) offshore parts of lakes and oceans.

Figure 17.1 shows a map of all recordings of dust records in the DIRTMAP 2 (*D*ust *I*ndicators and *R*ecords of *T*errestrial and *MA*rine *P*alaeoenvironments) database, including on-land (loess) and ice-core deposits. Clearly, marine sites dominate the map, and most of the terrestrial records comprise loess deposits. Unfortunately, hardly any lacustrine records are present in this compilation. The map clearly shows that the marine dust records are concentrated around the mid-latitude deserts, mainly offshore either sides of northern Africa in the Atlantic and Indian Oceans, respectively, as well as in the western North Pacific offshore the major Asian deserts.

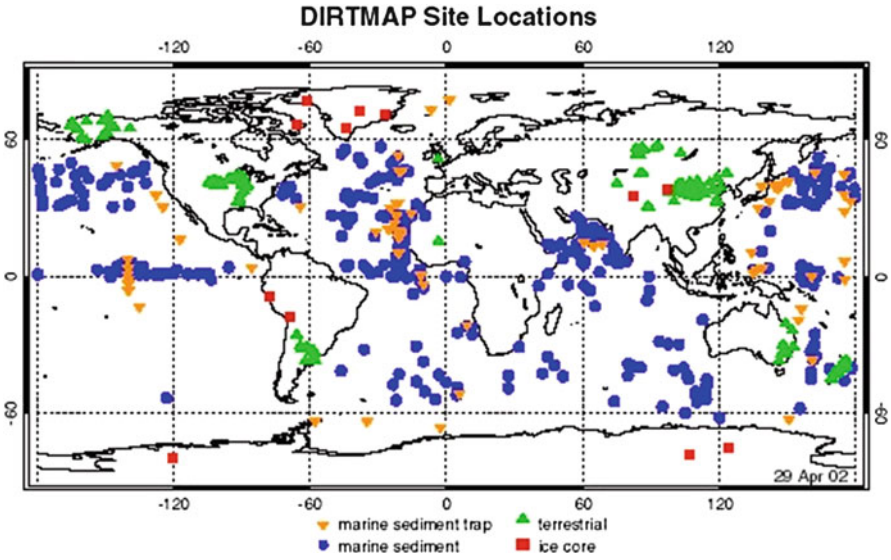

Fig. 17.1 Map of marine, terrestrial (loess deposits, peat bogs and lakes) and ice-core sites contained within the DIRTMAP 2 database. http://www.bridge.bris.ac.uk/projects/DIRTMAP. Note: DIRTMAP 3 is currently being compiled

The big advantages of subaquatic dust deposits are as follows:

- They are usually easy to date, thanks to carbonate-building organisms that deposit contemporaneously with the settling dust particles. These carbonate tests can be dated using, e.g. AMS ^{14}C dating $\delta^{18}O$. In addition, paleaeo-magnetic properties of the sediments can be used for dating.
- They reflect both wet and dry deposition of dust particles that were suspended in the atmosphere, both at low and high altitudes. This is a big advantage compared to, e.g. dust in ice cores, which are often at high altitudes and therefore only register long-distance/high-altitude dust.
- The proxy-derived inferences can be verified using modern analogue techniques. This is a big advantage compared to, e.g. loess deposits, which often do not have a modern analogue.
- These deposits cover large parts of the Earth's surface.

17.2 From Desert Source to Subaquatic Sink: Dust Transport Processes

The details of the processes of desert dust production, entrainment and deposition are dealt with in Chaps. 3, 5 and 8. To be able to interpret the various subaqueous deposits, these processes and their consequences for the resulting physical properties (e.g. particle-size distribution) of the deposited dust are very important. The whole suite of processes that eventually lead to dust deposition was conceptualised by Pye and Zhou (1989), see Fig. 17.2.

Pye and Zhou (1989) argued that there are essentially two end-members to atmospheric transport; low-level and high-level dust clouds travelling downwind. Gravitational settling causes the coarser-grained particles to be deposited closer to the source and finer-grained material further downwind. In addition to gravitational

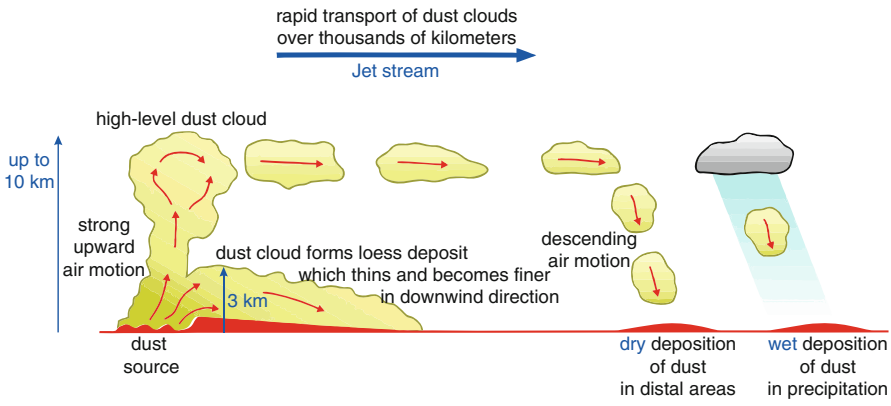

Fig. 17.2 Schematic diagram showing different dust transport mechanisms in the high- and low-level atmosphere (Redrawn from Pye and Zhou 1989)

settling, there is a part of the wind-blown sediment fraction that is washed out of the atmosphere by rain or snow. These processes were synthesised for the north African dust sources by Stuut et al. (2009) and are described in this book in Chap. 8.

17.3 Wind-blown Dust in Subaqueous Sedimentary Archives: A Recorder of Environmental Changes

17.3.1 Lacustrine Dust Archives

As opposed to the more regional character of dust deposited in marine sedimentary archives, lacustrine archives contain a more local signal of environmental conditions leading to dust generation, entrainment and finally deposition. Early recognition of the potential of lake deposits as archives of dust deposition dates back to the studies of, e.g. Grove (1972) and Bowler (1976). Well-established palaeo-environmental records derived from lacustrine deposits include the southern German Alpine lakes (Niessen et al. 1992), the German Maar records (Zolitschka et al. 2000; Sirocko et al. 2005), the Patagonian crater lakes (Mayr et al. 2007), the central North American lakes (Dean 1997) and the central Saharan Ounianga lakes (Kröpelin et al. 2008). Another advantage of lake sediments is that often they are varved, which is the result of seasonal differences in environmental conditions. For example, high-latitude lakes may be frozen over during winter, which leads to a seasonal banding of the sedimentary deposits on the lake floor.

Especially the Maar records are examples of lakes where wind-blown material is the only terrigenous input and thus where the dust can relatively simply be isolated from the biogenic sedimentary fraction that is produced in both the lake waters and on the lake floor. Sirocko et al. (2005) argue that the sediments that were retrieved from the various Maar lakes in central Germany are a two-component mixture of dark biogenic material produced in the lake and light-coloured quartz particles blown into the lake. The authors argue that during warm periods, organic-rich sediments are deposited as opposed to colder periods when deposition of wind-blown particles dominates. Thus, the greyscale of these sediments can be used to reconstruct variability in the input of the two individual components (Fig. 17.3).

The advantage of recording mere local environmental conditions may turn into a disadvantage in the case of small lake basins where very local conditions (like a nearby field of sand dunes) potentially dominate the depositional system. It is hard to say what the appropriate lake size should be in order to avoid such artefacts.

17.3.2 Marine Dust Archives

Marine sediment archives containing dust most likely record integrated signals from a larger dust-producing region, especially when the source-to-sink distance is

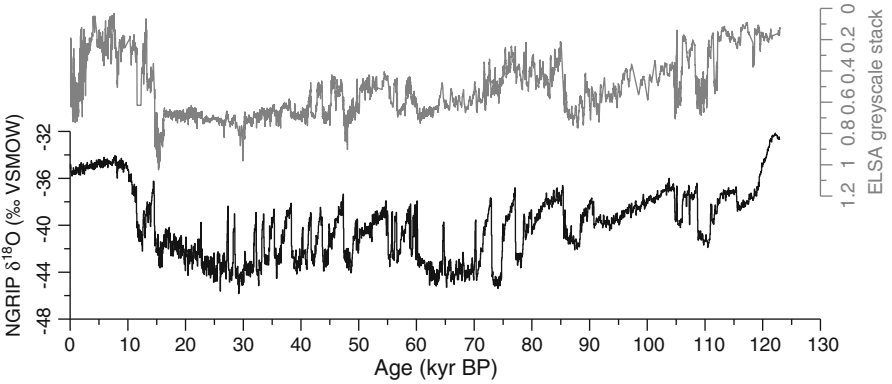

Fig. 17.3 Comparison of the ELSA greyscale stack (Sirocko et al. 2005) with the oxygen isotope record from the Greenland NGRIP ice core (NorthGRIP community members 2004). High values of $\delta^{18}O$ and low values of the greyscale (note reversed scale on greyscale axis) indicate warm conditions

relatively large (>1,000 km). The big advantage of such remote marine depositional sites is that the dust can only be transported to the site by winds (excluding potential sediment-transporting current systems).

Another advantage of marine dust archives is the age of the total stratigraphy, which obviously varies with sedimentation rates, and can be anywhere between several million years (Rea 1994) to several millennia (Mulitza et al. 2010); see Fig. 17.4.

The first recognition of the potential of wind-blown deposits in marine sediments was presented by Windom (1975). This was followed by many studies that focussed on dusty areas like downwind of northwest Africa and eastern Asia. Well-established palaeo-environmental/dust records from marine sediments include the ODP records by Rea and co-workers in the north Pacific (Rea and Janecek 1981; Rea and Bloomstine 1986; Hovan et al. 1989; Snoeckx et al. 1995), the ODP records by deMenocal and co-workers off Africa on both the Indian Ocean and equatorial North Atlantic sides (deMenocal et al. 1993, 2000a; deMenocal 1995) and shorter sediment cores from offshore southwest Africa (Stuut et al. 2002b), South America (Rea and Bloomstine 1986; Lamy et al. 2000; Stuut and Lamy 2004) and Australia (Hesse 1994). These records have shown on different temporal resolutions the importance of recognising and quantifying wind-blown dust in marine sediments in order to reconstruct the environmental conditions in the source region(s) of the dust particles through geologic history.

Sarnthein and co-workers (Koopmann 1979; Sarnthein et al. 1981) analysed a large set of sea-floor sediments from the equatorial North Atlantic Ocean, assuming that they had been deposited there recently. They isolated the terrigenous fraction by removing all biogenic components in these samples and analysed the particle-size distribution. In the absence of substantial rivers draining into the Atlantic Ocean presently, they interpreted this sediment fraction to reflect modern Saharan dust deposition. Figure 17.5 shows that the present Saharan dust plume can be

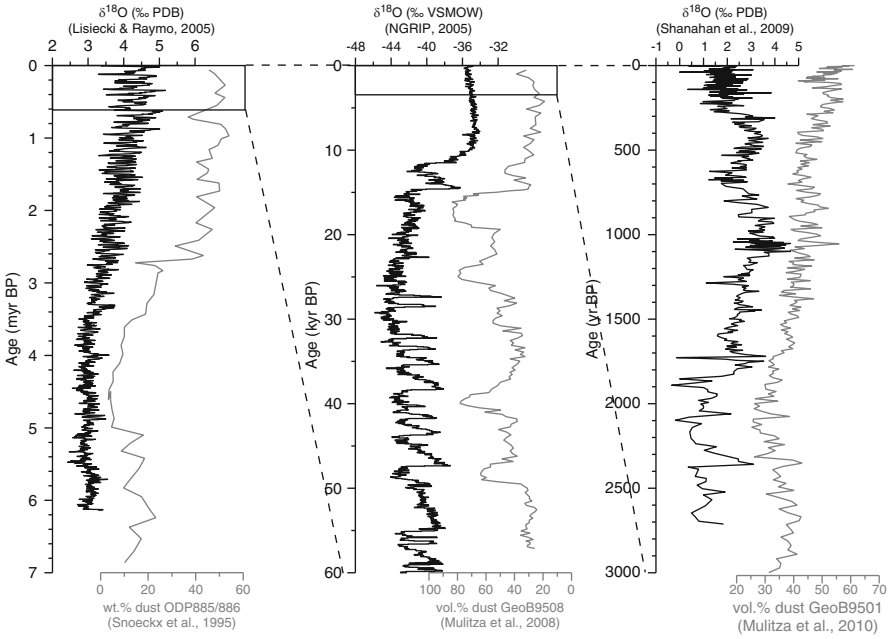

Fig. 17.4 Comparison of marine dust records at three different time scales. All *black* plots depict $\delta^{18}O$ records, which are used as global temperature proxy. From left to right these are the global $\delta^{18}O$ stack by Lisiecki and Raymo (2005), the $\delta^{18}O$ record from the Greenland NGRIP ice core (NorthGRIP community members 2004) and the $\delta^{18}O$ record from Lake Bosumtwi by Shanahan et al. (2009). Note the scales of the time axes changing from left to right from myr, kyr to yr before present. The *grey* records depict dust records defined as the non-soluble fraction of marine sediments from Snoeckx et al. (1995), Mulitza et al. (2008) and Mulitza et al. (2010), respectively. Note that the x-axis of the Mulitza et al. 2008 record is reversed

easily recognised in these sediments by a downwind decrease in both dust particle size and dust flux. The same conclusion can be drawn from satellite observations of the modern Saharan dust plume travelling westward over the equatorial North Atlantic Ocean; Figure 17.5 also shows how the aerosol index of the Total Ozone Mapping Spectrometer (TOMS) locates both the presently most active dust sources in northwest Africa but also how the modern Saharan dust plume over the Atlantic Ocean is centred at about 12°N. These downwind gradients in both flux and particle size are key issues in the role that wind-blown dust may have as a player of environmental change.

The sediment archive that can be found on the sea floor is always a mixture of various components like erosion products from land, plankton and algal remains from the surface ocean and biogenic components from the sea floor. The erosion products from land are transported to the ocean by rivers, winds and ice. On nearly all parts of the sea floor in the (sub)tropical oceans, the land-derived fraction is – in the absence of ice – a mixture of river load and wind-blown dust. Even when nowadays no active river systems are present, environmental conditions throughout

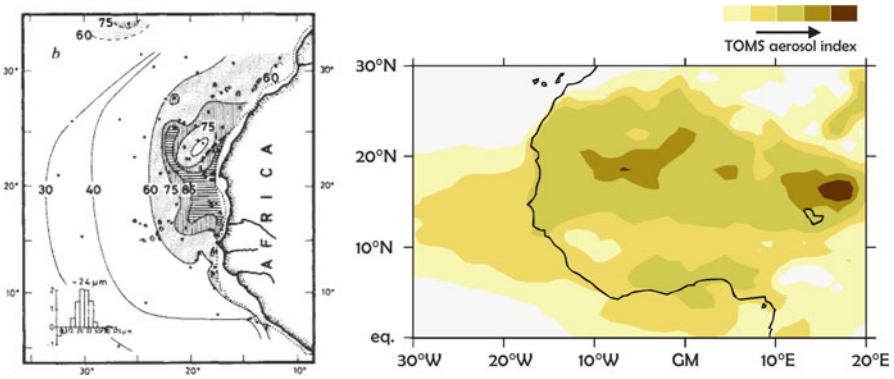

Fig. 17.5 Maps of the equatorial northwest Atlantic, showing dust flux and dust particle size of sea-floor sediments (Sarnthein et al. 1981 (*left*)), with each *black* dot indicating individual samples that were analysed for particle size, and an 8-year average of TOMS aerosol index data (TOMS data are available at http://toms.gsfc.nasa.gov) showing the position of the northwest African dust plume travelling westward (Mulitza et al. 2008 (*right*))

geologic history may have favoured river run-off. A classic example of this is the Sahara Desert in northwest Africa, which presently is hyper-arid and basically only producing dust, but which was characterised by the so-called African Humid Period about 10,000 years ago (e.g. deMenocal et al. 2000b) with increased rainfall at such magnitudes that present-day deserts were turned into grasslands with ample shrubs and trees (e.g. Tjallingii et al. 2008). Such humid periods occurred regularly through geologic time at a pacing of about 23,000 yrs, and the lakes that were filled with water during these wet phases now act as sources of dust (Prospero 1996; Prospero et al. 2002; Drake and Bristow 2006; Stuut et al. 2009). Undoubtedly, such high amounts of rainfall also caused significant river run-off, and evidence of this is found in large palaeo-river systems (Vörösmarty et al. 2000; Krastel et al. 2004). The terrigenous fraction of deep-sea sediments that was carried to sea in such intervals in geologic history most likely was dominated by river-transported sediments instead of dust.

17.4 Proxies Used in Subaquatic Sediments to Reconstruct Palaeo-environmental Conditions

17.4.1 Particle Size of Mineral Dust

The particle size of the wind-blown sediment fraction is intuitively related to wind vigour (e.g. Janecek and Rea 1985), and several studies therefore used the particle size of the wind-blown sediment fraction to reconstruct atmospheric circulation patterns in the past (Prins and Weltje 1999; Stuut et al. 2002b;

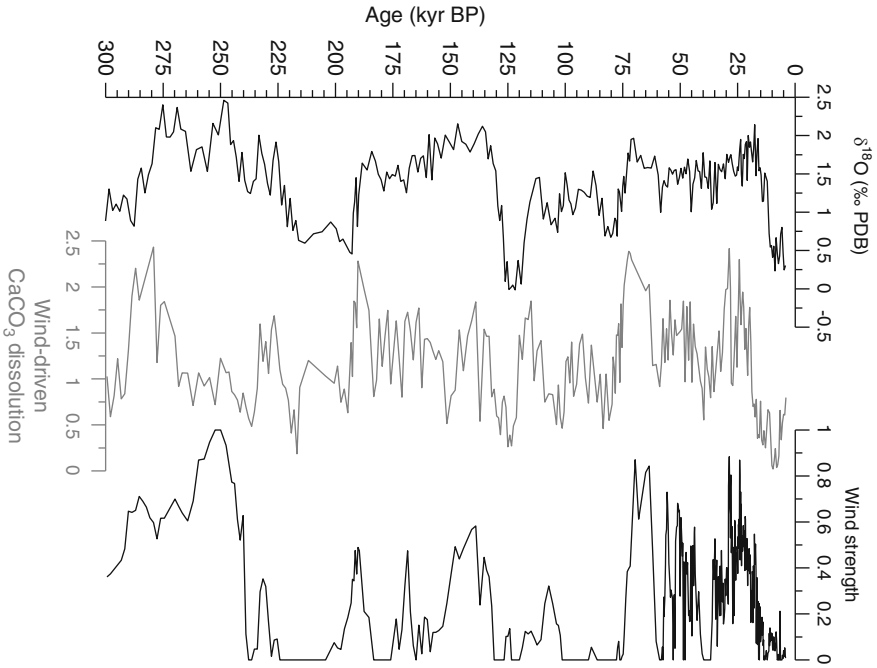

Fig. 17.6 Proxy records from core MD962094. Top: $\delta^{18}O$ record showing glacial-interglacial swings throughout the last 300 kyr BP. Middle: wind-driven carbonate dissolution record. *Bottom*: wind strength record, as reconstructed from the dust fraction (Redrawn from Stuut et al. 2002a; b)

Weltje and Prins 2003). Generally, throughout the Pleistocene, glacial periods were characterised by intensified atmospheric circulation due to increased latitudinal pressure gradients. These increased winds are often reflected in larger wind-blown particles. Presently, there are still lively discussions on the size of dust particles and how far they can be transported through the air, but the intuitively logical downwind decrease in both dust flux and particle size was beautifully demonstrated by Sarnthein et al. (1981) for the Saharan dust plume (Fig. 17.5).

The southeast Atlantic Ocean, offshore Namibia, is dominated by the trade wind-driven upwelling of deep waters, causing high primary productivity in the surface ocean. These same trade winds also carry dust from the Namib Desert, which settles on the sea floor. Stuut and co-workers demonstrated how the variability of the trade wind system varied throughout the late Quaternary based on the particle-size distributions of both the marine sediment fraction (Stuut et al. 2002a) and the land-derived sediment fraction (Stuut et al. 2002b). Generally, during glacial stages of the late Quaternary, atmospheric circulation intensified, leading to enhanced wind-driven upwelling, which is reflected in the particle size of the carbonate fraction. As the upwelled waters are cold, they are more corrosive to carbonate tests of unicellular plankton and will consequently influence their particle size. Simultaneously, the intensified winds had a larger carrying capacity, which enabled them to carry coarser-grained dust particles (Fig. 17.6).

Table 17.1 Grain-size-derived proxies for desert dust in marine sediments used in literature

Grain-size proxy	Proxy for	Location	Citation
Terrigenous sediment <63 μm	Total dust	Distal North Pacific Proximal Tasman Sea	Rea and Janecek (1981) Hesse (1994)
Terrigenous sediment >6 μm	Total dust	Eq. Atlantic Indian Ocean	Sarnthein et al. (1981) Clemens and Prell (1990)
Terrigenous sediment >60 μm	Total dust	Indian Ocean	De Deckker et al. (1991)
Bulk sediment >63 μm	Wind stress	Eq. Atlantic	Matthewson et al. (1995)
Moment statistics (mean, median) after Folk and Ward (1957)	Total dust	Indian Ocean	Prins and Weltje (1999)
Bulk sediment, unmixed with EMMA	Aridity	Indian Ocean	Prins and Weltje (1999)
Bulk sediment, unmixed with EMMA	Wind stress	Indian Ocean	Prins and Weltje (1999)
Terrigenous sediment 18–63 μm	Total dust	Eq. Atlantic	Nizou et al. (2011)
Terrigenous sediment >10 μm	Total dust	Eq. Atlantic	Meyer et al. (2013)

Similar to using the size of the wind-blown sediment fraction as a proxy for wind strength in the past, the flux of the wind-blown sediment fraction can be considered a proxy for palaeo-aridity in the source area. Following this approach, various palaeo-environmental reconstructions based on marine sediment cores were established in the Indian Ocean (Prins and Weltje 1999; Prins et al. 2000; Weltje and Prins 2003, 2007), southeast Atlantic (Stuut et al. 2002b, 2004; Stuut and Lamy 2004), southeast Pacific (Stuut and Lamy 2004; Stuut et al. 2006), equatorial North Atlantic (Holz et al. 2004, 2007; McGregor et al. 2009; Filipsson et al. 2011; McGee et al. 2013), Mediterranean (Hamann et al. 2008) and southeast Indian Ocean (Stuut et al. 2014).

As discussed before, the most intuitive relationship between wind strength and sedimentary deposits resulting from aeolian transport is the particle size of the deposited sediments. Several size-derived proxies were suggested to characterise dust in subaqueous sediments such as certain size fractions (Table 17.1). Most of these studies isolated the land-derived fraction by removing organic fractions (marine carbonate, organic matter, biogenic opal) and sometimes also authigenic or volcanic minerals (e.g. Rea and Janecek 1981), after which the grain-size distribution of the non-soluble fraction was analysed.

In an attempt to characterise and quantify the wind-blown portion within the land-derived sediment fraction, Prins and Weltje (1999) presented the end-member modelling approach, which is based on the assumption that every sediment transport mechanism leaves its own characteristic imprint on the grain-size distribution of

the material it transports; ice-rafted sediments tend to be completely unsorted as opposed to aeolian sediments, which are very well sorted. Based on this assumption, a numerical model was developed (Weltje 1997), with which a data set of grain-size distributions can be modelled and deconvolved into subpopulations – without a priori information about these subpopulations – that can subsequently be interpreted in terms of sediment transport mechanism. The end-member modelling algorithm (EMMA) does not prescribe anything in terms of shape of the grain-size distributions of the subpopulations and has been successfully applied to recognise ice-rafted sediments (e.g. Prins et al. 2002) and wind-blown dust (Stuut et al. 2002b, 2007, 2014; Weltje and Prins 2003, 2007). Using the end-member approach, the river-transported and wind-blown fractions can be distinguished and quantified downcore provided the source-to-sink distance is small enough for the aeolian fraction to be coarser grained than the river-derived sediment fraction, which is typically around 4–6 μm in deep-marine sediment archives (e.g. Prins and Weltje 1999).

Intuitively, it may seem more logical to assume that wind-blown sediments are relatively fine grained, but numerous studies on present-day dust have demonstrated that aeolian particles (including volcanic grains) can be up to 300 μm, even thousands of kilometres from their source (e.g. Ram and Gayley 1991). This observation of large wind-blown particles is fully accepted in the loess community (see, e.g. Chap. 16; Prins and Vriend 2007; Prins et al. 2007), but on land coarse-grained wind-blown deposits could be the result of sequential short-term suspension events (Fig. 17.2).

In the marine realm such short-term suspension events can be excluded, but nonetheless there is the issue of the so-called "giant" wind-blown particles (Betzer et al. 1988; Middleton et al. 2001), which are particles that can only be transported through the atmosphere, like particles from a dust outbreak in China, retrieved on the islands of Hawaii, >10,000 km from their source (Betzer et al. 1988), but which are too coarse grained to be explained using currently acknowledged atmospheric transport mechanisms. Potentially, there are turbulences in the atmosphere, which can keep relatively large particles suspended in air over thousands of kilometres. This observation is important as the particle size and shape are directly related to optical properties of the mineral dust. It is well established that small particles in the higher parts of the atmosphere reflect incoming radiation (Chap. 11), but in the lower parts of the atmosphere, larger particles may absorb solar energy that was reflected at the Earth's surface and would have otherwise been radiated into space (e.g. Otto et al. 2007; Satheesh et al. 2007).

The shape of the aeolian particles also plays a big role in their long-distance transport as platy minerals such as micas aerodynamically behave like much smaller particles (e.g. Stuut et al. 2005). At very large source-to-sink distances (several tens of thousands of kilometres), wind-blown particles usually are very small (e.g. Prospero and Bonatti 1969; Rea et al. 1985, this book: Chap. 18) and can be so small that they would only settle from the atmosphere as nuclei of ice crystals (Chap. 12 and, e.g. Franzén and Hjelmroos 1988).

Table 17.2 Other proxies for desert dust in marine sediments used in literature

Proxy	Proxy for	Location	Citation
Phytoliths	Aridity	Eq. Atlantic	Pokras and Mix (1985)
Freshwater diatoms	Aridity	Eq. Atlantic	(Pokras and Mix 1985)
Pollen	Aridity	SE Atlantic	Coetzee (1976)
Lipids from plant waxes	Aridity	Eq. Atlantic	Simoneit (1977)
Ti/Al (Ti in dust, Al in river mud)	Total dust	Indian Ocean	Weedon and Shimmield (1991)
Zr/Rb (Zr in dust, Rb in river mud)	Total dust	Eq. Atlantic	Matthewson et al. (1995)
Si/Al (Si in dust, Al in river mud)	Total dust	Eq. Atlantic	Mulitza et al. (2010)
Pb isotopes	Total dust	Eq. Atlantic	Abouchami and Zabel (2003)
He isotopes	Total dust	Eq. Atlantic	Mukhopadhyay and Kreycik (2008)
Sr/Nd isotopes	Provenance	Eq. Atlantic	Meyer et al. (2011; 2013)
Palygorskite (trace mineral)	Provenance	Sahara	Schütz and Sebert (1987)
Magnetic minerals	Aridity	Eq. Atlantic	Bloemendal et al. (1988)

Hesse (1994) presented a reconstruction of the Australian dust plume in the western Pacific Ocean throughout the last 350 kyr BP based on the <63 μm fraction of the terrigenous sediment fraction isolated using the methods described in Rea and Janecek (1981). However, this method was developed to characterise Asian dust in the distal parts of the northern Pacific Ocean, whereas the sediment cores off Australia were taken relatively close to the continent. Hence, there may well be a considerable river-derived fraction in the sediment archive that Hesse (1994) studied.

17.4.2 Other Proxies for Wind-blown Dust

Besides the particle-size distributions of the terrigenous sediment fraction, several other proxies were suggested useful to characterise dust in subaquatic sediment archives (see Table 17.2 and also Chap. 2). The first published detailed study of the composition of Saharan dust was done by Ehrenberg (1847), who received material that Charles Darwin had collected on his travels onboard HMS Beagle from 1831 to 1836. Ehrenberg recognised all kinds of biogenic material in the dust, which he classified as freshwater diatoms and plant-derived biogenic silica called phytoliths. These freshwater diatoms and phytoliths were later found in North Atlantic sediments (e.g. Kolbe 1957) and consequently used to reconstruct Saharan climate (Pokras and Mix 1985; Gasse et al. 1989; Alexandre et al. 1997) and south-western African climate (Jansen et al. 1992).

An alternative wind-blown land-derived organic fraction is pollen, and they have been used widely to reconstruct palaeo-environmental conditions in dry areas around the world, both in marine and lacustrine settings, in South America from

sediments in the eastern Pacific and in the numerous lakes of the Andes mountains (e.g. Groot and Groot 1966; Heusser 1983; Markgraf 1993), in Australia from sediments in the western Pacific and in Lynch's crater lake (e.g. Kershaw et al. 2003, 2007), in north Africa from equatorial Atlantic sediments and presently dry lakes (e.g. Dupont et al. 1989; Lézine 1989; Lézine and Casanova 1991) and in South Africa from marine sediments in the eastern Atlantic Ocean (e.g. Shi and Dupont 1997; Dupont and Wyputta 2003; Rommerskirchen et al. 2006) as wel as a desiccated lake (Partridge et al. 1993) and even Hyrax middens (Chase et al. 2011). Although there is much debate about the transport mechanism of pollen (fluvial versus aeolian), assemblages of the different pollen can be used to characterise vegetation type, and downcore variability in the different vegetation types can be interpreted in terms of environmental changes.

Homologous series of long-chain *n*-alkanes, *n*-alcohols and fatty acids are typical lipids found in dust (Lepple and Brine 1976; Schefuß et al. 2003). These lipids are the product of terrestrial higher plant epicuticular waxes (Eglinton and Hamilton 1967) and are used by these plants as a protective coating on leaves and stems. The wax particles are easily eroded off the surface of the leaves by wind, especially by a sandblasting effect, and can then become airborne (Simoneit 1977). Alternatively, decaying plant organic matter in soils can be lifted during dust storms and transported by wind. The plant waxes have been found in marine sediments up to 4 million years old and can be used to reconstruct environmental conditions in the source areas of the dust (Martinez-Garcia et al. 2011).

Next to these organic proxies for wind-blown deposits, many studies use the bulk chemistry of sediments as derived from core scanning and individual samples to characterise aeolian dust. Bulk chemistry is in fact related to the particle size but also potentially the density of the terrigenous particles (Bloemsma et al. 2012). Using the isotope chemical composition of the aeolian sediment fraction ($>10\ \mu m$), Meyer et al. (2011) managed to reconstruct the provenance changes of Saharan dust throughout several geologic stages with well-established contrasting palaeo-environmental conditions. Three periods were compared: (1) the Last Glacial Maximum, which occurred about 20 kyr BP, was characterised by extreme aridity and intensified atmospheric circulation; (2) the aforementioned African Humid Period, which occurred about 10 kyr BP, was characterised by increased rainfall and decreased atmospheric circulation relative to today; and (3) the present-day situation, which is characterised by relatively dry conditions and "normal" atmospheric circulation. All three periods obviously had an effect on the amount and size of the material transported by winds, which is reflected in their differing provenance (Meyer et al. 2011, 2013).

Other isotopes like the Pb series (^{204}Pb, ^{206}Pb, ^{207}Pb and ^{208}Pb) were used to characterise dust in sediment cores from the equatorial North Atlantic to reconstruct increased dust input during the Last Glacial Maximum ($\sim$18 kyr BP; Abouchami and Zabel 2003). Great care should be taken using Pb isotopes in modern mineral dust as combustion of long-chained hydrocarbons also emits considerable amounts of Pb that end up in the marine sediment archive (e.g. Erlenkeuser et al. 1974; Alleman et al. 2001).

Another marine archive with great potential for high-resolution dust records is tropical corals. Although tropical corals are very efficient in removing pollutants from their polyps, they seem to register dust that rains down on them in the He isotopes (there are nine, of which only ^{3}He and ^{4}He are stable) that they precipitate in their carbonates. Without comprehending exactly why and how corals do register these isotopes, Mukhopadhyay and Kreycik (2008) observed a close co-occurrence of ^{4}He in *Porites* corals from the Cape Verde Islands and the summer surface dust concentration (SDC) record from Barbados (Prospero and Lamb 2003). As *Porites* corals can grow several hundreds of years, they bear great potential for highly resolved long-term palaeo-aridity records.

Next to the chemical composition, also the mineralogical composition of marine sediments can be used to reconstruct amounts of dust being blown around. A classic example is the mineral palygorskite, which is typical for Saharan dust (Schütz and Sebert 1987) and of which the abundance in marine sediments can be used to quantify Saharan dust in the marine sediment archive (e.g. Coudé-Gaussen 1989; Scheuvens et al. 2013).

Related to the mineralogical proxies are various magnetic proxies, which are based on the magnetic properties of various minerals and mineral coatings in wind-blown dust. These coatings form under various environmental conditions with the iron oxide minerals haematite and goethite as main indicators of wetter or drier conditions (e.g. Bloemendal et al. 1988). As with all proxies, there are some pitfalls with magnetic proxies, related to, e.g. diagenetic (post-depositional) alterations of the magnetic minerals (Maher 2011) or occurrence of magnetic minerals produced by magnetotactic bacteria (Blakemore 1975).

17.5 Wind-blown Dust in the Ocean as a Player of Environmental Change

In the late 1990s, John Martin hypothesised that the ocean may play a crucial role in global climate. This so-called Fe hypothesis relates to the Fe-limited parts of the ocean (see Chap. 14), where many nutrients are available yet primary productivity is very low. Mineral dust may have played a role: as it carries Fe and other macro- and micronutrients, it may have stimulated plankton growth, which in turn may have led to lower atmospheric CO_2 concentrations. This hypothesis has been tested extensively by many so-called fertilisation experiments (see de Baar et al. 2005 for a synthesis of the results) which demonstrated that indeed primary productivity can be stimulated using dissolved Fe. However, the net effect of these experiments in terms of export of organic matter and hence actual CO_2 sequestration is still under debate. Also, so far there is only one known example of observed ocean fertilisation by mineral dust (Bishop et al. 2002) that indeed led to an increase in organic matter export from the surface ocean to the deep sea.

In a recent paper, Martinez-Garcia et al. (2011) demonstrated that there is indeed a coupling between dust input into the Southern Ocean and global climate through

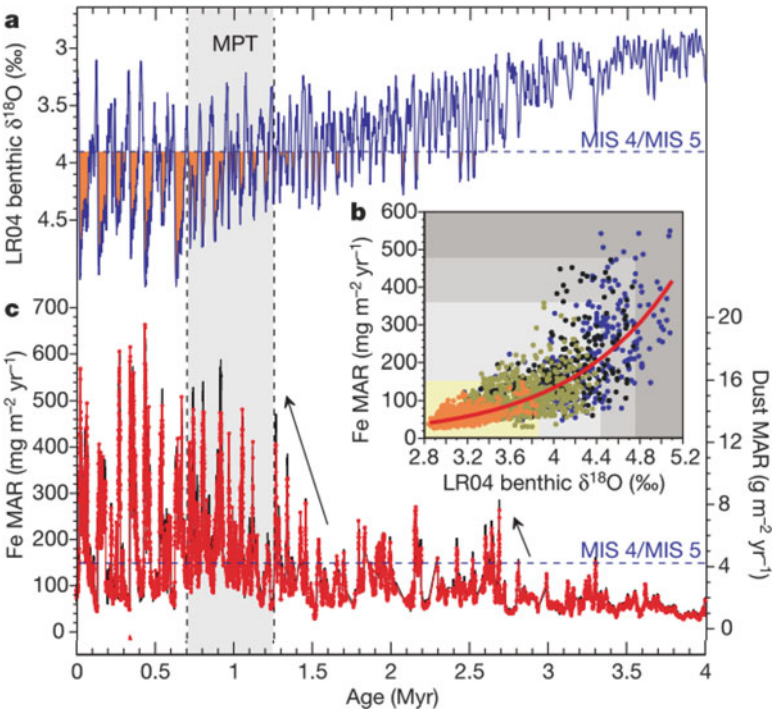

Fig. 17.7 Evolution of global ice volume and Southern Ocean dust and iron variability through the Pliocene and Pleistocene epochs. *a*, benthic $\delta^{18}O$ stack. *Orange* shading indicates the intervals where glaciations intensified. *b*, regression between benthic $\delta^{18}O$ and Fe mass accumulation rate (MAR). C, Fe MAR (*red line*) and dust MAR. From Martinez-Garcia et al. (2011)

plankton growth stimulation of dust and the resulting CO_2 effects throughout the last 4 million years. It was further hypothesised that mineral dust not only stimulates plankton growth through nutrient supply but also by increasing export of organic matter from the surface ocean to the deep sea through ballasting effects (Iversen and Ploug 2010), which comes down to relatively large and heavy mineral particles that sink to the sea floor at relatively high speed and on their way scavenge organic matter from the surface ocean downward. If this ballasting process is fast enough, there is less time for the organic tissue to be recycled and actual export of organic matter can be realised. Obviously, the speed of the downward transport from surface to deep ocean is directly related to the size of the dust particles that act as the anchors. In contrast, the bio-availability of the nutrients that are potentially supplied with the dust is most likely inversely related to the size of the dust particles; the faster they sink, the smaller the chance that the phytoplankton can actually benefit from the nutrients they carry. More research is needed to confirm this idea and picture in detail what the role of the particle size of the deposited dust on the ocean is, both in terms of nutrient supplier and in terms of carbon-pump accelerator (Fig. 17.7).

17.6 Conclusion

Subaqueous sediments form a great archive of mineral dust, and there are several well-established proxies to characterise and quantify dust back in time. In order to reconstruct the palaeo-environmental conditions that led to the deposition of these dust particles, these proxies have to be interpreted. There are many dust particle size-related proxies, based on the idea that particle-size distribution and wind carrying capacity are tightly coupled. However, care has to be taken with this approach as not only the horizontal but also the vertical distance of the transport path determines the particle-size distribution of the wind-blown deposits. There are still many open questions related to the particle size and chemical composition of mineral dust and its role in global climate.

References

Abouchami W, Zabel M (2003) Climate forcing of the Pb isotope record of terrigenous input into the Equatorial Atlantic. Earth Planet Sci Lett 213:221–234

Alexandre A, Meunier JD, Lezine AM, Vincens A, Schwartz D (1997) Phytoliths: indicators of grassland dynamics during the late Holocene in intertropical Africa. Palaeogeogr Palaeoclimatol Palaeoecol 136:213–229

Alleman LY, Church TM, Véron AJ, Kim G, Hamelin B, Flegal AR (2001) Isotopic evidence of contaminant lead in the South Atlantic troposphere and surface waters. Deep-Sea Res II Top Stud Oceanogr 48:2811–2827

Betzer PR, Carder KL, Duce RA, Merrill JT, Tindale NW, Uematsu M et al (1988) Long-range transport of giant mineral aerosol particles. Nature 336:568

Bishop JKB, Davis RE, Sherman JT (2002) Robotic observations of dust storm enhancement of carbon biomass in the North Pacific. Science 298:817–821

Blakemore R (1975) Magnetotactic bacteria. Science 190:377–379

Bloemendal J, Lamb B, King J (1988) Paleoenvironmental implications of rock-magnetic properties of late quaternary sediment cores from the eastern equatorial Atlantic. Paleoceanography 3:61–87

Bloemsma MR, Zabel M, Stuut JBW, Tjallingii R, Collins JA, Weltje GJ (2012) Modelling the joint variability of grain size and chemical composition in sediments. Sediment Geol 280:135–148

Bowler JM (1976) Aridity in Australia: Age, origins and expression in aeolian landforms and sediments. Earth Sci Rev 12:279–310

Chase BM, Quick LJ, Meadows ME, Scott L, Thomas DSG, Reimer PJ (2011) Late glacial interhemispheric climate dynamics revealed in South African hyrax middens. Geology 39:19–22

Clemens SC, Prell WL (1990) Late Pleistocene variability of Arabian Sea summer monsoon winds and continental aridity: Eolian records from the lithogenic component of deep-sea sediments. Paleoceanography 5:109–145

Coetzee JA (1976) A report on a pollen analytical investigation of recent river mouth sediments on the South West African coast. In: Sarnthein M, Seibold E, Rognon P (eds) Palaecology of Africa, vol 9. A.A. Balkema, Rotterdam, pp 131–135

Coudé-Gaussen G (1989) Local, proximal and distal Saharan dusts: characterization and contribution to the sedimentation. In: Leinen M, Sarnthein M (eds) Palaeoclimatology and palaeometeorology: modern and past patterns of global atmospheric transport. Kluwer Academic, Dordrecht 282:339–58

de Baar H, Boyd PW, Coale KH, Landry MR, Tsuda A, Asmmy P et al (2005) Synthesis of iron fertilization experiments: From the Iron Age in the Age of Enlightenment. J Geophys Res 110:24

De Deckker P, Corrège T, Head J (1991) Late Pleistocene record of cyclic eolian activity from tropical Australia suggesting the Younger Dryas is not an unusual climatic event. Geology 19:602–605

Dean WE (1997) Rates, timing, and cyclicity of Holocene eolian activity in north-central United States: evidence from varved lake sediments. Geology 25:331–334

deMenocal PB (1995) Plio-pleistocene African climate. Science 270:53–59

deMenocal PB, Ruddiman WF, Pokras EM (1993) Influences of high- and low-latitude processes on African terrestrial climate: Pleistocene eolian records from Equatorial Atlantic Ocean Drilling Program site 663. Paleoceanography 8:209–242

deMenocal P, Ortiz J, Guilderson T, Sarnthein M (2000a) Coherent high- and low-latitude climate variability during the Holocene warm period. Science 288:2198–2202

deMenocal PB, Ortiz J, Guilderson TP, Adkins J, Sarnthein M, Baker L et al (2000b) Abrupt onset and termination of the African humid period: rapid climate responses to gradual insolation forcing. Quat Sci Rev 19:347–361

Drake N, Bristow C (2006) Shorelines in the Sahara: geomorphological evidence for an enhanced monsoon from palaeolake Megachad. The Holocene 16:901–911

Dupont LM, Wyputta U (2003) Reconstructing pathways of aeolian pollen transport to the marine sediments along the coastline of SW Africa. Quat Sci Rev 22:157–174

Dupont LM, Beug HJ, Stalling H, Tiedemann R (1989) First palynological results from site 658 at 21 N off northwest Africa: pollen as climate indicators. Proc Ocean Drill Prog Sci Result 108:93–111

Eglinton G, Hamilton RJ (1967) Leaf epicuticular waxes. Science 156:1322–1335

Ehrenberg CG (1847) Passatstaub und Blutregen – Ein grosses organisches unsichtbares Wirken und Leben in der Atmosphäre. Abhandlungen der Königlichen Akademie der Wissenschaften zu Berlin, pp 269–460 (printed in 1849).

Erlenkeuser H, Suess E, Willkomm H (1974) Industrialization affects heavy metal and carbon isotope concentrations in recent Baltic Sea sediments. Geochim Cosmochim Acta 38:823–842

Filipsson HL, Romero OE, Stuut J-BW, Donner B (2011) Relationships between primary productivity and bottom-water oxygenation off northwest Africa during the last deglaciation. J Quat Sci 26:448–456

Folk RL, Ward WC (1957) Brazos River bar: a study in the significance of grain size parameters. J Sediment Petrol 27:3–26

Franzén L, Hjelmroos M (1988) A Coloured Snow Episode on the Swedish West Coast, January 1987 a Quantitative and Qualitative Study of Air Borne Particles. Geogr Ann Ser A Phys Geogr 70:235–243

Gasse F, Stabell B, Fourtanier E, van Iperen Y (1989) Freshwater diatom influx in intertropical Atlantic: relationships with continental records from Africa. Quat Res 32:229–243

Groot JJ, Groot CR (1966) Pollen spectra from deep-sea sediments as indicators of climatic changes in southern South America. Mar Geol 4:525–537

Grove AT (1972) The dissolved and solid load carried by some West African rivers: Senegal, Niger, Benue and Shari. J Hydrol 16:277–300

Hamann Y, Ehrmann W, Schmiedl G, Kruger S, Stuut J-BW, Kuhnt T (2008) Sedimentation processes in the Eastern Mediterranean Sea during the Late Glacial and Holocene revealed by end-member modelling of the terrigenous fraction in marine sediments. Mar Geol 248:97–114

Hesse PP (1994) The record of continental dust from Australia in Tasman sea sediments. Quat Sci Rev 13:257–272

Heusser CJ (1983) Quaternary pollen record from Laguna de Tagua Tagua, Chile. Science 219:1429–4132

Holz C, Stuut J-BW, Henrich R (2004) Terrigenous sedimentation processes along the continental margin off NW-Africa: implications from grain-size analyses of surface sediments. Sedimentology 51:1145–1154

Holz C, Stuut J-BW, Henrich R, Meggers H (2007) Variability in terrigenous sedimentation processes off northwest Africa and its relation to climate changes: Inferences from grain-size distributions of a Holocene marine sediment record. Sediment Geol 202:499–508
Hovan SA, Rea DK, Pisias NG, Shackleton NJ (1989) A direct link between the China Loess and Marine Delta-O-18 records – aeolian flux to the North Pacific. Nature 340:296–298
Iversen MH, Ploug H (2010) Ballast minerals and the sinking carbon flux in the ocean: carbon-specific respiration rates and sinking velocities of macroscopic organic aggregates (marine snow). Biogeosci Discuss 7:3335–3364
Janecek TR, Rea DK (1985) Quaternary fluctuations in the Northern Hemisphere trade winds and westerlies. Quat Res 24:150–163
Jansen JHF, Alderliesten C, Houston CM, De Jong AFM, Van der Borg K, Van Iperen JM (1989) Aridity in equatorial Africa during the last 225,000 years: a record of opal phytoliths/freshwater diatoms from the Zaire (Congo) deep-sea fan (NE Angola Basin). Radiocarbon 31:557–569
Kershaw AP, van der Kaars S, Moss PT (2003) Late Quaternary Milankovitch-scale climatic change and variability and its impact on monsoonal Australasia. Mar Geol 201:81–95
Kershaw AP, Bretherton SC, van der Kaars S (2007) A complete pollen record of the last 230 ka from Lynch's Crater, north-eastern Australia. Palaeogeogr Palaeoclimatol Palaeoecol 251:23–45
Kolbe RW (1957) Fresh-water diatoms from Atlantic deep-sea sediments. Science 126:1053–1056
Koopmann B (1979) Saharastaub in den sedimenten des subtropisch-tropischen Nordatlantic während der letzten 20.000 Jahre. Thesis. Type, Christian-Albrechts-Universität, Kiel
Krastel S, Hanebuth TJJ, Antobreh AA, Henrich R, Holz C, Kölling M et al (2004) Cap Timiris Canyon: A newly discovered channel system offshore of Mauritania. Eos 85:417–419
Kröpelin S, Verschuren D, Lezine A-M, Eggermont H, Cocquyt C, Francus P et al (2008) Climate-driven ecosystem succession in the Sahara: the past 6000 years. Science 320:765–768
Lamy F, Klump J, Hebbeln D, Wefer G (2000) Late quaternary rapid climate change in northern Chile. Terra Nova 12:8–13
Lepple FK, Brine CJ (1976) Organic constituents in eolian dust and surface sediments from Northwest Africa. J Geophys Res 81:1141–1147
Lézine A-M (1989) Late quaternary vegetation and climate of the Sahel. Quat Res 32:317–334
Lézine A-M, Casanova J (1991) Correlated oceanic and continental records demonstrate past climate and hydrology of North Africa (0–140 ka). Geology 19:307–310
Lisiecki LE, Raymo ME (2005) A Pliocene-Pleistocene stack of 57 globally distributed benthic δ18O records. Paleoceanography 20, PA1003
Maher BA (2011) The magnetic properties of quaternary aeolian dusts and sediments, and their palaeoclimatic significance. Aeolian Res 3:87–144
Markgraf V (1993) Climatic history of South America since 18,000 yr B.P.: comparison of pollen records and model simulations. In: Wright HE, Kutzbach JE, Webb T, Ruddiman WF, Street-Perrot FA, Bartlein PJ (eds) Global climate since the last glacial maximum. University of Minnesota Press, Minneapolis, pp 357–85
Martinez-Garcia A, Rosell-Mele A, Jaccard SL, Geibert W, Sigman DM, Haug GH (2011) Southern Ocean dust-climate coupling over the past four million years. Nature 476:312–315
Matthewson AP, Shimmield GB, Kroon D (1995) A 300 kyr high-resolution aridity record of the North-African continent. Paleoceanography 10:677–692
Mayr C, Wille M, Haberzettl T, Fey M, Janssen S, Lücke A et al (2007) Holocene variability of the Southern Hemisphere westerlies in Argentinean Patagonia (52° S). Quat Sci Rev 26:579–584
McGee D, deMenocal PB, Winckler G, Stuut JBW, Bradtmiller LI (2013) The magnitude, timing and abruptness of changes in North African dust deposition over the last 20,000 yr. Earth Planet Sci Lett 371–372:163–176
McGregor HV, Dupont L, Stuut J-BW, Kuhlmann H (2009) Vegetation change, goats, and religion: a 2000-year history of land use in southern Morocco. Quat Sci Rev 28:1434–1448
Meyer I, Davies GR, Stuut J-BW (2011) Grain size control on Sr-Nd isotope provenance studies and impact on paleoclimate reconstructions: An example from deep-sea sediments offshore NW Africa. Geochem Geophys Geosyst 12, Q03005

Meyer I, Davies GR, Vogt C, Kuhlmann H, Stuut J-BW (2013) Changing rainfall patterns in NW Africa since the Younger Dryas. Aeolian Res 10:111–123

Middleton NJ, Betzer PR, Bull PA (2001) Long-range transport of 'giant' aeolian quartz grains: linkage with discrete sedimentary sources and implications for protective particle transfer. Mar Geol 177:411–417

Mukhopadhyay S, Kreycik P (2008) Dust generation and drought patterns in Africa from helium-4 in a modern Cape Verde coral. Geophys Res Lett 35:L20820. doi:10.1029/2008GL035722

Mulitza S, Prange M, Stuut J-BW, Zabel M, von Dobeneck T, Itambi AC et al. (2008) Sahel megadroughts triggered by glacial slowdowns of Atlantic meridional overturning. Paleoceanography 23. doi:10.1029/2008PA001637

Mulitza S, Heslop D, Pittauerova D, Fischer HW, Meyer I, Stuut J-B et al (2010) Increase in African dust flux at the onset of commercial agriculture in the Sahel region. Nature 466:226–228

Niessen F, Lister G, Giovanoli F (1992) Dust transport and palaeoclimate during the Oldest Dryas in Central Europe — implications from varves (Lake Constance). Clim Dyn 8:71–81

Nizou J, Hanebuth TJJ, Vogt C (2011) Deciphering signals of late Holocene fluvial and aeolian supply from a shelf sediment depocentre off Senegal (North-West Africa). J Quat Sci 26:411–421

NorthGRIP Community Members (2004) High-resolution record of Northern Hemisphere climate extending into the last interglacial period. Nature 431:147–151

Otto S, de Reus M, Trautmann T, Thomas A, Wendisch M, Borrmann S (2007) Atmospheric radiative effects of an in situ measured Saharan dust plume and the role of large particles. Atmos Chem Phys 7:4887–4903

Partridge TC, Kerr SJ, Metcalfe SE, Scott L, Talma AS, Vogel JC (1993) The Pretoria Saltpan: a 200,000 year Southern African lacustrine sequence. Palaeogeogr Palaeoclimatol Palaeoecol 101:317–337

Pokras EM, Mix AC (1985) Eolian evidence for spatial variability of late Quaternary climates in tropical Africa. Quat Res 24:137–149

Prins MA, Vriend M (2007) Glacial and interglacial eolian dust dispersal patterns across the Chinese Loess Plateau inferred from decomposed loess grain-size records. Geochemistry, Geophysics, Geosystems, 8

Prins MA, Weltje GJ (1999) End-member modeling of siliciclastic grain-size distributions: the Late Quaternary record of eolian and fluvial sediment supply to the Arabian Sea and its paleoclimatic significance. In: Harbaugh J, Watney L, Rankey G, Slingerland R, Goldstein R, Franseen E (eds) Numerical experiments in stratigraphy: Recent advances in stratigraphic and sedimentologic computer simulations, vol 62, SEPM special publication. Society for Sedimentary Geology, Tulsa, pp 91–111

Prins MA, Postma G, Weltje GJ (2000) Controls on terrigenous sediment supply to the Arabian Sea during the late Quaternary: the Makran continental slope. Mar Geol 169:351–371

Prins MA, Bouwer LM, Beets CJ, Troelstra SR, Weltje GJ, Kruk RW et al (2002) Ocean circulation and iceberg discharge in the glacial North Atlantic: inferences from unmixing of sediment size distribution. Geology 30:555–558

Prins MA, Vriend M, Nugteren G, Vandenberghe J, Lu H, Zheng H et al (2007) Late Quaternary aeolian dust input variability on the Chinese Loess Plateau: inferences from unmixing of loess grain-size records. Quat Sci Rev 26:230–242

Prospero JM (1996) Saharan dust transport over the North Atlantic Ocean and Mediterranean: an overview. In: Guerzoni S, Chester R (eds) The impact of desert dust across the Mediterranean, vol 11. Kluwer, Dordrecht/Boston/London, pp 133–151

Prospero J, Bonatti E (1969) Continental dust in the atmosphere of the eastern equatorial Pacific. J Geophys Res 74:3362–3371

Prospero JM, Lamb PJ (2003) African droughts and dust transport to the Caribbean: climate change implications. Science 302:1024–1027

Prospero JM, Ginoux P, Torres O, Nicholson SE, Gill TE (2002) Environmental characterization of global sources of atmospheric soil dust identified with the Nimbus 7 total ozone mapping spectrometer (TOMS) absorbing aerosol product. Rev Geophys 40:1–31

Pye K, Zhou L-P (1989) Late Pleistocene and Holocene aeolian dust deposition in North China and the Northwest Pacific Ocean. Palaeogeogr Palaeoclimatol Palaeoecol 73:11–23
Ram M, Gayley RI (1991) Long-range transport of volcanic ash to the Greenland ice sheet. Nature 349:401–404
Rea DK (1994) The paleoclimatic record provided by eolian deposition in the deep sea: the geologic history of wind. Rev Geophys 32:159–195
Rea DK, Bloomstine MK (1986) Neogene history of the South Pacific tradewinds: evidence for hemispherical asymmetry of atmospheric circulation. Palaeogeogr Palaeoclimatol Palaeoecol 55:55–64
Rea DK, Janecek TR (1981) Mass-accumulation rates of the non-authigenic crystalline (eolian) component of deep-sea sediments from the western Mid-Pacific Mountains. In: Stout LN (ed) Initial reports of the Deep Sea Drilling Project Site 463, vol 62. NSF, Washington, DC, pp 653–659
Rea DK, Leinen M, Janecek TR (1985) Geologic approach to the long-term history of atmospheric circulation. Science 227:721–725
Rommerskirchen F, Eglinton G, Dupont L, Rullkötter J (2006) Glacial/interglacial changes in southern Africa: compound-specific $\delta^{13}C$ land plant biomarker and pollen records from southeast Atlantic continental margin sediments. Geochem Geophys Geosyst 7:21
Sarnthein M, Tetzlaff G, Koopmann B, Wolter K, Pflaumann U (1981) Glacial and interglacial wind regimes over the eastern subtropical Atlantic and North-West Africa. Nature 293:193–196
Satheesh SK, Dutt CBS, Srinivasan J, Rao UR (2007) Atmospheric warming due to dust absorption over Afro-Asian regions. Geophys Res Lett 34:L04805. doi:10.1029/2006GL028623
Schefuß E, Ratmeyer V, Stuut J-BW, Jansen JHF, Sinninghe Damsté JS (2003) Carbon isotope analyses of n-alkanes in dust from the lower atmosphere over the central eastern Atlantic. Geochim Cosmochim Acta 67:1757–1767
Scheuvens D, Schütz L, Kandler K, Ebert M, Weinbruch S (2013) Bulk composition of northern African dust and its source sediments – a compilation. Earth Sci Rev 116:170–194
Schütz L, Sebert M (1987) Mineral aerosols and source identification. J Aerosol Sci 18:1–10
Shanahan TM, Overpeck JT, Anchukaitis KJ, Beck JW, Cole JE, Dettman DL et al (2009) Atlantic forcing of persistent drought in West Africa. Science 324:377–380
Shi N, Dupont LM (1997) Vegetation and climatic history of southwest Africa: a marine palynological record of the last 300,000 years. Veg Hist Archaeobot 6:117–131
Simoneit BRT (1977) Organic matter in eolian dusts over the Atlantic Ocean. Mar Chem 5:443–464
Sirocko F, Seelos K, Schaber K, Rein B, Dreher F, Diehl M et al (2005) A late Eemian aridity pulse in central Europe during the last glacial inception. Nature 436:833–836
Snoeckx H, Rea DK, Jones CE, Ingram BL (1995) Eolian and silica deposition in the central North Pacific: results from Leg 145 Sites 885/886. In: Rea DK, Basov IA, Scholl DW, Allan JF (eds) Proceedings of the ODP, scientific results, vol 145D. Ocean Drilling Program, College Station, pp 219–230
Stuut J-BW, Lamy F (2004) Climate variability at the southern boundaries of the Namib (southwestern Africa) and Atacama (northern Chile) coastal deserts during the last 120,000 yr. Quat Res 62:301–309
Stuut J-BW, Prins MA, Jansen JHF (2002a) Fast reconnaissance of carbonate dissolution based on the size distribution of calcareous ooze on Walvis Ridge, SE Atlantic Ocean. Mar Geol 190:563–571
Stuut J-BW, Prins MA, Schneider RR, Weltje GJ, Jansen JHF, Postma G (2002b) A 300-kyr record of aridity and wind strength in southwestern Africa: inferences from grain-size distributions of sediments on Walvis Ridge, SE Atlantic. Mar Geol 180:221–233
Stuut J-BW, Crosta X, Van der Borg K, Schneider RR (2004) The relationship between Antarctic sea ice and South-western African climate during the Late Quaternary. Geology 32:909–912
Stuut J-BW, Zabel M, Ratmeyer V, Helmke P, Schefuß E, Lavik G et al. (2005) Provenance of present-day eolian dust collected off NW Africa. *Journal of Geophysical Research* 110, doi:10.1029/2004JD005161

Stuut J-BW, Marchant M, Kaiser J, Lamy F, Mohtadi M, Romero O et al (2006) The late Quaternary paleoenvironment of Chile as seen from marine archives. Geol Helv 61:135–151

Stuut J-BW, Kasten S, Lamy F, Hebbeln D (2007) Sources and modes of terrigenous sediment input to the Chilean continental slope. Quat Int 161:67–76

Stuut J-BW, Smalley I, O'Hara-Dhand K (2009) Aeolian dust in Europe: African sources and European deposits. Quat Int 198:234–245

Stuut J-BW, Temmesfeld F, De Deckker P (2014) A 550 kyr record of aeolian activity near North West Cape, Australia: inferences from grain-size distributions and bulk chemistry of SE Indian Ocean deep-sea sediments. Quat Sci Rev 83:83–94

Tjallingii R, Claussen M, Stuut J-BW, Fohlmeister J, Jahn A, Bickert T et al (2008) Coherent high- and low-latitude control of the northwest African hydrological balance. Nat Geosci 1:670–675

Vörösmarty CJ, Fekete BM, Meybeck M, Lammers RB (2000) Global system of rivers: its role in organizing continental land mass and defining land-to-ocean linkages. Glob Biogeochem Cycles 14:599–621

Weedon GP, Shimmield GB (1991) Late Pleistocene upwelling and productivity variations in the Northwest Indian Ocean deduced from spectral analyses of geochemical data from sites 722 and 724. Proc Ocean Drill Prog Sci Result 117:431–443

Weltje G (1997) End-member modelling of compositional data: Numerical-statistical algorithms for solving the explicit mixing problem. J Math Geol 29:503–549

Weltje GJ, Prins MA (2003) Muddled or mixed? Inferring palaeoclimate from size distributions of deep-sea clastics. Sediment Geol 162:39–62

Weltje GJ, Prins MA (2007) Genetically meaningful decomposition of grain-size distributions. Sediment Geol 202:409–424

Windom HL (1975) Eolian contributions to marine sediments. J Sediment Petrol 45:520–529

Zolitschka B, Brauer A, Negendank JFW, Stockhausen H, Lang A (2000) Annually dated late Weichselian continental paleoclimate record from the Eifel, Germany. Geology 28:783–786

Chapter 18
Ice Core Archives of Mineral Dust

Paul Vallelonga and Anders Svensson

Abstract The ice caps of Greenland and Antarctica provide an archive of dust deposition covering several glacial-interglacial climate cycles. Greenland ice core records extend back to approximately 130 ka ago, showing great changes in dust concentrations from interglacial (45 ng/g) to glacial (5,000 ng/g) climate periods. Strontium and Neodymium isotopic fingerprinting indicate that the Gobi and Taklamakan Deserts in central Asia are the predominant source of dust deposited in Greenland. Antarctic ice core records archive the past 8 glacial-interglacial cycles, with less dust deposited during interglacial (15 ng/g) and glacial (800 ng/g) climate periods in comparison to Greenland. Loess fields and glacial outwash plains in southern South America are the main sources of dust deposited in Antarctica, although there is evidence of other sources, such as Australia and local dust deflation zones in Antarctica, also contributing dust during interglacial periods. Dust concentrations in ice cores provide a detailed record of the manner in which climate variability influences the combined processes of dust deflation, transport and deposition processes, but the precise distinction of drivers and feedbacks within these processes remains an ongoing challenge.

Keywords Greenland • Antarctica • Dust • Provenance • Strontium isotope • Particle size distribution

P. Vallelonga (✉) • A. Svensson
Centre for Ice and Climate, Niels Bohr Institute, University of Copenhagen,
Juliane Maries vej 30, 2100, Copenhagen, Denmark
e-mail: ptravis@nbi.ku.dk; as@gfy.ku.dk

P. Knippertz and J.-B.W. Stuut (eds.), *Mineral Dust: A Key Player in the Earth System*, DOI 10.1007/978-94-017-8978-3_18,

18.1 Introduction

Snow and ice cover up to 25 % of the Earth's surface, approximately 15 million km^2 is on land and 25 million km^2 is sea ice that forms seasonally over the polar oceans. Snow is deposited in many areas but glaciers will only grow in areas where the annual snow accumulation exceeds the annual snow ablation. Although the largest and most persistent ice sheets are found at the poles, many glaciers and smaller ice sheets are found on lower latitude mountain ranges of sufficient height. As snow accumulates, it compacts the underlying years' snowfall and produces layers that become denser with depth. Fresh snow has a low density (300 kg/m^3) and rapidly compacts to firn (density 500–800 kg/m^3). At densities greater than 830 kg/m^3 the snow crystals have compressed into solid ice. The maximum possible density of ice is 910 kg/m^3, due to the trapping of air in the firn column, and subsequent presence of air bubbles and clathrates in the ice matrix.

Ice sheets and glaciers can be hundreds to thousands of metres thick, offering long climate records that are retrieved by drilling ice cores (Fig. 18.1). Deep ice cores in central Greenland and Antarctica can be up to 4 km long and have produced climate records covering the past 800 ka (thousands of years). Mountain glaciers are usually less than 300 m thick and offer climate records from a few hundred to a few thousand years long. Drilling operations are conducted in the summer, when weather and temperature conditions are favourable; mountain glacier cores can be drilled in a few weeks, deep drillings in Greenland and Antarctica usually require 3–5 years. The ice is recovered in sequential drilling "runs", returning 1–4 m of ice at a time.

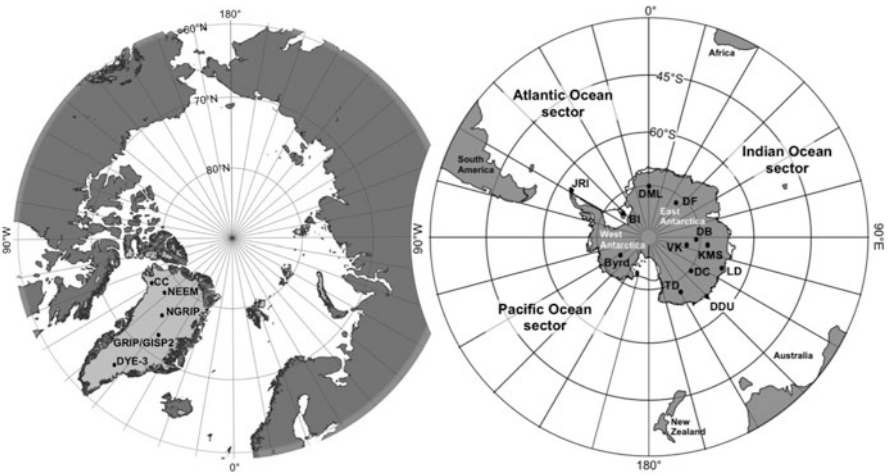

Fig. 18.1 Map of the north and south polar regions showing ice core drilling sites in Antarctica and Greenland. Antarctic locations include Berkner Island (BI), Byrd, Vostok (VK), Dome C (DC), Dronning Maud Land (DML), Dumont D'Urville (DDU), Talos Dome (TD), Law Dome (LD), Dome Fuji (DF), Dome B (DB) and Komsomolskaya (KMS). Greenland sites include Camp Century (CC), NEEM, NorthGRIP (NGRIP), GRIP/GISP2 and DYE-3

The borehole is stabilized using a dense non-freezing liquid which may potentially contaminate the dust record contained within the ice (Svensson et al. 2011). The outer contaminated section of the ice core is removed to ensure accurate dust measurements. This is done by various methods; mechanical scraping of the outer layers using steel or ceramic chisels (Vallelonga et al. 2002a); melting the outer layers by dipping them into baths of particle-free purified water (Delmonte et al. 2002a); or by continuously melting the ice on a hot surface that separates the inner pristine ice from the outer contaminated section (Bigler et al. 2011).

Ice core chronologies are constructed from a variety of parameters; these include ice flow models, absolute time markers and seasonal indicators (Wolff et al. 2010). Seasonal indicators include Oxygen isotope ratios ($\delta^{18}O$, related primarily to precipitation temperature), sea salts (usually greater in winter) and dust fluxes (spring peaks in Greenland ice). Seasonal indicators are difficult to measure in deep ice as they are diffused or thinned by ice flow. Absolute time markers include atmospheric nuclear bomb testing maxima in 1954 and 1963, as well as volcanic eruption products such as sulphate, fluoride, chloride, ash and tephra. On longer time scales, geomagnetic excursions and reversals can be detected by variability in the production of cosmogenic nuclides (^{10}Be, ^{36}Cl, ^{81}Kr). All of these chronological markers can then be incorporated into models of firn densification and ice flow, to produce a complete ice core chronology (Parrenin et al. 2007). Ice flow models are the bases for the longest Greenland and Antarctic ice core records.

Dust plays an important role in ice crystal structure, densification and possibly glacial dynamics. Inaccuracies in firn densification models are likely due to the absence of parameterizations for dust and impurity content. Recent observations have shown a correlation between impurity content and densification, which implies that impurities have an effect on the strength and/or structure of the ice crystals formed (Hörhold et al. 2012). Firn modelling is valuable for constructing age models for shallow and intermediate ice cores, and for interpreting gas records from deep ice cores. The information that can be retrieved from a well-tuned firn model include ice-gas age differences (Δage), past site elevation and temperature. There is also indirect evidence that impurities have an effect on larger scale dynamics of ice sheets; the Greenland NEEM deep ice drilling project has identified that ice folding preferentially occurs at the interface of the early glacial ice and late interglacial ice, which have different rheologies due to many factors including impurity concentrations (NEEM Community Members 2013).

Dust plays an important role in the formation and growth of glaciers, as it both affects and responds to climate changes and influences the formation and densification of snow strata. The effects of dust deflation and atmospheric transport on climate have been covered in Chaps. 5, 6, 7. The impacts of atmospheric dust loading on insolation and albedo have also been discussed in detail in Chaps. 11, 13 and 15. In this chapter we will discuss the methods used to produce dust records from ice cores, outline the dust flux records produced, and synthesize the current understanding of global variability in dust transport and deposition revealed by ice cores.

18.2 Dust Measurement Techniques

18.2.1 Coulter Counter

Most dust concentration and size data reported for snow and ice have been determined using Coulter Counter (CC) instruments. Ice samples are melted and mixed with filtered, particle-free electrolyte solution (usually NaCl). The sample is drawn through a small aperture, across which the electrical conductivity is continuously monitored. As each particle crosses the aperture, a change in conductivity across the aperture is recorded, with the magnitude of the conductivity change being proportional to the volume of displaced electrolyte, that is, the volume of the dust particle. The coulter counter is calibrated using latex beads of specified size and concentration, allowing the determination of both particle concentration and size. Although CCs are reliable and sensitive instruments, they are limited to discrete measurements with a minimum sample size of approximately 10 mL. The technique is slow (approximately 5 min per measurement) and CCs are sensitive to electromagnetic noise. The particle size range that can be determined is dependent upon the aperture size; the smallest aperture allows particle measurements between 0.6 and 10 μm diameters. As with most particle detectors, there is the difficulty of coincidence – the phenomenon of simultaneously counting two small particles, which are then counted as one particle, however as particle numbers in ice core samples are usually low, the coincidence effect is often negligible.

18.2.2 Laser Particle Detector

Laser particle detectors (LPD) have been in use since the 1980s and compensate for some limitations of CCs, the primary one being that LPDs sample continuously. The LPD detector consists of small optical cell, through which the melted ice sample is passed. A high-powered laser illuminates the optical cell, opposite a very sensitive light detector. The detector records scattering of light due to the presence of particles in the optical cell, thus allowing the determination of particle concentrations and size ranges. The sensitivity and particle size range depends on the instrument wavelength range and power; a 680 nm laser allows the determination of 0.9–15 μm particle diameters, appropriate for ice core measurements. Similar to CC, LPDs are calibrated using manufactured latex bead standards. There are concerns regarding such materials, as to whether they accurately represent the response from real dust particles. An alternative is to use standards produced from filtered desert dust, although they are expensive and less reproducible. CC and LPD techniques have been compared by parallel measurements of EPICA Dome C (EDC) samples (Ruth et al. 2008). Very good agreement was found for insoluble particle concentrations, although it appears that the LPD did not reproduce the full variance of the CC,

possibly due to the microsecond-long delay time between LPD measurements. CC remains the reference technique for dust particle determination in ice core samples.

18.2.3 Elemental Dust Proxies

Elements with a high crustal abundance are often used as a proxy for total dust flux when CC or LPD instruments are unavailable (see also Chap. 2). Calcium (measured as the soluble Ca^{2+} ion) is commonly used because it can be determined routinely using Ion Chromatography or Continuous Flow Analysis (CFA) techniques. Calcium is also present in seawater and marine inputs may disturb the dust-Ca signal in coastal ice core records; these can be corrected by determining the input of marine salts, usually from sodium (Na^{+}). The non-sea salt Ca^{2+} ($nssCa^{2+}$) concentration is then determined by substracting the sea salt ($ssCa^{2+}$) input as determined from the marine Ca^{2+}/Na^{+} ratio, employing the following equations:

$$\mathrm{nssCa^{2+}} = \frac{R_\mathrm{t}}{R_\mathrm{t} - R_\mathrm{m}} \left(\mathrm{Ca^{2+}} - R_\mathrm{m}\mathrm{Na^{+}}\right)$$

$$\mathrm{ssNa^{+}} = \mathrm{Na^{+}} - \frac{1}{R_\mathrm{t} - R_\mathrm{m}} \left(\mathrm{Ca^{2+}} - R_\mathrm{m}\mathrm{Na^{+}}\right)$$

where R_m and R_t are the respective Ca^{2+}/Na^{+} ratios in seawater (0.038 by mass) and crustal (1.78) sources (Fischer et al. 2007b). For inland sites, the sea salt correction is usually negligible. A detailed study of dust and marine salts and sources in EDC ice has been reported by Bigler et al. (2006).

Aluminium (Al), Iron (Fe), Scandium (Sc), Thallium (Tl) and Barium (Ba) are also used as dust proxies, and have been determined using Inductively-Coupled Plasma Mass Spectrometer (ICP-MS) and/or Thermal Ionization Mass Spectrometer (TIMS) instruments. Contamination controls are required in the preparation and analysis of these elements. As for Ca, a limitation of using single elements for dust proxies is the possible range of elemental abundances in different dust sources. Using a suite of elements as proxies can minimize this. Ruth et al. (2008) compared CC and LPD data with elemental proxies such as Al and Fe. In all cases, good agreement was found between the techniques, although ratios of glacial-interglacial concentrations varied by up to a factor of two between the techniques. Sample preparation is also an important consideration; elemental recoveries will vary depending on the duration and type of sample acidification. In the case of Fe, acidification at pH1 for 24 h will recover 40–80 % of the total Fe in dust particles, but acidification periods of up to a month using concentrated HCl are required to recover total Fe concentrations (Edwards et al. 2006). Traversi et al. (2004) also demonstrated that the recovery of Fe and Al is much greater for ICP-MS compared to CFA, on account of the brief acidification time (2–3 min) used in CFA analyses.

18.2.4 Provenance Techniques

Isotopic fingerprinting is the most selective technique available for determining the sources of dust deposited in polar ice cores. The technique is based on the variability of isotope ratios that result from radioactive decay of elements in the Earth's crust, as well as the varied ages and geochemistry of the continents. Radioactive decay chains have half-lives of billions of years, and are unaffected by chemical or physical transport processes such as dust deflation and dissolution. Two isotopic systems have been used for investigating dust provenance: strontium (Sr) and neodymium (Nd) (Grousset and Biscaye 2005); and lead (Pb) (Rosman 2001). ^{87}Sr and ^{143}Nd are the respective radioactive decay products of rubidium and samarium, so the ratios of ^{87}Sr and ^{143}Nd to stable ^{86}Sr and ^{144}Nd, respectively, will change over time. For Pb, three isotopes (^{206}Pb, ^{207}Pb, ^{208}Pb) are respective end-products of radioactive decay chains of ^{238}U, ^{235}U and ^{232}Th. For these isotopic systems to be effective, there must be sufficient variability between the different Potential Source Areas (PSAs) and the ice core dust to enable the viable PSAs to be distinguished. In the case of Pb, other emission sources such as volcanism or industrial activity can interfere with the interpretation (Vallelonga et al. 2002b). Isotope ratios are determined using sensitive instruments capable of separating the isotopes of an element and measuring their relative abundances. These measurements are routinely performed using TIMS and Multicollector ICP-MS instruments.

Ice core dust provenance has also been evaluated using Rare Earth Elements (REEs), determined by ICP-MS. REEs have the benefit of being relatively easy to measure and difficult to contaminate, so they can be determined at higher resolution and more quickly than Sr/Nd or Pb isotopes. Interpretation of REE provenance is complicated by overlapping PSA signatures as well as sample processing interferences; Rhodes et al. (2011) have found that REE signatures can be altered by some sample preparation techniques.

18.2.5 Visual Stratigraphy

Ice core dust content is often visible to the naked eye as a layering or banding in the ice (Alley et al. 1997). A profile of the visual ice core stratigraphy is best obtained after carefully preparing a clear flat ice core surface. Using an indirect light source and a digital camera the visual stratigraphy or 'linescan' profile can be obtained (Svensson et al. 2005; McGwire et al. 2008). Similar to dark field microscopy, in this profile transparent ice will appear dark whereas any impurities in the ice, such as air bubbles or dust particles, will cause light scattering and make the impurities appear white in the line scan image (Fig. 18.2). Continuous line scan profiles are available for the glacial part of the Greenland NorthGRIP (NGRIP) ice core (Svensson et al. 2005) and the Antarctic EPICA Dronning Maud Land (EDML) ice core (Faria et al. 2010).

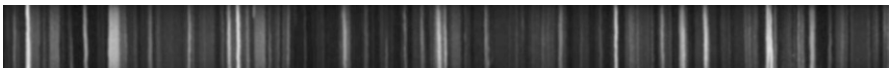

Fig. 18.2 Example of line scan image from the glacial part of the Greenland NGRIP ice core during the last glacial period (depth 1,836.45–1,837 m, approximately 26.1 ka ago). Brighter areas indicate greater dust concentrations

18.3 Dust Records

18.3.1 Southern Hemisphere

18.3.1.1 Antarctica

18.3.1.1.1 Early Discoveries

The first deep ice core drilling in Antarctica was the US "Byrd" program, drilled in West Antarctica in 1968. Thompson et al. (1975) reported microparticle concentrations in the Byrd core, identifying a correlation between temperatures (determined from the $\delta^{18}O$ isotope ratio) and particle concentrations. They observed particles smaller than 1 μm in diameter and attributed these to emissions from circum-Pacific volcanoes. On the assumption that Byrd dust originated from volcanoes, they were not able to explain the greater-than fourfold increase in dust concentrations during the Last Glacial Maximum (LGM) between 12 and 21 ka ago (Johnsen et al. 1972).

The Byrd record was followed by more detailed dust records from the first Dome C ice core, drilled in 1977 to a depth of 905 m (Petit et al. 1981; Royer et al. 1983), and the first Vostok ice core drilled in the early 1980s (De Angelis et al. 1984). The Dome C record spanned 32 ka, showing that dust flux variations occurred across Antarctica and were of a similar magnitude. Petit and co-workers used sea salts (Na, Cl), terrestrial elements (Mg, V) and a volcano proxy (Zn) to attribute the dust to continental sources. Considering dust records from Vostok and D10 (a site 260 km inland of Dumont D'Urville) they identified a smaller, 7-fold, concentration change over the deglacial transition.

18.3.1.1.2 Longer and More Detailed Records

De Angelis et al. (1987) reported Na and Al concentrations in a new Vostok record, extended to 2,200 m depth and approximately 160 ka, finding many novel features in the dust record. They confirmed the strong link between temperature and dust fluxes and showed that dust fluxes were lower during the early glacial period, when temperatures and global ice coverage were also less severe. They reported a dust peak at the end of the penultimate glacial period, approximately 150 ka ago. They also identified that "full" glacial conditions, with very high dust fluxes, were only

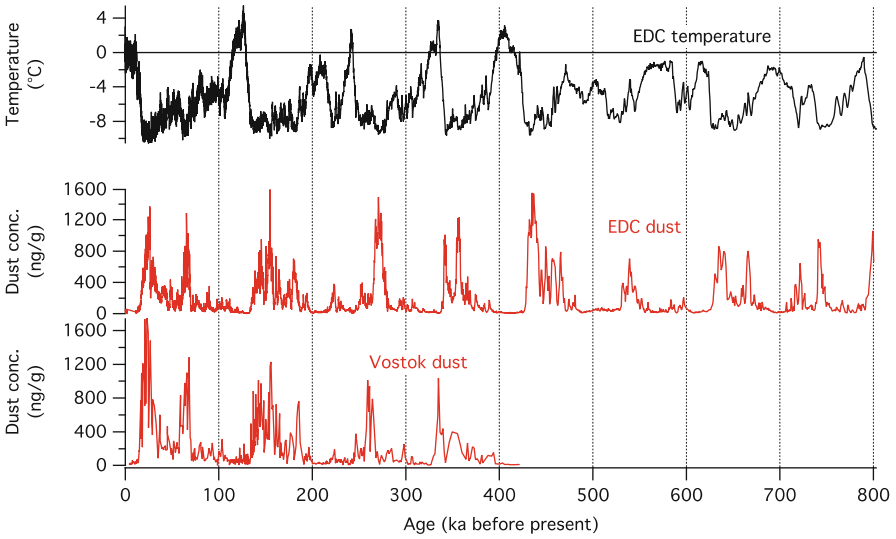

Fig. 18.3 Dust concentrations in EPICA Dome C and Vostok Antarctic ice cores. Also shown are reconstructed temperatures for EDC, relative to the average of the past 1,000 years

observed during the coldest parts of the glacial maxima – about 150, 60 and 20 ka ago. Petit et al. (1990) confirmed these findings and compared them to magnetic records from a Southern Ocean marine sediment record, revealing common dust fluxes to the Antarctic continent and Southern Ocean. The Vostok record was ultimately extended to an age of 420 ka at 3,623 m depth (Petit et al. 1999). It was found that dust peaks had occurred at each of the last four glacial maxima, and were all of approximately equal magnitude (Fig. 18.3).

A new drilling at Dome C under the European Project for Ice Coring in Antarctica (EPICA) covered 8 glacial cycles (780 ka) and is the longest ice core record currently available from Antarctica (Fig. 18.3). Dust fluxes were greater during the last 4 glacial maxima compared to the previous 4 maxima, corresponding to the Mid-Brunhes Event (MBE), a climate transition from cooler interstadials to warmer interstadials about 430 ka ago. Dust fluxes were observed to decrease by approximately 25 times from full glacial to interglacial conditions, with fluxes during glacial maxima regularly being greater than 12 mg/m^2/y. A strong correlation between dust fluxes and paleotemperatures was observed for the coldest climate periods, with much lower correlations (>0.2) during warmer climate periods. This was interpreted as a strengthening in the deflation of dust in southern South America and more efficient transport to deposition sites in Antarctica. The full EPICA Dome C dust record was published in 2008 (Lambert et al. 2008), with earlier evaluations of the last 27 ka (Delmonte et al. 2002a) and 220 ka (Delmonte et al. 2004a).

18.3.1.1.3 Coastal and Regional Variability

Several dust records are available from coastal zones of Antarctica, allowing comparisons between different sectors of Antarctica and the identification of variable dust inputs to different parts of Antarctica on centennial timescales. Delmonte et al. (2004b) reported deglacial dust records from Dome B, Dome C and Komsomolskaya (KMS) and identified a regional oscillation in dust size fraction. This was interpreted as a poleward migration of the Antarctic polar vortex, leading to less subsidence of upper-atmosphere air masses at the more-coastal locations of Dome C and KMS. In all three records, a "pre-Holocene dust minimum" was observed between 11.3 and 12.1 ka ago. Rather than dust, Fischer et al. (2007a) evaluated reported nssCa^{2+} fluxes at EDML, finding them to be approximately 3 times greater than those at EDC. This difference was attributed to the greater proximity of EDML to dust sources in southern South America compared to EDC. Using a simple box model of dust transport, the glacial-interglacial dust flux variability observed at EDML and EDC was attributed to changes in the strength of southern South American dust sources, rather than changes in the efficiency of atmospheric transport pathways.

Dust records from Talos Dome, a coastal site in Northern Victoria Land, feature some important differences to those from the East Antarctic Plateau. The Talos Dome dust record shows greater dust concentrations during the Holocene, attributed to local sources that were exposed since the deglaciation (Delmonte et al. 2010). Over the Holocene, these local source inputs slowly diminished due to changes in local atmospheric circulation resulting from the retreat of the Ross Ice Shelf (Albani et al. 2012) and the possible exhaustion of local dust sources. The Talos Dome dust record does not feature the pre-Holocene dust minimum observed in central East Antarctica, further hinting at different deglacial tendencies across Antarctica and especially in the coastal regions.

18.3.1.1.4 Recent Dust Flux Variations

The few studies available indicate that Antarctic dust fluxes have increased over the twentieth century. McConnell et al. (2007) determined Al fluxes in an ice core from James Ross Island, finding aluminosilicate dust fluxes to have increased since 1832, from approximately 12 (1832–1900) to 27 (1960–1991) mg/m^2/y. This confirmed two low-resolution dust particle records from West Antarctica (Thompson et al. 1994), showing stable dust concentrations between 1500 and 1900, and an approximate doubling over the twentieth century. Vallelonga et al. (2004) also observed a twentieth-century doubling in mineral dust concentrations (based on a suite of 11 crustal and marine elements) in a 500-year ice core record from Law Dome.

18.3.1.2 Southern Hemisphere Mountain Glaciers

Dust records are only available from a few mountain glaciers in the South American Andes. The longest dust records have been produced from the Sajama ice core in Bolivia (Thompson et al. 1998) and the Huascaran ice core in Peru (Thompson et al. 1995), covering the past 20–25 ka. Both records show synchronous temperature changes, but opposing dust trends, to Greenland ice core records. The Andean dust records show high concentrations during the Holocene and from 13 to 16 ka ago, and eight-fold lower concentrations during the glacial. The dust record reflects local hydrological conditions while the temperature record is a strong indication of fast-reacting atmospheric teleconnections between high and low latitudes.

18.3.2 Northern Hemisphere Dust Records

18.3.2.1 Greenland

Hamilton and Langway (1967) were the first to demonstrate annual dust cycles in polar ice using a central Greenland shallow ice core. Since then profiles of Greenland ice core dust concentrations from over the last glacial cycle have been obtained from all of the major Greenland ice coring sites (Fig. 18.1). Hammer et al. (1978) determined dust concentration profiles from sections of the 1,387 m long Camp Century ice core from Northwestern Greenland that covers the entire last glacial period (Dansgaard et al. 1969). A continuous dust concentration profile was obtained from the 2,037 m long Dye-3 ice core from southern Greenland that continuously reaches back some 40 ka (Hammer et al. 1985). In the early 1990s two deep ice cores were retrieved from Summit, Greenland: the 3,053 m long American-led GISP2 ice core (Grootes et al. 1993) and the 3,029 m long European-led GRIP ice core (Johnsen et al. 1992). Both ice cores continuously cover the last 100 ka, although earlier layering is folded and disturbed. Continuous dust records for the glacial section of those ice cores are available (Ram and Koenig 1997; Svensson et al. 2000).

In Fig. 18.4 the high resolution dust concentration record from the 3,085 m long Central Greenland NGRIP ice core (Ruth et al. 2003) is shown together with the Greenland temperature proxy '$\delta^{18}O$' from the same core (NGRIP members 2004). During the present interglacial period, the Holocene covering the last 11.7 ka, and the previous interglacial period, the Eemian about 130–115 ka, the average dust content of the ice has been very low, around 45 mg of dust per kilo of ice (45 ng/g). During the last glacial period the amount of dust that reached Greenland was much greater than during the interglacials. Within the last glacial the dust concentration of the ice is coupled to climate (Fig. 18.3) with the highest dust levels occurring during the cold Marine Isotope Stages (MIS) 2 and 4 and lower levels during the milder MIS3. On shorter time scales of centuries-to-millennium, the coupling to climate is even stronger with high dust concentrations during the colder periods (so-called stadials) and lower dust levels during the milder (so-called interstadial) periods. In

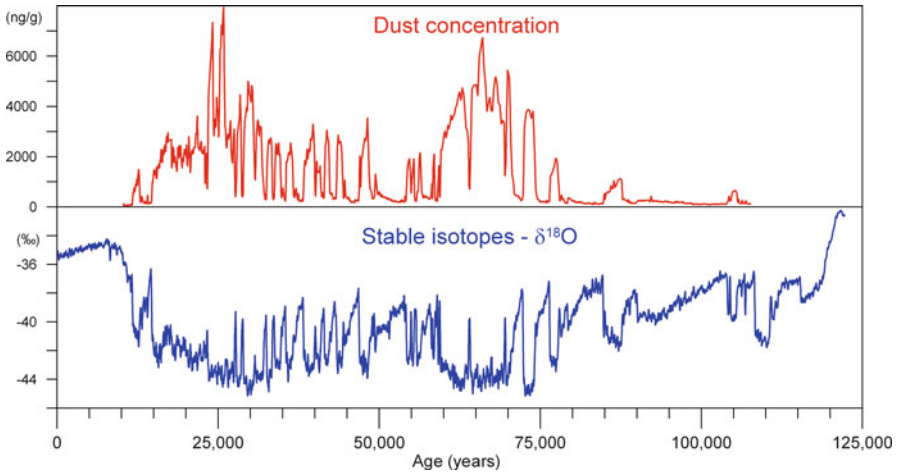

Fig. 18.4 The Greenland NGRIP ice core dust concentration profile (Ruth et al. 2003) together with the $\delta^{18}O$ temperature proxy from the same core (NGRIP members 2004). The more negative the $\delta^{18}O$ proxy, the colder it is

this respect, the dust concentrations follow the typical pattern of most Greenland chemical impurities (Mayewski et al. 1997). Close to the Last Glacial Maximum, at around 25 ka BP, the most extreme dust events occur with dust concentrations of 80–100 times that of interglacial and present day conditions.

The great dust concentration variability of the Greenland ice is thought to have several causes (Fuhrer et al. 1999; Fischer et al. 2007b): First of all, the continental dust sources may have varied in extent and productivity over time (see discussion Sect. 18.4.2). Secondly, the transport efficiency from the sources to Greenland is thought to have varied importantly with climate. During the coldest periods of the last glacial, the high latitude air masses have been relatively dry allowing for reduced wash-out of dust and more efficient long range transport. Furthermore, the latitudinal temperature gradient is thought to have been strong which has caused stronger winds for dust uplift and long-range transport. Finally, changes in amounts of Greenland precipitation influence the dust concentration of the ice. During the coldest glacial periods the snow accumulation was less than half of that of milder periods, so snow accumulation changes alone can thus account for a factor of two or more of the observed dust concentration variability depending on the relative amounts of wet and dry deposition.

At present day, the Greenland dust deposition shows a clear seasonal variability with most of the dust being deposited during springtime (Drab et al. 2002; Banta et al. 2008) (Fig. 18.5). By application of seasonally resolved measurements of various major chemical impurities that all show a strong seasonal pattern this dust-spring pattern can be traced throughout the Holocene period (Rasmussen et al. 2006).

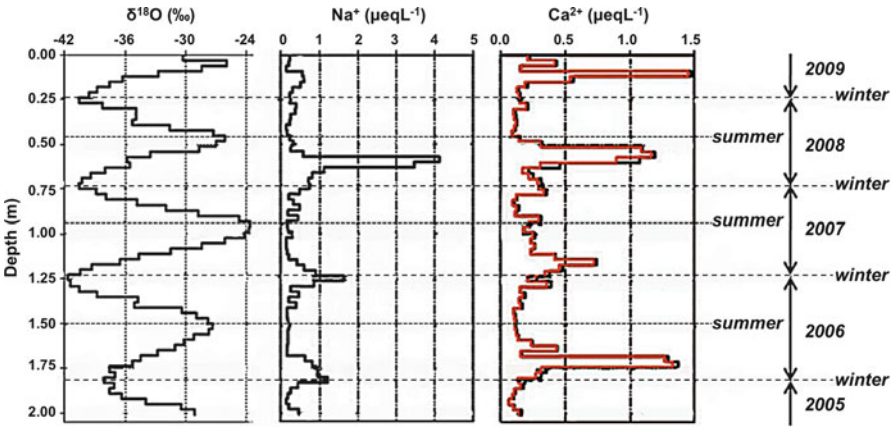

Fig. 18.5 Profiles of oxygen isotope ratios ($\delta^{18}O$), sodium (representing sea salt inputs) and calcium (representing dust inputs) in a snow pit from NEEM site in northwestern Greenland. The regular seasonal deposition of sodium (winter peak) and calcium (spring peaks) is clearly demonstrated. The red curve shows non-sea salt calcium while the black curve shows total calcium. Modified after Kuramoto et al. (2011)

During glacial times the seasonal arrival of dust to Greenland is more difficult to trace, but the dust generally expresses an annual cycle, and high dust levels are clearly visible in the visual stratigraphy of the ice (Fig. 18.2). Together with records of chemical impurities in the ice that also show a pronounced annual cycle, the dust signal has been applied for annual layer counting and dating of the Greenland ice (Andersen et al. 2006; Rasmussen et al. 2006).

18.3.2.2 Northern Hemisphere Glaciers

Few dust records are available for the lower latitudes of the northern hemisphere. Those regions where reliable ice core records are available include Mount Kilimanjaro in Africa and the Himalayas and Tibetan Plateau of central Asia. A 1 ka dust record from Dasuopu glacier in Tibet (Thompson et al. 2000) shows variability driven by changes in Asian monsoon intensity, in addition to a steady rise due to anthropogenic activity after 1900. The increase of dust due to anthropogenic activity has recently been questioned, based on a high-resolution dust record from Mount Everest (Kaspari et al. 2009). Older records from the Dunde ice cap (Thompson et al. 1989) demonstrate higher dust concentrations during the glacial, between 10 and 25 ka ago, approximately double the average Holocene dust level. Ice cores from Kilimanjaro, Tanzania (Thompson et al. 2002), demonstrate distinct periods of high dust fluxes over the past 12 ka, particularly during the "First Dark Age" approximately 4 ka ago.

18.4 Dust Provenance

18.4.1 Antarctica

The earliest investigations of insoluble particles in Antarctic snow and ice used elemental ratios to determine the source of particles to be primarily crustal, rather than volcanic or marine, in nature (Petit et al. 1981). Such an approach had been originally used to determine the inputs of anthropogenic elements to polar ice cores (Murozumi et al. 1969). The deserts of the Southern Hemisphere landmasses were considered the most likely sources of such dust, with the contribution also of continental shelves exposed during glacial periods of low-standing sea levels.

A definitive evaluation of Antarctic dust sources was not available until 1992, with a study of Sr and Nd isotopes in Dome C and PSA samples. Grousset et al. (1992) were the first to identify that South America was the dominant source of dust, despite their sampling of a limited range of PSAs and the availability of only one, composite, LGM sample from the first Dome C ice core (the analytical technique required 11 half-metre ice core sections for one measurement). Despite a limited number of samples from deserts and arid areas in Argentina, South Africa, Australia and Antarctica, they established a good agreement between the Argentinean samples and the Dome C composite sample, dated to 17 ± 1 ka BP. Exposure of the Argentine continental shelf during glacial periods was invoked as a possible explanation for the change in glacial-interglacial dust fluxes. They confirmed the continental source of Dome C dust by REEs; the shape of the REE pattern of the Dome C and continental dust samples were very similar, and clearly different to a volcanic sample from the South Shetland Islands.

In the last two decades, Sr and Nd isotopic provenance techniques have been expanded and complemented, but the primary findings have remained unchanged. Basile et al. (1997) expanded the initial study to Vostok and Dome C ice (sample size reduced to 7 kg) from the dustiest time periods of the last 160 ka: MIS2 (Dome C samples from 16–20 ka ago), MIS4 (Vostok samples from 60–62 ka ago) and MIS6 (Vostok samples from 158–167 ka ago). The field of PSAs was also expanded, with additional samples from Tierra del Fuego, the Argentine continental shelf, New Zealand and Antarctic moraines. They found that the Argentinean continental shelf was not the source of enhanced Antarctic glacial dust fluxes, and that the isotopic signature of dust deposited at Dome C and Vostok was identical. Delmonte et al. (2004a) expanded the PSA dataset to southern South America, southern Africa, New Zealand and the Antarctic Dry Valleys. They found a persistent common dust source for Dome C and Vostok over the last several glacial cycles, attributable to a mixture of southern South American sources (most likely Patagonia and the Puna Altiplano). Recent studies confirm the same source for glacial dust at Talos Dome (Delmonte et al. 2010) and Berkner Island (Bory et al. 2010). Strontium and Nd isotopes have been determined in only six interglacial samples (Delmonte et al. 2007), but these are clearly offset from glacial dust samples (Fig. 18.6). The isotopic offset indicates that other dust sources are active during interglacial periods, most

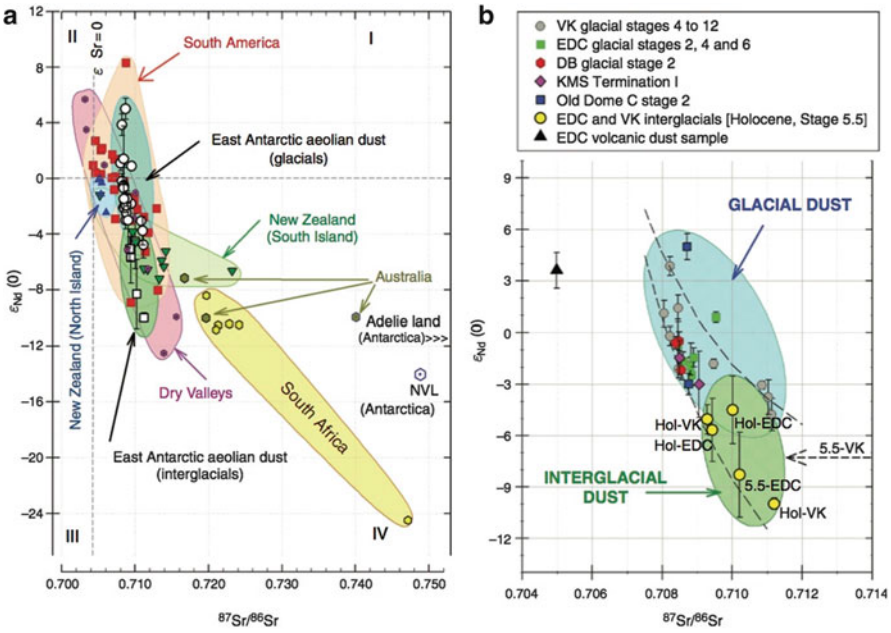

Fig. 18.6 Isotopic ratios of Sr ($^{87}Sr/^{86}Sr$) and Nd [$\varepsilon_{Nd}(0)$] in Antarctic dust and potential source areas (PSA) in the Southern Hemisphere. The blue fields in (**a**) and (**b**) show the signatures of East Antarctic glacial dust which are offset from East Antarctic interglacial dust (*green* fields). The *arrow* in panel (**b**) indicates an additional sample from stage 5.5 for which only Nd isotopes were measured. The volcanic dust sample (*black triangle*) was extracted from one EDC ice core section corresponding to stage 5.5. From Delmonte et al. (2007)

probably in Australia (Revel-Rolland et al. 2006; De Deckker et al. 2010) and/or within Antarctica.

Other techniques for identifying the provenance of Antarctic dust generally complement the initial findings based on the Sr/Nd isotopic system, or highlight periods of enhanced source variability. Lead isotopes can be used to identify different emission sources, such as industrial activity and dust deflation (Vallelonga et al. 2002b), as well as volcanism (Hinkley 2007). Ice from EDC and Law Dome contain mixtures of Pb from Antarctic volcanism and dust from southern South America (Vallelonga et al. 2005). A recent evaluation of Pb isotopes in Dome C ice (Vallelonga et al. 2010) identifies a second continental dust source in Antarctic ice, which can be attributed to Australian and/or local Antarctic sources. The geochemical composition of dust in EDC and EDML ice (Marino et al. 2009) confirms a common glacial dust source for these sites, compatible with a southern South American origin. REEs in EDC (Gabrielli et al. 2010) and EDML (Wegner et al. 2012) ice also demonstrate a change from a dominant glacial signature (southern South America) to a mixture of signatures during the deglacial and early Holocene, including Australian and New Zealand dust sources. Magnetization

(Lanci et al. 2008) and lithium solubility (Siggaard-Andersen et al. 2007) also indicate a change in the composition, and hence sources, of Antarctic dust from glacial to interglacial conditions.

18.4.2 Greenland

As for Antarctica, Greenland ice core dust has been characterized by a number of different provenance tracers, such as isotopes of Sr, Nd, and Pb, mineralogy (determined by X-ray Fluorescence), REEs and other trace elements (Biscaye et al. 1997). The ice core dust is compared to samples from PSAs that for Greenland are mainly North America, Eastern Asia, Northern Africa and the Middle East, exposed continental shelf areas as well as local Greenland sources. It is important to evaluate PSA sample size fractions that are comparable to those of Greenland dust because the characteristics of some tracers, such as Sr isotopes and trace elements, do vary with particle size (Chen et al. 2007; Feng et al. 2011).

During the second half of last glacial period, where dust concentrations of the ice are generally high, the Greenland dust has a very homogeneous composition in all tracers (Svensson et al. 2000). The dust appears to originate almost entirely from deserts and dry areas in eastern Asia, such as the Gobi and Taklimakan Deserts (Biscaye et al. 1997), although the number of samples from potential sources is rather limited (Muhs 2013). In milder climatic periods during the last glacial there may be a contribution originating from glacial sediments adjacent to Greenland (Burton et al. 2007).

During recent times, Asia is also a major dust source for Greenland (Bory et al. 2002) but in addition there is evidence for a significant Saharan contribution (Lupker et al. 2010; VanCuren et al. 2012). In general, more studies of both ice core samples and potential source area samples are needed in order to improve the understanding of Greenland dust provenance throughout time. Besides dust of terrestrial origin, the contributions of volcanic tephra (Abbott et al. 2012) and extraterrestrial dust (Maurette et al. 1987; Gabrielli et al. 2004; Lanci et al. 2012) have been intensively studied in Greenland ice cores (Fig. 18.7).

18.5 Dust Size Distributions

18.5.1 Antarctica

The first evaluation of dust size distributions in Antarctic ice was conducted by Petit et al. (1981) in Dome C ice. Petit and coworkers observed that dust particle size modes were consistently between 1 and 2 μm, with a tendency toward larger modes in LGM samples. The absence of large particles (>10 μm diameter) was interpreted

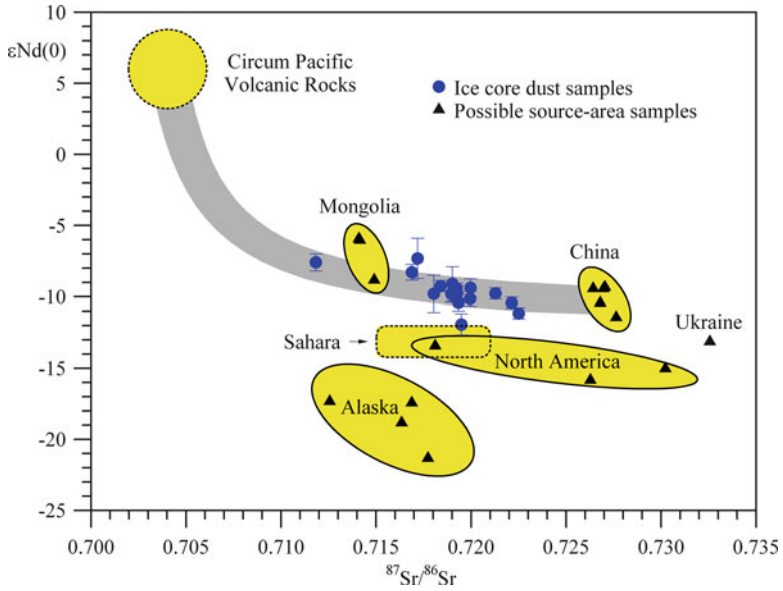

Fig. 18.7 An example of Greenland ice core dust provenance tracing based on the isotopic composition of Strontium (Sr) and Neodymium (Nd). Ice core dust is compared to dust from potential source areas in the Northern Hemisphere. Due to their different geological histories, the dust source areas have different isotopic fingerprints. A fraction of volcanic ash in the ice core samples will drag their isotopic signature in the direction of the 'Circum Pacific Volcanic Rocks'. The ice core dust samples that have been extracted from glacial Greenland ice (*blue dots*) are seen to have an isotopic composition most similar to a mixing of dust from the Asian source areas. Modified after (Biscaye et al. 1997) and (Svensson et al. 2000)

as an indication that the dust in Antarctic ice originated from very distant source locations. Delmonte et al. (2002b) reported particle size distributions in EDC ice over LGM-Holocene transition, observing a minor shift to larger D_v from LGM (1.90 ± 0.07 μm) to Holocene (2.07 ± 0.24 μm) conditions as well as an increase in dust size variability (LGM $\sigma_g = 1.60 \pm 0.03$ and Holocene $\sigma_g = 1.80 \pm 0.15$). This was interpreted as a change in atmospheric transport patterns from more-zonal Holocene winds to more-meridional winds during the LGM. More recent studies (Delmonte et al. 2004b) have identified opposite trends in deglacial dust size tendencies, which the authors related to the transport of finer aerosols in the upper atmosphere and shifts in the location of their subsequent subsidence onto the Antarctic ice sheet, as described in Sect. 18.3.1.1.

Despite these observations and the interpretations drawn from them, few studies have been conducted to unequivocally link ice core records to dust collected in the Antarctic atmosphere. Fattori et al. (2005) collected aerosols on stacked filters of varying porosity (0.4–10 μm range) and found a finer mode at coastal Terra Nova Bay (0.75 μm) compared to inland Dome C base (1 μm). The Terra Nova Bay sample had a smaller particle size mode due to the strong influence of fine sea salt

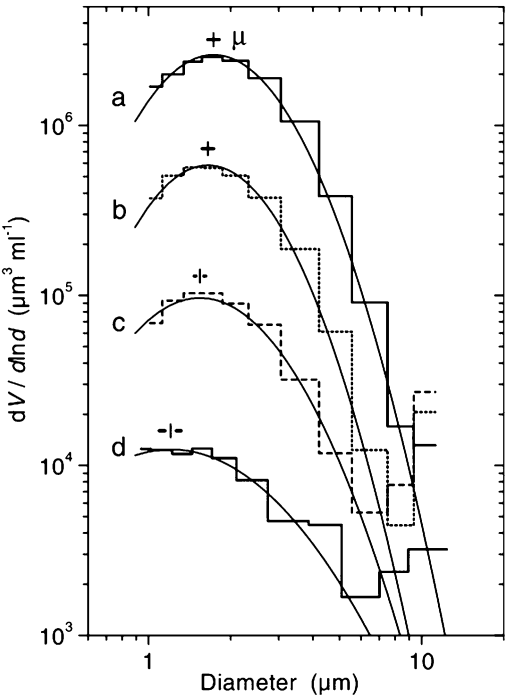

Fig. 18.8 Individual size distributions by volume from different climatic periods along with lognormal fits. *a*: 1,831.50–1,833.15 m (LGM); *b*: 2,075.70–2,077.35 m (Stadial 9); *c*: 2,121.90–2,123.55 m (Interstadial 10); *d*: 1,460.25–1,461.90 m (Preboreal). Indicated is the position of the mode and the uncertainty of the fit [*a*: (1.73 ± 0.02) μm; *b*: (1.65 ± 0.06) μm; *c*: (1.54 ± 0.05) μm; *d*: (1.21 ± 0.11) μm]. From Ruth et al. (2003)

particles. Gassó et al. (2010) also presented a combined study of dust collected from Antarctic air, satellite observations and modelling, although dust particle sizes were not presented. Such combined studies offer the best way forward to quantifying and interpreting changes in particle sizes reported for Antarctic ice.

18.5.2 Greenland

The earliest observations of size distributions of insoluble particles in Greenland ice showed a log-normal distribution similar to that reported for Antarctica. Thompson (1977) observed a greater proportion of coarse particles ($D_v > 1.65$ μm) in Holocene ice from Camp Century ice core, compared to LGM ice. Similar to the situation for Antarctica, more accurate measurements of DYE-3 and GRIP ice by Steffensen (1997) found the opposite result, of a small decrease in D_v from LGM (2.06 μm) to Holocene (1.84 μm) conditions. Most recently, Ruth et al. (2003) used laser particle counter data to confirm the shift toward a larger mode in the more-dust climatic periods of the LGM and late Greenland stadials (1.6–1.7 μm) compared to the Preboreal and Greenland interstadials (1.2–1.5 μm). These results were interpreted as being indicative of a faster atmospheric transport time during the LGM rather than changes in deflation sources or dust characteristics (Fig. 18.8).

18.6 Conclusion

The insoluble dust particles deposited in polar snow allow the investigation of changes in atmospheric and terrestrial conditions over the late Pleistocene. Greenland ice cores have shown great fluctuations in the atmospheric dust content of the Northern Hemisphere, linked closely to the volume of terrestrial ice and consequently the strength of the hydrological cycle. Dust transported to the high Northern latitudes is unequivocally sourced from central Asian deserts including the Gobi and Taklamakan. From Antarctic ice cores, it is clear that southern South America is the dominant source of dust in the Southern Hemisphere, and has been so for at least the last eight glacial-interglacial climate cycles. The very low concentrations of dust present in Antarctic Holocene snow and ice represent an ongoing analytical challenge, with suggestions of additional dust sources but few certainties regarding their locations. Australia, New Zealand and exposed rock areas in Antarctica are currently the most likely candidates for the currently unaccounted sources of dust in Antarctica. The size distributions of dust found in polar ice is reasonably well characterized but further research is required to explain the remarkable homogeneity of dust sizes and the evaluate the extent to which dust size distributions can be used to reconstruct atmospheric transport patterns and/or deflation source variability.

References

Abbott PM, Davies SM, Steffensen JP, Pearce NJG, Bigler M, Johnsen SJ et al (2012) A detailed framework of Marine Isotope Stages 4 and 5 volcanic events recorded in two Greenland ice-cores. Quat Sci Rev 36:59–77

Albani S, Delmonte B, Maggi V, Baroni C, Petit JR, Stenni B et al (2012) Interpreting last glacial to Holocene dust changes at Talos Dome (East Antarctica): implications for atmospheric variations from regional to hemispheric scales. Clim Past 8:741–750

Alley RB, Gow AJ, Meese DA, Fitzpatrick JJ, Waddington ED, Bolzan JF (1997) Grain-scale processes, folding, and stratigraphic disturbance in the GISP2 ice core. J Geophys Res 102:26819–26830

Andersen KK, Svensson A, Rasmussen SO, Steffensen JP, Johnsen SJ, Bigler M et al (2006) The Greenland Ice Core Chronology 2005, 15–42 ka. Part 1: constructing the time scale. Quat Sci Rev 25:3246–3257

Banta JR, McConnell JR, Edwards R, Engelbrecht JP (2008) Delineation of carbonate dust, aluminous dust, and sea salt deposition in a Greenland glaciochemical array using positive matrix factorization. Geochem Geophys Geosyst 9:19

Basile I, Grousset FE, Revel M, Petit J-R, Biscaye PE, Barkov NI (1997) Patagonian origin of glacial dust deposited in East Antarctica (Vostok and Dome C) during glacial stages 2, 4 and 6. Earth Planet Sci Lett 146:573–589

Bigler M, Röthlisberger R, Lambert F, Stocker TF, Wagenbach D (2006) Aerosol deposited in East Antarctica over the last glacial cycle: detailed apportionment of continental and sea-salt contributions. J Geophys Res 111, D08205. doi:10.1029/2005JD006469

Bigler M, Svensson A, Kettner E, Vallelonga P, Nielsen M, Steffensen JP (2011) Optimization of high-resolution continuous flow analysis for transient climate signals in ice cores. Environ Sci Technol 45:4483–4489

Biscaye PE, Grousset FE, Revel M, Van der Gaast S, Zielinski GA, Vaars A et al (1997) Asian provenance of glacial dust (stage 2) in the Greenland Ice Sheet Project 2 Ice Core, Summit, Greenland. J Geophys Res 102:26765–26781

Bory AJ-M, Biscaye PE, Svensson A, Grousset FE (2002) Seasonal variability in the origin of recent atmospheric mineral dust at NorthGRIP, Greenland. Earth Planet Sci Lett 196:123–134

Bory A, Wolff E, Mulvaney R, Jagoutz E, Wegner A, Ruth U et al (2010) Multiple sources supply eolian mineral dust to the Atlantic sector of coastal Antarctica: Evidence from recent snow layers at the top of Berkner Island ice sheet. Earth Planet Sci Lett 291:138–148

Burton GR, Rosman KJR, Candelone J-P, Burn LJ, Boutron CF, Hong S (2007) The impact of climatic conditions on Pb and Sr isotopic ratios found in Greenland ice, 7–150 ky BP. Earth Planet Sci Lett 259:557–566

Chen J, Li G, Yang J, Rao W, Lu H, Balsam W et al (2007) Nd and Sr isotopic characteristics of Chinese deserts: implications for the provenances of Asian dust. Geochim Cosmochim Acta 71:3904–3914

Dansgaard W, Johnsen SJ, Møller J, Langway CC Jr (1969) One thousand centuries of climatic record from Camp Century on the Greenland ice sheet. Science 166:377–381

De Angelis M, Legrand M, Petit JR, Barkov NI, Korotkevitch YS, Kotlyakov VM (1984) Soluble and insoluble impurities along the 950 m deep Vostok ice core (Antarctica) – climatic implications. J Atmos Chem 1:215–239

De Angelis M, Barkov NI, Petrov VN (1987) Aerosol concentrations over the last climatic cycle (160 kyr) from an Antarctic ice core. Nature 325:318–321

De Deckker P, Norman M, Goodwin ID, Wain A, Gingele FX (2010) Lead isotopic evidence for an Australian source of aeolian dust to Antarctica at times over the last 170,000 years. Palaeogeogr Palaeoclimatol Palaeoecol 285:205–223

Delmonte B, Petit J-R, Maggi V (2002a) Glacial to Holocene implications of the new 27000-year dust record from the EPICA Dome C (East Antarctica) ice core. Clim Dyn 18:647–660

Delmonte B, Petit J-R, Maggi V (2002b) LGM-Holocene changes and Holocene millennial-scale oscillations of dust particles in the EPICA Dome C ice core, East Antarctica. Ann Glaciol 35:306–312

Delmonte B, Basile-Doelsch I, Petit J-R, Maggi V, Revel-Rolland M, Michard A et al (2004a) Comparing the EPICA and Vostok dust records during the last 220,000 years: stratigraphic correlation and provenance in glacial periods. Earth-Sci Rev 66:63–87

Delmonte B, Petit JR, Andersen KK, Basile-Doelsch I, Maggi V, Ya Lipenkov V (2004b) Dust size evidence for opposite regional atmospheric circulation changes over east Antarctica during the last climatic transition. Clim Dyn 23:427–438

Delmonte B, Petit JR, Basile-Doelsch I, Jagoutz E, Maggi V (2007) Late quaternary interglacials in East Antarctica from ice core dust records. In: Sirocko F, Litt T, Claussen M (eds) The climate of past interglacials, vol 7. Elsevier, Amsterdam, pp 53–73

Delmonte B, Baroni C, Andersson PS, Schoberg H, Hansson M, Aciego S et al (2010) Aeolian dust in the Talos Dome ice core (East Antarctica, Pacific/Ross Sea sector): Victoria Land versus remote sources over the last two climate cycles. J Quat Sci 25:1327–1337

Drab E, Gaudichet A, Jaffrezo JL, Colin JL (2002) Mineral particles content in recent snow at Summit (Greenland). Atmos Environ 36:5365–5376

Edwards R, Sedwick P, Morgan V, Boutron C (2006) Iron in ice cores from Law Dome: a record of atmospheric iron deposition for maritime East Antarctica during the Holocene and Last Glacial Maximum. Geochem Geophys Geosyst 7(12):Q12Q01. doi:10.1029/2006GC001307

Faria SH, Freitag J, Kipfstuhl S (2010) Polar ice structure and the integrity of ice-core paleoclimate records. Quat Sci Rev 29:338–351

Fattori I, Becagli S, Bellandi S, Castellano E, Innocenti M, Mannini A et al (2005) Chemical composition and physical features of summer aerosol at Terra Nova Bay and Dome C, Antarctica. J Environ Monit 7:1265–1274

Feng J-L, Hu Z-G, Ju J-T, Zhu L-P (2011) Variations in trace element (including rare earth element) concentrations with grain sizes in loess and their implications for tracing the provenance of eolian deposits. Quat Int 236:116–126

Fischer H, Fundel F, Ruth U, Twarloh B, Wegner A, Udisti R et al (2007a) Reconstruction of millennial changes in dust emission, transport and regional sea ice coverage using the deep EPICA ice cores from the Atlantic and Indian Ocean sector of Antarctica. Earth Planet Sci Lett 260:340–354

Fischer H, Siggaard-Andersen M-L, Ruth U, Röthlisberger R, Wolff E (2007b) Glacial/interglacial changes in mineral dust and sea-salt records in polar ice cores: sources, transport, and deposition. Rev Geophys 45:RG1002. doi:10.29/2005RG000192

Fuhrer K, Wolff EW, Johnsen SJ (1999) Timescales for dust variability in the Greenland Ice Core Project (GRIP) ice core in the last 100,000 years. J Geophys Res 104:31043–31052

Gabrielli P, Varga A, Barbante C, Boutron C, Cozzi G, Gaspari V et al (2004) Determination of Ir and Pt down to the sub-femtogram per gram level in polar ice by ICP-SFMS using preconcentration and a desolvation system. J Anal At Spectrom 19:831–837

Gabrielli P, Wegner A, Petit JR, Delmonte B, De Deckker P, Gaspari V et al (2010) A major glacial-interglacial change in aeolian dust composition inferred from rare earth elements in Antarctic ice. Quat Sci Rev 29:265–273

Gassó S, Stein A, Marino F, Castellano E, Udisti R, Ceratto J (2010) A combined observational and modeling approach to study modern dust transport from the Patagonia desert to East Antarctica. Atmos Chem Phys 10:8287–8303

Grootes PM, Stuiver M, White JWC, Johnsen SJ, Jouzel J (1993) Comparison of oxygen isotope records from the GISP2 and GRIP Greenland ice cores. Nature 366:552–554

Grousset FE, Biscaye PE (2005) Tracing dust sources and transport patterns using Sr, Nd and Pb isotopes. Chem Geol 222:149–167

Grousset FE, Biscaye PE, Revel M, Petit JR, Pye K, Joussaume S et al (1992) Antarctic (Dome C) ice-core dust at 18 k.y. B.P.: Isotopic constraints on origins. Earth Planet Sci Lett 111:175–182

Hamilton WL, Langway CC Jr (1967) A correlation of microparticle concentrations with oxygen isotope ratios in 700 year old Greenland ice. Earth Planet Sci Lett 3:363–366

Hammer CU, Clausen HB, Dansgaard W, Gundestrup N, Johnsen SJ, Reeh N (1978) Dating of Greenland ice cores by flow models, isotopes, volcanic debris, and continental dust. J Glaciol 20:3–26

Hammer CU, Clausen HB, Dansgaard W, Neftel A, Kristinsdottir P, Johnson E (1985) Continuous impurity analysis along the Dye-3 deep core. In: Langway CC Jr, Oeschger H, Dansgaard W (eds) Greenland ice core: geophysics, geochemistry, and the environment. American Geophysical Union (AGU), Washington, DC, pp 90–94

Hinkley T (2007) Lead (Pb) in old Antarctic ice: some from dust, some from other sources. Geophys Res Lett 34, L08502. doi:10.1029/2006GL028736

Hörhold MW, Laepple T, Freitag J, Bigler M, Fischer H, Kipfstuhl S (2012) On the impact of impurities on the densification of polar firn. Earth Planet Sci Lett 325–326:93–99

Johnsen SJ, Dansgaard W, Clausen HB, Langway CC Jr (1972) Oxygen isotope profiles through the Antarctic and Greenland ice sheets. Nature 235:429–434

Johnsen SJ, Clausen HB, Dansgaard W, Fuhrer K, Gundestrup N, Hammer CU et al (1992) Irregular glacial interstadials recorded in a new Greenland ice core. Nature 359:311–313

Kaspari S, Mayewski PA, Handley M, Kang S, Hou S, Sneed S et al (2009) A high-resolution record of atmospheric dust composition and variability since a.d. 1650 from a Mount Everest ice core. J Clim 22:3910–3925

Kuramoto T, Goto-Azuma K, Hirabayashi M, Miyake T, Motoyama H, Dahl-Jensen D et al (2011) Seasonal variations of snow chemistry at NEEM, Greenland. Ann Glaciol 52:193–200

Lambert F, Delmonte B, Petit JR, Bigler M, Kaufmann PR, Hutterli MA et al (2008) Dust-climate couplings over the past 800,000 years from the EPICA Dome C ice core. Nature 452:616–619

Lanci L, Delmonte B, Maggi V, Petit JR, Kent DV (2008) Ice magnetization in the EPICA-Dome C ice core: implication for dust sources during glacial and interglacial periods. J Geophys Res 113(D14), D14207. doi:10.1029/2007JD009678

Lanci L, Delmonte B, Kent DV, Maggi V, Biscaye PE, Petit JR (2012) Magnetization of polar ice: a measurement of terrestrial dust and extraterrestrial fallout. Quat Sci Rev 33:20–31

Lupker M, Aciego SM, Bourdon B, Schwander J, Stocker TF (2010) Isotopic tracing (Sr, Nd, U and Hf) of continental and marine aerosols in an 18th century section of the Dye-3 ice core (Greenland). Earth Planet Sci Lett 295:277–286

Marino F, Castellano E, Nava S, Chiari M, Ruth U, Wegner A et al (2009) Coherent composition of glacial dust on opposite sides of the East Antarctic Plateau inferred from the deep EPICA ice cores. Geophys Res Lett 36(23), L23703. doi:10.1029/2009GL040732

Maurette M, Jéhanno C, Robin E, Hammer CU (1987) Characteristics and mass distribution of extraterrestrial dust from the Greenland ice cap. Nature 328:699–702

Mayewski PA, Meeker LD, Twickler MS, Whitlow S, Yang QZ, Lyons WB et al (1997) Major features and forcing of high-latitude northern hemisphere atmospheric circulation using a 110,000-year-long glaciochemical series. J Geophys Res Ocean 102:26345–26366

McConnell JR, Aristarain AJ, Banta JR, Edwards PR, Simões JC (2007) 20th-century doubling in dust archived in an Antarctic Peninsula ice core parallels climate change and desertification in South America. Proc Natl Acad Sci U S A 104:5743–5748

McGwire KC, McConnell JR, Alley RB, Banta JR, Hargreaves GM, Taylor KC (2008) Dating annual layers of a shallow Antarctic ice core with an optical scanner. J Glaciol 54:831–838

Muhs DR (2013) The geologic records of dust in the Quaternary. Aeolian Research 9:3–48. doi:10.1016/j.aeolia.2012.08.001

Murozumi M, Chow TJ, Patterson CC (1969) Chemical concentrations of pollutant lead aerosols, terrestrial dusts and sea salts in Greenland and Antarctic snow strata. Geochim Cosmochim Acta 33:1247–1294

NEEM Community Members (2013) Eemian interglacial reconstructed from a Greenland folded ice core. Nature 493:489–494

NGRIP Members (2004) High-resolution record of Northern Hemisphere climate extending into the last interglacial period. Nature 431:147–151

Parrenin F, Barnola J-M, Beer J, Blunier T, Castellano E, Chappellaz J et al (2007) The EDC3 chronology for the EPICA Dome C ice core. Clim Past 3:485–497

Petit J-R, Briat M, Royer A (1981) Ice age aerosol content from East Antarctic ice core samples and past wind strength. Nature 293:391–394

Petit JR, Mounier L, Jouzel J, Korotkevich YS, Kotlyakov VI, Lorius C (1990) Palaeoclimatological and chronological implications of the Vostok core dust record. Nature 343:56–58

Petit J-R, Jouzel J, Raynaud D, Barkov NI, Barnola J-M, Basile I et al (1999) Climate and atmospheric history of the past 420,000 years from the Vostok ice core, Antarctica. Nature 399:429–436

Ram M, Koenig G (1997) Continuous dust concentration profile of pre-Holocene ice from the Greenland Ice Sheet Project 2 ice core: dust stadials, interstadials, and the Eemian. J Geophys Res 102:26641–26648

Rasmussen SO, Andersen KK, Svensson AM, Steffensen JP, Vinther BM, Clausen HB et al (2006) A new Greenland ice core chronology for the last glacial termination. J Geophys Res 111, D06102. doi:10.1029/2005JD006079

Revel-Rolland M, De Dekker P, Delmonte B, Hesse PP, Magee JW, Basile-Doelsch I et al (2006) Eastern Australia: a possible source of dust in East Antarctica interglacial ice. Earth Planet Sci Lett 249:1–13

Rhodes RH, Baker JA, Millet M-A, Bertler NAN (2011) Experimental investigation of the effects of mineral dust on the reproducibility and accuracy of ice core trace element analyses. Chem Geol 286:207–221

Rosman KJR (2001) Natural isotopic variations in lead in polar snow and ice as indicators of source regions. In: Caroli S, Cescon P, Walton DWH (eds) Environmental contamination in Antarctica: a challenge to analytical chemistry. Elsevier Science B.V, New York, pp 87–106

Royer A, De Angelis M, Petit JR (1983) A 30 000 year record of physical and optical properties of microparticles from an East Antarctic ice core and implications for paleoclimate reconstruction models. Clim Chang 5:381–412

Ruth U, Wagenbach D, Steffensen JP, Bigler M (2003) Continuous record of microparticle concentration and size distribution in the central Greenland NGRIP ice core during the last glacial period. J Geophys Res 108(D3):4098. doi:10.1029/2002JD002376

Ruth U, Barbante C, Bigler M, Delmonte B, Fischer H, Gabrielli P et al (2008) Proxies and measurement techniques for mineral dust in Antarctic ice cores. Environ Sci Technol 42:5675–5681

Siggaard-Andersen M-L, Gabrielli P, Steffensen JP, Strømfeldt T, Barbante C, Boutron C et al (2007) Soluble and insoluble lithium dust in the EPICA DomeC ice core – implications for changes of the East Antarctic dust provenance during the recent glacial–interglacial transition. Earth Planet Sci Lett 258:32–43

Steffensen JP (1997) The size distribution of microparticles from selected segments of the Greenland Ice Core Project ice core representing different climatic periods. J Geophys Res 102:26755–26763

Svensson A, Biscaye PE, Grousset FE (2000) Characterization of late glacial continental dust in the Greenland Ice Core Project ice core. J Geophys Res 105:4637–4656

Svensson A, Nielsen SW, Kipfstuhl S, Johnsen SJ, Steffensen JP, Bigler M et al (2005) Visual stratigraphy of the North Greenland Ice Core Project (NorthGRIP) ice core during the last glacial period. J Geophys Res 110, D02108

Svensson A, Bigler M, Kettner E, Dahl-Jensen D, Johnsen S, Kipfstuhl S et al (2011) Annual layering in the NGRIP ice core during the Eemian. Clim Past 7:1427–1437

Thompson LG (1977) Variations in microparticle concentration, size distribution and elemental composition found in Camp Century, Greenland, and Byrd Station, Antarctica, deep ice cores. In: Proceedings of symposium on isotopes and impurities in snow and ice, International Association of Hydrological Sciences, Commission of Snow and Ice, I.U.G.G. XVI, General Assembly, Grenoble Aug–Sep, 1975. Washington, DC, pp 351–63

Thompson LG, Hamilton WL, Bull C (1975) Climatological implications of microparticle concentrations in the ice core from "Byrd" Station, Western Antarctica. J Glaciol 14:433–444

Thompson LG, Mosley-Thompson E, Davis ME, Bolzan JF, Dai J, Yao T et al (1989) Holocene-Late Pleistocene climatic ice core records from Qinghai-Tibetan Plateau. Science 246:474–477

Thompson LG, Peel DA, Mosley-Thompson E, Mulvaney R, Dal J, Lin PN et al (1994) Climate since AD 1510 on Dyer Plateau, Antarctic Peninsula: evidence for recent climate change. Ann Glaciol 20:420–426

Thompson LG, Mosley-Thompson E, Davis ME, Lin P-N, Henderson KA, Cole-Dai J et al (1995) Late glacial stage and Holocene tropical ice core records from Huascarán, Peru. Science 269:46–50

Thompson LC, Davis ME, Mosley-Thompson E, Sowers TA, Henderson KA, Zagorodnov VS et al (1998) A 25,000-year tropical climate history from Bolivian ice cores. Science 282:1858–1864

Thompson LG, Yao T, Mosley-Thompson E, Davis ME, Henderson KA, Lin P-N (2000) A high-resolution millennial record of the South Asian monsoon from Himalayan ice cores. Science 289:1916–1919

Thompson LG, Mosley-Thompson E, Davis ME, Henderson KA, Brecher H, Zagorodnov V et al (2002) Kilimanjaro ice core records: evidence of Holocene climate change in tropical Africa. Science 298:589–593

Traversi R, Barbante C, Gaspari V, Fattori I, Largiuni O, Magaldi L et al (2004) Aluminium and iron record for the last 28 kyr derived from the Antarctic EDC96 ice core using new CFA methods. Ann Glaciol 39:300–306

Vallelonga P, Van de Velde K, Candelone J-P, Ly C, Rosman KJR, Boutron CF et al (2002a) Recent advances in measurement of Pb isotopes in Polar ice and snow at sub-picogram per gram concentrations using thermal ionisation mass spectrometry. Anal Chim Acta 453:1–12

Vallelonga P, Van de Velde K, Candelone J-P, Morgan VI, Boutron CF, Rosman KJR (2002b) The lead pollution history of Law Dome, Antarctica, from isotopic measurements on ice cores: 1500 AD to 1989 AD. Earth Planet Sci Lett 204:291–306

Vallelonga P, Barbante C, Cozzi G, Gaspari V, Candelone J-P, Van de Velde K et al (2004) Elemental indicators of natural and anthropogenic aerosol inputs to Law Dome, Antarctica. Ann Glaciol 39:169–174

Vallelonga P, Gabrielli P, Rosman KJR, Barbante C, Boutron CF (2005) A 220 kyr record of Pb isotopes at Dome C Antarctica from analyses of the EPICA ice core. Geophys Res Lett 32, L01706

Vallelonga P, Gabrielli P, Balliana E, Wegner A, Delmonte B, Turetta C et al (2010) Lead isotopic compositions in the EPICA Dome C ice core and Southern Hemisphere potential source areas. Quat Sci Rev 29:247–255

VanCuren RA, Cahill T, Burkhart J, Barnes D, Zhao YJ, Perry K et al (2012) Aerosols and their sources at Summit Greenland – first results of continuous size- and time-resolved sampling. Atmos Environ 52:82–97

Wegner A, Gabrielli P, Wilhelms-Dick D, Ruth U, Kriews M, De Deckker P et al (2012) Change in dust variability in the Atlantic sector of Antarctica at the end of the last deglaciation. Clim Past 8:135–147

Wolff EW, Chappellaz J, Blunier T, Rasmussen SO, Svensson A (2010) Millennial-scale variability during the last glacial: the ice core record. Quat Sci Rev 29:2828–2838

Index

P. Knippertz and J.-B.W. Stuut (eds.), *Mineral Dust: A Key Player in the Earth System*, DOI 10.1007/978-94-017-8978-3,